Handbook of Integrated and Sustainable Buildings Equipment and Systems

Volume 1: Energy Systems

Edited by

Jorge E. Gonzalez and Moncef Krarti

Library of Congress Cataloging-in-Publication Data

Names: Gonzalez, Jorge E., 1965- editor. | Krarti, Moncef, editor. | American Society of Mechanical Engineers, issuing body.
Title: Handbook of integrated and sustainable buildings equipment and systems/ edited by Jorge E. Gonzalez and Moncef Krarti.
Description: New York : ASME Press, 2017- | Includes bibliographical references and index.
Identifiers: LCCN 2017010072 | ISBN 9780791861271 (volume 1 : alk. paper)
Subjects: LCSH: Buildings--Mechanical equipment--Handbooks, manuals, etc. | Sustainable buildings--Handbooks, manuals, etc. | Buildings--Energy conservation | Buildings--Heating--Handbooks, manuals, etc.
Classification: LCC TH6010 .H285 2017 | DDC 690.028/6--dc23
LC record available at https://lccn.loc.gov/2017010072

Table of Contents

Preface xiii

Editors xv

Contributors xvii

1 INTRODUCTION 1

1.1 Introduction 1

1.2 On the State of Building Energy in the U.S. and Global Energy Sector 3

1.3 On Building Energy Modeling 4

1.4 On Controls and Monitoring of Building Systems 5

1.5 On Passive Design Strategies 6

1.6 On Integrated Renewable Energy Generation and Energy-Efficient Technologies 8

1.7 On Integrated Power, Heating, Cooling, and Thermal Storage Equipment and Systems 10

1.8 Neighborhood and City-Scale Integrated Energy Strategies 14

1.9 Additional Topics for Future Consideration 16

1.9.1 Commercial Building Lighting and Window Designs 16

1.9.2 Data Centers 17

1.9.3 On the Subject of Climate Change and Sustainable Buildings 17

1.10 Recommendations and Next Steps on ISBES 18

References 20

2 BUILDING ENERGY SYSTEMS MODELING AND SIMULATION 23

2.1 Introduction 23

2.2 Basic Heat Transfer Concepts 24
2.2.1 Transient Heat Transfer from Building Envelope 26

2.3 Methods for Transient Building Envelope Energy Analysis 30
2.3.1 Finite Difference Methods 31
2.3.2 Interzone Temperature Profile Estimation (ITPE) Techniques 34
2.3.3 Conduction Transfer Function (CTF) Methods 41
2.3.4 Frequency-Domain Regression 44
2.3.5 Response Factors 53

2.4 Simplified Energy Analysis Methods 60
2.4.1 Variable Base Degree Days Method 60
2.4.2 Transient Thermal Network Analysis 67

2.5 Detailed Energy Analysis Methods 70
2.5.1 Heat Balance Method 70
2.5.2 Thermal Network Method 73
2.5.3 Weighting Factors 74

2.6 Whole-Building Energy Models 76
2.6.1 Inverse Modeling Methods 77
2.6.2 Forward Modeling Methods 81
2.6.3 Meta-Modeling Approach 86

2.7 Summary 89

References 89

3 CONVENTIONAL MECHANICAL SYSTEMS FOR EFFICIENT HEATING, VENTILATING, AND AIR CONDITIONING SYSTEMS 93

3.1 Introduction 93

3.2 Cooling Vapor Compression Systems 94
3.2.1 Refrigerants 96

3.3 Absorption Cooling Systems 97

3.4 Mechanical Cooling Equipment — Chillers 100

3.5 Heat Rejection Equipment 101
3.5.1 Cooling Towers 101
3.5.2 Air-Cooled Condensers 104

3.6 Recommendations for Chiller System Operation in Commercial Buildings 105

3.7 Cooling by Desiccant Equipment 106
3.7.1 Performance Equations for Liquid Desiccant Equipment 108

3.8 Summary for Cooling Equipment 109

3.9 Heat Generation and Transfer Equipment 109
3.9.1 Introduction 109
3.9.2 Furnaces and Boilers 110
3.9.3 Electric Resistance Heating 119
3.9.4 Electric Heat Pumps 120
3.9.5 Low-Temperature Radiant Heating Systems 121

3.10 Secondary Equipment: Air Handling Units 124
3.10.1 Fresh Air Ventilation Rates 126

3.11 High Efficiency System Integration 127
3.11.1 Chiller Water Loops and VAV Systems 127
3.11.2 Energy Recovery Systems 132

3.12 Future Trends of HVAC Mechanical Systems 133
3.12.1 Supervisory Control Systems 133
3.12.2 Heat Exchanger Materials 134
3.12.3 Surface Enhancing Heat Transfer 134

References 135

4 PASSIVE COOLING AND HEATING TECHNIQUES FOR BUILDINGS 139

4.1 Introduction 139

4.2 Overview of Passive Cooling 142

4.3 Overview of Passive Heating 143

4.4 Prescreening Feasibility of Passive Cooling and Heating Techniques 145

4.5 Natural Ventilation 147
4.5.1 Principle 147
4.5.2 Performance 148
4.5.3 Design Considerations 150

4.6 Night Cooling with Thermal Mass 154
4.6.1 Principle 154
4.6.2 Performance 154
4.6.3 Design Considerations 155

4.7 Direct/Indirect Evaporative Cooling 158
4.7.1 Principle 158
4.7.2 Performance 159
4.7.3 Design Considerations 160

4.8 Trombe Wall 162
4.8.1 Principle 162
4.8.2 Performance 163
4.8.3 Design Considerations 164

4.9 Sunspace 165
4.9.1 Principle 165
4.9.2 Performance 166
4.9.3 Design Considerations 167

4.10 Double Skin Facade 168
4.10.1 Principle 168
4.10.2 Performance 169
4.10.3 Design Considerations 170

4.11 Phase Change Material **173**
4.11.1 Principle 173
4.11.2 Performance 174
4.11.3 Design Considerations 177

4.12 Two Case Studies **179**
4.12.1 Houghton Hall Office Building in Luton, UK 179
4.12.2 RMI Headquarters Building: Amory Lovins Uber Solar Home in Colorado, US 180

References **184**

5 CONTROL STRATEGIES FOR BUILDING ENERGY SYSTEMS 189

5.1 Introduction **189**

5.2 Basic Control Principles **190**
5.2.1 Overview of Control System Components 190
5.2.2 Transfer Function Analysis 193
5.2.3 Control Modes 198
5.2.4 Intelligent Control Systems 201
5.2.5 Types of Control Systems 202

5.3 Supervisory Controllers **204**
5.3.1 Basic Components of an EMCS 204
5.3.2 Typical Functions of ECMS 206
5.3.3 Design Considerations of an EMCS 207
5.3.4 Communication Protocols 209

5.4 Control Applications **210**
5.4.1 Electrical Systems 211
5.4.2 Optimal Start of HVAC Systems 218
5.4.3 HVAC Equipment Operation 221
5.4.4 HVAC Systems with Thermal Storage 236

5.5 Summary **246**

References **246**

6 COMBINED COOLING, HEATING, AND POWER SYSTEMS FOR BUILDINGS 251

6.1 Introduction 252

6.2 State-of-the-Art Review of CCHP Technology 254

6.3 Prime Mover Options 260

6.4 Heat Recovery 261

6.5 Thermally Activated Cooling Systems 264

6.6 Thermal Energy Storage Requirements/Benefits 270

6.7 CCHP Sizing Options, Building Integration, Operation and System Controls: Case Studies 271

6.8 Economic and Feasibility Analysis 279

6.9 Future CCHP and Conclusion 284

Nomenclature 284

Useful Resources 285

Calculator 285

References 285

7 INTEGRATION OF SOLAR ENERGY SYSTEMS 291

7.1 Introduction to Integration of Solar Energy Systems 291

7.2 Photovoltaics 292

7.3 Daylighting 305

7.4 Passive Solar Heating and Cooling Load Avoidance 313

7.5 Solar Ventilation Air Preheating 319

7.6 Solar Water Heating **324**
7.6.1 Low Temperature Unglazed Collector 325
7.6.2 Glazed Flat Plate Collectors 326
7.6.3 Evacuated Tube Collectors 326
7.6.4 Parabolic Trough Collectors 327

7.7 Energy Systems Integration **335**
7.7.1 Building Level Challenges and Solutions 337
7.7.2 Substation-Level Challenges and Solutions 341
7.7.3 Grid-Level Challenges and Solutions 342
7.7.4 Utilities' Electrical Generation Systems 343

7.8 Conclusion **345**

References **346**

8 ENERGY STORAGE SYSTEMS FOR BUILDINGS 347

8.1 Introduction **347**

8.2 Sensible and Latent TES Systems for Buildings **348**
8.2.1 Energy Storage System Classification 348
8.2.2 TES for Building Air Conditioning 349
8.2.3 TES for Heating 358
8.2.4 TES and Heat Pumps 367
8.2.5 TES and CHP 370
8.2.6 Building with TES Integration Literature Summary 375
8.2.7 Materials for Sensible/Latent TES 379
8.2.8 Mathematical Modeling of Storage System 383

8.3 Sorption TES System for Buildings **385**
8.3.1 Working Principle of Sorption TES System 385
8.3.2 Sorption Working Pairs 392
8.3.3 Sorption TES Performance Improvement 397

8.4 Conclusions and Perspective **407**

Nomenclature **408**

Acknowledgments **409**

References **409**

9 AUTOMATED FAULT DETECTION AND DIAGNOSIS IN HVAC SYSTEMS 421

9.1 Introduction to Alarm Management and Fault Detection and Diagnosis 421
9.1.1 Process or System Fault Definition 422
9.1.2 Process Monitoring Method 424

9.2 Classification of Fault Detection Methods 425
9.2.1 Traditional Alarm Management—A Prismatic Approach 425
9.2.2 Most Commonly Used Fault Detection and Diagnosis Methods 427

9.3 Recent Advances in Fault Detection for HVAC Systems 436

9.4 Industrial and HVAC Applications of Fault Detection Methods 441
9.4.1 Hardware/Software Requirements 442
9.4.2 Business Models and Commercial Solutions 443
9.4.3 Review of Industrial and HVAC Implementations of FDD 443

9.5 Challenges in FDD Application to Buildings and HVAC Systems 450
9.5.1 Technology Platforms Related Challenges 450
9.5.2 Strategy or Approach Related Challenges 451

9.6 Case Study Fault Detection System for a District Cooling Systems 452
9.6.1 Process Layout and Specifications 452
9.6.2 FDD Design and Features 454
9.6.3 Implementation Results 455
9.6.4 Conclusions and Recommendations 461

9.7 Conclusions and Future Works 464

Acknowledgments 465

References 465

10 MODELING BUILDING AIR CONDITIONING ENERGY CONSUMPTION IN DENSE URBAN ENVIRONMENTS 475

10.1 Chapter Summary 475

10.2 Introduction 476

10.3 Case Study Sites 478

10.4 Description of the Summer 2010 Heat Wave Event 481

10.5 Methodology for Case Study 483
10.5.1 City Scale Model-uWRF 483
10.5.2 Building Energy Parameterization (BEP) 484
10.5.3 Building Energy Model (BEM) 485
10.5.4 Single Building Energy Model-EnergyPlus™ 488

10.6 Results and Discussion 490

10.7 Conclusions and Future Work 495

Acknowledgments 496

Nomenclature 496

References 497

Index 501

Preface

This *Handbook of Integrated and Sustainable Buildings Equipment and Systems* is a direct result of the American Society of Mechanical Engineers (ASME) initiative on Integrated/Sustainable Building Equipment and Systems (ISBES) which has the objective of filling voids in the literature and motivate advances on integrated mechanical systems in buildings. The main focus of this first Volume of the Handbook is on integrated energy systems in the built environment. The handbook includes current state of knowledge in areas of energy equipment and building energy modeling tools, and emerging topics in a wide range of areas encompassing combined heat and power, building energy storage systems, and advanced control strategies for mechanical energy systems in buildings. In addition, the integration of renewable energy and passive cooling and heating strategies as well as the latest advanced techniques to analyze energy demands at the neighborhood and city scales are addressed. The contributors have a diverse set of skills and extensive experience in building energy engineering. The main audience for the Handbook are practitioners building engineers and researchers seeking current and emerging topics in a single source.

The first handbook of the ISBES initiative highlights the state-of-the art in energy systems for buildings and has four different but very important focus areas:

- Developing and promoting innovative energy efficient design strategies;
- Integrating renewable energy generation into buildings and building systems;
- Integrating power generation systems into building heating and cooling systems; and
- Integrating energy strategies at neighborhood and city-scales.

A strategic workshop was convened on April 24, 2013 at the ASME Center for Research and Technology Development (CRTD) and ASME Emerging Technologies (ET) at the ASME offices in Washington, D.C. in order to identify and evaluate challenges and opportunities in topical areas related to ISBES. National technical experts and thought leaders from industry, government, and academia came together for a detailed one-day discussion of the four proposed ISBES-topical areas. The workshop

was proceeded by several technical sessions at the ASME International Conference and Exposition and at the International Energy Sustainability Conferences. These efforts resulted in a wealth of knowledge that was first summarized in a Special Issue in the ASME Journal of Solar Energy Engineering, and now expanded in this *Handbook of Integrated and Sustainable Buildings Equipment and Systems: Volume I: Energy Systems*. We hope this handbook will be the first of a series of contributions that will eventually cover most aspects of mechanical systems for sustainable buildings. Most importantly, we hope that ISBES related activities and products provide a point of encounter for continuous dialog in the very relevant subject of building systems.

We would like to thank the contributors at the initial workshop in 2013, to all authors that presented their works at the follow up technical conferences and journal publications, and to the authors of this Handbook, an effort that spanned over three years from the inception of ISBES initiative. Our special thanks to ASME Production Staff, Tara Collins and Mary Grace Stefanchik, for their encouragement and patient throughout this editorial process.

We hope the readers find the contents of this handbook useful to their practices and insightful to inspire new advances and developments of Energy Systems for Sustainable Buildings.

Jorge E. González and Moncef Krarti
(Editors)
May 2017

Editors

Jorge González
NOAA-CRES Professor of Mechanical Engineering
The City College of New York
New York, New York (USA)

Dr. González is the Director of the *Earth Science and Environmental Sustainability Graduate Initiative* and the NOAA CREST professor of Mechanical Engineering at the City College of New York. Dr. González earned his Doctorate (1994) and Bachelor (1988) degrees in Mechanical Engineering from the Georgia Institute of Technology and from the University of Puerto Rico-Mayagüez, respectively. He joined The City College of New York faculty in 2008 after tenures at Santa Clara University, California, as Professor and David Packard Scholar, and as Chairman and Professor of Mechanical Engineering at the University of Puerto Rico-Mayagüez. He teaches and conducts research in regional climate change, renewable energy, environmental sustainability, regional climate modeling, and urban remote sensing. Professor González is currently pioneering works in climate change detection in tropical coastal zones, and in developing next generational urban weather prediction systems. He holds six patents in solar energy equipment, aerosol detection, and energy forecasting for buildings, and was recognized as a prominent young researcher by the National Science Foundation with a prestigious CAREER Award. He has authored or co-authored more than 90 peer-reviewed publications, and 100s of conference presentations, and his research has attracted more than $25M in external funding. He is a Fellow Member of the American Society of Mechanical Engineering, and Vice-Chairman of the American Meteorological Society Board on the Urban Environment. He was recently appointed by the Mayor of the City as Member of the Climate Change Panel for the City of New York, and Senior Visiting Scientist of the Beijing Institute of Urban Meteorology.

Moncef Krarti
Professor, Civil Environmental and Architectural Engineering Department
University of Colorado at Boulder
Boulder, Colorado (USA)

Dr. Krarti, Professor, Building Systems Program, Civil, Environmental, and Architectural Engineering Department at the University of Colorado, has been very active in ASME from the last 25 years, especially in the ASME Solar Energy Division (SED). He has served both as Technical and Conference Chairs, and is a past president. He has been elected ASME Fellow in 2015 as testament of his leadership qualities within SED and ASME and also to his great research contributions in solar energy, energy efficiency in buildings and renewable energy systems modeling and analysis. He is the co-founder and the co-chair of the ASME Emergency Technologies Committee on Integrated Sustainable Building Equipment and Systems (ISBES) which initiated several activities including workshops, monographs, and handbooks. Prof. Krarti is considered a world expert in building energy management and has helped establish energy efficiency programs in several countries. He has been able to attract over $15 million in sponsored research and has contributed enormously in the fields of energy efficiency and renewable energy through his publications, research supervision of graduate students and undergraduate teaching. In particular, Prof. Krarti has published over 250 technical journals in wide of fields related to sustainable energy technologies. He authored three textbooks on building energy management and has been an invited keynote speaker in several national and international forums and conferences.

Contributors

Dr. Omar Abdelaziz
Oak Ridge National Laboratory
Oak Ridge, Tennessee (USA)
Email: abdelazizoa@ornl.gov

Ms. Cinthia Audivet
Universidad del Norte
Barranquilla, Colombia
Email: caudivet@uninorte.edu.co

Prof. Antonio José Bula-Silvera
Universidad del Norte
Barranquilla, Colombia
Email: abula@uninorte.edu.co

Mr. Ning Feng
University of Colorado-Boulder
Boulder, Colorado (USA)
Email: ning.feng@colorado.edu

Prof. Jorge E. González
The City College of New York
New York, New York (USA)
Email: jgonzalezcruz@ccny.cuny.edu

Dr. Estatio Gutierrez
The City College of New York
New York, New York (USA)
Email: estatio@yahoo.com

Dr. Bahman Habibzadeh
U.S. Dept. of Energy
Washington DC (USA)
Email: bahman.habibzadeh@ee.doe.gov

Res. Prof. Yunho Hwang
University of Maryland
College Park, Maryland (USA)
Email: yhhwang@umd.edu

Prof. Moncef Krarti
University of Colorado-Boulder
Boulder, Colorado (USA)
Email: krarti@colorado.edu

Dr. Ben Kroposki
National Renewable Energy Laboratory
Golden, Colorado (USA)
Email: benjamin.kroposki@nrel.gov

Dr. Gang Li
Ingersoll Rand
Shanghai (China)
Email: gangli166@gmail.com

Mr. Luis Ortiz
The City College of New York
New York, New York (USA)
Email: lortiz10@citymail.cuny.edu

Prof. Patrick Phelan
Arizona State University
Phoenix, Arizona (USA)
Email: phelan@asu.edu

Mr. Horacio Pinzón
Promigas S.A. E.S.P.
Barranquilla, Colombia
Email: horacio.Pinzon@promigas.com

Prof. Ming Qu
Purdue University
West Lafayette, Indiana (USA)
Email: mqu@purdue.edu

Prof. Marco E. Sanjuan
Universidad del Norte
Barranquilla, Colombia
Email: msanjuan@uninorte.edu.co

Ms. Jennifer Scheib
National Renewable Energy Laboratory
Golden, Colorado (USA)
Email: jennifer.scheib@nrel.gov

Mr. Yehisson Tibana
The City College of New York
New York, New York (USA)
Email: tibana13@gmail.com

Prof. Zhiqiang (John) Zhai
University of Colorado-Boulder
Boulder, Colorado (USA)
Email: john.zhai@colorado.edu

Dr. Andy Walker
National Renewable Energy Laboratory
Golden, Colorado (USA)
Email: andy.Walker@nrel.gov

1 Introduction

Jorge E. González and Moncef Krarti (Editors)

Abstract

This *Handbook of Integrated and Sustainable Buildings Equipment and Systems* is a direct result of the American Society of Mechanical Engineers (ASME) initiative on Integrated/Sustainable Building Equipment and Systems (ISBES) which has the objective of filling voids in the literature and motivate advances on integrated energy systems in buildings. The main focus of this Volume I of the Handbook is on integrated energy systems and is organized from the current state of knowledge in areas of energy equipment and building energy modeling tools, to emerging topics in a wide range of areas encompassing combined heat and power, building energy storage systems, and advanced control strategies for mechanical energy systems in buildings. In addition, the integration of renewable energy and passive cooling and heating strategies is particularly addressed, closing with advanced techniques to analyze energy demands at the neighborhood and city scales. The contributors have a diverse set of skills and extensive experience in building engineering. The main audience for the Handbook are practitioners building engineers and researchers with the intention of finding current and emerging topics in a single source. This first introductory chapter summarizes the current state of building energy in the global energy sector, and provides a brief synthesis of the strategic areas that the Handbook addresses consistent with the ASME ISBES initiative. The introduction also highlights areas of challenges and opportunities for each of the focus areas, and discusses other topics that may need to be address in the future, and not covered in this Handbook. We hope the readers find the content relevant and useful to their practice and insightful to inspire new advances and developments of Energy Systems for Sustainable Buildings.

1.1 Introduction

Although the United States and the developed world has made significant progress in increasing energy efficiency for the transportation and industrial sectors, the building sector energy efficiency has only been modestly improved and remains well below what building owners and

government policy leaders have hoped for. Automobiles, aircraft systems, and locomotion systems have all shown energy efficiency improvements twice those of building systems. In response to this shortcoming, the American Society of Mechanical Engineers (ASME) formed the Integrated/Sustainable Building Equipment and Systems (ISBES) Initiative as a new strategy to enhance building energy efficiency and reduce building energy use.

The initial focus of ISBES initiative is in energy systems for buildings and has four different but very important focus areas:

- Developing and promoting innovative energy efficient design strategies,
- Integrating renewable energy generation into buildings and building systems,
- Integrating power generation systems into building heating and cooling systems, and
- Integrating energy strategies at neighborhood and city-scales.

A strategic workshop was convened on April 24, 2013, at the ASME Center for Research and Technology Development (CRTD) and ASME Emerging Technologies (ET) at the ASME offices in Washington, D.C. for the purpose of identifying and evaluating the challenges and opportunities in the area of ISBES. National leaders from industry, government, and academia came together for a detailed 1-day discussion of each of the four proposed ISBES-topical areas. This *Handbook of Integrated and Sustainable Buildings Equipment and Systems: Volume I Energy Systems* is a direct result of this initiative, and was preceded by a special issue of the Journal of Solar Energy Engineering in 2013 [1]. The Handbook is organized from the current state of knowledge in areas of mechanical equipment and building energy modeling tools, to emerging topics in a wide range of areas encompassing combined heat and power, building energy storage systems, and advanced control strategies for mechanical systems in buildings. In addition, the integration of renewable energy and passive cooling and heating strategies is particularly addressed, closing with advanced techniques to analyze energy demands at the neighborhood and city scales. The contributors have a diverse set of skills and extensive experience in building engineering. The main audience for the Handbook are practitioners building engineers and researchers with the intention of finding current and emerging topics in a single source. This introduction summarizes the current state of building energy in the global energy sector, and provides a brief synthesis of the strategic areas that the Handbook

addresses consistently with the ASME ISBES initiative. The introduction also highlights areas of challenges and opportunities for each of the four focus areas, and discusses other topics that may need to be address in the future, and not covered in this Handbook. We hope the readers find the content relevant and useful to their practice and insightful to inspire new advances and developments of Mechanical Systems for Sustainable Buildings.

1.2 On the State of Building Energy in the U.S. and Global Energy Sector

Buildings represent the most energy intensive sector in the vast majority of countries. According to the US Department of Energy, building represented 40% of the total US energy used (Figure 1.1a; [2]). The total energy usage for US in 2014 was about 3 TW-yr (100 QBtu). This represents close to 1 TW-yr (40 QBtu) of the energy usage by the building sector alone, and hence the importance of focusing efforts in understanding and engineering strategies and technologies to reduce energy usage in buildings. Within buildings, mechanical systems represent the majority of the energy end-use (Figure 1.1b [3]), representing close to 50% for space heating and cooling, and for hot water. Further, the fraction of energy usage by US buildings compares favorably with the majority of the countries, as shown in Figure 1.2. It is clear, however, that buildings play a major role in the global world energy demand.

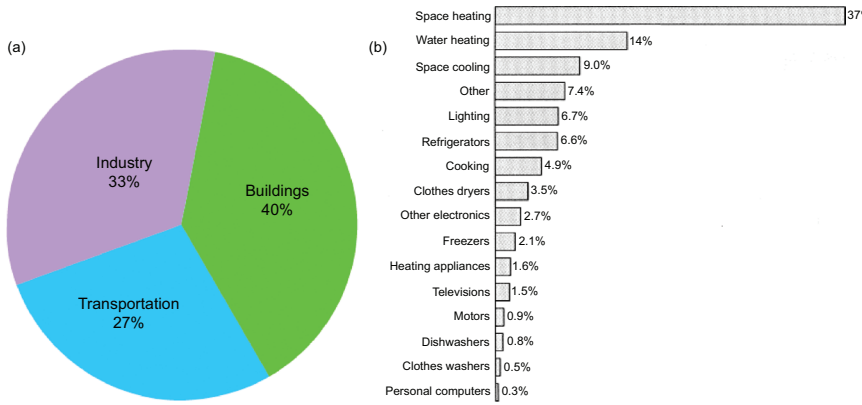

Figure 1.1. (a) Percentage of energy usage by key sectors in US [2], and (b) Distribution of energy usage within an average building [3].

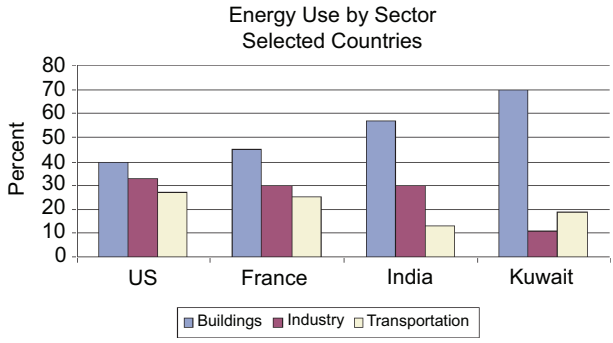

Figure 1.2. Percentage of energy usage by sector for different countries [4].

Efforts to reduce energy consumption via proven and innovative technologies and designs may go long ways in a sustainable path, and this is the primary objective of this Handbook. Key elements include integrated renewable energy technologies and energy-efficient mechanical systems, and combined heat and power systems.

1.3 On Building Energy Modeling

Building Energy Modeling remains the basis of useful design tools but is still highly assumption driven. In particular, building energy models are useful in setting design directions but are still far from providing accurate energy use predictions. Chapter 2 of this Handbook provides an overview of fundamental concepts useful to carry out an energy modeling and analysis of both new and existing buildings. The energy analysis concepts outlined are focused on modeling and evaluation of building envelope components thermal performance and their impacts on whole-building thermal loads for both heating and cooling systems under steady-state and transient conditions. In particular, basic modeling methods and techniques are presented for building thermal analysis. These modeling methods are then applied to develop forward and inverse models as well as detailed whole-building simulation tools that can be used to design, operate, and retrofit building energy systems. Finally, some of the commonly utilized whole-building energy simulation tools and their applications are presented.

Building design optimization remains a difficult and challenging. The use modeling is an area to bridge this gap. New building optimization

codes such as the US Department of Energy National Renewable Energy Laboratory BEopt™ (Building Energy Optimization) software (https://beopt.nrel.gov/) are becoming available to evaluate residential building designs and identify cost-optimal efficiency packages at various levels of whole-house energy savings along the path to zero net energy.

1.4 On Controls and Monitoring of Building Systems

Building systems control strategies provide significant energy-savings opportunities to various energy consuming equipment such boilers, chillers, and motors. A chapter (Chapter 5) is dedicated to this important topic providing basic concepts of HVAC system controls where typical supervisory controls including energy management and control systems (EMCs) are outlined. Several applications of EMCS are discussed to illustrate the types of controls that can be implemented for building energy systems and equipment. In the discussion of the applications for the supervisory controls, the benefits of using optimal control strategies to operate building energy systems are outlined and evaluated.

The energy efficiency optimization of complex HVAC systems in buildings is built-in interdependency into system components, with more variables are being monitored and controlled, and subsequently larger data sets are increasingly available for equipment, system, and user domains. This increase in complexity and real-time information is leading toward new techniques and technologies for equipment and system level monitoring, supervision, and fault detection, some of which have emerged in commercial applications. However, there is a wealth of opportunities to enhance and integrate new and on-going research in automated fault detection techniques that can be deployed by building management systems (BMS), or implemented as stand-alone HVAC control and supervision applications, to increase system performance, efficiency, and quality of service.

Chapter 9 presents a review of the different types of approaches of fault-detection techniques, state-of-the-art technologies, referenced applications to industrial and HVAC settings, commercial applications with embedded fault-detection ability, as well as challenges to be addressed in this field. The chapter also presents a case study to showcase the implementation of automated fault detection in a district cooling application.

Despite these advances, controls and monitoring will continue to rapidly evolve due mostly to the amount of new sensing capabilities, massive data gathered of the operations of components and systems, and controls for individual systems. Thus, addressing the integration of controls and control strategies and focusing on the following key questions will be essential on the following:

- How can various building control systems communicate with each other?
- How do integrated building strategies differ from individual building strategies?
- How are components in the system really working? (In some cases, fluids have been found to be flowing in the wrong direction.)
- How we best use building data for improved operation and fault detection?

The hope is that future efforts would answer these questions related to control systems, including building data management systems.

1.5 On Passive Design Strategies

Building has significant impacts on the environment and natural resources. Indeed, the construction, maintenance, and demolition of buildings consume tremendous natural resources and produce significant environment pollutions. Historically, humans have learned to utilize the natural resources to cool, heat, and ventilate spaces. Over the course of time, dwellings have evolved to respond to challenges associated to diverse and ever-changing climatic conditions. For instance, techniques and materials for constructing materials have been perfected through a long period of trial and error and the ingenuity of local builders who possess detailed knowledge about their specific location and climate. Passive architecture varies widely with the world's vast spectrum of climate, terrain, and culture. In particular, passive architecture contains significant information and knowledge on how to optimize the energy performance of buildings at low cost using local materials. Sun, earth, sky, and atmosphere are adequate, fundamental, and renewable resources that can be utilized to increase building indoor thermal comfort while reducing building energy use (Figure 1.3). Good understanding of heat transfer mechanisms (conduction, convection, radiation, evaporation, and condensation) between ground medium, surrounding environment,

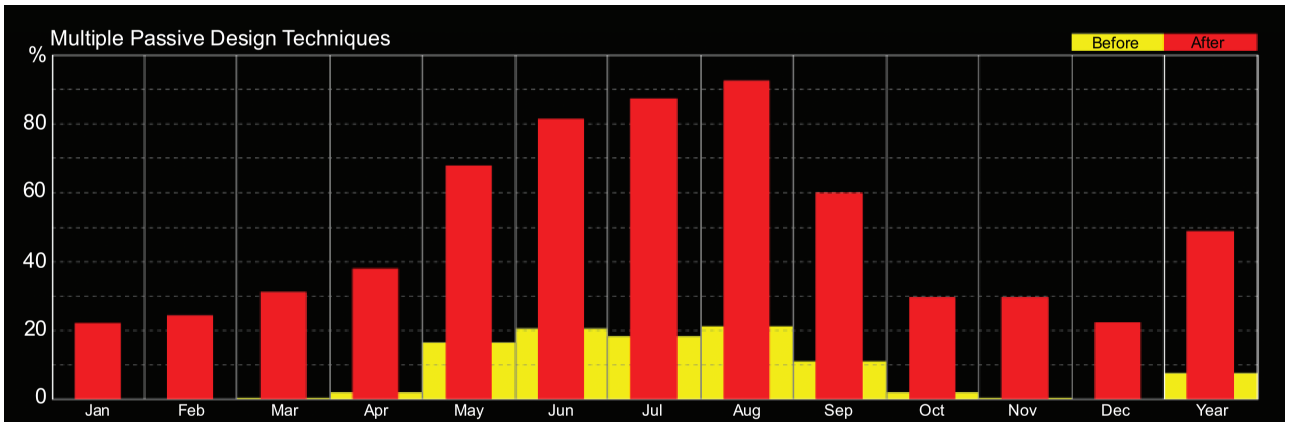

Figure 1.3. Potential savings of passive techniques used in Boulder, CO (from Zhai, Chapter 4).

and building elements facilitate proper design to fully take advantage of the cooling and heating capacity of ambient conditions (solar, air, sky, etc.). A chapter is therefore dedicated to this topic (Chapter 4) that introduces the general principles and considerations of designing and implementing passive cooling and heating techniques for sustainable building development. The Chapter discusses in detail seven commonly used passive cooling and heating techniques, focusing on presenting general principles, thermal and energy performance, and key design considerations of these techniques. The selected passive techniques are classified into three major categories based on their main functions:

1. Passive cooling techniques, including natural ventilation, night cooling and thermal mass, and evaporative cooling.
2. Passive heating techniques, including Trombe wall and sunspace.
3. Combined passive cooling and heating techniques, including double skin facade and phase change material.

1.6 On Integrated Renewable Energy Generation and Energy-Efficient Technologies

A key focus area of the ASME ISBES effort covers the challenging question of how the growing availability of renewable energy generation should be integrated into buildings and the current electrical grid. The application of more energy-efficient designs and the use of efficient technologies can greatly reduce electrical load of any individual building. Energy generation from renewable sources, when combined with storage options, can help meet building electrical load and can provide excess energy back to the electric utility. New electric utility metering policies are making the utility grid a “two-way street.”

Chapter 7 of the Handbook covers photovoltaics, daylighting, passive solar heating, and cooling, solar water heating and solar ventilation air preheating as the most relevant renewable energy technologies for building integrated options to an individual building or a group of buildings. The authors of Chapter 7 bring a unique collection and perspectives of research and practice in the field of renewables in the building sector.

The opportunities that building integrated renewable technologies can be significant and are currently growing. Examples include innovative approaches combining solar into air conditioning that can double the

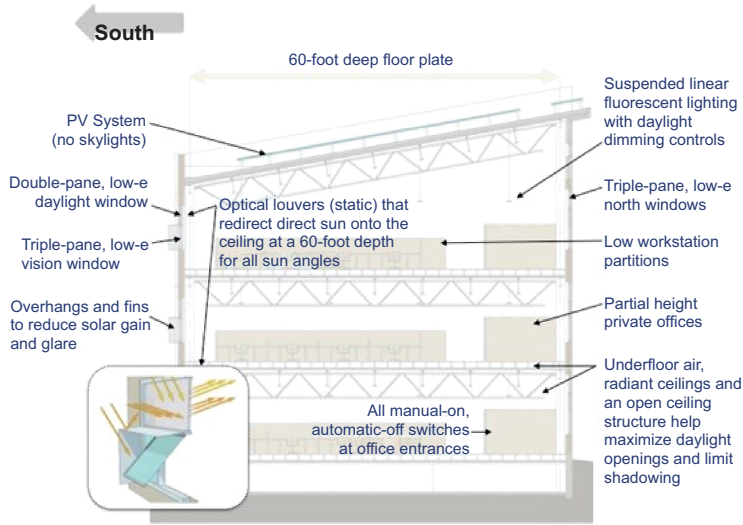

Figure 1.4. Sample of daylighting techniques into buildings' façade (from Walker, Chapter 7).

coefficient of performance (COP) over conventional systems. Hybrid solar collectors, combining photovoltaic electric generation and thermal collection, can achieve coefficients of performance over 1.0. Optimizing architectural designs and system selections can result in buildings that approach "net-zero" energy use.

There are, however, a large number of challenges and opportunities for integrating renewable energy systems into buildings that engineers and researchers should keep in mind as we advance into this emerging field, some were discussed in the ASME ISBES Workshop, and are outlined here.

- First cost remains a significant barrier to the acceptance of renewable energy technologies in buildings, and the cost of energy storage remains a major key problem in advancing renewables. Storage of electricity is still not highly evolved. Advances in battery technology are paving the way for electricity storage. Incentives remain key to support adoption of renewables in buildings. Appropriate utility rates, such as real-time pricing for electricity, would help promote more energy storage.
- The integration of solar technologies into building designs remains a challenge. Occupants' behavior can be a strong contributing

factor to design integration and energy performance. Additional efforts to improve user awareness and involvement is required in this regard.

- Solar energy can be a "local" generator of power in support of net-zero buildings. Utility company grids are the buffer when a building or system does not have electrical storage capacity. Strategies must be found to reduce the "pressure" of solar power production on the utility grid. One strategy is to schedule workloads to "follow" the sun (the availability of solar generated power) so that solar power can meet local loads before it is routed to the utility grid network. Utilities have their own codes and standards to meet in controlling the utility grid. They are likely to be more receptive to local solar power generation when they can see how it will improve their own load control (by peak-shaving for example). The growth of renewables also raises important questions about who will control energy flow. Control of energy flow has typically been highly "segregated" by the electric meter — utilities controlling flow on the power side of the meter while HVAC and electrical engineers controlling flow on the customer side of the meter. However, utilities traditionally have been reluctant to accept power generation from the customer side of the meter, while customers typically have been reluctant to hand over control of household and building systems to the utility even for significant price incentives to do so (to control peak loads).
- U.S. energy standards do not yet require renewables. However, voluntary compliance may not be enough. Implementation of energy standards such as ASHRAE 90.1 and 90.2 [5–6], will continue to take place at local and not federal levels of government. ASHRAE Std. 189.1 (Standard for the Design of High-Performance Green Buildings Except Low-Rise Residential Buildings) [7] has been adopted by some federal agencies, which may pave the way to main stream renewables.

1.7 On Integrated Power, Heating, Cooling, and Thermal Storage Equipment and Systems

This focus area covers the integration of power generation systems with the heating and cooling systems of buildings. Electrical power can be produced from traditional sources, like generators, to more innovative

sources, like fuel cells and micro-turbines, as well as solar and other renewable sources. The fundamental question for this focus area is how to integrate these systems into building elements and how to control their operation. As is the case with the previous focus area, energy storage remains a significant issue to be solved if these integrated systems are to become more common.

The Handbook presents a chapter detailing Combined Cooling, Heating, and Power (CCHP) components and systems (Chapter 6), complemented by a chapter in energy storage systems and coupled to CCHPs systems (Chapter 8). Buildings are characterized by the demand for power in the form of electricity as well as significant thermal heating and cooling loads — thus are excellent candidates for CCHP application. A properly designed building CCHP can meet the entire building thermal loads and offset significant electricity needs at higher primary energy efficiency compared with conventional technologies — based on heating equipment and purchased electricity from the grid.

A CCHP system is usually designed to provide power in the form of electricity while recovering the available waste heat to meet fully or partially heating and/or cooling loads. Chapter 6 of the Handbook provides an overview of the state-of-the-art in CCHP systems applied to commercial and residential buildings to maximize their primary energy efficiency. The chapter includes a discussion of available prime mover options ranging from classic technologies, such as internal combustion engines, to emerging technologies, such as thermoelectric generators. Different heat recovery concepts along with their limitations and design challenges are also addressed. These include gas-to-gas heat exchangers, gas-to-liquid heat exchangers, and condensing economizers, as well as advanced concepts, such as transport membrane condensers. The available heat pump technologies that can be matched with various types of prime movers to service the building heating and/or cooling loads are also outlined. The heat pump options include classic thermally activated technologies, such as the absorption and adsorption heat pumps, as well as other emerging technologies, such as thermo-acoustic heat pumps and the Vuilleumier cycle. A brief discussion on the economics and feasibility assessments of building CCHP systems, such as break even time, and life cycle cost of electricity generation is included.

Thermal energy storage (TES) systems could be used to reduce a building's peak power demand by shifting the peak heating or cooling loads to the low power demanding hours. Chapter 8, the handbook provides

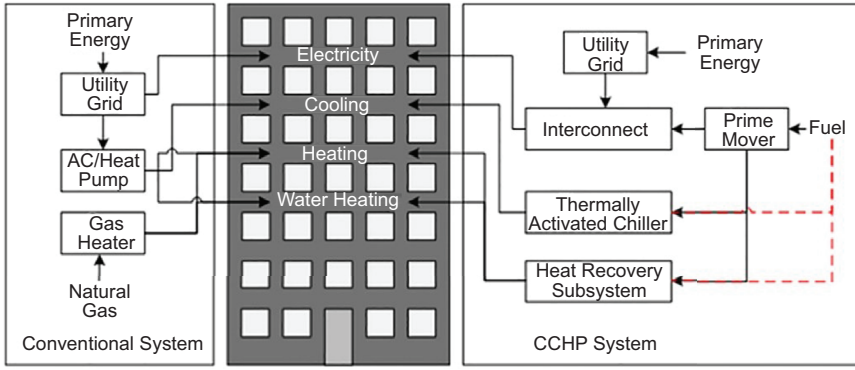

Figure 1.5. Conventional versus CCHP system building integration (from Chapter 6).

an overview of the recent energy storage research activities applicable to building applications. The information is divided into two storage technologies: sensible/latent TES and sorption TES. Sorption TES technology is summarized by improving working pair properties and enhancing sorption bed heat transfer. Investigation on the sensible/latent TES is tailored for building storage system classification, its energy saving potential, phase change material (PCM) property improvement, and mathematical modeling of PCM storage system. The opportunities and challenges in coupling TES with CCHP are also addressed in Chapters 6 and 8.

Below, we summarized additional discussions related to CCHP, from the 2013 ASME IBSES workshop, outlining broad challenges, and emerging opportunities, that the Handbook did not cover which may serve as roadmap for future research and development in combining power systems to building operations.

- Although already a mature technology, combined heat and power systems using microturbines coupled to traditional heat and cooling systems are a good example of integrating power and building systems that have been proven to offer significant energy cost savings. However, further integration of technologies into buildings with their environment is needed. For instance, connecting geothermal systems to building foundations represent an incremental innovation from known ground source heat pump technologies. Geothermal piping in concrete pilings and in

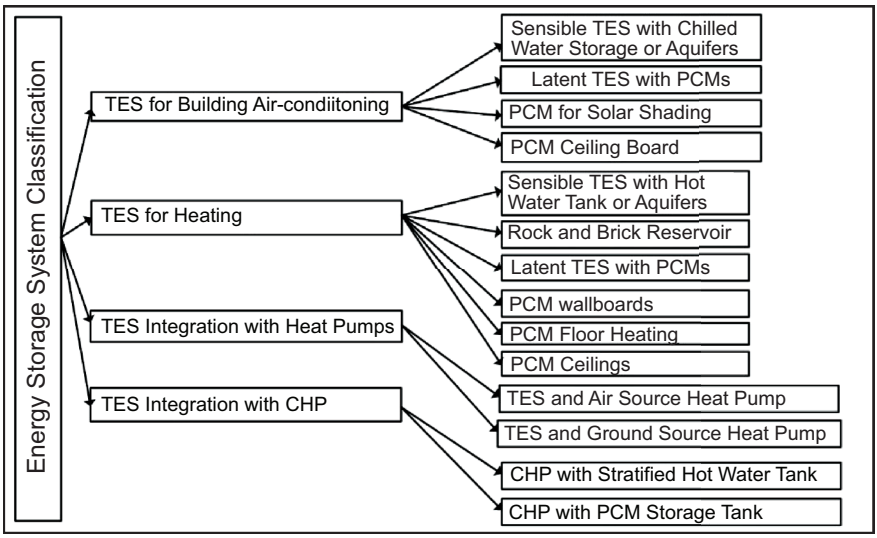

Figure 1.6. Sensible/latent TES system classification (from Chapter 8).

Figure 1.7. Installation of ground source heat pipe piping inside the foundation piles of buildings for a project in Abu Dhabi (Courtesy of M. Krarti [11]).

foundation walls has been used with success in Europe and Japan for over 10 years, with initial estimates that building energy use could be reduced by 20% to 30% [8].

- "Breathing walls" and double-skin facades are examples of dramatically new concepts currently being researched for combined heat (cooling) and power generation [9].
- Air source heat pump technologies continue to receive attention. In Europe, combining domestic hot water systems with air source heat pumps has shown significant energy savings. "Earth tubes" (air intake pipes buried in the earth so as to take advantage of the lower earth temperatures) have been proposed as a way to present more temperate air-to-air source [10–11].

1.8 On Neighborhood and City-Scale Integrated Energy Strategies

This Focus Area covers diverse issues around the concept of combining several buildings together and viewing them as integrated urban environment on a neighborhood or city-wide scale. Such groupings might be used to increase efficiency and reduce overall building energy use, accept and optimize renewable technologies, generate power, or reconfigure utility company grids and grid management. Key aspects of this emerging topic are:

- Cities could be a source of sustainability but this would require a holistic approach tied to local, regional, and global processes. Urban "heat islands" reduce air quality, by increasing ground-level ozone, and increasing the demand for air conditioning, further increasing the demand for electricity and increased carbon dioxide (CO_2) emissions related to that energy production.
- Current Building Energy Models (BEM) are based on using a single building responding to typical weather records. This approach tends to ignore the complex interactions of multiple buildings in an urban setting including the width of "street canyons," shading of solar radiation by adjoining buildings; higher air temperatures within urban heat islands; and variations caused in natural ventilation by urban environments. Better urban modeling could improve the ability of models to predict the effects of extreme weather conditions, such as local or regional brown-outs or black-outs from excessive air conditioning demands. As cities become denser, it is anticipated

that there will be an increase in energy demands from cities in the future, making it imperative to develop new methodologies to quantify energy demands from buildings in very dense urban environments.

- Renewable energy technologies need to be studied carefully as strategies in the urban environment. In some cases, aspects of a renewable technology might actually make the situation worse. Heat from PV collectors and humidity from green roofs are two examples that merit further study [12]. Models show that significantly increasing the use of green roofs (rooftop grass or landscaping) in a humid urban environment can increase humidity and increase the "heat island" effect [13–14]. This suggests that individual building-level renewable applications may improve single building performance but widespread use of such technologies, in an urban setting, may have the opposite effect.
- Integrated Energy Master Plans (IEMPs), at the campus, city, or county level, offer an opportunity to significantly reduce greenhouse gases and increase building efficiency at affordable costs within 10 to 30 years. Currently, European cities have the lead in such projects, but both Canada and the United States have important projects moving forward. District heating and cooling technology fits this approach well but challenges in the United States are large where district systems in place tend to be old and leaky. A district heating and cooling system, supplemented by heat recovery from municipal wastewater and high-efficiency natural gas boilers could be an effective technology suitable for a neighborhood scale. Sidewalks and roadways can provide the "easements" necessary to facilitate installation. City of Phoenix, the old Austin Airport, and the Smart Village Campus in Egypt are recent examples of successful district cooling/heating system installation, whereas Honolulu is considering a district cooling system using sea water. It should be noted that the design team for a district heating and cooling system needs to be highly diverse. In particular, the project architect and mechanical engineer are key members of the team and need to work collaboratively. Moreover, building operators must be included if the project is to have long-term success.
- Energy performance ratings and metrics are under development for neighborhoods and cities such as LEED for Neighborhood Development, of the U.S. Green Building Council (LEED-ND), a collaborative program providing credits and levels of certification (Certified, Silver, Gold, and Platinum) for neighborhood-level designs and implementations [15]. In this case, Neighborhood

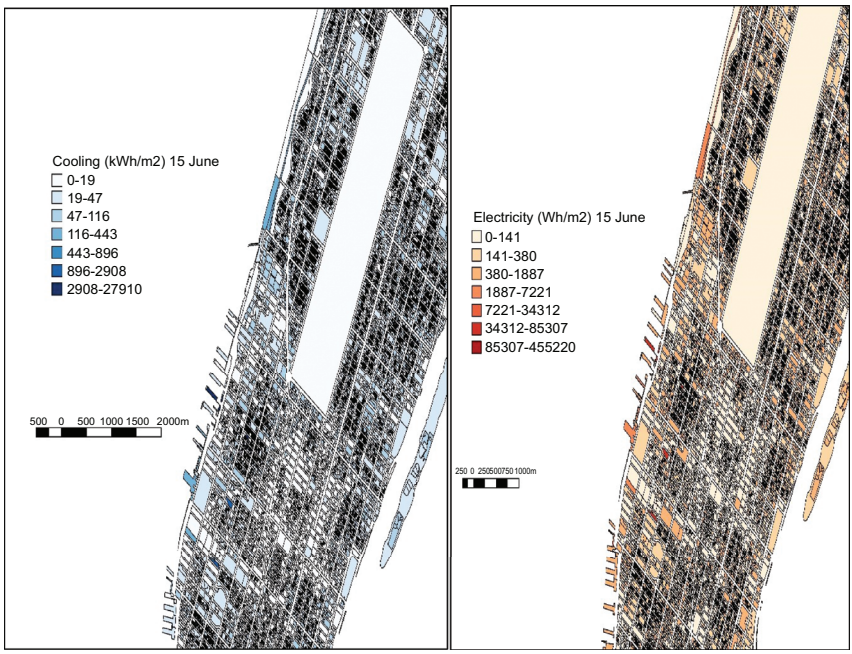

Figure 1.8. City Scale Building Energy Modeling, for the case of Lower Manhattan, New York City left represents the peak cooling demand for June 15 2016, and right represents the lighting and equipment demand. (from Krarti et al. [16]).

> Pattern and Design credits focus on connecting people to place, shared public spaces, and nearby goods and services.

A chapter is dedicated to this emerging topic (Chapter 10) with focus on energy modeling for cities, which addresses some of the key topics outlined above. The chapter outlines a modeling strategy to address the urban heat island and its impacts on energy demand which is associated mostly to the air conditioning needed to maintain indoor human comfort conditions.

1.9 Additional Topics for Future Consideration

1.9.1 Commercial Building Lighting and Window Designs

Advances in lighting fixtures and design requirements is an additional topic that is gaining traction in the building energy efficiency arena.

Current standards for ambient and task lighting are outdated and do not account adequately for the design and operation of lighting devices. Building fenestration (windows) is an area of opportunity that is receiving new attention. The design goal of envelope systems including window elements is to change buildings from the traditional energy "losers" into energy "neutral" systems. Another design goal is to try to "harvest" the thermal energy passing through windows.

1.9.2 Data Centers

Buildings dedicated to the management and processing of information, such as data centers, are emerging energy efficiency challenges and opportunities. Energy use accounts for about 70% of data center operating costs. This high cost is a significant barrier to worldwide adoption of IT services. In 2012, Hewlett Packard completed a data center demonstration prototype in Palo Alto, CA, which achieved 30% reduction in total energy use and 80% reduction in overall operating costs through integrated management of IT, power, and cooling [17]. By more carefully scheduling critical versus non-critical IT loads in data centers, it is possible to shift and thus better match IT workloads to the availability of renewable power. A "Net Zero" data center can be achieved with or without onsite energy storage. In the former case, the objective is to minimize the onsite storage capacity required by the work load scheduling, and in the latter case, the electricity grid can be viewed as virtual energy storage.

1.9.3 On the Subject of Climate Change and Sustainable Buildings

Modeling energy in buildings and urban environment needs to be connected to climate change assessments. Warming temperatures may provide new baseline for design weather conditions. Further, increasing the reliability and resiliency of urban electrical grids provides a strong incentive in support of this design and building management approach. This approach is important in addressing the increasing likelihood of significant weather events, such as extreme heat and cold events, and high wind conditions. The need for resiliency may drive greater integration of power into buildings and new design tools and techniques. More frequent extreme weather events (hurricanes, heat waves, and extreme cold) are causing more frequent power outages. Current building codes and standards are based on historic records over the past 100 years, which may not be

good predictors of changing future events. Building codes and standards may have to be revised accordingly. Integrating power generation into more buildings may become popular as a strategy to increase reliability (from an owner's point of view). Future building design may need to emphasize the following strategies: long life (with durable materials), loose fit (modularity to facilitate adding innovations as they become available), and low energy (to reduce energy demand, reduce energy cost, and increase sustainability). Diversity of energy supply is another strategy to enhance buildings' resiliency to extreme weather events.

1.10 Recommendations and Next Steps on ISBES

The following are combined recommendations from the 2013 ASME workshop that both designers and researchers as well as the general public should consider in moving forward to foster ISBES and to craft the vision of a highly sustainable community of buildings (Figure 1.9).

- Sensing, metering, and communications among building systems needs to be improved. Accessibility of more sub-metered data and the interoperability among data sets should be a focus of further research. Low cost or "virtual" sensors to facilitate diagnostics and control should also be further developed. Building energy management systems and building control strategies need to be enhanced so that advanced, integrated buildings can demonstrate persistent improved energy performance over much longer periods after commissioning.
- Integration of solar technology into buildings suggests several research areas requiring new skills and innovative design approaches including: rethinking windows as a source of thermal energy or to generate power, additional technologies and techniques to use the building envelope to store energy, or further innovations in electro/chemical or flow batteries for storage.
- Professional organizations, such as ASME, ASHRAE, AHRI, IEEE, UL, DOE, IEA, IIR, and SEPA, should work collaboratively when addressing the topic of Integrated/Sustainable Building Equipment and Systems. Joint technical committees should be established and include all of the above as well as members from the climate change community, which could help to focus decision making and prioritize research topics by drafting a research road maps for the future.

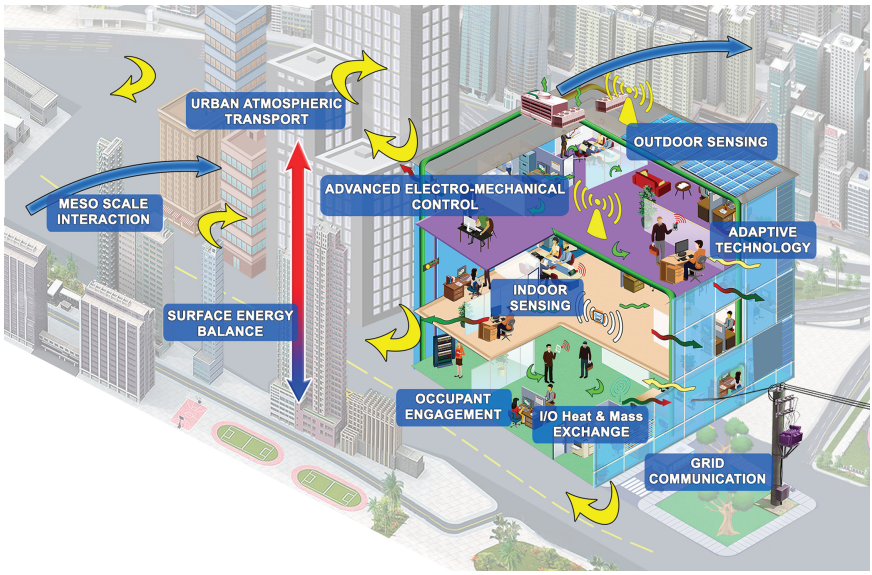

Figure 1.9. Vision of sustainable community of buildings using highly integrated energy systems.

- Organizations should collaborate for indexing and cataloging sources of urban "thermal pollution" from pavements, cars, solar PV panels, various roofing materials, and other common sources. Also, there is a need to benchmark larger integrated building energy models.
- Modeling and simulation tools need to be improved so that time required for data input are appropriate to complete the analysis of the project performance and its alternative designs in timely manner. Current tools take too long and show too great a variance in output results. Existing codes and standards need to be enhanced to recognize the benefits of integrated, energy-efficient building designs.
- There is a need for thermal metering standards so that flow meters can meet "revenue grade" standards. These are important for district heating systems and other energy systems with fluid flows. Opportunities for contributing via collaborations to international building energy codes should not be overlooked, particularly for warm climates, both humid and dry.
- At the city scale, improving our understanding of complex heat flux in cities will require: advanced surface and vertical sensors, data mining and visualization techniques, managing of

climate data records, and improved modeling tools. To date, the engineering community has had little involvement in the energy sustainability of cities. Fundamental, experimental, and applied research is needed to better understand energy/mass/momentum fluxes at the adequate temporal and spatial scales. Collaborations with international, federal, and state agencies may lead to funded research in this area.

References

[1] Krarti, M., and Gonzalez, J. E. 2013. Special Issue of ASME JSEE on Integrated/Sustainable Building Equipment and Systems Notes From Guest Editors. *Journal of Solar Energy Engineering,* **135**, p. 1.

[2] U.S. Department of Energy. Building Energy Data Book. 2010. http://buildingsdatabook.eren.doe.gov/ChapterIntro1.aspx?1. Downloaded 12/18/2016.

[3] U.S. Department of Commerce, *Statistical Abstract of the United States,* USDOE, Washington, DC, 2001.

[4] International Energy Agency. 2008. Worldwide Trends in Energy Use and Efficiency: *Key Insights from IEA Indicator Analysis*. https://www.iea.org/publications/freepublications/publication/Indicators_2008.pdf

[5] American Society of Heating, Refrigeration, and Air Conditioning (ASHRAE). Standard 90.1-2001 — Energy Standard for Buildings Except Low-Rise Residential Buildings (IESNA cosponsored; ANSI approved; Continuous Maintenance Standard). Atlanta, GA.

[6] American Society of Heating, Refrigeration, and Air Conditioning (ASHRAE). Standard 90.2-2007 — Energy Efficient Design of Low-Rise Residential Buildings. Atlanta, GA.

[7] American Society of Heating, Refrigeration, and Air Conditioning (ASHRAE) *ANSI/ASHRAE/IES/USGBC Standard 189.1-2014, Standard for the Design of High-Performance Green Buildings*. Atlanta, GA.

[8] Aposteanu, A., Berre, I., Bertani, R., Clauser, C., Jaudin, F., Kujbus, A., Sanner B., and Urchueguia, J. (Authors). 2014. Geothermal Technology Roadmap. European Technology Platform on Renewable Heating and Cooling. http://www.rhc-platform.org/fileadmin/Publications/Geothermal_Roadmap-WEB.pdf. Secretariat of the Geothermal Panel of the RHC-Platform (EGEC) (Editors).

[9] Zhai, J. 2016. Breathing Wall: Concept and Thermal Performance. Cityscape, **18**. https://www.questia.com/library/journal/1P3-4133091671/breathing-wall-concept-and-thermal-performance
[10] http://www.homeintheearth.com/tech_notes/earth-tubes/
[11] Kwag, B. C., and Krarti, M. 2013. Performance of Thermoactive Foundations for Commercial Buildings. *Journal of Solar Energy Engineering,* **135**, doi: 10.1115/1.4025587.
[12] Lebassi, B., González, J. E., and Bornstein, R. On the Environmental Sustainability of Building Integrated Solar Technologies in a Coastal City. *Journal of Solar Energy Engineering,* **135**, doi: 10.1115/1.4025507.
[13] Sailor, D. 2008. A Green Roof Model for Building Energy Simulation Programs. *Energy Buildings,* **40**, pp. 1466–1478.
[14] Vázquez-Morales, W., Jazcilevich, A., García-Reynoso, A., Caetano, E., Gómez, G., and Bornstein, R. D. 2016. Influence of Green Roofs on Early Morning Mixing Layer Depths in Mexico City. *Journal of Solar Energy Engineering,* **138**, doi: 10.1115/1.4025507. doi: 10.1115/1.4034807.
[15] U.S. Green Building Council. LEED for Neighborhood Development Prerequisites and Credits. http://www.usgbc.org/articles/leed-nd-credits-and-points
[16] Krarti, A., L. Ortiz, L., and J.E. González. (2017). On the Spatio-Temporal End-User Energy Demands of a Dense Urban Environment. *J. of Solar Energy Engineering*, http://doi:10.1115/1.4036545
[17] Ortiz, L., J.E. González, E. Gutierrez, and M. Arend. (2017). Forecasting Building Energy Demands with a Coupled Weather-Building Energy Model in a dense urban environment. *J. of Solar Energy Engineering*, **139** (1), http://dx.doi.org/10.1115/1.4034909.
[18] Martin, A. et al. 2012. "Towards the design and operation of net-zero energy data centers." *Thermal and Thermomechanical Phenomena in Electronic Systems (ITherm), 2012. 13th IEEE Intersociety Conference on*. IEEE, 2012.

2 Building Energy Systems Modeling and Simulation

Moncef Krarti

Abstract

This chapter provides an overview of fundamental concepts useful to carry out an energy analysis of both new and existing buildings. The energy analysis concepts outlined in this chapter is focused on modeling and evaluation of building envelope components and their impact on thermal loads for heating and cooling systems under steady-state and transient conditions. In particular, basic modeling methods and techniques are presented for building thermal analysis. These modeling methods are then applied to develop forward and inverse models and simulation tools used to design, operate, and retrofit building energy systems. Finally, some of the commonly utilized whole-building energy simulation tools and their applications are presented.

2.1 Introduction

To determine design thermal heating and cooling loads, analyze energy consumption, and estimate the cost effectiveness of energy conservation measures suitable for buildings, a myriad of calculation methods and simulation tools can be utilized. The existing energy analysis methods vary widely in complexity and accuracy. To select the appropriate building energy analysis method, several factors should be considered including speed, cost, versatility, reproducibility, sensitivity, accuracy, and ease of use [1]. Currently, there are over hundreds of energy analysis tools and methods that are used worldwide to estimate heating and cooling thermal loads and to predict the potential savings of energy conservation measures for both residential and commercial buildings. In the United States, DOE provides an up-to-date listing of selected building energy software [2].

In this section, some of the most relevant energy analysis techniques and methods for both commercial and residential buildings are described. In particular, simplified thermal analysis methods, such as variable-based degree-day and thermal network techniques are introduced with some

applications to estimate thermal performance indicators of buildings. In addition, detailed energy modeling and simulation techniques suitable for designing and retrofitting building envelope systems are presented. First, an overview of fundamental principles of building physics is provided including heat transfer through building envelope under steady-state and transient conditions. Then, simplified and advanced energy analysis methods suitable for buildings are introduced. Finally, a brief description of various forward and inverse modeling techniques for whole-building energy performance analysis is presented. The methods and techniques presented in this chapter are the basis of a wide range of whole-building simulation tools used to design, operate, and retrofit various energy systems suitable for residential and commercial buildings.

2.2 Basic Heat Transfer Concepts

Heat transfer from the building envelope can occur through various mechanisms including conduction, convection, and radiation. In this section, fundamental concepts of heat transfer are briefly reviewed. These concepts and associated metrics are typically used to characterize the thermal performance of various components of the building envelope and are useful to estimate heating and cooling thermal loads.

The steady-state heat transfer from a multi-layered wall or roof can be found by determining first its overall *R*-value:

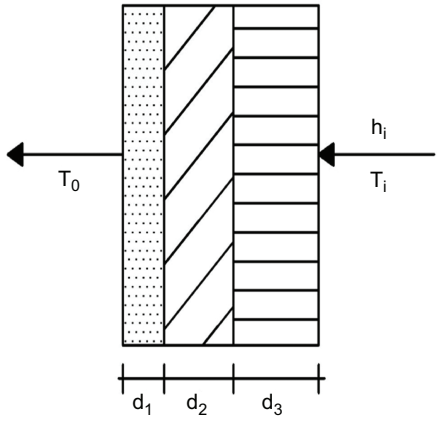

Figure 2.1. Heat transfer from a multi-layered wall.

$$R_T = \sum_{j=1}^{N_L} R_j \tag{2.1}$$

Where:

- R_j is the R-value of each homogeneous layer part of the construction of the wall or roof assembly. It includes the R-value due to convection at both inner and outer surfaces of the wall or roof.
- N_L is the number of layers (including the convection boundary layers) that are part of the wall or roof assembly. For instance, in the wall assembly presented in Figure 2.1, N_L = 5 (3 conductive layers and 2 convective layers).

The overall U-value of the wall or roof can be defined simply as the inverse of the overall R-value:

$$U_T = \frac{1}{R_T} \tag{2.2}$$

It should be noted that practitioners usually prefer to use R-values rather than U-values since the U-values are small especially when insulation is added to the wall or roof assembly. For doors and windows, the use of U-values is more common since these components have low R-values.

Under steady-state conditions, it is possible to estimate the R-value of the wall by measuring three temperatures as indicated in Figure 2.2: the indoor air temperature, $T_{o,}$ the outdoor air temperature, T_i and, the indoor surface temperature, $T_{i,s}$.

Since the steady-state heat flux through the wall can be estimated using the equivalent thermal network shown in Figure 2.2:

$$\dot{q} = \frac{A}{R_T}.(T_i - T_o) = Ah_i(T_i - T_{i,s}) \tag{2.3}$$

Thus, the R-value of the wall, R_T, can be expressed as follows as a function of the indoor heat convection coefficient, h_i, and the temperatures, T_i, T_o, and $T_{i,s}$:

$$R_T = \frac{1}{h_i}\frac{(T_i - T_{i,s})}{(T_i - T_o)} \tag{2.4}$$

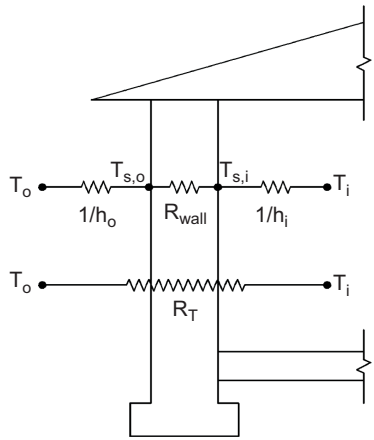

Figure 2.2: Temperature measurements for overall wall thermal resistance estimation.

Alternatively, the *U*-value of the wall can be obtained through measurements of the temperatures, T_i, T_o, and $T_{i,s}$:

$$U_T = h_i \frac{(T_i - T_o)}{(T_i - T_{i,s})} \tag{2.5}$$

The field testing for estimating the *R*-value or *U*-value of the wall should be conducted when there is a large difference between the indoor and outdoor temperatures and when there is very little solar radiation hitting the wall. Thus, it is recommended to perform the temperature measurements in a cold night. Table 2.1 summarizes the percent error in estimating the wall *R*-value using temperature measurements for various indoor-outdoor temperature differences ($T_i - T_o$). It is clear from Table 2.1 that the larger the difference between indoor and outdoor air temperatures, the more accurate is the estimation of the wall *R*-value using the field test illustrated in Figure 2.2. In particular, an indoor-outdoor temperature of at least 4°C or 7°F is required to achieve an accuracy of 5% or less in estimating the wall/roof *R*-value especially when the building envelope is poorly insulated.

2.2.1 Transient Heat Transfer from Building Envelope

In most building simulation analysis tools, heat transmission through building envelope is modeled using one-dimensional (1-D) transient heat conduction analysis. Transient 1-D heat conduction through a homogeneous wall layer having constant and uniform thermal properties is subject to Eq. (3.1):

Table 2.1. Percent Error for *R* Value Estimation Based on Temperature Measurements.

$[T_i - T_o]$ (°F)	$[T_i - T_o]$ (°C)	$R = 2.5$	$R = 5$	$R = 10$
40	22.2	0.98%	0.54%	0.28%
35	19.4	1.12%	0.61%	0.32%
30	16.7	1.30%	0.72%	0.38%
25	13.9	1.56%	0.86%	0.45%
20	11.1	1.95%	1.07%	0.56%
15	8.3	2.60%	1.43%	0.75%
10	5.6	3.90%	2.15%	1.13%
5	2.8	7.81%	4.29%	2.25%
4	2.2	9.76%	5.37%	2.81%
3	1.7	13.01%	7.16%	3.75%
2	1.1	19.52%	10.74%	5.63%
1	0.6	39.04%	21.47%	11.25%
0.5	0.3	78.08%	42.95%	22.50%
0.1	0.1	390.39%	214.73%	112.50%

where,

$$\frac{\partial^2 T}{\partial x^2} = \frac{1}{\alpha}\frac{\partial T}{\partial t} \tag{2.6}$$

- $\alpha = \dfrac{k}{\rho \cdot Cp}$ is the thermal diffusivity of the homogeneous wall layer (m^2/s)
- T = temperature (°C)
- x = vector space of x (m)
- c_p = specific heat (J/kg×°C)
- k = thermal conductivity (W/m×°C)
- ρ = density (kg/m^3)
- t = time (sec)

In some cases, two-dimensional (2-D) and three-dimensional (3-D) heat conduction solutions are utilized (i.e., ground-coupled heat transfer and thermal bridges in walls and roofs). Figure 2.3 shows a 3-D rectangular slab-on-grade floor model with partial insulation along the perimeter of the foundation. The slab model presented in Figure 2.3 (a) accounts for the above grade walls by assuming that the steady-state wall temperature varies gradually along the wall thickness from indoors to outdoors as shown in Figures 2.3(b) and 2.3(c) for both sections A and B [3].

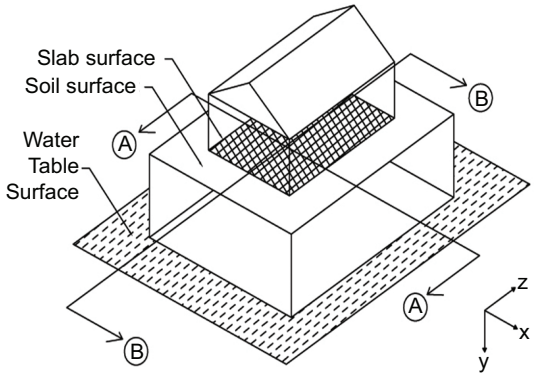

Figure 2.3a. A rectangular slab-on-grade floor foundation model with partial floor insulation. (a) slab-on-grade floor foundation for a typical building above soil medium.

(*Continued*)

(a) Slab-on-grade floor foundation for a typical building above soil medium

(b) Section A of building shown the variations of the temperature and the U-value along the soil-slab surface

(c) Section B of building shown the variations of the temperature and the U-value along the soil-slab surface

Under transient conditions, the temperature distribution within the ground medium, *T(x,y,z)* is subject to the diffusion equation:

$$\nabla T(x,y,z,t) = \frac{1}{\alpha_s}\frac{\partial T}{\partial t} \tag{2.7}$$

where ∇ is the Laplacian operator. Throughout this section, ∇ is assumed to be given in the three-dimensional Cartesian form, that is:

$$\nabla = \frac{\partial^2}{\partial x^2} + \frac{\partial^2}{\partial y^2} + \frac{\partial^2}{\partial z^2} \tag{2.8}$$

In Eq. (2.7), t is time and α_s is the soil thermal diffusivity assumed to be constant (i.e., isotropic soil).

Fourier's law of heat conduction expresses the heat flux variation along any surface and is directly depend on the material thermal conductivity

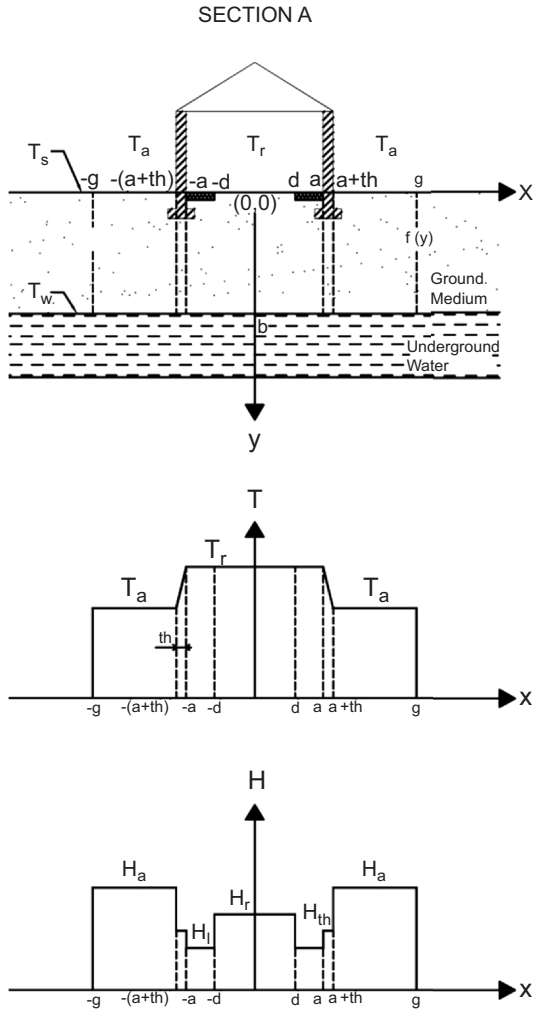

Figure 2.3b. A rectangular slab-on-grade floor foundation model with partial floor insulation. (b) Section A of building shown the variations of the temparature and the *U*-value along the soil-slab surface.

(*Continued*)

and temperature gradient across the thickness of the material as shown by Eq. (2.9):

$$q = -k\frac{\partial T(x,t)}{\partial x} \tag{2.9}$$

where q is heat flux expressed in W/m^2.

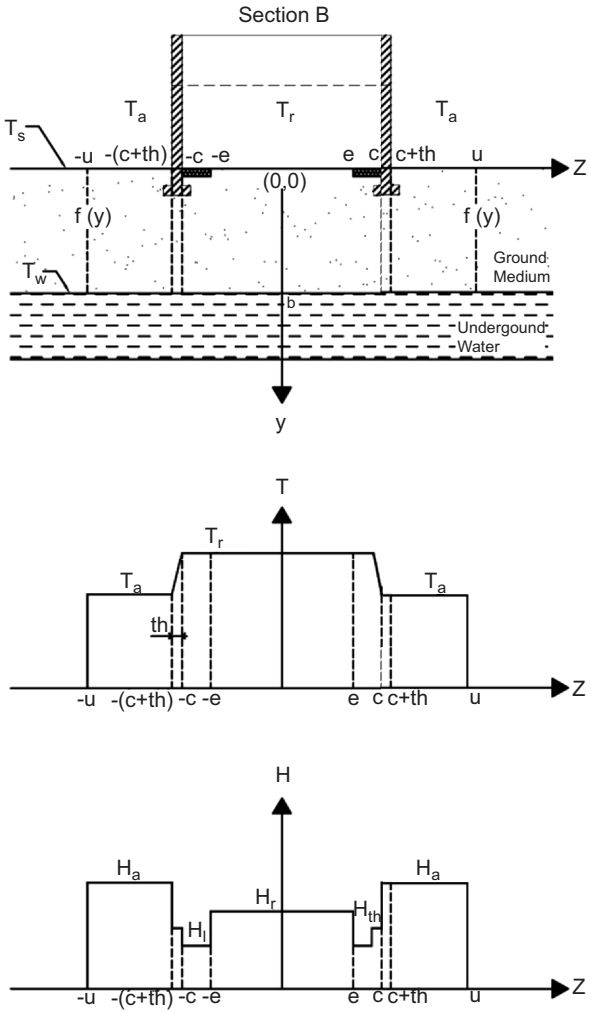

Figure 2.3c. A rectangular slab-on-grade floor foundation model with partial floor insulation. (c) Section B of building shown the variations of the temperature and the *U*-value along the soil-slab surface.

2.3 Methods for Transient Building Envelope Energy Analysis

Several methods and techniques are considered to solve the transient heat conduction equations such as those shown by Eqs. (2.6) and (2.7) and ultimately determine heat transfer through building envelope systems.

Some of these methods are easy to implement into whole-building simulation tools as discussed in this section.

2.3.1 Finite Difference Methods

One commonly used methods to solve heat conduction equations and to determine transient temperature profile and heat transfer rates through building envelope components is the finite difference numerical technique. This approach involves dividing the wall into a series of thin sections through a discretization scheme and performing an energy balance on the thin section. This method of solution is flexible and can be used to model almost any building envelope system. Moreover, the numerical analysis method can be easily implemented in a standalone algorithm. However, the finite difference method requires generally significant computational time efforts especially when applied to determine the long-term performance of building energy systems. A brief description of the explicit formulation of the finite different technique is outlined in this section to solve the transient 1-D heat conduction equation within a building wall.

Spatial Discretization: A common spatial discretization scheme for a building wall is described by Figure 2.4. The wall is divided into N sections of thickness Δx. An energy balance on any node i is given by the following relationship.

$$C_i \frac{dT_i}{dt} = \frac{T_{i-1} - T_i}{R_{i-}} + \frac{T_{i+1} - T_i}{R_{i+}} \tag{2.10}$$

The resistance R_{i-} is the resistance to the *left* of node i and the resistance R_{i+} is the resistance to the *right* of node i. The thermal performance of the wall can be represented by the RC-network as illustrated in Figure 2.5. For this wall, each capacitance in the network is identical and equal to the mass times specific heat of the wall segment. The resistance between each interior node is identical and equal to the conduction resistance R_{cond}.

$$C = \rho c \Delta x \tag{2.11}$$

$$R_{cond} = \frac{\Delta x}{k} \tag{2.12}$$

The resistance between the exterior nodes 1 and N are slightly different, because these resistances must account for both heat conduction

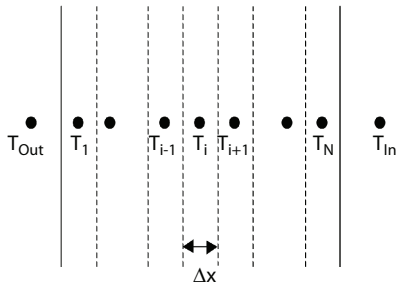

Figure 2.4. Finite difference analysis in a plane wall.

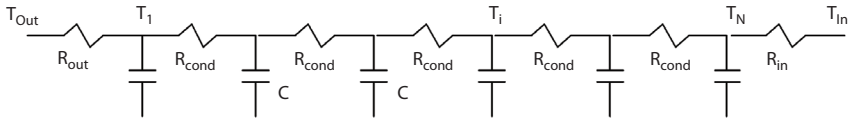

Figure 2.5. An RC network model for a thick wall.

through a distance $\Delta x/2$ and heat convection at the surface. The resistances at the outer and inner surfaces, R_{out} and R_{in}, respectively, are given by the following equations.

$$R_{in} = \frac{\Delta x}{2k} + \frac{1}{h_{in}} \tag{2.13}$$

$$R_{out} = \frac{\Delta x}{2k} + \frac{1}{h_{out}} \tag{2.14}$$

Time Discretization for the Explicit Finite Difference Formulation: The differential equations above apply at any value of time, t. For the purpose of developing the difference equations, consider the solution at some time $t = p\Delta t$ where Δt is the time step for calculations and p is an integer. An approximate estimation of the derivative of temperature with respect to time at some time p is provided as follows:

$$\frac{dT_i^p}{dt} = \frac{T_i^{p+1} - T_i^p}{\Delta t} \tag{2.15}$$

This representation approximates the derivative at some time $t = p\Delta t$, by looking ahead in time. Such an approach is known as *Euler*, or *explicit*, representation of the derivative. Alternative formulations will be discussed later.

For any node in the wall, the RC network equations can be written using this expression for the first derivative to give the following difference equation.

$$C_i \frac{T_i^{p+1} - T_i^p}{\Delta t} = \frac{T_{i-1}{}^p - T_i^p}{R_{i-}} + \frac{T_{i+1}{}^p - T_i^p}{R_{i+}} \tag{2.16}$$

Substituting and rearranging, the temperature of node i at time $p+1$ can be solved in terms of temperatures at time p.

$$T_i^{p+1} = \frac{\Delta t}{C_i}\left(\frac{T_{i-1}{}^p}{R_{i-}} + \frac{T_{i+1}{}^p}{R_{i+}}\right) + \left[1 - \frac{\Delta t}{C_i}\left(\frac{1}{R_{i-}} + \frac{1}{R_{i+}}\right)\right] T_i^p \tag{2.17}$$

It is noted that the left side of this equation involves temperature at time step $p+1$ while the right side of the equation involves only temperatures at time step p. Such a formulation gives very simple numerical calculations. Given initial values for all the temperatures (every analysis problem requires initial conditions), the temperature of any spatial node at the end of the first time step can be directly (*explicitly*) calculated using this equation. The temperature of any node at the end of the second time step can be directly calculated from the temperatures at time step 1. This formulation is particularly convenient for spreadsheet calculations.

The heat flux at any point in the wall at any time can be readily calculated from the temperature profile. In general, the heat flux between any two temperature nodes can be calculated using the resistance between them.

$$q_{ij}{}^p = \frac{T_i^p - T_j{}^p}{R_{ij}} \tag{2.18}$$

Stability Constraint for the Explicit Finite Difference Method: Unfortunately, Eq. (2.17) cannot be applied with an arbitrary time step size. If the time step is too large, the right-most term can be negative, which not only violates the Second Law of Thermodynamics, but causes numerical instability in the solution. To ensure a stable solution (i.e., a solution that does not blow up to infinity), the time step must be chosen such that this right term is positive. In other words,

$$\Delta t_{i,\max} < \frac{C_i}{1/R_{i-} + 1/R_{i+}} \tag{2.19}$$

In general, it is wise to calculate this term for each node and select a time step less than the smallest value. While a solution may be stable for

some time steps greater than this limit, the solution is guaranteed to be stable for time steps less than this limit.

For the *special case* of an interior node (not located at a surface or interface between materials), the resistance to the left of node i is the same as the resistance to the right of node i, giving $R_{i-} = R_{i+} = R_{cond}$. Substituting and rearranging, the temperature of node i at time $p+1$ can be solved in terms of temperatures at time p.

$$T_i^{p+1} = \frac{\Delta t}{R_{cond} C}\left(T_{i-1}^{\,p} + T_{i+1}^{\,p}\right) + \left(1 - \frac{2\Delta t}{R_{cond} C}\right) T_i^{p} \tag{2.20}$$

The equations for the end nodes are slightly different because the resistances are different. To ensure a stable solution for this special case, the time step must be chosen such that this right term is positive. In other words,

$$\Delta t_{i,\max} < \frac{R_{cond} C}{2} \tag{2.21}$$

In general, it is wise to select a time step no more than about half this maximum value.

2.3.2 Interzone Temperature Profile Estimation (ITPE) Techniques

Analytical solutions for estimating heat transfer in building envelope systems have been considered by several authors [3–8]. In particular, the Interzone Temperature Profile Estimation (ITPE) technique, initially developed by Krarti et al. [7], has been applied to solve several types of two- and three-dimensional steady-state and transient heat conduction problems. The ITPE formalism includes analytical solutions combined with solving a linear systems of equations and can be applied to generate coefficients for conduction transfer functions (CTFs) for building envelope systems in detailed building simulation tools. In particular, the ITPE technique has been used to calculate heat transfer from a variety of building foundations as well as heat gain from refrigerated warehouses [9–10].

Because of its analytical formalism, the ITPE methodology has two significant advantages compared to numerical methods (such as finite difference or finite element methods) including:

- *Higher flexibility*: The ITPE can be used to develop flexible model building envelope system with continuously variable input parameters. For instance, the model can handle any geometric dimensions, any soil thermal properties, and any thermal insulation placement and R-value.
- *Lower computational requirements*: The ITPE is an efficient calculation method and does not require large computational efforts without any significant impact on its accuracy. By way of comparison, The ITPE technique requires at most one minute of CPU time of 60-MHZ computer to calculate three-dimensional heat losses from a building slab-on-grade floor while a finite difference solution for the same floor needs at least 10 hours of the same CPU time for annual simulation period [11]. However, the ITPE results were found to agree well with those obtained with Bahnfleth's solution as well as other numerical models and experimental data [9,12].

Using the building foundation model of Figure 2.3, the ITPE has been applied to solve the 3-D heat equation shown by Eq. (2.7). Assuming steady-periodic conditions, the solution $T(x,y,z,t)$ of Eq. (1) can be found by applying the complex temperature technique [3]:

$$T(x,y,z\ t) = T_{ss}(x,y,z) + Re[T_t(x,y,z)e^{i\omega t}] \tag{2.22}$$

In the above equation, T_{ss} is the mean of the periodic temperature variation over one cycle (such as one day or one year) and T_t is the *complex* amplitude of the annual temperature fluctuations. A real amplitude and a phase shift can be obtained by taking respectively the modulus and the argument of the complex value of T_t.

Both T_{ss}(x,y,z) and T_t(x,y,z) can be obtained from a complex temperature solution I (x,y,z) of the following Helmholtz equation.

$$\nabla \mathfrak{I} = \delta^2\, \mathfrak{I} \tag{2.23}$$

with the following boundary conditions:

$$\Im(x,0,z) = A^*(x,z) \quad \text{for } y = 0 \tag{2.24-a}$$

$$\Im(x,b,z) = T_w \quad \text{for } y = \text{b} \tag{2.24-b}$$

$$\Im(\pm g,y,z) = \Im_s\left(\frac{\sinh\delta(b-y)}{\sinh\delta b}\right) + \Im_w\left(\frac{\sinh\delta y}{\sinh\delta b}\right) \quad \text{for x} = \pm\text{g} \tag{2.24-c}$$

$$\Im(x,y,\pm u) = \Im_s\left(\frac{\sinh\delta(b-y)}{\sinh\delta b}\right) + \Im_w\left(\frac{\sinh\delta y}{\sinh\delta b}\right) \quad \text{for z} = \pm\text{u} \tag{2.24-d}$$

$$\frac{\partial\Im}{\partial z} = H(x,z)(\Im - \Im_\infty(x,z)) \quad \text{for y = 0 and 0} \le \text{x} \le \text{g and 0} \le \text{z} \le \text{u} \tag{2.24-e}$$

where,

$$H(r) = \begin{cases} H_r & \text{x} \le d \text{ and z} \le e \\ H_i & \text{d} \le \text{x} \le \text{a and e} \le \text{z} \le \text{c} \\ H_{th} & \text{a} \le \text{x} \le \text{a} + \text{th and c} \le \text{z} \le \text{c} + \text{th} \\ H_a & x > a + th \text{ or z} > \text{c} + \text{th} \end{cases}$$

and

$$\Im_\infty(r) = \begin{cases} \Im_r & \text{x} \le d \text{ and z} \le e \\ \Im_r & \text{d} \le \text{x} \le \text{a and e} \le \text{z} \le \text{c} \\ \Im_{th} & \text{a} \le \text{x} \le \text{a} + \text{th and c} \le \text{z} \le \text{c} + \text{th} \\ \Im_a & x > a \text{ or z} > \text{c} \end{cases}$$

where $A^*(x, z)$ is an unknown function to be determined using the ITPE approach. H_r, H_i and H_a are the ratio between the equivalent conductance at the boundary surface and the soil thermal conductivity (i.e., for instance, $H_a = U_a/k_s$).

To find the expression for the temperature field $\Im(x, y, z)$, it can be first noted that Eq. (2.23) can be reduced to the following equation:

$$\nabla\theta = \delta^2\theta \tag{2.25}$$

with,

$$\theta(r) = \Im(r) - \Im_w e^{-\delta y}$$

and the following boundary conditions:

$$\theta(x,0,z) = A(x,z) \qquad \text{for } y = 0 \tag{2.26-a}$$

$$\theta(x,b,z) = 0 \qquad \text{for } y = \text{b} \tag{2.26-b}$$

$$\theta(\pm g, y, z) = \theta_s \left(\frac{\sinh \delta(b-y)}{\sinh \delta b} \right) \quad \text{for x} = \pm\text{g} \tag{2.26-c}$$

$$\theta(x, y, \pm u) = \theta_s \left(\frac{\sinh \delta(b-y)}{\sinh \delta b} \right) \quad \text{for z} = \pm\text{u} \tag{2.26-d}$$

$$\frac{\partial \theta}{\partial y} = H(x,z)(\theta - \theta_\infty(x,z)) \text{ for } y = 0 \text{ and } 0 \le x \le g \text{ and } 0 \le z \le u \tag{2.26-e}$$

thus

$$H(r) = \begin{cases} H_r & \text{x} \le d \text{ and z} \le e \\ H_i & \text{d} \le \text{x} \le \text{a and e} \le \text{z} \le \text{c} \\ H_{th} & \text{a} \le \text{x} \le \text{a} + \text{th and c} \le \text{z} \le \text{c} + \text{th} \\ H_a & x > a \text{ or z} > \text{c} \end{cases}$$

and

$$\theta_\infty(r) = \begin{cases} \theta_r & \\ \theta_r & \\ \theta_r \left[\dfrac{\sinh \delta(\text{th} - \text{MAX(x} - \text{a; z} - \text{c))}}{\sinh \delta.th} \right] + \theta_a \left[\dfrac{\sinh \delta.\text{MAX(x} - \text{a; z} - \text{c)}}{\sinh \delta.th} \right] & \\ \theta_a & \end{cases}$$

$$\begin{array}{c} \text{x} \le d \text{ and z} \le e \\ \text{d} \le \text{x} \le \text{a and e} \le \text{z} \le \text{c} \\ \text{a} \le \text{x} \le \text{a} + \text{th and c} \le \text{z} \le \text{c} + \text{th} \\ x > a \text{ or z} > \text{c} \end{array}$$

with $\theta_s = \dfrac{H_a \theta_a}{\left(H_a + \delta \coth \delta b\right)}$ and $\theta_a = \Im_a - \Im_w e^{\delta b}$ and $\theta_i = \Im_i - \Im_w e^{-\delta b}$ $(1 - \delta/H)$

Using the separation of variables technique, the solution, $\theta(x,y,z)$, is expressed as:

$$\theta(x,y,z) = \frac{4}{ug}\sum_{n=1}^{\infty}\sum_{m=1}^{\infty} A_{n,m}.\cos\mu_n x \cos\rho_m z.\frac{\sinh\nu''_{n,m}(b-y)}{\sinh\nu''_{n,m}b}$$

$$+\frac{4}{ub}\theta_s\sum_{n=1}^{\infty}\sum_{m=1}^{\infty}\frac{-(-1)^n\nu_m}{\rho_n\nu'^2_m}.\cos\rho_n z\sin\nu_m y.\frac{\cosh\mu''_{n,m}x}{\cosh\mu''_{n,m}g} \qquad (2.27)$$

$$+\frac{4}{gb}\theta_s\sum_{n=1}^{\infty}\sum_{m=1}^{\infty}\frac{-(-1)^n\nu_m}{\mu_n\nu'^2_m}.\cos\mu_n x\sin\nu_m y.\frac{\cosh\rho''_{n,m}z}{\cosh\rho''_{n,m}u}$$

Where,

$$\nu_n = \frac{n\pi}{b}; \qquad \nu'_m = \sqrt{\delta^2 + \nu_m{}^2}; \; \mu_n = \frac{(2n-1)\pi}{2g}; \qquad \rho_n = \frac{(2n-1)\pi}{2u};$$

$$\mu''_{n,m} = \sqrt{\delta^2 + \rho_n{}^2 + \nu_m{}^2}; \quad \rho''_{n,m} = \sqrt{\delta^2 + \mu_n{}^2 + \nu_m{}^2};$$

$$\nu''_{n,m} = \sqrt{\delta^2 + \mu_n{}^2 + \rho_m{}^2};$$

and, $A_{n,m}$ are Fourier coefficients that are determined using the heat flux continuity at the boundary surface $y = 0$ and $0 \le x \le g$ and $0 \le z \le u$. Only the final expression of the system of equations for the coefficients, $A_{n,m}$ is provided here.

$$A_{p,k} = \alpha_{p,k} + \sum_{n=1}^{\infty}\sum_{m=1}^{\infty}\beta_{n,p,m,k}.A_{n,m} \qquad (2.28)$$

The expressions for the coefficients $\alpha_{p,k}$ and $\beta_{n,p,m,k}$ for Eq. (2.28) are provided below:

if k ≠ p

$$\alpha_{p,k} = \frac{1}{(H_a + \nu''_{p,k}\coth\nu''_{p,k}b)(\rho_k\mu_p)} *$$

$$\left\{
\begin{array}{l}
\left[
\begin{array}{l}
(-1)^{p+k} H_a\theta_a + (H_{th}.(\theta_r - \frac{\theta_a - \theta_r}{th} * a) - H_a\theta_a).\sin\mu_p(a+th).\sin\rho_k(c+th) + \\
(H_t\theta_r - H_{th}.(\theta_r - \frac{\theta_a - \theta_r}{th} * a)).\sin\mu_p a.\sin\rho_k c + (H_r\theta_r - H_t\theta_r).\sin\mu_p d.\sin\rho_k e
\end{array}
\right] \\
+ 4 * \frac{H_{th}.\sin\rho_k c}{th.\rho_k.\mu_p^2}\left([\theta_a - \theta_r].\cos\mu_p(a+th) + [\theta_a - \theta_r].th\mu_p\sin\mu_p(a+th) + [\theta_r - \theta_a].\cos\mu_p a\right) \\
+ 4 * \frac{H_{th}.\sin\mu_p c}{th.\rho_k^2.\mu_p}\left([\theta_a - \theta_r].\cos\rho_k(c+th) + [\theta_a - \theta_r].th.\rho_k\sin\rho_k(c+th) + [\theta_r - \theta_a].\cos\rho_k c\right) \\
+ \frac{2}{b}\theta_s(-1)^{p+k}(\mu_p^2 + \rho_k^2)\sum_{m=1}^{\infty}\frac{\nu_m^2}{\nu'^2_m(\mu_p^2 + \rho_k^2 + \nu_m^2 + \delta^2)} \\
+ \frac{4.H_{th}}{2\mu_p.\rho_k^2.th.(\mu_p + \rho_k)^2.(-\mu_p + \rho_k)^2} * \\
\left[
\begin{array}{l}
\{[\mu_p^2.\rho_k^3 - \mu_p^3.\rho_k^2 - \mu_p^4.\rho_k + \mu_p.\rho_k^4] * [\theta_r a - \theta_r c + \theta_a c - \theta_a a] - \theta_r.th * [\mu_p^2.\rho_k^3 + \mu_p^3.\rho_k^2 - \mu_p^4.\rho_k - \mu_p.\rho_k^4]\} \\
* \{\cos((\rho_k - \mu_p).a) - \cos((\rho_k - \mu_p).(a+th))\} + \\
\{[\theta_r - \theta_a] * [3\mu_p^2.\rho_k^2 - 2\mu_p.\rho_k^3 - \mu_p^4]\} * \{\sin((\rho_k - \mu_p).(a+th)) - \sin((\rho_k - \mu_p).a)\} + \\
\{[\theta_r - \theta_a] * [-3\mu_p^2.\rho_k^2 + 2\mu_p.\rho_k^3 + \mu_p^4]\} * \{\sin((\rho_k + \mu_p).(a+th)) - \sin((\rho_k + \mu_p).a)\} + \\
\{[\mu_p^2\rho_k^3 + \mu_p^3\rho_k^2 - \mu_p^4\rho_k - \mu_p\rho_k^4].[\theta_r a - \theta_r c + \theta_a c - \theta_a a - \theta_a th]\}\{\cos(\rho_k + \mu_p)(a+th) - \cos(\rho_k + \mu_p)a)\} \\
+ \{\theta_a.th * [\mu_p^4.\rho_k - 2\mu_p^2.\rho_k^3 + \rho_k^5] * [\cos(\mu_p a + \mu_p th - \rho_k c - \rho_k th) - \cos(\mu_p a + \mu_p th + \rho_k c + \rho_k th)\} \\
+ \{[\theta_r - \theta_a].[2\mu_p^2.\rho_k^2 - \mu_p^4 - \rho_p^4] * [\sin(\mu_p a + \mu_p th - \rho_k c - \rho_k th) + \sin(\mu_p a + \mu_p th + \rho_k c + \rho_k th)\} \\
+ \{[\theta_r - \theta_a].[\mu_p^4 + \rho_p^4 - 2\mu_p^2.\rho_k^2] * [\sin(\mu_p a + \rho_k c + \rho_k th) + \sin(\mu_p a - \rho_k c - \rho_k th)]\} \\
+ \{\theta_a.th * [-\mu_p^4.\rho_k + 2\mu_p^2.\rho_k^3 - \rho_k^5] * [\cos(\mu_p a - \rho_k c - \rho_k th) - \cos(\mu_p a + \rho_k c + \rho_k th)\}
\end{array}
\right] \\
+ \frac{4.H_{th}}{2\mu_p^2.\rho_k.th.(\mu_p + \rho_k)^2.(\mu_p - \rho_k)^2} * \\
\left[
\begin{array}{l}
\{[\mu_p^2.\rho_k^3 - \mu_p^3.\rho_k^2 - \mu_p^4.\rho_k + \mu_p.\rho_k^4] * [\theta_r a - \theta_r c + \theta_a c - \theta_a a] - \theta_r.th * [\mu_p^2.\rho_k^3 + \mu_p^3.\rho_k^2 - \mu_p^4.\rho_k - \mu_p.\rho_k^4]\} \\
* \{\cos((\rho_k - \mu_p).a) - \cos((\rho_k - \mu_p).(c+th))\} + \\
\{[\theta_r - \theta_a] * [3\mu_p^2.\rho_k^2 - 2\mu_p^3.\rho_k^1 - \rho_k^4]\} * \{\sin((\rho_k - \mu_p).(c+th)) - \sin((\rho_k - \mu_p).c)\} + \\
\{[\theta_r - \theta_a] * [-3\mu_p^2.\rho_k^2 + 2\mu_p^3.\rho_k^1 + \rho_k^4]\} * \{\sin((\rho_k + \mu_p).(c+th)) - \sin((\rho_k + \mu_p).c)\} - \\
\{[\mu_p^2\rho_k^3 + \mu_p^3\rho_k^2 - \mu_p^4\rho_k - \mu_p\rho_k^4].[\theta_r a - \theta_r c + \theta_a c - \theta_a a - \theta_a th]\}\{\cos(\rho_k + \mu_p)(c+th) - \cos(\rho_k + \mu_p)c)\} \\
+ \{\theta_a.th * [\mu_p.\rho_k^4 - 2\mu_p^3.\rho_k^2 + \mu_p^5] * [\cos(\mu_p a + \mu_p th - \rho_k c - \rho_k th) - \cos(\mu_p a + \mu_p th + \rho_k c + \rho_k th)\} \\
+ \{[\theta_r - \theta_a].[2\mu_p^2.\rho_k^2 - \mu_p^4 - \rho_p^4] * [\sin(\mu_p a + \mu_p th - \rho_k c - \rho_k th) + \sin(\mu_p a + \mu_p th + \rho_k c + \rho_k th)\} \\
+ \{[\theta_r - \theta_a].[\mu_p^4 + \rho_p^4 - 2\mu_p^2.\rho_k^2] * [\sin(\mu_p a + \rho_k c + \mu_p th) + \sin(\mu_p a - \rho_k c - \mu_p th)]\} \\
+ \{\theta_a.th * [-\mu_p.\rho_k^4 + 2\mu_p^2.\rho_k^3 - \mu_p^5] * [\cos(\mu_p a - \rho_k c - \mu_p th) - \cos(\mu_p a + \rho_k c + \mu_p th)\}
\end{array}
\right]
\end{array}
\right\}$$

if k = p

$$\alpha_{p,k} = \frac{1}{(H_a + \nu''_{p,k}\coth\nu''_{p,k}b)(\rho_k\mu_p)} *$$

$$\left\{
\begin{array}{l}
\left[
\begin{array}{l}
(-1)^{p+k} H_a\theta_a + (H_{th}.(\theta_r - \frac{\theta_a - \theta_r}{th} * a) - H_a\theta_a).\sin\mu_p(a+th).\sin\rho_k(c+th) + \\
(H_i\theta_r - H_{th}.(\theta_r - \frac{\theta_a - \theta_r}{th} * a)).\sin\mu_p a.\sin\rho_k c + (H_r\theta_r - H_i\theta_r).\sin\mu_p d.\sin\rho_k e
\end{array}
\right] \\
+ 4 * \frac{H_{th}.\sin\rho_k c}{th.\rho_k.\mu_p^2}\left([\theta_a - \theta_r].\cos\mu_p(a+th) + [\theta_a - \theta_r].th\mu_p\sin\mu_p(a+th) + [\theta_r - \theta_a].\cos\mu_p a\right) \\
+ 4 * \frac{H_{th}.\sin\mu_p c}{th.\rho_k^2.\mu_p}\left([\theta_a - \theta_r].\cos\rho_k(c+th) + [\theta_a - \theta_r].th.\rho_k\sin\rho_k(c+th) + [\theta_r - \theta_a].\cos\rho_k c\right) \\
+ \frac{2}{b}\theta_s(-1)^{p+k}(\mu_p^2 + \rho_k^2)\sum_{m=1}^{\infty}\frac{\nu_m^2}{\nu'^2_m(\mu_p^2 + \rho_k^2 + \nu_m^2 + \delta^2)} \\
+ \frac{4.H_{th}}{2\mu_p.\rho_k^2.th.(\mu_p + \rho_k)^2} * \\
\left[
\begin{array}{l}
\{[\theta_r a - \theta_r c + \theta_a c - \theta_a a] - \theta_r.th\} * \{\cos((\rho_k - \mu_p).a) - \cos((\rho_k - \mu_p).(a+th))\} + \\
\{[\theta_r - \theta_a]\} * \{\sin((\rho_k - \mu_p).(a+th)) - \sin((\rho_k - \mu_p).a)\} + \\
\{[\theta_r - \theta_a]\} * \{\sin((\rho_k + \mu_p).(a+th)) - \sin((\rho_k + \mu_p).a)\} + \\
\{.[\theta_r a - \theta_r c + \theta_a c - \theta_a a - \theta_a th]\}\{\cos(\rho_k + \mu_p)(a+th) - \cos(\rho_k + \mu_p)a)\} \\
+ \{\theta_a.th * [\cos(\mu_p a + \mu_p th - \rho_k c - \rho_k th) - \cos(\mu_p a + \mu_p th + \rho_k c + \rho_k th)\} \\
+ \{[\theta_r - \theta_a] * [\sin(\mu_p a + \mu_p th - \rho_k c - \rho_k th) + \sin(\mu_p a + \mu_p th + \rho_k c + \rho_k th)\} \\
+ \{[\theta_r - \theta_a].*[\sin(\mu_p a + \rho_k c + \rho_k th) + \sin(\mu_p a - \rho_k c - \rho_k th)]\} \\
+ \{\theta_a.th * [\cos(\mu_p a - \rho_k c - \rho_k th) - \cos(\mu_p a + \rho_k c + \rho_k th)\}
\end{array}
\right] \\
+ \frac{4.H_{th}}{2\mu_p^2.\rho_k.th.(\mu_p + \rho_k)^2} * \\
\left[
\begin{array}{l}
\{*[\theta_r a - \theta_r c + \theta_a c - \theta_a a] - \theta_r.th*\} * \{\cos((\rho_k - \mu_p).a) - \cos((\rho_k - \mu_p).(c+th))\} + \\
\{[\theta_r - \theta_a]\} * \{\sin((\rho_k - \mu_p).(c+th)) - \sin((\rho_k - \mu_p).c)\} + \\
\{[\theta_r - \theta_a]\} * \{\sin((\rho_k + \mu_p).(c+th)) - \sin((\rho_k + \mu_p).c)\} - \\
\{[\theta_r a - \theta_r c + \theta_a c - \theta_a a - \theta_a th]\}\{\cos(\rho_k + \mu_p)(c+th) - \cos(\rho_k + \mu_p)c)\} \\
+ \{\theta_a.th * [\cos(\mu_p a + \mu_p th - \rho_k c - \rho_k th) - \cos(\mu_p a + \mu_p th + \rho_k c + \rho_k th)\} \\
+ \{[\theta_r - \theta_a] * [\sin(\mu_p a + \mu_p th - \rho_k c - \rho_k th) + \sin(\mu_p a + \mu_p th + \rho_k c + \rho_k th)\} \\
+ \{[\theta_r - \theta_a].*[\sin(\mu_p a + \rho_k c + \mu_p th) + \sin(\mu_p a - \rho_k c - \mu_p th)]\} \\
+ \{\theta_a.th * [\cos(\mu_p a - \rho_k c - \mu_p th) - \cos(\mu_p a + \rho_k c + \mu_p th)\}
\end{array}
\right]
\end{array}
\right\}$$

And

$$\beta_{n,p,m,k} = \frac{-4}{ug}\frac{\left[F_{n,p}^{a+th}G_{m,k}^{c+th}\cdot(H_{th} - H_a) + F_{n,p}^{a}G_{m,k}^{c}\cdot(H_i - H_{th}) + F_{n,p}^{d}G_{m,k}^{e}\cdot(H_r - H_i)\right]}{(H_a + \nu''_{p,k}\coth\nu''_{p,k}b)}$$

where

$$F_{n,p}^{x} = \begin{cases} \dfrac{\sin(\mu_n - \mu_p)x}{2.(\mu_n - \mu_p)} + \dfrac{\sin(\mu_n + \mu_p)x}{2.(\mu_n + \mu_p)} & ;\mathrm{n} \neq \mathrm{p} \\ \dfrac{1}{2}\left(x + \dfrac{\sin 2\mu_p x}{2.\mu_n} \right) & ;\mathrm{n} = \mathrm{p} \end{cases}$$

$$G_{m,k}^{z} = \begin{cases} \dfrac{\sin(\rho_m - \rho_k)z}{2.(\rho_m - \rho_k)} + \dfrac{\sin(\rho_m + \rho_k)z}{2.(\rho_m + \rho_k)} & ;\mathrm{m} \neq \mathrm{k} \\ \dfrac{1}{2}\left(z + \dfrac{\sin 2\rho_k z}{2.\rho_k} \right) & ;\mathrm{m} = \mathrm{k} \end{cases}$$

The system of equations expressed by Eq. (2.28) is solved by truncating the sums to a finite number of terms, respectively, N and M. A linear system of (N*M) × (N*M) equations with (N*M) × (N*M) unknowns is obtained and is solved by the Gauss-Jordan Matrix Solver. The accuracy of the solution provided by Eq. (2.27) depends on the truncation numbers N and M; the higher these numbers, the more accurate is the solution but the more computational effort is required.

The heat flux along the slab surface can be obtained from the third boundary condition of Eq. (2.26-e) and the 3-D temperature solution of Eqs. (2.27) and (2.28):

$$q(x,z) = \frac{4}{ug} U_{conv} \sum_{n=1}^{\infty} \sum_{m=1}^{\infty} \left[A_{n,m}. - \frac{(-1)^{n+m}\theta_i}{\mu_n \rho_m} \right].\cos \mu_n x.\cos \rho_m z \qquad (2.29)$$

The total slab heat loss is obtained by integrating the 2-D heat flux, *q(x,z)*, of Eq. (2.29) over the entire slab surface (i.e., y = 0 and $-a \leq x \leq a$ and $-c \leq z \leq c$):

$$Q_{total} = \iint_S \frac{4}{ug} U_{conv} \sum_{n=1}^{\infty} \sum_{m=1}^{\infty} \left[A_{n,m}. - \frac{(-1)^{n+m}\theta_i}{\mu_n \rho_m} \right].\cos \mu_n x.\cos \rho_m z.dxdz \qquad (2.30)$$

2.3.3 Conduction Transfer Function (CTF) Methods

One of the most popular methods to predict transient heat conduction transfer in whole-building energy simulation programs is the conduction

transfer function (CTF) method. The CTF method was introduced by Stephenson and Mitalas [13] using inverse Laplace transforms and Z-transforms to estimate transient heat conduction transfer through building walls. Hittle and Bishop [14] developed a root-finding method, referred to as the Laplace method, to increase the accuracy of the CTF method while improving its computational efficiency. To estimate CTF coefficients more accurately, other methods have been proposed including the state space method [15–16] and finite difference [17].

Several whole-building energy simulation programs use the CTF method including BLAST [14], TRNSYS [18], and EnergyPlus [19]. In particular, EnergyPlus uses the state space method for calculating CTF coefficients.

CTF Method Overview: Transient 1-D heat conduction through a building envelope system can be formulated by a partial differential equation as noted by Eq. (2.6) and can be solved numerically using the conduction transfer function (CTF) method. The basic form of the CTF solution is shown in Eq. (2.31) for estimating heat flux at the inner surface of a building envelope layer:

$$q''_{i,t} = \sum_{m=1}^{M} X_m T_{i,t-m+1} - \sum_{m=1}^{M} Y_m T_{o,t-m+1} + \sum_{m=1}^{k} F_m q''_{i,t-m} \qquad (2.31)$$

where, k is the order of the conduction transfer functions, M is a finite number defined by the order of the conduction transfer functions, and X, Y, and F are the conduction transfer functions (CTFs). Moreover, T_i and T_0 are the interior and exterior surface temperatures. A similar CTF equation can be defined for calculation heat flux at the exterior surface.

The linear relationship can reduce computational effort and make it easy to use for computer programming. Furthermore, CTF coefficients are temperature independent for non-phase change and homogeneous materials, and they are calculated for typical materials.

State Space Method for Calculating CTFs: The state space method to solve heat equations was first introduced by Ceylan and Myers [15] and later refined by Seem [16]. The basic form of the state space expression is shown as follows:

$$\dot{x}(t) = A \cdot x(t) + B \cdot u(t) \qquad (2.32)$$

$$y(t) = C \cdot x(t) + D \cdot u(t) \tag{2.33}$$

where A, B, C and D are (n x n), (n x p), (m x n) and (m x p) matrices. x is the vector of state variables, and u is the vector of inputs, y is the output vector and t is the time.

This form can be applied to solve a transient heat equation. To use the state space method, a finite difference grid is applied within layers in the building elements. The state variables are the nodal temperature, the environmental temperatures are the input variables and heat fluxes at the surface are the output variables. Seem presented a method for calculating transfer functions for multi-dimensional heat transfer [16].

Stability of Linear System: If the input (u_i) and output (y_i) variables for a system are expressed using the state (x_i) at t_o for i=1, 2, 3…as indicated in Eq. (3.18), the system is called a linear system [20].

$$\left.\begin{array}{l} x_i(t_0) \\ u_i(t), t \geq t_0 \end{array}\right\} \rightarrow y_i(t), t \geq t_0 \tag{2.34}$$

A linear system can be described by a set of equations such as Eq. (2.32) and Eq. (2.33) if the number of state variables is finite. The set of equations for the linear system is then called a state space equation.

The response of a linear system can be decomposed into two responses: the zero-state response and the zero-input response. Solutions for the two responses can be determined separately and the sum of these two solutions yields the solution for the complete response. Therefore, the stability analysis for a linear system can be performed separately for the zero-input response and for the zero-state response. The stability conditions associated to both the zero-input response and the zero-state response constitute the stability conditions for the linear system [20].

According to the theorem of stability for zero-state response, the state-space equation [Eq. (2.32) and Eq. (2.33)] is bounded-input and bounded-output stable if and only if every eigenvalue has a negative real part [20]. If the input $u(t)$ is identically zero, the output is called the zero-input response. For zero-input response, Eq. (2.32) provides the following equation:

$$\dot{x}(t) = A \cdot x(t) \tag{2.35}$$

According to the theorem of stability, Eq. (2.35) is stable if and only if all eigenvalues of A have a magnitude less than or equal to 1 [20]. Therefore, Eq. (2.32) and Eq. (2.33) are stable if and only if every eigenvalue of A has a negative real part and its magnitude is less than or equal to 1 from the stability conditions of both zero-state response and zero-input response.

2.3.4 Frequency-Domain Regression

The frequency-domain regression (FDR) method, described in details by Krarti et al. [21–22], Cheng and Wang [23–24], and Khlifi and Krarti [25] can be applied to determine the conduction transfer functions for building envelope systems. In this section, the basic approach of the FDR method is first briefly outlined. Then, the FDR approach is validated using known results for heat transfer problems for multi-layered walls as well as for slab-on-grade floors using the ITPE technique [25].

Overview of FDR: The basic approach for estimating heat flux at the inner surface of any building envelope layer using the conduction transfer function (CTF) technique is summarized in the following expression:

$$Q_{in}(t) = \sum_{i=1}^{n} \gamma_i T_{in}(t - i\Delta t) - \sum_{i=1}^{n} \alpha_i T_{out}(t - i\Delta t) - \sum_{l=1}^{m} \beta_l Q_{in}(t - l\Delta t) \quad (2.36)$$

In Eq. (2.36), m is the order of the conduction transfer functions, n is a finite number defined by the order of the conduction transfer functions, and γ_i, α_i, and β_i are the CTF coefficients. Moreover, T_{in} and T_{out} are the interior and exterior surface temperatures. A similar CTF equation can be defined for calculating the heat flux at the exterior surface. The CTF technique, using the linear relationship outlined in Eq. (2.36), reduces computational time and is easy to implement in a computer algorithm. The following section describes a calculation method for determining the CTF coefficients.

The indoor and then the outdoor temperatures are set to zero in Eq. (2.36) to simplify the calculation procedure. For instance, by setting the indoor temperature to zero, the heat flux $Q(t)$ from a building envelope surface at a given time t, can be estimated from present and past values of outdoor surface temperatures and from the past values of heat flux:

$$Q(t) = \sum_{i=0}^{n} \alpha_i T(t - i\Delta t) - \sum_{l=1}^{m} \beta_l Q(t - l\Delta t) \tag{2.37}$$

with, Δt is the time step. α_i and β_i are coefficients characterizing the heat flux from the surface. Note that when the flux $Q(t)$ is expressed only as a function of the present and past values of temperatures (i.e., ; l = 1, 2, …, m), the coefficients (i=1,2,…n) are the thermal response factors as defined by Mitalas and Stephenson [13].

Using the z-transform of Eq. (2.37), the heat flux $Q(z)$ can be expressed as function of $T(z)$ as follows:

$$Q(z) = \frac{\sum_{i=0}^{n} \alpha_i z^{-i}}{1 + \sum_{l=1}^{m} \beta_l z^{-l}} T(z) \tag{2.38}$$

or

$$\frac{Q(z)}{T(z)} = G(z) = \frac{\sum_{i=0}^{n} \alpha_i z^{-i}}{1 + \sum_{l=1}^{m} \beta_l z^{-l}} \tag{2.39}$$

The function $G(z)$ is known as the z-transfer function of the building envelope surface and z is the back-shift operator. In the particular case of $z = 1/j\omega$, a frequency transfer function can be obtained:

$$G(\omega) = \frac{Q(\omega)}{T(\omega)} = \frac{\sum_{i=0}^{n} \alpha_i (j\omega)^i}{1 + \sum_{l=1}^{m} \beta_l (j\omega)^l} = \frac{\tilde{A}(\omega)}{1 + \tilde{B}(\omega)} = G_R(\omega) + jG_I(\omega) \tag{2.40}$$

$G_R(\omega)$ and $G_I(\omega)$ are respectively, the real part and the imaginary part of the frequency transfer function $G(\omega)$. For reference, Table 2.2 illustrates selected cycles and frequencies and their logarithmic values used to express variations in outdoor and indoor air temperatures.

Note that a similar frequency transfer function can be obtained when z is substituted by $e^{j\omega\Delta t}$ as proposed by Chen and Wang [23] to estimate CTFs for walls and roofs and Krarti et al. [21] for building foundations.

Table 2.2. Selected Frequencies and Their Logarithmic Values Used to Express Variations in Outdoor and Indoor Air Temperatures.

Period	Frequency, ω (rad/s)	-ln(ω)
1 min	0.105	2.256
10 min	1.05×10^{-2}	4.560
30 min	3.49×10^{-3}	5.658
1 hr	1.745×10^{-3}	6.351
3 hr	5.818×10^{-4}	7.450
6 hr	2.909×10^{-4}	8.143
12 hr	1.454×10^{-4}	8.836
24 hr	7.272×10^{-5}	9.529
1 month	2.424×10^{-6}	12.930
1 yr	1.992×10^{-7}	15.429
2 yr	9.962×10^{-8}	16.122
Steady-state	0	∞

The coefficient α_i and β_i can be determined using the error function (see details in [21, 24]). A set of linear system of equations can be expressed as follows:

$$E(X) = \sum_{k=1}^{N} \left| \tilde{A}(\omega_k) - G(\omega_k)[1 + \tilde{B}(\omega_k)] \right|^2 \tag{2.41}$$

where X is a vector defined by:

$$X^T = \left[\beta_0 \quad \beta_1 \quad \beta_2 \quad \beta_3 \ldots\ldots \beta_m \quad \alpha_1 \quad \alpha_2 \quad \alpha_3 \ldots\ldots \alpha_n \right] \tag{2.42}$$

The set of frequency ω_k (k=1, ... N) is selected from a suitable range depending on the properties of the building envelope component, typically from 10^{-2} to 10^{-10} rad/s. By minimizing the error function, the coefficients α_i and β_i (i.e., the vector X) can be found. It can be shown that X is solution of a system of linear equations [24]:

$$M.X = Y \tag{2.43}$$

With

$$Y^T = \left[S_0 \quad W_1 \quad -S_2 \quad -W_3 \quad S_4 \ldots\ldots 0 \quad U_1 \quad 0 \quad U_3 \quad 0 \ldots\ldots \right] \tag{2.44}$$

and

$$M = \begin{bmatrix} V_0 & 0 & -V_2 & 0 & V_4 & ... & W_1 & S_2 & -W_3 & -S_4 & W_5 & .... \\ 0 & V_2 & 0 & -V_4 & 0 & ... & S_2 & W_3 & S_4 & -W_5 & -S_6 & .... \\ -V_2 & 0 & V_4 & 0 & -V_6 & ... & W_3 & -S_4 & W_5 & S_6 & -W_7 & .... \\ 0 & -V_4 & 0 & V_6 & 0 & ... & S_4 & -W_5 & -S_6 & W_7 & S_8 & .... \\ V_4 & 0 & V_6 & 0 & V_8 & ... & W_5 & S_6 & -W_7 & -S_8 & W_9 & .... \\ : & : & : & : & : & : & : & : & : & : & : & .... \\ W_1 & -S_2 & -W_3 & S_4 & W_5 & ... & U_2 & 0 & -U_4 & 0 & U_6 & .... \\ S_2 & W_3 & -S_4 & -W_5 & S_6 & ... & 0 & U_4 & 0 & -U_6 & 0 & .... \\ -W_3 & S_4 & W_5 & -S_6 & -W_7 & ... & -U_4 & 0 & U_6 & 0 & -U_8 & .... \\ -S_4 & -W_5 & S_6 & W_7 & -S_8 & ... & 0 & -U_6 & 0 & U_8 & 0 & .... \\ W_5 & -S_6 & -W_7 & S_8 & W_9 & ... & U_6 & 0 & -U_8 & 0 & U_{10} & .... \\ : & : & : & : & : & : & : & : & : & : & : & : \end{bmatrix} \tag{2.45}$$

and

$$V_i = \sum_{k=1}^{N} \omega_k^i, \qquad S_i = \sum_{k=1}^{N} \omega_k^i . G_{R,k},$$

$$W_i = \sum_{k=1}^{N} \omega_k^i . G_{I,k}, \qquad U_i = \sum_{k=1}^{N} \omega_k^i (G_{R,k}^2 + G_{I,k}^2) \tag{2.46}$$

$$G_{R,k} = G_R(\omega_k), \qquad G_{I,k} = G_I(\omega_k)$$

Eq. (2.43) provides a system of ($n + m + 1$) linear equations with ($n + m + 1$) unknowns: the coefficients a_i ($n + 1$ unknowns) and the coefficients b_l (m unknowns). This linear system can be solved using the Gauss-Jordan elimination method [26]. The set of frequencies ω_k is selected based on where it is most important to have accurate estimation of the conduction transfer function.

Application for CTF Estimation for 1-D Heat Transfer for Walls: The FDR method is applied first to evaluate its accuracy in performing transient heat conduction analysis for one-dimensional (1-D) walls

compared with the commonly used response factor technique. Table 2.3 provides details of a multi-layered wall used to compare the FDR method prediction accuracy against the response factor technique based on the direct root-finding method [5]. The wall consists of an outside convective layer, a layer of face brick, an insulation layer, a layer of common brick, and an inside convective layer.

A polynomial transfer function can be estimated for the multi-layered wall of Table 2.3 using the state-space method. The conduction transfer function, for the multi-layered wall of Table 2.3, has been estimated by Ouyang and Haghighat [27]. This conduction transfer function was found to take the following expression [24]:

$$G(z) = \frac{\begin{array}{c} -4.9035.10^{-5} z^{-5} + 2.35096.10^{-7} z^{-4} - 6.9965.10^{-10} z^{-3} \\ +1.38768.10^{-12} z^{-2} - 1.77507.10^{-15} z^{-1} + 1.13961.10^{-18} \end{array}}{\begin{array}{c} z^{-5} + 3.19462.10^{-3} z^{-4} + 3.59719.10^{-6} z^{-3} + 1.49979.10^{-9} z^{-2} \\ +1.21286.10^{-13} z^{-1} + 2.30188.10^{-18} \end{array}} \quad (2.47)$$

Figure 2.6 compares the variation of the amplitude of heat conduction through the multi-layered wall as a function of the frequency of outdoor air temperature fluctuations l obtained using the FDR method and that obtained using the state-space method referred to as theoretical.

Figure 2.7 compares the variation of the phase angle of the wall heat conduction as a function of outdoor air temperature frequency obtained the FDR method and that obtained using the state-space method referred to as theoretical.

Table 2.3.Details of Wall Construction Used in the Validation Analysis.

Description	**L(mm)**	k**(W m^{-1}K^{-1})**	ρ**(kg m^{-3})**	c_p**(Jkg^{-1}K^{-1})**	R**(m^{2}K. W^{-1})**
Outside surface film					0.05
Face brick	89	1.73	2235	1106	0.0514
Insulation	127	0.0744	24	992	1.707
Common brick	89	1.73	2235	1106	0.0514
Inside surface film					0.16

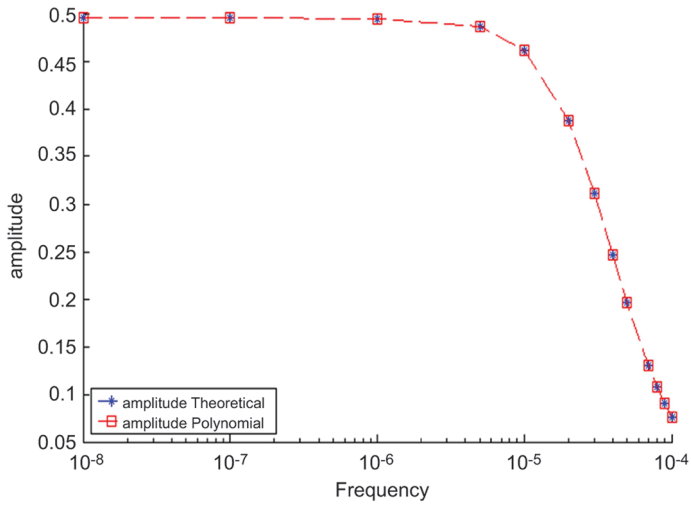

Figure 2.6. Frequency analysis of amplitude of heat conduction for 1-D wall.

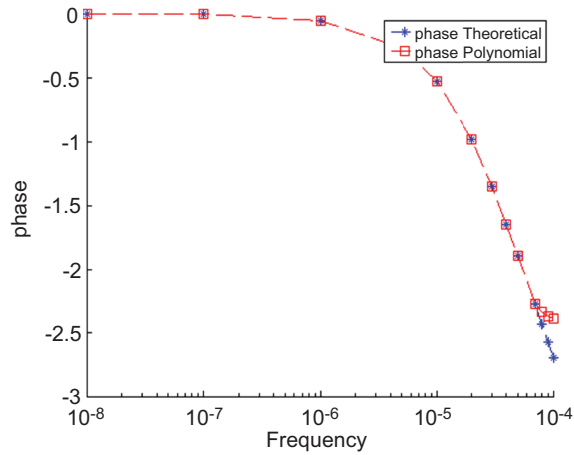

Figure 2.7. Frequency analysis of phase angle of heat conduction for 1-D wall.

Using the response factors of the wall, the wall heat loss can be determined at any time step using information on outdoor temperatures and heat losses at previous time steps. Assuming that the indoor air temperature is constant, the heat transfer through the wall can be as expressed as a function of the CTF coefficients and the solar-air temperature as follows [28]:

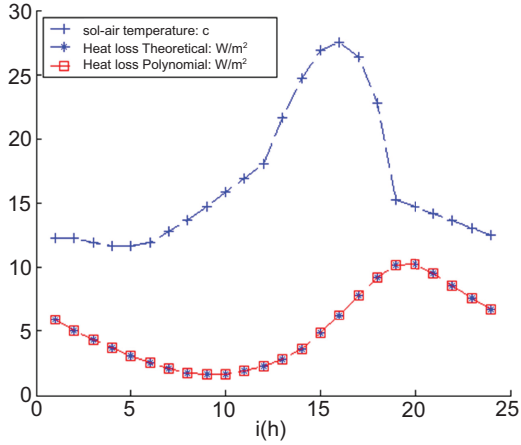

Figure 2.8. Comparison of heat loss calculated with FDR and response factor technique through 1-D wall.

$$Q(i.\Delta t) = \sum_{k=0} b_k T_a(i.\Delta t - k.\Delta t) - \sum_{k=1} d_k Q(i.\Delta t - k.\Delta t) - T_r \sum_{k=0} c_k \qquad (2.48)$$

Using a variation of the solar-air temperature during a cycle of 24 hours as depicted in Figure 2.8 and a constant room air temperature of 20^{o}C, the hourly variation of the heat loss per unit wall area can be estimated using Eq. (2.48). Figure 2.8 compares the wall heat transfer obtained using CTF coefficients obtained from the FDR method and from the response factor technique (using the ITPE solution). The results of Figure 2.8 clearly indicate that the two methods provide the same variation of wall heat loss due to the solar-air temperature. According to the results of Figure 2.8, there is a shift of about 3 hours between when the solar air temperature and the wall heat loss reach their maximum. This time shift is due to thermal mass of the wall.

Application for Estimating Heat Transfer from Slab-On-Grade Floor: In this section, the FDR method is considered to evaluate the impact of fluctuations in both indoor and outdoor air temperatures on the magnitude and phase angle of total slab heat losses or gains. The solution for ground-coupled heat transfer is first obtained using 3-D ITPE technique [3, 7, 25, 29]. Then, the FRD method as outlined above is used to estimate coefficients for the conduction transfer functions (CTFs) for slab foundations based on the results of the frequency analysis is carried out using the ITPE solution.

Figure 2.9 compares the results obtained by the FDR method and those obtained by the ITPE technique for the normalized amplitude of the ground-coupled 3-D heat transfer from a slab-on-grade floor as a function of the frequency of indoor air temperature fluctuations. In particular, Figure 2.9 illustrates the results for the case where the thickness of the above-grade walls is accounted for [25]. Good agreement is obtained by the FDR method when compared with the ITPE results.

Figure 2.10 compares the FDR and ITPE results for the Nyquist diagram for the normalized ground-coupled 3-D heat transfer from the slab-on-grade floor to illustrate the variation of both amplitude and phase angle of slab heat loss as a function of the frequency of indoor air temperature variations.

Figure 2.11 compares the results obtained by the FDR method and those obtained by the ITPE technique for the normalized amplitude of the ground-coupled 3-D heat transfer from a slab-on-grade floor as a function of outdoor air temperature. Specifically, Figure 2.11 illustrates the results for the case where the thickness of the above-grade walls is accounted for [25]. Good agreement is obtained by the FDR method when its predictions are compared with the ITPE results.

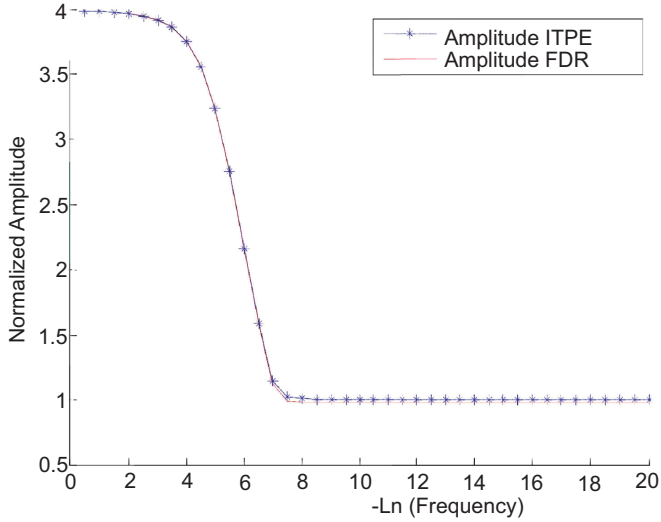

Figure 2.9. Amplitude for 3-D total slab heat losses as a function of frequency of indoor air temperature obtained by FDR and ITPE techniques.

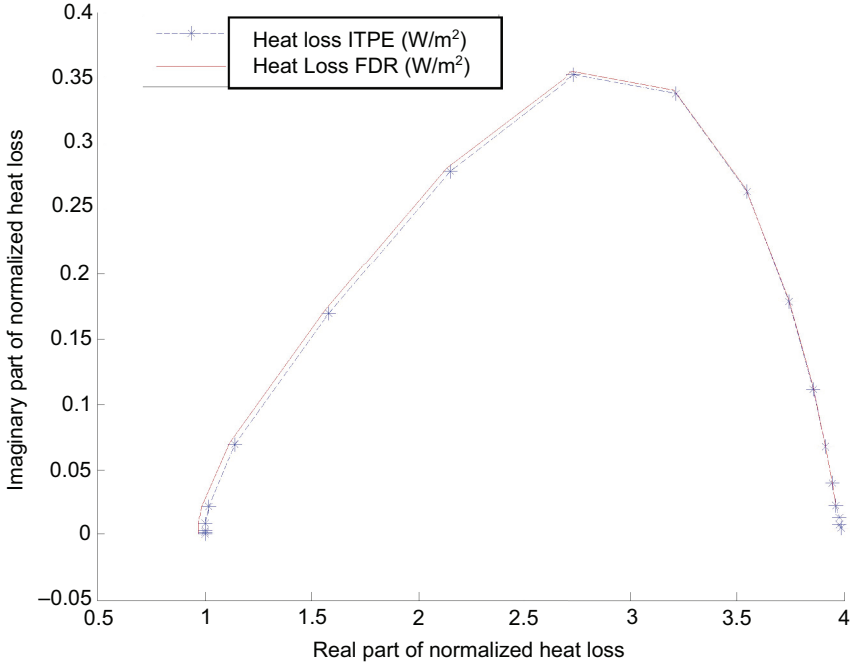

Figure 2.10. Comparison of the frequency characteristics obtained by FDR and ITPE methods for 3-D slab heat losses due to indoor temperature variations using the Nyquist diagram.

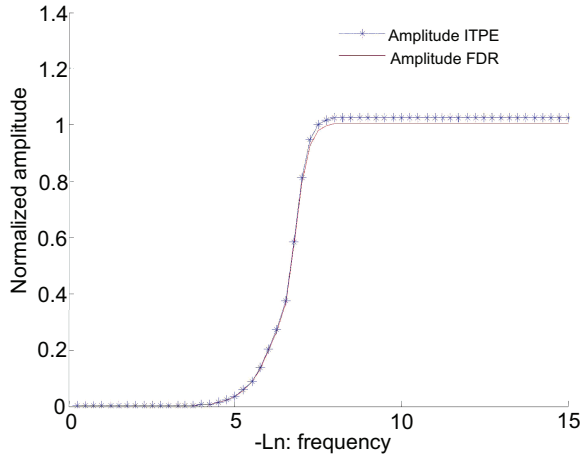

Figure 2.11. Amplitude for 3-D total slab heat losses as a function of frequency of outdoor air temperature obtained by FDR and ITPE techniques.

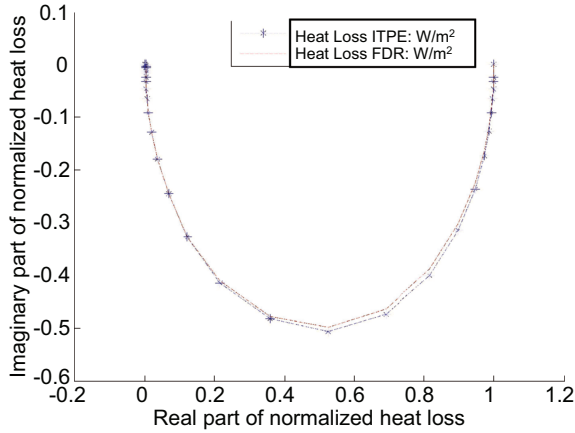

Figure 2.12. Comparison of the frequency characteristics obtained by FDR and ITPE methods for 3-D slab heat losses due to outdoor temperature variations using the Nyquist diagram.

Figure 2.12 compares the FDR and ITPE results for the Nyquist diagram for the normalized ground-coupled 3-D heat transfer from the same slab-on-grade floor used in Figure 2.11 to illustrate the variation of both amplitude and phase angle of slab heat loss as a function of the frequency of outdoor air temperature variations. Good agreement between both methods is obtained.

In summary, the FDR method can predict accurately the frequency response of slab foundations to both indoor and outdoor air temperature fluctuations. Moreover, FDR methodology offers a better alternative of numerical methods to couple detailed foundation heat transfer models into whole-building simulation programs. As indicated in Figures 2.9–2.12, the frequency analysis indicates that the foundation heat transfer is sensitive to only low frequency fluctuations in outdoor air temperatures (i.e., only monthly outdoor air temperatures affect slab heat loss) but is very sensitive to almost any fluctuations in indoor air temperatures (i.e., hourly and monthly indoor air temperatures affect significantly the slab heat loss).

2.3.5 Response Factors

Another formulation of the conduction transfer conduction (CTF) method used in whole building energy analysis tools to estimate the

heat transfer through building envelope components (i.e., walls, roofs, and floors), is the use of response factors to compute outside and inside surface transmission heat fluxes using current and past indoor and outdoor temperatures. As noted in Figure 2.13, the heat fluxes at the outside and inside wall surfaces are driven by the wall thermal properties but also on the outside and inside wall surfaces.

By approximating the time-variations of temperatures as series of triangular pulses as illustrated in Figure 2.14, the outside and inside surface heat fluxes caused by any arbitrary indoor and outdoor temperature variations can be determined as indicated by Eq. (2.49) and Eq. (2.50):

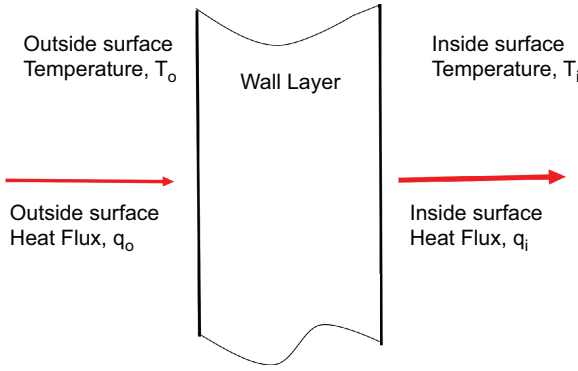

Figure 2.13. Heat fluxes at wall inside and outside surfaces.

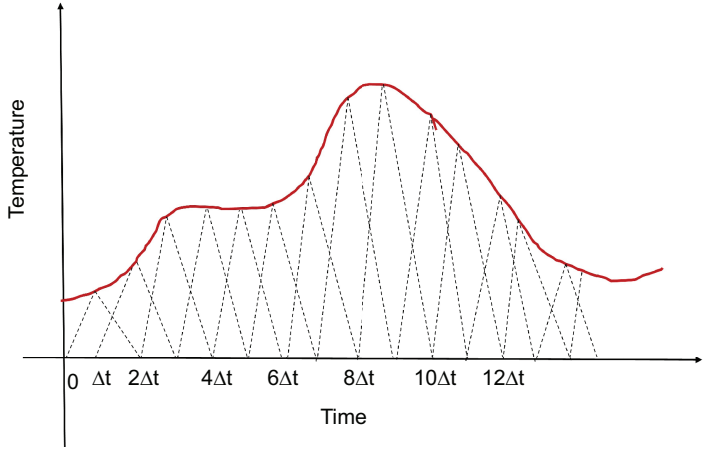

Figure 2.14. Approximation of temperature time variation using unit triangular pulses.

$$q_o(t) = \sum_{n=1}^{\infty} X_n T_o(t-(n+1)\Delta t) - \sum_{n=1}^{\infty} Y_n T_i(t-(n+1)\Delta t) \qquad (2.49)$$

$$q_i(t) = \sum_{n=1}^{\infty} Y_n T_o(t-(n+1)\Delta t) - \sum_{n=1}^{\infty} Z_n T_i(t-(n+1)\Delta t) \qquad (2.50)$$

Where,

- $q_o(t)$ is the current value of the transmission heat flux at the outside surface
- $q_i(t)$ is the current value of the transmission heat flux at the inside surface
- $T_o(t - (n + 1)\Delta t)$ are the current and past values for the outside surface temperatures
- $T_i\ (t - (n + 1)\Delta t)$ are the current and past values for the inside surface temperatures
- Δt is the time step considered in the analysis, typically 1 hour

Using steady-state analysis, it can be shown that independently of the building envelope thermal properties, the response factors follow the general expression as shown in Eq. (2.51) where R is the total *R*-value and U is the U-value of the building envelope assembly:

$$\sum_{n=1}^{\infty} X_n = \sum_{n=1}^{\infty} Y_n = \sum_{n=1}^{\infty} Z_n = U = \frac{1}{U} \qquad (2.51)$$

Response factors represent the heat fluxes due to temperature triangular unit pulse subjected at t = 0 at one of the surface while the other surface is maintained at a constant reference temperature (i.e., T = 0). Figure 2.15 illustrates the Y response factors as the values of the inside surface heat flux at various time steps due to a rectangular unit pulse variation of the outside surface temperature.

Using the Laplace transform of the one-dimensional heat conduction equation as provided by Eq. (2.6), the response factors can be estimated for any layer of building envelope. In particular, close form solutions can be found for homogeneous layer with uniform thermal properties as shown by Eq. (2.52) through (2.54) for both X response factors and Eq. (2.55) through Eq. (2.57) for Y response factors. For uniform layers, it can be shown that the values for the Z response factors are equal to those of Y response factors.

$$X_1 = \frac{1}{\Delta t}\left[\frac{C}{3} + \frac{\Delta t}{R} - 2\sum_{n=1}^{\infty} \frac{Ce^{-\Delta t \beta_n}}{(\pi n)^2}\right] \qquad (2.52)$$

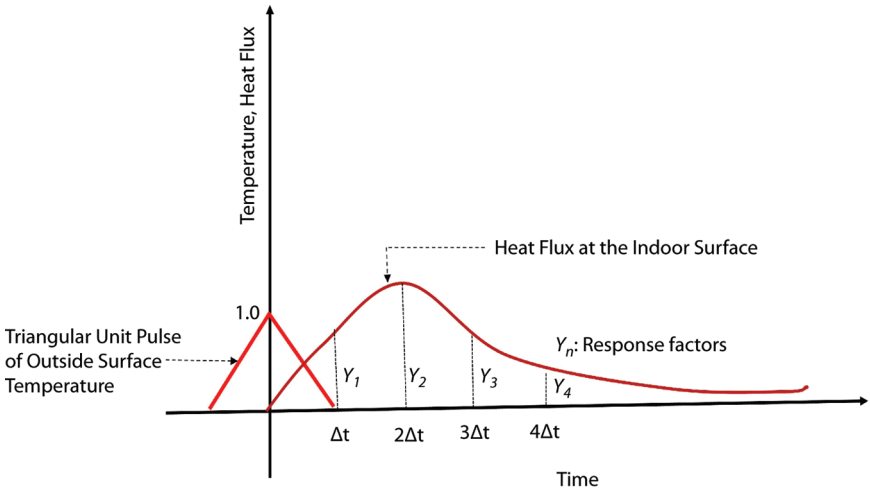

Figure 2.15. Definition of response factors due to a unit pulse of the outside surface temperature.

$$X_2 = \frac{1}{\Delta t}\left[\frac{C}{3} + 2\sum_{n=1}^{\infty}\frac{C(e^{-2\Delta t\beta_n} - 2e^{-\Delta t\beta_n})}{(\pi n)^2}\right] \tag{2.53}$$

And for $m \geq 3$:

$$X_m = -\frac{1}{\Delta t}\left[2\sum_{n=1}^{\infty}\frac{C(e^{-m\Delta t\beta_n} - 2e^{-(m-1)\Delta t\beta_n} + e^{-(m-2)\Delta t\beta_n})}{(\pi n)^2}\right] \tag{2.54}$$

Similarly,

$$Y_1 = -\frac{1}{\Delta t}\left[\frac{C}{6} - \frac{\Delta t}{R} + 2\sum_{n=1}^{\infty}\frac{(-1)^n Ce^{-\Delta t\beta_n}}{(\pi n)^2}\right] \tag{2.55}$$

$$Y_2 = \frac{1}{\Delta t}\left[\frac{C}{6} + 2\sum_{n=1}^{\infty}\frac{(-1)^n C(-e^{-2\Delta t\beta_n} + 2e^{-\Delta t\beta_n})}{(\pi n)^2}\right] \tag{2.56}$$

And for $m \geq 3$:

$$Y_m = -\frac{1}{\Delta t}\left[2\sum_{n=1}^{\infty}\frac{(-1)^2 C(e^{-m\Delta t\beta_n} - 2e^{-(m-1)\Delta t\beta_n} + e^{-(m-2)\Delta t\beta_n})}{(\pi n)^2}\right] \tag{2.57}$$

With

$$\beta_n = \frac{(\pi n)^2}{RC} \tag{2.59}$$

Where

- R is the thermal resistance of the homogeneous layer (i.e., $R = \frac{\Delta x}{k}$ with Δx is the thickness and k is the thermal conductivity of the layer).
- C is the thermal capacitance of the homogeneous layer (i.e., $\rho \Delta x c_p$ with ρ is the density, Δx is the thickness and c_p is the specific heat of the layer).

For multi-layered walls, roofs, and floors, the response factors can be calculated using the Laplace transform of the heat conduction equation. A detailed description of the calculation process for multi-layered walls can be found in several references [4–5, 13, 30].

To illustrate some applications of the response factors listed in Table 2.4 for a concrete wall, select wall properties and heat transfer through a wall are estimated.

- Estimation of thermal conductivity of the wall if the wall thickness is 7.5 cm (0.25 ft)

Since the U-value of the wall is $U = \sum X_n = \sum Y_n \approx 2.0$ Btu/hr.°F. ft^2 and since the R-value of an homogeneous wall is $R = 1/U = d/k$ (where d is its thickness and k is its thermal conductivity):

$$k = d.U = 0.25 * 2 = 0.50 \text{ Btu/hr.°F.ft}$$

- Estimation of the time constant of the wall if the concrete density is 120 lbm/ft^3 and the specific heat is 0.20 Btu/lbm·°F:

The time constant of a wall is defined as:

$$\tau = R.C = \rho.c_p.d/U = 120 * 0.20 * 0.25/2 = 3.0 \text{ hrs.}$$

Thus, it will take several hours to charge the wall (at least $2\tau = 6$ hours).

- Calculation of heat flux at the inside and outside surfaces of the wall when the outside temperature is one triangular unit pulse (at t = 1) and the inside temperature is constant and equal to zero:

Table 2.4. X and Y Response Factors for a Concrete Layer.

X_1=6.180774	X_2=-3.588095	X_3=-0.4404840	X_4=-0.1171224	X_5=-0.03140926
Y_1=0.311360	Y_2=1.095936	Y_3=0.43270	Y_4=0.117080	Y_5=0.0314092

By definition of the response factors as outlined by Eqs. (2.49) and (2.50), the heat fluxes across inside (q_i) and the outside (q_o) surfaces due to a unit pulse (at the outside surface) are given by:

$$q_i\,(n.\Delta t) = -Y_n \quad \text{and} \quad q_o\,(n.\Delta t) = -X_n$$

The profiles of both the inside and outside surfaces heat fluxes are provided in Figure 2.16 (q_i in yellow).

- Calculation of the wall heat flux under steady-state conditions with the inside surface temperature is set at 70°F while the temperature at the outside surface is maintained at 0°F.w

The steady-state heat flow is given as:

$$q_i = q_o = U\Delta t = 2 * (70 - 0) = 140 \text{ Btu/hr.ft}^2$$

It should be noted that large set of response factors is needed for walls or slabs with high thermal capacitance since any sudden temperature variation can have a significant impact several hours after the change. In this case, several response factors have to be calculated and stored to estimate heat fluxes at any time as shown in Eqs. (2.49) and (2.50). Table 2.5 lists response factors for a R-11 wood frame wall and an 8-in concrete uninsulated wall.

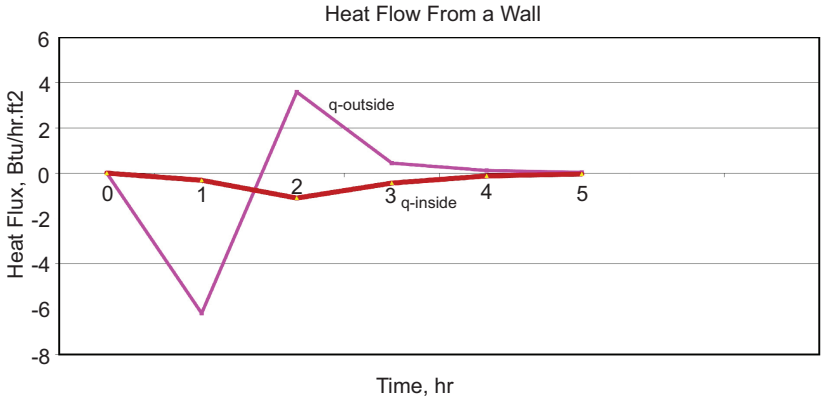

Figure 2.16. Time variation of inside and outside wall surface heat fluxes.

Table 2.5. Response factors for wood frame and concrete walls.

n	Wood Frame R-11 Wall			8-in Concrete Wall		
	X	Y	Z	X	Y	Z
1	0.5707337260	0.04498966410	0.4278753996	2.2132558823	0.0000476876	0.7773964405
2	0.4788596332	0.04301747310	0.3225956559	0.8019668460	0.0048133433	0.1180156916
3	0.0010346086	0.00268453060	0.0138370087	0.1993563175	0.0211568922	0.0421135984
4	0.0000237536	0.00011768620	0.0006007524	0.1272786260	0.0323558077	0.0302988626
5	0.0000010026	0.00000511150	0.0000260850	0.0939759091	0.0350728966	0.0241539739
6	0.0000000435	0.00000022190	0.0000011326	0.0753490254	0.0337515213	0.0202459972
7				0.0633016080	0.0309645236	0.0174151920
8				0.0545101054	0.0278185792	0.0151761724
9				0.0475272313	0.0247533042	0.0133096101
10				0.0416924953	0.0219268985	0.0117086973
11				0.0366821885	0.0193819087	0.0103156371
CR	0.043420643			0.8822238445		
U	0.090814695			0.397458762		

2.4 Simplified Energy Analysis Methods

For residential and small commercial buildings, simplified energy analysis methods can be used to evaluate the whole-building energy performance as well as to design of heating and cooling systems and assess the cost-effectiveness of several energy efficiency measures. In this section, two simplified analysis methods are described including the variable-base degree day method and the thermal network technique.

2.4.1 Variable Base Degree Days Method

The degree-days method provides an estimation of the heating and cooling loads of a building due to transmission losses through the envelope and any solar and internal heat gains. The degree-days method is based on steady-state analysis of the heat balance across the boundaries of the building. A building is typically subject to several heat flows including conduction, infiltration, solar gains, and internal gains as illustrated in Figure 2.17. The net heat loss or heat gain at any instant is determined by applying a heat balance (i.e., first law of Thermodynamics) to the building. For instance, for heating load calculation, the instantaneous heat balance provides [31]:

$$\dot{q}_H = BLC.(T_i - T_o) - \dot{q}_g \tag{2.60}$$

Where:

- BLC is the building load coefficient as defined in Eq. (2.61) to include the effects of both transmission and infiltration losses:

$$BLC = \sum_{j=1}^{N_E} U_{T,j}.A_j + \dot{m}_{\text{inf}}.c_{p,a} \tag{2.61}$$

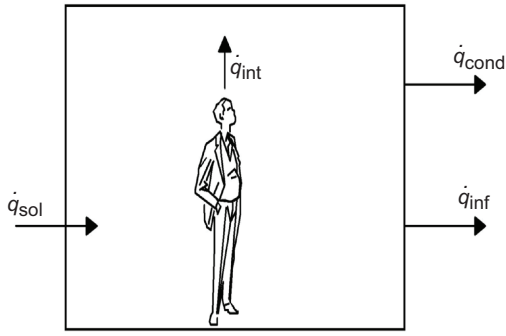

Figure 2.17. A simplified heat balance model for a building.

- q_g is the net heat gains due solar radiation, q_{sol}; internal gains (people, lights, and equipment), q_{int}; and in some cases the ground losses, q_{grd}, if they are significant:

$$\dot{q}_g = \dot{q}_{sol} + \dot{q}_{int} - \dot{q}_{grd} \tag{2.62}$$

This equation can be rearranged to introduce the balance temperature, T_b, for the building:

$$q_H = BLC.\left[\left(T_i - \frac{q_g}{BLC}\right) - T_o\right] = BLC.(T_b - T_o) \tag{2.63}$$

With the balance temperature defined as:

$$T_b = T_i - \frac{q_g}{BLC} \tag{2.64}$$

Therefore, the balance temperature adjusts the interior temperature set-point by the amount of temperature increase due a reduction in the building heating load resulting from the internal gains. Before the oil crisis, the transmission and the infiltration losses were significant (and thus the BLC value was high relative to the internal gains). It is estimated that the net internal gains contributes to about 3°C (or 5°F) in most buildings. Therefore, the balance temperature was assumed to be 18°C (or 65°F) for all the buildings. However, with the increase in thermal efficiency of the building envelope and the use of more equipment within the buildings, the internal heat gains are more significant and thus can contribute in reducing the heating load of the buildings.

By integrating the instantaneous heating load over the heating season, the total building heating load can be determined. Note only the positive values of q_H are considered in the integration. In practice, the integration is approximated by the sum of the heating loads averaged over short time intervals (one hour or one day).

If hourly averages are used, the seasonal total building heating load is estimated as:

$$Q_H = \sum_{j=1}^{N_{h,H}} \dot{q}^{+}_{H,j} = BLC. \sum_{i=1}^{N_{h,H}} (T_b - T_{o,j})^{+} \tag{2.65}$$

The sum is performed over the number, $N_{h,H}$, of hours in the heating season. From Eq. (2.65), a parameter that characterizes the heating load of the building can be defined as the heating degree-hours (DH_H) which is function of only the outdoor temperatures and the balance or

base temperature, T_b, which varies with the building heating set-point temperature and the building internal gains:

$$DH_H(T_b) = \sum_{j=1}^{N_{h,H}} (T_b - T_{o,j})^+ \tag{2.66}$$

If daily averages are used, the seasonal total building heating load is estimated as:

$$Q_H = 24. \sum_{i=1}^{N_{d,H}} \dot{q}^+_{H,i} = 24.BLC. \sum_{i=1}^{N_{d,H}} (T_b - T_{o,i})^+ \tag{2.67}$$

The sum is performed over the number, $N_{d,H}$, of days in the heating season. Similar to the heating degree-hours defined by Eq. (2.66), the heating degree-days (DD_H) can be introduced for a base temperature, T_b:

$$DD_H(T_b) = \sum_{i=1}^{N_{d,H}} (T_b - T_{o,i})^+ \tag{2.68}$$

The total energy use, E_H, to meet the heating load of the building can be estimated by assuming a constant efficiency of the heating equipment over the heating season (for instance several heating equipment manufacturers provide the annual fuel use efficiency rating or AFUE for their boilers or furnaces).

Using heating degree-hours is used, $DH_H(T_b)$, the total energy use, E_H, is estimated as follows:

$$E_H = \frac{Q_H}{\eta_H} = \frac{BLC.DH_H(T_b)}{\eta_H} \tag{2.69}$$

When heating degree-days is used, $DD_H(T_b)$, E_H, is calculated using Eq. (2.70):

$$E_H = \frac{Q_H}{\eta_H} = \frac{24.BLC.DD_H(T_b)}{\eta_H} \tag{2.70}$$

The variable base degree-hours and degree-days methods stated by Eq. (2.69) and (2.70) can also be applied to determine the cooling load by estimating the cooling season degree-hours, DH_C, and degree-days, DD_C, using respectively, Eq. (2.71) and Eq. (2.72):

$$DH_C(T_b) = \sum_{j=1}^{N_{h,C}} (T_{o,j} - T_b)^+ \tag{2.71}$$

$$DD_C(T_b) = \sum_{i=1}^{N_{d,C}} (T_{o,i} - T_b)^+ \quad (2.72)$$

Where $N_{h,c}$ and $N_{d,c}$ are the number of hours and days, respectively, in the cooling season.

Figure 2.18 illustrates the concept of both heating and cooling degree-days based on the variation of the average daily outdoor air temperature over one year.

It should be noted that the variable base degree-hours and degree-days methods can provide remarkable accurate estimation of the annual energy use due to heating especially for buildings dominated by losses through the building envelope including infiltration. Unfortunately, the degree-hours or degree-days method is not as accurate for calculating the cooling loads due to several factors including effects of building thermal mass that delays the action of internal gains, mild outdoor temperatures in summer resulting in large errors in the estimation the cooling degree-days, and the large variation in infiltration or ventilation rates as occupants open windows or economizer cycles are used [32].

In several homes, the heating set-point is set back during unoccupied hours typically during daytime as outlined in Figure 2.19. Instead of using Eq. (2.66) with no setback, the heating degree-hours when temperature setback is implemented can be estimated as follows:

$$DH(T_{\mathrm{b,\,setback}}) = \sum_{j=1}^{N_{h,OCC}} (T_{\mathrm{b}} - T_{\mathrm{o,j}})^+ + \sum_{j=1}^{N_{\mathrm{h,UNOCC}}} (T_{\mathrm{b,setback}} - T_{\mathrm{o,j}})^+ \quad (2.73)$$

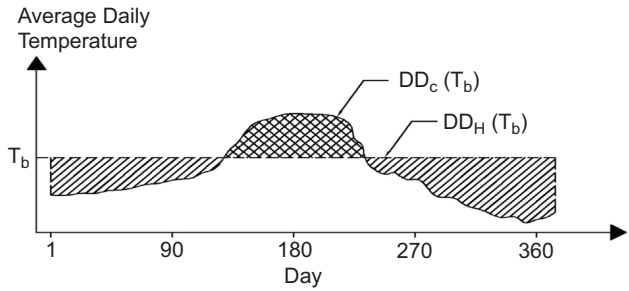

Figure 2.18. Heating and cooling degree-days associated with a balance temperature, T_b.

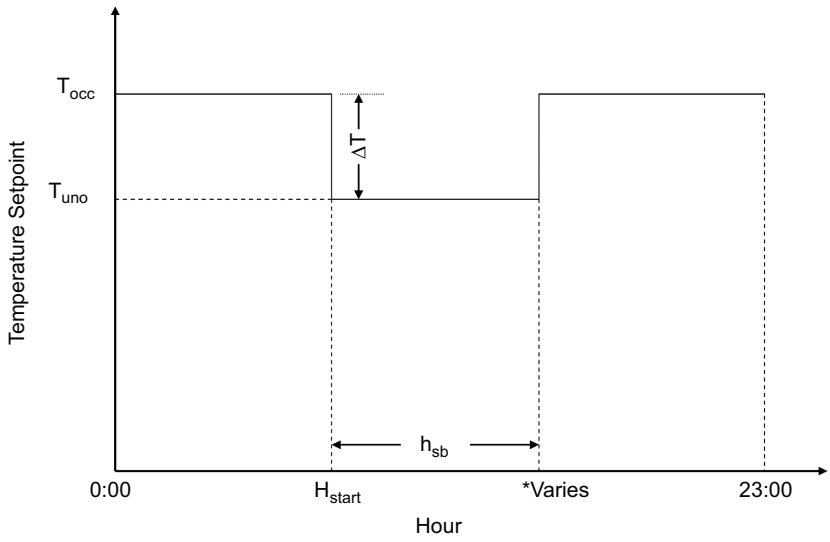

Figure 2.19. Heating temperature setting with a setback temperature, ΔT.

where

- T_b = base temperature during occupied period (°F or °C)
- $T_{b,setback}$ = base temperature adjusted for setback period during unoccupied period (°F or °C)
- $N_{h,\ UNOCC}$ = number of hours during the heating season when the home is unoccupied
- $N_{h,\ OCC}$ = number of hours during the heating season when the home is occupied

As illustrated in Figure 2.19, the temperature setback, $T_{b,setback}$ can be defined as a function of the balance temperature, T_b, and the setback temperature difference:

$$T_{b,setback} = T_b - \Delta T \tag{2.74}$$

In residential buildings, setbacks are typically implemented during weekdays to accommodate typical daytime work schedules as illustrated in Figure 2.20. In this case, the heating degree-hours can be estimated as follows:

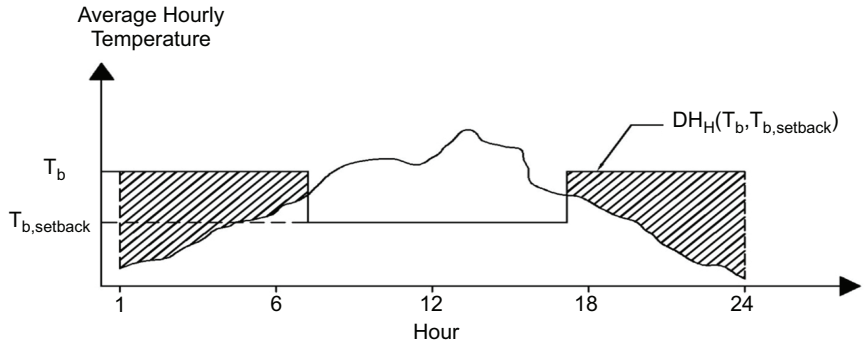

Figure 2.20 Heating degree-hours for a balance temperature, T_b, and a set-back temperature, $T_{b,setback}$.

$$DH(T_{\text{b, setback}}) = \sum_{j=1}^{N_{h,WE}} (T_{\text{b}} - T_{\text{o,j}})^{+} + \sum_{j=1}^{N_{\text{h,WD, OCC}}} (T_{\text{b}} - T_{\text{o,j}})^{+} + \sum_{j=1}^{N_{\text{h.WD, UNOCC}}} (T_{\text{b.setback}} - T_{\text{o,j}})^{+} \quad (2.75)$$

where

- $N_{\text{h,WD, UNOCC}}$ = number of weekday hours during unoccupied period
- $N_{\text{h,WD, OCC}}$ = number of weekday hours during occupied period
- $N_{\text{h,WE}}$ = number of weekend hours

The temperature setback reduces the heating degree-hours and thus the energy use required to heat the home. To estimate the reduction of the heating degree-hours due to a temperature setback, the fraction f_{DH}, is defined as the ratio of the degree-hours with setback estimated using Eq. (2.75) to the degree-days without setback calculated using Eq. (2.66):

$$f_{\text{DH}} = \frac{DH(T_{\text{b,setback}})}{DH(T_{\text{b}})} \quad (2.76)$$

It should be noted if there is no setback, then $f_{DH} = 1$. Otherwise, a correlation can be utilized to provide the fraction f_{DH} as function of the differential temperature setback and the duration of setback period expressed in hours [33]:

$$f_{DH} = a \exp(-m\Delta T_{setback}) + b \exp(-nh_{setback}) \tag{2.77}$$

where

- $\Delta T_{setback}$ = setback temperature difference (°F or °C)
- $h_{setback}$ = the number of setback hours. It assumed that the setback starts in the morning at 8:00 am.
- *a, b, n,* and *m* = correlation coefficients defined in Table 2.6 for several US climate zones and sites

A simplified but less accurate method that the correlation presented by Eq. (2.77) to estimate the fraction, f_{DH}, can be used:

$$f_{DH} = \frac{24 - h_{setback}}{24} + \frac{h_{setback}}{24} \frac{(T_{b,setback} - T_{H,o})}{(T_b - T_{H,o})} \tag{2.78}$$

where

- $T_{H,o}$ = average heating season outdoor ambient air temperature (°F or °C)

Table 2.6: Model Coefficients for Eq. (2.77).

Zones	Locations	R^2	a	b	m	n
1A	Honolulu, HI	0.783	0.0623	0.9481	0.5229	0.0016
1A	Miami, FL	0.951	0.1491	0.8975	0.1600	0.0075
2A	Savannah, GA	0.914	0.1970	0.8686	0.0613	0.0113
2B	Tucson, AZ	0.937	0.1773	0.8751	0.0730	0.0087
3A	Charleston, SC	0.906	0.1997	0.8711	0.0594	0.0121
3A	Little Rock, AR	0.894	0.2410	0.8284	0.0412	0.0126
3B	San Diego, CA	0.885	0.1336	0.9476	0.2127	0.0126
4A	Kansas City, MO	0.887	0.2991	0.7637	0.0268	0.0124
4B	Albuquerque, NM	0.896	0.2624	0.8011	0.0337	0.0119
4C	Eugene, OR	0.895	0.2434	0.8317	0.0464	0.0135
5A	Chicago, IL	0.876	0.3277	0.7337	0.0217	0.0126
5A	Hartford, CT	0.881	0.2840	0.7793	0.0273	0.0122
5B	Boulder, CO	0.888	0.2357	0.8198	0.0310	0.0100
6B	Eagle, CO	0.892	0.2674	0.7805	0.0234	0.0091
4 – 6	Any Location	0.851	0.2623	0.7990	0.0307	0.0115

2.4.2 Transient Thermal Network Analysis

The degree-day method presented above assumes steady-state heat transfer processes. In most buildings, convection heat transfer is generally steady state, however, conduction and radiation heat transfer is often transient and vary with time. The time scale associated with these transients in residential buildings is on the order of hours, which is the same general time scale for changes in the driving potentials of outdoor temperature and solar radiation. Therefore, in calculating the heat transfer into a building through walls and roofs, the calculations must account for transient effects. Straight steady-state heat transfer calculations are a crude simplification especially for building with significant thermal mass. In residential buildings, simplified transient analysis techniques can be utilized to estimate the mass effect and predict the time variation of indoor temperature. In this section, the RC thermal network technique is first introduced and then applied to estimate the thermal mass and the time constant of a residential building.

An entire building can be represented by a thermal RC network. In the simplest case, building heat transfer can be represented by two temperature nodes, a single capacitance, and a single resistance as shown in Figure 2.21. The two temperatures are the indoor and outdoor temperatures, the capacitance represents the entire thermal mass of the building, and the resistance represents the heat transfer path between the indoor and outdoor temperatures. Additional heat flow paths are added to account for internal heat gains and heat addition by the HVAC system.

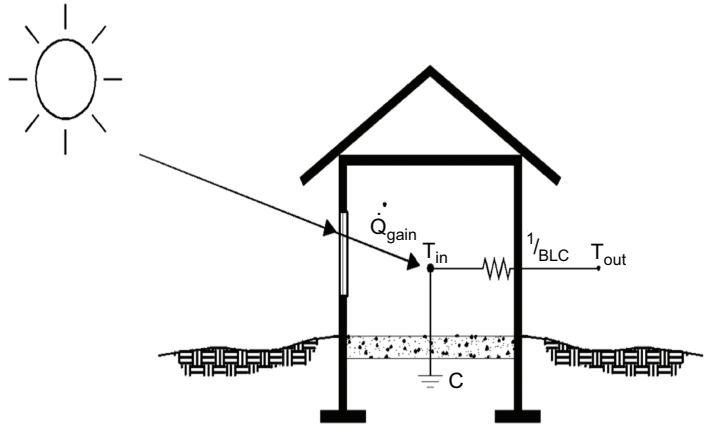

Figure 2.21. Thermal network model for a home.

Mathematically, the thermal network for the house shown in Figure 2.21 can be expressed using a simple expression [31]:

$$C\frac{dT_{in}}{dt} = BLC(T_{out} - T_{in}) + Q_{gain} \tag{2.79}$$

Where $C = mc_p$ is the capacitance of the home including the mass of all the envelope components (i.e., floor and walls) as well as furniture and interior partitions). Notice that, if the HVAC system is controlled to maintain the indoor temperature at a constant value, this equation reverts back to a simple and familiar steady-state equation.

$$C\frac{dT_b}{dt} = BLC(T_{out} - T_b) \tag{2.80}$$

Where T_b is the balance temperature of the building defined earlier for the variable-base degree-day method as follows:

$$T_b = T_{in} \quad Q_{gain}/BLC \tag{2.81}$$

The time constant, τ, of a building is defined as the ratio of the building capacitance, C, over the building load coefficient, BLC:

$$\tau = \frac{C}{BLC} \tag{2.82}$$

Thus, the differential equation, Eq. (2.80), can be expressed simply as:

$$\frac{dT_b}{dt} = -\frac{T_{in} - T_{out}}{\tau} \tag{2.83}$$

If the outdoor air temperature, T_{out}, is constant, the solution to the differential equation is given below with $T_{b,0} = T_b(t = 0)$:

$$\frac{T_b(t) - T_{out}}{T_{b,0} - T_{out}} = e^{\frac{-t}{\tau}} \tag{2.84}$$

Therefore, the indoor air temperature variation with time, $T_{in}(t)$, can be estimated as follows:

$$T_{in}(t) = T_{out} + \frac{Q_{gain}}{BLC} + \left[T_{in}(t = 0) - T_{out} - \frac{Q_{gain}}{BLC}\right]e^{\frac{-t}{\tau}} \tag{2.85}$$

In particular, when there is no internal gains (i.e., $Q_{gain} = 0$), the indoor air temperature variation with time, $T_{in}(t)$, can be simply estimated as follows:

$$T_{in}(t) = T_{out} + \left[T_{in}(t = 0) - T_{out}\right]e^{\frac{-t}{\tau}} \tag{2.86}$$

The RC thermal network model presented above can be used to estimate the thermal mass of a building by measuring the indoor air temperature during a period where the internal gains are small and the outdoor air temperature remains constant. A cold winter night during a period when the heating system is shut off (or during a set-back period) can be adequate cool-down testing period especially if the outdoor temperature does not vary significantly. Figure 2.22 shows the time variation of both outdoor and indoor temperature variations for a home during a cool-down period.

The time constant can be estimated as the slope of the time variation of the variable Y defined as:

$$Y = Ln\left[\frac{T_{in}(t) - T_{out}}{T_{in}(t=0) - T_{out}}\right] \tag{2.87}$$

Based on Eq. (2.87), Y varies linearly with t with a constant of variation $a = -1/\tau$ with τ is the building time constant. Using linear regression, the slope a can be obtained as illustrated by Figure 2.23 for the testing data presented in Figure 2.22 for the period between 2:15 am and 3:45 am when the outdoor temperature remains constant at about 56°F.

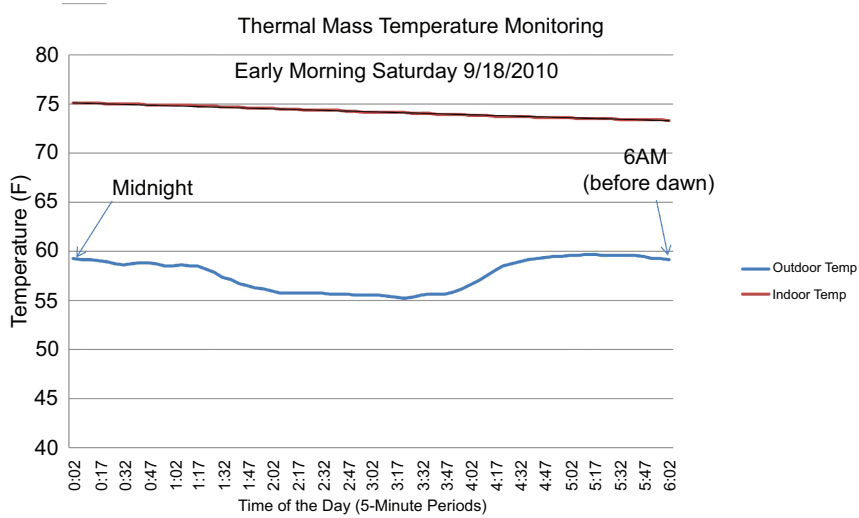

Figure 2.22. Indoor and outdoor temperature variations during a cool-down period.

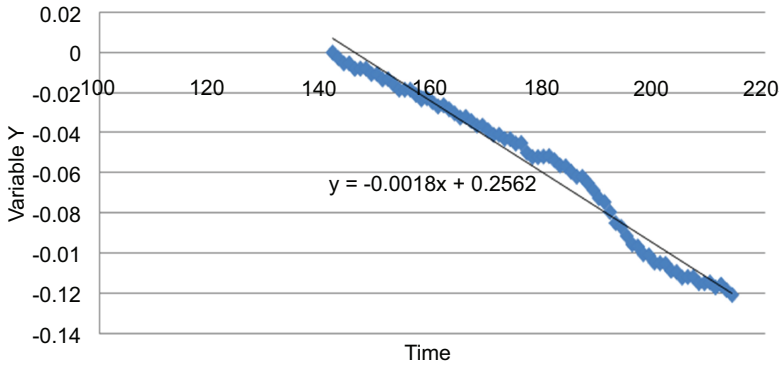

Figure 2.23. Estimation of the home time constant through Regression of Y vs. time.

Based on the value of the slope a ($a = -0.0018\ \text{min}^{-1}$) as shown in Figure 3.13, the time constant can be estimated to be $\tau = -1/a = -1/(0.0018\text{min}^{-1}) = 555.6$ min = 9.25 hr. This time constant indicate that the home has a rather significant level of thermal mass. The capacitance of the home can be estimate using Eq. (2.82) based on the BLC value.

2.5 Detailed Energy Analysis Methods

To model transient behavior of building energy systems, detailed modeling techniques are typically used. A wide range of techniques has been considered for the development of whole-building energy simulation tools. In this section, three methods for detailed building energy analysis are briefly described including heat balance, thermal networks, and weighting factors based techniques.

2.5.1 Heat Balance Method

Figure 2.24 shows the basic heat balance elements considered to model building thermal zones. The calculation procedure denoted in the top part of Figure 2.24, inside the blue dashed box, is applied to all exterior walls. The indoor air heat balance module ultimately collects convective heat transfer from all interior surfaces, thermal load from infiltration and ventilation, then compute indoor air temperature.

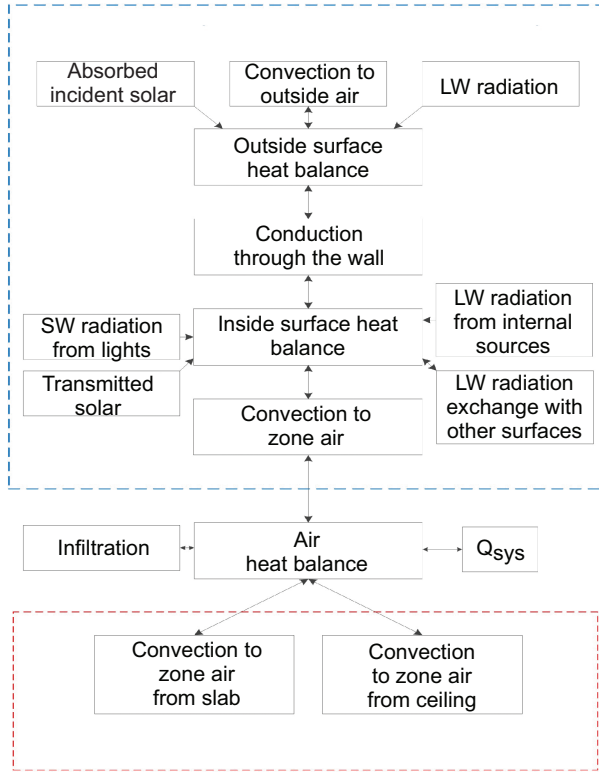

Figure 2.24. Schematic of heat balance calculation procedure.

The heat balance on the outside surfaces can be expressed using Eq. (2.88). The net heat flux from outside to inside of the wall is taken to be positive in the direction. The first three terms (solar radiation heat flux, convective exchange flux, and long-wave radiation flux exchange) can be combined together by using the concept of a sol-air temperature. Instead of a sol-air temperature, the heat balance method implemented in EnergyPlus considers each of these heat flux components separately. The direct and diffuse solar radiation is influenced by location, surface azimuth and tilt angle, and material properties. The long-wave radiation flux exchange term calculates radiation exchange between the surface, the sky, and the ground.

$$q''_{\text{sol}} + q''_{\text{conv}} + q''_{\text{LWR}} - q''_{\text{ko}} = 0 \tag{2.88}$$

Where,

- q''_{sol} = absorbed direct and diffuse solar radiation heat flux,
- q''_{conv} = convective exchange flux with outside air,
- q''_{LWR} = long-wave radiation flux exchange with outdoor air and surroundings,
- q''_{ko} = conductive flux (q/A) into wall.

Heat conduction through the opaque wall can be solved by various methods as discussed in Section 2.3. For instance, Energyplus uses Conduction Transfer Function (CTF) to solve transient heat transfer through various building envelope components.

The inside surface heat balance involving the inside facades of the surfaces can be written as Eq. (2.89) involving several heat transfer components:

$$q''_{LWX} + q''_{SW} + q''_{LWS} + q''_{ki} + q''_{conv} = 0 \tag{2.89}$$

Where,

- q''_{LWX} = net long-wave radiant flux exchange between zone surfaces,
- q''_{SW} = net short-wave radiation flux to surface from lights,
- q''_{LWS} = long-wave radiation flux from equipment in zone,
- q''_{ki} = conductive flux through the interior surface,
- q''_{conv} = convective heat flux to zone air.

The air heat balance technique is applied to determine the heating and cooling thermal load for each thermal zone. The indoor air heat balance combines convective heat transfer from building envelope surfaces, air infiltration, and internal loads. The air heat balance can be written as indicated by Eq. (2.90) with relevant heat transfer components:

$$\rho c_p \frac{\left(T_{air}^{n+1} - T_{air}^{n}\right)}{\Delta t} = Q_{conv} + Q_{internal} + Q_{vent} + Q_{inf} + Q_{sys} \tag{2.90}$$

where,

- ρ = density of air (kg/m^3),
- c_p = specific heat (J/kg-°C),
- Δt = timestep (sec),
- T_{air} = zone air temperature (°C),

- Q_{conv} = convective heat transfer rate (W),
- $Q_{internal}$ = convective parts of internal loads (W),
- Q_{vent} = sensible load caused by ventilation (W),
- Q_{inf} = sensible load caused by infiltration (W),
- Q_{sys} = heat transfer to/from HVAC system (W).

2.5.2 Thermal Network Method

Thermal networks have been widely used to simulate the thermal performance of the building envelope as briefly noted in Section 2.4.2. In particular, 3R-2C models have been successfully applied to simulate the building envelopes for transient building load predictions [16, 34–37]. For instance, Dewson et al. have demonstrated that a 3R-2C model is capable of capturing accurately thermal behavior of a test solar cell [35]. Moreover, Fux et al. have shown that a 3R-2C thermal network model can accurately predict the room air temperature compared to the measured average room air temperature for a lodging building in the Swiss Alps [37]. A generic 3R-2C thermal network model is modified to have a virtual node at wall surface exposed to surroundings. A virtual node, a wall surface node, has no thermal capacitance so that the surface temperature can react quickly to the environment conditions. If a generic 3R-2C thermal network model is used, Sol-air temperature must be employed instead T_0 and Q_{solar}. Figure 2.25 depicts a thermal network of exterior wall connecting the indoor space to the outdoor environment. All resistances and capacitances are assumed to be time invariant.

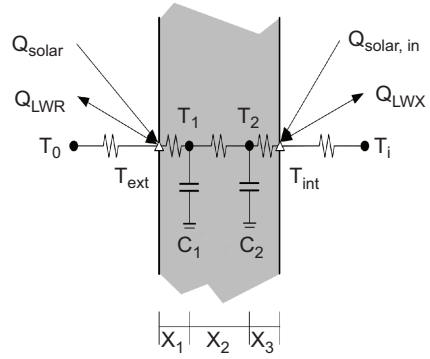

Figure 2.25. Description of RC thermal network for a single layer exterior wall.

Convection and long-wave radiation exchanges occur at both sides while short-wave solar radiation is considered only at the outer surface of an exterior wall. Note that the thermal capacity at surface nodes (virtual air film nodes) is neglected so that it can rapidly reacts to the surroundings. The transient heat balance analysis for both nodes yields the following difference equations:

$$k\frac{\mathrm{T_1}-\mathrm{T_{ext}}}{x_1}A+\mathrm{h_o A}(\mathrm{T}_o-\mathrm{T_{ext}})+\mathrm{Q_{LWR}}+Q_{\mathrm{solar}}=0 \qquad (2.91)$$

$$k\frac{\mathrm{T_{ext}}-\mathrm{T_1}}{x_1}A+k\frac{\mathrm{T_2}-\mathrm{T_1}}{x_2}A=C_1\frac{\mathrm{dT_1}}{\mathrm{dt}}$$

$$k\frac{\mathrm{T_1}-\mathrm{T_2}}{x_2}A+k\frac{\mathrm{T_{int}}-\mathrm{T_2}}{x_3}A=C_2\frac{\mathrm{dT_2}}{\mathrm{dt}}$$

$$k\frac{\mathrm{T_2}-\mathrm{T_{int}}}{x_3}A+h_{\mathrm{i}}\mathrm{A}(T_{\mathrm{i}}-T_{int})+\mathrm{Q_{LWX}}+\mathrm{Q_{solar,in}}=0$$

where,

- k = thermal conductivity of materials (W/m-^{o}C),
- x = distance between nodes (m),
- C = thermal capacitance of materials (J/^{o}C),
- A = area of surfaces (m^2),
- T_{o} = the outdoor air temperature (°C),
- T_{i} = the zone air temperature (°C),
- T = the surface temperature of exterior walls (°C),
- h_{o} = the convective coefficient at outer surface of exterior walls (W/m^2-^{o}C),
- h_{i} = the convective coefficient at inner surface of exterior walls (W/m^2- ^{o}C),
- Q_{LWR} = net longwave radiation (W),
- Q_{solar} = exterior solar radiation incident (W),
- $Q_{\mathrm{solar,in}}$ = transmitted solar radiation incident (W),
- Q_{LWX} = longwave radiant heat exchange between surfaces (W).

2.5.3 Weighting Factors

Weighting factors can be used to estimate thermal loads as function of several variables such as temperatures and internal gains from people,

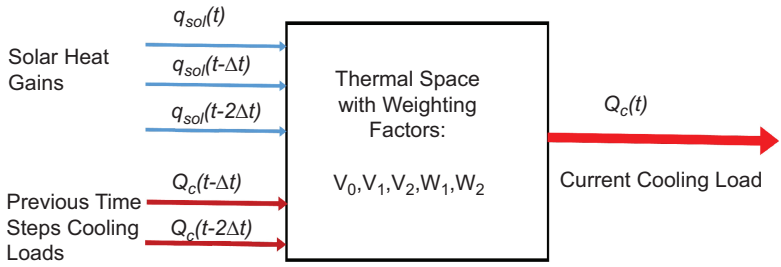

Figure 2.26. Estimation of current loads from solar heat gains and previous time step cooling loads.

equipment, and lighting. Specifically, a set of weighting factors are defined for each space and thermal zone to compute the heating and cooling load due either air-temperature or internal heat gains. Figure 2.26 illustrates the concept of the weighting factors of a space to estimate the current cooling load from previous time step cooling load and current and previous two time steps of solar heat gains [30].

Using the case shown in Figure 2.26, the general expression to estimating the thermal space cooling load, $Q_c(t)$, using the weighting factors [v_0, v_1, v_2, w_1, w_2] as well solar gains [$q_{sol}(t)$, $q_{sol}(t-\Delta t)$, $q_{sol}(t-2\Delta t)$] and previous time steps cooling [$Q_c(t-\Delta t)$, $Q_c(t-2\Delta t)$] is provided by Eq. (2.95):

$$Q_c(t) = v_0 q_{sol}(t) + v_1 q_{sol}(t-\Delta t) + v_2 q_{sol}(t-2\Delta t) - w_1 Q_c(t-\Delta t) + w_2 Q_c(t-2\Delta t) \quad (2.95)$$

It should be noted that Eq. (2.95) can be applied for any time step and any time-variation of solar heat gains. Under steady-state conditions, Eq. (2.95) can be reformulated as follows:

$$\frac{Q_C}{q_{sol}} = \frac{v_0 + v_{10} + v_2}{1 + w_1 + w_2} = f_{c,sol} \quad (2.96)$$

The fraction, $f_{c,sol}$, represents the fraction of the solar heat gain that appears as space cooling load under steady-conditions.

It should be noted that different sets of weighting factors are defined for each type of internal heat gains. Table 2.7 lists weighting factors for an air conditioned wood frame home with R-11 insulated walls and an uninsulated roof.

Table 2.7. Weighting Factors for Estimating Cooling Loads from Internal Heat Gains due to Solar, Lighting, People, Equipment, and Conduction.

Weighting factors	Solar	Lighting	People/equipment	Conduction
v_0	0.399	0.39712	0.39712	0.63131
v_1	−0.5013	−0.3903	−0.3903	−0.695
v_2	0.10884	0.03824	0.03824	0.11655
w_1	1.42473	1.17458	1.17458	1.17458
w_2	−0.434	−0.2398	−0.2398	−0.2398

2.6 Whole-Building Energy Models

Generally, whole-building energy analysis tools can be classified into either forward or inverse methods. In the forward approach as depicted in Figure 2.27, the energy predictions are based on a physical description of the building systems such as geometry, location, construction details, and HVAC system type and operation. Most of the existing detailed energy simulation tools such as DOE-2, TRNSYS, and EnergyPlus follow the forward modeling approach. In the inverse approach illustrated in Figure 2.28, the energy analysis model attempts to deduce representative building parameters [such as the building load coefficient (BLC), the building base-load, or the building time constant] using existing energy use, weather, and relevant performance data. In general, the inverse models are less complex to formulate than the forward models. However, the flexibility of inverse models is typically limited by the formulation of the representative building parameters and the accuracy of the building performance data. Most of the existing inverse models rely on regression analysis such as the variable-base degree-day models or the change-point models [38] tools or connectionist approach [39] to identify the building parameters. It should be noted that tools based on the forward or inverse approaches are suitable for other applications. Among the common applications are verification of energy savings actually incurred from energy conservation measures, diagnosis of equipment malfunctions, and efficiency testing of building energy systems.

Energy analysis tools can also be classified based on their ability to capture the dynamic behavior of building energy systems. Thus, energy analysis tools can use either steady-state or dynamic modeling approaches. In general, the steady-state models are sufficient to analysis seasonal or annual building energy performance. However, dynamic models may be required to assess the transient effects of building energy systems such as

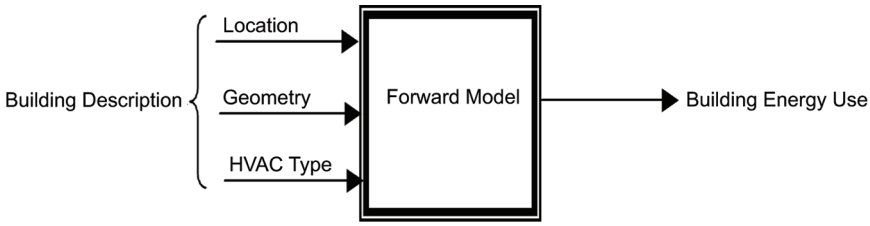

Figure 2.27. Basic approach of a typical forward energy analysis mode.

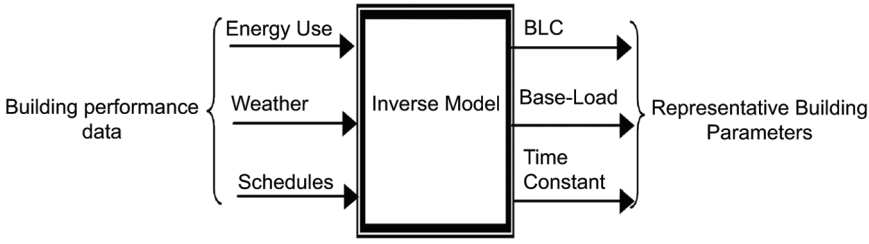

Figure 2.28. Basic approach of a typical inverse energy analysis model.

those encountered for thermal energy storage systems and optimal start controls.

In this section, selected energy analysis tools commonly used in the US and Europe are described. These tools are grouped into three categories:

- *Inverse methods:* using both steady-state and dynamic modeling approaches and include variable-base degree-day methods.
- *Forward methods:* including either steady-state or dynamic modeling approaches, are often the basis of detailed energy simulation computer programs.

2.6.1 Inverse Modeling Methods

As discussed in the introduction, methods using the inverse modeling approach rely on existing building performance data to identify a set of building parameters. The inverse modeling methods can be valuable tools in improving the building energy efficiency. In particular, the inverse models can be used to:

- help detect malfunctions by identifying time periods or specific systems with abnormally high energy consumption,
- provide estimates of expected savings from a defined set of energy conservation measures, and
- measure and verify savings achieved by energy retrofits.

Typically, regression analyses are used to estimate the representative parameters for the building and/or its systems (such as building load coefficient or heating system efficiency) using measured data. In general, steady-state inverse models are based on monthly and/or daily data and include one or more independent variables. Dynamic inverse models are usually developed using hourly or sub-hourly data to capture any significant transient effect such as the case where the building has a high thermal mass to delay cooling or heating loads.

Steady-State Inverse Models: These models generally attempt to identify the relationship between the building energy consumption and selected weather-dependent parameters such as monthly or daily average outdoor temperatures, degree-hours, or degree days. As mentioned earlier, the relationship is identified using statistical methods (based on linear regression analysis). The main advantages of the steady-state inverse models are:

- Simplicity: steady-state inverse models can be developed based on a small data set such as energy data obtained from utility bills.
- Flexibility: steady-state inverse models have a wide range of applications. They are particularly valuable in predicting the heating, cooling energy end-uses for both residential and small commercial buildings.

However, steady-state inverse models have some limitations since they cannot be used to analyze transient effects such as thermal mass effects and seasonal changes in the efficiency of the HVAC system. Steady-state inverse models are especially suitable for measurement and verification (M&V) of energy savings accrued from energy retrofits. In this section, only simplified methods based on steady-inverse modeling are briefly presented. These simplified models have been used to determine the energy impact of selected energy efficiency measures and are based on the degree-day method.

Using steady-state analysis, the building energy use per billing period is correlated to either the average outdoor temperatures or to heating or cooling degree-days (obtained for the billing period). Thus the energy

consumption is estimated for each billing period using the following expressions depending if outdoor temperature or degree-day is used:

Eq. (2.97) provides a temperature-base model while Eq. (2.98) outlines a degree-day based model for evaluating residential building heating loads:

$$E_H = 24 \times \frac{BLC}{\eta_H} \times (T_{b,H} - \overline{T}_o) + E_{base,H} \tag{2.97}$$

$$E_H = 24 \times \frac{BLC}{\eta_H} \times DD_H(T_{b,H}) + E_{base,H} \tag{2.98}$$

Eq. (2.99) provides a temperature-base model while Eq. (2.100) outlines a degree-day based model for evaluating residential building cooling loads:

$$E_C = 24 \times \frac{BLC}{COP_C} \times (\overline{T}_o - T_{b,C}) + E_{base,C} \tag{2.99}$$

$$E_C = 24 \times \frac{BLC}{COP_C} \times DD_C(T_{b,C}) + E_{base,C} \tag{2.100}$$

where,

- $E_{H/C}$ represents the annual building energy use during heating or cooling season
- BLC is the building loss coefficient
- η_H is the average seasonal energy efficiency of the heating system
- COPC is the average seasonal coefficient of performance of the cooling system
- $T_{b,\,H/C}$ is the building balance temperature for heating or cooling energy use.
- DD_H is the heating or cooling degree-days (based on the balance temperature).
- $E_{base,H/C}$ is the base-load for building energy use. It represents the non-heating or non-cooling energy use.

Through regression analysis, the balance temperature and the building load coefficient (assuming known the heating or cooling system efficiency) can be determined. One the building parameters are estimated, the models of Eqs. (2.97)–(2.100) can be used to establish an energy use model for the building and to determine any energy savings attributed to measures that affect one of the three parameters, balance temperature,

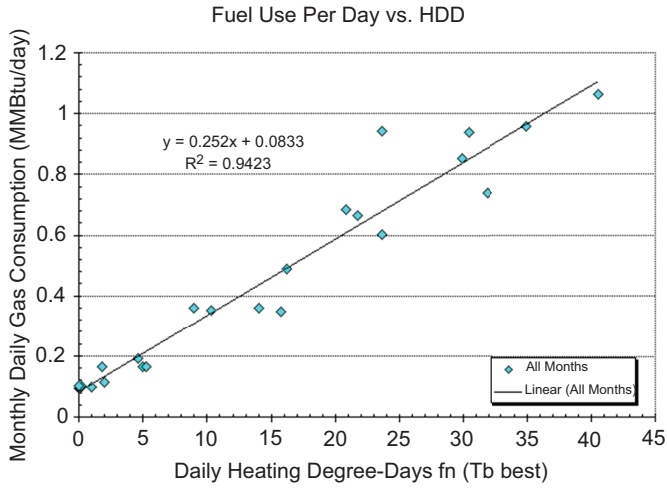

Figure 2.29. Analysis of gas consumption as a function of monthly heating degree-days.

building load coefficient, or heating/cooling system efficiency. Figure 2.29 illustrates the use of the heating model outlined by Eq. (2.98) to correlate the natural gas usage as a function of the heating degree-day for a residential building [40].

Dynamic models: Steady-state inverse models are only suitable for predicting long-term building energy use. Therefore, energy use data is collected for a relatively long time period (at least one season or one year) to carry out the regression analysis. In the other hand, dynamic inverse models can be used to predict short-term building energy use variations using data collected for a short period of time such as one week. Generally, a dynamic inverse model is based on a building thermal model that uses a specific set of parameters. These building model parameters are identified using typically some form of a regression analysis.

An example of a dynamic model relating building cooling energy use to the outdoor air temperatures at various time steps (typically hours) is presented by Eq. (2.101):

$$E_C^n + b_1 E_C^{n-1} + ... + b_N E_C^{n-N} = a_0 T_o^n + a_1 T_o^{n-1} + ... + a_M T_0^{\,n-M} \qquad (2.101)$$

Other examples of dynamic inverse models include equivalent thermal network analysis, Fourier series models, and artificial neural networks. These models are capable of capturing dynamic effects such as building thermal mass dynamics. The main advantages of the dynamic inverse models include the ability to model complex systems that depend on several independent parameters. Their disadvantages include their complexity and the need for more detailed measurements to fine-tune the model. Unlike steady-state inverse models, dynamic inverse models usually require a high degree of user interaction and knowledge of the modeled building or system.

2.6.2 Forward Modeling Methods

Forward modeling methods are generally based on physical description of the building energy systems. Typically, forward models can be used to determine the energy end-uses as well as predict any energy savings incurred from energy conservation measures. Selected existing US energy analysis tools that use the forward modeling approach are described in the following sections [28].

Steady-state methods: Steady-state energy analysis methods that use the forward modeling approach are generally easy to use since most of the calculations can be performed by hand or using spreadsheet programs. Most of steady-state forward tools are based on one form of degree-day methods. As described earlier, the degree-day method used seasonal degree-day computed at a specific set-point temperature (or balance temperature) to predict the energy use for building heating. Typically, these degree-days methods are not suitable for predicting building cooling loads. In the US, the traditional degree method day using a base temperature of 65°F has been replaced by the variable-base degree-days method and is applied mostly to residential buildings. In Europe, heating degree-days using 18°C as the base temperature is still used for both residential and commercial buildings.

The variable-base degree-day methods predict seasonal building energy used for heating with one variation of the following formulation:

$$FU = \frac{24.BLC.f_{DH}.DD_H(T_b)}{\eta_H} \tag{2.102}$$

Where:

- FU represents the fuel use (gas, fuel oil, or electricity depending on the heating system).
- BLC is the building loss coefficient including transmission and infiltration losses through the building envelope.
- f_{DH} is a correction factor to include various effects such night set-back effects, and free heat gains. A simplified method to estimate this factor has been presented earlier in this chapter.
- T_b is the building heating balance temperature.
- $DD_H(T_b)$ is the heating degree days calculated at the balance temperature T_b.

Variable-base degree-days methods provide generally good predictions of the fuel use for residential buildings dominated by transmission loads. However, they are not recommended for buildings dominated by internal loads and/or with involved HVAC system operation strategies.

Dynamic methods: Dynamic analytical models use numerical or analytical methods to determine energy transfer between various building systems. These models consist generally of simulation computer programs with hourly or sub-hourly time steps) to estimate adequately the effects of thermal inertia – due for instance to energy storage in the building envelope and/or its heating system. The important characteristic of the simulation programs is their capability to account for several parameters that are crucial to accurately energy use especially for buildings with significant thermal mass, thermostat setbacks or setups, explicit energy storage, or predictive control strategies. A typical calculation flow chart of detailed simulation programs is presented in Figure 2.30 [31].

Detailed computer programs require high-level of expertise and are generally suitable to simulate large buildings with complex HVAC systems and involved control strategies that are difficult to model by simplified energy analysis tools.

In general, an energy simulation program requires a detailed physical description of the building (including building geometry, building envelope construction details, HVAC equipment type and operation, and occupancy schedules). Thermal load calculations are based on a wide range of algorithms depending on the complexity and the flexibility of the simulation program. To adequately estimate energy savings from energy efficiency measures, energy simulation tools have to be calibrated using existing measured energy data (utility bills, for instance).

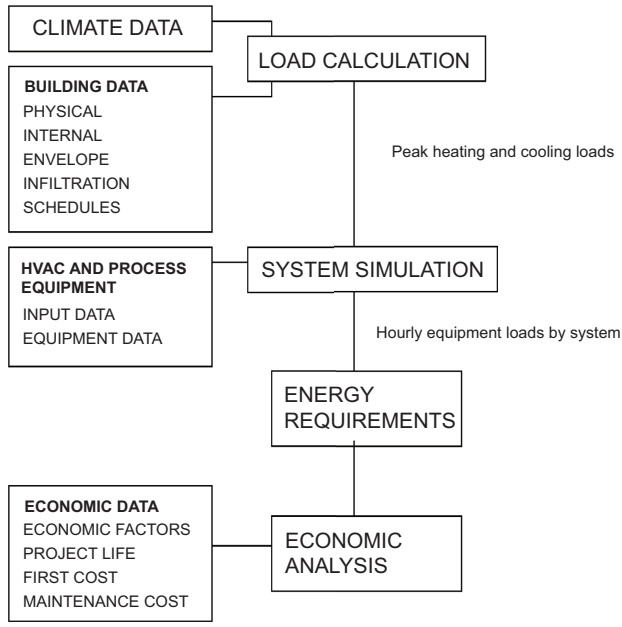

Figure 2.30. Flow chart of complete building model.

While energy simulation programs are generally capable of modeling most of the building energy systems, they are often not sufficiently flexible and have inherent limitations. To select the appropriate energy simulation program, it is important that the user be aware of the capabilities of each simulation available to him/her. Some of the well-known simulations programs are briefly presented below:

- DOE-2 (version DOE-2.1). DOE-2 was developed at the Lawrence Berkeley National Laboratory (LBNL) by the US Department of Energy and is widely used because of its comprehensiveness [30]. It can predict hourly, daily, monthly, and/or annual building energy use. DOE-2 is often used to simulate complex buildings. Typically, significant efforts are required to create DOE-2 input files using a programming language called Building Description Language (BDL). Several tools are currently available to facilitate the process of developing DOE-2 input files. Among energy engineers and professionals, DOE-2 has become a standard building energy simulation tool in the US and several other countries using interfaces such eQUEST and VisualDOE. Figure

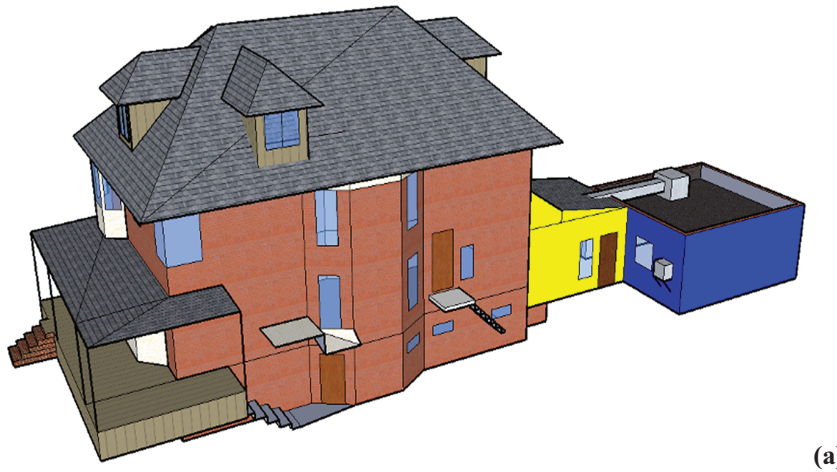

(a)

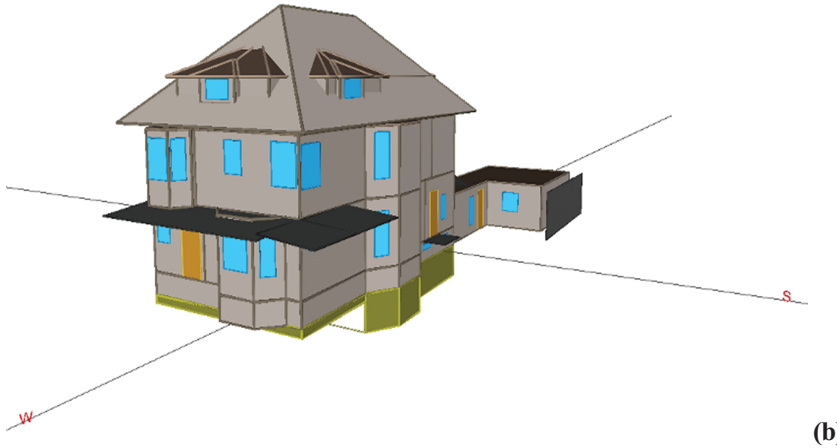

(b)

Figure 2.31. Three-dimensional models for a residential building (a) CAD rendering and (b) eQUEST rendering (Kalinic, 2009).

2.31 shows a 3-D rendering of a residential building modeled using eQUEST.

- EnergyPlus builds on the features and capabilities of both DOE-2 and BLAST [19]. It first version is expected to be issued in year 2000. EnergyPlus uses new integrated solution techniques to correct one of the deficiencies of both BLAST and DOE-2 – the inaccurate prediction of space temperature variations. Accurate prediction of space temperatures is crucial to properly analyze energy efficient systems. For instance, HVAC system performance and occupant comfort are directly affected by space

temperature fluctuations. Moreover, EnergyPlus have several features that should aid engineers and architects to evaluate a number of innovative energy efficiency measures that cannot be simulated adequately with either DOE-2 or BLAST. These features include:

- Free cooling operation strategies using outdoor air,
- Realistic HVAC systems controls,
- Effects of moisture adsorption in building elements,
- Indoor air quality with a better modeling of contaminant and air flows within the building.

Several interfaces for EnergyPlus have been developed over the last few years. A complete list of the interfaces is periodically updated in the EnergyPlus website [19]. Figure 2.32 illustrates a 3-D rendering of a large residential building modeled using EnergyPlus.

- TRNSYS provides a flexible energy analysis tool to simulate a number of energy systems using user-defined modules [18]. While TRNSYS can be used to model heating and cooling thermal loads for homes, it is widely used for modeling active solar systems including PV and solar hot water heating systems. Figure 2.33 illustrates a thermal model for a home using TRNSYS. A good knowledge of computer programming (Fortran) is required to properly use TRNSYS simulation tool.

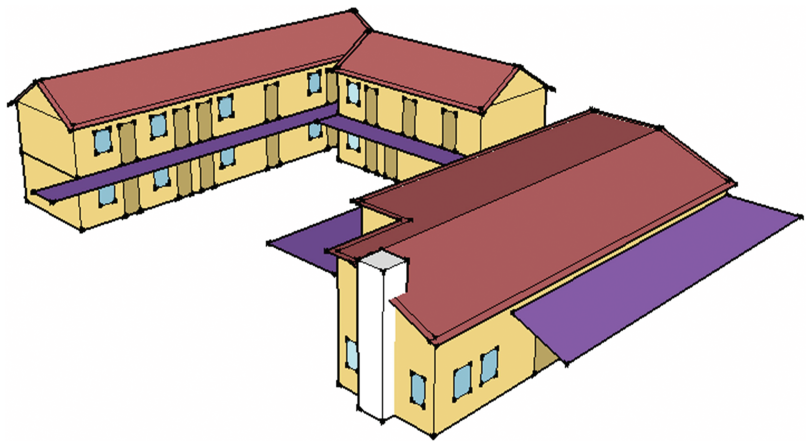

Figure 2.32. Three-dimensional model for a large building using EnergyPlus.

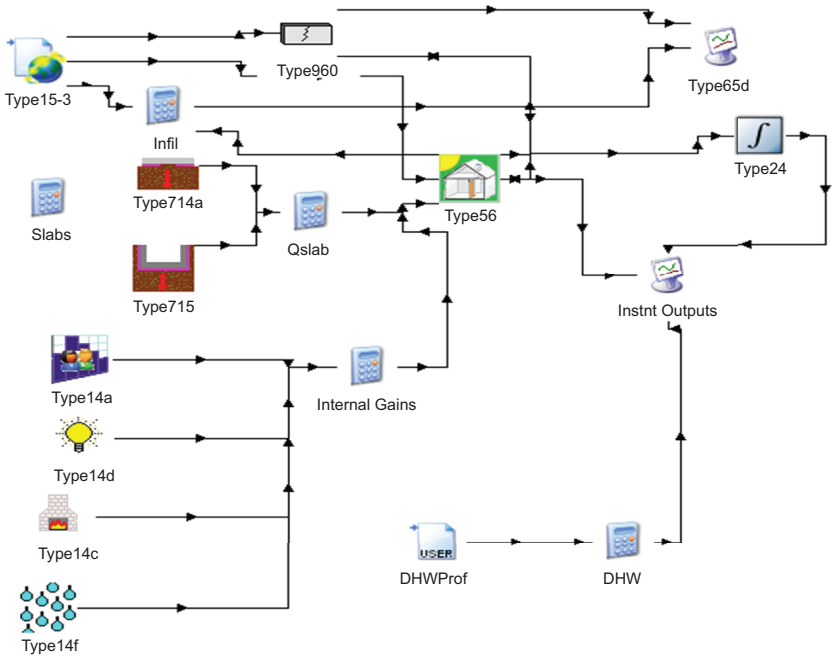

Figure 2.33. A thermal model for a house using TRNSYS simulation tool.

2.6.3 Meta-Modeling Approach

For several applications, the use of direct simulation tools may not be suitable. A recent modeling approach, referred to as meta-modeling, has been proposed and applied to building energy analysis. The meta-modeling can replace and emulate detailed simulation analysis tools but with the main advantage of significant reduction in computational efforts with little reduction in prediction accuracy. The meta-modeling has been used to calibrate detailed simulation model of existing buildings using metered data.

Figure 2.34 illustrates the structure of a Bayesian-Emulator approach to identify input parameters to calibrate building energy models using measured output data. The approach main features include:

- User estimation of input parameters including prior belief distribution probability functions for the unknown parameters.
- A sampling process for selecting sets of input parameters specific to the building energy model.

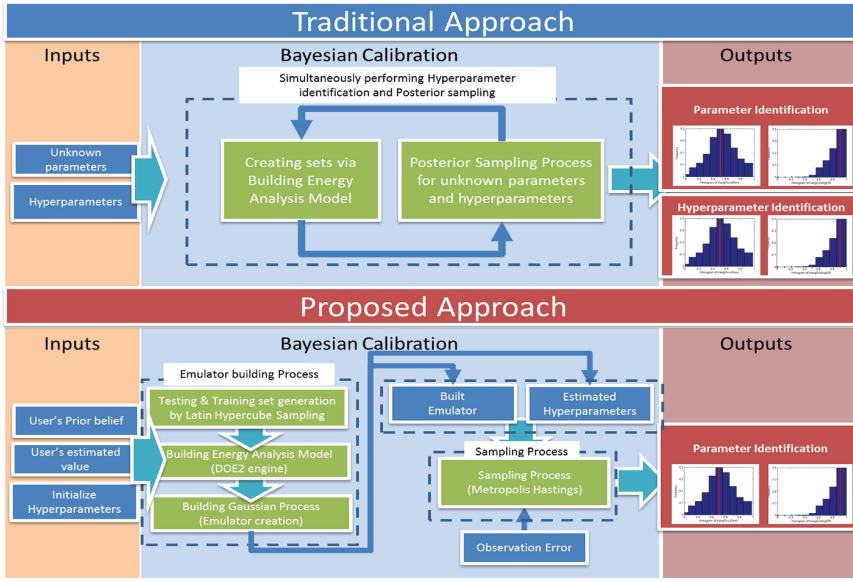

Figure 2.34. Comparison of proposed and traditional Bayesian based approaches for parameter identification.

- A development of a Gaussian Process (GP) emulator for the building energy model using the sampling input and output data.
- Through a Gaussian process, hyperparameters for the building energy model are determined.
- Through another sampling procedure, the unknown parameters are identified by posterior distribution probability functions using both the building energy model emulator and the hyperparameters.

In particular, Figure 2.34 compares the basic features for both the proposed Bayesian-Emulator approach and the traditional Bayesian parameter identification approaches. Specifically, the approach develops a GP emulator of the detailed building energy model to reduce the computational efforts associated with the use of a whole-building simulation analysis tool such as DOE-2 or EnergyPlus outlined earlier. Initially, user's estimated values for the unknown model input parameters and prior belief distributions are considered for the emulator development process. Then, the building energy model input parameters are processed using a sampling approach to generate testing and training building energy model input sets for the GP emulator. It has been shown that the use of the emulator instead of the detailed energy model can reduce

significantly the computational efforts while provide accurate estimation of the unknown input parameters. Specifically, the emulator reduces the computing time for the Bayesian optimization including the posterior sampling procedure and the identification of the unknown building energy model input parameters and their posterior distribution.

Recently, Kang and Krarti [41] has evaluated the benefits of using the Bayesian-Emulator instead of the traditional Bayesian approach for the calibration of detailed energy models of existing buildings. Several methods exist to implement the traditional Bayesian approach [42–43]. In their comparative analysis, Kang and Krarti have obtained the posterior distributions and likelihood functions for the unknown input parameters directly from DOE-2 simulation runs and measured data [43]. Three sampling set sizes have been used to determine the accuracy level and CPU time obtained by both the traditional Bayesian and the Bayesian-Emulator approaches as illustrated in Figure 2.35. Moreover, Figure 2.35 compares the accuracy levels for both approaches for the three considered sampling set sizes (100, 1000, and 10000) using PRRMSE indicators. As indicated by Figure 2.35, the Bayesian-Emulator approach significantly reduces the CPU time for the identification of the unknown input parameters compared to the traditional Bayesian approach by two orders of magnitude from 40 hours to just 5 minutes when a 10000 sampling set is used. However, the accuracy of the traditional approach is actually slightly better than that of the Bayesian-Emulator approach especially for a sampling size of 1000 [41]. This slightly lower accuracy of the Bayesian-Emulator approach is

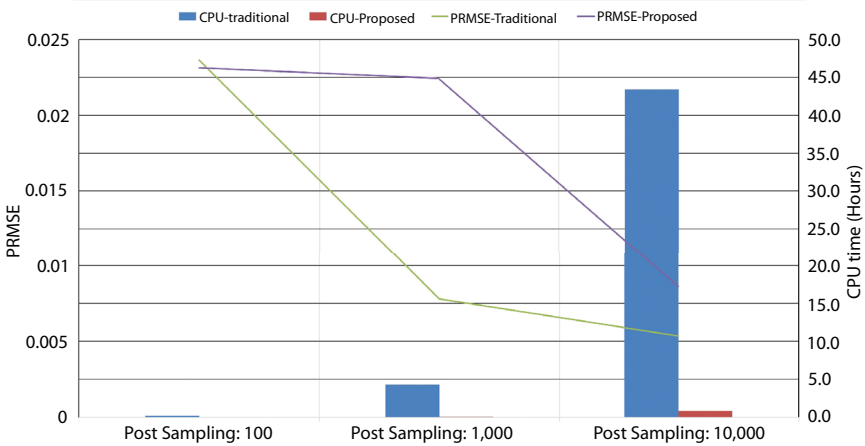

Figure 2.35. Comparison of CPU time and PRMSE for the traditional Bayesian and proposed Bayesian-Emulator approaches.

expected and is attributed to the prediction errors associated with the use of an emulator instead of the detailed building energy simulation model.

2.7 Summary

In this chapter, suitable thermal analysis methods and techniques are presented to assess the energy performance of buildings. In particular, fundamental heat transfer concepts as well as thermal comfort metrics are reviewed and applied to estimate the characteristics of various energy systems of a building. Moreover, simplified as well as detailed analysis tools are described with a brief discussion of the general analysis procedures used by these tools. Depending on the building type and project requirement as well as available time and budget, the energy modeler should select the proper tool to carry out the energy analysis of the building and to estimate the potential energy and cost savings for energy efficiency measures.

References

[1] Sonderegger, R.C., 1985. Thermal Modeling of Buildings as a Design Tool, *Proceedings of CHMA 2000*, Vol. 1.

[2] DOE, 2015. US Department of Energy, Energy Efficiency for Buildings, Directory of Building Energy Software, Washington D.C., An updated list, Website: http://apps1.eren.doe.gov/buildings/tools_directory/.

[3] Khlifi, A. and Krarti, M., 2014. Impact of Above-Grade Walls on Three-Dimensional Heat Transfer from Slab-on-Grade Floor Building Foundations, *ASME Journal of Solar Energy Engineering*, 136(1).

[4] Mitalas, G.P., 1968. Calculation of Transient Heat Flow Through Walls and Roofs, *ASHRAE Trans*., 74.

[5] Kusuda, T., 1969. Thermal Response Factors for Multi-Layer Structures of Various Heat Conduction Systems, *ASHRAE Trans*., 75.

[6] Delsante, A.E., Stokes, A.N., and Walsh, P.J., 1983. Application of Fourier Transforms to Periodic Heat Flow into the Ground under a Building, *International Journal of Heat Mass Transfer* 26, 121–132.

[7] Krarti, M., Claridge, D.E., and Kreider, J.F., 1988. ITPE Technique Applications to Time Varying Two-Dimensional Ground-Coupling Problems, *International Journal of Heat Mass Transfer*, 31(9), 1899–1911.

[8] Hagentoft, C.E., 1996. Heat Losses and Temperature in the Ground under a Building With and Without Ground Water Flow-I. Infinite Ground Water Flowrate, *Building and Environment*, 31, 3–11.

[9] Krarti, M., Claridge, D.E., and Kreider, J.F., 1995. Frequency Response Analysis of Ground-Coupled Building Envelope Surfaces. *ASHRAE Transactions*, 101, 355–364.

[10] Krarti, M., Alanzi, A., and Chuangchid, P., 2002. Cooler Floor Heat Gain in Refrigerated Structures—Final Report, ASHRAE, Atlanta, GA.

[11] Bahnfleth, W.P. and Petersen, C.O., 1990. Three-Dimensional Modeling of Heat Transfer from Slab Floors, *ASHRAE Transactions*, 96, 2.

[12] Yuill, G.K. and Wray, C.P., 1987. Verification of a Microcomputer Program Implementing the Mitalas Below-Grade-Heat Loss Model, *ASHRAE Transactions*, 93(1), 434–446.

[13] Stephenson, D.G. and Mitalas, G.P., 1969, Cooling Load Calculations by Thermal Response Factors, *ASHVE Trans*., 73.

[15] Ceylan, H.T. and Myers, G.E., 1979. Long-Time Solutions to Heat Conduction Transients with Time-Dependent Inputs, *ASME Journal of Heat Transfer*, 102, 115–121.

[16] Seem, J.E., 1987. *Modeling of heat transfer in buildings*. Wisconsin Univ., Madison (USA).

[17] Burch, D.M., Seem, J.E., Walton, G.N., and Licitra, B.A., 1992. Dynamic Evaluation of Thermal Bridges in Typical Office Building, *ASHRAE Transaction*, 98(1), 291–304.

[18] Klein, S.A., Beckman, W.A., Mitchell, I.W., 1994. *TRNSYS—A transient system simulation program*. Solar Energy Laboratory. University of Wisconsin, Madison, WI.

[19] EnergyPlus User's Guide (2010), Engineering Reference—The Reference to EnergyPlus Calculations, DOE.

[20] Chen, C., 1998. *Linear system theory and design*, 3rd edition, Oxford University Press.

[21] Krarti, M., Claridge, D.E., and Kreider, J.F., 1993. *Energy Calculations for Basements, Slabs, and Crawl Space*, Project 666-RP Final report. ASHRAE, Atlanta, GA.

[22] Krarti, M., Chaungchid, P., and Ihm, P., 2001. Foundation heat transfer module for EnergyPlus Program. *Proceedings of IBPSA Conference*, Rio de Janeiro, Brazil, 931–938.

[23] Chen, Y. and Wang, S., 2001. A Frequency Domain Regression Method for Estimating CTF Models of Building Multi-Layer Constructions, *Applied Mathematical Modeling*, 25, 579–592.

[24] Chen, Y. and Wang, S., 2005. A New Procedure for Calculating Periodic Response Factors Based on Frequency Domain

Regression Method, *International Journal of Thermal Sciences*, 44, 383–392.
[25] Khlifi, A. and Krarti, M., 2012. A Frequency-Domain Regression Method for Estimating Building Foundation Heat Transfer, *Journal of Building Performance Simulation*, 5(2).
[26] SIAM, 1994. *Lapack User's Guide*, V. 2.0, Philadelphia, P.A.
[27] Ouyang, K. and Haghighat, F., 1991. A Procedure for Calculating Thermal Response Factors of Multiplayer Walls–State-Space Method, *Building and Environment*, 26(2), 173–177.
[28] ASHRAE, 2013. *Handbook of Fundamentals*. American Society of Heating, Refrigerating and Air Conditioning Engineers, Atlanta, 111.
[29] Krarti, M., 2000. Foundation Heat Transfer. *Advance in Solar Energy*, Vol. 13, editor Y. Goswami and K. Boer, ASES, Boulder, CO.
[30] DOE, 1982. DOE-2 Engineers Manual, Response Factors Section by W.F. Buhl and R.B. Curtis, Report by Lawrence Berkeley Laboratory, LBL-11353, Berkeley, CA.
[31] Krarti, M., 2011. *Energy Audit for Building Systems: An Engineering Approach*—Second Edition, book, CRC Press, 600 pages.
[32] Claridge, D.E., Krarti, M., and Bida, M., 1987. A Validation Study of Variable-Base Degree-Day Cooling Calculations, *ASHRAE Transactions*, 93(2), 90–104.
[33] Kearns, P.A. and Krarti, M., 2011. Residential Energy Analysis: Regression Analysis of Heating Degree Days with Temperature Setback for Selected ASHRAE Climate Zones, *Proceedings of ASME Energy Sustainability Conference 2011*, Washington DC.
[34] Braun, J.E. and Chaturvedi, N., 2002. An Inverse Gray-Box Model for Transient Building Load Prediction, *HVAC&R Research*, 8(1), 73–99.
[35] Dewson, T., Day, B., and Irving, A.D., 1993. Least Squares Parameter Estimation of a Reduced Order Thermal Model of an Experimental Building, *Building and Environment*, 28(2), 127–137.
[36] Wang, S. and Xu, X., 2006. Parameter Estimation of Internal Thermal Mass of Building Dynamic Models Using Genetic Algorithm, *Energy Conversion and Management*, 47(13), 1927–1941.
[37] Fux, S.F., Benz, M.J., and Guzzella, L., 2011. Comparing control-oriented thermal models for a passive solar house. In submitted to CISBAT conference.
[38] Kissock, K., Reddy, T.A., and Claridge, D.E., 1998. Ambient-Temperature Regression Analysis for Estimating Retrofit Savings in Commercial Buildings, *ASME J. Solar Energy Engineering*, 120(3), 168–176.

[39] Kreider, J.F., Blanc, S.L., Kammerud, R.C., and Curtiss, P.S., 1997. Operational Data as the Basis for Neural Network Prediction of Hourly Electrical Demand, *ASHRAE Transactions*, 103-2.

[40] Kalinic, N., 2009. Measurement and Verification of Savings from Implemented ECMs, MS Report, University of Colorado, Boulder, CO.

[41] Kang, Y. and Krarti, M., 2016. Bayesian-Emulator Based Parameter Identification for Calibrating Energy Models for Existing Buildings, *Building Simulation*, 9(4), 411–428.

[42] Pavlak, G.S., 2014. Building-to-Grid Integration through Commercial Building Portfolios Participating in Energy and Frequency Regulation Markets. University of Colorado at Boulder—PhD Thesis.

[43] Higdon, D., 2004. Combining Field Data and Computer Simulations for Calibration and Prediction. 2, *SIAM Journal on Scientific Computing*, 26, 448–466.

3 Conventional Mechanical Systems for Efficient Heating, Ventilating, and Air Conditioning Systems

Jorge E. González and Antonio José Bula-Silvera

Abstract

This chapter provides a concise overview of mechanical systems used for heating, ventilation and air conditioning (HVAC) in residential and commercial applications with emphasis on energy efficient equipment. Components and systems considered include vapor compression systems, chill water systems, heat rejection systems, radiant heating systems, gas-fired heating systems, ventilation systems, design processes and strategies, equipment sizing, review of codes and standards, system integration, and future trends of these technologies. The focus of the chapter is on primary mechanical HVAC systems.

3.1 Introduction

This chapter describes the equipment used to produce a cooling or heating effect in residential and commercial buildings. For cooling, there are three main systems widely used; a) the vapor compression system, b) the absorption system, and c) the evaporative cooling process. Commonly heating systems include; a) furnaces and boilers, b) vapor compression heat pumps, and c) radiant heating systems.

The chapter first presents the details of the vapor compression and absorption cycles, followed by heat rejection equipment, evaporative cooling systems, and finally heating systems. The chapter closes with system integration strategies. Components over which the designer has little control (e.g., the internal design of a chiller or expansion device) are not discussed in the chapter.

3.2 Cooling Vapor Compression Systems

Figure 3.1 shows the ideal cycle schematically on a Temperature-Entropy, or *T-s*, diagram. This process is called *ideal* because pressure and temperature drop are ignored, superheating in the evaporator and sub-cooling in the condenser that are present in real equipment are ignored, and compressor inefficiencies are omitted. In this ideal cycle, also known as Carnot Refrigeration Cycle, heat from the buildings is extracted in the evaporator unit as a two-phase flow mix of the refrigerant (process 4-1). The heat from the building is used to evaporate the mix before entering the compressor. Ideally, the compression process (process 1-2) takes place isentropically before entering the condensation process (process 2-3) where the total heat is released to the environment. The refrigeration effect is eventually obtained in the expansion valve (process 3-4) where the refrigerant is cooled down as a saturated low pressure mix.

The most common measure of refrigeration cycle performance is the coefficient of performance (COP). For the ideal VC cycle, it is given by;

$$COP = \frac{h_1 - h_4}{h_2 - h_1} \tag{3.1}$$

The enthalpies in Eq. (3.1) are identified with the subscripts in Figure 3.1.

Figure 3.2 shows an actual vapor compression air conditioning system with typical operating equipment. For actual systems, each mechanical

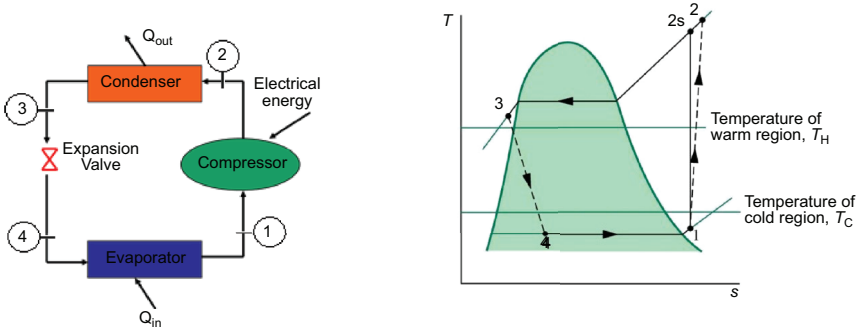

Figure 3.1. Ideal refrigeration cycle and corresponding schematic arrangement of mechanical equipment and T-S diagram.

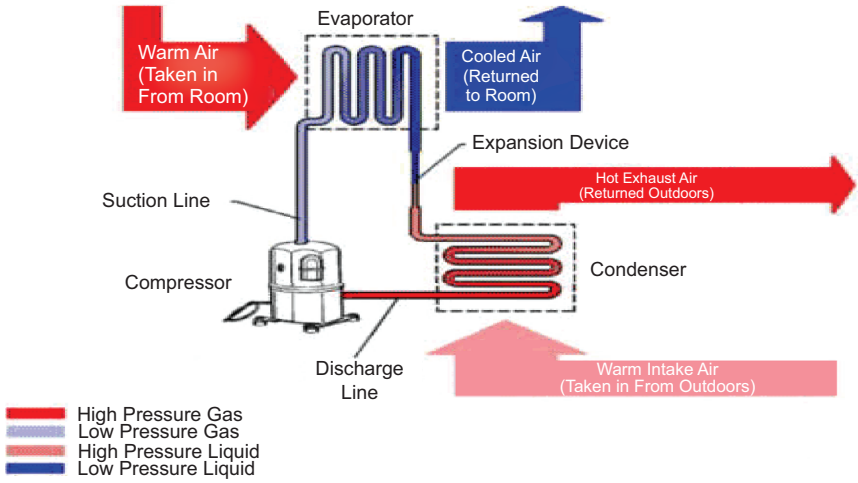

Figure 3.2. VC cycle equipment with typical operating equipment.

component in Figure 3.2 has thermodynamic irreversibilities associated with it.

These may include:

1. *Compressor* — friction losses, heat losses, or heat gains
2. *Condenser* — friction losses, sub-cooling to ensure pure liquid at throttling valve inlet
3. *Evaporator* — friction losses, superheating to ensure pure vapor at compressor inlet
4. *System losses* — pressure drops, heat gains, and heat losses in refrigerant lines; compressor shaft friction

These effects distort the ideal cycle shown in Figure 3.1 (solid lines) to the real cycle shown in Figure 3.1 (dashed lines). Analysis of a real cycle requires considerably more data than for the ideal cycle. To complete the analysis, the following are required:

- Compressor efficiency
- Liquid and vapor line heat loss coefficients
- Liquid and vapor line pressure drop values
- Compressor heat loss or gain rate
- Condenser and evaporator pressure drops

- Amount of refrigerant superheating at evaporator outlet
- Amount of refrigerant sub-cooling at condenser outlet

The most significant factors of those listed are the compressor efficiency, compressor suction line heat gains and pressure losses, and condenser and evaporator pressure drops.

3.2.1 Refrigerants

The key requirement of a refrigerant is that it has properties that match the needs of building cooling systems. As a compressed vapor, a refrigerant must not have excessive pressures at temperatures needed for heat rejection to the environment on a hot summer day. It is desirable to have the evaporator pressure below atmospheric pressure to avoid refrigerant contamination to the ambient. The evaporator temperature at this pressure should be near 40°F (5°C) to produce cooled air in direct-expansion equipment at temperatures in the range of 50°F to 55°F (10°C to 13°C); chillers and ice makers will operate at lower temperatures. With these thermal restrictions plus the concerns listed earlier, it is not surprising that only a few inexpensive refrigerants exist that meet all criteria.

During the early 1990s, 90 percent of all refrigerants used consisted of R11, R12, R22, and R502 (an azeotropic mixture of R22 and R115; an azeotrope is a mixture that cannot be separated by distillation and that has properties different from either constituent). These refrigerants, known as chlorofluorocarbons (CFCs), are chemically stable for terrestrial applications, inexpensive, and nontoxic compounds. However, they have been shown to destroy the stratospheric ozone layer which protects us from ultraviolet (UV) solar radiation. Hence, damaging UV flux levels are predicted to increase at the earth's surface in the future. To avoid these serious problems, the use of these common CFCs is being phased out worldwide.

Refrigerants 11 and 12 are the most destructive to the ozone layer and have been the first to be phased out following the Montreal Protocol [1]. They have been replaced by R22, R123, and R134a. Some of these replacements, in turn, are likely to be replaced by more benign compounds in the future, these known as natural refrigerants such as air and CO_2 [2]. Some of the compounds proposed for the first round of replacements have problems, including toxicity, higher cost, reduced equipment capacity, and incompatibility with existing compressor seal designs and lubricating

oils. Thermodynamic properties for several common refrigerants are given in charts and tables and are available in the open literature [3].

The method of identifying CFC refrigerants with the numbering system used above is based on the number of fluorine atoms (right digit of number), number of hydrogen atoms plus 1 (center digit), and number of carbon atoms minus 1 (left digit, unless zero, which is suppressed). For example, the chemical formula for dichlorodi-fluoromethane is CCl_2F_2. Therefore, the first digit is zero (suppressed); the center digit is 1 since there are no hydrogen atoms. The right digit is 2 since there are two fluorine atoms. The symbol is R12. Inorganic compounds are numbered by adding 700 to their molecular weight. Therefore, ammonia (MW = 17) is numbered R717. Mixtures of refrigerants use a serial numbering system beginning with 500 are not related to the chemical composition.

3.3 Absorption Cooling Systems

The closed absorption system is a heat operated unit using a refrigerant which is alternatively absorbed and liberated at certain temperatures and pressures. The main components of this system are absorber, generator, condenser and evaporator. Figure 3.3 shows the principal features of these systems. The basic operation is as follows.

In the evaporator the refrigerant is evaporated under low pressures as it is sprayed on the tubes through which chilled water flows. The chilled water is then delivered to the heat exchanger coil; however, the air is cooled to be discharged to the room space for air-conditioning as it is needed. In the absorber, the concentrated solution absorbs the vaporized refrigerant from the evaporator at the same low pressure. As the solution is sprayed on the cooling tubes within the absorber container, it is cooled down and the pressure is lowered to be capable of absorbing more vapor. Any absorption heat produced is suppressed by cooling water. The absorbent solution is diluted due to the absorption of the vaporized refrigerant, being reduced to a weak solution with less capacity of absorbing water vapor. In the regenerator, the diluted solution pumped from the absorber is heated and concentrated by dispelling some refrigerant vapor, so that the solution again is capable of absorbing refrigerant vapor. This separation occurs because the concentration of the refrigerant in the absorber decreases

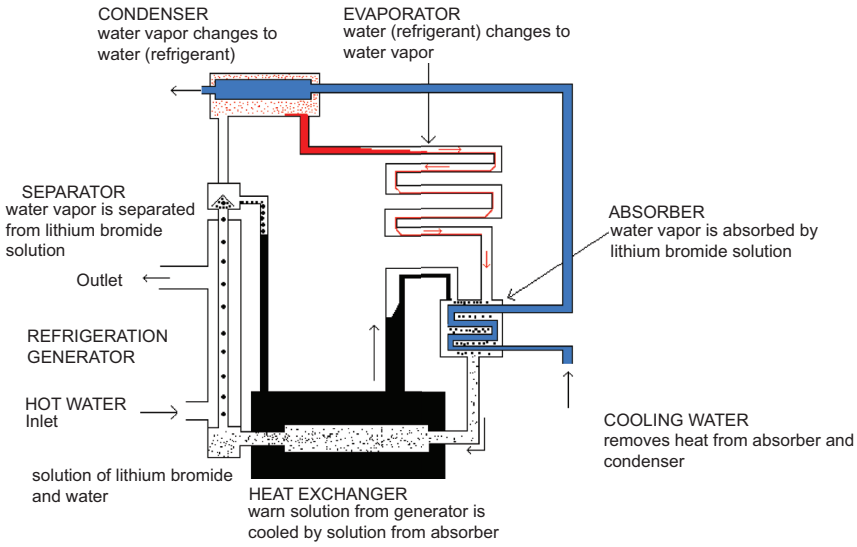

Figure 3.3. Closed absorption single-effect cooling cycle.

with temperature and is called regeneration. The heat must be given from outside and may come from gas, oil, solar energy, or combinations of them. The heat source will depend on the boiling temperature of the refrigerant in the weak solution. The strong solution at the high temperature is cooled through a heat exchanger with the weak solution from the absorber before being brought into the absorber. This process serves to pre-heat the weak solution which will be eventually brought to higher temperatures at the regenerator. In the condenser, the high temperature vapor produced in the regenerator is condensed on the surface of the cooling tubes through the cooling tower water flow. The liquid refrigerant then enters into the evaporator by a throttling process, being evaporated to take heat out of the chilled water. The cycle is thus completed.

The absorbent solution is usually a salt with strong power to absorb moisture. The desirable properties for the refrigerant are high heat of vaporization, low specific heat capacity, and good thermal stability, while for the absorbent, chemical stability, high boiling point and low heat capacity are advantageous. The most common refrigerant/absorbent pairs are water (refrigerant)/lithium bromide (H_2O/LiBr) and ammonia (refrigerant)/water (NH_3/H_2O).

The performance of closed-absorption machines is usually expressed by the Coefficient of Performance (*COP*). The *COP* of an absorption

chiller is defined as the ratio of the room cooling effect (Q_{evap}) to the input energy to the regenerator (Q_{gen}):

$$COP = \frac{Q_{evap}}{Q_{gen}} \tag{3.2}$$

Typical values of *COP*s for commercially available absorption chillers ranges between 0.5 and 1.5. Commercial units are available for the H_2O/LiBr absorbent/refrigerant pair. Companies such as Carrier Corporation, U.S.A.; Arkla, U.S.A.; and Yazaki, Japan; build chillers operated by gas burners and have modified these units to be operated by hot water from solar collectors. Units of NH_3/H_2O are not commonly found for domestic applications due to the toxicity of NH_3. Arkla-Servel and Bryant, U.S.A. have marketed aqua-ammonia air conditioning units which can be used outside of commercial or industrial buildings.

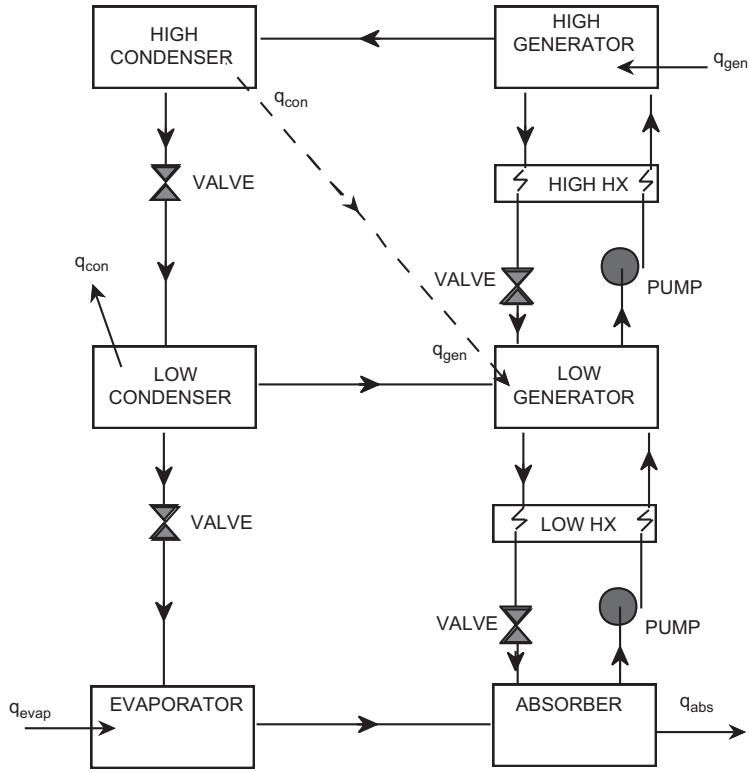

Figure 3.4. Double-effect closed absorption cooling cycle.

Since the advent of closed absorption machines more than 30 years ago, improvements in the simple absorption cycle have taken several forms. The most significant being the incorporation of multiple effects generators. It was proposed some years ago an absorption chiller which operated with two regenerators. In this chiller, most of the refrigerant is desorbed in a high temperature regenerator. This high temperature refrigerant exchanges heat with the weak solution at a lower pressure and the weak solution is further regenerated. Figure 3.4 shows a typical two-stage absorption chiller.

3.4 Mechanical Cooling Equipment — Chillers

A *chiller* is an assembly of equipment used to produce chilled water for cooling of spaces within buildings. The equipment comprising a chiller depends on whether the absorption cycle (AC) or vapor compression (VC) cycle is used. Heat exchangers between the heat rejection subsystem and cooling distribution subsystem are also included in the chiller assembly. Figure 3.5 is a simple diagram of a liquid chiller based on the VC cycle.

In USCS units, the rate of refrigeration is often expressed as *tons of cooling*. This unit of cooling effect is equivalent to 12,000 Btu/h (3.5 kW). It was originally defined on the basis of melting of 1 ton (2000 lb_m) of ice (heat of fusion 144 Btu/lb) per day (24 h), giving a cooling rate equal to 12,000 Btu/h (3515 W).

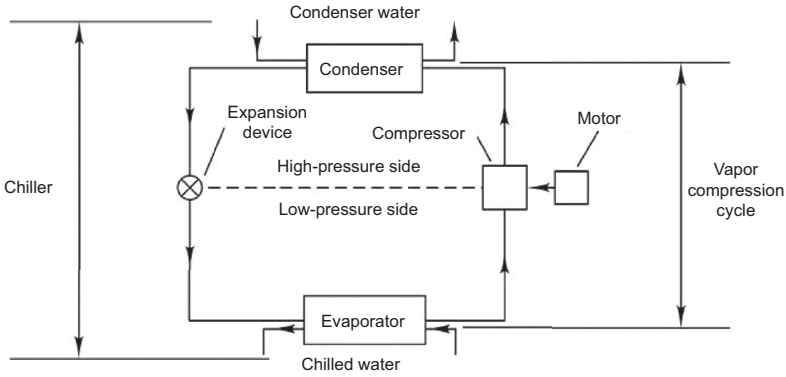

Figure 3.5. Schematic diagram showing essential components of basic liquid chiller and relation to vapor compression cycle. (With permission CRC Press [4].)

3.5 Heat Rejection Equipment

All cooling equipment must reject to a heat sink the total of the heat removed from the cooled building spaces and the compressor work (or the absorber heat input for an absorption system). There are two standard methods for rejecting heat. A *cooling tower* passes condenser water in direct contact with outdoor air to cool the water by evaporation. An *air-cooled condenser* cools refrigerant directly by flowing outdoor air over the outer surface of tubes in which the condensing refrigerant flows. In this section, we describe both forms of heat rejection to outdoor air from central plant cooling systems. Although other heat sinks are used, outdoor air is by far the most common.

3.5.1 Cooling Towers

Moderate to large chillers [larger than 150 to 200 tons (525 to 700 kW)] use water as a condenser cooling medium. The lower condensing temperatures achieved with water causes the chiller to operate more efficiently than if an air-cooled condenser were used. The most common method of producing cooling water for a condenser is by use of a cooling tower. A cooling tower is a direct-contact heat exchanger in which heat picked up by a cooling water loop from a refrigerator, air conditioner, or industrial process is transferred to atmospheric air [3]. The condenser in commercial HVAC systems transfer heat generated by the compressor into a water loop. Warm water is pumped to the cooling tower and is cooled via evaporating cooling. Air inlets allow the flow of cooler and dryer air from the surroundings into the interior of the cooling tower. Heat and mass transfer takes place when water droplets from the condenser unit enter in contact with incoming air reducing water's temperature via evaporative cooling process (Figure 3.6). Cooled water is collected at the bottom of the tower where it will be pumped back to the cycle while warm and moist air is released to the atmosphere. Additional water is added to the system to replace water loss due to evaporation.

Cooling towers eject a partition of sensible and latent heat from commercial buildings. The effectiveness of a heat exchanger is the ratio of the actual heat transfer rate to the maximum possible heat transfer rate determined by the maximum possible cooling effect. The maximum heat transfer rate is limited by the enthalpy difference between inlet air and outlet air if it were saturated at the temperature of the warm inlet water [4]. The effectiveness (ε), is defined as:

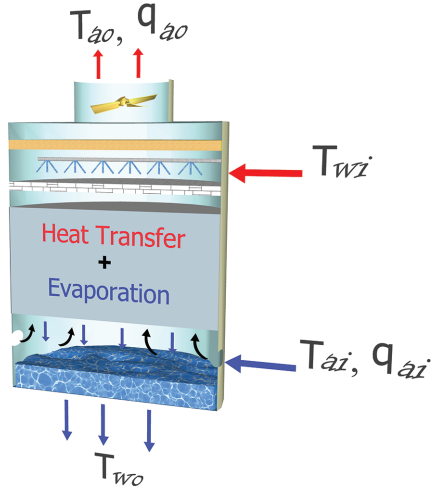

Figure 3.6. Schematic of a wet cooling tower.

$$\varepsilon = \frac{Q^*}{m_a (h_{sai} - h_{ai})}. \tag{3.3}$$

The heat exchange between the refrigerant and the water in the condenser is modeled to determine the water temperature that enters the cooling tower. The heat exchange in the condenser is represented by:

$$Q^* = C_{min}(T_{wo,cond} - T_{wi,cond}) = C_{min}(T_{Refi} - T_{wi,cond}), \tag{3.4}$$

$$T_{w_i,cond} = T_{w_o,CT} = T_{wb,air}, \tag{3.5}$$

$$T_{w_o,cond} = T_{w_i,CT}.$$

where C_{min} is the minimum specific heat between the water and the refrigerant, and T_{Refi} is the refrigerant temperature entering the condenser. The minimum magnitude at which water temperature can be decreased inside the cooling tower is equal to the wet bulb temperature of the outside air. The wet bulb temperature, $T_{wb,air}$, is calculated from the following Eq. (3.5):

$$T_{wb,air} = T \operatorname{atan}[0.151977(RH\% + 8.313659)^{1/2}] + \operatorname{atan}(T + RH\%) - \operatorname{atan}(RH\% - 1.676331) + 0.00391838(RH\%)^{\frac{3}{2}} \operatorname{atan}(0.023101 RH\%) - 4.686035, \tag{3.6}$$

Air energy balance relates the cooling tower inlet and outlet conditions that combined with the effectiveness definition provides an expression that estimates the enthalpy of the outlet air based on the effectiveness magnitude, inlet air enthalpy and saturated inlet air enthalpy. The mixing ratio equation, which is related to temperature by the vapor pressure term, completes an equation system that determines the magnitude of the outlet temperature and specific humidity

$$Q^* = m_a(h_{ao} - h_{ai}), \tag{3.7}$$

$$h_{ao} = h_{ai} + \varepsilon(h_{sai} - h_{ai}), \tag{3.8}$$

$$C_p T_{ao} + q_{vao}(C_{pw} + L) = h_{ai} + \varepsilon(h_{sai} - h_{sai}), \tag{3.9}$$

$$q_{vao} = 0.62198\frac{e}{P-e}, \tag{3.10}$$

$$e = 6.11 \times 10^{\frac{7.5T_{ao}}{237.7+T_{ao}}}. \tag{3.11}$$

where h_{sai} is the enthalpy of saturated air at the inlet conditions. *Mechanical draft* towers use fans or blowers to cause air to counterflow upward against the down-flowing water droplets. Figure 3.7 shows a *forced-draft* cooling tower. In this equipment, air is forced to flow against the water droplet stream by use of an external centrifugal fan.

Figure 3.7. Photograph of induced draft cooling tower installation. (Courtesy of SPX Cooling Technologies, Inc., Overland Park, KS. With permission CRC Press [4].)

3.5.2 Air-Cooled Condensers

Small chillers [less than 100 tons (350 kW)] often use air-cooled condensers rather than water-cooled condensers and cooling towers, discussed above. Air-cooled condensers are simply cross-flow heat exchangers with refrigerant flowing and condensing inside of finned tubes. Fans force air over the exterior surface of the tubes and the fins. These condensers have modest maintenance requirements but may result in higher energy consumption and shorter compressor life, because condensing pressures are relatively high on summer days given typical air-to-refrigerant temperature differences, as discussed below.

Although much of the heat transfer involves isothermal phase change, some initial desuperheating and final liquid sub-cooling are usual. Figure 3.8 is a photograph of an air-cooled condenser. The effectiveness-Number of Transfer Units ($\in$-NTU) method can be used to calculate the performance of an air-cooled condenser of this type by dividing it into three heat exchange sections — two sensible and one latent [6].

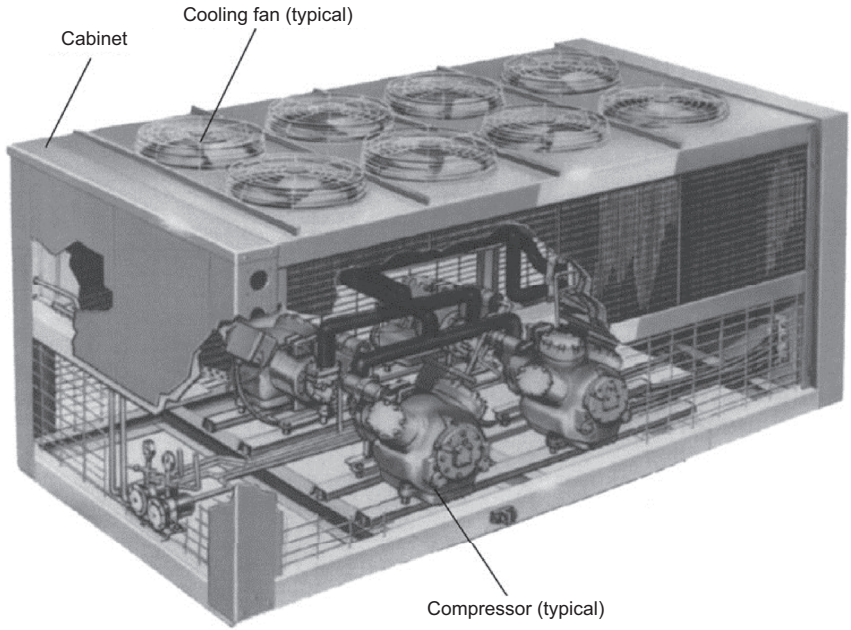

Figure 3.8. Photograph of air-cooled condenser bank located above compressor. (Courtesy of United Technologies/Carrier, Farmington, CT. With permission CRC Press [4].)

The design of air-cooled condensers requires the specification of:

1. *Heat rejection rate* — determined by chiller or air conditioner peak heat discharge rate.
2. *Airflow rate* — a balance between excessive pressure drop for high flow rates and high initial cost for large heat transfer surface. Usual values are 600 to 1200 ft^3/min per ton [80 to 160 L/s per kW]. Fan power consumption is typically 0.1 to 0.2 hp/ton (20 to 40 W/kW).
3. *Temperature difference* (refrigerant to entering air) — affected by decision in item 2 and heat rate from item 1. Typical values are 15°F to 40°F (8°C to 22°C).
4. *Noise* — large air-cooled condensers can be noisy. They should be located so that noise produced is not a nuisance to building occupants.
5. *Unobstructed airflow* — a supply of outdoor air is needed for proper operation. Short-circuiting of warm air leaving the condenser back to the condenser inlet must be avoided. The area near the condenser air inlet must be kept clean so that the coils do not become blocked off or fouled.

In addition to problems associated with high-temperature operation, air-cooled condensers require special controls to avoid excessive sub-cooling. High altitude also causes a reduction in air-cooled condenser capacity since the mass flow rate is reduced (because of lower air density), even though the fan produces the same volumetric flow.

A small cooling effect (up to 20% to 25% of full load) can be achieved by opening all valves in the refrigerant loop when the compressor is off. The free migration of refrigerant between the indoor evaporator (warm) and the outdoor condenser (cool) can produce some cooling without operating the compressor for a small fraction of the year.

3.6 Recommendations for Chiller System Operation in Commercial Buildings

Taking into account the part-load characteristics of chillers, cooling towers, fans, and pumps, Braun et al. [7] have prepared a set of rules for minimizing the energy consumption of chiller plants in commercial buildings. In a case study, the authors showed that chiller energy consumption could

be reduced from 26% to 43% compared with conventional fixed-speed equipment, if these rules are followed.

- If the cooling tower is constructed of several cells with variable-speed drives, operate all cells at the same speed.
- If the cooling tower is constructed of several cells with multiple-speed fans, increment the lowest-speed fans first when additional tower capacity is needed.
- Variable-speed condenser water pumps should be controlled with their associated chillers to give peak pump efficiency. If chillers have more than one fixed-speed pump, all pumps should be controlled so that they all operate at the same speed (assuming the common practice that the several pumps are all the same model). As described earlier, *great care must be used if cooling tower water flow is to be modulated*, since flow imbalance and freezing may occur.
- Multiple-chiller plants should be operated so that they all have the same chilled water set points and so that condenser and evaporator flows are proportional to each chiller's cooling capacity. There is not much difference in energy consumption for multiple-chiller plants operated in series or parallel.
- Parallel air handlers should all operate with the same air set points.
- Optimal sequencing of multiple chillers depends on the specific characteristics of the chillers. No general rules exist.

This relatively compact and simple set of rules was found because all the key characteristics of an *optimally operating chiller plant* — chilled water temperature, supply air temperature, cooling tower airflow rate, and cooling tower water flow rate (if allowed to vary) — are related nearly linearly to cooling load and wet-bulb temperature. Since control of building relative humidity (rarely done except for critical applications) imposes an additional constraint on the chiller plant, humidity control will always consume more energy than not controlling it will under typical commercial building conditions.

3.7 Cooling by Desiccant Equipment

Dehumidification processes can be used for cooling purposes. Excessive temperature reductions in refrigeration systems will lead to dehumidification by condensation if the temperature is below the dew point of the moist air. Air

can also be dehumidified, however, without cooling by use of hygroscopic materials which absorb or adsorb part of the water present in humid air. These hygroscopic materials are known as desiccants, and may be liquids or solids. If used for cooling, the dehumidification process must be associated with an air cooling process. The dehumidification in desiccants systems is usually associated with heat release and thus temperature increase of the air. The cooling of the air can be achieved by means of a *VC* or absorption system. Cooling of the air can also be achieved by addition of moisture by means of heat and mass exchange between air and atomized water or evaporative cooling.

Dehumidification can also be achieved by absorbing water vapor by a hygroscopic liquid. The important requirements of the liquid are its miscibility (i.e., capacity for dilution) with water and a water vapor pressure in the solution significantly lower than the partial pressure of water in moist air. The boiling point of the liquid must be much higher than that of water in order to be recycled and reused. Liquids that have been commercially used as liquid desiccants include calcium chloride, lithium chloride, and triethylene glycol. Kathabar, U.S.A. manufactures a line of liquid desiccant dehumidifiers for industrial applications. Figure 3.9 shows the basic processes of a liquid desiccant dehumidifier system. Room air is brought in contact with the warm liquid desiccant. The air goes to sensible or evaporative cooling process, while the dilute solution

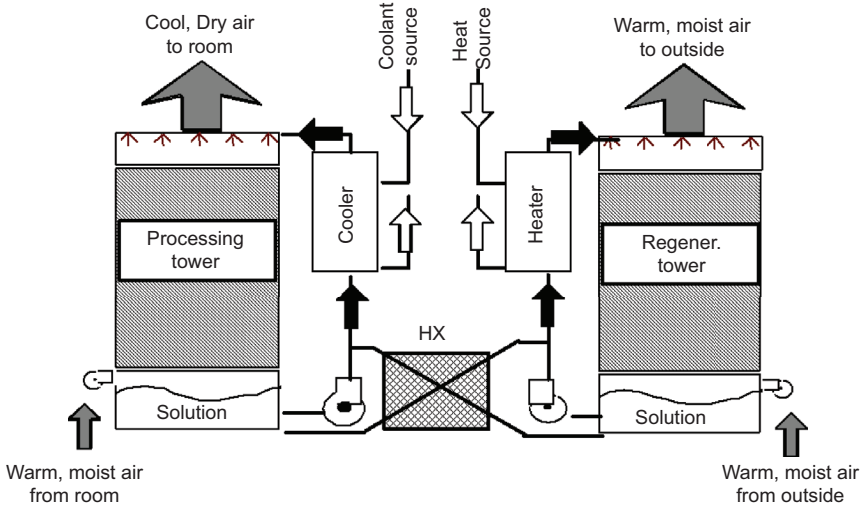

Figure 3.9. Basic liquid-desiccant machine.

of liquid desiccant goes to regenerator, in which exchanges heat to desorb the moisture gained which is then released into the environment. A heat exchanger is placed between the absorption and the desorption towers to pre-heat the liquid desiccant prior to the regeneration. Typical regeneration temperatures for liquid desiccant range from 60°C to 80°C, which are suitable for solar heating applications.

3.7.1 Performance Equations for Liquid Desiccant Equipment

In open absorption systems, flows of heat and mass take place to and from the system. Among these, dehumidification systems take the air in, either from outside or from the building, and absorb its moisture in a solid or liquid desiccant, cooling it also by exchange of sensible heat. The desiccant is then regenerated by using low-grade heat, such as that provided by solar collectors. Stevens et al. [8] have described a computationally efficient model of liquid-desiccant heat and mass exchangers derived from an effectiveness model of a cooling tower. The inlet solution and water conditions and the system *NTU* were needed, as well as an assumption of the exit conditions for the solution. A specific heat for saturated moist air was obtained from:

$$c_{P,sat} = \frac{dh_{T_s,sat}}{dT_s}. \tag{3.12}$$

Then, an effectiveness was calculated as:

$$\varepsilon = \frac{1 - e^{-NTU(1-m^*)}}{1 - m^* e^{-NTU(1-m^*)}} \tag{3.13}$$

where a capacitance ratio was defined by:

$$m^* = \frac{\dot{m}_a c_{sat}}{\dot{m}_{s,i} c_{P,s}}. \tag{3.14}$$

The outlet air enthalpy was expressed as:

$$h_{a,o} = h_{a,i} + \varepsilon(h_{T_s,sat} - h_{a,i}). \tag{3.15}$$

Using an energy balance, the outlet solution enthalpy could be obtained. An effective saturation enthalpy is defined as:

$$h_{T_s,sat,eff} = h_{a,i} + \frac{h_{a,o} - h_{a,i}}{1 - e^{-NTU}}. \tag{3.16}$$

With the corresponding effective humidity ratio, the outlet air humidity ratio can be calculated with:

$$\omega_{a,o} = \omega_{T_s,sat,eff} + \left(\omega_{a,i} - \omega_{T_s,sat,eff}\right) e^{-NTU}. \tag{3.17}$$

Mass balances and the known states can be used to calculate the outlet air temperature, the outlet solution mass flow rate, and new values for its concentration and temperature. Therefore, the previous procedure called for an iterative scheme. This approach has been used to model the solar-assisted hybrid air conditioning system [9]. In this case, first, an absorber inlet solution temperature was obtained such that the air leaving the absorber has the desired humidity for the supply air. Then, a regenerator inlet solution temperature was found to ensure that the moisture released in the regenerator was equal to the moisture added in the absorber.

3.8 Summary for Cooling Equipment

This chapter has so far considered the quantitative aspects of the design of mechanical and evaporative cooling central plants. Vapor compression and absorption cycles are both competitive and should be considered by the designer. Evaporative processes using water can reduce energy consumption in many ways, including reducing cooling loads, meeting part of the sensible load, or improving the performance of air-cooled condensers on chiller plants. Part-load performance of mechanical or evaporative cooling equipment must be considered to find the annual energy consumption needed for system optimization.

3.9 Heat Generation and Transfer Equipment

3.9.1 Introduction

This section discusses equipment used for producing heat from fossil fuels, electricity, or solar power. The emphasis is on design-oriented information including system characteristics, operating efficiency, the significance of part-load characteristics, and criteria for selecting from the vast array of heat-producing equipment available.

The heating plants discussed in this section are often called the *primary systems*. Systems intended to distribute heat produced by the primary

systems are called *secondary systems* and include duct and pipes, fans and pumps, terminal devices, and auxiliary components. Such secondary systems for heating and cooling are described elsewhere in this Handbook and are best understood after the primary heating and cooling systems described in this and the next chapters are well comprehended. The terms *primary* and *secondary* are equivalent to the terms *plant* and *system* used by some building analysts and HVAC system modelers.

The various and most common heat generation or transfer systems are:

- Furnaces & Boilers
- Heat pumps
- Radiant heating systems

The primary sources of heat for building heating systems are fossil fuels, natural gas, and various grades of fuel oil and coal. Electricity is used under certain circumstances for heat in commercial buildings, although the economic penalties for so doing are significant. Solar power can be converted to heat for applications in commercial buildings including perimeter zone heating and service water heating.

3.9.2 Furnaces and Boilers

Fossil fuel–fired *furnaces and boilers* — are devices that convert the chemical energy in fuels to heat. Furnaces heat airstreams that are used in turn for heating the interior of buildings. Forced-air heating systems supplied with heat by furnaces are the most common type of residential heating system in the United States and most parts of the develop countries. Boilers are pressure vessels used to transfer heat, produced by burning a fuel, to a fluid. The most common fluid used for this purpose in buildings is liquid water or water vapor. The key distinction between furnaces and boilers is that air is heated in the former and water is heated in the latter.

The fuels used for producing heat in boilers and furnaces include natural gas (i.e., methane), propane, fuel oil (at various grades numbered through 6), wood, coal, and other fuels including refuse-derived fuels. It is beyond the scope of this book to describe in detail the design of boilers and furnaces or how they convert chemical energy to heat. Rather we provide the information needed by HVAC designers for these two classes of equipment. Since boilers and furnaces operate at elevated temperatures

(and pressures for boilers), they are hazardous devices. As a result, a body of standards has been developed to ensure the safe operation of this equipment. We briefly describe this aspect of this equipment as well.

3.9.2.1 Furnaces

Modern furnaces use forced convection to remove heat produced within the firebox from its outer surface. There are very many designs to achieve this; four residential classifications based on airflow type are shown in Figure 3.10. The *upflow* furnace shown in Figure 3.10 has a blower located below the firebox heat exchanger with heated air exiting the unit at the top. Return air from the heated space enters this furnace type at the bottom. The upflow design is used in full-size mechanical rooms where sufficient floor-to-ceiling space exists for the connecting ductwork. This is the most common form of residential furnace.

Downflow furnaces work in reverse: Air flows downward as it is heated by passing over the heat exchanger. This design is used in residences without

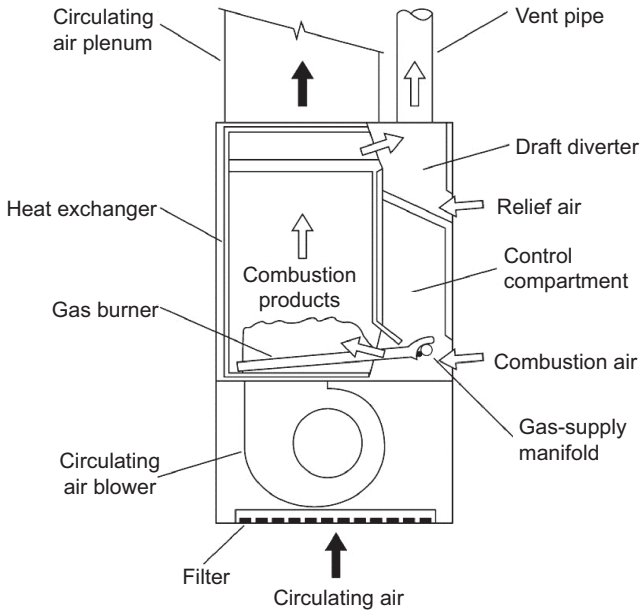

Figure 3.10. Examples of furnace for residential space heating: vertical. (With permission CRC Press [4].)

basements or in upstairs mechanical spaces in two-story buildings. *Horizontal* furnaces use a horizontal airflow path with the air mover located beside the heat exchanger. This design is especially useful in applications where vertical space is limited, for example, in attics or crawl spaces of residences.

The combustion side of the heat exchanger in gas furnaces can be at either atmospheric pressure (the most common design for small furnaces) or superatmospheric pressures produced by combustion air blowers. The latter are of two kinds: forced-draft (blower upstream of combustion chamber) or induced-draft (blower downstream of combustion chamber) furnaces that have better control of parasitic heat losses through the stack. As a result, efficiencies are higher for such *power combustion furnaces*.

In addition to natural gas, liquefied propane gas (LPG) and fuel oil can be used as energy sources for furnaces. LPG furnaces are very similar to natural gas furnaces. The only differences between the two arise due to the difference in energy content (1000 Btu/ft^3 for natural gas and 2500 Btu/ft^3 for propane) and supply pressure to the burner. Gas furnaces can be adapted for LPG use, and vice versa in many cases. Fuel oil burner systems differ from gas burner systems owing to the need to atomize oil before combustion. The remainder of the furnace is not much different from a gas furnace except that heavier construction is often used.

In terms of performance, the steady-state efficiency η_{furn} is defined as the fuel supplied less flue losses, all divided by the fuel supplied:

$$\eta_{furn} = \frac{(\dot{m}h)_{fuel} - (\dot{m}h)_{fuel,out}}{(\dot{m}h)_{fuel}} \tag{3.18}$$

in which the subscripts identify the fuel input and flue gas exhaust mass flow rates $\dot{m}$ and enthalpies h. Gas flows are usually expressed in cubic feet per hour (liters per second). Efficiency values are specified by the manufacturer at a single value of fuel input rate. Of course, one could use either greater or lesser flow rates, but the design flow rate is that at which the manufacturer's efficiency value applies. At higher fuel input rates, the furnace could overheat with hazardous results. Industry standards dictate the temperature limits allowable in furnaces and thereby limit the fuel input rates.

This instantaneous efficiency is of limited value in selecting furnaces owing to the fact that furnaces often operate in a cyclic, part-load mode where instantaneous efficiency may be lower than that at peak operating

conditions. Part-load efficiency is low since cycling causes inefficient combustion, cyclic heating and cooling of the furnace heat exchanger mass, and thermal cycling of the distribution ductwork. A more useful performance index is the *annual fuel utilization efficiency* (AFUE), which also accounts for other loss mechanisms over a season. These include stack losses, cycling losses, infiltration, and pilot losses [6]. An ASHRAE standard (103-1982R) is used for finding the AFUE for residential furnaces.

Table 3.1 shows typical values of AFUE for residential furnaces. The table shows that efficiency improvements can be achieved by eliminating

Table 3.1. Typical Values of AFUE for Furnaces.

Type of Gas Furnace	**AFUE, Percent**
1. Atmospheric with standing pilot	64.5
2. Atmospheric with intermittent ignition	69.0
3. Atmospheric with intermiteent ignition and automatic vent damper	78.0
4. Same basic furnace as type 2, except with power vent	78.0
5. Same as type 4 but with improved heat transfer	81.5
6. Direct vent with standing pilot, preheat	66.0
7. Direct vent, power vent, and intermittent ignition	78.0
8. Power burner (forced-draft)	75.0
9. Condensing	92.5
Type of Oil Furnace	**AFUE, Percent**
1. Standard	71.0
2. Same as type 1 with improved heat transfer	76.0
3. Same as type 2 with automatic vent damper	83.0
4. Condensing	91.0

Source: ASHRAE, *Handbook of Systems and Equipment*, American Society of Heating, Refrigerating and Air-Conditioning Engineers, Atlanta, GA, 2000.

standing pilots, by using a forced-draft design, or by condensing the products of combustion to recover latent heat normally lost to the flue gases. Efficiency can also be improved by using a vent damper to reduce stack losses during furnace-off periods. Although this table is prepared from residential furnace data, it can be used for commercial-size furnaces as well. Few data have been published for commercial systems since this has not been mandated by law, as it has been for residential furnaces. The AFUE has the shortcoming that a specific usage pattern and equipment characteristics are assumed. In the next section, we discuss a more accurate method for finding annual performance of heat-producing primary systems.

The AFUE can be used to find the annual energy consumption directly from its definition below. The fuel consumption during an average year $Q_{\text{fuel,yr}}$ is given by

$$Q_{fuel,yr} = \frac{Q_{yr}}{AFUE}[MBTu/yr; GJ/yr] \tag{3.19}$$

where Q_{yr} is the annual heat load. By using this approach it is a simple matter to find the savings one might expect, on average, by investing in a more efficient furnace.

In addition to energy consumption, the designer must be concerned with myriad other factors in furnace selection. These include:

- Air-side temperature rise; duct design and airflow rate affected
- Airflow rate; duct design affected
- Control operation (for example, will night or unoccupied day-night setback be used? Is the fan controlled by thermal switch or time-delay relay?)
- Safety issues (combustion gas control, fire hazards, high-temperature limit switch)

3.9.2.2 Boilers

A boiler is a device made from copper, steel, or cast iron to transfer heat from a combustion chamber (or electric resistance coil) to water in the liquid phase, vapor phase, or both. Boilers are classified both by the fuel used and by the operating pressure. Fuels include gas, fuel oils, wood, coal, refuse-derived fuels, and electricity. In this sub-section we focus

on fossil fuel-fired boilers. Boilers produce either hot water or steam at various pressures. For building applications, hot water is more widely used mechanism to transfer heat. Boilers for buildings are classified as:

- *Low-pressure*: Steam boilers with operating pressures below 15 psig (100 kPa). Hot-water boilers with pressures below 150 psig (1000 kPa); temperatures are limited to 250°F (120°C).
- *High-pressure*: Steam boilers with operating pressures above 15 psig (100 kPa). Hot-water boilers with pressures above 150 psig (1000 kPa); temperatures are above 250°F (120°C).

Heat rates for steam boilers are often expressed in pound-mass of steam produced per hour (or kilowatts). The heating value of steam for these purposes is rounded to 1000 Btu/lb_m. Steam boilers are available at heat rates of 50 to 50,000 lb_m/h of steam (15 to 15,000 kW).

Water boilers are available in the same range of sizes as steam boilers: 50 to 50,000 kBtu/h (15 to 15,000 kW). Hot water is used in buildings for space and water heating.

Since the energy contained in steam and hot water within and flowing through boilers is very large, an extensive codification of regulations has evolved to ensure safe operation. In the United States, the ASME Boiler and Pressure Vessel Code governs construction of boilers. For example, the code sets the limits of temperature and pressure on low-pressure water and steam boilers listed above.

Large boilers are constructed from steel or cast iron. Cast-iron boilers are modular and consist of several identical heat transfer sections bolted and gasketed together to meet the required output rating. Steel boilers are not modular but are constructed by welding various components together into one assembly. Heat transfer occurs across tubes containing either the fire or the water to be heated. The former are called *fire-tube boilers*, and the latter are *water-tube boilers*. Either material of construction can result in equally efficient designs. Small, light boilers of moderate capacity are sometimes needed for use in buildings. For these applications, the designer should consider the use of copper boilers. Figure 3.11 is a photograph of a steam boiler.

The HVAC engineer must specify boilers based on a few key criteria. In this section we list these but do not discuss the internal design of boilers and their construction. Boiler selection is based on the following criteria:

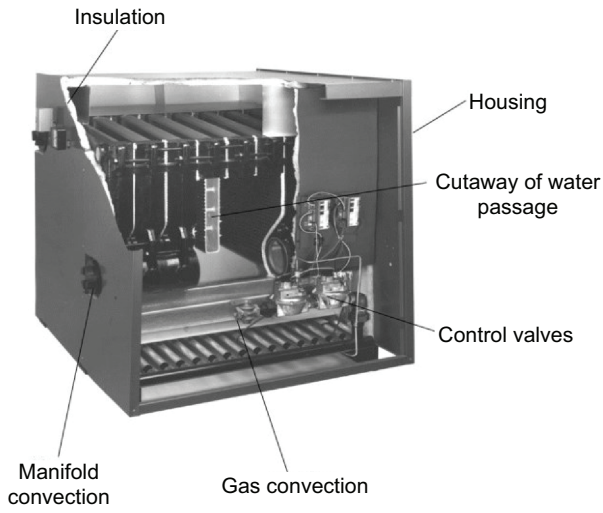

Figure 3.11. Cutaway photograph of boiler. (With permission CRC Press [4].)

- *Boiler fuel*: type, energy content, heating value including altitude effects if gas-fired (no effect for coal or fuel oil boilers)
- *Required heat output*: net output rating, kBtu/h (kW)
- *Operating pressure and working fluid*
- *Efficiency and part-load characteristics*
- *Other*: space needs, control system, combustion air requirements, safety requirements, ASME code applicability

The boiler heat output required for a building is determined by summing the *maximum heating requirement* of all zones or loads serviced by the boiler during peak demand for steam or hot water and adding to that (1) parasitic losses including piping losses and (2) initial loop fluid warm-up. Simply adding all the *peak heating unit capacities* of all the zones in a building can result in an oversized boiler, since not all zones require peak heating simultaneously. Additional boiler capacity may be needed to recover from night setback in massive buildings. This transient load is called the *pickup* load and must be accounted for in both boiler and terminal heating unit sizing.

Boilers are often sized by their *sea-level input* fuel ratings. Of course, this rating must be multiplied by the applicable efficiency to determine the gross output of the boiler. In addition, if a gas boiler is not to be located at sea level, the effect of altitude must be accounted for in the rating. Some boiler designs

use a forced-draft burner to force additional combustion air into the firebox, to offset part of the effect of altitude. Also enriched or pressurized gas may be provided at high altitude so that the heating value per unit volume is the same as that at sea level. If no accommodation to altitude is made, the output of a gas boiler drops by approximately 4% per 1000 ft (13% per 1 km) of altitude above sea level. Therefore, a gas boiler located in Denver, Colorado (5000 ft, 1500 m), will have a capacity of only 80% of its sea-level rating.

Table 3.2 shows the type of data provided by manufacturers for the selection of boilers for a specific project. Reading across the table, the fuel input needs are first tabulated for the 13 boiler models listed. Column 5 is the sea-level boiler output at the maximum design heat rate. Columns 6 to 9 convert the heat rate to steam and hot-water production rates. Column 10 expresses the heat rate in still a different way, by using units of boiler horsepower (=33,475 Btu/h or 9.8 kW). Columns 11 to 14 provide information needed for designing the combustion air supply system and the chimney.

According to the Boiler Efficiency Institute [10], the efficiency of a steam boiler η_{boil} can be found from field measurements by

$$\eta_{boil} = \frac{\dot{Q}_{steam}}{\dot{m}_{fuel}\left(HHV\right)} \tag{3.20}$$

where

$\dot{Q}_{steam}$ is the steam output rate, Btu/h (kW)
$\dot{m}_{sfuel}$ is the fuel supply rate, lbm/h (kg/s)
HHV is higher heating value of fuel, Btu/lb (kJ/kg)

An additional efficiency is defined for boilers, the combustion efficiency. It can be determined experimentally to ascertain the condition of the fuel combustion equipment, including burners, heat transfer surfaces, and combustion air supply equipment. As noted earlier, efficiency under specific test conditions has very limited usefulness in calculating the annual energy consumption of a boiler because of significant dropoff of efficiency under part-load conditions. For small boilers [up to 300 kBtu/h (90 kW)], the Department of Energy has set forth a method for finding the AFUE. The annual energy consumption must be known in order to perform economic analyses for optimal boiler selection.

For larger boilers, data specific to a manufacturer and an application must be used to determine annual consumption. Efficiencies of fossil fuel

Table 3.2. Example of Manufacturer's Boiler Capacity. (From Ref [4].)

Boiler Unit Number, Steam, or Water (1)	IBR Burner Capacity: Light Oil, gal/h (2)	IBR Burner Capacity: Gas, kBtu/h (3)	IBR Burner Capacity: Min. Gas Press. Req'd., inWG (4)	Gross IBR Output, Btu/h (5)	Net IBR Ratings: Steam, ft^2/h (6)	Net IBR Ratings: Steam, Btu/h (7)	Net IBR Ratings: Water, Btu/h (8)	Net Heat Transfer Area, ft^2/H_2O (9)	Boiler hp (10)	Net Firebox Volume, ft^3 (11)	Stack Gas Volume, ft^3/min (12)	Positive Pressure in Firebox, inWG (13)	IBR Chimney Size Vent Dia., in (14)
486°F	6.30	882	5.5	720,000	2,250	540,100	626,100	4,175	21.5	11.02	395	0.34	10
586°F	8.25	1,155	7.0	940,000	2,940	705,200	817,400	5,450	28.1	14.45	517	0.35	10
686°F	10.20	1,428	5.5	1,160,000	3,625	870,200	1,008,700	6,725	34.6	18.08	640	0.35	10
786°F	12.15	1,701	6.0	1,380,000	4,355	1,044,700	1,200,000	8,000	41.2	21.61	762	0.36	12
886°F	14.10	1,974	6.5	1,600,000	5,115	1,227,900	1,391,300	9,275	49.6	25.14	884	0.37	12
986°F	16.05	2,247	7.0	1,820,000	5,875	1,409,800	1,582,600	10,550	54.3	28.67	1,006	0.38	14
1086°F	18.00	2,520	6.5	2,040,000	6,600	1,583,900	1,773,900	11,825	60.9	32.20	1,128	0.39	14
1186°F	19.95	2,793	7.0	2,260,000	7,310	1,754,700	1,965,200	13,100	67.5	35.73	1,251	0.40	14
1286°F	21.95	3,073	7.0	2,460,000	8,025	1,925,500	2,156,500	14,375	74.1	39.26	1,376	0.41	14
1386°F	23.90	3,346	6.5	2,700,000	8,735	2,096,300	2,347,800	15,650	80.6	42.79	1,498	0.42	14
1486°F	25.90	3,626	7.5	2,920,000	9,445	2,267,100	2,539,100	16,925	87.2	46.32	1,623	0.43	16
1586°F	27.85	3,899	7.5	3,140,000	10,160	2,437,900	2,730,900	18,200	93.8	49.85	1,746	0.44	16
1686°F	29.75	4,165	8.5	3,350,000	10,835	2,600,900	2,913,000	19,420	100.1	53.38	1,865	0.45	16

Source: Courtesy of Weil-McLain, Inc., Michigan City, IN. With permission.
Note: 1 bhp = 33,475 Btu/h – 9.8 kW.

boilers vary with heat rate depending on the internal design. If the boiler has only one or two firing rates, the continuous range of heat inputs needed to meet a varying heating load is achieved by cycling the boiler on and off. However, as the load decreases, efficiency decreases since the boiler spends progressively more time in transient warm-up and cooldown modes, during which relatively less heat is delivered to the load. At maximum load, the boiler cycles very little, and efficiency can be expected to be near the rated efficiency of the boiler. Part-load effects can reduce average efficiency to less than one-half of the peak efficiency. Of course, for an oversized boiler, the average efficiency is well below the peak efficiency since it operates at part load for the entire heating season. This operating-cost penalty persists for the life of a building long after the designer who oversized the system has forgotten the error.

3.9.3 Electric Resistance Heating

Electricity can be used as the heat source in both furnaces and boilers. Electric units are available in the full range of sizes from small residential furnaces (5 to 15 kW) to large boilers for commercial buildings (200 kW to 20 MW). Electric units have four attractive features:

- Relatively lower initial cost
- Efficiency near 100%
- Near-zero part-load penalty
- Flue gas vents not necessary

The high cost of electricity (both energy and demand charges) diminishes the apparent advantage of electric boilers and furnaces, however. Nevertheless, they continue to be installed where first cost is a prime concern. The prudent designer should consider the overwhelming life cycle costs of electric systems, however. Electric boiler and furnace sizing follows the methods outlined above for fuel-fired systems. In many cases, the thermodynamic and economic penalties of pure resistance heating can be reduced by using electric heat pumps, the subject of next subsection.

Environmental concerns must also be taken into account in considering electric heating. Low conversion and transmission efficiencies (relative to direct combustion of fuels for water heating) result in relatively higher CO_2 emissions. Also SO_2 emissions from coal power plants are an environmental concern.

3.9.4 Electric Heat Pumps

Actual heat pump systems depart significantly from the Carnot cycle method. Most system in common use today are of the vapor compression type. The method of analysis is of vapor-compression heat pumps is the same as vapor compression cooling systems described earlier in this chapter. Also, the previous discussion of concerning the departure of actual systems from ideal conditions apply for vapor-compression heat pump systems. As shown in Figure 3.12, a typical vapor-compression heat pump for space heating has the basic components of the vapor compression cooling system: compressor, condenser, expansion valve, and evaporator. The objective of the system, however, is different. In a heat pump system, $\dot{Q}_{in}$ comes from the outside, and $\dot{Q}_{out}$ is directed to the building as the desired effect. A net work input, electrical in most cases, is needed to accomplish this goal. The COP of a simple vapor compression system

$$COP = \frac{h_2 - h_3}{h_2 - h_1} \tag{3.21}$$

Where the values of the enthalpies correspond to those of Figure 3.12. The COP of electrical heat pump systems can never be less than unity.

Many sources of heat transfer to the refrigerant passing through the evaporator are available including outside air, the ground, large water

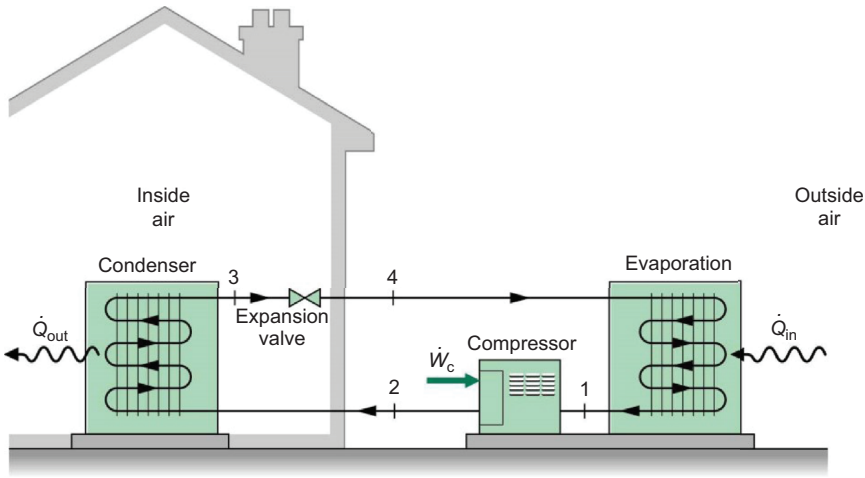

Figure 3.12. Air-source vapor compression heat pump system. (From Ref [11].)

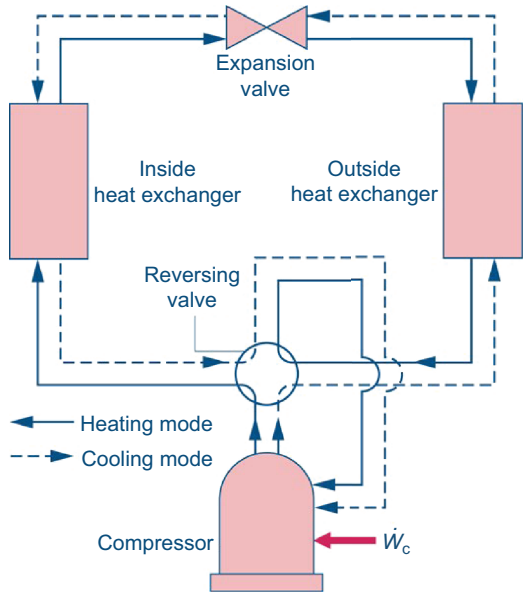

Figure 3.13: Air-to-air reversing heat pump compression system. The solid (dashed) lines show the operation on heating (cooling) mode. (From Ref [11].)

bodies such as lakes or rivers, or well water. Liquid water circulated through solar collectors and stored in insulate tanks can also be used as heat source for heat pumps. Industrial heat pumps employ waste heat to warm liquid or gas streams as the low temperature source and are capable of achieving high condenser temperatures.

In the most common type of vapor-compression systems for space heating, the evaporator communicates thermally with the outside air. Such are source heat pumps also can be used to provide cooling the summer with the use of a reversing valve, as shown in Figure 3.13.

3.9.5 Low-Temperature Radiant Heating Systems

Heating systems in many parts of the world use warmed floors and/or ceilings for space heating in buildings. Although this system is less commonly used in the United States, the good comfort and quiet operation provided by this approach make it worth considering for some applications. Radiant systems are well suited to operation with heat pump, solar, and

other low-temperature systems. In this section, we discuss the principles of low-temperature space heating. This is distinct from high-temperature radiant heating using either electricity or natural gas to provide a high-temperature source from which radiation can be directed for localized heating.

Figure 3.14 shows how a radiant floor might be configured in a residence. The same concept can also be used in the ceiling in both residential and commercial buildings. The term *radiant* is a misnomer since between 30% (ceilings) and 50% (floors) of the heat transferred from "radiant" panels is actually by convection. However, we use the industry's nomenclature for this heating system.

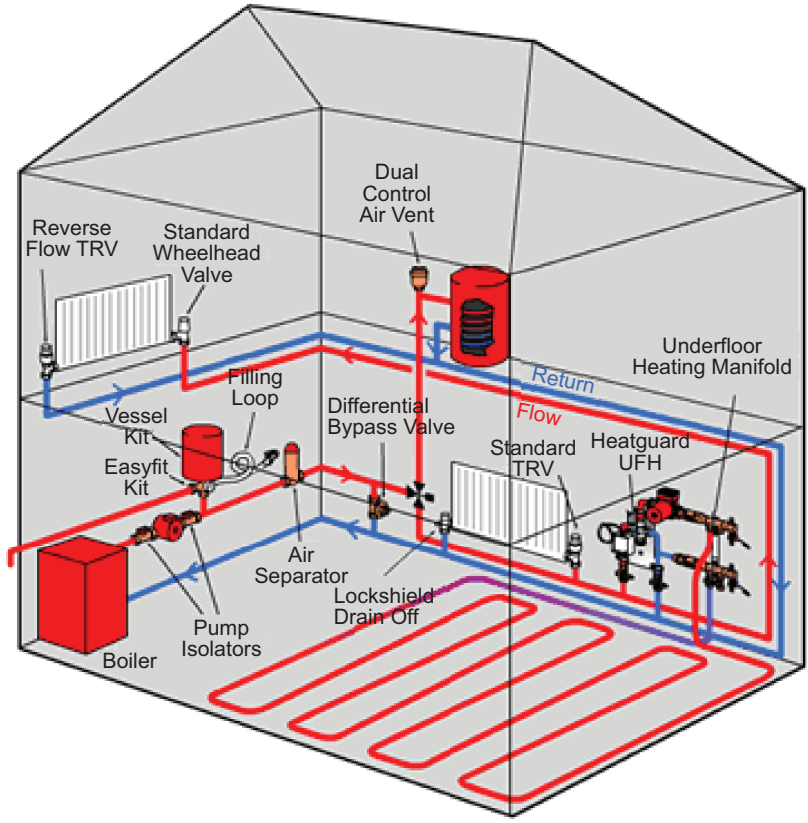

Figure 3.14. Sample of residential radiant floor heating system.

The radiation heat output of radiant panels is given by the Stefan-Boltzmann equation,

$$\dot{Q}_{h-u} = \varepsilon_{eff} F_{h-u} \sigma \left(T_h^4 - T_u^4 \right) \tag{3.22}$$

where

$\varepsilon_{eff} = \dfrac{1}{\dfrac{1}{\varepsilon_h} + \dfrac{1}{\varepsilon_u}}$ is the effective emittance of space; subscripts h and u refer to heated and unheated (by radiant panels) surfaces of space; ε_{eff} is approximately 0.8

$F_{h\text{-}u}$ = if the geometric view factor between heating surface and unheated surfaces. In most cases this value could be considered to be 1 due to the internal characteristic of the radiant surface (inside the building) to be an enclosure.

T_h = heating surface temperature

T_u = mean of unheated surface temperatures

σ = Stefan-Boltzmann constant.

The convection from the heating surface can be found by using standard free-convection expressions [12–13].

The designer's job is to determine the panel area needed, its operating temperature, the heating liquid flow rate, and construction details. The panel size is determined based on standard heat load calculations. Proper account should be made of any losses from the back of the radiant panels to unheated spaces. Panel temperatures should not exceed 85°F (29.5°C) for floors and 115°F (46°C) for ceilings.

Water temperatures are typically 120°F (49°C) for floors and up to 155°F (69°C) for ceilings. Panels can be piped in a series configuration if pipe runs are not excessively long (the final panels in a long series run will not perform up to specifications due to low fluid temperatures). Long series loops also have excessively high pressure drops. If large areas are to be heated, a combination of series and parallel connections can be used. Manufacturer's advice should be sought regarding the number of panels that can be connected in series without performance penalties.

If radiant floors are to be built during building construction rather than used as prefabricated panels in ceilings, the following guidelines can be used: Tubing spacing for a system of the type shown in Figure 3.14 should be between 6 and 12 in. (15 and 30 cm). The tubing diameter ranges

between 0.5 and 1.0 in. (1.2 and 2.5 cm). Flow rates are determined by the rate of heat loss from the panel, which in turn depends on the surface temperature and hence the fluid temperature. This step in the design is iterative. Panel design follows this process:

1. Determine the room heat load.
2. Decide on the location of panels (roof or floor).
3. Find panel heat flux, including both radiative and convective contributions at 80°F (27°C) for floor panels and 110°F (43°C) for ceiling panels.
4. Divide heat load by heat flux to find needed panel area.
5. If panel area exceeds available floor or ceiling area, raise panel temperature (not exceeding temperatures noted earlier) and repeat steps 3 and 4.
6. If the panel area is still insufficient, consider both floor and ceiling panels to improve thermal quality of room insulation.

Control of radiant heating systems has proved to be a challenge in the past due to the large time constant of these systems. Both under- and overheating are problems. If the outdoor temperature drops rapidly, this system will have difficulty responding quickly. On the other hand, after a morning warm-up followed by high solar gains on a sunny winter day, the radiant system may overshoot. The current generation of "smart" controls should help improve the comfort control of these systems. Radiant heating systems are becoming widely popular in residential systems and commercially available. Companies such as Warmboard Inc. (http://www.warmboard.com), or RadiantTec (http://www.radiantec.com) provide comprehensive systems in The United States.

3.10 Secondary Equipment: Air Handling Units

Secondary systems are those that meet the HVAC needs of specific zones. They consist of air and liquid handling equipment, duct and pipe systems, and heating and cooling terminal devices including coils, mixing boxes, and baseboard heating units.

The energetic or economic measure of the effectiveness of the HVAC system depends almost solely on its efficiency of operation at part-load conditions since the system spends so much of its time at less than peak-load conditions. The proper design of HVAC systems is subject to several criteria:

1. Standards of comfort — temperature, humidity, air motion, noise, cleanliness
2. Standards of economic and energetic efficiency — low initial and operating costs and energy consumption subject to the criteria in item 1
3. Standards of safety — embodied in codes and laws applicable to buildings
4. Desires of the owner as specified initially in the architectural program and on an ongoing basis during the design process at design meetings
5. Effective communication between all design professionals and ongoing documentation of the design process

Air is the medium used in the majority of HVAC systems to condition spaces of many types. Either air can be supplied from a central plant or a heated or cooled liquid can heat or cool air within a space. The earliest methods for cooling a building used natural or mechanical ventilation with outdoor air.

Ventilation is defined as the supply or removal of air from a space by mechanical or natural means. Meeting comfort conditions will often require conditioning of this air by heating or cooling it or by humidifying or dehumidifying it or by both. Ventilation serves two purposes:

- Addition or removal of heat and/or humidity from occupied spaces
- Supply of fresh air to meet health requirements

Systems of the type shown in Figure 3.15 are commonly used for supplying air for both purposes in buildings, and are referred as Air Handling Units (AHU). When the AHU in Figure 3.15 is used for cooling, the air leaves the cooling coil (connected to the primary system chiller) at about 55°F (13°C) in conventional systems. Ordinarily some dehumidification is also achieved in the cooling coil. The heating coil is not active. On the other hand, when heating is required, the air delivery temperature for heating is approximately 90 to 105°F (32 to 40°C) or above in conventional systems. During heating, the cooling coil is inactive in this simple system.

The supply air fan draws air through the coils and causes it to flow into the space to be conditioned. According to the conservation of mass, the amount of air supplied to the space must also be removed from it, except for differences which may be caused by infiltration or exfiltration. The return air duct and fan serve to remove air from the zone. Under conditions

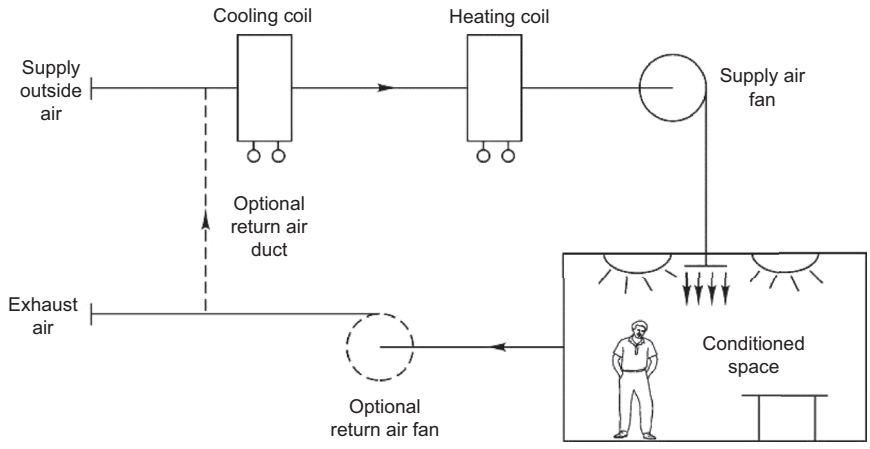

Figure 3.15. Simplified secondary HVAC system for a single zone.

of significant heating or cooling, considerable energy and cost have been expended to condition room air. Instead of discarding this air after a single pass through the space, a portion can be reused. This is the purpose of the return air duct. The amount of room air that must be discarded depends on the fresh air supply requirements, which we discuss next.

3.10.1 Fresh Air Ventilation Rates

The requirement for fresh air in buildings is set by the need to dilute indoor contaminants so that their concentration never exceeds established threshold levels. Building occupants and materials are the main source of pollutants that require control. (The amount of oxygen consumed by human metabolism is very small in typical occupancy densities in buildings and is not the main determinant for fresh air supply.) Contaminants in buildings include radon, formaldehyde, various other organic compounds, particulates, carbon dioxide, tobacco smoke, odors, and nitrogen oxides. Since the control of each contaminant in a building is impossible from a practical point of view, carbon dioxide concentration can be taken as an approximate surrogate for all other contaminants, at least those related to human activity. To maintain a minimum CO_2 concentration indoors, C_i in the presence of its evolution by humans requires a ventilation rate $\dot{V}$ given by

$$C_i = C_0 + \frac{\dot{V}_g}{\dot{V}} \tag{3.23}$$

Table 3.3. Fresh Air Ventilation Requirements.

Application	ft^3/min per Person	L/s per Person
Dining rooms	20	10
Hotel room	30 (per room)	15 (per room)
Offices, conference rooms	20	10
Public smoking lounge	60	30
Retail stores	0.20–0.30 $ft^3/(min \cdot ft^2)$	1.0–1.5 $L/(s \cdot m^2)$
Auditorium	15	8
School classroom	15	8
Hospital patient room	25	13
Residential living areas	0.35 air change/h but >15ft^3/min per occupant	0.35 air change/h but >7.5 L/s per occupant

Source: Courtesy of ASHRAE, *Standard 62–1999: Ventilation for Acceptable Indoor Air Quality*, American Society of Heating, Refrigerating and Air-Conditioning Engineers, Atlanta, GA, 1999b.

Where

C_o = outdoor volumetric concentration of CO_2; dimensionless, for example, percent or parts per million commonly used

$\dot{V}_g$ = generation rate of CO_2 by occupants, ft^3/min (L/s)

$\dot{V}$ = needed outdoor ventilation rate, ft^3/min (L/s)

Given the known rate of evolution and the threshold level of CO_2 to be permitted (about 0.1%) and a measure of conservatism, ASHRAE Standard 62-1999 [15] specifies that each person in a building should be supplied with at least 15 ft^3/min (7.5 L/s) of fresh air. Table 3.3 shows the amount of fresh air to be supplied based on the type of space and level of activity. "Fresh" air can be either outdoor air or treated indoor air with minimal contaminant levels. In some cities, outdoor air is quite contaminated and unsuitable for use in buildings. In such cases, other techniques such as particulate control by mechanical filtration, electronic filtration, air washing to remove gaseous contaminants, or use of activated charcoal are needed to provide fresh air.

3.11 High Efficiency System Integration

3.11.1 Chiller Water Loops and VAV Systems

In order to take advantage of the new technologies developed for HVAC systems, including air handling units, pumping systems and high efficiency refrigeration equipment, different schemes have been designed.

The variable air volume system (VAV) associated to variable speed dual cooling loop system, will be discussed.

An air conditioned area has a variable cooling load during the day, week, and year. This creates a necessity to follow the cooling load with the required amount of air. A typical air cooling load for a specific area can have the profile presented in Figure 3.16.

A single unit system, associated to that cooling profile can be represented according to Figure 3.17. The equation representing the sensible heat removed from the conditioned area can be written as:

$$\dot{Q}_s = 1.2\dot{V}\Delta T \tag{3.24}$$

Where

$\dot{Q}_s$ = sensible heat to be removed from the conditioned space (W)

$\dot{V}$ = standard volumetric flow required to remove the heat, (L/s)

ΔT = Temperature difference between the conditioned space and the supply air (°C)

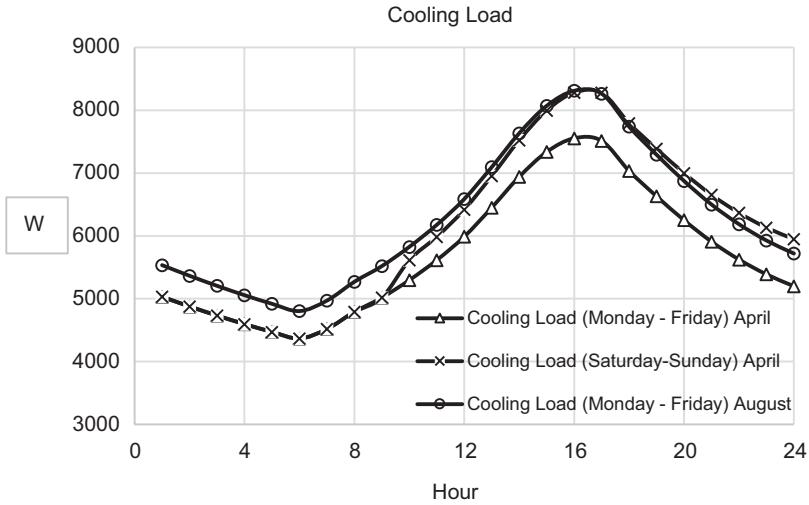

Figure 3.16. Typical cooling load in for different schedules.

And the latent heat removed can be written as:

$$\dot{Q}_L = 3010\dot{V}\Delta w \tag{3.25}$$

Where

$\dot{Q}_L$ = latent heat to be removed from the conditioned space (W)
$\dot{V}$ = standard volumetric flow required to remove the heat, (L/s)
w = humidity difference between the conditioned space and the supply air (kg of water vapor/kg of dry air)

For a fixed volume system, the cooling load is managed by changing the supply air temperature. According to Eq. (3.24), this is obtained by changing the temperature difference. For a variable air system, this is attained by changing the amount of air being supplied to the space. This requires to introduce some control elements in the system, and they are presented in Figures 3.17 and 3.18. The amount of air required by the room is modified by introducing a Variable Air Volume Box, VAV Box. This box receives a signal from a temperature controller that is sensing the temperature inside the conditioned space. If the temperature rises over the temperature set point, the signal being sent by the temperature

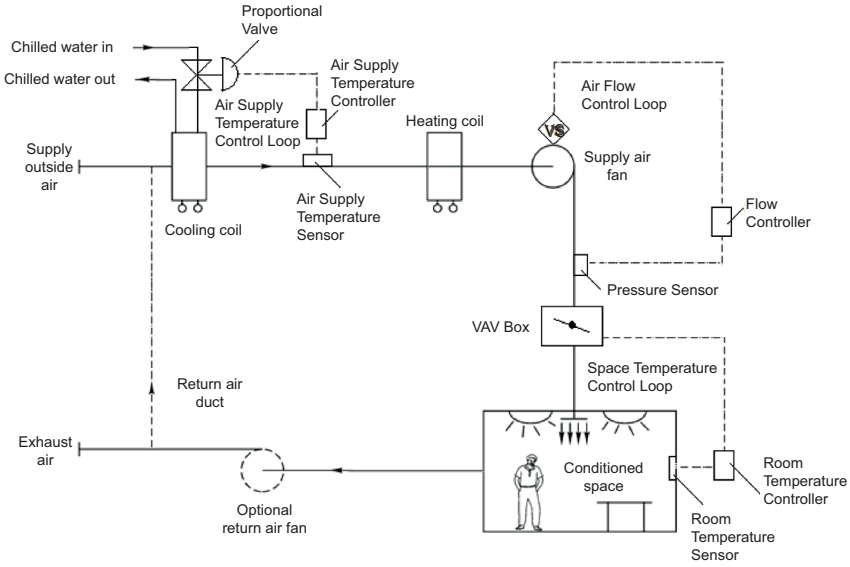

Figure 3.17. Variable air volume system control loops.

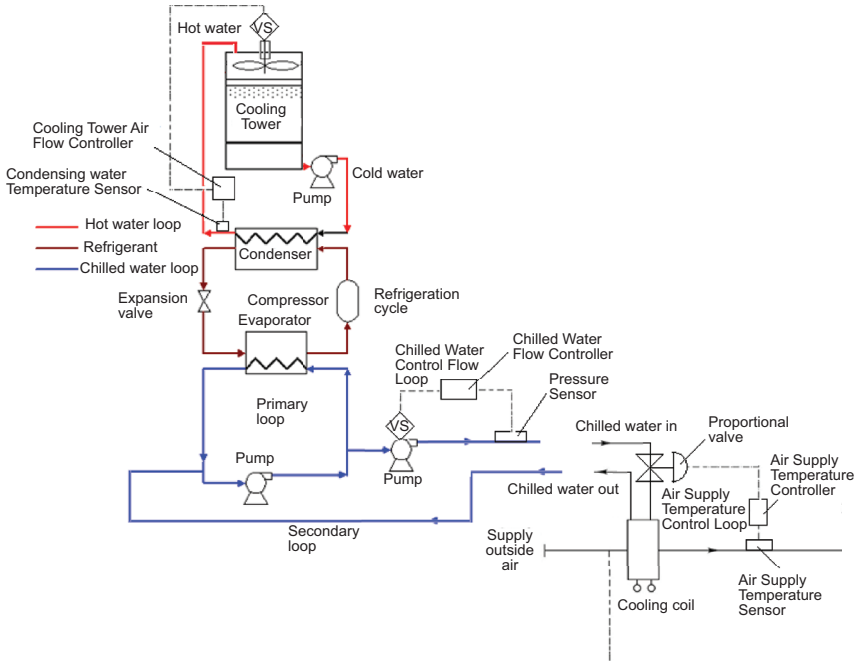

Figure 3.18. Variable air volume system control loops with chill water cooling system.

sensor is interpreted by the controller and the VAV Box is opened by an electro-mechanical device allowing more air to flow in the space. On the other hand, if the temperature drops below the temperature set point, the VAV Box is closed. At all times, the temperature of the supplied air remains constant. This is the first control loop: Space Temperature Control Loop.

As the VAV Box closes, this increases the temperature upstream the VAV Box. If no action is taken, the fan will accommodate itself to the new pressure condition, nevertheless, the energy consumption will remain high due to the high pressure in the duct. The second loop: Air Flow Control loop, consists of a pressure sensor and a flow controller that changes the fan speed. The VAV Box closes because the temperature of the room is below the set point, this increases the pressure upstream the VAV Box. The Flow controller receives the signal from the pressure sensor indicating that the air flow can be reduced and the speed fan is then reduced. If the room temperature increases, the VAV Box opens, the pressure upstream the VAV Box decreases and the flow controller increases the fan speed.

The power required by the fan is proportional to the flow and proportional to the second power of the speed in the duct. If the flow is reduced, energy is saved because the flow is reduced to the required value and the pressure drop in the duct is also reduced.

The third loop, the Air Supply Temperature Control Loop is used to maintain a constant supply temperature. If the air flow is reduced, the air supply temperature will decrease. A temperature sensor send that signal to the air supply temperature controller, indicating that the proportional valve located at the inlet of chiller water to the cooling coil can be proportionally closed. If the flow increases, the system increases the chilled water flow through the cooling coil.

The fourth control loop is established between the building and the pump moving the chilled water from the facilities room. As the proportional valves (there is one proportional valve for each different air handling unit), close due to temperature drop in the conditioned space, the pressure at the exit of the pump increases. A pressure sensor located at the discharge of the pump (it needs to be located before any other valve or flow restrictor element) sends a signal to the chilled water flow controller. This controller reduces then, the speed of the pump.

The fifth control loop is internal to the refrigerating machine, and depends on the technology being used. The manufacturers have proprietary technology for their equipment.

The sixth and final control loop is located at the cooling tower. The water flow going through the condenser, for most of the equipments, is constant independently of the cooling load. As the temperature of the water coming from the condenser decreases, a temperature sensor sends a signal to the cooling tower air flow controller, and this reduces the speed of the cooling tower fan.

As it is noticed, the control cascade is able to accommodate to the cooing load of the building, and it achieves the desired energy consumption reduction. Alvarez et al. [15, 16], performed an energy analysis to the following system.

The results obtained showed that using a VAV system operating with the control loops discussed, achieved savings up to 43% in energy consumption for ventilation and up to 18% in energy consumption for entire system (Table 3.4).

TABLE 3.4. Chiller and System Energy Performance (From Alvarez et al. [15]).

Chiller (Only)					System (Chiller plus pumps and cooling tower)	
% Load	**TON**	**kW**	**EER**	**kW/TON**	**kW**	**kW/TON**
100.0	85.9	63.8	16.2	0.7	78.7	0.9
72.6	63.4	45.1	16.8	0.7	56.1	0.9
50.0	43.0	30.0	17.2	0.7	37.5	0.9
22.6	19.4	13.5	17.3	0.7	16.8	0.9

3.11.2 Energy Recovery Systems

The energy savings can also be achieved by the introduction of energy recovery systems, especially in zones where the humidity is extremely high. A schematic showing how the system is installed is presented in Figure 3.19.

The air being exhausted from the conditioned space, is used to remove part of the sensible and, occasionally, part of the latent heat of the outside air being used for ventilation purposes. This is achieved by having a heat exchanger. According to Figure 3.19, the temperature at T_4 (Conditioned space temperature) is lower than T_1 (Outside air temperature), and this

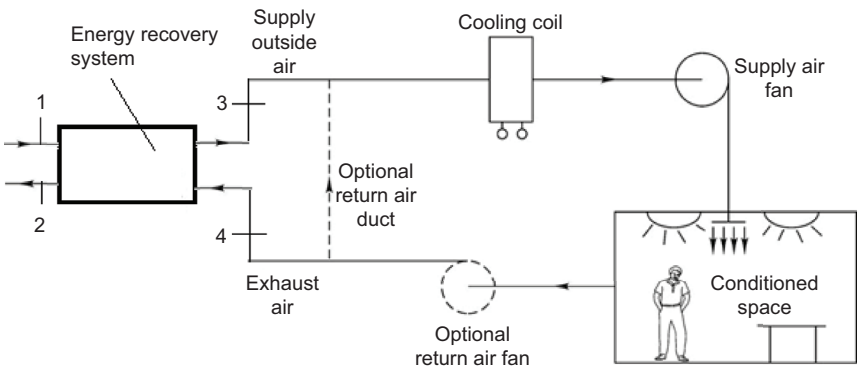

Figure 3.19. Energy recovery system for a cooling HVAC system for a single zone.

energy potential is used to remove sensible heat. In case T_4 is lower than the dew point at point 1, humidity will be removed from the ventilation air.

Some other systems, have a rotary enthalpy wheel. In this case, the wheel is made out of an adsorbent material, able to remove humidity from the outside air being used for ventilation. In order to bring the rotary enthalpy wheel back to an operational condition, the wheel is heated to remove the humidity adsorbed in the process. The ventilation air suffers a temperature increment and a humidity reduction. Because of that, the exhaust air used to cool down the air as it comes out of the rotary wheel.

The final effect of this recovery system, is to reduce the cooling power required by the air handling unit.

3.12 Future Trends of HVAC Mechanical Systems

3.12.1 Supervisory Control Systems

The air conditioning systems have been taking advantage of the electronic developments in order to have more efficient equipment, able to follow the thermal load and accommodate to the user requirements. These abilities require an increment in the complexity of the control system, a supervising control strategy to manage the different control loops, automatic systems with the programmed knowledge to respond to the building necessities, and at the end, the air conditioning systems become a complex system that is difficult to trouble shoot in case of failure.

The new trends will require development of supervisory systems, able to oversee the operation in real time, which will have to learn to recognize if the system is operating adequately or if it is presenting a malfunctioning condition. The supervisory will have to be flexible enough to learn from any building, and the operational knowledge will be proprietary for that building. Nevertheless, the logic behind the learning process have to be applicable for any building, it has to be flexible enough to accept as many signals coming from the field, and it will have to be able to make decisions identifying if a failure is present or it is in front of a non-common operation in between the operational conditions. This system will require centralizing every single signal from the field, and it will have to analyze it in a statistical manner among many other signals, and it will have to be able to recognize patterns, create thresholds, and finally make a decision to report if a failure has been detected.

Traditional systems, where an operator can check every signal will no longer be viable, humans are not able to follow hundreds of signals [17] and they are not able to recognize failure patterns when hundreds of signals are present [18].

3.12.2 Heat Exchanger Materials

Heat exchangers are required to perform at different conditions, especially in refrigeration equipment where variable flow is used (refrigerant, air, water). For the fluids involved, this represents a change in the heat transfer mode, either at the evaporator or the condenser. In order to keep the heat transfer coefficients at a level capable of removing the heat even at low speeds, change in the materials performance or "behavior" can be considered [19].

New materials are being developed and used for this purpose [20, 21] and the results have shown these new materials used to manufacture heat exchangers are able to improve the heat transfer conditions at the outer surface of the air side.

For internal conditions, researchers have been working to enhanced heat transfer conditions, and experiments are being developed for pool boiling [22]. Still, research needs to be done in order to have pipes able to enhance the heat transfer process at different mass flow rates.

The last developments in materials have brought a new important characteristic, expected to enhance heat transfer: plasmons. Many different options are being considered, and the most extreme but the most beneficial for the planet would be a non-moving parts air conditioning system. Think about walls, made out of especial materials absorbing heat from inside the building, reflecting shortwave near the visible and infrared spectrum, and emitting in the middle infra-red wavelengths. This situation will allow cooling buildings in the middle of the summer, and helping to reduce the energy consumption from mechanical refrigeration systems. This initiative has been led by the US Department of Energy through the Sun Shot program [23].

3.12.3 Surface Enhancing Heat Transfer

Heat transfer can be enhanced by changing the surface characteristics of the heat exchangers. Many different options have been considered,

depending on the fluid phase: either gas, liquid or a multiphase flow. In the case of a evaporator, one of the main ideas is to increase nucleation sites, boundary layer break-up and reattachment as well as interfacial turbulence. These surface enhancements look for a size reduction and an increment in the heat transfer coefficient, even at very small flows [24]. Fins have also been improved, and micro fins are used to improve the heat transfer characteristics [25].

New developments associated to nano structures will create smaller and more efficient heat exchangers, and mainly, they will be able to handle variable flow equipment. This will allow not only guarantee the temperature but humidity control as well.

References

[1] The 1987 Montreal Protocol on Substances that Deplete the Ozone Layer. United Nations Development Program. Downloaded on Sep 5, 2016: http://ozone.unep.org/en/handbook-montreal-protocol-substances-deplete-ozone-layer/27571

[2] Bolaji, B. O., and Huan, Z. (2013). Ozone Depletion and Global Warming: Case for the Use of Natural Refrigerant — A Review. Renewable and Sustainable Energy Reviews, (18), 49–54.

[3] ASHRAE (2009). ASHRAE Handbook-Fundamentals. American Society of Heating, Refrigerating, and Air Conditioning Engineers Inc., Atlanta, GA. 544pp.

[4] Kreider, J. F., Curtiss, P., and Rabl, A. (2009). Heating and Cooling of Buildings: Design for Efficiency. 2nd Revised Edition. CRC Press, Boca Raton.

[5] Stull, R. (2011). Wet-Bulb Temperature from Relative Humidity and Air Temperature. Journal of Applied Meteorology and Climatology, 50, 2267–2269, doi:10.1175/JAMC-D-11-0143.1.

[6] ASHRAE (2000). Handbook of Systems and Equipment. American Society of Heating, Refrigerating and Air-Conditioning Engineers, Atlanta, GA.

[7] Braun, J. E., Mitchell, J. W., Klein, S. A., and Beckman, W. A. (1987). Performance and Control Characteristics of a Large Cooling System. ASHRAE Transactions, 93(pt. 1), 1830–1852.

[8] Stevens, D. I., Braun, J. E., and Klein, S. A. (1989). An Effectiveness Model of Liquid-Desiccant System Heat/Mass Exchangers. Solar Energy, 42, 449–455.

[9] Hernández, H. R., González, J. E., and Khan, A. Y. (1997). A Parametric Study of Solar-Assisted Air Conditioning and Dehumidification Systems Operating in the Caribbean Region, Solar Engineering, 327–334.
[10] David, F., and Maples, G. (1991). Boiler Efficiency Improvement, 5th ed. Boiler Efficiency Institute, Auburn University, Auburn, Ala.
[11] Moran, M. J., and Shapiro, H. N. (2008). Fundamentals of Engineering Thermodynamics. 6th Ed. Wiley, NY.
[12] Rohsenow, W. M., Hartnett, J. P., and Ganic, E. N., (Eds.), Handbook of Heat Transfer Fundamentals, McGraw-Hill.
[13] Bergman, T. L., Lavine, A. S., Incropera, F. P., and DeWitt, D. P. Fundamentals of Heat and Mass Transfer, 7th Edition. John Wiley & Sons.
[14] ASHRAE Standard 62-1999. Ventilation for Acceptable Air Quality Standards. American Society of Heating, Refrigerating, and Air Conditioning Engineers Inc., Atlanta, GA.
[15] Alvarez, O., Sanjuan, M., Amaya, F., and Bula, A. (2013). VAV System Operating in an Educational Building under Tropical Conditions: Energy Analysis. In ASME 2013 7th International Conference on Energy Sustainability collocated with the ASME 2013 Heat Transfer Summer Conference and the ASME 2013 11th International Conference on Fuel Cell Science, Engineering and Technology (pp. V001T14A002–V001T14A002). American Society of Mechanical Engineers.
[16] Alvarez, O., Sanjuan, M., Amaya, F., and Bula, A. (2013). VAV System Operating in an Educational Building under Tropical Conditions: Modeling and Simulation. In ASME 2013 International Mechanical Engineering Congress and Exposition (pp. V011T06A023–V011T06A023). American Society of Mechanical Engineers.
[17] Smith, C. A., and Corripio, A. B. (2005). Principles and Practice of Automatic Process Control. New York: Wiley.
[18] Portnoy, I., Melendez, K., Pinzon, H., and Sanjuan, M. (2016). An Improved Weighted Recursive PCA Algorithm for Adaptive Fault Detection. Control Engineering Practice, 50, 69–83.
[19] Huang, L. (2015). A Survey of Optimization Formulations and Techniques for the Design of Heat Exchangers Using Lower GWP Refrigerants. ASHRAE Transactions, 121, 1MM.
[20] Ryu, H. Y., Yoon, S. H., Han, D. H., Hafeez, H., Paluvai, N. R., Lee, C. S., and Park, J. G. (2016). Fabrication of Hydrophobic/Hydrophilic Switchable Aluminum Surface Using poly (N-isopropylacrylamide). Progress in Organic Coatings, 99, 295–301.

[21] Ganesan, P., Vanaki, S. M., Thoo, K. K., and Chin, W. M. (2016). Air-Side Heat Transfer Characteristics of Hydrophobic and Super-Hydrophobic Fin Surfaces in Heat Exchangers: A Review. International Communications in Heat and Mass Transfer, 74, 27–35.
[22] Van Rooyen, E., and Thome, J. R. (2013). Pool Boiling Data and Prediction Method for Enhanced Boiling Tubes with R-134a, R-236fa and R-1234ze (E). International Journal of Refrigeration, 36(2), 447–455.
[23] US Department of Energy SunShot Initiative. (2012). Sun-Shot Vision Study. Washington, DC.
[24] Guo, S. P., Wu, Z., Li, W., Kukulka, D., Sundén, B., Zhou, X. P., and Simon, T. (2015). Condensation and Evaporation Heat Transfer Characteristics in Horizontal Smooth, Herringbone and Enhanced Surface EHT Tubes. International Journal of Heat and Mass Transfer, 85, 281–291.
[25] Yeom, T., Simon, T., Zhang, T., Zhang, M., North, M., and Cui, T. (2016). Enhanced Heat Transfer of Heat Sink Channels with Micro Pin Fin Roughened Walls. International Journal of Heat and Mass Transfer, 92, 617–627.

4 Passive Cooling and Heating Techniques for Buildings

Zhiqiang (John) Zhai and Ning Feng

Abstract

Sun, earth, sky, and atmosphere are adequate, fundamental and renewable resources that can be taken advantage of to increase building comfort while reduce building energy use. Passive cooling and heating techniques not only save building energy consumption but also demonstrate significant comfort and health benefits, as well as human preference. This chapter introduces the general principles and considerations of utilizing passive cooling and heating techniques for sustainable building development. Seven commonly used passive cooling and heating techniques are further discussed in details. The chapter focuses on presenting general principles, thermal and energy performance, and key design considerations of these techniques.

4.1 Introduction

Building has significant impacts on the environment and natural resources. The construction, maintenance, and demolition of buildings consume tremendous natural resources and energy and produce significant environment pollutions. The emerging world energy and environment crises demand a substantial revolution of building design philosophies, strategies, technologies, and construction and management methods. Historically, human are smart enough to utilize natural forces and resources to cool, heat, and ventilate spaces. Over the course of time, dwellings have evolved to respond to challenges of climate, building materials and cultural expectations in a given place through a long period of trial and error and the ingenuity of local builders who possess specific knowledge about their place on the planet. Passive architecture varies widely with the world's vast spectrum of climate, terrain and culture. It contains significant information and knowledge

on how to optimize the energy performance of buildings at low cost using local materials.

Sun, earth, sky, and atmosphere are adequate, fundamental and renewable resources that can be taken advantage of to increase building comfort while reduce building energy use (Table 4.1). Good understanding of heat transfer mechanisms (conduction, convection, radiation, evaporation, and condensation) between earth ground, environment, and building elements will facilitate proper designs that fully use the cooling and heating capacity of ambient conditions (solar, air, sky etc.).

In addition to saving on energy, passive cooling and heating techniques typically demonstrate significant comfort and health benefits, as well as human preference. For instance, research has shown that the acceptable thermal comfort range for naturally ventilated buildings is noticeably larger than for buildings with standard mechanical HVAC systems. The generally high level of occupant control associated with passive buildings is also thought to contribute to the acceptance of warmer indoor temperature. Furthermore, passive systems have been shown to consistently outperform mechanical systems with respect to complaints of Sick Building Syndrome (SBS) and its associated symptoms. Generally, when building occupants are more satisfied with their working environment, their productivity and job satisfaction also increase. The advantages of using passive techniques are, hence, significant beyond the energy benefit.

This chapter first introduces the general principles and considerations of utilizing passive cooling and heating techniques for sustainable building development. A brief checklist is presented to prescreen the feasibilities of using passive cooling and heating techniques for specific projects.

Seven commonly used passive cooling and heating techniques are then discussed in details. The chapter focuses on presenting general principles, thermal and energy performance, and key design considerations of these techniques. The introduced passive techniques are classified into three categories based on the functions:

1. Passive cooling techniques: including natural ventilation; night cooling and thermal mass; and evaporative cooling.
2. Passive heating techniques: including Trombe wall and sunspace.
3. Combined passive cooling and heating techniques: including double skin façade and phase change material.

Table 4.1. Heat Transfer Mechanisms and Sources for Passive Cooling and Heating.

	Conduction	Convection	Radiation	Evaporation
Passive cooling	Adjust insulation	Reduce infiltration	Reduce solar gain	Use evaporative cooling
	Use earth cooling	Use ventilation	Use radiant cooling	
Passive heating	Increase insulation	Reduce infiltration Reduce external airflow	Increase solar gain	
Source	Atmosphere; earth	Atmosphere	Sun; sky	Atmosphere

4.2 Overview of Passive Cooling

Before the technology of refrigeration, people use many natural methods to keep themselves cool such as wind through windows, water evaporating from pools and fountains and stone or earth for storing extra heat. People developed these ideas thousands of years ago which are being called "passive cooling" in today's terminology [1]. Passive cooling is defined as *"Passive cooling is a building design approach that focuses on heat gain control and heat dissipation in a building in order to improve indoor thermal comfort with low or none energy consumption. This approach works either by preventing heat from entering the interior (heat gain prevention) or by passively removing heat from the building (natural cooling). Natural cooling utilizes on-site energy, available from the natural environment, combined with the architectural design of building components (e.g., building windows), rather than mechanical systems, to dissipate heat."* [2] People are able to reduce the capital cost and operation cost of the equipment and even eliminate the cooling energy by adopting passive cooling [1].

Passive cooling can be implemented in a number of approaches with different heat sinks (Figure 4.1): natural ventilation, double-skin façade, night pre-cooling, earth cooling, and evaporative cooling. Proper natural cooling design must rely on a detailed study of the local climate, integrated building design strategies, and often advanced computational

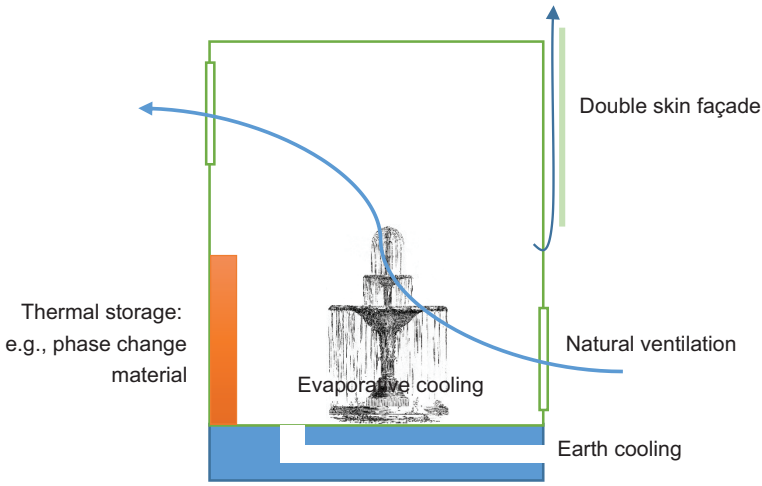

Figure 4.1. Illustration of passive cooling techniques.

analysis. A successful passive design is intrinsically integrated with the architectural design making an integrated building design process necessary. Natural ventilation is one of the most popular and important passive cooling strategies that can be generally divided into two categories: wind-driven natural ventilation and buoyancy-driven natural ventilation. Wind-driven natural ventilation uses the air pressure differential across the building, caused by wind, to drive ventilation air through the building. This type of design is highly dependent upon the external site weather conditions. Buoyancy-driven natural ventilation, also called the stack effect, uses the principle of thermal stratification in buildings to induce airflow through the building. This technique is different from wind-driven natural ventilation in that it does not rely on the ambient wind for motivating ventilation air. Buoyancy-driven flow is typically used with atriums, clerestories, solar chimneys, and courtyards.

Night cooling and earth cooling are two other important and widely used passive cooling techniques that use night-time cool ambient air and the earth as heat sinks to remove the heat stored during the daytime. Evaporative cooling is most appropriate in dry semi-arid to arid climates, and consists of using the latent heat of evaporation of water to cool incoming air. Evaporative cooling systems are used quite often in the Southwest United States. It should be noted that passive cooling systems can be combined with conventional mechanical ventilation technologies, for example, solar-assisted ventilation systems. The adoption of passive systems can largely reduce the size and energy use of active ventilation systems.

4.3 Overview of Passive Heating

Passive heating utilizes the solar and thermal energy to keep occupants' comfort without the use of mechanical systems. Passive solar heating is one of primary passive heating methods focusing on the effective use of solar energy. When integrated properly, these passive strategies can collectively contribute to the heating, cooling, and daylighting of nearly any building. The types of buildings that benefit from the application of passive heating may range from barracks to large maintenance facilities.

Typically, passive solar heating involves [3]:

- Collection of solar energy through properly-oriented (e.g., south-facing) glazing;

- Storage of this energy in "thermal mass," comprised of building materials with high heat capacity such as concrete slabs, brick walls, and tile floors;
- Distribution of the stored energy back to the living space, when required, through the mechanisms of natural convection and radiation

Passive solar design is the act of designing a building envelope, primarily the orientation and fenestration, to capture the solar to heat a building. Some of the first examples of passive solar design were in ancient Greece, 2500 years ago. Passive solar heating systems usually have a low initial cost and short-term payback period, both of which are common with many active solar heating systems. Passive solar heating will bring user comfort a lot which is another benefit. If properly designed, passive solar buildings are able to provide a delightful place to live and work as well as contributing to increased satisfaction and user productivity [3]. A variety of different passive solar techniques are currently used in building design, including: direct gain systems, thermal storage walls, and sunspaces (Figure 4.2).

Direct gain systems allow the direct solar radiation to strike surfaces in a building. The heat from solar radiation is stored in these surfaces and then released later during the day. The main disadvantage to this approach is that the large amount of direct solar radiation in the living space can cause UV deterioration and sun fading of fabrics and dyes, as well as causing glare and thermal discomfort for the occupants. Thermal storage walls are thus proposed that are typically located at the south façade of a building,

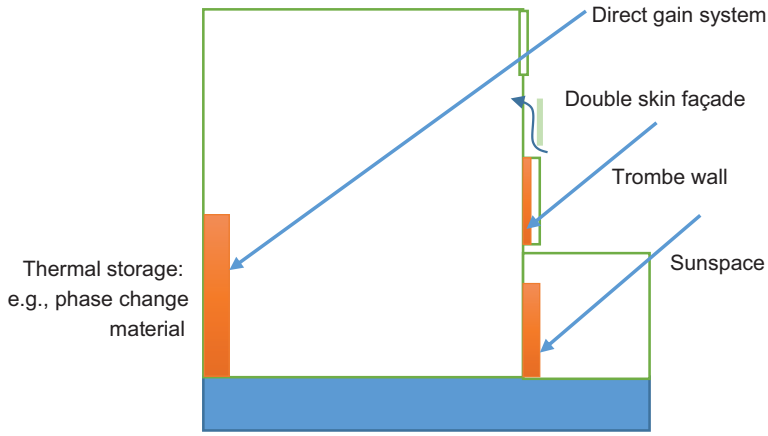

Figure 4.2. Illustration of passive heating techniques.

which receive direct solar radiation and transfer the heat through the wall by conduction at a delayed time step. The conducted heat is distributed to the space by convection and radiation. This approach is a response to the drawbacks of the direct gain system and can provide far greater comfort in the room. Integrated design of these two systems can ensure that heat is introduced to the space at the desired time of a day. Another direct heating design with passive solar is the sunspace. While, a sunspace will generally not provide all of the required heating, it can make a positive contribution. Sunspaces have the added benefit of connecting the outdoor and indoor environments, as well as providing additional livable space.

4.4 Prescreening Feasibility of Passive Cooling and Heating Techniques

Passive cooling and heating techniques use natural resources to condition building living spaces, and thus are highly sensitive to environmental conditions. Similar design strategies may be applicable for one project but the other, even at the same location under the same climate. Surrounding buildings and environments (e.g., water body, terrain, landscaping, etc.) will all play an important role in determining appropriate passive cooling and heating strategies and techniques for a specific project. In addition, due to the large variation (or instability) of climatic conditions with time, passive techniques typically are difficult to maintain strictly specified indoor environment conditions (e.g., temperature, humidity, acoustics, lighting etc.) to the level that most mechanical systems can achieve. Buildings with rigorous environmental control needs such as hospitals, clean-rooms, laboratories may not be suitable for using passive cooling, heating and ventilation techniques. Table 4.2 presents a check list to prescreen the feasibility of using passive strategies for specific building projects. The shaded blocks represent the feasibility of project environment conditions (e.g., climate) and design conditions (e.g., function, indoor environment quality need, and budget) for passive technique applications. Note that "low" or "high" value of some conditions may be good for one passive technique while unideal for another passive technique. As a result, multiple appropriate values (low, medium, high) are selected for various possible passive solutions for different heating, cooling and ventilation needs.

A host of computational tools are developed to assist the design of passive cooled and heated buildings at different design stages. Simple tools, such as Ecotect and Climate Consultant, can determine the viability

Table 4.2. Prescreening Checklist for Feasibility of Using Passive Strategies.

	Passive Cooling			Passive Heating		
	Low	**Medium**	**High**	**Low**	**Medium**	**High**
Climate						
Temperature						
Relative humidity						
Solar						
Precipitation						
Micro-climate						
Terrain						
Landscape						
Shadow						
Air pollution						
Noise						
Indoor Environment Requirement						
Thermal comfort						
Air quality						
Lighting quality						
Acoustic quality						
Building Function						
Activity type/ intensity						
Schedule variation						
Occupant age						
Space availability for systems						
Budget						
First cost						
Utility rate						
Maintenance cost						

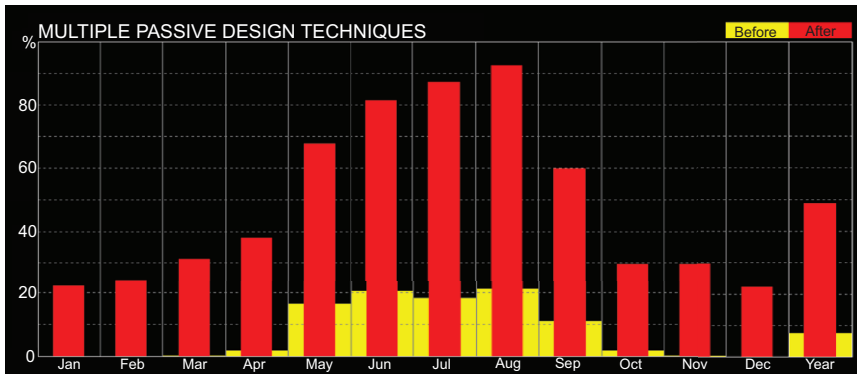

Figure 4.3. Potential savings of passive techniques used in Boulder, CO estimated by Ecotect.

and potential saving of specific passive techniques by analyzing climate data (Figure 4.3). This conclusion, however, does not consider specific project features (e.g., orientation, geometry, indoor design criteria, human activities etc.) and surrounding environment conditions (e.g., surrounding buildings, atmospheric quality etc.). Passive design is truly case-dependent. Although rules-of-thumb can be found in literature for various passive techniques and these rules are of great value for preliminary design, an in-depth design and optimization of passive cooling, heating and ventilation techniques requires advanced simulation tools to quantify and compare the performance of different solutions. It is important, however, to note that advanced models are only as accurate as the inputs, which can be difficult in the case of passive designs with many unknowns or uncertainties. For example, weather data that most simulation programs require may not account for the local climatic variations (e.g., wind speed and direction). A proper passive design will only occur through a detailed analysis of microclimate, site conditions, and building design.

4.5 Natural Ventilation

4.5.1 Principle

With an increased awareness of human comfort and the environmental impacts of energy use, natural ventilation has become an attractive approach for reducing energy use and for providing acceptable indoor

environmental quality. It plays an important role in maintaining a healthy, comfortable, and productive indoor climate rather than the more prevailing approach of using mechanical ventilation [4].

Natural ventilation is the process of supplying and removing air through an indoor space by natural means, that is, without the use of a fan or other mechanical system [5]. Air is driven by pressure differences between the building and its surroundings or among different building zones. Natural wind and buoyancy effect caused by temperature difference and humidity difference are the two main reasons causing pressure differences. The amount of ventilation depends on the size and placement of openings in the building. Transom windows, louvers, grills, or open plans are techniques to complete the airflow circuit through a building. Smoke and fire transfer requirements challenge the designer when designing a natural ventilation system.

4.5.2 Performance

4.5.2.1 Energy Consumption

There are many researches focusing on the energy usage reduction by taking advantage of natural ventilation. In favorable climates and buildings types, natural ventilation can be used as an alternative to air-conditioning systems, saving 10% to 30% of total energy consumption. A 30% reduction of the cooling energy consumption and 40% reduction of the installed cooling capacity were predicted for a UK low-energy office building with a night stack ventilation air exchange of 10 per hour [6]. 40% reduction of the daily cooling demand was simulated for a high thermal mass office building in Belgium [7]. Night ventilation air changes of 8 per hour can reduce cooling requirements by 12% to 54%, depending on the temperature set-point [8]. The primary energy consumption of naturally ventilated office buildings in Denmark was compared with mechanical ventilation systems. The naturally ventilated buildings consumed 40 kWh/m2 per year, whereas the mechanical systems consumption varied from 50 kWh/m^2 per year (VAV system) to 90 kWh/m^2 per year (CAV). The primary energy conservation for naturally ventilated office buildings in Belgium was calculated to be 8 kWh/m^2 per year [9]. Studies conducted for the 23 story Liberty Tower of Meiji University in Tokyo showed that about 17% of energy consumption for cooling is saved by using the natural ventilation system [10].

4.5.2.2 Thermal Comfort and Health

Besides offering benefits of energy usage reductions, many research and field experiments have shown that the occupants' thermal response in naturally ventilated spaces depend in part on the outdoor climate and may differ from thermal responses in buildings with centralized HVAC systems because of different thermal experiences, changes in clothing, availability of control and shifts in occupant expectations. The acceptable thermal comfort range for naturally ventilated buildings is significantly larger than for buildings with standard mechanical HVAC systems. According to this, ASHRAE Standard 55 has been revised to include an adaptive thermal comfort standard specifically for naturally ventilated buildings, which allows for increasing indoor temperatures as outdoor temperature increases. Figure 4.4 is the acceptable operative temperature ranges for naturally conditioned spaces from ASHARE Standard 55-2010 "Thermal Environmental Conditions for Human Occupancy" [11]. This adaptive model relates acceptable indoor operative temperature ranges to mean monthly outdoor temperature (defined as arithmetic average of mean monthly minimum and maximum air temperature). This information can be found easily by examining readily available climate data. Natural ventilation systems have been shown to consistently outperform mechanical systems with respect to complaints of Sick Building Syndrome and its associated symptoms.

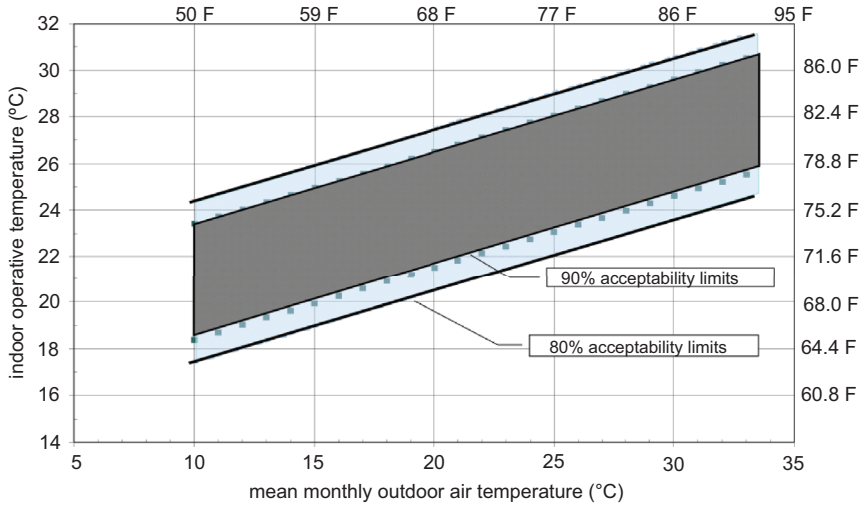

Figure 4.4. Comfort zone in naturally ventilated spaces [11].

Sepannen and Fisk [12] in a review of 18 different studies on SBS and ventilation systems, found that prevalence of SBS symptoms was 30% to 200% higher in air conditioned buildings as compared to naturally ventilated ones.

4.5.3 Design Considerations

Natural ventilation can be divided into: wind driven vs buoyancy driven (stack) natural ventilation according to driving forces; cross vs single-sided natural ventilation according to opening settings. Figure 4.5 illustrates the rule of thumb for the space depths penetrable by cross and single-sided ventilation. This rule of thumb indeed matches the prescriptive requirements for natural ventilation in ASHRAE 62.1 standard "Ventilation for Acceptable Indoor Air Quality" [13]. ASHRAE 62.1 further requires the openable area of wall openings directly to the outdoors is a minimum of 4% of the net occupiable floor area being naturally ventilated.

Wind-driven natural ventilation: when wind blows across a building, the wind hits the windward wall causing a direct positive pressure and after the wind moves around the building and leaves the leeward wall it leaves a negative pressure (Figure 4.6). If there are any openings on the windward and leeward walls of the building at the same time, fresh air will rush in the windward wall opening and exit the leeward wall opening. Thus the pressures on the windward and leeward walls can be balanced [5]. In summer and/or shoulder seasons when outdoor air temperature is appropriate, wind can be used to remove indoor heat and provide fresh air; while in winter, ventilation is normally reduced to the level that is sufficient to remove excess moisture and pollutants.

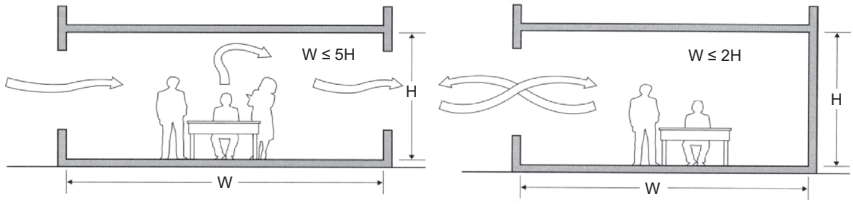

Figure 4.5. Rule of thumb for the maximum space depths for cross and single-sided.

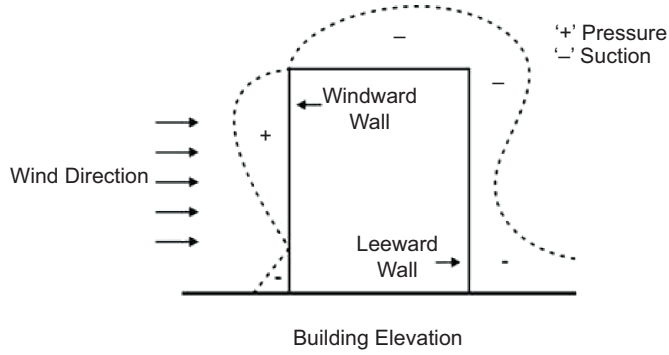

Figure 4.6. Diagram of wind driven ventilation [5].

The air volume flow rate induced by wind can be calculated via:

$$Q_{wind} = K \times A \times V \tag{4.1}$$

where Q_{wind} is the volume of airflow (m^3/h); A is the area of smaller opening (m^2); V is the outdoor wind speed (m/h); K is the coefficient of effectiveness. The coefficient of effectiveness depends on the angle of the wind and the relative size of entry and exit openings. It ranges from about 0.4 for wind hitting an opening at a 45-degrees angle of incidence to 0.8 for wind hitting directly at a 90-degrees angle.

Buoyancy driven natural ventilation: both temperature gradient (known as stack ventilation) and humidity disparity (known as cool tower) can induce airflow, due to the air density difference caused by temperature and humidity. Stack ventilation is the most commonly used ventilation strategy when outdoor wind is not sufficient. In stack ventilation, the temperature difference between warm air inside the building and cool air outside can move the air in the building to rise and exit at upper openings, while air is supplemented from outside via lower openings.

The airflow rate induced by the stack effect can be estimated as:

$$Q_{stack} = C_d * A * [2gh(T_i - T_o)/T_i]^{1/2} \tag{4.2}$$

where Q_{stack} is the volume of ventilation rate (m^3/s); C_d is the discharge coefficient (e.g., 0.65); A is the net area of inlet opening (m^2), which equals area of outlet opening; g is the acceleration due to gravity (9.8 m/s^2); h is the vertical distance between inlet and outlet midpoints

(m); T_i = average temperature of indoor air (K); T_o = average temperature of outdoor air (K).

Similarly, buoyancy caused by differences in humidity can allow a pressurized column of wet and cool air to naturally enter a space and repel the dry and warm indoor air from the top. Cool tower ventilation is most effective where outdoor humidity is low and evaporation can be directly applied. Prediction of airflow rate induced by humidity difference can be somewhat involved. The following equation (3) for estimating the airflow rate in humidity-based ventilation is based on the expression developed by Thompson, with the coefficient from the data measured at Zion National Park Visitor Center that has a cool tower of 7.4 m tall, 2.4 m^2 cross section, and a 3.1 m^2 opening [4].

$$Q_{\text{cool tower}} = 0.49 * A* [2gh (T_{db} – T_{wb})/T_{db}]^{1/2} \quad (4.3)$$

where $Q_{\text{cool tower}}$ is volume of ventilation rate (m^3/s); 0.49 is an empirical coefficient calculated with data from Zion Visitor Center, UT, which includes humidity density correction, friction effects, and evaporative pad effectiveness; A is the free area of inlet opening (m^2), which equals area of outlet opening; g is the acceleration due to gravity (9.8 m/s^2); h is the vertical distance between inlet and outlet midpoints (m); T_{db} = dry bulb temperature of outdoor air (K); T_{wb} = wet bulb temperature of outdoor air (K).

In design practice, stack ventilation and cool tower can be combined by having a cool tower deliver evaporative air to a space, and then relying on the increased buoyancy of the warm air to exhaust heat through upper stacks. In the design of a naturally ventilated building, climate conditions, location topography and vegetation, and surrounding objects all need be carefully evaluated. Wind data collected at local airports may not tell much about microclimates that can be heavily altered by natural and man-made obstructions around the building site. Window openings should be accessible and operable by the occupants. A naturally ventilated structure often includes an articulated plan and large window and door openings, while an artificially conditioned building is sometimes best served by a compact plan with sealed windows.

When designing ***wind driven natural ventilation***, several important factors need be considered during design process.

1. Building orientation is the most important factor that determines how much air can flow through a building. Generally, building

should be oriented so that the windward wall is perpendicular to the summer wind to maximize the ventilation.

2. Building shape is one crucial factor to capture wind and bring ventilation to a building. Good building shape design can create proper wind pressures around the building that can effectively drive the air flow through the openings of the building. Naturally ventilated buildings should not be too deep as it will be difficult to distribute fresh air to all portions of the building. It is important to avoid obstructions between the windward inlets and leeward exhaust openings. Avoid partitions in a space oriented perpendicular to the airflow. Buildings that rely on natural ventilation often have an articulated open floor plan.
3. Window typology and operation are critical to enhance and balance air-conditioning needs. Proper window design can achieve the same amount of ventilation but with less openings (and thus costs). When wind flow does not ideally prevails perpendicular to a building wall, optimal location, type and opening direction of windows can act as a scoop to direct the wind into the space.

When designing ***buoyancy driven natural ventilation***, the use and creation of indoor-outdoor temperature difference (indoors be warmer than outdoors) is the critical factor. Several design hints are:

1. Design low inlets and high outlets;
2. Increase vertical distance between inlets and outlets;
3. Use skylights or ridge vents as exhaust;
4. Provide adequate up-flow channel (e.g., atrium);
5. Use solar chimney to increase indoor-outdoor temperature gradient;
6. Do not compromise the function as fire exits of enclosed staircases.

Natural ventilation are typically supplemented with mechanical ventilation, due to the variation and unreliability of climate and stack effect, called hybrid ventilation. Hybrid ventilation allows a building to capitalize on the benefits of natural ventilation, with insurance that the building can operate at a desirable thermal comfort level during extreme outdoor conditions. Thus hybrid ventilation can be implemented in a wider range of climates, where purely natural ventilation is insufficient to provide all the cooling needs of a space. Other methods to enhance natural ventilation performance include solar chimneys and wind towers. A solar chimney

may be an effective solution where prevailing breezes are not dependable enough to rely on wind-induced ventilation and where keeping indoor temperature sufficiently above outdoor temperature to drive buoyant flow would be unacceptably warm. The chimney is isolated from the occupied space and can be heated as much as possible by the sun or other means. Air is simply exhausted out the top of the chimney creating suction at the bottom which is used to extract stale air. Wind towers, often topped with fabric sails that direct wind into the building, are a common feature in historic Arabic architecture. The incoming air is often routed past a fountain to achieve evaporative cooling as well as ventilation. At night, the process is reversed and the wind tower acts as a chimney to vent room air. More design strategies and parameters for natural ventilation can be found in AM10 Natural Ventilation in Non-Domestic Buildings [14].

4.6 Night Cooling with Thermal Mass

4.6.1 Principle

Night cooling with thermal mass is an effective application of natural (and hybrid) ventilation strategy, especially for areas with dramatic diurnal temperature swings. Night cooling method ventilates a building during the cool night and remove heat stored in building structural elements (e.g., walls and floors) during the day. Thermal mass is importantly necessary for this approach to store heat (from solar, outdoors, internal heats) and release them at a later time when outside is cool and ventilation (opening) is on either by a passive approach or by the use of mechanical ventilation system. The thermal mass of the building is cooled mainly by convection during the night, and then the cooled/discharged mass can act as a heat sink and reduce the rate of indoor temperature rise at the following day. Night cooling can affect internal conditions during the day in several aspects, such as reducing the peak air temperatures, reducing air temperature throughout the day especially during morning hours. It can also flatten diurnal air temperature swing. The energy impact of this technique can cause a reduction in the cooling load both in air-conditioned buildings and those naturally ventilated.

4.6.2 Performance

Setting controls for night cooling can save a significant amount of energy, depending on location. Studies indicate cost savings range from

5% in Phoenix, Arizona, to 18% in Denver, Colorado, for a typical office building. Night precooling also reduces peak demand. Simulation analyses show that precooling a 100,000 ft^2 three-story building in Sacramento, California, would reduce energy use by 12.6% and cause a peak demand reduction of 31.3%. Most of the studies conclude that the use of night ventilation in free floating buildings may decrease the next day peak indoor temperature up to 3K. Research on night cooling applications for residential buildings shows that night ventilation may decrease the cooling load up to 40kWh/m^2/year with an average contribution close to 12kWh/m^2/year [15].

Given that the free energy offered by night ventilation techniques increases as a function of the initial cooling needs of the buildings, those with high cooling loads benefit much higher absolute contribution than buildings presenting a low cooling demand. By investigating the correlation between the cooling needs of buildings and the energy contributions of night ventilation, researchers found the correlation is almost linear. In parallel, the uncertainty associated to the evaluation of the energy contribution of night ventilation decreases seriously for higher air flow rates. Given the dissimilarity of the energy amount stored in buildings and the variability of the night ventilation capability for each individual building the percentage energy contribution of night ventilation is independent of the initial cooling load of buildings.

4.6.3 Design Considerations

Night cooling with thermal mass is most appropriate and effective for climates with large diurnal air temperature range, where the cool night air can be used to remove the heat accumulated and stored during the hot day in the building mass. For a high-mass, well-insulated and shaded building, closed during the daytime and ventilated only during the night, a drop of the indoor maximum below the outdoor maximum of about 45% to 55% of the outdoor range is possible. At night the indoor temperatures are higher than outdoors. Figure 4.7 shows the climatic boundaries, in terms of the outdoor maximum daily temperatures, under which night cooling is applicable.

Generally, night cooling is very efficient in arid and desert regions where the maximum temperature is below about 36°C. In desert regions with daytime temperatures above 36°C, night ventilation alone would not

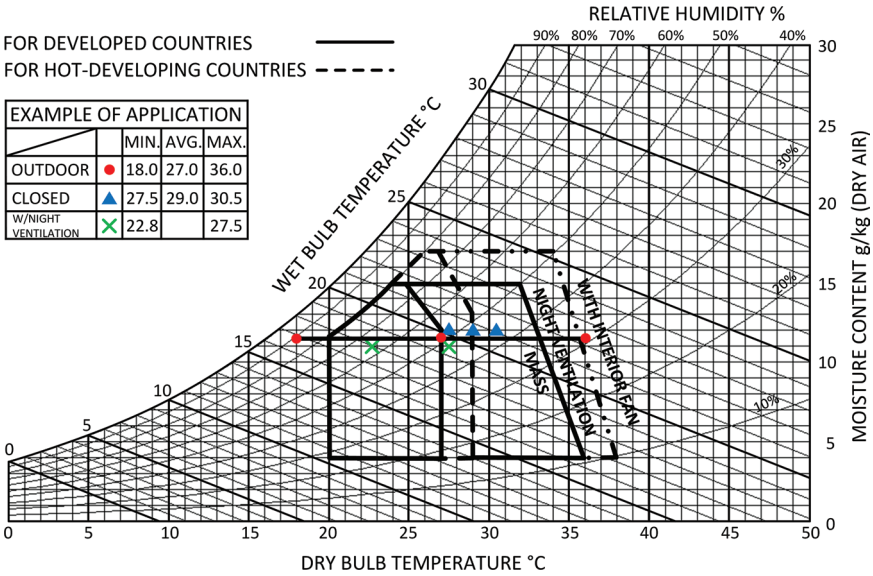

Figure 4.7. Climate boundaries for using night cooling technique [16].

maintain the indoor daytime temperature at an acceptable level and other passive cooling systems should be applied during the hot hours, such as evaporative cooling or compression or absorption air-conditioning. But even in this case the application of night ventilation can significantly reduce the length of the periods and duration of the time when the additional cooling systems will be used.

In reviewing the distribution of temperature ranges of many regions in the world, Givoni [17] found a quantitative relationship between the vapor pressure (vp) and the diurnal ranges (T_{swing} (K)):

$$T_{swing}\,(K) = 26 - 0.83 * (vp)\,(mm\ Hg) \qquad (4.4)$$

He gave some examples in his paper that in a very dry desert with a summer vapor pressure of about 7 to 8 mm Hg, the expected diurnal temperature range would be about 20 K, and in arid regions with a vapor pressure of about 12 mm Hg the expected range would be about 16 K, while in a humid region with vapor pressure of 22 mm Hg the expected

range would be only about 8 K. It should be noted, however, that this is only a statistical relationship and in any given location the actual temperature range should be taken into account. As a general principle it can be estimated that in arid and desert regions, with a summer diurnal temperature range of 15 to 20°K, the expected reduction of the indoor maximum temperature can be about 6 to 8°K below the outdoor maximum. On very hot days, which usually have a larger diurnal range, the drop of the indoor temperature, during the time of the outdoor maximum, may be up to about 10°K [16].

Thermal mass is an inevitable element in night cooling design which indeed determines the performance of night ventilation. A building can maintain daytime temperatures lower than the outdoor level only when it has sufficient thermal mass and thermal resistance, and is protected from absorbed and penetrating solar radiation. In such a building the diurnal temperature swing is very small, about 10% to 20% of the outdoor temperature range. High thermal mass and materials with high thermal resistance are recommended along with the application of this technique.

Night cooling won't work without proper control and operation strategies. In principle, a building should be cooled down 1 to 2°K during the night below the lowest comfort level that can be accepted during the daytime. If this is not accomplished, and it is controlled at the same comfort level as applied during the daytime then the benefits of night cooling will be disappointing. To get effective night cooling it should be cooled down deliberately to lower temperatures.

It should be noted that the acceptable temperature range is reduced with higher humidity, reflecting the corresponding decrease of the outdoor range with higher humidity. Increasing the indoor air speed by internal fans can extend the indoor comfort range, without elevating the indoor temperature. It is also possible to use air handler and economizer to flush the building with night air to cooling down the building mass. In general, the use of mechanical-ventilation systems resolves a number of problems associated with natural systems. They require much smaller openings, can be easier to control and provide sound absorption and security. However, they consume electricity and heat the air (systems can have fan gains of up to 2°C). Therefore, careful monitoring is required when used for night ventilation.

4.7 Direct/Indirect Evaporative Cooling

4.7.1 Principle

Evaporative cooling is an effective, economical, environmentally friendly, and healthy cooling approach that is widely used in residential and commercial buildings. Evaporative cooling is different from traditional air conditioning systems that use vapor-compression or absorption refrigeration cycles with chemical refrigerant. Instead, it uses water as the working fluid and provide excellent cooling by employing water's large enthalpy of vaporization. The temperature of dry air can be reduced significantly by passing through water. Evaporative cooling has the additional attractiveness of low energy consumption, easy maintenance, installation and operation. Evaporative cooling is commonly used in cooling water towers, air washes, evaporative condensers, fluid cooling and also to soothe the temperature in places where several heat sources are present [18].

There are basically two types of evaporative cooling, direct evaporative cooling (DEC) and indirect evaporative cooling (IEC). The combination of DEC and IEC technique is also very popular in the practical applications. In ***direct evaporative cooling***, water evaporates directly into the air thus brings down the dry-bulb air temperature as well as adding the moisture to the airstream until the air is close to saturation. Therefore, the ideal status of air after a direct evaporative cooler is that the dry-bulb temperature can reach the wet-bulb temperature and the humidity of air may come close to 100%. The air can be cooled either by direct contact with a liquid surface or a wet solid surface or else with the use of spray systems. ***Indirect evaporative cooling*** removes the heat from the primary air by crossing the secondary airstream in a heat exchanger. The secondary air is cooled by water in either direct approach or indirect approach. In the direct approach, the secondary airstream passes through a cooling tower and circulates through one side of the heat exchanger. While for the indirect approach, the secondary air which is always the return air from the rooms can be wetted directly and removes the heat from the conditioned supply air on the dry side in an air-to-air heat exchanger. IEC does not add moisture to the primary air, but both of the dry bulb and web bulb air temperatures of the primary air are reduced. IEC is much flexible in the application than DEC, as it is also applicable even in the climate with high web-bulb temperature. In practice, combination of IEC and DEC is becoming more and more popular and proved to be an efficient passive cooling strategy, which is also called two-phase cooling. The primary air is sensibly cooled

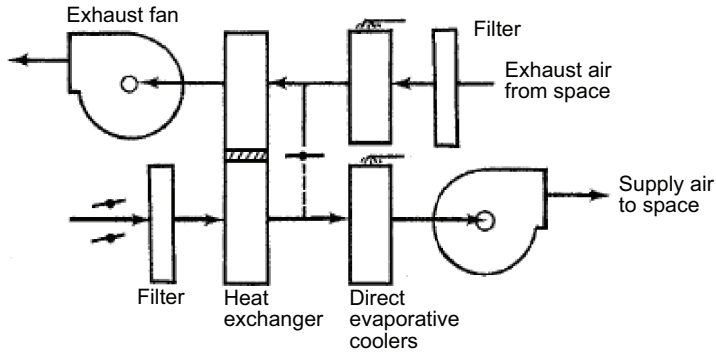

Figure 4.8. Sketch of an indirect-direct evaporative cooling system [19].

first by IEC in phase one and then cooled by directly adding the moisture to the main air stream in phase two which is DEC (Figure 4.8).

4.7.2 Performance

The effectiveness of an evaporative cooling is defined as the rate between the real decrease of dry bulb temperature and the maximum theoretical decrease that dry bulb temperature could have if the cooling were 100% efficient. In DEC, saturation will be a key factor in determining evaporative cooler performance. The theoretical temperature that the air can reach is the web bulb temperature of the entering air. Therefore, the direct saturation efficiency can be expressed as

$$\varepsilon_e = 100\frac{t_1 - t_2}{t_1 - t_s'} \tag{4.5}$$

where
ε_e = direct evaporative cooling saturation efficiency, %
t_1 = dry-bulb temperature of entering air, °F
t_2 = dry-bulb temperature of leaving air, °F
t_s'= thermodynamic wet-bulb temperature of entering air, °F

In IEC, the effectiveness of the heat exchanger is important. The performance is defined as web-bulb depression efficiency (WBDE) as follows:

$$WBDE = 100\frac{(t_1 - t_2)}{(t_1 - t_s')} \tag{4.6}$$

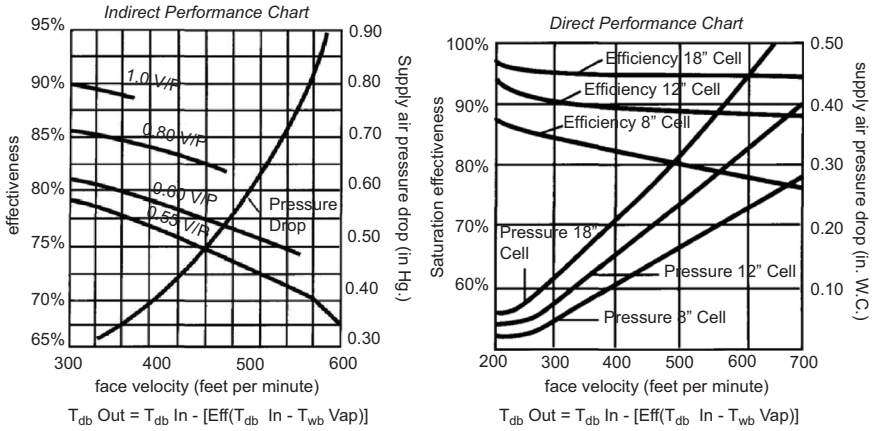

Figure 4.9. The performance charts of direct and indirect evaporative cooling [20].

where
WBDE = wet-bulb depression efficiency, %
t_1 = dry-bulb temperature of entering primary air, °F
t_2 = dry-bulb temperature of leaving primary air, °F
t'_s = wet-bulb temperature of entering secondary air, °F

The performance charts of direct and indirect evaporative cooling are shown in Figure 4.9.

4.7.3 Design Considerations

Evaporative cooling varies in applicability and efficiency with the relative humidity of the outside air. It is much suitable in the dry climate. This constraint should be especially paid attention to when using DEC, as the performance is directly determined by the web-bulb temperature of the air. IEC can be somehow flexible to the climate. The following three climate types are mostly suitable for the application of evaporative cooling:

- Desert: comfort during the entire cooling season
- Steppe: comfort during the dry period of the hot season and moderate relief cooling during more humid periods
- Savanna: only relief cooling during the hot season

The most commonly used evaporative cooling equipment or units are packaged direct evaporative air coolers, air washers, indirect evaporative air coolers, evaporative condensers, vacuum cooling apparatus and cooling towers exchange sensible heat for latent heat. The details of these equipment or units can be referred to ASHRAE Handbook—HVAC application [21].

Air passing through a direct evaporative cooler's wetted media is free of pollutants, minerals and bacteria. A properly designed system, operating within the recommended face velocities, will not have water carryover. For example, the maximum face velocity for a rigid-type media is about 700 fpm while the systems are often designed for around 500 fpm. The primary air passing through an indirect evaporative cooler will not take any additional moisture. Besides acting as a scrubber for removing water-soluble gases, the wetted media has some particulate removal capability. That capability depends on media type and thickness. A 12 in. rigid media has an ASHRAE Standard 52 dust spot efficiency of about 16%, which is equivalent to a fiber furnace filter. Water added in the evaporative systems also acts as an air washer by cleaning the inlet air stream of airborne particulates and soluble gases, which could be a significant benefit to downstream filter elements. Studies show that evaporative cooling also reduces NO_x, emissions because of the increase in moisture added to the air.

Evaporative cooler makeup water are recommended to be supplied from a drinking water quality source. Untreated surface water sources should be avoided due to the risk of a high concentration of nutrients and other pollutants. Two criteria for evaporative coolers are 500 mg/L of TDS and a pH in the range of 6.5 to 8.5. By using drinking quality water for makeup, the outside air to be conditioned will be the most likely source of nutrients. Depending on efficiency, upstream filtration can significantly reduce the concentration of these potential nutrients. A water bleed, required for scale control, also will keep nutrients that might penetrate upstream filtration from concentrating in the recirculating water. Besides moisture and nutrients, algae need light to grow. Evaporative coolers that have the wetted media attached or in close proximity to inlet louvers can be particularly susceptible to algae. Providing a barrier of shade cloth or awnings will inhibit algae growth. Prevention of legionellosis is a health and safety concern for owners and operators of facilities and those who manage water-based evaporative cooling systems. ASHRAE 188: Prevention of Legionellosis Associated with Building Water Systems should be used for compliance.

Evaporative cooling is not considered or recognized as a viable humidification technology. Yet, there are quality and economic advantages when compared with other options such as steam injection, infrared, air injection (atomizing), or ultrasonic. Maintenance and equipment costs are moderate compared to the other four. In a 100% outside air-makeup system, the thermal energy cost to humidify is essentially equal for all technologies. However, when humidification by wetted media is incorporated in an economizer system using a mixture of outside and return air, the energy content of the return air provides a significant portion and sometimes all of the energy to humidify.

The operating costs for evaporative condensers are normally less than a cooling tower designed to dissipate the same heat load because the air flow for evaporative condensers will be about equal for equivalent service and the recirculating water pumping cost will usually be less. The fan static pressure for the evaporative cooler will usually be between 0.2 in. and 0.8 in. of water which is also true for the cooling tower. Comparison of brake horsepower requirements for equivalent service indicate that the evaporative cooler will generally be equal to or lower than the cooling tower. The rate of recirculating water in an evaporative cooler is less than half of the recirculating rate required for a cooling tower exchanger combination designed for equivalent service.

Maintenance requirements for evaporative coolers are comparable with shell and tube heat exchangers. If proper fouling resistances are used to determine the cooling surface, the frequency of cleaning can be reduced to practically any level desired. Even cleaning of the outside tube surface can be accomplished either chemically or mechanically without shutting down the unit.

4.8 Trombe Wall

4.8.1 Principle

Thick adobe or stone walls can absorb and store sun heat during the day and release it slowly and evenly at night to heat building inside. The performance of this thermal storage wall can be largely improved by attaching a layer of glazing outside the wall – an enhanced method for passive heating. Named after French inventor Felix Trombe in the late 1950s, this energy storage Trombe wall generally is a very thick, solar

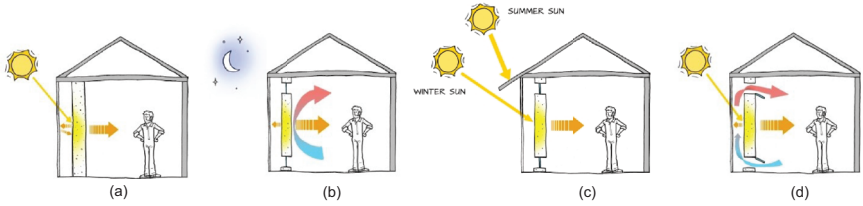

Figure 4.10. Trombe wall design and operation.

facing wall, typically painted in dark and made of material with large density and specific heat (for energy storage). A pane of glass or plastic glazing, installed a few inches in front of the wall, helps hold in the heat. The wall heats up slowly during the day and cools gradually during the night, transferring heat to the inside at a delayed time. Tromble wall takes advantage of the unique transmittance properties of regular glass at different radiation wavelengths: transmit most solar energy at low wavelength but block most thermal energy at high wavelength. As the result, the transmitted solar energy is trapped in the cavity between the glazing and the wall, gradually transporting into the indoor space via the storage wall. Trombe wall is a very useful passive heating system, particularly for buildings with large heating loads and for building retrofit. They require little or no effort to operate, and are ideal for spaces where silence and privacy are desirable. They are often easily built from readily available materials and very reliable. Rooms heated by a Trombe wall often feel more comfortable than those heated by forced-air systems, even at lower air temperatures, because of the radiantly warm surface of the wall. A successful Trombe wall with properly design window systems can optimize heat gain and minimize heat loss during cold time, and avoids excess heat gain in hot time (Figure 4.10) [22].

4.8.2 Performance

Trombe wall performance varies mostly with wall materials. For an 8-in-thick (20-cm) concrete wall, heat may take about 8 hours to reach the interior of the building. This implies that rooms receive slow heating for many hours after the sun sets, greatly reducing the need for conventional heating (during no-sun period). The performance of Trombe walls is diminished if the wall interior is not directly open to the interior zones. Based on previous experience with Trombe walls, the heat delivered by a Trombe wall in a residence was reduced by over 40% because kitchen

cabinets were placed on the interior of the wall [23]. National Renewable Energy Lab of US monitored and analyzed the energy performance of the Trombe wall in a visitor center over a two year period. The analysis consisted of measured electrical end uses, Trombe wall temperature profiles, and thermographic pictures to determine the performance of the Trombe wall. They found the thermal distribution of the Trombe wall at 8:30 p.m. on December 16, 2000 is generally homogeneous, with internal wall surface temperature ranging from 90°F to 96°F (32°C to 36°C). The wall temperature typically peaks between 8 and 9 p.m. The Visitor Center electric radiant heating system used 22,680 kWh (81.6 GJ) over the year, with the Trombe wall contributing 20% of the total heating to the building. The Trombe wall imposed a heating load on the building for only two of the 151 days of the 2001 to 2002 heating season. For the other 149 heating days, the wall was a net positive. The peak heat flux through the wall was 11.2 W/ft^2 (89 W/m^2), or 8.3 kW over the entire Trombe wall area. The average efficiency of the wall (defined as the heat delivered to the building divided by the total solar radiation incident on the exterior of the wall) was 13%.

4.8.3 Design Considerations

Trombe walls are particularly well-suited to sunny climates that have high diurnal (day-night) temperature swings, such as the mountain-west. They do not work well in either cloudy climates or where there isn't a large diurnal temperature swing. For instance in New Mexico, where homes have been built out of adobe (dried mud) bricks for hundreds of years, even an unglazed south wall will deliver some heat into the house – if one add a frame and layer of glazing on the outside of the wall the performance improves dramatically.

A typical unvented Trombe wall consists of a 4- to 16-in. (10 to 41 cm) thick, solar-facing masonry wall with a dark, heat-absorbing material on the exterior surface and faced with a single or double layer of glass. The glass is placed from ¾ to 2 in. (2 to 5 cm) from the masonry wall to create a small airspace. Heat from sunlight passing through the glass is absorbed by the dark surface, stored in the wall, and conducted slowly inward through the masonry. High transmission glass maximizes solar gains to the masonry wall. As an architectural detail, patterned glass can limit the exterior visibility of the dark concrete wall without sacrificing transmissivity. Using low-E glazing can prevent heat from re-radiating out through the glass of a Trombe wall

and greatly reduce the amount of heat lost. Applying a spectrally selective surface or low-E coating to the wall itself can also improve performance by reducing the amount of infrared energy radiated towards the glass.

Trombe walls typically do not have additional insulation. The system works with material that is both very heavy (high heat capacity) and fairly conductive (low R-value per inch). The hint is to choose the right material and size the wall thickness so that the solar heat penetrates through it to the inner surface by a desired later time. In general 6 to 10 in. is good for adobe wall, whereas 10 to 16 in. may be needed for concrete or brick wall. Water may also be used as the thermal storage medium but it usually requires a container (e.g., tube). When water tank is used, 8 or more inches of thickness is often suggested.

To avoid overheating at hot times of day or hot seasons of the year, Trombe walls may be used in conjunction with overhangs, eaves, and other building design elements to evenly balance solar heat delivery. An overhang is typically built that extends out over the Trombe wall above it. This will shade the wall from direct sun during the summer, but allow full solar exposure in the winter.

Top and bottom vents can be installed through the masonry wall to deliver more heat into the house during the daytime hours. Warm air in the space between the glazing and wall surface rises and enters the room, being replaced by air from the house entering through the lower vents in a convective loop. These vents should be closed at night so that the air circulation doesn't reverse, with air next to the glazing cooling off and pulling in warm air from the room through the upper vents and delivering chilled air to the room through lower vents. Vents through the glazing can also be installed and seasonally opened and closed. In the summer months – when one don't need the Trombe wall to deliver heat into the house – these vents are left open. Screens on the vents keep out insects and other unwanted visitors.

4.9 Sunspace

4.9.1 Principle

Sunspace is one popular passive solar system, due to its potential as an energy collecting system and its multiple functions and pleasant

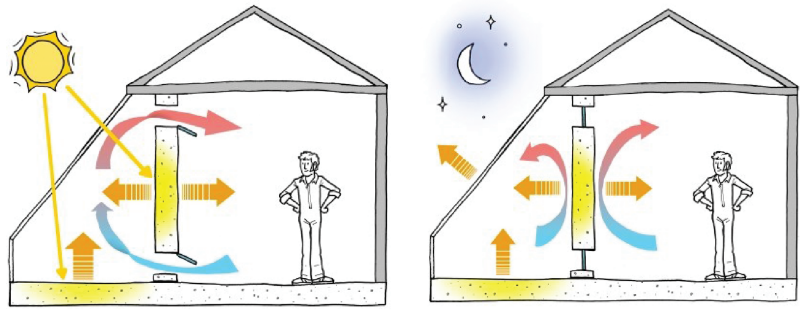

Figure 4.11. Sunspace design and operation.

appearance. Sunspaces represent additional space (and thus value) with positive architectural qualities. Sunspaces, as a retrofitting technique produced by glazing in balconies or as newly built extensions, can be one of the most useful techniques to store solar energy and therefore extensively used.

The main principle of south-facing sunspaces and conservatories is similar to the Trombe wall but with a large and functional air "cavity". The greenhouse effect of glass allows solar beam penetrate through the external glazing but keep the heat inside. Part of the heat is stored in the thermal storage media (e.g., wall and floor), which will be redistributed back to the space at a later time (e.g., at night). Part of the heat can be directly carried into the space via the air convection through the vent openings at the wall when heating is needed immediately (Figure 4.11) [24].

4.9.2 Performance

Sunspace generally is less efficient in collecting solar heat than direct solar gain via windows and Tromble walls, mostly due to the stronger convection and radiation heat loss in larger air space between the glazing and the wall. Increase thermal resistance of sunspace glazing by using multi-pane glasses (either air-filled or inert gas filled) can reduce the heat loss although it does slightly decrease the solar transmittance.

Good orientation of a sunspace is critical. Ideally, sunspace should face due south, but 30 degrees east or west of due south will provide about 90% of the maximum static solar collection potential. The optimum orientation will depend on site-specific and local landscape features.

Research compared the performance of sunspace with south, north, east, and west orientations in the cold period of a year, and found orientation alteration from north to south can improve the results almost up to 7°C [25, 26].

4.9.3 Design Considerations

Sunspace performance heavily depends on climate conditions and system designs. In southern latitudes, passive solar design can provide space heating in winter, but overheating problems in summer should be overcome by using effective solar control and passive cooling systems, such as night ventilation and earth-to-air heat exchangers. In temperate and northern climates, although the conditions are more favorable, it may still need pay attention to the climate variations by using effective shading devices, ventilation and sufficient thermal insulation to ensure a comfortable built environment. In very cold climates, double glazing is needed to reduce heat losses through the glass to the outside. For all climates except those with very cool summers, operable or mechanized windows should be considered at top and bottom. These allow the sunspace to avoid overheating by passively venting hot air out the top of the glazing and pulling cool air in through the bottom of the glazing.

Angle and type of sunspace window glazing determine the performance of sunspace. Although tilted glazing collects more heat in winter, it also loses more heat at night and may be covered with snow in winter, as well as causing overheating in warmer weather. Vertical glazing is commonly used that maximizes heat gain in winter when the solar angle is low and heat is needed most. It is also easy to shade and produces less heat gain in summer. Compared with tilted glazing, vertical glazing is less expensive, easier to install and insulate, and not as prone to leaking, fogging, breaking, and other glazing failures. Vertical glazing is also often more aesthetically compatible with the retrofit of existing homes. Glazing sometime is also implemented on the common wall that separates the sunspace from the indoors, allowing daylighting to the indoor spaces. Movable insulation is usually desired, especially at night at cold climates, to reduce the heat loss from the inside to the sunspace.

Massive materials (e.g., masonry or concrete) are required to flatten temperature swing and store energy for a later use. Wall and floor are typically the best locations for thermal mass which have direct exposures to the solar. In general, for insulated and uninsulated masonry common

walls, the suggested wall thicknesses are, 8 to 12 in. and 4 to 6 in., respectively. If water is used as thermal storage, the rule of the thumb is 2 gallons of water for each square foot of glazing.

Operable vents are often designed at the top of sunspaces where temperature is the highest and at the bottom where temperature is the lowest. The vents can circulate air between sunspace and indoors, or directly exhaust hot air to outsides. They can be operated manually or with thermostatically controlled motors. Mechanical fans (e.g., ceiling fan) can be used to accelerate the air circulation to the entire house when natural convection is not adequate [27].

4.10 Double Skin Facade

4.10.1 Principle

Modern architecture is dominated by transparent buildings. The large glazed areas result in high building heating and cooling loads, leading to high levels of energy consumption and therefore significant financial and environmental burdens. The double skin facade (DSF) is one potential response to these problems. Compared to a single-skin façade, a DSF consists of an external glazing offset from an internal glazing integrated into a curtain wall, often with a controllable shading system located in the cavity between the two glazing systems. Typically, the external glazing is a single layer of heat-strengthened safety or laminated safety glass, while the interior layer consists of single- or double-pane glass with or without operable windows.

Air can flow through the cavity via natural or mechanical ventilation and is used to help moderate building thermal loads. Most commonly, outdoor air flows into the bottom of the cavity and exhausts from the top of the cavity outdoors. During the cooling season, throttling flaps at the inlet and outlet of the cavity remain open to allow airflow through the cavity to exhaust heat that builds up in the cavity. If the DSF includes dynamic sun shades in the cavity, they are usually deployed during the cooling season. Consequently, instead of heating the building interior, the solar radiation heats the air in the cavity, causing the air to buoyantly rise out of the cavity. Thus, the DSF reduces the heat gain of the building. Because the buoyancy of the heated air increases with cavity height, DSFs are typically used in multistory buildings on one or more sides of the building that receive appreciable sun. In addition,

when combined with operable windows that open into the air cavity, a DSF can provide natural ventilation to cool spaces adjacent to the DSF without (or with much lower levels of) mechanical cooling when the outdoor air enthalpy is less than the indoor air enthalpy. During heating season, the DSF cavity inlet and outlet vents close to prevent airflow, trapping solar gains in the cavity and reducing daytime heat losses through the façade. In addition, the sunshades remain open during the day to allow more solar radiation to enter the building and are closed at night to retain heat (i.e., the reverse of the operational scheme during cooling season).

4.10.2 Performance

A good deal of research has been done one the thermal performance of DSF. Generally, it is believed that DSF can achieve better energy performance than a single-skin façade. This is due to (1) additional thermal buffer zone/layer created between inside and outside; (2) proper airflow controls depending on indoor and outdoor conditions. However, the actual performance of DSF buildings vary significantly with building type, scale, and location.

The following validated formulae provide quick estimate on the most important parameters for predicting energy performance of DSF buildings.

1. The airflow rate as a function of opening size and h/d ratio for a single story high cavity with a roller shading device for buoyancy-driven airflow DSF:

$$\dot{V} = \left(-6.2 * h/d + 647.5\right) A_{opening} \sqrt{\Delta T}_{Average} \tag{4.7}$$

For a five-story (15 m) high cavity:

$$\dot{V} = 1375 * A_{opening} \sqrt{\Delta T}_{Average} \tag{4.8}$$

where h/d is the cavity height/depth ratio; $A_{opening}$ is the area in m^2 of one opening for cavities with two equal size openings, or the smaller of two openings for cavities with different size openings; ΔT is the average cavity temperature minus outdoor air temperature in °C; and $\dot{V}$ is the airflow rate through the cavity in m^3/hr. Note that $A_{opening}$ is the equivalent opening area that has the same resistance performance as a physical opening.

2. The peak cavity air temperature to the average cavity air temperature:

$$T_{PeakCavityAir\text{-}1\text{-}Story} = 2.43\left(T_{AverageCavityAir}\right)^{0.78} \quad (4.9)$$

$$T_{PeakCavityAir\text{-}5\text{-}Stories} = 3.68\left(T_{AverageCavityAir}\right)^{0.69} \quad (4.10)$$

It is interesting to notice that the difference between peak cavity air temperature and outdoor air temperature is about 1.87 of that between average cavity air temperature and outdoor air temperature, independent of cavity height.

4.10.3 Design Considerations

A double skin façade consists of an external façade and an internal façade that form an internal cavity. Apart from this basic design, the cavity dimensions, openings, materiality, construction types, airflow paths, and control systems vary considerably. Different DSF designs are better suited to specific climates and design goals. Figure 4.12 shows a typical DSF configuration that was tested in Belgium. The primary parameters of a DSF design include:

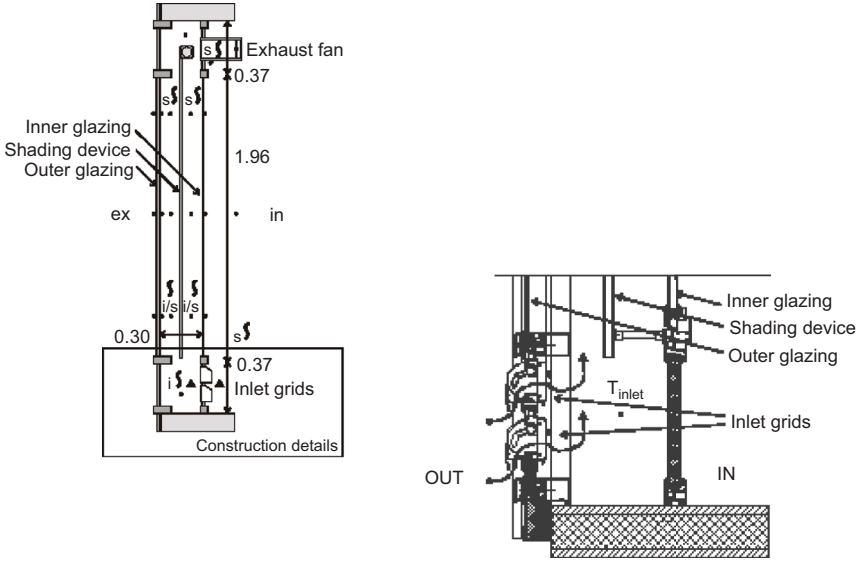

Figure 4.12. Vliet test cell cavity details with louvered cavity opening.

a. Cavity Depth

DSF cavities have been built with depths from a few inches up to 4 or 5ft. Most studies that have considered a variety of cavity widths have determined that this variable does not have a large effect on the overall thermal performance of the DSF. Some considerations in deciding on the cavity depth include: (a) making the cavity volume large enough to allow for sufficient airflow through operable windows to meet ventilation requirements; (b) providing adequate space for the shading device and other structural elements; (c) allowing for easy access to the cavity interior for maintenance and cleanness purposes, etc.

b. Cavity Width

DSF exists both with cavities extending the whole width of a building and with cavities stratified into one to two meter wide sections. The effect of cavity width on airflow has not been studied extensively, but it is likely that structural and aesthetic considerations would largely determine this design decision. It has been suggested, however, that creating narrow cavities will produce shafts that will allow fire and contaminants to propagate more quickly throughout the building.

c. Cavity Height and Opening Locations

Another design consideration is the height of the cavity: whether it extends the whole height of a building, or is divided at each floor. Most existing DSFs have cavities that are divided along the height of the façade, although some have perforated catwalks at each floor for maintenance access that still allow air to flow through them. A taller cavity will produce a stronger buoyancy force, creating a greater airflow rate. However, the fire hazard resulting from a large vertical cavity with no divisions might be prohibitive. Also, air contaminants and noise pollution could flow readily from floor to floor. If the cavity is divided at each floor, there are typically air inlets and outlets near the top and bottom of each section. For a full building height cavity, there could be a single bottom inlet and a single top outlet. This configuration creates the strongest buoyancy-driven airflow due to the tall cavity height. Alternatively, there could be a number of inlets along the exterior façade with one main outlet at the cavity's peak. This will increase the airflow into the cavity, which is desirable in the case with operable windows.

d. Opening Structure

The cavity openings could be quite simple, or complex with controlled louvers and wind shields meant to reduce the effect of wind pressure on airflow through the cavity. If no wind shields exist, the airflow within the cavity will often be driven by wind pressure, forcing the air to flow predominantly in the downward direction. Two sets of automatically controlled louvers allow one or two grids to be open, providing precise control over the airflow rate through the cavity.

e. Cavity Materiality

Most DSF's for new buildings are designed with the goal of maximizing the transparency of the building, in which case both the interior and exterior facades will be mostly glazed. Typically, the interior facade is the thermal barrier, while the exterior facade is a higher transmittance single pane glazing. This is the logical configuration if outdoor air is drawn into the cavity through openings on the exterior façade. If indoor air is cycled through the cavity, conversely, the exterior façade should be the thermal barrier. In the renovation of an existing masonry building a glazed exterior façade could be placed as a screen in front of the original building. In such case the exterior glazing and cavity could protect the original building and operable windows from pollutants, noise, wind, insolation, rain, and vandalism. In either case, the glazing could be clear, allowing as much insolation in as possible, or tinted or etched to filter out the sun as desired.

f. Shading Device

One frequently sited reason for the implementation of a DSF is the potential for positioning a shading device within the cavity. This reduces maintenance costs over locating it on the exterior of the building, and more effectively prevents solar gains than when it is located within the building. Generally, all the options exist as for conventionally located shading devices: roller shades, louvered blinds, fixed versus manually or automatically controlled, horizontal versus vertical fins, etc. The designer should consider how the device will affect airflow within the cavity, and how solar gains absorbed by the shade will be radiated relative to the interior façade. The roller shade positioned in the center of the cavity, shown in Figure 4.12, will allow air to flow freely against the interior façade. Daylight might be more difficult to control precisely with this design, however.

g. Airflow Control

The airflow through the cavity can be naturally driven (with buoyancy and wind pressure), mechanically driven, or a combination of both. Operable windows could allow airflow into the building, or the cavity air could be completely closed off from the building's interior. The airflow could be bi-directional, or it might always flow in the same direction. Additionally, depending on the application seasons and purposes, the cavity inlet could draw in outdoor air, indoor air, or alternate between the two; and the cavity outlet could discharge the air to the outdoors, to the building's interior, or to preheat for the HVAC system.

4.11 Phase Change Material

4.11.1 Principle

Shifting part of the peak load to off-peak time by adding building thermal mass is a promising approach to managing the building load demand. However as promising as this approach may be, when common building materials are used, large masses of these materials are required. Phase change materials (PCMs), on the other hand, can absorb large amounts of heat during the phase change process without being so massive. For example, Benard et al. [28] found that for the same thermal performance, a wall outfitted with PCMs would only need about one-twelfth of the weight of a concrete wall. When PCMs are placed in building walls, they absorb a major part of the heat transferred from hot outside environment in the daytime and release the absorbed heat during the night and early morning hours. As a result, part of the peak space-cooling load is reduced and shifted to off-peak hours. For real applications, PCMs should be able to work in daily cycles, which means the PCM melted in the daytime should solidify at night and/or during early morning hours and then be ready for the next melting process. PCMs can be generally categorized as organic, inorganic, etc. Table 4.3 lists the main characteristics of inorganic and organic phase change materials [29].

According to the methods of energy storage, there are two kinds of phase change energy storage building envelopes. One is the passive phase change energy storage building envelope, which is based on indoor air temperature or solar radiation changes; the other is the active phase change energy storage building envelope, which is combined with heating

Table 4.3. Classification and Properties of PCMs [29].

Classification	Inorganic	Organic
Category	Crystalling hydrate, molten salt, metal or alloy	High aliphatic hydrocarbon, acid/esters or salts, alcohols, aromatic hydrocarbons, aromatic ketone, lactam, freon, multi-carbonated category, polymers
Advantages	Higher energy storage density, higher thermal conductivity, nonflammable, inexpensive	Physical and chemical stability, good thermal behavior, adjustable transition zone
Disadvantages	Supercooling, phase segregation, corrosive	Low thermal conductivity, low density, low melting point, highly volatile, flammable, volume change
Methods for improvement	Mixed with nucleating and thickening agents, thin layer arranged horizontally, mechanical stir	High thermal conductivity additives, fire-retardant additives

or cooling equipment and the heat transfer can be controlled actively. Table 4.4 lists some applications of PCM in building envelopes.

4.11.2 Performance

PCM is an effective passive technique to reduce the effect of heat wave; resulting in a reduced and delayed thermal zonal load. Several studies show promising conceptual and real examples of PCM integration into building applications [31–35]. Several experimental studies [36–38] conducted over summer or winter days in the University of Kansas revealed that PCM has significant reduction in peak and daily loads. The average reduction in peak heating load for all walls ranges from as low as 5.7% to as high as 15% depending on the thermal properties of PCM, PCM design configurations, PCM concentrations, and the time period of the

Table 4.4. Illustration of a Few Passive and Active PCMs Applications in Building [30].

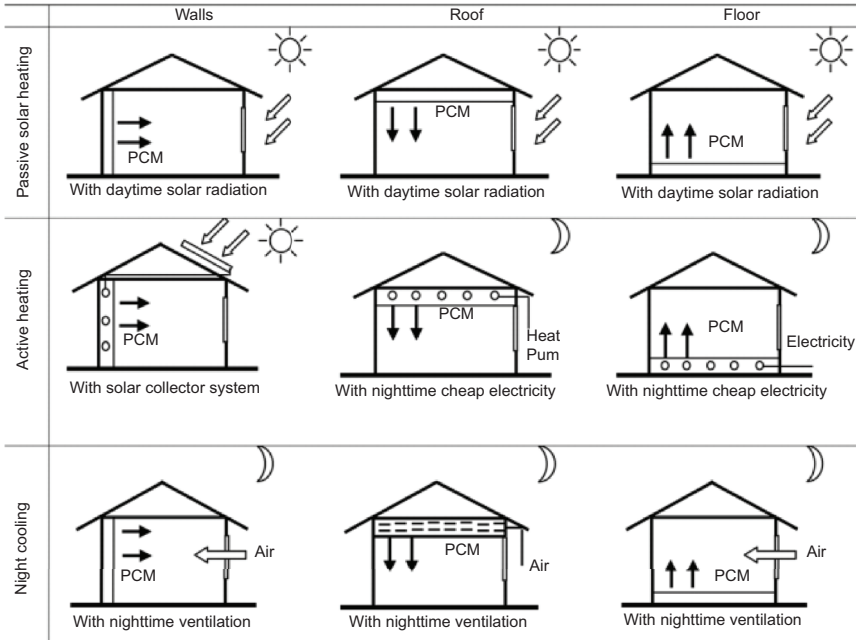

study. Experimental testing at Arizona State University on the PCM panels installed on every surface of the test shed on the interior side showed a reduction of 27% in peak cooling load and a reduction of 19% in annual cooling energy in Phoenix, AZ. Since no internal heat gain are imposed except the solar radiation from a single east window, the high surface area of PCM has to exclusively handle the cooling load generated by the heat transfer from outside climate through exterior envelope. At Natural Exposure Testing facility located in Charleston in south California, two testing campaigns in summer and winter have been conducted to evaluate the performance of different PCM panels divided into two wall groups under real climatic conditions [17]. Results from one wall group show a reduction in heat gain that ranges between 21.8% and 22.9% in summer. In winter, the reduction in heat gain ranges from 5.7% to 15.4% and a reduction in heat loss from 25.5% to 27.7% have been reported.

Simulation tools have also been used to evaluate the energy performance of PCM in buildings. The US National Renewable Energy Laboratory (NREL) research team has used EnergyPlus to simulate the

PCM integrations into different envelope systems using a typical house as per America benchmark protocols under Phoenix, AZ weather file [39]. The results show that PCM has minor effect on reducing the peak cooling load in the cooling season of Phoenix. For the best PCM application in the wall, a maximum reduction of around 8% in peak cooling was achieved in the month of May with only 4% peak cooling reduction in July. A couple of hospital spaces including administration office space, group treatment and patient rooms have been individually simulated using EnergyPlus for Oregon State Hospital in Junction City [40]. PCM layers with different thermal properties are integrated into these spaces for three envelope options: 1) external walls only, 2) external walls and ceiling, 3) all surfaces. The charging occurs naturally during the day but discharging is performed using night flush via integrated economizer with HVAC system. Average reduction of 15%, 17% and 28% in annual cooling energy, and 9.5%, 11%, 12% reduction in peak cooling load are achieved for external walls only, external walls and ceiling deign option, and all surfaces option respectively.

In general, these various studies indicated that the PCM's performance is highly dependent on many factors including the PCM's thermal properties (i.e., latent heat, melting temperature, and melting range), zonal thermostat set-points, PCM's design configurations and integration mechanism, the insulation level of the wall assembly, PCM's surface areas, exposure to internal heat and solar gains, charging and discharging strategies and the climate. Recent studies at University of Colorado at Boulder indicated that PCM performs relatively better when it is located in direct contact with the controlled indoor environment. On annual bases, the maximum saving for the tested latent heat case is 6% and 2.4% for cooling and heating loads, respectively. PCM shows improved performance during transition season when compared to winter or summer seasons. For the month of May (a transition month in Colorado), a maximum savings of 10% and 23% are achieved for heating and cooling loads, respectively. A closer look at PCM layer level indicated that the diurnal cycle during this month was the main reason for the improved PCM's performance. As the result, the charging and discharging cycles occur on a daily bases; driven mainly by the climate. Multiple PCM layers – one for cooling and another for heating were found to provide slightly better performance. For this design, the order of PCM layers relative to the indoor environment was not sensitive.

PCM shows improved performance when integrated with other passive strategies such as natural ventilation, night cooling, direct solar

gain techniques and PCM-enhanced Trombe wall etc. The Colorado study showed that the reduction in annual heating loads for a south wall with PCM is only 0.59% compared to 7.2% when a cavity is used (Trombe wall). Ideally, the charging and discharging process should occur on a daily bases for maximum benefits. In mild climates, the PCM should be flushed with outside cooled air via natural ventilation during night to prepare the PCM for the next hot day cycle. In winter cold climates, solar harvesting techniques should be fully exploited to store the solar heat for later night use.

4.11.3 Design Considerations

Selecting proper PCM properties is the first important step for designing a successful PCM-enhanced building. In general, optimal melting temperature of PCM is found to hover around the thermostat set-points: 1°C below the cooling set-point for maximum savings in annual cooling load while at heating set-point of 22°C for maximum savings in annual heating load. The corresponding melting range should be 0.1 to 1°C and 2°C for maximum savings in annual cooling and heating loads, respectively.

The following general guidelines for choosing desirable thermo-physical, kinetic and chemical properties of PCMs can be followed:

1. Thermo-physical properties:
- melting temperature in the desired operating temperature range (temperature range of application),
- high latent heat of fusion per unit volume so that the required volume of the container to store a given amount of energy is smaller,
- high specific heat to provide additional significant sensible heat storage,
- high thermal conductivity of both solid and liquid phases to assist the charging and discharging energy of the storage system,
- small volume change on phase transformation and small vapor pressure at operating temperature to reduce the containment problem,
- congruent melting of the phase change material for a constant storage capacity of the material with each freezing/melting cycle.

2. Kinetic properties:
- high nucleation rate to avoid super cooling of the liquid phase,

- high rate of crystal growth, so that the system can meet demand of heat recovery from the storage system.

3. Chemical properties:

- complete reversible freeze/melt cycle,
- no degradation after a large number of freeze/melt cycle,
- no corrosiveness to the construction materials,
- non-toxic, non-flammable and non-explosive material for safety.

PCM can be integrated into different building enclosures; ceiling, floor, or walls. The PCM can be thermally activated (i.e., charging or discharging) using passive strategies such as solar radiation from the sun, internal heat gain, or using outside cooled air via natural ventilation. Active systems can also be used to thermally activate the PCM especially when the energy is available at low cost. To be fully exploited, PCM should go through a charging and discharging cycle at least one time a day. Multiple cycles can be achieved through active systems which demand tuned control algorithms for optimizing the charging and discharging process to meet the zone demand.

PCM can be integrated into either passive or active building's systems. Passive systems perform their intended function using explicit inherited properties with no or negligible external aid. On the other hand, active systems are those associated with using mechanical, electrical and electronic equipment to perform their intended function. One of the simplest and easiest solutions is when PCM incorporated into drop ceiling of a zone. Hybrid (automatic or manually) controlled windows are installed to recharge the PCM when outside air is favorable. PCM can also be embedded into floor systems. The PCM-enhanced concrete floor is charged by the direct exposure to the solar radiation during the day. During the night, the PCM is then naturally discharged to meet the heating demand.

Wall system is perhaps one of the most common integration mechanisms for PCM in buildings. In addition to PCM-enhanced multilayer wall systems, PCM can be integrated into ventilated cavity walls (similar to Tromble wall with top and bottom vents). PCM can be utilized in south wall for solar collection and consequently discharged when heat demand is required. Different design, operational strategies and controlled mechanism can be used to passively or actively charge and discharge the PCM. Air is commonly used as a heat transfer medium but embedded pipes can be integrated into the PCM-enhanced wall. Using the

embedded pipes, water can be utilized to quickly charge and discharge the PCM.

4.12 Two Case Studies

4.12.1 Houghton Hall Office Building in Luton, UK

Houghton Hall is a three story office building located in Luton, UK (Figure 4.13). Among a number of passive building techniques used such as daylighting, passive solar, and shading, natural and hybrid ventilation is the main feature of this building. Each of the building's floors is open to a central atrium, and five stacks with fans for ventilation assistance are located in the roof of the atrium.

The building has two sets of vents, upper-level and view-level. Approximately half of the view windows shown in the above photo are operable, and these serve as view-level vents. Above each view-level vent is a smaller upper-level vent. Figure 4.14 illustrates some of the natural ventilation modes experienced into the building. Because the vents in this building are user-operated, a number of different combinations of wind- and buoyancy-driven ventilation are experienced. The upper-level vents are opened in the spring of every year and left open until fall. The view-level vents are user-operated during the occupied hours but are closed at 5pm for security purposes. The exhaust vents located in the five stacks have louvers that are controlled based on wind direction as well as temperature in the atrium. The louvers open and the assisting fans

Figure 4.13. Houghton Hall (south façade and internal atrium view).

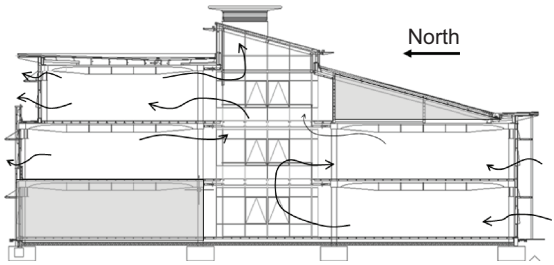

Figure 4.14. Natural ventilation in Houghton Hall.

switch on if the atrium temperature is higher than 26C. If the temperature drops below 26C, the fans turn off. The louvers close when the atrium temperature drops below 22C. Rain or high wind detected causes the louvers to close.

The operable windows in this building are horizontally pivoting that open approximately 10°. Experimentation regarding the effective area of the vents in this building was conducted. The net effective area was found to be approximately 30% of the gross window area. Table 4.5 provides the detailed information about Houghton Hall.

The monitoring program in this building was implemented over an 18 month period, with the first 6 months used for resolving problems. During this time, temperature and humidity loggers were placed throughout the building, primarily at desk height, with vertical arrays in some areas. CO2 measurements were also taken throughout this period, as well as the following external conditions: temperature, humidity, barometric pressure, direct and diffuse solar radiation, and wind speed. Electric energy data loggers monitored overall energy usages as well as the energy used by a variety of different consumers (lifts, fans, lights, etc.). Figure 4.15 shows one of measured indoor air temperature against the outside air temperatures, showing the effectiveness of natural/hybrid ventilation for this building.

4.12.2 RMI Headquarters Building: Amory Lovins Uber Solar Home in Colorado, US

Amory Lovins' 4000-square-foot Uber Solar Home in Colorado, US, also served as the headquarter for Rocky Mountain Institute, is a showcase

Table 4.5. Houghton Hall Information.

Parameter	Value	Units
Floor area	2600	m^2
Floor height	3.9	M
Loads		
Electric	3	kW/zone
Occupancy	25	people/zone
Glazing		
Type	Double-pane, tinted, argon-filled	
U-value	2.2	W/m^2-K
Area (SE)	64	percent
Area (NE,SW)	44	percent
Area (NW)	32	percent
Thermal mass	Exposed concrete soffits in each zone	
Inlet vent area (gross)	1.0	%
Outlet vent area (gross)	0.3	%

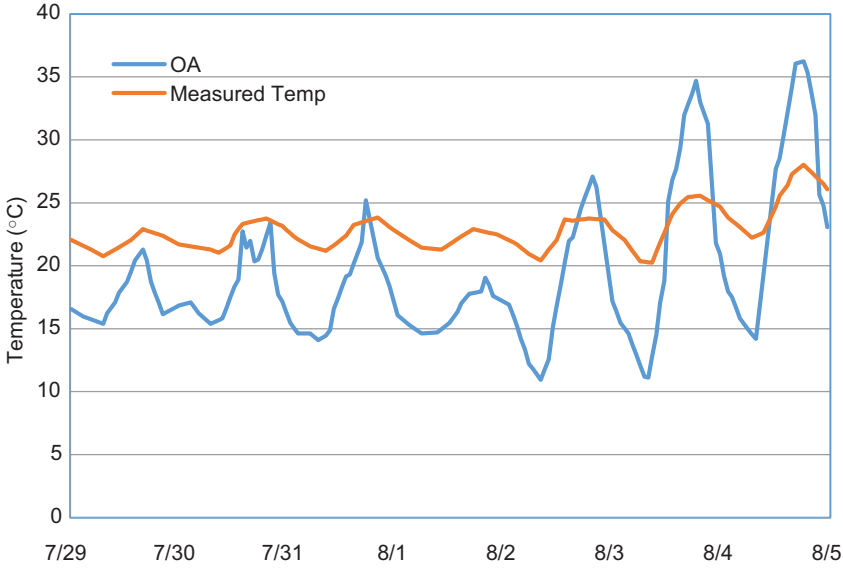

Figure 4.15. Measured indoor and outdoor air temperatures.

for green architecture and ultra-efficient housing, especially for the high-elevation mountain climate. The building was completed in 1984 for \$500k, or \$130/ft^2. The main passive features are passive solar heating and superinsulation (Figures 4.16 and 4.17). With no heating system, the house, instead, relies on greenhouse "furnace" and 1 million pounds of heat-storing thermal mass for heating needs. Other green features include: tracking PV, solar thermal water heater, daylighting, efficient appliances. Masonry taken from local area helps building blend in with surroundings. The energy savings paid off the extra cost of green features within

Figure 4.16. Amory Lovins' uber solar home.

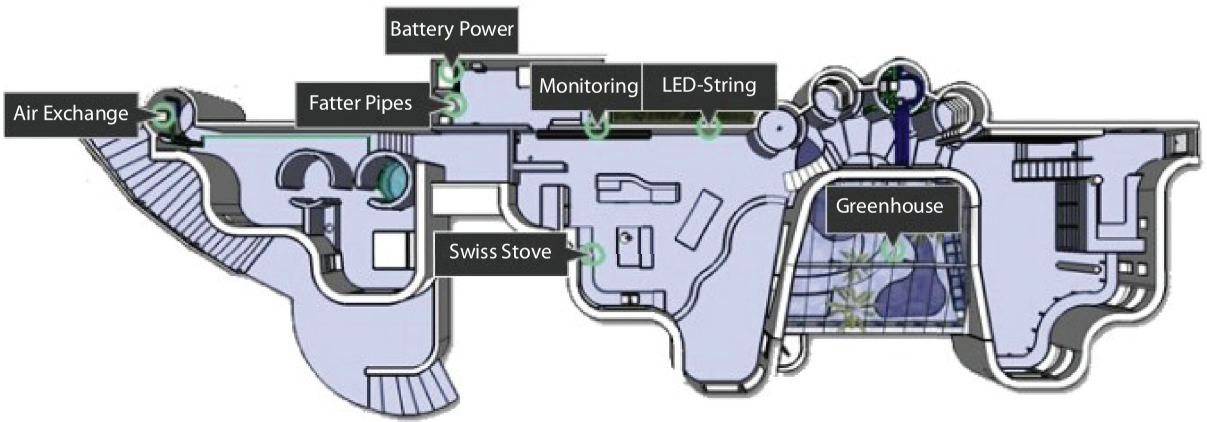

Figure 4.17. Floorplan of Amory Lovins' uber solar home.

10 months. The house saves 99% space/water heating, 90% household electricity, and 50% household water.

Surrounded by the 16-in.-thick stone walls and the hill earth that keep the interior temperature fairly constant, the house also implements a greenhouse (sunspace) that forms the central living room let in light, and store heat in a small jungle of plants, from guavas to coffee to bananas. The stored heat can then be used for night heating.

In the recent renovation, more passive and active solar systems including solar tubes, solar hot water and photovoltaic panels were used. This paves the directional road to the net-zero-energy house but also reveals the notable cost associated with active systems (although most of his renovation project components were donated by industry). For instance, the new photovoltaic panels nearly doubles the amount of solar electricity the house produces, to 9.7 kW, enough for the house's needs. The PV panels, which were donated to Mr. Lovins, retail for about $30,000, not including installation.

References

[1] Oikos, "Which passive cooling strategy is right for you," [Online]. Available: http://www.oikos.com/esb/51/passivecooling.html.

[2] Wikipedia, "Passive cooling," [Online]. Available: http://en.wikipedia.org/wiki/Passive_cooling.

[3] Judt Fosdick T. C. H., "Passive solar heating," [Online]. Available: http://www.wbdg.org/resources/psheating.php.

[4] Walker A., "Natural ventilation," [Online]. Available: http://www.wbdg.org/resources/naturalventilation.php?r=wbdg_approach.

[5] "Natural ventilation," [Online]. Available: http://gbtech.emsd.gov.hk/english/utilize/natural.html.

[6] Kolokotroni M. and Aronis A., "Cooling-Energy Reduction in Air-Conditioned Offices by Using Night Ventilation," Applied Energy, vol. 63, no. 4, pp. 241–253, 1999.

[7] Gratia E., and Herde A. D., "Natural Cooling Strategies Efficiency in an Office Building With A Double-Skin Facade," Energy and Buildings, vol. 36, no. 11, pp. 1139–1152, 2004.

[8] Blondeau P., Sperandio M., and Allard F., "Night Ventilation for Building Cooling in Summer," Solar Energy, vol. 61, no. 5, pp. 327–335, 1997.

[9] Schulze T., and Eicker U., "Controlled Natural Ventilation for Energy Efficient Buildings," Energy and Building, vol. 56, pp. 221–232, 2013.
[10] Kolokotroni M., and Aronis A., "Cooling-Energy Reduction in Air-Conditioned Offices by Using Night Ventilation," Applied Energy, vol. 63, pp. 241–253, 1999.
[11] ASHRAE, Thermal Environmental Conditions for Human Occupancy, 2010.
[12] Seppanen O., and Fisk J. W., "Association of Ventilation Type With SBS Symptoms in Office Workers," International Journal of Indoor Environment and Health, vol. 12, no. 2, pp. 98–112, 2002.
[13] ASHRAE, Ventilation for Acceptable Indoor Air Quality, 2013.
[14] CIBSE, AM10 Natural Ventilation in Non-Domestic Buildings, CIBSE, 2005.
[15] Santamouris M., Sfakianaki A., and Pavlou K., "On the Efficiency of Night Ventilation Techniques Applied to Residential Buildings," Energy and Buildings, vol. 42, pp. 1309–1313, 2010.
[16] Givoni B., "Comfort, Climate Analysis and Building Design Guidelines," Energy and Buildings, vol. 18, pp. 11–23, 1992.
[17] Givoni B., Climate and Architecture, London: Applied Science Publishers, 1976.
[18] Camargo J. R., Ebinuma C. D., and Cardoso S., "Three Methods to Evaluate the Use of Evaporative Cooling for Human Thermal Comfort".
[19] ASHRAE, ASHARE Handbook—HVAC Systems and Equipment, ASHRAE, 2012.
[20] "Evaporative cooling design guidelines manual for New Mexico schools and commercial buildings".
[21] ASHRAE, ASHRAE Handbook—HVAC application, ASHRAE, 2011.
[22] "Trombe Wall," SuryaUrza Enterprises, [Online]. Available: http://suryaurza.com/blog/2013/04/20/trombe-wall/.
[23] Torcellini P., and Pless S., The World Renewable Energy Congress VIII and Expo, Denver, Colorado, August 29–September 3, 2004. http://www.nrel.gov/docs/fy04osti/36227.pdf.
[24] National Renewable Energy Laboratory (NREL). Building a Better Trombe Wall: NREL Researchers Improve Passive Solar Technology. National Renewable Energy Laboratory. Available at http://www.nrel.gov/docs/legosti/fy98/22834.pdf. NREL/FS-130-22834; December 1998.

[25] Mihalakakou G. and Ferrante A., "Energy Conservation and Potential of a Sunspace: Sensitivity Analysis," Energy Conversion and Management, vol. 41, pp. 1247–1264, 2000.
[26] Mihalakakou G., "On the Use of Sunspace for Space Heating/Cooling in Europe," Renewable Energy, vol. 26, pp. 415–429, 2002.
[27] S. C. Information, "Sunspace Design Basics".
[28] Benard C., Body Y., and Zanoli A., "Experimental Comparison of Latent and Sensible Heat Thermal Walls," Solar Energy, vol. 34, pp. 475–487, 1985.
[29] Fang Y., "A Comprehensive Study of Phase Change Materials for Building Walls Applications," PhD thesis.
[30] Wang X., Zhang Y., Xiao W., Zeng R., Zhang Q., and Di H., "Review on Thermal Performance of Phase Change Energy Storage Building Envelope," Chinese Science Bulletin, vol. 54, no. 6, pp. 920–928, 2009.
[31] Baetens R., Jelle B. P., and Gustavsen A., "Phase Change Materials for Building Applications: A State-of-the-Art Review," Energy and Buildings, vol. 42, pp. 1361–1368, 2010.
[32] Khudhair A. M., and Farid M. M., "A Review on Energy Conservation in Building Applications With Thermal Storage by Latent Heat Using Phase Change Materials," Energy Conversion and Management, vol. 45, pp. 263–275, 2004.
[33] Zhang Y., Zhou G., Lin K., Zhang Q., and Di H., "Application of Latent Heat Thermal Energy Storage in Buildings: State-of-the-Art and Outlook," Building and Environment, vol. 42, pp. 2197–2209, 2007.
[34] Tyagi V. V., and Buddhi D., "PCM thermal Storage in Buildings: A State of Art," Renewable and Sustainable Energy Reviews, vol. 11, pp. 1146–1166, 2007.
[35] Pasupathy A., Velraj R., and Seeniraj R. V., "Phase Change Material-Based Building Architecture for Thermal Management in Residential and Commercial Establishments," Renewable and Sustainable Enegy Reviews, vol. 11, pp. 39–64, 2008.
[36] Zhang M., Medina M. A., and King J. B., "Development of a Thermally Enhanced Frame Wall With Phase-Change Materials for On-Peak Air Conditioning Demand Reduction and Energy Savings in Residential Buildings," International Journal of Energy Research, vol. 29, pp. 795–809, 2005.
[37] Medina M. A., King J. B., and Zhang M., "On the Heat Transfer Rate Reduction of Structral Insulated Panels (SIPs) Outfitted With Phase Change Materials (PCMs)," Energy, vol. 33, pp. 667–678, 2008.

[38] Lee K. O., “Using Hydrated Salt Phase Change Materials for Residential Air Conditioning Peak Demand Reduction and Energy Conservation in Coastal and Transitional Climates in the State of California: University of Kansas,” 2013.
[39] Tabares-Velasco P. C., Christensen C., and Bianchi M., “Verification and Validation of EnergyPlus Phase Change Material Model for Opaque Wall Assemblies,” Building and Environment, vol. 54, pp. 186–196, 2012.
[40] Affiliated Engineers, “Preliminary Analysis of PCM Strategies,” [Online]. Available: www.phasechange.com/Research%20Library/OSH_JC_PCM_Analysis.pdf.

5 Control Strategies for Building Energy Systems

Moncef Krarti

Abstract

This chapter describes control strategies which can provide significant energy-saving opportunities to various energy-consuming equipment, such as boilers, chillers, and motors. First, basic concepts of HVAC system controls are presented. Then, typical supervisory controls including energy management and control systems (EMCs) are outlined. Finally, several applications of EMCS are discussed to illustrate the types controls that can be implemented for building energy systems and equipment. In the discussion of the applications for the supervisory controls, the benefits of using optimal control strategies to operate building energy systems are evaluated.

5.1 Introduction

Currently, almost all new buildings have some control systems to manage the operation of various building equipment including HVAC systems. More elaborated control systems can operate simultaneously several mechanical and electrical equipment dispersed throughout the facility. In particular, these energy management control systems can be used to reduce and limit the energy demand of the entire facility. In the last decade, most of the advances in the HVAC equipment are due to the modern electronic controls which are now cheap, flexible, and reliable.

The development of energy management and control systems (EMCS) is mostly attributed to the introduction of computerized building automation systems. In fact, energy management represents one of several tasks performed by an integrated building automation system (IBAS). Among other tasks of the IBAS include fire safety, vertical transportation control, and security regulation. Advanced IBAS include logic for interaction between lighting, HVAC, and security systems. For instance, if an automated occupancy sensor detects presence of people in specific spaces during late hours (during night or week-ends), the information can be used to adjust indoor temperature (for comfort) and to reinstate elevator

service (to ensure that people can leave the building). Moreover, EMCS can provide facility operators with recommendations on maintenance needs (such as lighting fixtures replacement) and alarms for equipment failures (such as motors when they burn out).

The use of energy-efficient equipment does not always guarantee energy savings. Indeed, a good management of the operation of this equipment is a significant factor to reduce whole building energy use. Generally, building energy loads are continuously changing with time due to fluctuations in weather and changes in equipment use and occupancy. Thus, effective energy management requires the knowledge of the facility loads. Two approaches are typically applied:

- *Load Tracking*: the operation of equipment is modulated to respond to the actual needs in the facility. As an example, the compressor in a centrifugal chiller may change speed to match the cooling demand. The actual needs of a facility can be determined by a continuous monitoring. As an example, the load on the chiller can be estimated if the chiller water flow, and chilled water supply and return temperatures are monitored.
- *Load Anticipation*: In some applications, the needs of a facility have to be predicted to be able to modulate adequately the operation of equipment. For instance, in cooling plants with thermal energy storage system, it is beneficial to anticipate the future cooling loads to be able to decide when and how much to charge and discharge the storage tank. Load prediction can be achieved by analyzing the historical pattern variations of the loads.

Using monitored data and other parameters characterizing the building, energy control systems enable operators and managers to operate efficiently HVAC and lighting systems to maintain comfort level. In the following sections, building energy control systems and some of their applications are presented and discussed.

5.2 Basic Control Principles

5.2.1 Overview of Control System Components

Control systems are used to match equipment operation to load requirements by changing system variables. A typical control system includes four elements as briefly described below:

1. Controlled variable is the characteristic of the system to be controlled (for instance, the indoor temperature is often the controlled variable in HVAC systems).
2. Sensors which measure the controlled variable (for instance thermocouple can be used to measure indoor temperatures). Table 5.1 lists some sensors commonly to control HVAC systems.
3. Controllers that determine the needed actions to achieve the proper setting for the controlled variable (for instance, the damper position of the VAV box terminal can be modulated to increase the air supply in order to increase the indoor temperature of the zone if it falls below a set-point).

Table 5.1. Types of Sensors Used for HVAC Systems Controls.

Variable to sense	Types of sensors
Temperature	• Bi-metallic strip • Sealed bellows • Bulb and capillary sensors
Pressure	• Variable resistance • Capacitance
Liquid flow	• Orifice • Venturi tube • Flow nozzles • Vortex shedding sensors • Positive displacement flow sensors • Turbine-based flow sensors • Magnetic flow sensors • Ultrasonic flow sensors
Air flow	• Hot wire anemometers • Pitot static tube
Relative humidity	• Resistance relative humidity sensor • Capacitance relative humidity sensor • Temperature condensation • Condensation and wetting • Quartz crystal relative humidity sensor • Hydrostatic sensors • Ultrasonic sensors • Capacitance sensors

4. Actuators are the controlled devices which need to be activated in order to complete the actions set by the controllers (to vary the air supplied by a VAV box, the position of the damper is changed by an actuator through direct linkages to the damper blades)

Generally, two categories of control systems can be distinguished including closed loop and open loop systems. In a closed loop system (also known as a feedback control system), the sensors are directly affected by (and thus sense) the actions of the actuators. A typical control of a heating coil is an example of a closed loop system. However, in an open loop system (also called a feed forward control system), the sensors do not directly sense the actions of the controllers. The use of timer to set the temperature of the heating coils would be an example of an open loop system since the time may not have a direct connection with the thermal load on the heating coils.

Figure 5.1 shows the various components and terms discussed above as well as an equivalent control diagram for a closed-loop control system for a heating coil.

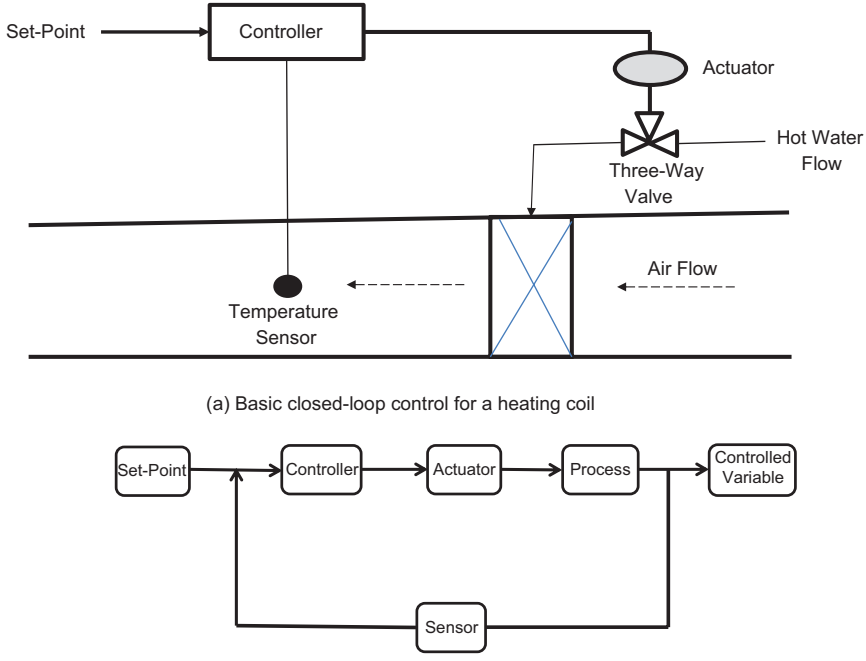

Figure 5.1. Typical representations for a heating coil control system.

5.2.2 Transfer Function Analysis

In HVAC controls, the analysis of control systems can be carried out using transfer functions connecting input to output signals. For instance, Figure 5.2 shows the relationship between the input function $u(t)$ and the output $y(t)$ after a process function, $g(t)$, typically referred to as a response function.

For linear processes, the output function, y(t) can be estimated from the input function, u(t), using the following expression:

$$y(t) = \int_{-\infty}^{\infty} u(t-\tau)g(\tau)d\tau \tag{5.1}$$

As a notation, the relation of Eq. (1) can be written simply as:

$$y(t) = u(t) * g(t) \tag{5.2}$$

For instance, in case the process can be represented by a constant response function, that is, $g(t) = K$. Then, from Eq. (5.1), the output function is proportional to the input signal as shown by Eq. (5.3):

$$y(t) = K.u(t) \tag{5.3}$$

In general, the relationship between the input and output involved linear differential functions such as the relationship provided by Eq. (5.4):

$$a\frac{d^2y}{dt^2} + b\frac{dy}{dt} + c\,y = \alpha\frac{du}{dt} + \beta u \tag{5.4}$$

In order to find the relationship between the input and output functions, and thus define the function $g(t)$, the Laplace transform analysis is used. The Laplace transform function for any function $f(t)$ is defined as $F(s)$ as follows:

$$F(s) = \int_0^{\infty} f(t)e^{-st}dt \tag{5.5}$$

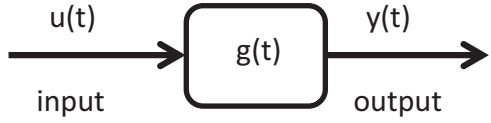

Figure 5.2. Time domain input-output relation through a response function g.

Through the Laplace transform, any linear differential equation can be simplified. For instance Eq. (5.4) can be transformed in the Laplace domain as follows:

$$a\,s^2Y(s) + bsY(s) + cY(s) = a\,s\,U(s) + b\,U(s) \tag{5.6}$$

Thus,

$$Y(s) = \frac{\alpha\, s + \beta}{a\,s^2 + b\,s + c} U(s) \tag{5.7}$$

Therefore, the response function G(s) in the Laplace Transform can be written as:

$$G(s) = \frac{Y(s)}{U(s)} = \frac{\alpha\, s\, +\, \beta}{a\,s^2 + b\,s + c} \tag{5.8}$$

Figure 5.3 illustrates the input-output relationship through the function G in the Laplace transform domain. The function G is called a transfer function to find the output Y(s) from the input U(s) by simple multiplication operator in the Laplace transform domain:

$$Y(s) = G(s)\; U(s) \tag{5.9}$$

The output function Y(s) can then be converted into the time domain, y(t), using the inverse of the Laplace transform as shown by Eq. (5.10):

$$f(t) = \int_0^\infty G(s)e^{st}\,ds \tag{5.10}$$

Table 5.2 summarizes for typical response functions their associated Laplace transforms as well as Transfer functions.

When two signals are used as input variables, u_1 and u_2, first the sum of the output signals, X, from two transfer functions, G_1 and G_2, are added before the resultant is applied to a third transfer function, G_3, to obtain the output signal, y, as shown in Figure 5.4 using the Laplace Transform analysis.

Using the transfer functions G_1, G_2, and G_3, the output y(s) can be determined from the $U_1(s)$ and $U_2(s)$ as indicated by Eqs. (5.11) and (5.12):

$$Y(s) = G_3(s)\,X(s) \tag{5.11}$$

Figure 5.3. Transform domain input-output relation through a response function G.

Table 5.2. Laplace Transforms for Selected Response Functions.

Time domain response function	Laplace transform function, G(s)	Input-output relationship
δ(t) [impulse function at t = 0]	1	$y(t) = u(t)$
e^{-at}	$\frac{1}{s+a}$	$\frac{dy}{dt} + a\,y = u$
$\sin(\omega t)$	$\frac{\omega}{\omega^2 + s^2}$	$\frac{d^2y}{dt^2} + \omega^2 y = \omega u$
δ(t – T) [impulse function at t = T]	e^{sT}	$y(t) = u(t–T)$
H(t) [Integrator]	$\frac{1}{s}$	$y(t) = \int_0^t u(\tau)\,d\tau$

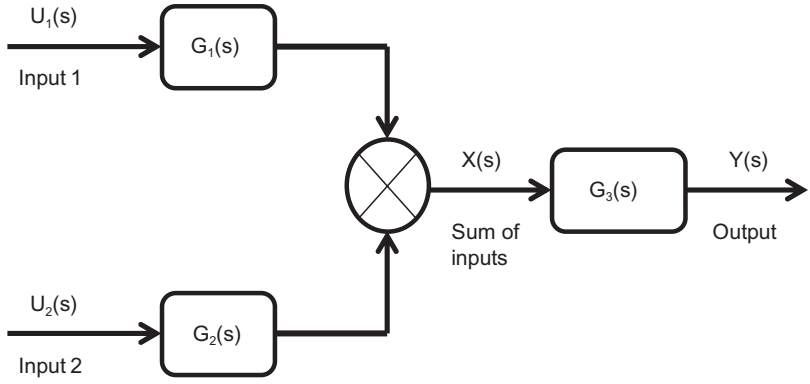

Figure 5.4. Interconnection between two input signals and the output functions.

And

$$X(s) = G_1(s)\ U_1(s) + G_2(s)U_2(s) \tag{5.12}$$

Thus, the output can be directly obtained from the input signals U_1 and U_2:

$$Y(s) = G_1(s)\ G_3(s)\ U_1(s) + G_2(s)\ G_3(s)\ U_2(s) \tag{5.13}$$

The output from the two input variables is simply the sum of the output signals from each input variable obtained by the transfer functions $G_1\ G_3$ and $G_2\ G_3$.

Another common interconnection is when there is a feedback loop from the output to the input to estimate the error function as shown in Figure 5.5 and expressed in terms of transfer functions

$$E(s) = U(s) - G_2(s)\ Y(s) \tag{5.14}$$

And

$$Y(s) = G_1(s)\ E(s) \tag{5.15}$$

Thus,

$$Y(s) = G_1(s)\ U(s) - G_1(s)\ G_2(s)\ Y(s) \tag{5.16}$$

Therefore,

$$Y(s) = \frac{G_1(s)}{1 + G_1(s)G_2(s)}(U)s \tag{5.17}$$

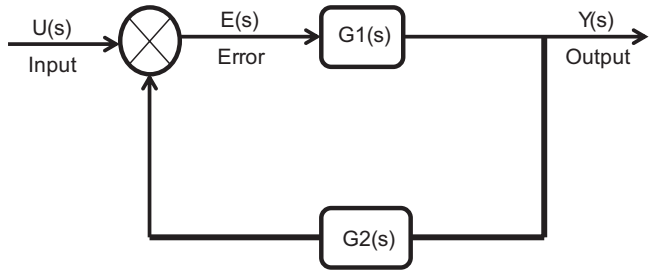

Figure 5.5. Error signal obtained input and the output signals.

Then, the error transfer function can be estimated by substituting Eq. (5.17) into Eq. (5.14):

$$E(s) = \frac{1}{1 + G_1(s)G_2(s)} U(s) \tag{5.18}$$

As an application of the two interconnected transfer functions shown by Figures 5.4 and 5.5, the transfer function for any linear control scheme can be developed. For instance, the transfer function diagram for the control process of Figure 5.1 is shown in Figure 5.6.

The input-output transfer function for the control process can be derived to be:

$$Y(s) = \frac{G_1(s)G_2(s)G_3(s)}{1 + G_1(s)G_2(s)G_3(s)G_4(s)} U(s) \tag{5.19}$$

Moreover, the error transfer function can be shown to have the following expression:

$$E(s) = \frac{1}{1 + G_1(s)G_2(s)G_3(s)G_4(s)} U(s) \tag{5.20}$$

In the following section, common control modes for HVAC systems are described in details.

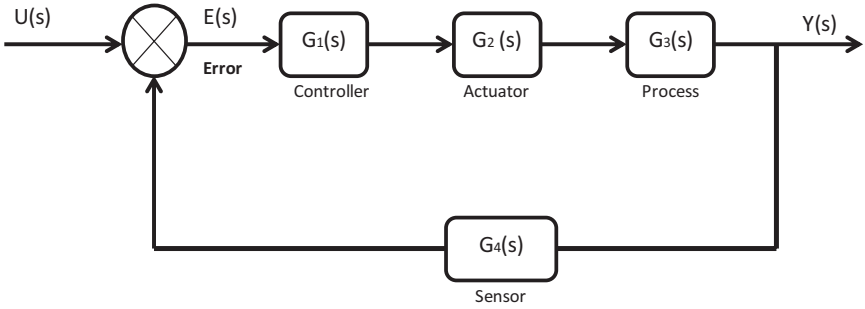

Figure 5.6. Transfer function diagram for input and the output signals for control process of Figure 5.1.

5.2.3 Control Modes

Each control system can use different control modes to achieve the required objectives of the control actions. Four control modes are commonly used in operating HVAC systems. These four control modes are:

1-Two-position: This control mode allows only two values (on-off or open-closed) for the controlled variable and is best suited for slow-reacting systems. Figure 5.7(a) shows the effect of two-position control on the time variation of the controlled variable (such as the air temperature due to on-off valve position in a heating coil). In order to avoid rapid cycling, a control differential can be used. Due to the inherent time lag in the sensor response and to the thermal mass of the HVAC system, the controlled variable fluctuates with an operating range (called operating differential) with higher amplitude than the control differential. Thus, the operating

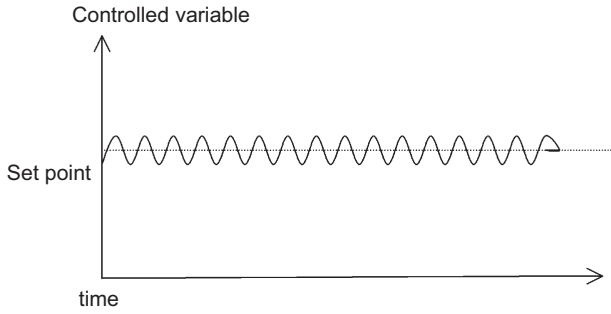

(a) Two-position action when no control differential is used (rapid cycles)

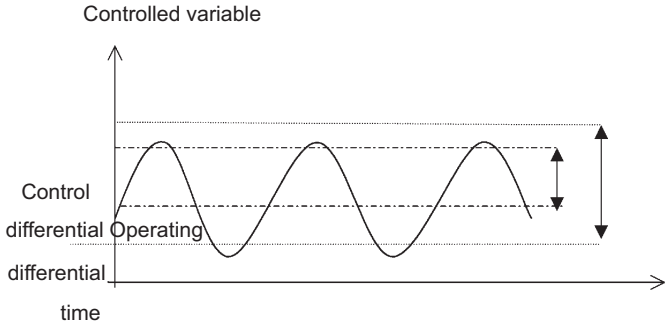

(b) Two-position action with a control differential

Figure 5.7. Effect of two-position control on the time variation of a controlled variable.

differential is always higher than the control differential as illustrated in Figure 5.7(b).

Examples of two-position controls are domestic hot-water heating, residential space-temperature controls, and HVAC system electric preheat elements.

2-Proportional: This mode has a linear relationship between the incoming sensor signal and the controller's output. The relationship is established within an operating range for the sensor signal. The set point of a proportional controller is the sensor input which results in the controller output to be at the midpoint of its range. Mathematically, the controller output, *u*, is given by the following equation for a proportional control:

$$u = K_p e + u_0 \tag{5.21}$$

The offset or error, e, is the difference between the set point and the value of the controlled variable. The proportionality constant, K_p, is called the proportional gain constant. The controller bias, u_0, is the value of the controller output when no error exists.

As depicted by Eq. (5.21), the proportional control is not capable of reducing the error since an error is required to produce any controller action. Therefore, the controlled variable fluctuates within a throttling range as depicted in Figure 5.8.

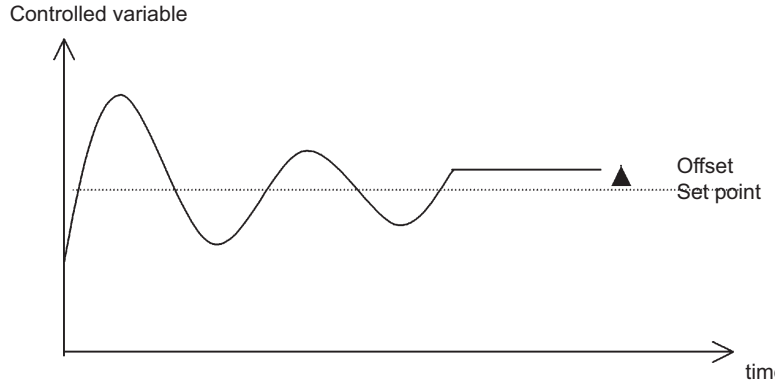

Figure 5.8. Proportional control effect on the time variation of a controlled variable.

It should be noted that when the gain constant is very large, unstable system can be obtained.

Generally, proportional controllers are used with slow stable systems that have small offset.

3-Integral: This control mode is typically incorporated with a proportional control mode to provide an automatic means to reset the set point in order to eliminate the offset. The combination of the proportional and integral actions is called 'proportional-plus-integral" or simply PI control. Mathematically, the PI control can be expressed as follows:

$$u = K_i \int e.dt + K_p e + u_0 \tag{5.22}$$

where K_i is the integral gain constant (also known as the reset rate) and has the effect of adding a correction to the controller output whenever an error exists. For HVAC systems, typical K_p/K_i ratio is less than 60 minutes.

The PI control can be applied to fast-acting systems that require large proportional bands for stability. Typical applications include mixed-air controls, heating or cooling coil controls, and chiller-discharge controls.

4-Derivative: This control action is used to speed up the response of the system in case of sudden changes. The derivative control mode is included in a combination of proportional-plus-integral-plus derivative (PID) control modes for fast-acting systems that tend to be unstable such as duct static-pressure controls. The mathematical model for the PID control is given by Eq. (5.23):

$$u = K_d \frac{de}{dt} + K_i \int e.dt + K_p e + u_0 \tag{5.23}$$

where, K_d is the derivative gain constant. The derivative term generates a corrective action proportional to the time rate of change of the error. The ratio K_d/K_p is typically less than 15 minutes for most HVAC applications. If the system has a uniform offset, the derivative term has little effect. The use of PID controls is typically less common than the PI controls for HVAC systems since no rapid control responses are needed.

To illustrate the action of P, PI, and PID control modes, Figure 5.9 compares the response of the system to an input step change. As expected the proportional control results in an offset and the controlled variable

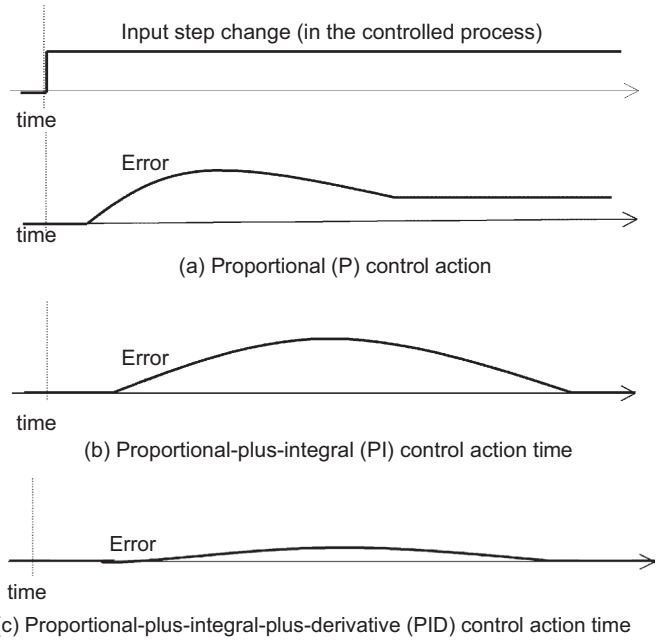

Figure 5.9. Comparison of the reaction of three control modes to an input step change.

does not reach the set point. The correction term due to the PI control slowly forces the controlled variable to reach the set point value. Finally, the derivative term of the PID control provides a faster action to allow the controlled variable to attain the set point.

In addition to these conventional control modes, other intelligent controllers have been investigated in various engineering fields including HVAC equipment controls as will be discussed in the following section.

5.2.4 Intelligent Control Systems

In the future, it is expected that intelligent control systems will be commonly available to operate HVAC systems. A number of research studies are applying intelligent system methodologies so that control systems have human-like capabilities such as pattern recognition, adaptation, learning, reasoning, and associative memory to operate complex systems that convention control techniques cannot handle. Various intelligent control environments have been considered for HVAC systems including:

- **Expert Controls:** Rule-based expert systems are based on human-like reasoning and can be powerful to solve practical engineering problems. Indeed, expert control systems have been applied to self-tuning, structured knowledge based adaptive control, fault diagnosis, and scheduling and planning. However, rule-based expert systems are not yet suitable to process numerical knowledge and thus to provide precise solutions. The development of an expert system environment that can deal with both qualitative and quantitative knowledge, and to automatically explore knowledge, is still in the realm of future expert control research.
- **Fuzzy Controls:** Since the development of fuzzy logic in the 1960s, fuzzy control has been one of the most attractive strategies in controlling complex systems with imprecise and/or uncertain knowledge of system information and behavior. Fuzzy logic can be applied to system modeling, estimation, optimal control, and adaptive control with the requirements of only system fuzzy knowledge and input/output data. Applications of fuzzy logic in expert systems are becoming attractive to establish intelligent expert control systems with fuzzy knowledge representation and fuzzy reasoning.
- **Artificial Neural Networks:** Similar to biological neural networks, artificial neural networks consist of large number of simple non-linear processing elements, typically called nodes or neurons, which are interconnected with adjustable weights. Well-trained neural network models can provide both qualitative and quantitative knowledge and has powerful functions in learning and self-organization. These features make neural networks more suitable in dealing with numerical data than expert systems.

5.2.5 Types of Control Systems

To achieve the actions of the control systems discussed above, several types of energy sources are used. In particular, the following types of control systems are used in HVAC applications:

- Pneumatic devices are used with low-pressure compressed air at 0 to 20 psig. Pneumatic systems are common in older installations.
- Electric devices using 24 to 120 volts or even higher voltage sources.
- Electronic devices with low direct current voltages varying from 0 to 10V. These devices are being installed in new commercial buildings especially with direct digital control (DDC) systems.

- Hydraulic systems when large forces are required with pressure larger than 100 psi.
- Self-generated energy derived from the change of state of the controlled variable or from the energy available in the process plant.

For HVAC retrofit applications, it is recommended that direct digital control (DDC) systems be considered. Indeed, currently developed DDC systems use the latest digital technology including features such as intelligent controllers, high speed communication networks, and sophisticated control algorithms. All these features allow more energy-efficient control strategies to be implemented. Moreover, digital devices present additional advantages compared with pneumatic or electric devices as outlined below:

- Little or no maintenance is required for digital devices.
- Calibration of digital devices can be performed through remote instructions issued over a network. Some digital devices have the advantage to be continuously self-calibrating.
- Better accuracy is obtained from digital controls compared to pneumatic or electric devices.

While DDC devices have been used since the 1980s, it is only recently that manufacturers have developed systems that house interposing devices (such as relays, transducers, and hard-wired logic) in the same package with the electronic devices. These new DDC systems are suitable for retrofitting applications since it is now economical to convert existing pneumatic and electric analog controls to DCC systems. The best candidates for DDC retrofitting are air handling units (AHUs), heat exchangers, distribution pumps, and cooling towers. In general, the larger the equipment size, the faster the payback period. Replacing the controls for small HVAC equipment such as package unitary systems (including unit ventilators, heat pumps, and fan coils) may not be cost-effective.

Retrofit of pneumatic controllers can be made using electronic-to-pneumatic (E/P) transducers to convert signals so electronic and pneumatic control components can be combined in the same control loop. For instance, the controller and the sensor in an existing pneumatic HVAC control system can be converted into electronic devices while the actuator can remain pneumatic. The pressure output of the E/P transducer should match the electric signal. The use of E/P transducers allows retrofit of control systems with minor interruption in the operation of the controlled system.

5.3 Supervisory Controllers

Supervisory controllers can interact with all the subsystems housed inside a building to effectively meet building needs with appropriate operator input. Typically, supervisory controllers are called building automation system (BAS), building management systems BMS), Energy Management System (EMS), or more commonly Energy Monitoring and Control Systems (EMCS).

5.3.1 Basic Components of an EMCS

To control and operate equipment for heating, ventilating, and air conditioning, or for lighting and process equipment, an energy monitoring (or management) and control system (EMCS) can be used. A typical EMCS is configured into a network that includes sensors and actuators at the bottom level, microprocessor controllers in the middle, and a computer at the top with a modem to allow remote monitoring and control of the building energy systems. For a typical commercial building, an EMCS system can be cost-effective in reducing the energy use for HVAC and lighting systems.

Energy management is often just one element of an integrated building automation system (IBAS) which regulates security, fire safety, lighting, HVAC systems, and elevators. Advanced IBAS systems include logic for interaction between various systems such as HVAC, lighting, and security systems. Indeed, the automated occupancy count information obtained for different spaces in a facility can be used to adjust indoor temperature settings, reduce or turn-off lights, and ensure proper elevator operation.

The size of an EMCS system is typically classified based on the total number of points connected to a system. Five size categories are generally considered for EMCS systems:

- Large EMCS systems with more than 2000 points.
- Medium EMCS systems with 500 to 2000 connected points.
- Small EMCS systems with 200 to 1000 points.
- Small centralized EMCS systems with 50 to 500 points.
- Micro EMCS systems with less than 100 points.

A typical EMCS system is depicted in Figure 5.10 and includes a central control unit (CCU), a processing memory, storage devices, input-output

devices, a central communication controller (CCC), data transmission medium (DTM), a field interface devices (FID), multiplexers, instruments, and controls. A brief description of the major components of an EMCS system is presented in the following sections.

- The central control unit (CCU) consists generally of a computer with memory for the operating system software, command software, and implementation of application algorithms. In particular, computations and logical decision functions for central supervisory control and monitoring are performed by the CCU. However, data and programs are stored in and retrieved from the memory or storage devices such as magnetic tape and disk systems. Typically, the CCU has input-output (I/O) ports for specific equipment such as printers and terminals.
- The central communications controller (CCC) is typically a computer with enough memory to execute specific programs required to reformat, transfer, and perform error checks on data coming from the CCU or the field interface devices (FIDs). The CCC may have back-up capabilities in case of CCU failure.

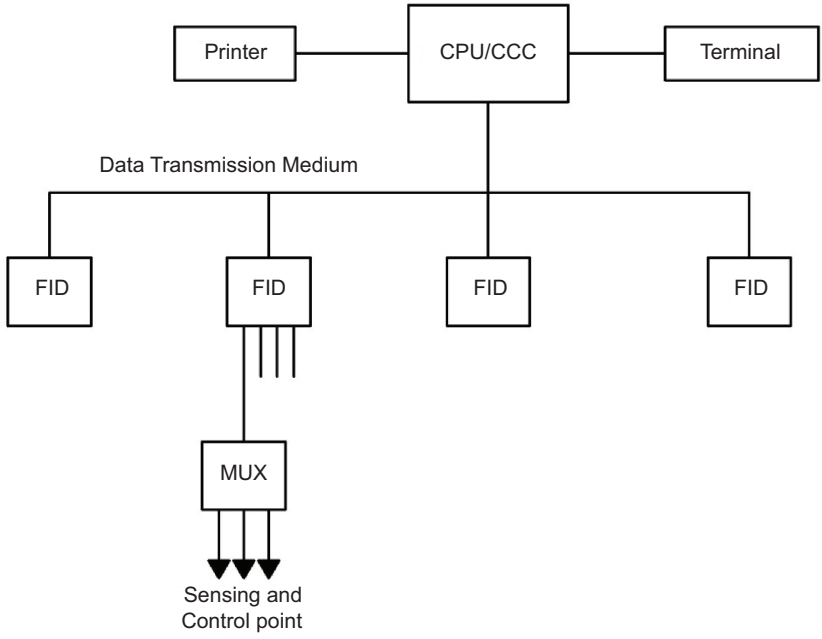

Figure 5.10. Typical EMCS components and configuration.

- Field interface devices (FIDs) consist generally of computer devices with memory, I/O, communications, and power supply. The FIDs record the monitored and controlled data, perform calculations and logical operations, accept and process system commands. They should be capable of operating in case of CCU failure.
- A multiplexer (MUX) is a device that communicates between the data environment and its associated FID. The MUX is functionally part of the FID and can thus be in the same enclosure.
- The data transmission medium (DTM) is the communications link that allows transferring data between the CCU and its associated FIDs such as telephone lines, optical fibers, or coaxial cables.

5.3.2 Typical Functions of ECMS

Several control operations and functions can be performed by an EMCS including but not limited to:

i. Equipment operation such start-stop, on-off, and open-close controls.
ii. Alarm functions such as abnormal equipment status, high or low parameter values (temperature, pressure, refrigerant level, etc.
iii. Computer programming and table look-up functions for energy management and equipment use optimization including enthalpy economizer controls, chiller plant optimization, load shedding based on demand monitoring, lighting control by zones.
iv. Monitoring of operation conditions such as temperatures, pressures, energy end-uses.

Other functions and applications of EMCS are being developed and implemented in some facilities. Some of these applications are discussed in the following sections:

EMCS can be used with expert systems to make intelligent operating decisions based on stored and accumulated knowledge. For instance, integrated EMCS/expert systems can be used to diagnose faults and inefficiencies in HVAC and lighting systems. Typically, an EMCS/expert system would be programmed with basic information about the building equipment and their design operation characteristics. Over time, actual operating data would be recorded and used to train the expert system and thus

improve its diagnostic accuracy. If a fault were detected, the EMCS/expert system would notify the building operator of the probable problems and suggest remedial actions or simply initiate automatically countermeasures in case of serious problems. As an example, if the indoor temperature for a specific space is noted to be rising significantly beyond the throttling range, the EMCS/expert system would examine all the relevant sensor readings (such as airflow rates, fan energy use, and cooling water flow and temperature). Then, the EMCS/expert system would indicate using its knowledge base that the probable causes for the problem are faulty fan operation or leakage in chilled water pipe (70% faulty fan and 30% chilled water pipe leakage).

Another function of EMCS that has been implemented in several buildings especially in the last decade is the maintenance of acceptable indoor air quality (IAQ) levels. Indeed, the cost of sensors for monitoring air pollution compounds such carbon monoxide (CO), carbon dioxide (CO_2), and volatile organic compounds (VOC) have decreased sufficiently enough to be incorporated in commercial and institutional buildings. For instance, CO_2 demand controlled ventilation has been implemented in several spaces including classrooms, conference rooms, theaters, and auditoriums.

5.3.3 Design Considerations of an EMCS

When an EMCS is recommended for a facility, it is important to consider some practical issues to ensure a successful design and operation. In particular, it is recommended to:

- Allow redundancy into the control systems in case of system failure. In particular, it is important that the local control devices are able to manage and operate the system for a reasonable period of time when the central control unit malfunctions or needs servicing.
- Provide clear information about the system operation. For instance color graphic displays are preferred to numerical data for the use of facility operators and managers.
- Perform a thorough commissioning of all the components and functions of the EMCS under various operating conditions (peak cooling and peak heating modes as well as part-load conditions).
- Train the operating staff to use the EMCS to their best advantage. In particular, the operators should understand the EMCS capabilities and benefits.

The selection of an EMCS for a given facility depends typically on the required functions and on economic considerations. The desired functions and controls from an EMCS are based on several aspects including the building type, HVAC system zoning, occupancy profiles, accuracy requirements, and the objectives of the owners. For instance, owner-developers may be more interested in having an EMCS with the lowest first cost rather than a system that provides a high-quality environment which may be one of the main objectives of owner-occupants. Moreover, high-rise buildings tend to have centralized systems with built-up fans and associated controls. In the other hand, low-rise buildings use typically package rooftop fan systems with local controls.

The cost benefits of the EMCS can be evaluated after identification of all the desired controls. Some of the important factors that affect the cost of an EMCS include:

i. System size and number of control points
ii. Degree of automation in the control functions
iii. Accuracy requirements for sensors and controls

To ensure that the control systems conserve energy and save operating cost, it is important to follow basic principles in their design including:

1. The energy-consuming equipment should be operated only when needed. For instance, heating temperature set-points should be set back during unoccupied periods. The heating equipment should be operated only to maintain these set-back temperatures (typically between 50°C and 55°C to prevent freezing damages for various components of the HVAC system),
2. The simultaneous heating and cooling should be avoided. Proper zoning and HVAC system selection can minimize—if not eliminate—the need for providing heating and cooling at the same time.
3. The outdoor air intake should be controlled. In the United States, only minimum requirement ASHRAE Standard 62-1999 for ventilation need to be supplied to the building when no economizer cycles are used.
4. The heating and cooling should be provided efficiently. In particular, only actual heating and cooling load requirements should be met. In addition, free cooling/heating or low-cost energy sources should be considered first to maintain comfort within the building.

Finally, it should be noted that energy control systems should be designed to be simple and easy to operate and maintain.

5.3.4 Communication Protocols

A communication protocol consists of a set of rules that have to be applied to exchange data between two parts of an EMCS system. Most manufacturers of building automation systems have their proprietary communication protocols. Therefore, building owners are forced to purchase only equipment from the original manufacturer if he wants to expand the existing automation system. Due to the lack of interoperability between communication protocols from various manufacturers, it is almost impossible to take advantage of a facility-wide approach to control optimization and energy savings. A single manufacturer does not provide all the best possible control strategies for electrical demand limiting, heating and cooling optimization, and similar energy-saving options. Moreover, several control sub-systems in a building including HVAC controls, lighting/daylighting interface, fire alarm and life safety, security, and communication systems are generally manufactured by different companies. Integrating all these subsystems is a difficult task without a common communication protocol.

As a solution to the limitations and the difficulties inherent to proprietary protocols, a number of open communication protocols have been developed in recent years. These open protocols have some interoperability capabilities and thus allow building owners and managers to keep the open door to competition on any future expansion projects. One of the most widespread and widely accepted open protocols is the BACnet, a data communication protocol for Building Automation and Control networks [1]. BACnet is a non-proprietary open protocol standard that supports various communication networks ranging from high speed Ethernet local area networks (LANs) to low cost networks. Since ASHRAE developed BACnet, no one specific company or consortium has an advantage or an influence on future development of the standard. Any changes for BACnet are published for public review and comment after discussions on an ASHRAE open committee that includes representatives from industry, academia, and government.

To design a BACnet device, a manufacturer needs to identify the BACnet objects and services required to achieve the intended functionality for the device. A BACnet object is a standard data structure defined with a set of properties and data types. In its current version, BACnet standard defines

several types of objects such as loops, tables, schedules, commands, and programs. BACnet services are the programmed actions that use the data objects to achieve the function of the device. Services, defined by the current version of the BACnet standard, include alarm and event services (to notify of any alarm and event), file access services (to read and write files), object access services (to read or write the properties of objects), remote device management services (to troubleshoot and maintain devices), and virtual terminal services (to allow interaction between a terminal and the device). Moreover, the BACnet device has to conform to a set of specifications using a series of conformance classifications. Each conformance classification adds functional services to the device. Thus, each BACnet device design would have a protocol implementation conformance statement (PICS) prepared by the manufacturer to identify the BACnet options available in the device.

In the last few years, some manufacturers have developed BACnet control devices. However, the integration and the application of these devices in real installations have not yet been documented.

5.4 Control Applications

Energy management and controls systems can be used to perform several functions and tasks. Early building automation systems were limited to simple functions, such as simple on/off programming including duty cycling and load shedding. Currently, more complex functions and controls can be achieved by EMCS. Some of these controls are now available in standard program packages such as:

- Duty cycling for motor loads to provide sequential shut-down for short periods for equipment such as supply fans of small air handling units. However for large motors, frequent duty cycling is not generally recommended due to adverse effects on belts, bearings, and motor drives.
- Demand shedding to limit electrical loads. However, it is generally difficult to identify loads that can be shed without affecting the building performance especially for HVAC systems that are not generally needed when electrical demand is high. Therefore, equipment not related to HVAC systems such plug loads or lighting fixtures are typically considered for demand shedding. In particular, programmable lighting controls can be combined with

other energy-saving lighting measures including dimming and occupancy sensors.
- Partial space conditioning to allow systems to cool only a small portion of the building by controlling supply-air dampers serving various zones. With the use of variable frequency drives, it is now possible to adjust fan speed to match small loads for most central fan systems.

For buildings, supervisory controllers have evolved to perform several functions including but not limited to:

- Maintain acceptable indoor quality environment in occupied spaces of buildings including thermal comfort, air quality, and visual comfort.
- Reduce energy consumption and thus energy and operating costs for buildings.
- Add some flexibility by allowing the use of some equipment while others are turned off either for regular maintenance or for repair.
- Assist in diagnostic analysis of faults specific to energy systems hardware by through a series of adjustments in control strategies.

The applications for supervisory controllers to improve the energy efficiency of building energy systems vary significantly and can range from single energy system to the entire building set of equipment and sub-systems. The following sections present some of these applications spanning a wide range of building energy systems.

5.4.1 Electrical Systems

5.4.1.1 Motor Duty Cycling Controls

Frequent turning on and off HVAC systems (and in particular fan motors) may be actually detrimental and may not be cost-effective over the life cycle of the equipment due to added maintenance and repair costs. However, on/off cycling of motor loads can be performed safely without long term damages when minimum on and off times are respected. The National Electrical Manufacturers Association (NEMA) provides a set of recommendations for minimum on/off times of duty cycling of motor loads [2]. Some of these recommendations are summarized in Table 5.3. It is highly recommended however, that the motor manufacturers be directly

Table 5.3. Allowable Number of Start per Hour and Minimum Off-Time for Motor Loads [2].

Motor size HP (kW)	2-pole motors		4-pole motors		6-pole motors	
	Max. Starts/hr	Min. Off-time (sec)	Max. Starts/hr	Min. Off-time (sec)	Max. Starts/hr	Min. Off-time (sec)
2.0 (1.5)	11.5	77	23.0	39	26.1	35
5.0 (3.75)	8.1	83	16.3	42	18.4	37
7.5	7.0	88	13.9	44	15.8	39
15.0	5.4	100	10.7	50	12.1	44
20.0 (15.0)	4.8	110	9.6	55	10.9	48
25.0 (18.75)	4.4	115	8.8	58	10.0	51
30.0 (22.5)	4.1	120	8.2	60	9.3	53
40.0 (30.0)	3.7	130	7.4	65	8.4	57
50.0	3.4	145	6.8	72	7.7	64

consulted to determine their suggested minimum off-time and allowable number of starts per hour.

To fully benefit from duty cycling energy cost savings (due mostly to reduction in demand charges), two methods can be used. In the first method known as parallel duty cycling, all the motors are cycled on and off at the same time. This method can provide energy cost savings when the duty period is less than the demand period (typically 15 minutes in most utility rates). However, when the duty period exceeds the demand period, there is no reduction in demand changes if all the motors are cycled on and off at the same time. In this case, it is recommended to use the second method of duty cycling called staggered duty cycling which alternates the on and off times of the motors.

Most mechanical equipment manufacturers recommend extended duty cycling periods (higher than typical demand periods of 15 minutes). Therefore, staggered duty cycling approach should be considered in most applications to ensure the safety of HVAC equipment while reducing operating costs.

For example, a 33% reduction in the annual energy use and costs due to staggered duty cycling of three identical 2-pole fan motors, each rated at 30 kW [40 hp] if the motor has a cycle of 20 minutes on and 10 minutes

off as the minimum duty cycle. Indeed, at any given time, only two out of the three motors are operating.

5.4.1.2 Daylighting

The use of daylighting controls to reduce the reliance on electrical lighting systems to maintain visual comfort within indoor spaces is one effective approach to significantly reduce the energy consumption in commercial buildings. A typical daylighting control system is illustrated in Figure 5.11, include a photo-sensors to measure the illuminance level at various locations within the daylight space, controllers to determine the required luminance output for the electrical lighting fixtures, and a set of control strategies. Two common conventional control strategies are used for daylighting systems including stepped and dimming controls as outlined in Figure 5.12.

Energy Savings from Daylighting Controls: Several Studies indicated that daylighting can offer a cost-effective alternative to electrical lighting for commercial and institutional buildings. Through sensors and controllers, daylighting can reduce and even eliminate the use of electrical lighting required to provide sufficient illuminance levels inside office spaces. Recently, a simplified calculation method has been developed by Krarti et al. [3] to estimate the reduction in the total lighting energy use due to daylighting with dimming controls for office buildings. The method

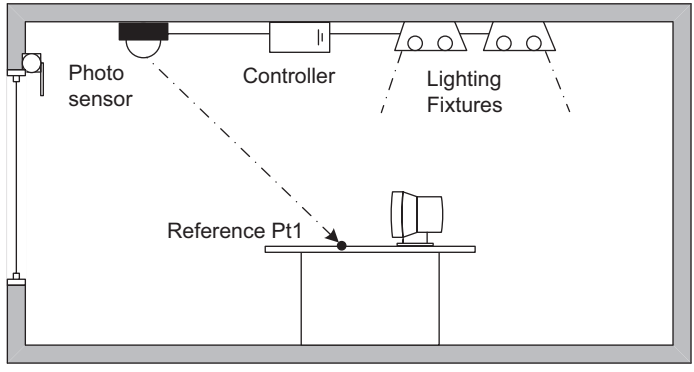

Figure 5.11. Typical Daylighting Control System for an indoor space.

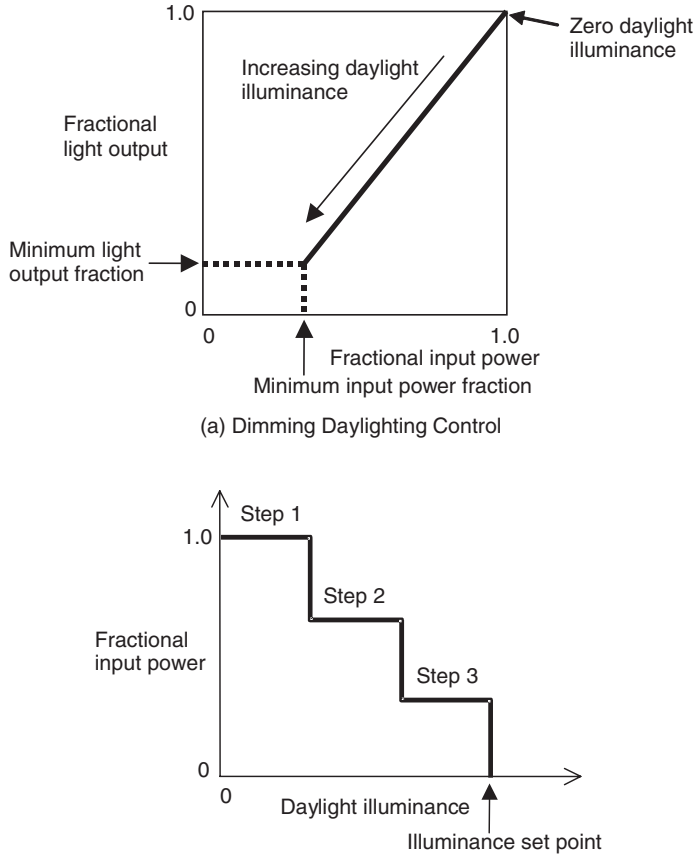

Figure 5.12. Conventional (a) Dimming and (b) Stepped Control Strategies for Daylighting Systems.

has been shown to apply for office buildings in the United States as well as in Egypt [4]. The simplified calculation method is easy to use and can be used as a pre-design tool to assess the potential of daylighting in saving electricity use associated with artificial lighting for office buildings.

To determine the percent savings, f_d, in annual use of artificial lighting due to implementing daylighting using daylighting controls in office buildings, Krarti et al. [3] found that the following equation can be used:

$$f_d = b\left[\, 1 - \exp(-a\tau_w A_w / A_p)\right] \frac{A_p}{A_f} \qquad (5.24)$$

where,

- Aw/Ap: window to perimeter floor area ratio. This parameter provides a good indicator of the window size relative to the daylit floor area.
- Ap/Af: perimeter to total floor area ratio. This parameter indicates the extent of the daylit area relative to the total building floor area. Thus, when Ap/Af = 1, the whole building can benefit from daylighting.
- *a* and *b*: coefficients that depends only on the building location and is given by Table 5.4 for various sites throughout the world.
- τ_w is the visible transmittance of the glazing

Table 5.4. Coefficients a and b of Eq. (5.24) for Various Locations Throughout the World.

Location	a	b	Location	a	b
Atlanta	19.63	74.34	Minneapolis	18.16	71.98
Chicago	18.39	71.66	Omaha	18.94	72.30
Denver	19.36	72.86	Casper	19.24	72.66
Phoenix	22.31	74.75	Portland	17.79	70.93
New York City	18.73	66.96	Montreal	18.79	69.83
			Quebec	19.07	70.61
Washington D.C.	18.69	70.75	Vancouver	16.93	68.69
			Regina	20.00	70.54
Boston	18.69	67.14	Toronto	19.30	70.48
Miami	25.13	74.82	Winnipeg	19.56	70.85
San Francisco	20.58	73.95	Shanghai	19.40	67.29
			K-Lumpur	20.15	72.37
Seattle	16.60	69.23	Singapore	23.27	73.68
Los Angeles	21.96	74.15	Cairo	26.98	74.23
Madison	18.79	70.03	Alexandria	36.88	74.74
Houston	21.64	74.68	Tunis	25.17	74.08
Fort Worth	19.70	72.91	Sao Paulo	29.36	71.19
Bangor	17.86	70.73	Mexico91	28.62	73.63
Dodge City	18.77	72.62	Melbourne	19.96	67.72
Nashville	20.02	70.35	Roma	16.03	72.44
Oklahoma City	20.20	74.43	Frankfurt	15.22	69.69
			Kuwait	21.98	65.31
Columbus	18.60	72.28	Riyadh	21.17	72.69
Brismarck	17.91	71.50			

As an alternative to conventional controls, Seo et al. [5] have developed an optimal daylighting controller. The optimal controller relies on an outdoor sensor to regulate the operation of the indoor lighting fixtures as outlined in Figure 5.13. Moreover, the optimal controller considers the actual lamp performance data to estimate the spatial illuminance distribution due to the electrical lighting system within an indoor space. Moreover, the optimal controller can determine the optimal settings for each fixture or lighting circuit within the space to maintain the desired indoor illuminance levels at specific reference points such as workplaces. In addition, the optimal daylighting controller can utilize only one outdoor photo-sensor or can forgo totally any sensing system to maintain desired indoor illuminance levels. Indeed, once the lighting system for an indoor space is designed, the performance of the lighting system can be predicted using detailed lighting simulation tools.

The lighting and daylighting simulation tool presented in [5] is utilized to optimize the design of lighting circuiting layouts in buildings. Specifically, a space with five possible lighting circuit layout options is considered as illustrated in Figure 5.14. The lighting circuiting options in Figure 5.14 indicate how the lamps are physically wired. Each lighting circuit has its own controller. For instance, the lamps in Option 1 are all wired to the same circuit and are connected to one controller. Thus, in Option 1, the entire space is one lighting zone controlled by one controller/photo-sensor system. In Option 4, there are 3 lighting circuits associated to 3 lighting zones. Each lighting zone is controlled by one controller. It should be noted that each lamp illuminance output affects lighting level in all 3 zones. For the analysis described in this section, it is assumed that the photo-sensor (i.e., the reference point) in each lighting zone is located in the middle of the zone.

Table 5.5 compares lighting energy use savings obtained using optimized daylighting controls with various window orientations and circuiting layouts for a building space located in Golden, CO. As indicated in Table 5.5, the lighting energy savings due to daylighting controls are the highest (67.2%) in layout 5 when the windows are south facing. When the windows are north facing, lighting energy savings ranging from 0.2% to 40% are obtained depending on the circuiting layouts. For east- and west-orientated windows, lighting energy savings of 18% to 50% can be achieved. The results outlined in Table 5.5 indicate that layout 5 provides the most energy savings up to 40% relative to layout 1. For layout 2, the lighting energy savings relative to layout 1 range from 1.4% to 6.6% depending on the orientation of the windows. It should be noted that daylighting control performance for layouts 4 and 5 are similar for east and west

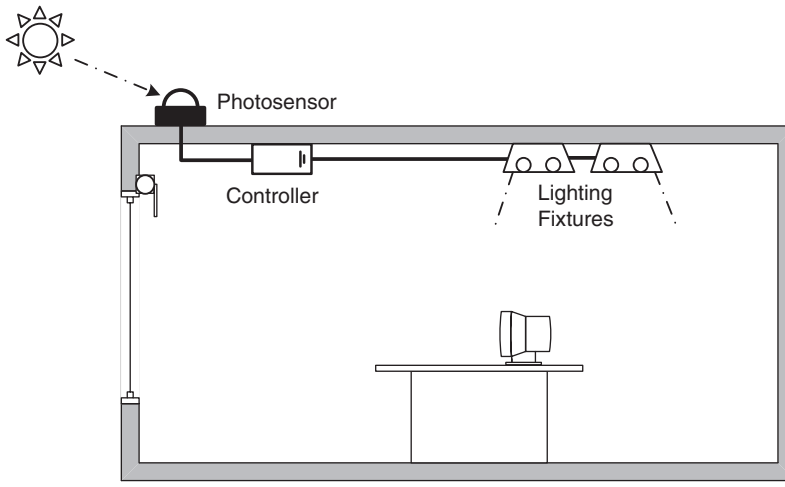

Figure 5.13. Daylighting Control System for n indoor space using an outdoor photo-sensor.

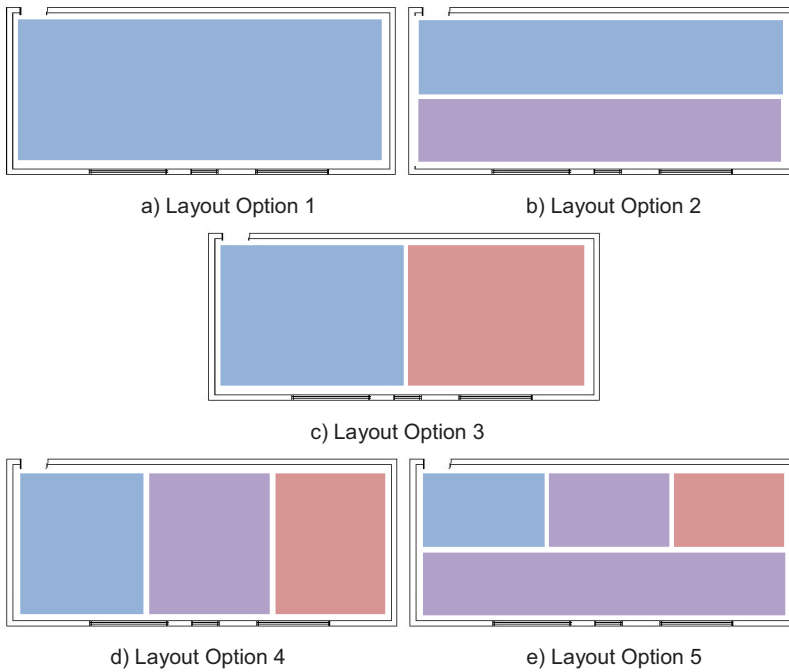

Figure 5.14. Lighting circuiting layout options for optimal daylighting controller.

Table 5.5. Summary of Parametric Simulation Results for 4 Window Orientations and 5 Circuiting Layouts (Golden, CO).

(a) Lighting energy saving relative to no daylight control

	Layout 1	Layout 2	Layout 3	Layout 4	Layout 5
West	28.5 %	33.2%	38.1%	49.4%	50.4%
North	0.2%	2.5%	8.4%	29.7%	40.2%
East	18.6%	19.8%	29.7%	43.1%	45.2 %
South	46.5%	49.9%	57.5%	61.6%	67.2 %

(b) Lighting energy saving relative to layout 1

	Layout 2	Layout 3	Layout 4	Layout 5
West	6.6%	13.4%	29.2%	30.7%
North	2.3%	8.2%	29.6%	40.0%
East	1.4%	13.6%	30.1%	32.6%
South	6.3%	20.5%	28.2%	38.7%

orientations. However, layout 5 outperforms layout 4 for both south and north orientations.

5.4.2 Optimal Start of HVAC Systems

After the energy crisis of the 1970's, engineers found that building utility bills can be reduced by 12% to 34% by merely implementing an occupied thermostat setback [6]. During the cooling season, the unoccupied zone temperature set-point is raised while during the heating season, the set-point is lowered. In some mild climates, the indoor temperatures are allowed to float during night periods rather than defined by a night set-point. However, the winter night setback is typically set between 13°C (55°F) and 15.5°C (60°F). Thus, building indoor temperature is colder than its occupied set-point in the early mornings. Due to the building thermal mass, the heating system has to be turned on earlier than the scheduled occupied time to achieve thermal comfort when people first enter the building.

The amount of time a building takes to recover from its night setback to its occupied set-point is usually referred to as the building recovery time. The length of the recovery period depends on several factors including outdoor ambient temperatures, indoor temperatures, and building thermal characteristics. Therefore, the recovery period can vary daily throughout

the heating season especially in climates with sudden changes in the outdoor temperatures. However, the recovery time is typically set to be the same throughout the entire heating season by building operators to simplify the start controls of the heating system. This recovery time is defined as the earliest time the heating system needs to be started for the coldest day of the year. While, this approach may achieve thermal comfort at the start of the occupancy periods throughout the heating season, it does not ensure optimal start times for the heating system especially during mild winter mornings.

With an energy management and control systems (ECMS), algorithms can be developed to determine the optimum start times and thus the best recovery periods. Several algorithms have been suggested in the literature. Typically, the recovery times are adjusted daily based on outdoor ambient temperatures and initial building zone temperatures (which may not be necessarily close to the set-point temperatures during unoccupied periods). In the following sections, some of the simplified algorithms for estimating building recovery times are presented.

Method 1: A linear relationship between recovery times, t, and outdoor ambient temperatures, T_{amb}:

$$t = a_0 + a_1 T_{amb} \tag{5.25}$$

Where,

$$a_0 = \tau_{\max} + \frac{\tau_{\max} T_{amb,\max}}{T_{amb,zero} - T_{amb,\max}}$$

and,

$$a_1 = -\frac{\tau_{\max}}{T_{amb,zero} - T_{amb,\max}}$$

with:

- t_{max} is the maximum recovery period
- $T_{\text{amb,max}}$ is the outdoor ambient temperature during the time when the maximum recovery period is obtained.
- $T_{\text{amb,zero}}$ is the outdoor ambient temperature during the time when the recovery period is zero.

It should be noted that the approach presented by Eq. (5.25) is relatively easy to implement since it does not require any regression analysis to determine the relation coefficients a_0 and a_1.

Method 2: A linear relationship between the recovery time, t, and both outdoor ambient temperature, T_{amb}, and initial zone temperature, $T_{zone,initial}$

$$t = a_0 + a_1 T_{amb} + a_2 T_{zone,initial} \tag{5.26}$$

Where the coefficients a_0, a_1, and a_2 are determined based on a regression analysis. This approach is first developed and implemented by Jobe and Krarti [7]. To determine the regression coefficients, it is recommended that data for at least 5 days be used.

Method 3: A quadratic relationship between the recovery time, t, and both outdoor ambient temperature, T_{amb}, and initial zone temperature, $T_{zone,initial}$, using a weighting function in the form of:

$$\tau = a_0 + w a_1 T_{amb} + (1-w).[a_2 T_{zone,initial} + a_3 T^2_{zone,initial}] \tag{5.27}$$

Where the weighting parameter w is defined as follows:

$$w = 1000^{-(T_{zone,initial} - T_{setnight}) \,/\, (T_{zone,final} - T_{setnight})}$$

with

- $T_{setnight}$ is the night (or unoccupied) setback temperature
- $T_{zone,final}$ is the occupied set-point temperature

The approach presented by Eq. (5.27) is proposed by Seem et al. [8] based on results from computer simulations.

A comparative analysis performed by Jobe and Krarti [7] between the three approaches indicated that all three methods can reduce the start-up time for the heating system and thus save energy compared to the common approach that relies on setting the maximum recovery time throughout the entire heating season. Table 5.6 summarized the daily average reduction time in recovery period for two educational buildings located in Colorado using the three approaches discussed above.

It is clear from the results presented in Table 5.6 that the approach described as method 2 provides the highest recovery time reduction while providing adequate thermal comfort within the two buildings. For the two buildings used in the comparative analysis, the recovery time was found to vary rather linearly with outdoor ambient temperatures. Therefore, and since method 3 places more emphasis on indoor air

Table 5.6. Daily Average Reduction in Recovery Periods for Two Buildings Located in Colorado [7].

Building # method #	Maximum recovery period (min)	Predicted recovery period (min)	Reduced start-up time (min)	Percent reduction from maximum recovery Period
Building 1				
Method 1	90	64	26	29%
Method 2	90	53	37	41%
Method 3	90	77	13	14%
Building 2				
Method 1	75	19	56	74%
Method 2	75	19	56	74%
Method 3	75	28	47	62%

temperatures [refer to Eq. (5.27)], it may not be adequate for the considered buildings.

5.4.3 HVAC Equipment Operation

5.4.3.1 Outdoor Air Intake Controls

Due to the increase in the number of occupant complaints regarding poor indoor air quality (IAQ) and the increase in buildings diagnosed with sick building syndrome, the control and measurement of outside air intake rates has come to the forefront of attention of many HVAC engineers and designers. The majority of HVAC system designers today rely on the ASHRAE "Ventilation Rate Procedure" described in ASHRAE Standard 62 [9], *Ventilation for Acceptable Indoor Air Quality*. ASHRAE Standard 62 specifies minimum ventilation rates as a function of building use and occupancy to provide adequate IAQ for conditioned spaces.

Unfortunately, the necessary monitoring equipment and control logic to maintain minimum outdoor intake rates are often nonexistent or are used improperly if they are installed. Consequently, several commercial buildings, and in particular those with Variable Air Volume (VAV) systems, have been found to have inadequate ventilation [10]. The use of appropriate airflow measurement or VAV control techniques is critical

to maintain minimum outside air intake rates. In a recent work [11], theoretical and experimental analyses have been performed to determine the accuracy of various techniques for outside airflow measurement and control applicable to VAV systems.

In economizer systems, the size of the outside air duct must be large enough to safely provide 100% of the design flow. This large size, however, results in very low airflow velocities during minimum outside air intake rate mode which can make measurement difficult with pressure-based airflow measurement devices.

Table 5.7 summarizes the results of an experimental comparative analysis performed by Krarti et al. [12] to evaluate some of the control techniques for outdoor air intake under repeatable laboratory conditions. Specifically, Table 5.7 provides the average value, the standard deviation, the root mean square of the outdoor air intake flow rate, and the validity of each measurement and control method tested in a laboratory set-up. In particular, three measurement techniques are used to determine the air flow rates: averaging pitot-tube array station (P), electronic thermal anemometer (E), and CO_2 concentration balance technique (C). For more details on these measurement techniques, the testing set-up, and the experimental results, the reader is referred to Krarti et al. [12].

The percentages listed in Table 5.7 in the column labeled "validity" were calculated from Eq. (5.28):

$$validity = \frac{n_v}{n} \tag{5.28}$$

where: n_v = the number of valid data points

Each test presented in Table 5.7 is subject to errors from the airflow measurement and the control technique used. Each 10-second data point, x_i, recorded during testing was considered valid if it met the following two conditions:

1) $\left|x_i - set\ point\right| \le \left(set\ point \cdot 10\%\right)$

and

2) $\frac{e_i}{x_i} < 15\%$

Table 5.7. Summary of Comparative Results for the Control and Measurement Techniques Tested by Krarti et al. [12].

					Outside Air Intake Rate Measurements					
					Averaging Pitot-tube Array			Electronic Thermal Anemometry		
System Description	Measurement Control[1]	Case	Set-point (cfm)	Validity	mean (cfm)	stdev (cfm)	RMS (cfm)	mean (cfm)	stdev (cfm)	RMS (cfm)
Fixed Damper Position	-NA-	1-A	1,600	14%	656	658	1,150	682	564	1,048
Fixed Damper Position	-NA-	1-B	2,400	23%	1,410	678	1,199	1,407	680	1,199
Fixed Damper Position	-NA-	1-C	3,200	26%	2,178	819	1,309	2,124	870	1,513
Plenum Pressure Control	-NA-	2-A	1,600	100%	1,630	69	75	1,544	70	89
Plenum Pressure Control	-NA-	2-C	3,200	100%	3,288	94	129	3,279	88	118
Direct Control with Economizer Duct	P	3-A	1,600	100%	1,635	38	52	1,546	46	71
Direct Control with Economizer Duct	P	3-C	3,200	100%	3,192	50	51	3,225	47	53
Direct Control with Economizer Duct	E	4-A	1,600	94%	1,695	55	110	1,637	55	67
Direct Control with Economizer Duct	E	4-C	3,200	100%	3,228	49	57	3,263	50	80
Volume Tracking	E	5-A	1,600	0%	2,427	439	936	2,436	458	953

(*Continued*)

Table 5.7. Summary of Comparative Results for the Control and Measurement Techniques Tested by Krarti et al. [12].

					Outside Air Intake Rate Measurements					
					Averaging Pitot-tube Array			Electronic Thermal Anemometry		
System Description	Measurement Control[1]	Case	Set-point (cfm)	Validity	mean (cfm)	stdev (cfm)	RMS (cfm)	mean (cfm)	stdev (cfm)	RMS (cfm)
Direct Control with Dedicated Duct	P	6-A	1,600	100%	1,639	39	56	1,634	47	58
Direct Control with Dedicated Duct	P	6-B	2,400	100%	2,430	41	51	2,457	51	77
Direct Control with Dedicated Duct	E	7-A	1,600	100%	1,643	36	56	1,640	43	58
Direct Control with Dedicated Duct	E	7-B	2,400	100%	2,404	39	40	2,428	42	50
Injection Fan	P	8-A	1,600	100%	1,621	31	37	1,622	36	42
Injection Fan	P	8-B	2,400	100%	2,429	28	40	2,440	36	54
Injection Fan	E	9-A	1,600	100%	1,622	38	44	1,617	36	40
Injection Fan	E	9-B	2,400	100%	2,418	33	37	2,427	32	42
Direct Control	C	-NA-[2]	1,600	75%	1,632	137	141	1,605[2]	119[2]	119[2]

[1]P = Averaging Pitot-tube Array, E = Electronic Thermal Anemometer, C = CO_2 Concentration Balance
[2]A different system setup was used for testing the concentration balance measurement technique
[3]Value is for CO_2 concentration balance measurement technique, not electronic thermal anemometry

where: e_i = *the predicted error for the airflow measurement in the laboratory*

The first condition attempts to account for the accuracy of the control technique by requiring the data point to be within 10% of the set point. The second condition attempts to account for the accuracy of the airflow measurement technique by requiring the predicted error of the data point to be less than 15%.

In summary, accurate measurement and control of outside air intake rates in VAV systems is possible when careful attention is paid to proper installation and operation of system equipment. In systems where uniform airflow profiles exist, the use of an averaging Pitot-tube array or an electronic thermal anemometry, depending upon the expected velocities, for the direct measurement of outside airflow rates allows for direct control of minimum outside air intake rates. When these conditions are not met, the installation of a separate, dedicated minimum outside air duct, or the use of the concentration balance airflow measurement technique provide adequate alternatives. However, calculating the outside airflow rate using a temperature balance will not provide accurate results for all building operating conditions. Plenum pressure control in systems where measurement of the outside airflow rate is not possible should provide adequate control of minimum outside air intake rates. The traditional CAV control strategy of a fixed minimum outside air damper position, and the more robust volumetric fan tracking technique are not capable of accurately controlling outside airflow rates in VAV systems.

5.4.3.2 Demand Ventilation Controls

In order to ensure that ventilation is provided only occupants are present in spaces, demand controlled ventilation or DCV controls have been developed. Strategies for the use of CO_2-based DCV controls have been suggested evaluated by several studies. Most of these studies [13–18] have focused on the potential energy savings of the CO_2-based demand controlled ventilation systems, with CO_2 concentration reported as a measure of the IAQ performance. Strategies with both constant-air-volume (CAV) and variable-air-volume (VAV) HVAC systems have been developed. In computer simulation modeling, researchers compared the performance of several ventilation strategies, including constant outdoor airflow at the ASHRAE Standard 62, minimum outdoor airflow at the

typical rate with temperature-based economizer, DCV with a step-flow control algorithm, DCV with a step-flow control and a temperature-based economizer, and DCV with On-off control. The on-off control used an algorithm in which outdoor airflow is set at 100% if the high CO_2 set-point is exceeded and at 0% if the CO_2 concentration drops below the low set-point.

Other researchers used DCV control strategies and/or variations of these strategies in real buildings. In summary, control strategies applied in fields so far include:

1. The ASHRAE Standard 62 (20 cfm/person in office buildings).
2. The on/off control strategy [19–20].
3. The proportional control strategy [21–23].
4. The step-flow control strategy [24–25].

Alawi and Krarti [26] have evaluated the effect of various CO_2-based demand controlled ventilation strategies on HVAC system energy consumption under controlled and repeatable test conditions. Three control strategies were evaluated: (i) the base case control strategy that controls the outside/re-circulated damper to provide a fixed outside air fraction equivalent to 20 cfm/person; (ii) the ON/OFF control strategy that opens and closes the damper as a function of the CO_2 level deviation from the set-point; (iii) a PID controller that controls the damper position according to the error involved in the control process. Another control strategy was also evaluated with the damper controlled proportionally to the zone CO_2 concentration level.

The main findings of Alawi and Krarti experimental analysis include [26]:

- ASHRAE minimum outdoor air ventilation rate (20 cfm/person) is needed to maintain an acceptable indoor air quality of less than 1000 ppm of CO_2 concentration within an office space. The experiments performed at lower ventilation rates showed that these rates do not guarantee that the CO_2 concentration level is kept below the limit (1000 ppm).
- A PID controller can maintain acceptable indoor CO_2 level with the minimum outdoor air requirements, followed by the proportional control and lastly the ON/OFF control. A reduction of about 33% can be obtained when applying the PID controller instead of the

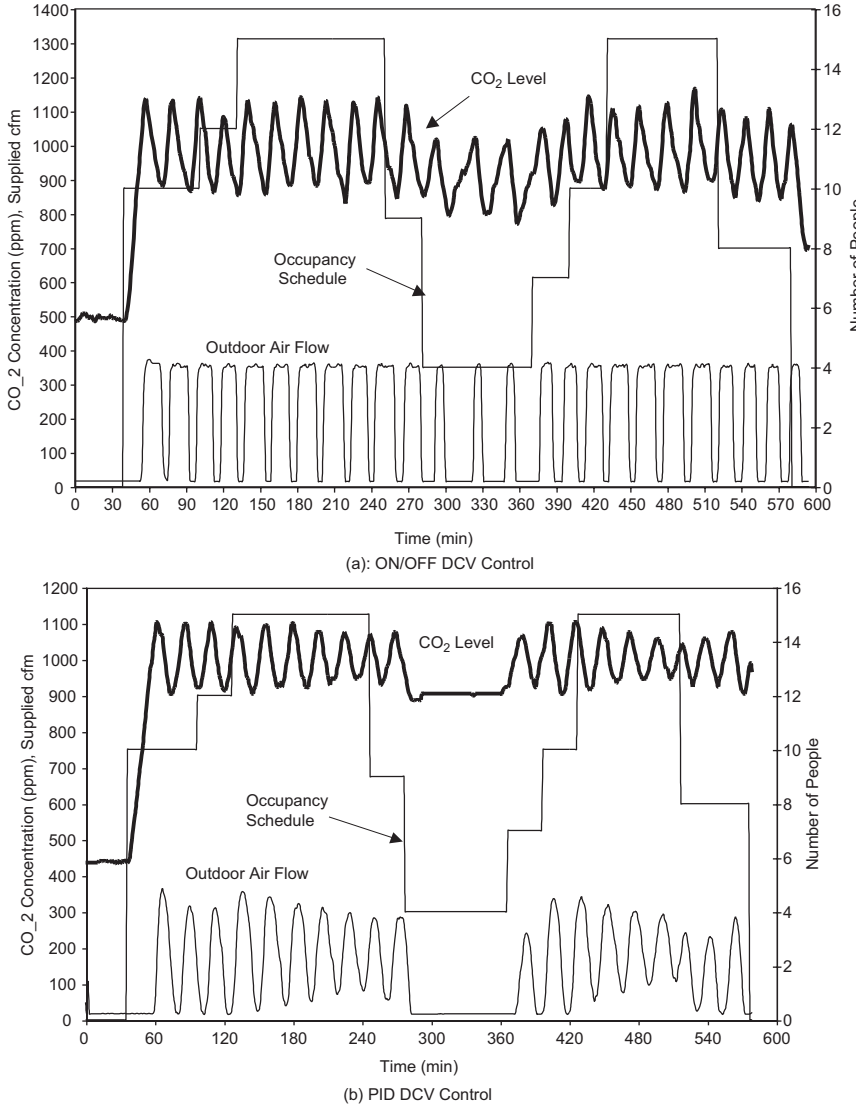

Figure 5.15. Outdoor air flow and CO_2 variations using DCV controls.

ON/OFF control strategy. Figure 5.15 compares the performance of both ON/OFF and PID DCV controls to maintain acceptable indoor air quality within an office space.

- The one-zone controls to maintain both indoor CO_2 concentration and temperature settings indicate that the ON/OFF control strategy

provides the minimum outdoor air requirements followed by the PID controller (as designed and implemented in their study) with a percent reduction of about 48.4% and 39.6%, respectively. The two-zone experiments, however, showed that the PID provided the lowest requirement of outside air by about 22.4%. Table 5.8 summarizes the experimental results to assess the performance of various DCV control strategies [26].

5.4.3.3 Radiant Slab Heating Systems

Radiant floor panel heating systems are widely used in several European and Asian countries. They consist of embedded hot water coils in floor slabs of residential and commercial buildings to provide space heating as illustrated in Figure 5.16 [27]. Control strategies of radiant floor

Table 5.8. Comparative Analysis of Various DCV Control Strategies.

One-zone Controls of CO_2 and Temperature Set-points

Parameters	Base case	On/Off	PID
Total volume of air (ft^3)	108,101	55,794	65,248
% Reduction in volume of air	–	48.4	39.6
Maximum CO_2 level (ppm)	860	956	983
Duration CO_2 exceeds limit (min)	0	2.1	35.1
Average outside temperature (F)	80.9	81.9	84.2

Two-zone Controls of CO_2 and Temperature Set-points

Parameter	Base case	On/Off	PID
Total volume of air (ft^3)	245,974	299,602	190,858
% reduction in volume of air*	–	–21.8	22.4
Maximum CO_2 level (ppm)	855	1007	965
Duration CO_2 exceeds limit (min)	0	72.3	13.8
Average outside temperature (F)	80.5	68.2	80.3

*A (−) sign indicates an increase in the volume or energy consumption

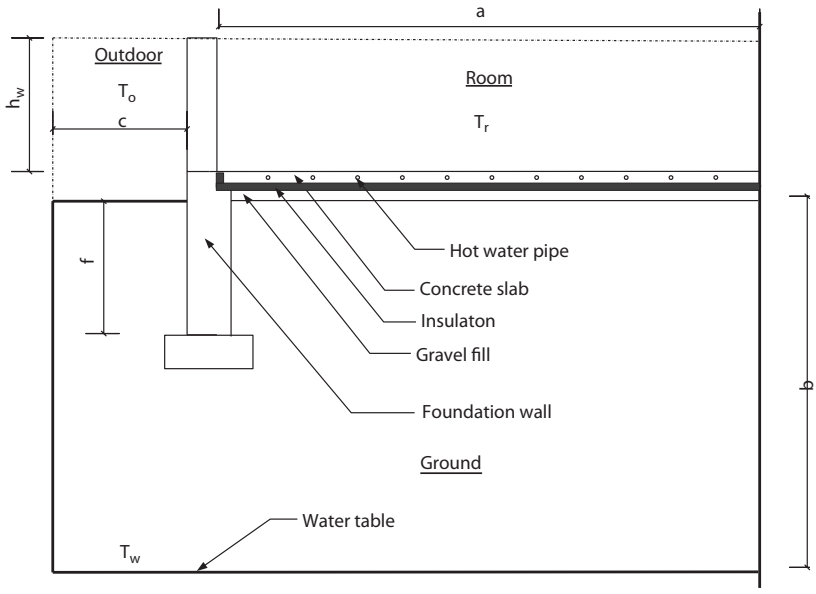

Figure 5.16. Ground-coupled heat transfer for a typical hot water radiant floor heating.

heating systems on slab-on-grade foundation are more challenging than those utilized to operate conventional hot air-heating systems. Due to the inherent time lag of ground-coupled heat transfer, the control of radiant floor heating system can be difficult in order to maintain indoor space temperature and thermal comfort within acceptable range.

Conventional control strategies for radiant floor heating panels typically maintain space temperature using mostly temperature or heat flux modulation techniques. Temperature-modulation control sets the supply water temperature to be proportional to outdoor temperature or to the difference between a desired set-point and room air temperatures. Although flux-modulation control attempts to ensure that a slab delivers heat to the space at a rate per unit area proportional to the difference between the room air temperature and the slab surface temperature. The heat flux provided to the slab is proportional to the difference between the supply and return water temperatures. Typically, three temperatures are considered for the radiant slab systems to in maintain indoor thermal comfort: mean air temperature (MAT), mean radiant temperature (MRT), and operative temperature (OT). Based on a detailed analysis of Ihm and Krarti [28], Figure 5.17 presents the total heating energy use and the number of hours when thermal comfort

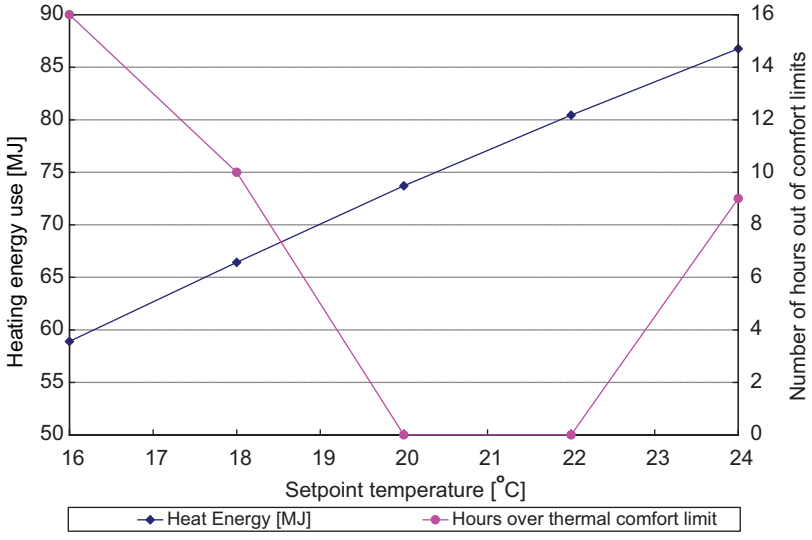

(a) : MAT-based control

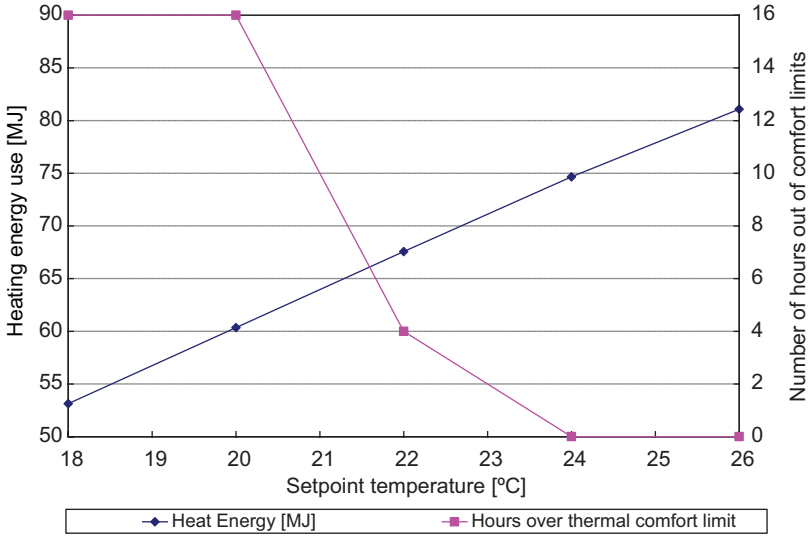

(b) : MRT-based control

Figure 5.17. Comparative of the three conventional controls for radiant slab heating system. (*Continued*)

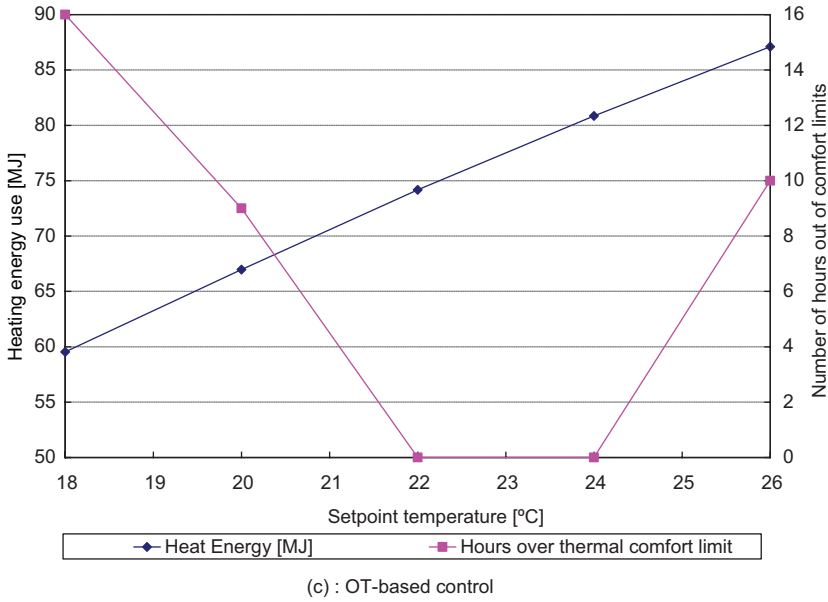

Figure 5.17. Comparative of the three conventional controls for radiant slab heating system.

levels exceed the acceptable range (i.e., $-0.5 \leq PMV \leq +0.5$) for the three conventional controls during a cold day in Denver, CO. As shown in Figure 5.17, total heating energy use is generally proportional to the increasing set-point temperature for all three control strategies. Depending on the control strategy, lower set-point temperature can save some heating energy use at the expense of a reduction in indoor thermal comfort. To further evaluate the performance of control strategies, the set-point temperatures are selected based on both achieving low energy use and satisfying building thermal comfort. Therefore, the set-point temperatures are chosen as 20°C for MAT-based control, 24°C for MRT-based control, and 22°C for OT-based control for further analysis.

Due to the dynamic characteristics of the radiant floor systems, optimal controls could be more appropriate than conventional controls to reduce energy consumption while maintaining building thermal comfort. The controlled variable to optimize building energy use is selected as time-varying indoor set-point temperature during one day to minimize the total daily operating cost taking into account the constraint of maintaining indoor space temperatures within a range defined by upper and lower temperature limits.

For the optimal control strategies, the objective function is constrained by the condition that thermal comfort has to be maintained during the occupied hours within acceptable levels. That is, the space indoor temperature should be kept within pre-defined indoor set-point temperature limits. Simmonds [29] used optimal controls to demonstrate that additional energy savings could be achieved by HVAC system if the control is based on maintaining the Fanger's predicted-mean-vote (PMV) index rather than the dry bulb temperature within a thermal comfort range. In general, a PMV value within ±0.5 is acceptable for thermal comfort according to ASHRAE [30]. Thus, desired PMV values can be used as constraints of the objective function to keep proper indoor thermal comfort conditions during the occupied period using the following condition:

$$-0.5 \leq PMV \leq +0.5 \tag{5.29}$$

Thus, the optimal control seeks to minimize the total energy use of radiant floor heating systems for any 24-hour period as a function of the building thermal characteristics, HVAC system, and outdoor environment with Eq. (5.29) as a constraint.

In the analysis discussed by Ihm and Krarti [28], the objective function to be minimized is defined as the total energy cost of heating the building constrained by thermal comfort (PMV) as expressed by the following equation:

$$C = \sum_{k=1}^{24} \{E_k + P(PMV_k)\} \tag{5.30}$$

Where,

- C: Total energy cost during a day combined penalty
- k: Hour
- E_k: Total energy use in a building at hour k
- P: Penalty when it PMV violates with the thermal comfort range.
- PMV_k: Thermal comfort index (Predicted Mean Vote) at hour k

Figure 5.18 shows the set-point temperature and MAT variation for both optimal and MAT-based controls when the slab thickness is 5 cm. The predicted set-point temperatures by optimal control vary at each hour while those of conventional MAT-based control are set to be 20°C

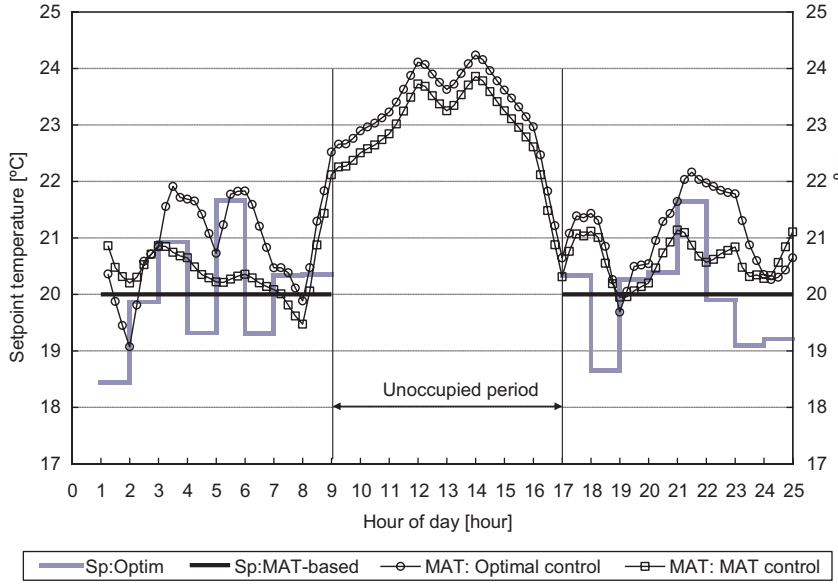

Figure 5.18. Comparison of setpoint temperature and MAT variation for both optimal and MAT-based controls for 5 cm thickness slab on Jan 21 in Denver, CO.

during the occupied hours of day [28]. The total heating energy use associated with in optimal control (46.9 MJ) is less than that required by the MAT-based control (70.0 MJ). It should be noted that the maximum heating energy for the optimal control is higher than that for the MAT control. However, the optimal control uses more effectively the high thermal mass of slab-on-grade floor and the ground to reduce total heating energy while maintaining acceptable thermal comfort levels for the occupants.

Several thermal comfort models have been proposed to predict the thermal sensation of people using personal, environmental, and physiological variables that influence thermal comfort. EnergyPlus incorporates three thermal comfort models including: (i) Fanger comfort model using the predicted mean vote (PMV) developed by Fanger [31], (ii) Pierce two-node model using the predicted mean vote modified by effective temperature (PMVET) developed by J. B. Pierce Foundation [32], and (iii) KSU two-node model using the thermal sensation vote (TSV) developed by Kansas State University [32]. The performance of the optimal controls for radiant slab systems depend on the thermal comfort model considered

in the optimization. Table 5.9 summarizes the total building heating energy savings attributed to optimal controls relative to the MAT-based control. It indicates that optimal controls can reduce total building energy by 26.9% based on Fanger model, by 29.5% based on KSU two-node model, and by 7.7% based on Pierce two-node model. The lower savings obtained for the Pierce model is expected since it has a 9-point thermal sensation scale (4 to –4) rather than the 7-point thermal scale (3 to –3) of Fanger and KSU models.

The potential savings associated with optimal controls depend on the thermal mass of the slab floor. Table 5.10 summarizes the total building heating energy savings attributed to optimal controls relative to MAT-based controls for various slab thickness values. The results indicate that optimal controls can reduce total building energy by 30.1% for 5-cm slab, by 26.9% for 10-cm slab, and by 22.7% for 15-cm slab.

5.4.3.4 Cooling/Heating Central Plant Optimization

Cooling and heating central plants offer several opportunities to reduce energy operating costs through optimal or near-optimal controls for individual equipment (local optimization) and for the entire HVAC system (global optimization). Although optimal controls have been developed

Table 5.9. Comparison of the Performance for MAT-Based and Optimal Controls for Three Thermal Comfort Models.

Comfort model	Optimal control total heating energy [MJ]	Savings [%]
Fanger	54.7	26.9
KSU	52.2	29.5
Pierce	57.7	7.7

Table 5.10. Comparison of the Performance for MAT-Based and Optimal Controls for Various Values of Slab Thickness.

Slab thickness	MAT control total heating energy [MJ]	Optimal control total heating energy [MJ]	Percent saving in total building energy [%]
5 cm	70.0	46.9	30.1
10 cm	74.0	54.7	26.9
15 cm	74.5	59.8	22.7

and implemented for various components of cooling and heating central plants, global optimization remains considerably a complex endeavor and only few strategies have been suggested and tested.

In this section, some of the local optimal control strategies are discussed. Moreover, operating strategies for entire cooling/heating plants are briefly discussed.

(a) Single Chiller Control Improvement

Before replacing an existing chiller, it may be more cost-effective to consider other cooling alternatives or simple operating strategies to improve cooling plant energy performance. In particular, a significant improvement in the overall efficiency of a chiller can be obtained through the use of automatic controls to:

- Supply chilled water at the highest temperature that meets the cooling load.
- Decrease the condenser water supply temperature (for water-cooled condensers) when the outside air wet bulb temperature is reduced.

(b) Controls for Multiple Chillers

When a central cooling plant consists of several chillers, a number of control alternatives exist to meet a building cooling load. Effective controls would select the best alternative for operating and sequencing the chillers to minimize the cooling plant operating costs.

Simple guidelines can be followed to operate multiple chillers at near-optimal performance. Typically, chiller operating variables such as chilled water temperature and condenser water flow rate are adjusted to ensure optimal controls. Some of the near-optimal control guidelines to operate electrically driven central chilled water systems are summarized below [33]:

- Multiple chillers should be controlled to supply identical chilled water temperatures.
- For identical chillers, the condenser water flow rates should be controlled to provide identical leaving condenser water temperatures.
- For chillers with different capacities but similar part-load performance, each chiller should be loaded so the at the same load fraction. The load fraction for a given chiller can be set as the ratio of its capacity to the sum total capacity of all operating chillers.

To determine the optimal chiller sequencing, a detailed analysis is generally needed to account for several factors including the capacity and the part-load performance of each chiller and the energy use associated with all power-consuming devices such as distribution pumps.

(c) Controls for Multiple Boilers

The use of an array of small modular boilers provides more energy efficient heating system than a single large boiler especially under part-load operation conditions. Indeed, each of the modular boilers can be operated close to its peak capacity and thus its highest energy efficiency. To optimally operate multiple boilers, it is important to know when to change the number of boilers on-line and/or off-line. The mere addition of a second boiler on-line when one boiler cannot handle the load may not provide the minimum operating cost. Indeed, the increase of firing rate (due to additional heating load) on any given boiler can cause a decrease in thermal efficiency due to higher flue-gas temperatures and thus higher thermal losses. However, the addition of a second boiler on-line increases the standing losses due to auxiliaries and the thermal losses through the added casing and piping of the second boiler. Therefore, a detailed analysis is needed to determine the changeover points for the multiple boilers. These changeover points depend on the characteristics of each boiler [33].

5.4.4 HVAC Systems with Thermal Storage

5.4.4.1 Precooling of Building Thermal Mass

The storage capabilities of a building structure can be used to shift a portion of on-peak cooling loads to off-peak periods and thus reduce electrical demand and energy charges. This measure can be achieved by precooling the building thermal mass. Reported studies [34−35] have shown that when an effective control strategy is used, up to 35% in energy cost savings can be achieved when an effective control strategy is used to determine when and how much to precool the building. Some additional savings in operating costs can be achieved if free cooling is used for precooling when cool outdoor air temperature is introduced to the building during the night using the air handling fans. In some cases, the cost of operating air handling fans may be less than the reduction in operating costs for mechanical cooling during occupied periods.

Pre-cooling building thermal mass is an example of the application of the EMCS to reduce operating costs. Pre-cooling of the building thermal mass can be effective at lowering building operating costs. This strategy can have a large impact when chillers have high loads during periods of high occupancy and high outdoor temperatures (which typically coincide with on-peak periods in rate structures). By reducing the on-peak cooling load it is possible to reduce chiller energy use during these critical periods, thereby reducing energy costs.

The pre-cooling control strategy is illustrated in Figure 5.19 and compared with conventional night setup control. Precooling starts with a constant temperature set point tpre, typically during the night. The warm-up period is then used to reset the zone air temperature set point so that the cooling system turns off without calling for heating. During this time, the zone air is warmed by lighting and equipment loads. The occupied set point, tocc, is set at the low end of the comfort region so that the building mass charge is held as long as cooling capacity is available. This set point is maintained until the limit on cooling capacity is reached. After this point, temperatures in the zones float up and the building thermal mass provides additional cooling.

Based on long-term simulation analysis, the annual energy cost savings associated with pre-cooling has been estimated for various time-of-use utility rates [36]. For time-of-use rates, on-peak to off-peak ratio for energy and demand charges is defined as follows:

Re: ratio of on-peak to off-peak energy charges:

$$R_e = \frac{PeakEnergyRate(\$/kWh)}{Off - PeakEnergyRate(\$/kWH)} \tag{5.31}$$

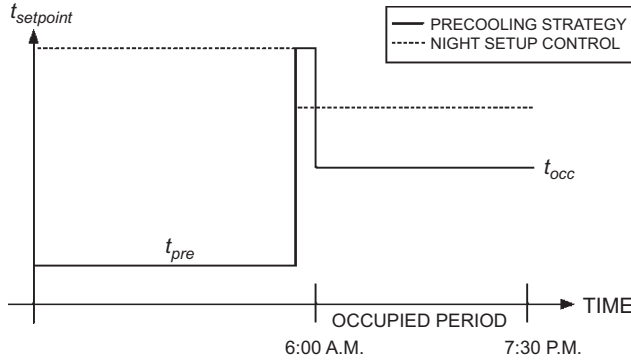

Figure 5.19. Typical indoor air temperature set points for precooling controls.

Rd: ratio of on-peak to off-peak demand charges:

$$R_d = \frac{PeakDemandRate(\$/kW)}{Off - PeakDemandRate(\$/kW)} \tag{5.32}$$

Figures 5.20 and 5.21 show the variation of the annual energy cost savings for a typical office building located in four US locations due to a 4-*hr* pre-cooling period as a function of R_d and R_e, respectively. The office building has a heavy thermal mass of 105 lbm/ft^2 (513.7 kg/m^2) and the time-of-use rate has an 8-*hr* on-peak period [36].

Using detailed simulation analysis for 16 US climates, Katipamula et al. [37] estimated the potential energy savings associated with precooling of commercial buildings. The results of the simulation analysis are summarized in Table 5.11 for most of the building types in all 16 climates. The potential savings using pre-cooling strategies can be substantial for most building types and climates where economizer cooling potential is modest and the annual sensible load is dominant.

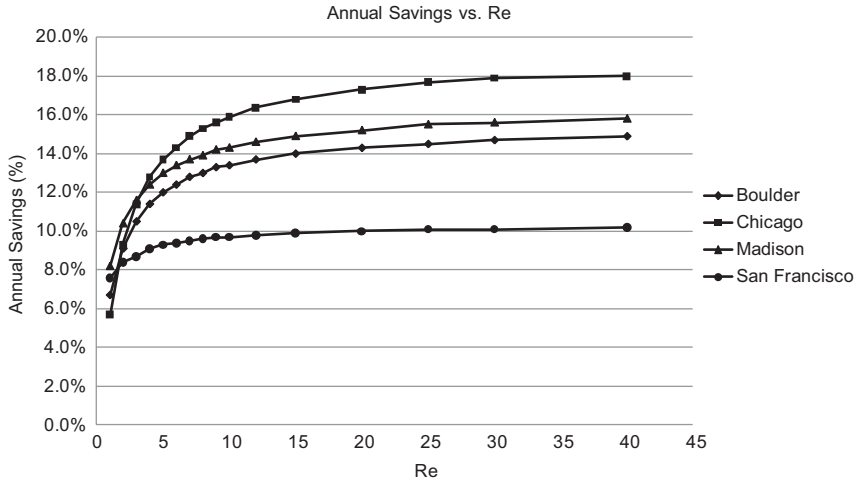

Figure 5.20. Annual energy cost savings due to pre-cooling relative to conventional controls as a function of R_e.

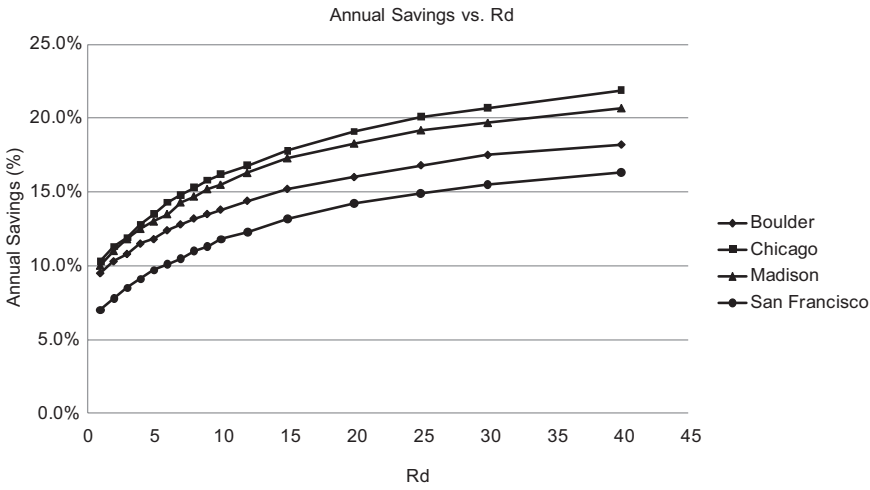

Figure 5.21. Annual energy cost savings due to pre-cooling relative to conventional controls as a function of R_d.

Table 5.11. Pre-Cooling Energy Savings Potential for 16 US Climates.

Building type	Minimum	Maximum	Average
Office, small	59%	77%	70%
Medium	13%	52%	37%
large	21%	61%	40%
Retail, standalone	56%	73%	66%
strip mall	45%	63%	56%
Primary school	46%	55%	51%
Secondary school	32%	49%	43%
Hotel, large	16%	57%	44%
Supermarket	59%	78%	68%
Warehouse	50%	81%	69%
Outpatient	65%	83%	78%
Hospital	48%	76%	64%

5.4.4.2 Passive and Active Thermal Energy Storage Systems

There are two common approaches to store cooling thermal energy in buildings: active and passive systems. The active systems consist of ice or chilled water storage tanks, commonly known as thermal energy storage (TES) systems, which are charged at night and discharged during the day. The passive systems utilize the thermal mass of the building materials to pre-cool the building at night when the electrical rates are low. Both active and passive systems have been used to shift some of the cooling loads from on-peak to off-peak utility rate periods. Several benefits can be incurred from reducing on-peak electrical demands. From a building owner's point of view, the prime motivation for load shifting is to avoid high energy rates and to reduce the overall demand charges. From the power utility's perspective, however, the benefit of active or passive storage systems is their effectiveness in reducing peak electricity demand [38].

Some studies have considered the use of both passive and active TES systems to reduce or even eliminating on-peak cooling demands and thus reduce demand charges associated with operating the cooling system [38−40]. Optimal control takes advantage of the building thermal capacitance to minimize the operating cost over a specified period of time such as a day while meeting some required constraints. Building loads are shifted to off-peak hours by proper adjustment of space temperature set points (thermostat settings) throughout the day.

The control strategies for both passive and actives TES systems can include:

- Conventional controls without load shifting (i.e., no pre-cooling of building thermal mass and no utilization of ice storage system)
- Pre-cooling of building thermal mass (typically unoccupied periods) to reduce peak cooling loads [41].
- Chiller-priority control strategy through the operation during on-peak periods of first the chiller (with a capacity smaller than the peak cooling load) and then the ice storage tank to meet any thermal load above the chiller capacity [40–41].
- Storage-priority control strategy through the operation during on-peak periods of first the ice storage and then the chiller to meet cooling thermal loads. The storage-priority control is set so the ice tank is not discharged prematurely [34–40].

- Optimal control is that control trajectory that minimizes the combined energy and demand charges over the simulation period. The objective function to be minimized is the total cost (i.e., including both energy and demand) of the cooling system. The total cost of the cooling system is represented mathematically as [40, 42]:

$$C = r_{d,o}\, P_{\max,o} + r_{d,1}\, P_{\max,1} + \sum_{k=0}^{K} r_{e,\gamma(k)} P(k) \Delta t \tag{5.33}$$

where:
C = The combined cost including both energy and demand charges,
$r_{d,0}$ = Off-peak demand charge \$/kW,
$r_{d,1}$ = On-peak demand charge \$/kW,
$P_{max,v}$ = Peak demand incurred in rate period v (v = 0 for off-peak, and v = 1 for on-peak),
r_e = Energy charge \$/kWh,
K = Total number of hours in the simulation period,
$P(k)$ = Total cooling and non-cooling plant power consumption at k,
$g(k)$ = 0 if k is during off-peak period, and 1 if k falls during on-peak period, and.
Dt = Time interval of one hour.

- For the case where only energy charges are minimized, the cost function is reduced to [40]:

$$C_{\text{energy}} = \sum_{k=0}^{K} r_{e,\gamma(k)} P(k) \Delta t \tag{5.34}$$

- On the other hand, if only the demand charges are minimized, the cost function becomes [40]:

$$C_{\text{demand}} = r_{d,0}\, P_{\max,0} + r_{d,1}\, P_{\max,1} \tag{5.35}$$

- Thus, the optimal control that seeks to minimize the combined energy and demand charges has the following cost function:

$$C = C_{\text{energy}} + C_{\text{demand}} \tag{5.36}$$

- The electrical energy cost represents the total cooling plant power consumption multiplied by the energy charge \$/kWh. The electric demand cost on the other hand, is generally based on the customer's maximum electrical power over 1 month. The maximum electrical power $P_{\max}$ is defined as the maximum value of electrical power

consumed in the building during on-peak period of the day. Because the simulation period of this research study is assumed to be a day (i.e., 24-hour period), the electrical demand cost (i.e., demand charge multiplied by P_{max}) is discounted by a factor of 30 to reflect the charges associated to one day in a typical month (i.e., average demand daily cost).

Under controlled laboratory testing conditions, Hajiah and Krarti [43] have performed a series of experimental analysis to compare the performance optimal controls for passive and active TES systems against that of conventional controls. The results of the experimental analysis for the three control strategies are summarized in Table 5.12. The results indicate significant cost savings can be achieved using the optimal controls compared to the conventional control strategy especially for the demand cost optimal control. Indeed, when charges are optimized, 13.2% savings in demand charges are obtained with 9.9% savings in total charges. When total charges are minimized, more 10.8% cost savings can be achieved.

The ice storage system optimal controller achieved total cost savings of 10.8% relative to the conventional control (system operating during occupancy hours only with no pre-cooling). However, higher savings of 28.1% in the total daily operating cost are obtained with the use of the combined optimal controller (i.e., use of both pre-cooling and ice storage) relative to the conventional control. This result illustrates clearly the advantage of using both passive thermal energy storage system (i.e., building thermal mass) and an active thermal energy storage system (i.e., ice storage tank) to minimize total building energy costs.

Table 5.12. Cost Savings Obtained for Optimal TES Control, Optimized Pre-Cooling, and Optimal Control Using Both Building Thermal Mass and Ice Storage System.

Control type	Energy cost ($)	Demand cost ($)	Total cost ($)	Savings in total cost (%)
Conventional (no TES system)	106.1	34.4	140.4	—
Optimized pre-cooling	91.3	28.2	119.5	14.9
Optimized ice Storage System	96.0	29.3	125.3	10.8
Optimized pre-cooling and ice storage system	81.0	20.0	101.0	28.1

Model predictive controls applied to commercial buildings require short-term weather forecasts to optimally adjust set points in a supervisory control environment. Predictive control strategies for both passive and discrete thermal storage systems have been field-tested [44]. Morgan and Krarti [44] investigated performance of various control strategies for combined passive and discrete TES systems in a Colorado elementary school equipped with an ice storage system. The predictive optimal control strategies were developed using an EnergyPlus-based simulation environment [45]. The simulation environment was found to be effective in defining and implementing predictive optimal controls for both passive and discrete TES systems for the buildings. Figures 5.22 and 5.23 show examples of the field testing results for the building energy use performed by Morgan and Krarti [44].

5.4.4.3 Neural Network Controls of Thermal Energy Storage Systems

Several model-based optimal TES control strategies have been proposed in the literature [34, 38, 40, 46]. These optimal control strategies are generally obtained through optimization techniques and computer simulations and are difficult to implement in the field. An optimal TES controller using self-learning neural networks has been proposed and tested in full-scale laboratory conditions [47].

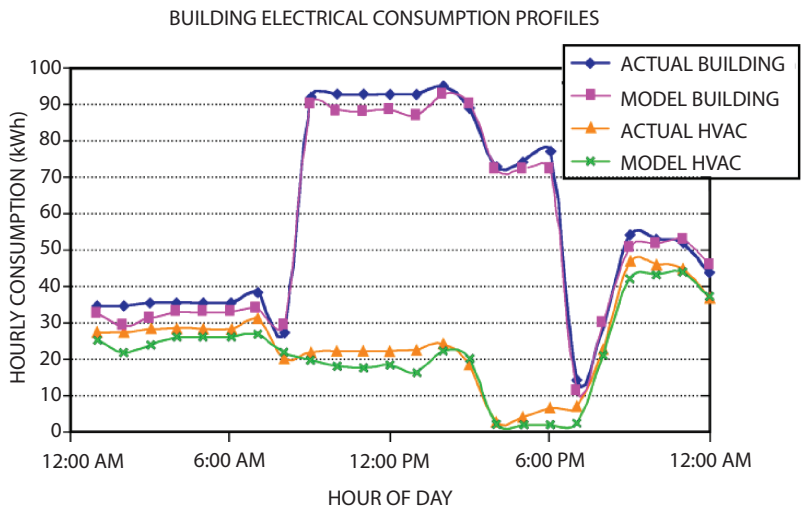

Figure 5.22. Building electricity use profiles for 6 hour predictive optimal control.

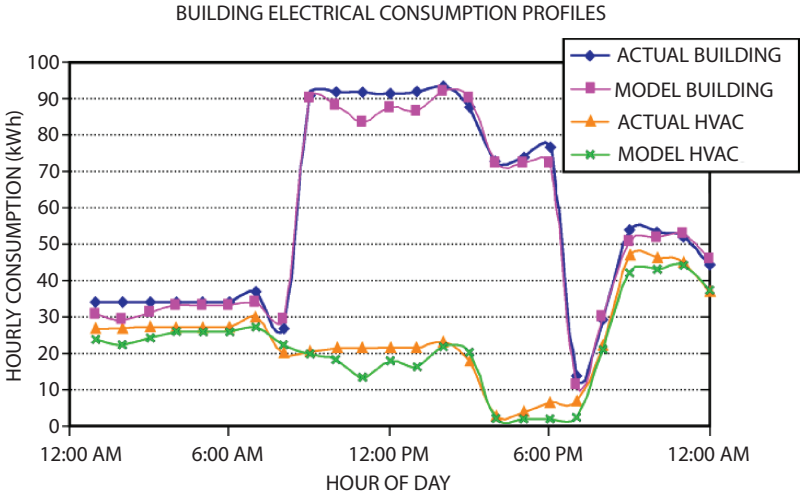

Figure 5.23. Building electricity use profiles for 24 hour predictive optimal control.

The NN-based optimal controller is developed to minimize the operating cost of the cooling plant within a 24-hour period. In addition to NN-based equipment models for the chiller and the TES system, the NN-based optimal controller utilizes a training network and a predictor network. The equipment models are based on feed-forward networks while the training and the predictor networks use recurrent networks that compute output vectors sequentially in time. The training network learns the relationship between the controlled and uncontrolled variables and the cooling plant operating conditions (such as electrical power consumption for the chiller and charging/discharging rates for the TES system). The training network weights are then passed to the predictor network to act as the activation functions. The main goal of the predictor network is to find acceptable set-points for the control variables that minimize operating cost. Massie [47] used two control variables to control the TES system: chiller set-point temperature and the primary loop three-way valve position. Then, charging/discharging rates for the TES system can be determined using values for the chiller set-point temperatures and the three-way valve positions.

Using laboratory conditions, the NN-based optimal controller has been implemented and found to be capable of operating an ice-storage system for least cost under various utility rate structures [47]. Figure 5.24 illustrates the performance of NN-based optimal controller for a typical office building under a strong price incentive. Specifically, the utility rate

is characterized by demand and energy charge ratios of 5 (i.e., ratios of on-peak to off-peak charges). The on-peak period starts at 8:00 AM and ends at 7:00 PM. As depicted in Figure 5.24, the non-cooling electrical load between 7:00 PM and 22:00 PM is dominant compared to the cooling electrical load associated with the cooling plant operation. Due to the strong incentive for load shifting, the NN-based optimal controller begins charging the ice storage system at the start of the off-peak period (i.e., 7:00 PM) by lowering the chiller set-point temperature to its lowest value (26°F [–3.3°C]). The charging process continues until the end of the off-peak period (i.e., 8:00 AM). Between 8:00 AM and 12:00 noon, the NN-controller opts to use the chiller to fully meet the building cooling load instead of discharging the ice storage system. This action is justified by the fact that the non-cooling load profile allows for additional power consumption (from the chiller) during the period between 8:00 AM and 12:00 noon without any increase in the on-peak demand charges. Starting

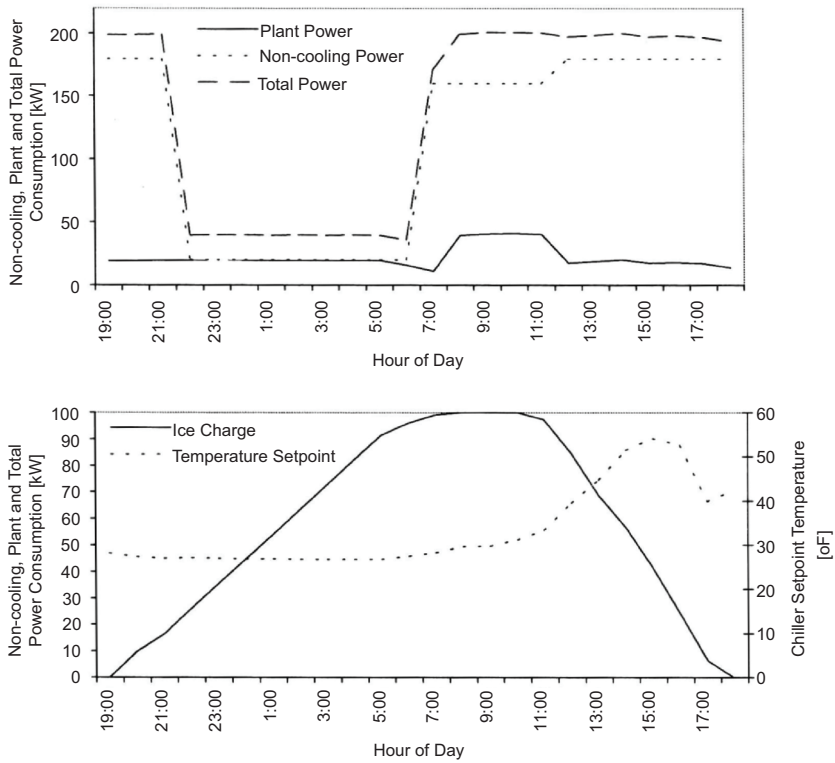

Figure 5.24. NN-based Optimal Control Strategy for a typical office under strong price incentive (Massie, 1998).

from 12:00 noon when the non-cooling load returns to its maximum value, the NN-controller utilizes the ice storage system as well as the chiller to meet the building cooling load.

5.5 Summary

In this chapter, an overview of basic components and applications of HVAC control systems has been presented. In particular, the energy cost savings incurred by various functions of energy management and control systems (ECMS) have been illustrated through selected examples and applications. In addition to being knowledgeable of the currently available control systems and applications, the reader should be aware of the development in the intelligent control systems especially those applicable to HVAC systems.

References

[1] Bushby, S.T., and Newman, H.M. (1991). The BACnet Communication Protocol for Building Automation Systems, *ASHRAE Journal*, 33(4), 14.

[2] NEMA (1994). *Energy Management Guide for Selection and Use of Polyphase Motors, Standard MG-10-1994*, National Electrical Manufacturers Association, Rosslyn, VA.

[3] Krarti, M., Erickson, P., and Hillman, T. (2005). A Simplified Method to Estimate Energy Savings of Artificial Lighting Use from Daylighting, *Building and Environment*, 40, 747–754.

[4] Al Mohimen, M., Hanna, G., and Krart, M. (2005). Analysis of Daylighting Benefits for Office Buildings in Egypt, *ASME Solar Energy Engineering*, 127.

[5] Seo, D., Ihm, P., and Krarti, M. (2011). Development of an Optimal Daylighting Controller, *Building and Environment*, 46(5), 1011.

[6] Bloomfield, D.P., and Fisk, D.J. (1977). The Optimization of Intermittent Heating, *Building and Environment*, 12, 43.

[7] Jobe, T., and Krarti, M. (1997). Field Implementation of Optimum Start Heating Controls, *Proceedings for ASME Solar Engineering*, 305.

[8] Seem, J.E., Armstrong, P.R., and Hancock, C.E. (1989). Comparison of Seven Methods for Forecasting the Time to return from Night Setback, *ASHRAE Transactions*, 95(2), 439.

[9] ASHRAE (2004). Ventilation for Acceptable Indoor Air Quality, Standard 62-2004, American Society of Heating, refrigerating and Air-Conditioning Engineers, Inc., Atlanta, GA.

[10] Sterling, E.M., Collet, C.W., and Turner, S. (1992). Commissioning to Avoid Indoor Air Quality Problems, *ASHRAE Journal*, 34(10), 28.
[11] Krarti, M., Brandemuehl, M., and Schroeder, C. (1999). *Techniques for Measuring and Controlling Outside Air Intake Rates in Variable Air Volume Systems*. Final Report for ASHRAE RP-980, American Society of Heating, Refrigerating, and Air Conditioning Engineering, Atlanta, GA.
[12] Krarti, M., Schroeder, C., Jeanette, E., and Brandemuehl, M. (2000). Experimental Analysis of Measurement and Control Techniques of Outside Air Intake Rates in VAV Systems, *ASHRAE Transactions*, 106(Pt. 2), 234–255.
[13] Knoespel, P., Mitchell, J., and Beckman, W. (1991). Macroscopic Model of Indoor Air Quality and Automatic Control of Ventilation System, *ASHRAE Transactions*, (97), 1020–1030.
[14] Sorensen, B. (1996). Simulation of a Small VAV Plant, *Proceedings of Indoor Air*, (2), 199–204.
[15] Emmerich, S., Mitchell, J., and Beckman, W. (1994). Demand-Controlled Ventilation in a Multi-zone Office Building, *Indoor Environment*, (3), 331–340.
[16] Kusuda, T. (1976). Control of Ventilation to Conserve Energy while Maintaining Acceptable Indoor Air Quality, *ASHRAE Transactions*, (82), 1169–1181.
[17] Ogasawara, S., Taniguchi, H., and Sukehira, C. (1979). Effect of Energy Conservation by Controlled Ventilation: Case Study in a Department Store, *Energy and Buildings*, (2), 3–8.
[18] Vaculik, F., and Plett, E. (1993). Carbon Dioxide Concentration-Based Ventilation Control, *ASHRAE Transactions*, (99), 1536–1547.
[19] Woods, J., Winakor, G., Maldonado, E., and Kipp, S. (1982). Subjective and Objective Evaluation of a CO_2-Controlled Variable Ventilation System, *ASHRAE Transactions*, (88), 1385–1393.
[20] Davidge, B. (1991). Demand Controlled Ventilation Systems in Office Buildings, Proceedings of the 12th AIVC Conference Air Movement and Ventilation Control within Buildings, pp. 157–171.
[21] Fleury, B. (1992). Demand Controlled Ventilation: A Case Study, Proceedings of the 13th AIVC Conference Ventilation for Energy Efficiency and Optimum Indoor Air Quality, pp. 343–346.
[22] Donnini, G., Haghighat, F., and Hguyen, V. (1991). Ventilation Control of Indoor Air Quality, Thermal Comfort, and Energy Conservation by CO_2 Measurement, Proceedings of the 12th AIVC Conference Air Movement and Ventilation Control within Buildings, pp. 311–331.

[23] Haghighat, F., and Donnini, G. (1992). IAQ and Energy-Management by Demand Controlled Ventilation, *Environmental Technology*, (13), 351–359.
[24] Fehlmann, J., Wanner, H., and Zamboni, M. (1993). Indoor Air Quality and Energy Consumption with Demand Controlled Ventilation in an Auditorium, Proceedings of the 6th International Conference on Indoor Air Quality and Climate, vol. (5), pp. 45–50.
[25] Zamboni, M., Berchtold, O., Filleux, C., Fehlmann, J., and Drangsholt, F. (1991). Demand Controlled Ventilation—An Application to Auditoria, Proceedings of the 12th AIVC Conference Air Movement and Ventilation Control within Buildings, pp. 143–145.
[26] Alalawi, M., and Krarti, M. (2002). Experimental Analysis of Demand Ventilation Controls, *ASHRAE Transactions*, 108(Part 2), 105–135.
[27] ASHRAE (2012). *Handbook of Systems and Equipment*. American Society of Heating, Refrigerating and Air-Conditioning Engineers, Inc., Atlanta, GA.
[28] Ihm, P., and Krarti, M. (2005). Optimal Control Strategies for Heated Radiant Floor Systems, *ASHRAE Transactions*, 111(Part 1).
[29] Simmonds, P. (1993). Thermal Comfort and Optimal Energy Use, *ASHRAE Transactions*, 99(1), 1037–1048.
[30] ASHRAE (2014). *Handbook of Fundamentals*. American Society of Heating, Refrigerating and Air-Conditioning Engineers, Inc., Atlanta, GA.
[31] Fanger, P.O. (1970). *Thermal Comfort*. Copenhagen, Danish Technical Press.
[32] Berglund, L. (1978). Mathematical Models for Predicting the Thermal Comfort Response of Building Occupants. *ASHRAE Transactions*, 84(1).
[33] ASHRAE (2007). *Handbook of HVAC Applications*. American Society of Heating, Refrigerating and Air-Conditioning Engineers, Inc., Atlanta, GA.
[34] Braun, J.E. (1992). A Comparison of Chiller-Priority, Storage-Priority, and Optimal Control of an Ice System, *ASHRAE Transactions*, 98(1), 893–902.
[35] Morris, F.B., Braun, J.E., and Treado, S.J. (1992). Experimental and Simulated Performance of Optimal Control of Building Thermal Storage, *ASHRAE Transactions*, 100(1), 402.
[36] Morgan, S., and Krarti, M. (2006). Impact of Electricity Rate Structures on Energy Cost Savings of Pre-Cooling Controls for Office Buildings. *Energy and Buildings*, 38.

[37] Katipamula, S., Armstrong, P.R., Wang, W., Fernandez, N., Cho, H., Goetzler, W., Burgos, J., Radhakrishnan, R., and Ahlfeldt, C. (2010). Cost-Effective Integration of Efficient Low-Lift Baseload Cooling Equipment: FY08 Final Report. PNNL-19114.

[38] Kintner-Meyer, M., and Emery, A.F. (1995). Optimal Control of an HVAC System Using Cold Storage and Building Thermal Capacitance, *Energy and Buildings*, 23(1), 19–31.

[39] Liu, S., and Henze, G.P. (2006). Experimental Analysis of Simulated Reinforcement Learning Control for Active and Passive Building Thermal Storage Inventory—Part 1: Theoretical Foundation, *Energy and Buildings*, 38(2), February 2006, 142–147.

[40] Henze, G.P., and Krarti, M. (1999). The Impact of Forecasting Uncertainty on the Performance of a Predictive Optimal Controller for Thermal Energy Storage Systems, *ASHRAE Transactions*, 105(1).

[41] Braun, J.E. (1990). Reducing Energy Costs and Peak Electrical Demand Through Optimal Control of Building Thermal Storage, *ASHRAE Transactions*, 96(2).

[42] Henze, G.P., and Krarti, M. (1996). Ice Storage System Controls for the Reduction of Operating Cost and Energy Use, *ASME Solar Engineering Journal*.

[43] Hajiah, A., and Krarti, M. (2012). Optimal Controls of Building Storage Systems Using Both Ice Storage and Thermal Mass—Part I: Simulation Environment, *Energy Conversion and Management*, 64, 499–508.

[44] Morgan, S., and Krarti, M. (2010). Field Testing for Optimal Controls of TES Systems, *ASHRAE Transactions*, 116(Part 1).

[45] Zhou, G., Ihm, P., Krarti, M., Liu, S., and Henze, G.P. (2005). Integration of an Internal Optimization Module within EnergyPlus. IBPSA Proceedings.

[46] Drees, K.H., and Braun, J.E. (1994). Modeling and Control of Area-Constrained Ice Storage Systems. Report No. 1796-2 HL 94-21. Johnson Controls, Inc.

[47] Massie, D., (1998). Optimal Neural Network-Based Controller for Ice Storage Systems, Ph.D. Dissertation, University of Colorado.

6 Combined Cooling, Heating, and Power Systems for Buildings

Ming Qu, Omar Abdelaziz, Patrick Phelan, and Bahman Habibzadeh

Abstract

Combined Cooling, Heating and Power (CCHP) is an efficient, clean, and reliable approach to generating power and thermal energy simultaneously from a single fuel source on site. A CCHP system is usually designed to provide power in the form of electricity while recovering the available waste heat for serving heating and/or cooling load. We start this chapter with an overview of the state-of-the-art in CCHP systems applied to commercial and residential buildings to maximize their primary energy efficiency. We continue with a discussion of available prime mover options ranging from classic technologies, such as internal combustion engines, to emerging technologies such as thermoelectric generators. We also discuss different heat recovery concepts along with their limitations and design challenges. These include gas-to-gas heat exchangers, gas-to-liquid heat exchangers, and condensing economizers, as well as advanced concepts such as transport membrane condensers. We then present the available heat pump technologies that can be matched with the different prime movers to service the building heating and/or cooling load. These heat pump options include classic thermally activated technologies such as the absorption and adsorption heat pumps as well as other emerging technologies such as thermo-acoustic heat pumps and the Vuilleumier cycle.

A properly designed building CCHP can meet the entire building thermal load and offset significant electricity consumption at higher primary energy efficiency compared to conventional technologies — heating equipment and purchased electricity from the grid. To guide the design if building CCHP, we first address the two approaches to sizing CCHP and identifying system configurations: electric load following and thermal load following. We also present sample thermal and electric load profiles for different types of buildings and present a step-by-step CCHP system design and integration for a health care facility. Furthermore, we discuss several of the system integration challenges. Finally, we present a quick discussion on the economic and feasibility assessment of building CCHP systems.

6.1 Introduction

Combined Cooling, Heating, and Power (CCHP), also known as trigeneration, is the sequential or simultaneous on-site generation of power, heating, and cooling from a single fuel source in a single integrated system. Compared to conventional systems, CCHP systems synergistically use the maximum potential of fuel for the end-use application. In a conventional system, electricity is supplied from the grid for the various electric loads; heating is supplied through fossil-fired equipment, electric heater or electric heat pump; and cooling is provided by using electric air conditioning. On the other hand, a CCHP system will use a fuel to run a prime mover for the generations of electricity and the waste heat from the prime mover can be used directly for heating, or for cooling by using thermally activated cooling technologies.

Compared with residential or small commercial buildings, large commercial buildings are considered as the primary market for CCHP due to the electricity pricing and the electric/thermal load balance. In a large office building, lighting and cooling are required throughout the year. This can be significantly reduced using a CCHP system that is sized to the lighting electric load (base electric load) and waste heat is used to run absorption chillers for cooling. Additional waste heat may be used for water heating and reheat coil as needed throughout the year. There is currently a significant effort to introduce CCHP into midsize and small commercial buildings as well as residential buildings as part of the Smart Grid initiatives and electric reliability due to the aging of the transmission lines and the lead-time required for expanding existing utility scale infrastructure [1]. However, for CCHP to be cost effective and more efficient than conventional systems in small to midsize buildings, the prime mover has to be more efficient than the average grid efficiency, and the waste heat recovery efficiency needs to be greatly improved. Furthermore, feasibility would greatly depend on the energy storage capability (electric or thermal) to decouple electric and thermal loads since these loads do not always coincide as in large buildings. A subset of CCHP technologies, Combined Heat and Power (CHP), is more favorable in applications with less cooling demand and to reduce the primary investment cost since the thermally activated air conditioning unit is no longer needed. Several CHP systems have been introduced in residential and small commercial applications. CHP system also has been used in large scale applications especially industrial processes.

A comparison between conventional and CCHP energy flows in buildings is summarized in Figure 6.1. The building would still rely on electricity from the utility grid and additional fuel firing to compensate for the imbalance between thermal and electric loads during transient building operation and as schedule and occupants change. If a perfect energy storage system is sized, designed, and installed, the building can operate completely off the grid relying mainly on the "single fuel". Some prime movers would provide an additional flexibility in the ability to handle different fuel types at different times which can be considered as a means for risk mitigation in case the primary fuel supply is interrupted.

Overall, CCHP systems enable energy cascading that ensures the primary energy is fully utilized for the application of interest. In building applications, CCHP can be used to serve both electric and thermal loads — though they might not always coincide for small and mid-size buildings, which emphasizes the need for energy storage. The main challenge for widespread use of CCHP in buildings is the cost effectiveness, reliability, and perceived risks by the end users. This chapter outlines a review of CCHP technology, discusses prime mover options, heat recovery unit designs, heat pump options, and thermal energy storage requirements and benefits. The chapter also presents CCHP sizing options, building integration, operation and system controls and a typical economic and feasibility analysis.

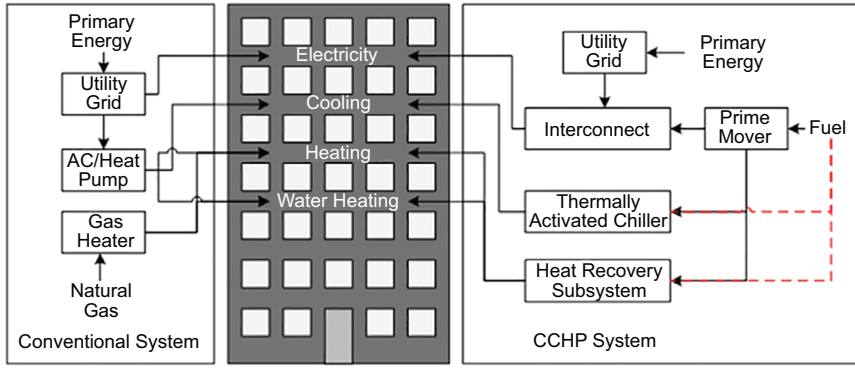

Figure 6.1. Conventional versus CCHP system building integration.

6.2 State-of-the-Art Review of CCHP Technology

There are five basic elements in a typical CCHP system: prime mover, electricity generator, heat recovery system, thermally activated equipment for generating cooling, and a control system. Figure 6.2 is a general diagram for typical CCHP systems. As depicted, in a typical CCHP, fuel is first fed to a power generation unit (PGU) like an engine or gas turbine to convert to shaft energy. The shaft energy is then used as the driving force of the electrical generator to produce electricity. Due to the limit of the PGU efficiency, the waste heat from PGU is recovered by a heat recovery unit to produce steam or hot water. The steam or hot water can be used in four ways. First, it can be directly used for domestic hot water required by buildings. Second, it can be used as the heat source in an air handler for space heating. Third, it can drive an absorption or adsorption chiller to produce chilled water, which is used as the cooling source in air handlers to cool or dehumidify the air for space cooling. Fourth, it can be used as the heat source in desiccant units to dehumidify the air for buildings. Since absorption/ adsorption chillers and desiccant units are thermally activated, the exhaust gas from the prime mover can also be directly used as the heat resource to drive them for space cooling. As an alternative to the combustion, electricity can be obtained through a chemical reaction in fuel cells. A fuel cell is an electrochemical device that converts fuel to direct current

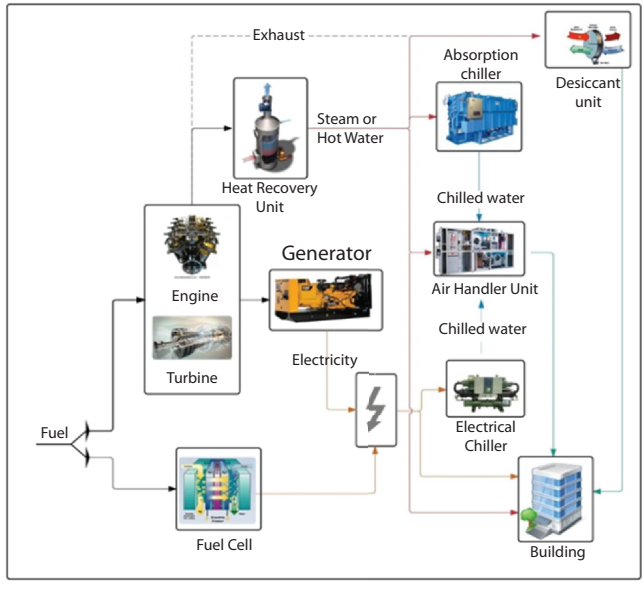

Figure 6.2. General diagram for typical CCHP systems.

electricity, with heat and water as by-products. As shown in Figure 6.2, CCHP systems can fully use one fuel in a cascading manner to provide a complete energy package of cooling, heating, and power for buildings.

Accordingly, a simplified schematic diagram of a CCHP system can be presented as Figure 6.3. The total fuel input, $\dot{Q}_{fuel}$, is the fuel gas used by the power generation unit (PGU). The outputs of PGU include electric power, W_E and waste heat. The waste heat can be recovered by heat recovery unit (HRU) and converted as thermal energy, $\dot{Q}_{th}$, which is used for an absorption chiller for chilled water generation and heating water for space cooling and heating. If the thermal energy from the PGU is not adequate, the thermal energy from other resources, $\dot{Q}_{th\_others}$ will be needed to provide enough heating and cooling for buildings. If the electricity generated on site cannot meet building demands, additional electricity will be bought from power grids.

As one of system indicators, the overall efficiency of CCHP, $\eta_{overall}$ is defined as the ratio of the sum of the net useful power output, W_E in kW and the net useful thermal outputs, $\dot{Q}_{th}$ in kW and the total fuel input, $\dot{Q}_{fuel}$, in kW.

$$\eta_{overall} = \frac{W_E + \dot{Q}_{th}}{\dot{Q}_{fuel}} \tag{6.1}$$

In CCHP systems, the net useful thermal outputs could be in various forms including process hot water, steam, domestic hot water, and chilled water. With their high efficiency, CCHP systems with have been widely

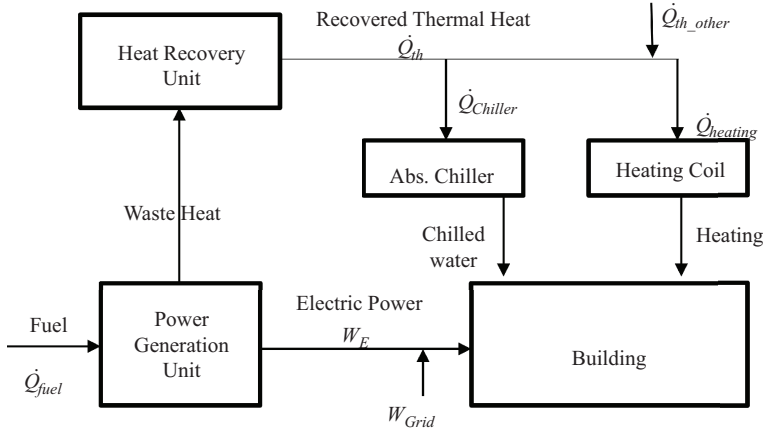

Figure 6.3. Schematic diagram of a simplified CCHP system.

utilized in industrial, commercial, and other applications in the U.S., especially in the past 30 years [2]. However, commercial and institutional applications currently account for only 13 percent of the existing capacity of CHP[1] in the U.S. Such low installation of CCHP in commercial and residential buildings is because (in part) the design of CCHP is limited by the magnitude, duration, and coincidence of the electrical and thermal requirements from an application. Commercial and residential buildings typically have oscillating electrical and thermal demands due to different occupancy schedules. The pronounced changes in the energy demands make the design, operation, and control of CCHP systems more sophisticated and difficult. In addition, the fluctuations in electrical and thermal loads require CCHP systems to be operated at partial load conditions on the most of the time, in which they run at low efficiency.

The majority of the CCHP systems in the commercial sector are for hospitals, schools, university campuses, hotels, nursing homes, office buildings and apartment complexes. Those applications typically are large buildings with multiple use occupancies and/or longer daily operating hours and particularly in urban areas where higher electrical and somewhat lower gas rates prevail [3]. According to the estimations from the US Department of Energy (DOE), however, of the ~130 GW of CHP technical potential, approximately half is at commercial and institutional facilities, as indicated in Figure 6.4. [4]. Many studies were conducted to evaluate the performance of CCHP systems for commercial and residential buildings in various locations by using modeling and simulation [3,5–10]. They found that CCHP systems can be more beneficial when operated at full load. Hospitals have been considered as a favorable commercial application for CCHP systems. It is generally agreed that CCHP systems for hospitals can achieve significant benefits in energy, economics, and the environment. Fuel-cell-based CCHP systems for hospitals can potentially reduce operational cost twice as much as that by micro-turbine-based CCHP systems. The simple payback for CCHP systems in hospital facilities ranges from 15 months to 7 years [6,8,9,11]. Data centers are another favorable application in the commercial sector. For both fuel-cell-based and gas-turbine-based CCHP systems, the savings on primary energy, operating cost, and CO_2 emissions in data center facilities range from 20%–30% of primary energy savings, 45% to 56% of operational

[1] We use the acronyms CHP and CCHP interchangeably, with the understanding that CCHP systems can provide either heating or cooling.

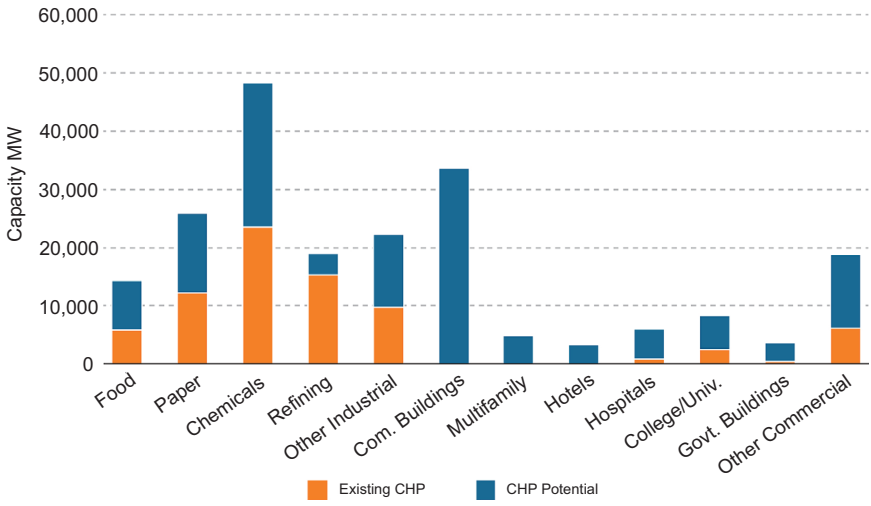

Figure 6.4. Technical potential for additional CCHP at existing industrial and commercial facilities [4].

costs, and 20% to 45% of CO_2 emissions [12,13]. For other commercial buildings like restaurants, primary schools, supermarkets, and hotels, CCHP systems are not always beneficial. It was concluded that buildings with a relatively higher fraction of thermal load covered by the CCHP system show improved feasibility [6].

According to their electric generating capacity, CCHP systems can be categorized into two groups: micro-CCHP and large-scale CCHP for systems with capacities less than 50 kW_e and larger than 50 kW_e, respectively. Micro-CCHP systems are mainly used for residential buildings and commercial buildings with relative small capacities. Most CCHP systems for residential applications are between 1 kW_e and 10 kW_e [7,10,14,15]. Those studies indicated that CCHP systems for residential applications currently have high initial cost.

Micro-CCHP systems are typically based on internal combustion engines (ICE), micro gas turbines (MGT), micro Rankine cycles (mRC, i.e., a steam turbine), Stirling Engines (SE), thermophotovoltaics (TPV), and fuel cell technologies. Internal combustion systems have a relatively high electric efficiency typically ranging from 25 to 35%, and a thermal efficiency of 50% to 70%. On the other hand, external combustion systems

have a relatively low electric efficiency, typically between 5% to 20%, and a higher thermal efficiency from 70% to 90%. It was found that all the available micro-CCHP technologies deliver values of $\eta_{overall}$ higher than 75%. Generally, mRC- and SE-based systems are more suitable for applications with a low ratio of the electric-to-thermal power, often called the 'C ratio', while ICE and MGT systems are more suitable for applications with relatively high C ratio from 0.3 to 0.7. In addition, external combustion systems have high reliability, low noise, and potentially high values of the total CHP efficiency, compared to internal combustion systems [16,17]. TPV-based micro CHP systems are a combination of photovoltaics and a surface radiant burner, which recovers most heat not converted into electric energy. Although most TPV CCHP systems have a low electric efficiency, approximately 2% to 5%, the potential $\eta_{overall}$ is always higher than 90%. Fuel cell micro CCHP systems are either based on low-temperature polymer electrolyte membrane fuel cells (PEFC or PEMFC), or on high-temperature solid oxide fuel cells (SOFC). Due to the high initial cost and technical challenges, fuel cell micro CCHP systems are still at the demonstration and research phases [17].

Large-scale CCHP systems are typical for large commercial or mix-used applications. In many commercial applications, the thermal load is not coincident with the electrical load due to strong dependency on season variations and also due to the limited operating hours based on the occupancy schedules. Although there appear quite a few newly emerging technologies in CCHP, reciprocating internal combustion engines (RICE), steam turbines (ST), combustion turbines (CT), Stirling engines (SE), and fuel cells are the primary prime movers used in CCHP systems for commercial buildings. According to a report published in 2000, among the capacity of existing CCHP installations in the commercial sector, 42.8% came from combined cycle power plants, consisting of a combustion turbine and a heat recovery steam generator (HRSG), which have high efficiency and are typically used in relatively large installations. Boilers powered by solid fuels and steam turbines make up 27% of total capacity. Combustion turbines make up about 19% of installed capacity. Reciprocating engines make up 10% of capacity but represent 79% of the total number of installations. Reciprocating engines are commonly used in smaller installations, with the average size for operating engine CCHP systems at 0.7 MWe. The average size for all operating commercial sector CCHP is 5 MWe [18]. Natural gas is the most common type of fuel, comprising over 72% of the total capacity. The next popular fuel type is waste, which is dominated by landfill gas and biogas from sewage

treatment facilities. Coal, oil, wood, and other fuel types make up the remaining 15% of installed CCHP capacity buildings [19].

As so-called tri-generation, CCHP systems include thermally driven cooling or dehumidification components for space air conditioning in addition to cogeneration systems, which can only provide electricity and heating for buildings. It is concluded by recent researchers that overall efficiency of CCHP systems can be higher than that for cogeneration systems due to the thermally activated cooling technologies. The major thermally activated technologies in CCHP systems are absorption chillers, adsorption chillers, and desiccant dehumidifiers. Those cooling systems can be driven by the various forms of thermal energy such as steam, hot water, and flue gas from prime movers or from heat recovery units. Due to the different temperature elevations of the thermal energy and the operating temperatures required by the cooling systems, appropriate temperature matching between the thermal energy resource and the thermally driven cooling technology must be made to implement CCHP. Table 6.1 shows the key system parameters and characteristics in various CCHP systems

Table 6.1. Characteristics and Key Parameters in CCHP Systems [19].

Prime Mover*	Capacity Range	Electric Efficiency (%)	Electric Power to Thermal Ratio (C ratio)	Overall Efficiency (%)	Recoverable Temperature (°C)	Matched Cooling Technologies
RICE	3kW–6MW	25–43	0.5–0.7	70–92	~80	1E† absorption, adsorption or dehumidification
ST	50kW–500MW	7–20	0.1–0.5	60–80	~540	3E†/2E† absorption
CT	250kW–50MW	25–42	0.2–0.8	65–87	~540	3E†/2E† absorption
SE	1kW–1.5MW	~40	1.2–1.7	65–85	~90	1E† absorption, adsorption or dehumidification
FC	5kW–2MW	37–60	0.8–1.1	85–90	~480 (SOFC)	3E†/2E† absorption
					~60(PEM)	1E† absorption, adsorption or dehumidification
MT	15–300kW	22–35	1.2–1.7	60–95	~320	3E†/2E† absorption

* CT: combustion turbines; FC: fuel cells; MT: micro turbines; RICE: reciprocating internal combustion engines; SE: stirling engines; ST: steam turbines.

†#E refers to the number of effects for an absorption system e.g., 1E is single effect absorption chiller.

based on different prime movers. The best pairs of recoverable energy and thermally activated cooling technologies are also shown in Table 6.1.

6.3 Prime Mover Options

The prime mover is one of the major components of CCHP systems and the type of the prime mover is directly related to the CCHP application. The prime movers which are commonly used for the CHP applications can also be considered for the CCHP. They are mostly being classified based on their marketability, size and efficiency. The focus of this chapter is CCHP for residential and commercial applications. This will limit the size of the prime movers in small to medium range that can be referred to micro turbines, reciprocating engines and fuel cells. American Society of Heating, Refrigerating, and Air-Conditioning Engineers (ASHRAE) has categorized Diesel, Spark ignition and Stirling engines under reciprocating engines, and likewise all types of fuel cells are being considered under one category.

Some emerging prime movers, which are still in the development stage, are not included in the ASHRAE handbook. Figure 6.5 shows a

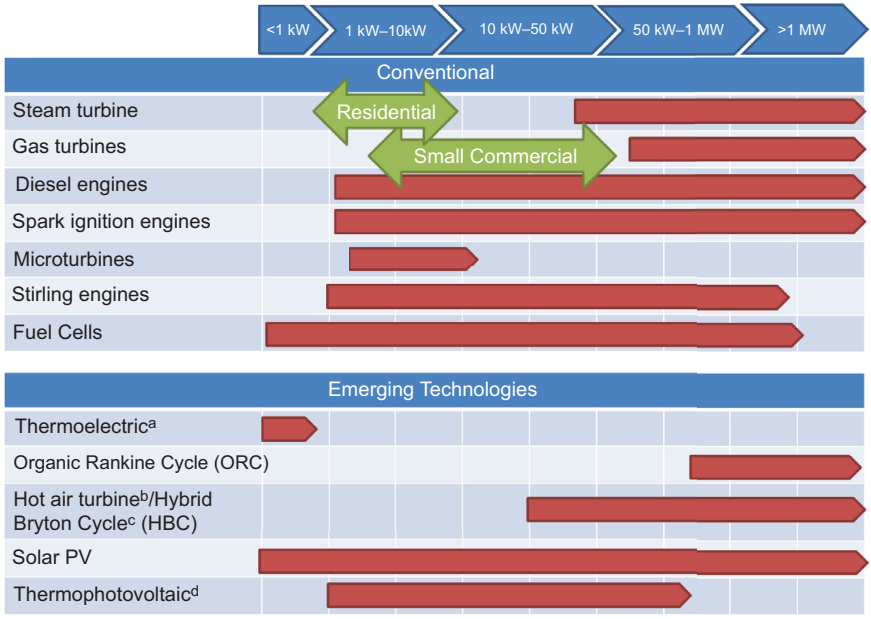

Figure 6.5. Capacity range of conventional and emerging prime mover technologies.

broad range of prime movers suitable for residential and commercial CCHP, categorized based on the electric power range. To have a better representation reciprocating engines are expanded into three categories.

Residential and small commercial applications of CCHP limit the fuel cell prime movers to Proton Exchange Membrane fuel cell (PEMFC), Phosphoric Acid fuel cell (PAFC) and Solid Oxide fuel cell (SOFC). Based on Figure 6.5, Rankine and Brayton cycles are not good candidates for smaller applications unless in the micro scale such as the micro Rankine Cycle (mRC) [16] and/or the Hybrid Brayton Cycle (HBC) [20].

Matching the cooling technology of the CCHP with the prime mover is one logical process of down-selecting the prime movers. For this purpose, the range of the output temperature can be used. Also other thermo-physical specification of the prime movers is important in selecting the prime movers as listed in Table 6.2. Beyond matching the prime mover with the CCHP and power demand, other environmental and end-user friendly aspects of the prime movers are also desirable. Nevertheless, economical concern and durability of the system is always a big consideration. A list of qualitative measures on such issues for the few most commonly used prime movers has been provided by [21]. These concerns could play even an even bigger role if CCHPs are going to be part of future homes. Introduction of more stringent environmental regulations might add new criteria in the selection of the prime movers. Table 6.2 lists the applicable prime movers for CCHP systems with the best fit to residential and small commercial buildings. Data provided for the emerging technologies is limited to recent research and development in that field.

6.4 Heat Recovery

Efficient heat recovery is essential to realizing the high overall efficiencies that CCHP systems can offer. The thermal efficiency η_{th} of a heat recovery unit is directly related to the effectiveness of the unit. The effectiveness ε of a heat exchanger is defined as Equation 6.2, where $\dot{Q}_{\max}$ is determined in part by the maximum temperature difference between the inlet of the hot and cold fluids for exchanging heat.

$$\varepsilon = \frac{\text{Actual heat transfer rate}}{\text{Maximum possible heat transfer rate}} = \frac{\dot{Q}_{act}}{\dot{Q}_{\max}} \qquad (6.2)$$

Table 6.2. Prime Movers for Small Buildings.

Technology	Recip. Engines[1,2]	Mictroturbine[1,2]	Stiring engine[2]	Fuel Cells[1,2]	Thermoelectric[3]	Organic Rankie Cycle (ORC)[4]
Electric Efficiency (HHV)	27–41%	22–28%	40	30–63%	5%	8–24%
Typical Capacity (kW)	5–1000	15–300	1–1500	5–2000	0.5–1	280–1200
Typical Power to Heat Ratio	0.5–1.2	0.5–0.7	1.2–1.7	1-2	0.01–0.04	0.25
Cost of the Prime Mover ($/kW)	350–1600	900–1500	1300–2000	2500–3500		1000–2000
Typical online Availability	96–98%	98-99%		95%	>98%	>75%
Hours to Overhauls	30,000–60,000	40,000-80,000		32,000-64,000		20,000
Startup Time	10 sec	60 sec		3 hrs-2 days		
Fuels	NG, biogas LPG	NG, liquid fuel		H_2,NG, Propane, Methanol	Liquid Fuel, Biofuel, NG	Geothermal, Waste heat, Biofuel, solar
Power Density (kW/m^2)	35–50	5–70		5–20	0.025	
NOx (lb/MWh)	0.06–0.8	0.08–0.2	0.5	0.0025–0.004		
CO_2 (lb/MWH)	1100–1400	1600	1500	950–1100		
Typical Outout Temperature (°C)	370–540	200–350	60–200	260–370	<200	250–300
Noise	Loud	Fair	Fair	Quiet	Quiet	Fair
Part Load Performance	Good	Fair	Good	Good	Fair	Fair
Life Cycle (year)	20	10	10	10–20		20

Note: 1-EPA [22], 2- [19], 3- [23], 4- [24,25].

A variety of heat exchanger types available includes double-pipe, shell-and-tube, and plate-and-frame. Generally, the flow pattern of the two fluids exchanging heat, such as the exhaust gases from a turbine and potable water for domestic use, are arranged such that the fluids are

in parallel flow, counter flow, or cross flow. Usually the counter-flow arrangement leads to the highest effectiveness, ε.

Table 6.3 provides the thermal and electrical performance characteristics of a variety of existing CHP systems potentially applicable for buildings, based on the following prime movers: microturbines, IC engines, and fuel cells. These particular examples were selected from a longer list of candidate prime movers described in [26], and are meant to give a snapshot of existing CHP technologies. The specified heat exchanger (HX) exhaust temperatures are relevant for water heating applications, but in general the exhaust temperatures are substantially higher and suggest that higher-quality heat could be recovered and used for other purposes.

Naturally, the location of the heat recovery unit depends on the type of prime mover, and on the temperature of the exhaust or other waste heat streams. For microturbines, typically a heat exchanger package can be purchased together with the power generation unit. For IC engines, in addition to the high-temperature exhaust heat, lower temperature waste heat is available from jacket cooling water and from the lube oil

Table 6.3. Electrical and Thermal Performance Characteristics for Select CHP Technologies, Based on HHV.

Type & Capacity	Total Efficiency (%)	Electrical Efficiency (%)	Thermal Efficiency (%)	Power to Heat Ratio	Exhaust Temp. (°C)	HX Exhaust Temp. (°C)	Total Installed Cost ($/kW$_e$)
30 kW$_e$ Microturbine	70.0%	22.0%	48.0%	0.46	277	88	4,300
65 kW$_e$ Microturbine	70.4%	23.8%	46.6%	0.51	311	88	3,220
100 kW$_e$ Internal Combustion Engine	80.0%	27.0%	53.0%	0.51	649	N/A	2,900
300 kW$_e$ Molten Carbonate Fuel Cell	82.0%	47.0%	35.0%	1.0	371	49	10,000

cooling system via a closed-loop water cooling system. Approximately 30 to 50% of the waste heat is available from the exhaust, while the remainder is from the cooling systems. For fuel cells, in general there are four potential sources of waste heat: the exhaust gas (including water condensation), cooling of the fuel cell stack, combustion of the anode off-gases, and heat generated by the reformer. The quantity and quality of the waste heat available from fuel cells depends on the type of fuel cell used, with proton exchange membrane (PEM) fuel cells offering the lowest temperature waste heat, and phosphoric acid, solid oxide, and molten carbonate fuel cells providing higher temperature waste heat.

Comprehensive references for the design of heat exchangers are available elsewhere, such as Thulukkanam, 2013 [27]. Depending on the type of CHP system and the temperature of the waste heat stream, either gas-to-gas, gas-to-liquid, or liquid-to-liquid heat exchanger may be needed. Gas-to-liquid heat exchangers, appropriate for transferring heat from the exhaust of a microturbine or internal combustion engine, generally include finned tubes to increase the surface area exposed to the exhaust gases. A useful general discussion of heat exchangers for CHP systems is provided in [28]. Heat recovery from fuel cells, being a relatively recent form of CHP, is still the subject of ongoing research [29,30].

6.5 Thermally Activated Cooling Systems

There exist several established thermally activated cooling technologies. Ranked by technical maturity, these technologies can be categorized as:

1. Absorption Heat Pump for heating and cooling
2. Adsorption Heat Pump for heating and cooling
3. Standalone Solid Desiccant Air Conditioning, A/C
4. Standalone Liquid Desiccant A/C
5. Ejector Heat Pump
6. Ground-Coupled Solid Desiccant A/C
7. Evaporative Liquid Desiccant A/C
8. Duplex-Stirling Heat Pump
9. Vuilleumier Heat Pump for heating and cooling options.

An absorption cycle, shown in Figure 6.6, utilizes a binary mixture of refrigerants such as ammonia–water or water–LiBr. The single-effect

cycle consists of an absorber, a generator or desorber, a condenser, an evaporator, and an electric solution pump, with the possibility of additional components, such as internal heat exchangers, to enhance efficiency.

An external heat source, such as a gas burner in a direct-fired system, steam or hot water in an indirect-fired system, or waste heat, is used in the generator, also called desorber. Heat transferred to the generator allows the refrigerant to desorb from the absorbent, creating a high pressure vapor. In cases where a volatile absorbent is used (e.g., ammonia–water), a rectifier is needed to reduce the concentration of the volatile absorbent (e.g., water) in the vapor to the condenser. A number of advanced cycles have been proposed in the literature to improve the COP starting from single effect with COP ~0.5 to 0.7 to Generator–Absorber heat [31] eXchange (GAX) with COP ~ 0.9 to 1.2 [32], double-effect with COP ~ 1.1 to 1.4 [33], triple-effect with COP ~ 1.3 to 1.7, compression-absorption [34] with 12% greater efficiency than vapor compression cycles [35], two-stage absorption [36] and more recently an expander-compressor cycle operating with low heat sources [37] and several waste heat/renewable energy operated absorption systems.

Absorption systems are characterized by a relatively high degree of complexity and large size. This is mainly due to the low vapor density in Water/LiBr chillers and added components for the Ammonia/Water systems. Further complexity arises from the need to mitigate corrosion

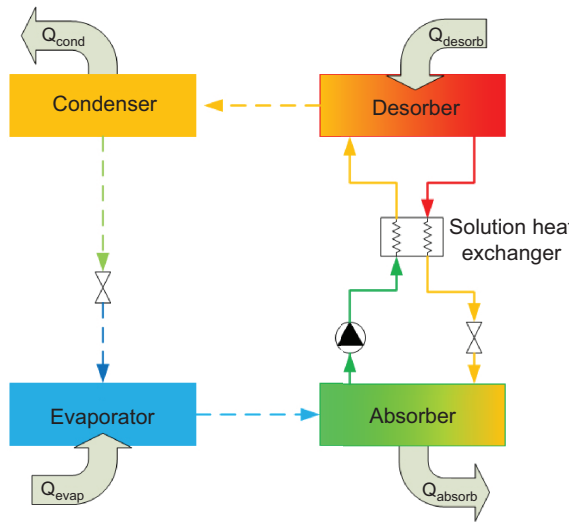

Figure 6.6. Schematics of single-effect absorption cycle.

issues and added measures to avoid solution crystallization in Water/LiBr chillers. Water/LiBr absorption chillers are considered economically attractive in large commercial buildings due to peak-demand reduction and low fuel costs. Availability of waste heat from the prime mover would further improve its feasibility. However, this technology has suffered market share decline in the United States over the last several decades while maintaining their popularity in foreign markets. On the other hand, small scale ammonia-water heat-only or reversible products are available in Europe and emerging in the United States as an alternative to gas-fired heating. Current gas prices in the United States make it infeasible except for high demand applications. The use of waste heat from the prime mover improves the economic viability and allow for shorter payback cycle. A summary of cost estimate for absorption chillers compared to vapor compression chillers was presented by [38] and summarized in Table 6.4.

An adsorption system uses multiple beds of adsorbents such as silica-gel in a silica gel-water system, to provide continuous capacity, and does not use any mechanical energy but only thermal energy. An adsorption refrigeration system usually consists of four main components: a solid adsorbent bed, a condenser, an expansion valve and an evaporator as shown in Figure 6.7. The solid adsorbent bed is linked to the evaporator. It desorbs refrigerant when heated and adsorbs refrigerant vapor when cooled such that the bed works like a thermal compressor to drive the refrigerant around

Table 6.4. Cost Estimates for Absorption and Vapor-Compression Chillers.

Chiller Type	Chiller Cost Estimates				
	(Bhatia 2010)			(Trane 2010)	
	$/ton (300 tons)	$/ton (500 tons)	$/ton (1,000 tons)	$/ton	Range (tons)
Electric Centrifugal	$340	$340	$350	$250–$230	300–2,500
Electric Rotary Screw (Water Cooled)	-	-	-	$300–$240	70–450
Electric Rotary Screw (Air Cooled)	-	-	-	$420	70–400
Single-Effect Absorption	$520	$430	$365	$350	90–1,600
Double-Effect Absorption	$625	$625	$625	$500	350–1,000

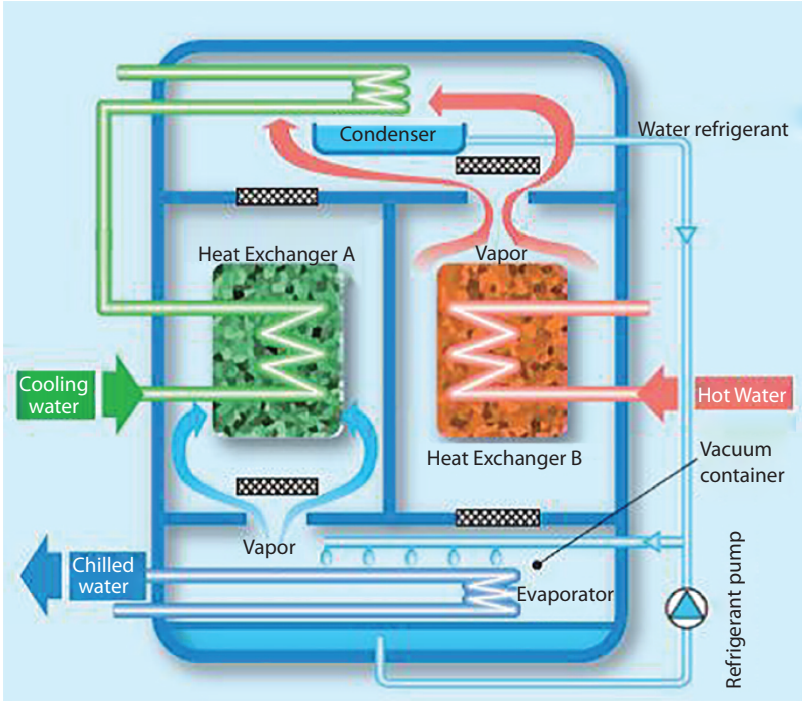

Figure 6.7. Schematic of an adsorption chiller [41].

the system to heat or cool a heat transfer fluid or to provide space heating or cooling. When the bed becomes saturated with refrigerant, it is isolated from the evaporator and connected to the condenser. The refrigerant vapor is condensed to a liquid, followed by expansion to a lower pressure in the evaporator where the low pressure refrigerant is vaporized producing the refrigeration effect (i.e., cooling the refrigerator air). When further heating no longer produces desorbed refrigerant from the adsorbent bed, the refrigerant vapor from the evaporator is reintroduced to the bed to complete the cycle. To obtain a continuous and stable cooling effect, generally two (or multiple) adsorbent beds are used, where one bed is heated during desorption while the other bed is cooled during adsorption. To achieve high efficiency, heat of adsorption needs to be recovered to provide part of the heat needed to regenerate the adsorbent. A recent literature review of conventional adsorption cycle was presented by [42].

Adsorptive beds of the chillers can be regenerated at relatively low temperatures using waste heat or solar energy as heat source. These chillers can also be employed in CCHP systems. The overall thermal and

electrical efficiency in these systems can be above 70% [43]. Some of the recent adsorption system performance enhancement technologies include heat pipes [44] and consolidated compound adsorbents [45,46] designed a prototype of icemaker with specific cooling power of 770 W/kg and a COP of 0.39, at −20 °C evaporation temperature. Space cooling COP range from 0.5 to 0.7 [47] while the space heating COP range from 1.1 to 1.4 [48].

Adsorption systems are known to suffer from low COP and low specific cooling power [42,49]. Although commercial adsorption systems for air-conditioning applications between 35 and 350 kW are reported to be available [41,50], household-scale systems are not yet commercially available. Wang et al. concluded that there is still a strong research need for advanced refrigerant/adsorbent pairs, advanced cycles and design to overcome the system transient effects [42]. Their review acknowledged the lower system efficiency and lower specific capacity compared to absorption and vapor compression refrigeration systems. Consequently, it is unlikely for adsorption refrigeration to be considered as a replacement for vapor compression refrigeration system in the near future.

Solid desiccant air-conditioning technology is mostly used for space-cooling applications in hot-humid climate zones. They are used to supplement existing vapor-compression cooling systems which otherwise would overcool the air to remove humidity and then reheat it to reach desired interior conditions. Solid desiccant dehumidification provides greater independent control of latent and sensible loads, making it an energy efficient option to achieve desired indoor air conditions. Standalone solid desiccant A/C relies on using solid desiccant materials that have a high affinity for water. As moist air crosses the desiccant bed, water vapor is adsorbed by diffusion. As the bed adsorbs the water vapor it becomes saturated; at which state it needs to be regenerated. Regeneration is a process in which the desiccant bed temperature is increased thereby increasing its water vapor pressure above that of the ambient air and allows it to diffuse to ambient or exhaust air streams. They are used in conventional A/C applications when latent loads are large and waste heat, even low grade is available to regenerate the solid desiccant bed. In HVAC systems, solid desiccant subsystems are used to dry the incoming air, thereby facilitating a secondary sensible cooling step accomplished with a different cooling technology. In hot-humid climates, standalone solid desiccant air conditioners may offer

significant energy and cost savings to satisfy large latent loads, but for most systems, the low COP of standalone solid desiccant systems offers no primary energy savings over vapor-compression systems [38]. The need for an additional sensible cooling system increases the cost and complexity over other technologies and as such acts as a market barrier. At low sensible heat ratio, solid desiccant systems can offset their cost by decreasing the required capacity of the sensible cooling system.

Standalone liquid desiccant A/C employs liquids that have a high affinity for water. These liquids can remove water from moist air when exposed to an airstream [51]. In HVAC systems, liquid desiccant air conditioners (LDACs) use liquid desiccants to dry the incoming air. As the desiccant liquid become loaded with water, it requires regeneration; a process that uses a heat source, e.g. waste heat (even low grade), to increase the liquid temperature and thereby increase the water vapor pressure above that of the ambient air. Unless coupled with other technologies, however, desiccants cannot provide sensible cooling and, therefore, do not provide a complete space-cooling function in most climates and applications. Use of a liquid desiccant (rather than solid desiccant) may facilitate coupling with a sensible cooling system [38]. Furthermore, new developments involve the use of direct and indirect evaporative cooling in tandem with liquid desiccant to provide the required sensible cooling in which case the system would provide all the space cooling needs.

The ejector heat pump cycle is similar to a reverse ranking cycle with a condenser, expansion device and an evaporator. However, the compressor is replaced with a pump, a generator, and an ejector. The pump raises the pressure of most of the liquid from the condenser to a higher pressure; the generator then boils the liquid to a high pressure high temperature superheated vapor. The superheated vapor is expanded through a jet ejector, where it entrains some low pressure vapor from the evaporator, with the combined reduced pressure stream of vapor flowing to the condenser. The liquid outflow from the condenser is split, with most of it flowing back to the circulating pump and the remainder flowing through an expansion valve to the evaporator. A schematic of the ejector heat pump cycle is shown in Figure 6.8. Rahamathulla et al. compiled available research on ejector heat pumps. Their review indicated that cooling COPs range from 0.2 to 0.4 and heating COPs range from 1.1 to 1.3 [52].

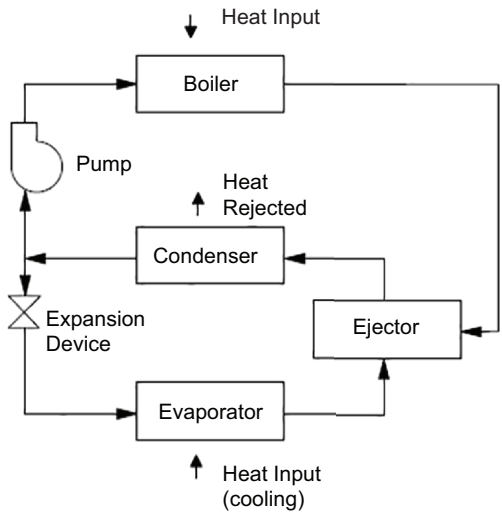

Figure 6.8. Schematic of an ejector cycle [53].

6.6 Thermal Energy Storage Requirements/Benefits

It has long been recognized that thermal energy storage (TES) can be beneficial for application of CCHP to buildings, in that it reduces or eliminates the need to meet the electrical and thermal loads simultaneously [54,55]. Rather, with TES energy can be stored for later use. This is especially important for buildings, as opposed to industrial applications, because the thermal loads in buildings including space heating and cooling, and water heating, tend to fluctuate and have strong seasonal variation. Some types of buildings, such as restaurants, spas, etc. do have large and consistent thermal loads, but here we focus our discussion on typical residential and commercial buildings where TES could potentially enable cost-effective application of CCHP.

Thermal energy storage materials, systems, and analysis have been widely covered in the literature [56], and thus only a brief discussion is given here. For CCHP, options exist to store high-temperature heat, such as the waste heat from a gas turbine exhaust greater than 500°C. However, that is rarely done in a building environment due to safety concerns and the fact that the heat will likely be used to meet space heating and domestic water heating requirements. Instead, usually

sensible heat storage in liquid water is considered as the primary heat storage medium [57], given that it can be directly used to provide domestic hot water. Other heat storage materials, however, have been examined, particularly phase change materials [58]. A hybrid thermal/electrical energy storage system has been considered [59], but in general the electric grid is treated effectively as infinite electrical energy storage. Cold storage, especially in the form of ice, has potential for CCHP systems, although cold storage does not seem to have been as widely investigated as hot storage.

The optimal design of CCHP systems including TES remains challenging. Generally speaking, relatively sophisticated models have been applied to optimize such systems. Typical building energy models with 1-hour time step have been found to yield large errors, compared with simulations based on 5-minute time steps, because of the rapidly varying nature of building electrical and thermal loads [60]. A somewhat simpler approach, termed the "extended ATD_e method" where ATD, Aggregated Thermal Demand, has been presented [57], as well as design guidelines [61]. In general studies have found positive impacts of incorporating TES in CCHP systems. For example, TES improved the operating cost savings of six of eight different types of commercial buildings located in Chicago, Illinois [62]. The two exceptions were hospitals and small hotels, both of which had much larger electrical loads than thermal loads. For single-family residential homes, the inclusion of TES may be essential to achieve cost effectiveness [61].

6.7 CCHP Sizing Options, Building Integration, Operation and System Controls: Case Studies

The goal of CCHP systems is to maximize the system operational savings and also to minimize the cost of the project. CCHP system can be operated on a topping, bottoming or combined cycle. A typical topping cycle recovers heat from operation of a prime mover and uses this thermal energy for space heating and cooling, while a bottoming cycle recovers heat from the process of the thermal energy production for space heating and cooling, to generate power. A combined cycle uses thermal output from a prime mover to generate additional shaft power where its exhaust waste heat can be used through heat recovery devices or thermal activated cooling equipment to meet the thermal demands.

In most cases, according to Eq. (1), the more thermal energy, $\dot{Q}_{th}$, is recovered, the higher the CCHP system efficiency is. Therefore, the design of CCHP system should first select the thermal components of the system based on the building heating and cooling demands, then select a generator based on thermal output to meet building electrical demands. As we can see, a good match between the thermal and electric output of a CCHP system with the thermal and electric loads of a building would induce higher efficiency and more energy savings. It is essential to assess the electrical and thermal loads for an application to optimize the CCHP design. Conventional heating and power plant are sized by maximum projected demands to cover seasonal peaks, however, CCHP selection is affected by maximum, minimum demands, and seasonal and diurnal profiles. In practice, half-hourly or hourly data should be used. Additionally, commercial and residential buildings have large time-dependent changes in the magnitude of their loads and in general the electric and thermal loads are non-coincident. Therefore, the heat and power demand profiles for buildings must be known to provide the necessary information on the magnitude, duration, and coincidence of building thermal and electrical loads for CCHP design. For an existing building, although monthly energy bills can yield approximate consumption profiles, they will not be helpful on how energy consumption profiles vary on a daily or hourly basis. To obtain sufficient data, particularly with respect to energy consumption, specific energy surveys, temporary metering and audits will be necessary. On the other hand, for new buildings, the heat and power demand profiles have to be estimated. The estimation could be based on one or a combination of the following data sources: 1) data from a dynamic simulation model of the building, 2) benchmark data from similar buildings, 3) projected occupancy patterns, and 4) empirical data from energy models or consumption codes.

To illustrate the design process, a data center located in San Diego, California is considered. The data center houses servers, computers, and other telecommunication equipment. In addition, some spaces in the data center are used as offices. Due to the location and equipment-dominated use feature, the data center has little heating load throughout the year. Therefore, for the data center, we only use electric demand and cooling demand to show how to size the CCHP system.

As illustrated in the beginning of this chapter, to achieve the highest overall system efficiency, the first step of the CCHP design is to select the

thermal components of the system according to the needs. For the data center, cooling demand is the only thermal demand in the CCHP. Thus, the thermally driven cooling component in the CCHP shall be selected first. For the data center, the majority of the cooling load is sensible cooling to reduce the air temperature in the spaces hosting tens of thousands of servers or other electrical devices, while ventilation is not required for the equipment. Double-effect Li-Br absorption chillers are selected as the proper thermally driven cooling component for the data center because of their higher COP and current availability on the market.

To design the CCHP, dynamic building simulations to identify a comprehensive electric and cooling demand is needed first. Figure 6.9 is the actual hourly electric and cooling demand of the data center in San Diego, California. We can observe that the facility has a night time peak electric demand at the range of 4 to 4.5 MW_e and a day time peak electric demand approximately 5 MW_e. For the cooling demand, there is no obvious day and night pattern; the cooling demand is at the range of 2.5 to 6 MW_{th}. The facility in the summer has a higher cooling load, as expected.

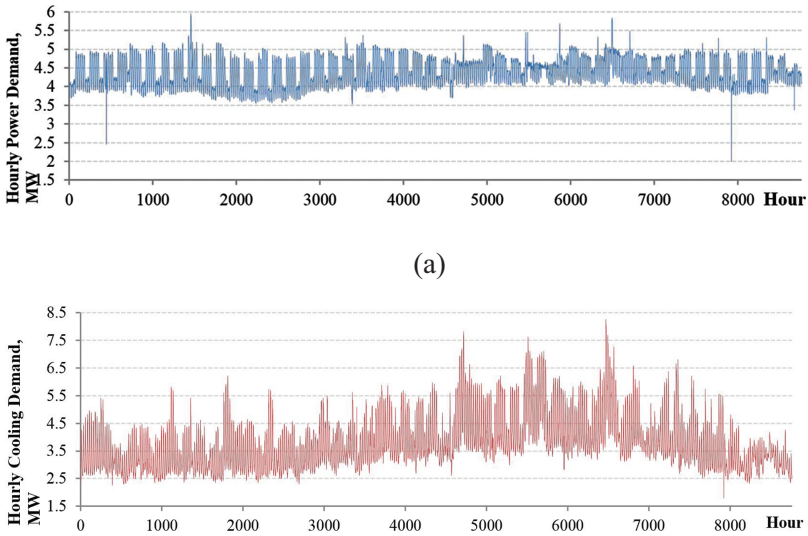

Figure 6.9. Hourly electric and cooling demand for a datacenter in San Diego, California (a) power (b) cooling.

Although dynamic data can provide us the detailed thermal and electric loads, in practice the load duration curve (LDC) is used as the basic tool for sizing and evaluating building electric power and thermal systems. A LDC is similar to a load curve as shown in Figure 6.9, but the demand data is ordered in descending order of magnitude, rather than chronologically. The LDC in descending order shows the capacity utilization requirements indicated as the frequency with which electric demand equals or exceeds a given value. Based on the electric demand obtained from the simulation, we can draw the LDC for the electric demand on an annual basis as shown in Figure 6.10. In the electric demand LDC graph, the base load and peak load of the electric demand could be identified. The base load is 3.5 MW_e and is determined by using the demand at the "knee" of the curve. The peak load is 6 MW_e, which is the maximum of the electric demand at the far left of the LDC. A CCHP system can achieve the highest efficiency of electric generation when it is sized at the base load but due to different electricity rate, however, it might not be the most economic choice. For the data center, the most economic size of the CCHP is predicated as 4.5 MW because of its shortest payback. Therefore, economic analyses shall be carried out to size the CCHP. Similarly, the cooling LDC can be drawn as shown in Figure 6.11. The base cooling and the peak cooling loads are also identified. As you may notice, Figure 6.10 and Figure 6.11 separate the electric load and the cooling load.

However, we need to consider simultaneously the variations of the electric and cooling demands during the design of the CCHP to achieve higher system efficiency and better economic benefits. Therefore, a two-dimensional load duration curve, which is able to show the relation of the frequency and the simultaneous loads, is needed. In the two-dimensional

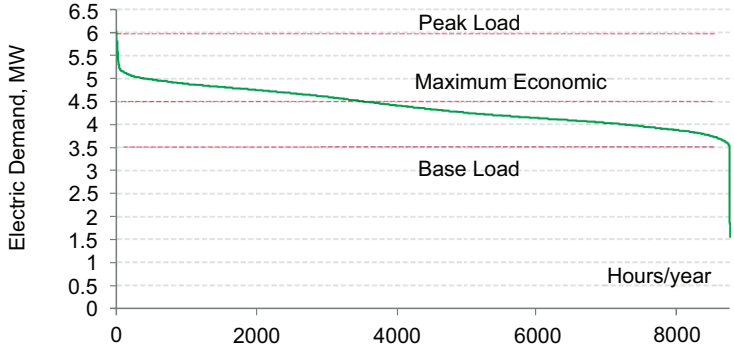

Figure 6.10. Electric load duration curve of a datacenter in San Diego, California.

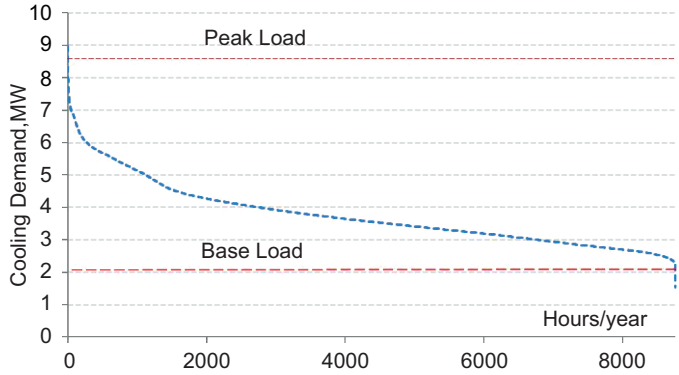

Figure 6.11. Cooling load duration curve of a datacenter in San Diego, California.

LDC, one of the demands must be broken into discrete periods and the other demand is created for each discrete period in the same way as the one used in a one-dimensional LDC.

Typically, the greater the load fluctuation, the greater the number of discrete periods required for accurate representation. Since the data center has a relatively stable load profile as shown in Figure 6.9, three discrete periods are used to represent the facility loads in the two-dimensional LDC. Figure 6.12 is the two-dimensional LDC for the data center with three discrete periods of the electric demand. The electric demand at each discrete period indicates the mean value of all the demands within the

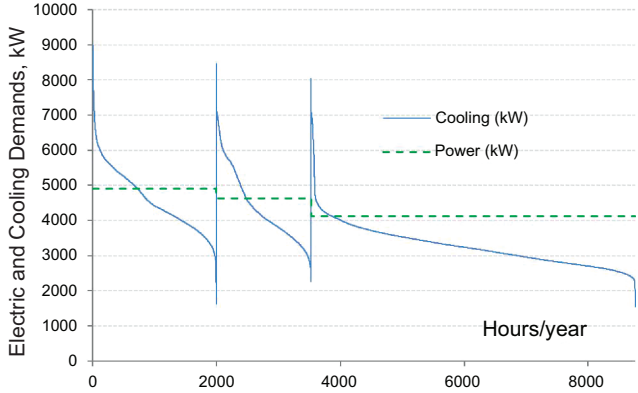

Figure 6.12. Two-dimensional LDC with 3 discrete periods for a datacenter in San Diego, California.

discrete period. According to Figure 6.12, the CCHP can select three power generators to meet the electric demands: 4.2 MW_e, 0.4 MW_e, and 0.4 MW_e. The 4.2 MW_e generator, which serves as the primary engine, will run all year long. On the other hand, one 0.4-MW_e generator will run approximate 40% of the year to provide the excess power when the facility needs more than 4.2 MW_e at the discrete periods with the highest and the medium demands. The second 0.4-MW_e generator will be operated approximate 20% of the year to provide the excess electricity when the facility electric demand is higher than 4.6 MW_e at the discrete period with the highest demand level in Figure 6.12.

Since the difference between the highest and the medium value is relatively small (300–400 kW), a two-dimensional LDC with a smaller number of discrete periods could be sufficient to represent the facility actual load profiles. Accordingly, Figure 6.13 is the two-dimensional LDC with only 2 discrete periods. According to Figure 6.13, we can use just two power generators to meet the electric demands of 4.2 MW_e and 0.8 MW_e, replacing the two 0.4-MW_e generators used in the previous design. This CCHP with fewer generators could be a better choice to save initial cost and simplify the operation and control of CCHP. However, the final design of a CCHP shall be made by the consideration of life cycle assessment with respects of energy, environment, and economic analyses. The LDC method is convenient and intuitive for preliminary sizing and analysis of a CCHP system if only one or two loads need to be considered simultaneously. However, we often have some facilities with more than two different loads such as electric power, heating water, domestic hot water, and chilled water, that all need to be considered simultaneously

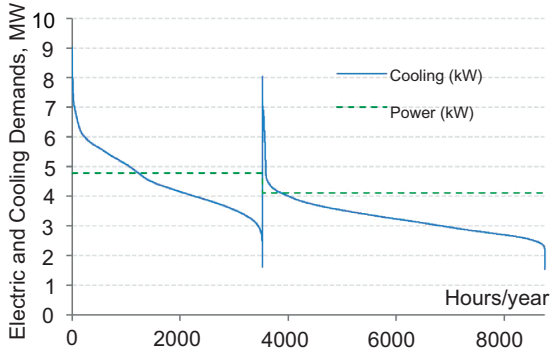

Figure 6.13. Two-dimensional LDC with 2 discrete periods for a datacenter in San Diego, California.

while performing the CCHP analysis. These loads make the design of CCHP complicated. In such cases, the LDC method becomes very limited and unacceptably cumbersome for those building to analyze or design a CCHP system. For such situations, computer screening programs should be used to assist in the design of CCHP.

A Li-Br double-effect (2E) absorption chiller typically has a COP of 1.0 to 1.2. It can be driven by various thermal resources including steam, hot water, direct fired, or exhaust gas. Table 6.5 summarizes the rated thermal resources for various types of absorption chiller based on data provided by manufacturer's brochures. According to Table 6.5, various system configurations can be identified for the CCHP. Either steam turbines or gas turbines can provide 400°C to 500°C exhaust gas required by the 2E absorption chillers. Comparably, natural gas is a much cleaner fuel source and natural gas turbines have relatively high overall system efficiency, so that the electric power generators used in the CCHP for the data center will be gas turbines with capacities of 4.2 MW_e and 0.8 MW_e, which are determined by using Figure 6.13 (the two-dimensional LDC with 2 discrete periods).

According to Table 6.1, we assume 35% electrical efficiency for the 4.2MW_e gas turbine. If the chiller is driven by steam or hot water, a heat recovery steam generator or a gas-water heat exchanger will be needed to recover the energy in the flue gas at 500°C to steam at 800 kPa or hot water at 170°C for driving the 2E absorption chiller. The outlet of the steam from the double-effect chiller is condensed at about 95°C or the outlet of hot water after the 2E chiller is at approximate 130°C. These outlet streams still contain a lot of energy that can be used for various heating demands or as the heat resource for driving a single-effect (1E) hot water absorption chiller to produce chilling power. Since the data center primarily has power and cooling demands, we will use the hot water out of the 2E absorption chiller to drive a 1E hot water absorption chiller for producing more chilled water. After the 1E hot water absorption chiller, the outlet of the hot water is around 88°C and it can be continuously used for various heating demands.

On the other hand, the 2E absorption chiller can also directly use the flue gas from the turbine as a heat resource to produce chilled water. Based on Table 6.5, the outlet of the flue gas from the 2E absorption chiller will be around 170°C, at which the flue gas is not able to drive a 1E flue gas absorption chiller, but the flue gas can exchange its energy to hot water used for driving a 1E hot-water driven absorption chiller. Figure 6.14 is a system schematic energy diagram for the CCHP, as an example of the possible system configurations. If we only consider the electric power and chilled water produced by the CCHP,

Table 6.5. Thermal resource rated conditions for absorption chillers [63].

	Exhaust Gas Absorption Chiller		Steam Absorption Chiller		Hot water Absorption Chiller	
	1E	2E	1E	2E	1E	2E
Inlet Condition	300 °C (572° F)	500 °C (932 °F)	100kPa (14.5psi)	800 kPa (116psi)	98 °C (208 °F)	170° C (338 °F)
Outlet Condition	130 °C (266 °F)	170 °C (338° F)	Condensation 95 °C (203 °F)	Condensation 95 °C (203 °F)	88 °C (190 °F)	130 °C (266 °F)

the total efficiency of the CCHP will be 76%. If we also include the hot water produced, the total efficiency of the CCHP could be as high as 99%.

CCHP building integration was shown to be dependent on available technology, climate, load profile, and utility costs. A recent study by Medrano et al. showed that annual electric and natural gas utility bills can be reduced by 61%, 24%, and 56% for hospital, college, and medium office buildings, respectively when using high temperature fuel cells [8]. The same study showed that using micro-turbine generators result in less energy and utility savings, but provide a more favorable payback due to the lower initial cost compared to the high temperature fuel cells. Other factors to include while investigating CCHP building integration are the location which dictates utility

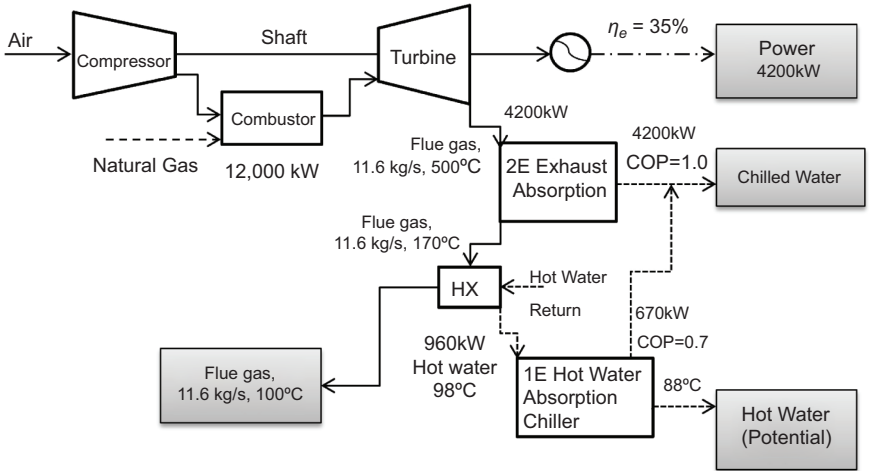

Figure 6.14. System schematic diagram of the CCHP with 2E exhaust absorption chiller.

costs, climate, and load profiles. For example, a building in Boston, MA has higher electricity cost than a similar building in Los Angeles, CA and has higher heating load while the similar Building in Los Angeles would have significantly higher cooling loads. As such, only heat recovery might be useful in Boston while a heat recovery with a thermally driven cooling device is needed in Los Angeles. When comparing the system complexity with the utility costs, it would be more apparent that the CHP system in Boston would be more cost effective than the CCHP system in Los Angeles.

6.8 Economic and Feasibility Analysis

Determining the feasibility of a CCHP system is largely a matter of conducting an economic analysis of the proposed system to see if it leads to an acceptable payback, or return on investment. Such a feasibility analysis consists usually of two or more stages, with the first stage being the simplest analysis and subsequent stages adding more complexity. The methodologies for analyzing a CHP system (i.e., one that provides electric power and heating) versus a CCHP system (one that provides electric power, heating, and cooling) are identical. A number of useful references are available that describe these analyses in some detail including a simple CHP screening analysis and feasibility analysis [64], a CHP Level 1 Feasibility Analysis Data Tool [65] and a CHP Level 2 Feasibility Analysis Overview and Checklist [66]. The US EPA also provides a spreadsheet calculation tool for the Level 1 Feasibility Analysis [67]. One free software tool is RETScreen, available from Natural Resources Canada [68]. Within the USA, comprehensive documentation on CHP technologies, analysis, state-by-state incentives and policies, and technical assistance for preparing feasibility analyses is available through the EPA Combined Heat and Power Partnership [22].

In general, detailed historical information is required for the facility to which the CCHP system will be applied, including electricity usage and demand, natural gas usage, the heating and cooling loads, electricity and natural gas costs (including demand charges and any time-of-use rates), and the daily profiles for electricity usage and demand, natural gas usage, and the heating and cooling loads. The first step, therefore, in any CCHP feasibility analysis is to assemble all this historical data, preferably for a period of at least one year to accurately represent seasonal energy use. Additional information may be required post-installation on what rate the local utility is willing to pay for any excess generated electricity returned

to the grid. It should be noted that the rates utilities typically pay for excess generation are much lower than the corresponding rates that the utilities charge their customers for utility-supplied electricity.

Detailed feasibility analyses require computer simulation, and go well beyond the one- and two-dimensional load demand curves described above in Section 7. Here, we will instead focus on a relatively simple spreadsheet approach, illustrated by an example calculation based on an actual CCHP feasibility analysis conducted for an installation in the southwestern USA. This facility is a residential development that includes a dining hall, fitness center, and a swimming pool/hot tub, making it an attractive candidate for CCHP because of its relatively consistent heat load. The option to provide cooling was not considered in this analysis. The detailed electricity and natural gas usage prior to CCHP installation is given in Table 6.6. Not surprisingly, natural gas consumption peaks in the winter, while electricity peaks in the summer. The "kW coincidence factor" is the fraction of time that the peak electric demands for the separate loads of fitness center, dining hall, and pool/spa occur simultaneously and here is taken to be 0.8.

Based on the values shown in Table 6.6, a 130 kW_e natural gas turbine with heat recovery is proposed as the CCHP system, and the following assumptions are applied:

1. The 130 kW_e turbine runs 16 hours/day
2. The turbine heat rate is 9225 kWh/Btu, and the recoverable heat rate is 5535 Btu/kWh

Table 6.6. Detailed Electricity and Natural Gas Usage for the Example Facility before CCHP Installation.

	Electricity								Natural Gas	
	Fitness Center		Dining Hall		Pool/Spa		Totals			
Month	kW	kWh	kW	kWh	kW	kWh	kW	kWh	Therms	MMBtu
Jan.	78	34,880	62	21,000	22	2,920	130	58,800	9,500	950
Feb.	86	40,240	73	26,880	32	2,800	152.8	69,920	8,000	800
Mar.	87	37,200	68	24,120	36	2,720	152.8	64,040	7,000	700
Apr.	92	35,280	77	26,640	48	2,440	173.6	64,360	5,000	500
May	87	36,800	86	27,480	27	2,280	160	66,560	4,000	400
Jun.	93	43,360	92	32,880	47	2,960	185.6	79,200	2,000	200
Jul.	96	43,920	96	37,440	46	3,560	190.4	84,920	500	50
Aug.	97	41,600	89	34,440	32	3,320	174.4	79,360	500	50
Sep.	96	44,320	89	33,240	39	3,640	179.2	81,200	1,500	150
Oct.	90	39,920	80	27,600	31	3,160	160.8	70,680	3,000	300
Nov.	79	32,400	65	20,640	32	2,600	140.8	55,640	6,000	600
Dec.	74	32,560	56	21,240	30	2,560	128	56,360	8,500	850

3. For direct heating, the natural gas burner efficiency is 0.75
4. Coincidence factor is 0.9 for turbine heat recovery
5. Turbine maintenance costs of $0.009/kWh
6. Electricity rate schedule after CCHP installation is equivalent to APS E-32S (APS = Arizona Public Service), for an average cost of $0.138/kWh
7. Natural gas costs are $7.10/MMBtu for the turbine, $8.40/MMBtu for direct heating
8. Any excess electricity is sold back to the utility at the rate of $0.040/kWh during the summer, and $0.035/kWh during the winter.

The electric output of the 130 kW_e gas turbine is presented on a monthly basis in Table 6.7. Since the output does not cover the entire electric load, additional electricity will have to be purchased from the utility, Arizona Public Service (APS), and those additional kWhs are also calculated in Table 6.7. The heat output, on the other hand, is presented in Table 6.8, which includes the additional natural gas that has to be purchased from the gas utility to meet the entire heat load. In this case, the natural gas utility is Southwest Gas Corporation (SWG). The electricity and natural gas usage before and after the CCHP installation is given in Figure 6.15. Finally, the monthly and total operating costs for the system after CCHP installation is given in Table 6.9.

Finally, these operating costs are compared to the initial capital costs to determine the cost effectiveness of the CHP system. Here, we determine the simple payback through the usual formula:

Table 6.7. Electric Output from the 130 kWe Gas Turbine.

Month	kW	Days in Month	Assumed Daily Operating Hours	kWh	Remaining kW from APS	Remaining kWh from APS	Excess kWh to be Sold to APS
Jan.	130	31	16	64,480	0	0	5,680
Feb.	130	28	16	58,240	23	11,680	0
Mar.	130	31	16	64,480	23	182	440
Apr.	130	30	16	62,400	44	1,960	0
May	130	31	16	64,480	30	2,080	0
Jun.	130	30	16	62,400	56	16,800	0
Jul.	130	31	16	64,480	60	20,440	0
Aug.	130	31	16	64,480	44	14,880	0
Sep.	130	30	16	62,400	49	18,800	0
Oct.	130	31	16	64,480	31	6,200	0
Nov.	130	30	16	62,400	11	86	6,760
Dec.	130	31	16	64,480	0	0	8,120
TOTALS		**365**		**759,200**		**93,109**	**21,000**

Table 6.8. Heat Output from the 130 kWe Gas Turbine.

Month	Recoverable Heat (MMBTU)	Heat Load (MMBTU)	Remaining NG Usage from SWG (MMBTU)	NG Usage for the CHP Turbine (MMBTU)	Total NG Usage (MMBTU)
Jan.	357	713	522	595	1,117
Feb.	322	600	413	537	950
Mar.	357	525	272	595	867
Apr.	345	375	86	576	661
May	357	300	0	595	595
Jun.	345	150	0	576	576
Jul.	357	38	0	595	595
Aug.	357	38	0	595	595
Sep.	345	113	0	576	576
Oct.	357	225	0	595	595
Nov.	345	450	186	576	761
Dec.	357	638	422	595	1,017
TOTALS	**4,202**	**4,163**	**1,899**	**7,004**	**8,903**

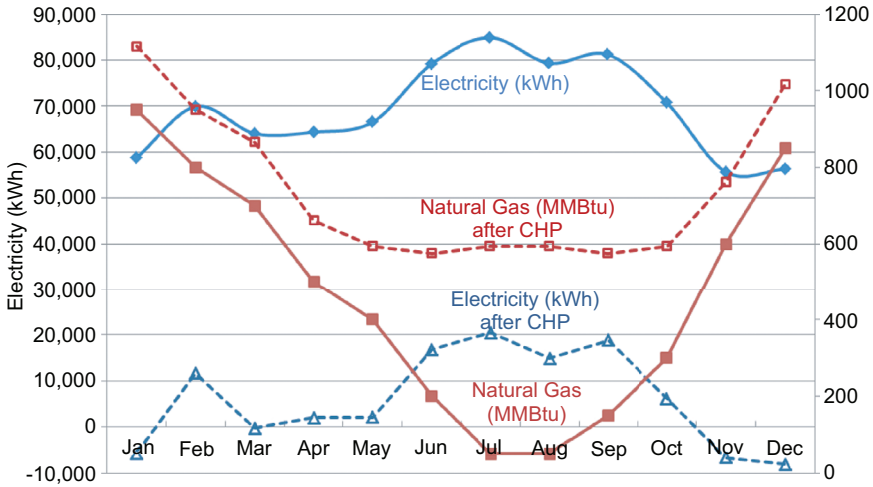

Figure 6.15. Electricity and natural gas usage before and after installation of the 130 kWe gas turbine CCHP system.

$$\text{Simple Payback}\left(\text{Yr}\right)=\frac{\text{Initial Cost}\left(\$\right)}{\text{Operating Cost}\left(\$\right)/\text{Yr}} \tag{6.3}$$

A summary of the cost analysis is provided in Table 6.10. Including the CCHP incentive of $52,000 from the natural gas utility, SWG, the simple payback is a presumably attractive 3.9 years.

Table 6.9. Electric and Natural Gas Costs after the 130 kWe Gas Turbine is Installed.

Month	APS Net Costs	SWG Costs for Remaining NG Usage	SWG Costs for NG Usage for the CHP Turbine	Total SWG Costs	Turbine Maintenance Costs
Jan.	-$156	$4,711	$4,540	$9,251	$580
Feb.	$1,039	$3,731	$4,101	$7,832	$524
Mar.	$284	$2,454	$4,540	$6,994	$580
Apr.	$681	$772	$4,394	$5,166	$562
May	$590	$0	$4,540	$4,540	$580
Jun.	$2,239	$0	$4,394	$4,394	$562
Jul.	$2,573	$0	$4,540	$4,540	$580
Aug.	$1,894	$0	$4,540	$4,540	$580
Sep.	$2,243	$0	$4,394	$4,394	$562
Oct.	$1,058	$0	$4,540	$4,540	$580
Nov.	-$75	$1,675	$4,394	$6,069	$562
Dec.	-$242	$3,808	$4,540	$8,348	$580
TOTALS	**$12,128**	**$17,152**	**$53,455**	**$70,607**	**$6,833**

Table 6.10. Cost Analysis for the 130 kWe Gas Turbine With Heat Recovery.

Annual Electricity Costs after CHP Installation:	$12,128
Annual Natural Gas Cost: Turbine	$53,455
Annual Natural Gas Cost: Heating	$17,152
Annual Natural Gas Costs after CHP Installation:	$70,607
Annual Maintenance Costs:	$6,833
Total Annual Costs after CHP Installation:	$89,568
Annual Cost Savings after CHP Installation:	$58,432

Initial Capital Cost:	$278,500
Total Incentive from SW Gas:	$52,000
Initial Capital Cost - Incentive:	$226,500
Simple Payback Year	**3.9**

6.9 Future CCHP and Conclusion

With advancing the technologies and market transformation for CCHP systems, CCHP systems should be rapidly expanded due to various important benefits, which include reducing fuel and energy consumptions, greenhouse gas emissions and air pollution, and overall energy costs, and improving total system efficiency, overall facility reliability and safety, as well as enabling carbon neutral for biofuel based system. To achieve those benefits, more future work and investigations are needed by focusing on the performance improvement of the CCHP systems including:

1. Increasing overall energy efficiency of CCHP system through maximizing the utilization of the thermal energy in a cascade;
2. Developing novel end-use devices in CCHP systems to deeply utilize thermal energy beyond the typical CCHP operation scenarios for higher overall system efficiency;
3. Developing advanced components and subsystems beyond the conventional art to minimize the energy losses among the subsystems;
4. Optimizing system design through advanced control strategies to maximize overall system efficiency;
5. Developing cost effective CCHP systems for both residential and commercial buildings by using advanced technologies like fuel cells, organic Rankine cycle based-systems, and others;
6. Investigating the use of new efficient and environmentally friendly working fluids to reduce the negative impacts from buildings on our environment;
7. Connecting to the grids using smart grids to increase power generation efficiency and reduce the infrastructure costs.

Furthermore, it is necessary to educate engineers and the public in a system approach that integrate design, technology management, economics, and marketing of CCHP. New technologies in the field and the supports from government will very much promote the deployment of CCHP to make US toward sustainability.

Nomenclature

$\eta_{overall}$	overall efficiency of CCHP
W_E	the net useful electric power output from generator, kW

W_{Grid}	electric power from grids, kW
$\dot{Q}_{th}$	net useful thermal outputs, kW
$\dot{Q}_{th\_others}$	other thermal energy inputs, kW
$\dot{Q}_{fuel}$	total fuel input, kW
η_{th}	thermal efficiency of heat recovery
ε	effectiveness of a heat exchanger, dimensionless
$\dot{Q}_{max}$	maximum possible heat transfer rate, kW
$\dot{Q}_{act}$	Actual heat transfer rate, kW

Useful Resources

https://doe.icfwebservices.com/chpdb/

http://energy.gov/eere/amo/chp-technical-assistance-partnerships-chp-taps

http://www3.epa.gov/chp/

http://www.energy.gov/eere/amo/chp-deployment

http://energy.gov/eere/amo/combined-heat-and-power-basics

http://www1.eere.energy.gov/manufacturing/distributedenergy/chp_database/

http://chpassociation.org/

http://northwestchptap.org/

Calculator

http://www.energygroove.net/energy-cost/micro-combined-heat-power-calculator/

http://www3.epa.gov/chp/basic/calculator.html

http://www.tech-4-you.com/ESC/Calculators/

References

[1] MIT. *The Future of the Electric Grid, an Interdisciplinary MIT Study*. Cambridge, MA: Massachusetts Institute of Technology, 2011.

[2] Greene, D. L., Duleep, K. G., and Upreti, G. *Status and outlook for the US non-automotive fuel cell industry: Impacts of government policies and assessment of future opportunities.* ORNL/TM-2011/101, Oak Ridge, TN: Oak Ridge National Laboratory, 2011.

[3] Meckler, M., and Hyman, L. B. *Sustainable On-Site CHP Systems: Design, Construction, and Operations.* 1. New York: The McGraw-Hill Companies, 2010.
[4] ICF International. *Internal estimates by ICF International and CHP Installation Database developed by ICF International for Oak Ridge National Laboratory and the U.S. DOE.* 2012. http://www.eea-inc.com/chpdata/index.html.
[5] Mago, P. J., and Smith, A. D. "Evaluation of the potential emissions reductions from the use of CHP systems in different commercial buildings." *Building and Environment* 53 (2012): 74–82.
[6] Mago, P. J., Hueffed, A., and Chamra, L. M. "Analysis and optimization of the use of CHP-ORC systems for small commercial buildings." *Energy and Buildings* 42, no. 9 (2010): 1491–1498.
[7] Gu, Q., Ren, H., Gao, W., and Ren, J. "Integrated assessment of combined cooling heating and power systems under different design and management options for residential buildings in Shanghai." *Energy and Buildings* 51 (2012): 143–152.
[8] Medrano, M., Brouwer, J., McDonell, V., Mauzey, J., and Samuelsen, S. "Integration of distributed generation systems into generic types of commercial buildings in California." *Energy and Buildings* 40, no. 4 (2008): 537–548.
[9] Pagliarini, G., Corradi, C., and Rainieri, S. "Hospital CHCP system optimization assisted by TRNSYS building energy simulation tool." *Applied Thermal Engineering* 44 (2012): 150–158.
[10] Ren, H., and Gao, W. "Economic and environmental evaluation of micro CHP systems with different operating modes for residential buildings in Japan." *Energy and Buildings* 42, no. 6 (2010): 853–861.
[11] Ziher, D., and Poredos, A. "Economics of a trigeneration system in a hospital." *Applied Thermal Engineering* 26, no. 7 (2006): 680–687.
[12] Xu, D., and Qu, M. "Energy, environmental, and economic evaluation of a CCHP System for a data center based on operational data." *Energy and Buildings* 67 (2013): 176–186.
[13] Guizzi, G. L., and Manno, M. "Fuel cell-based cogeneration system covering data centers' energy needs." *Energy* 41, no. 1 (2012): 56–64.
[14] Ebrahimi, M., Keshavarz, A., and Jamali, A. "Energy and exergy analyses of a micro-steam CCHP cycle for a residential building." *Energy and Buildings* 45 (2012): 202–210.
[15] Alanne, K., Saari, K., Kuosa, M., Jokisalo, J., and Martin, A. R. "Thermo-economic analysis of a micro-cogeneration system based

on a rotary steam engine (RSE)." *Applied Thermal Engineering* 44 (2012): 11–20.
[16] Barbieri, E. S., Spina, P. R., and Venturini, M. "Analysis of innovative micro-CHP systems to meet household energy demands." *Applied Energy* 97 (2012): 723–733.
[17] Maghanki, M. M., Barat, G., Gholamhassan, N., and Reza, J. G. "Micro combined heat and power (MCHP) technologies and applications." *Renewable and Sustainable Energy Reviews* 28 (2013): 510–524.
[18] Onsite Sycom. *The Market and Technical Potential for Combined Heat and Power in the Commercial/Institutional Sector.* DOE, 2000.
[19] Wu, D. W., and Wang, R. Z. "Combined cooling, heating and power: A review." *Progress in Energy and Combustion Science* 32 (2006): 459–495.
[20] Vitaliy, C. "Hybrid Brayton Cycle Model and Facility Commissioning." 2013. http://mspace.lib.umanitoba.ca/bitstream/1993/23292/3/Churilov_Vitaliy.pdf (accessed Sept. 4, 2014).
[21] Colella, W. "Design options for achieving a rapidly variable heat-to-power ratio in combined heat and poer (CHP) fuel cell system (FCS)." *Journal of Power Sources*, no. 106 (2002): 388–396.
[22] EPA CHP Partnership. *Combined Heat and Power Partnership.* 2014. http://www.epa.gov/chp/index.html (accessed Dec. 9, 2014).
[23] Moser, W. *Intelligent Heat Transfer with Thermoelectric Generators*. Jyväskylä, Finland: BIOENERGY 2007, 2007.
[24] Arvay, P., Muller, M. W. R., Ramdeen, V., and Cunningham, G. *Economic Implementation of the Organic Rankine Cycle in Industry*. ACEEE Summer Study on Energy Efficiency in Industry, 2011.
[25] Quoilin, S., Van Den Broek, M., Declaye, S., Dewallef, P., and Lemort, V. "Techno-economic survey of Organic Rankine Cycle (ORC) systems." *Renewable and Sustainable Energy Reviews* 22 (2013): 168–186.
[26] U.S. Environmental Protection Agency Combined Heat and Power Partnership. "Catalog of CHP Technologies." 2014.
[27] Thulukkanam, T. *Heat Exchanger Design Handbook.* 2nd. Boca Raton, FL: CRC Press, 2013.
[28] Mississippi Cooling, Heating, and Power (Micro-CHP) and Bio-Fuel Center. "Cooling, Heating, and Power for Buildings (CHP-B) Instructional Module." 2004.
[29] Hwang, J. J., Zou, M. L., Chang, W. R., Su, A., Weng, F. B., and Wu, W. "Implementation of a heat recovery unit in a proton exchange

membrane fuel cell system." *International Journal of Hydrogen Energy* 35 (2010): 8644–8653.
[30] Gao, X., Andreasen, S. J., Chen, M., and Kær, S. K. "Numerical model of a thermoelectric generator with compact plate-fin heat exchanger for high temperature PEM fuel cell exhaust heat recovery." *International Journal of Hydrogen Energy* 37 (2012): 8490–8498.
[31] Vliet, G. C., Lawson, M. B., and Lithgow, R. A. "Water–lithium bromide double-effect absorption cooling cycle analysis." *ASHRAE Transactions* 88 (1988): 811–882.
[32] Altenkirch, E., and Tenckhoff, B. Absorptionkaeltemaschine Zur kontinuierlichen erzeugung von kaelte und waerme oder acuh von arbeit. Germany Patent 278076. 1911.
[33] Grossman, G., Wilk, M., and DeVault, R. C. "Simulation and performance analysis of triple-effect absorption cycles." *ASHRAE Transactions* 100, no. 1 (1994): 452–462.
[34] Hultén, M., and Berntsson, T. "The compression/absorption cycle—influence of some major parameters on COP and a comparison with the compression cycle." *International Journal of Refrigeration* 22, no. 2 (1999): 91–106.
[35] Hong, D., Tang, L., He, Y., and Chen, G. "A novel absorption refrigeration cycle." *Applied Thermal Engineering* 30, no. 14–15 (2010): 2045–2050.
[36] Fan, Y., Luo, L., and Souyri, B. "Review of solar sorption refrigeration technologies: Development and applications." *Renewable and Sustainable Energy Reviews* 11, no. 8 (2007): 1758–1775.
[37] Wang, R. Z., Yu, X., Ge, T. S., and Li, T. X. "The present and future of residential refrigeration, power generation and energy storage." *Applied Thermal Engineering* 53, no. 2 (2013): 256–270.
[38] Navigant Consulting, Inc. *Energy Savings Potential and RD&D Opportunities for Non-Vapor-Compression HVAC Technologies.* Washington, D.C.: U.S. Department of Energy; Energy Efficiency and Renewable Energy, 2014.
[39] Bhatia, A. "1." *Overview of Vapor Absorption Cooling Systems.* Coninuing Education and Development, Inc. 2010. http://www.cedengineering.com/upload/Vapor%20Absorption%2Machines.pdf (accessed Dec. 13, 2013).
[40] Trane. *Cost Estimates* (2010).
[41] Mayekawa. 1. 2009. http://www.mayekawa.com/products/heat_pumps/ (accessed Dec. 13, 2014).
[42] Wang, D. C., Li, Y. H., Li, D., Xia, Y. Z., and Zhang, J. P. "A review on adsorption refrigeration technology and adsorption deteriorationin

physical adsorption systems." *Renewable Sustainable Energy Reviews* 14, no. 1 (2010): 344–353.

[43] Wang, R. Z., Kong, X. Q., Wu, J., Huangfu, Y., and Wu, D. "Performance research of a micro CCHP system with adsorption chiller." Edited by R. Radermacher. *International Sorption Heat Pump Conference*. Broomfield, Colorado, USA: Center for Environmental Energy Engineering, 2005.

[44] Yang, G. Z. et al. "Research on a compact adsorption room air conditioner." *Energy Conversion and Management* 47, no. 15–16 (2006): 2167–2177.

[45] Tamainot-Telto, Z., and Critoph, R. E. "Advanced solid sorption air conditioning modules using monolithic carbon-ammonia pair." *Applied Thermal Engineering* 23, no. 6 (2003): 659–674.

[46] Lu, Z. S., Wang, R. Z., Wang, L. W., and Chen, C. J. "Performance analysis of an adsorption refrigerator using activated carbon in a compound adsorbent." *Carbon* 44, no. 4 (2006): 747–752.

[47] RHC. *Strategic Research Priorities for Cross-Cutting Technology.* Brussels, Belguim: Secretariat of the European Technology Platform on Renewable Heating and Cooling, 2012.

[48] Schossig, P. *Fuel Driven Heat Pumps*. Nuremberg: Heat Pump Centre, 2012.

[49] Wang, R. Z., and Oliveira, R. G. "Adsorption refrigeration—An efficient way to make good use of waste heat and solar energy." *Progress in Energy and Combustion Science* 32, no. 4 (2006): 424–458.

[50] Tassou, S. A., Lewis, J. S., Ge, Y. T., Hadawey, A., and Chaer, I. "A review of emerging technologies for food refrigeration applications." *Applied Thermal Engineering* 30, no. 4 (2010): 263–276.

[51] Dieckmann, J., Roth, K. W., and Brodrick, J. "Emerging technologies: Liquid desiccant air conditioners." *ASHRAE Journal*, April (2004): 58–59.

[52] Rahamathullah, M. R., Palani, K., Aridass, T., Venkatakrishnan, P., Sathiamourthy, and Palani, S. "A review on historical and present developments in ejector systems." *International Journal of Engineering Research and Applications* 3, no. 2 (2013): 10–34.

[53] Fischer, S., and Labinov, S. *Not-In-Kind Technologies for Residential and Commercial Unitary Equipment.* Oak Ridge, TN: Oak Ridge National Laboratory, 2000.

[54] Dincer, I. "On thermal energy storage systems and applications in buildings." *Energy and Buildings* 34 (2002): 377–388.

[55] ASHRAE. "HVAC Systems and Equipment (SI)." In *ASHRAE Handbook.* 2012.

[56] Dincer, I., and Rosen, M. *Thermal Energy Storage: Systems and Applications.* 2nd. Hoboken, NJ: Wiley, 2010.
[57] Martinez-Lera, S., Ballester, J., and Martinez-Lera, J. "Analysis and sizing of thermal energy storage in combined heating, cooling and power plants for buildings." *Applied Energy* 106 (2013): 127–142.
[58] Mongibello, S., Capezzuto, M., and Graditi, G. "Technical and cost analyses of two different heat storage systems for residential micro-CHP plants." *Applied Thermal Engineering*, 2013: in press.
[59] Bianchi, M., De Pascale, A., and Melino, F. "Performance analysis of an integrated CHP system with thermal and electric energy storage for residential application." *Applied Energy* 112 (2013): 928–938.
[60] Hawkes, A., and Leach, M. "Impacts of temporal precision in optimisation modelling of micro-combined heat and power." *Energy* 30 (2005): 1759–1779.
[61] Bianchi, M., De Pascale, A., and Spina, P. R. "Guidelines for residential micro-CHP systems design." *Applied Energy* 97 (2012): 673–685.
[62] Smith, A. D., Mago, P. J., and Fumo, N. "Benefits of thermal energy storage option combined with CHP system for different commercial building types." *Sustainable Energy Technologies and Assessments* 1 (2013): 3–12.
[63] Broad. *Broad Air Conditioning Brochure*. Changsha. 2009.
[64] ASHRAE. "Chapter 7: Combined Heat and Power Systems." In *HVAC Systems and Equipment,* 7.39. Atlanta, GA: American Society of Heating, Refrigerating and Air-Conditioning Engineers, 2012.
[65] —. "Level 1 Feasbility Analysis Data Tool." www.epa.gov/chp /documents/chp_phase1_data_request_form.xls (accessed Dec. 9, 2014).
[66] —. "Level 2 Feasibility Analysis Overview and Checklist." http:// www.epa.gov/chp/documents/level_2_studies_september9.pdf (accessed Dec. 9, 2014).
[67] —. "Sample Comprehensive Level 1 Feasibility Analysis—Ethanol Facility." 2016. http://www.epa.gov/chp/documents/sample_fa _ethanol.pdf (accessed Dec. 9, 2014).
[68] Natural Resources Canada. *RETScreen International.* http://www .retscreen.net/ang/home.php (accessed Dec. 9, 2014).

7 Integration of Solar Energy Systems

Andy Walker, Jennifer Scheib, Ben Kroposki, and Ming Qu

Abstract

Photovoltaics, daylighting, passive solar heating and cooling, solar water heating, and solar ventilation air preheating are arguably the most relevant renewable energy technologies for implementation integral to an individual building or campus of buildings. This chapter provides an introduction to the operating principal of each technology, components and systems, applications, recent cost data, and examples.

7.1 Introduction to Integration of Solar Energy Systems

Almost all of the energy efficiency measures discussed in the earlier chapters of this book are less expensive than a solar energy system to provide the same amount of energy saved. But as the saying goes "you cannot save yourself rich" and having installed efficient systems and sophisticated controls, we need some source of energy to power them. On-site renewable energy (RE) systems offer several advantages, especially when operated in concert with a larger utility system. The main reasons to consider RE is cost-effectiveness, but other reasons are as diverse as: reduction of atmospheric emissions; compliance with regulations requiring RE; enhanced energy security through on-site energy source; enhanced reliability through redundant energy supply; abate risks related to fuel availability and cost, or risk of fuel-spills during delivery; score points in a sustainability rating system; or as a mitigation measure in a larger environmental-permitting process. Renewable energy technologies used on buildings include daylighting; solar photovoltaics; solar water heating; solar ventilation air preheating; passive solar heating and cooling load avoidance; wind power; biomass heat (or cogeneration as discussed in Chapter 8); anaerobic digestion of waste; and geothermal heat. Ground source heat pumps are also often considered, in-part, RE systems. Hydroelectric power on the water supply to a building has also been demonstrated. However, of these, the solar technologies, including photovoltaics, daylighting, passive solar heating and cooling, solar water heating and solar ventilation air preheating, are integral to the building — the others may be thought of as energy supplies exterior to the building

itself. A vast preponderance of on-site RE generation projects employ these technologies and they are the topic of this chapter.

We cover the operating principle of each type of solar energy system, list components and provide schematic diagram of how components are assembled into systems; provide information for a cost estimate and life cycle cost calculation, describe how system size may be optimized to minimize life cycle cost, and we stress the importance of operations and maintenance (O&M) over a long performance period. Significant emphasis is placed on integration of solar energy into the conventional building energy system, both within the building and from the perspective of the larger utility system, so that savings may be realized without compromising the reliability of the system. Case studies are presented to exemplify application of each technology.

7.2 Photovoltaics

Photovoltaic (PV) modules convert sunlight into electricity, and other components of a system condition the power to be compatible with the electrical system of a building. PV gets its name from the process of converting light — photons, into electricity — voltage. This process is called the PV effect.

The photovoltaics industry has grown tremendously in recent years, with US cumulative capacity increasing from 18 MW in 2000 to over 36,000 MW consisting of over 1 million systems by the end of 2016. As of January 2016 the U.S. solar industry employed 209,000 workers. Globally, PV installations are going in at a rate of 57,000 MW per year [1]. Photovoltaic technology is the most widely deployed renewable technology on buildings with geographically diverse applicability and a range of options from large ground mounted systems, to building-specific rooftop and facade options.

Figure 7.1 is a map of the solar resource across the globe and Figure 7.2 shows the solar resource across the US. Both maps show the resource on the horizontal orientation, which is a benchmark, and a good indicator of the overall generation potential of different orientations and tracking options commonly considered for photovoltaics. The map shows the resource is highest in the southwestern US, like the desert of southern California and Arizona, and lowest in the northwest, west of the Cascade

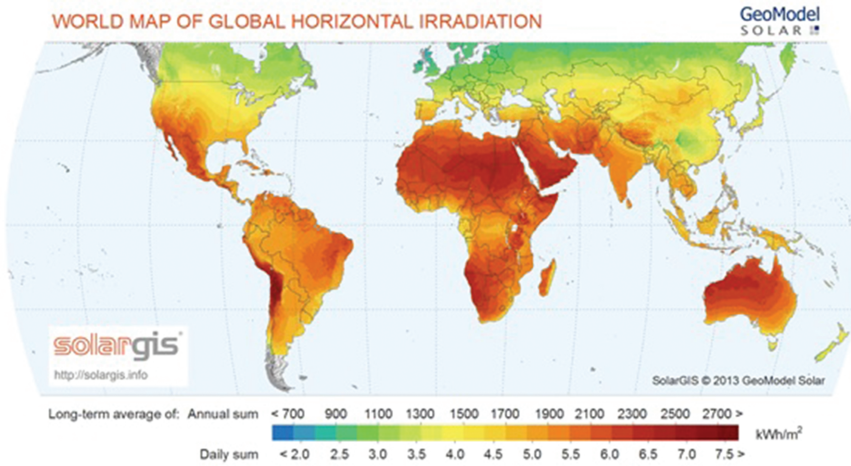

Figure 7.1. Map of solar radiation on the horizontal, a measure of PV generation potential for photovoltaics (SolarGIS © 2015 GeoModel Solar. For more information see http://geomodelsolar.eu/) [2].

mountains, and is almost as low in the northeastern US. The value shown here is in units of kilowatt hours per square meter per day (kWh/m^2/day).

In the US, the average is about 5 kWh/m^2/day, varying from 3.4 in Quillayute, Washington to 6.6 in Daggett CA. Solar energy is available in all parts of the country, but you would need 50% more area than average in the cloudiest places to get the same amount of energy. Alaska is lower.

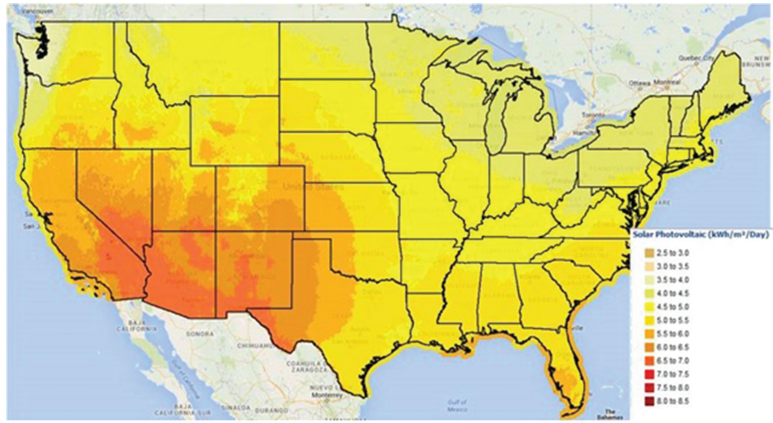

Figure 7.2. Map of solar insolation at orientation of tilt equal to the local latitude, appropriate for fixed-tilt photovoltaics [3].

In summer, there would be a lot of sun in Alaska, but in winter very little. Hawaii is great for PV because there the sun shines at about the same intensity all year long. Since, as we will see, PV modules are rated at an insolation value of 1 kW/m^2, the value in units of kWh/m^2/day may be thought of as hours per day that a system will deliver its rated capacity, or "sun hours".

The solar resource varies throughout the day and the year. Seasonal changes are totally predictable, as is the angle that the sun will be incident on a surface throughout the day, but fluctuations due to clouds within a day are largely unpredictable. The variable and intermittent nature of the solar resource introduces challenges to how PV is integrated into a larger energy system, as we discuss toward the end of this chapter.

PV cells convert sunlight directly into electricity and can be used for very simple applications such as powering watches and cell phones, to off-grid applications such as water pumping, to distributed-generation applications such as net-zero buildings, and on to utility-scale grid connected power generation. An individual PV cell is usually small, typically producing about 3 watts of power. Cells are connected together to form larger units called modules rated at 200 or 300 Watts. Modules, in turn, can be connected is series to form series strings of the desired voltage, and series strings are wired in parallel to form complete arrays for the desired amount of power. In this way, PV systems can be built to meet almost any electric power need, small or large.

The short-circuit operating current of a PV module is not that much greater than its normal operating current (you cannot say that of any other type of generator!). For example a PV module with a short circuit current of 6.5A might have maximum power output at 6.0 A. But as a load (resistance) is imposed on the module, the voltage increases until it approaches the voltage that can be supported by the diode that is central to the operation of the PV module. Figure 7.3 shows the equivalent circuit diagram of a PV cell. The current-voltage relationship for the PV module power output in Equation 1 thus involves William Shockley's 1956 expression for the current passed by a diode. In fact, solar cells were one of the first applications investigated for the diode which went on to be the basis of transistors and computers.

$$i = i_{light} - i_o\left[e^{\frac{q(v+iR_{series})}{kT}} - 1\right] - \frac{v+iR_{series}}{R_{shunt}} \qquad (7.1)$$

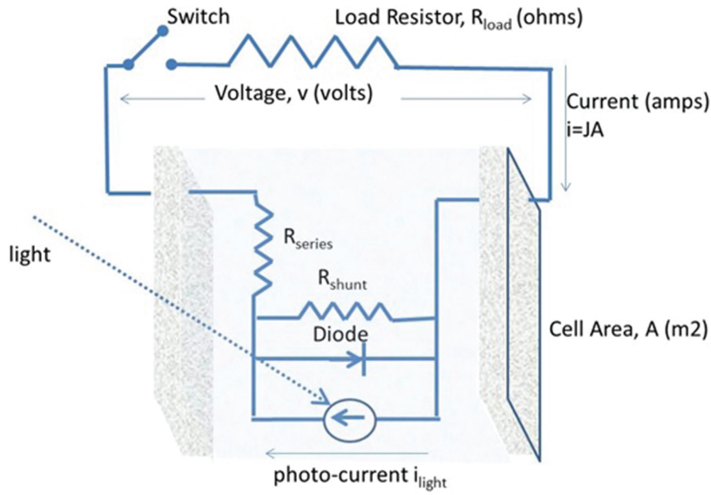

Figure 7.3. Equivalent circuit diagram for a PV cell [4].

Where i is the current output of the cell (amps); i_{light} is the light induced electric current (depends on the photon flux; photons/second over the area of the cell); the second term is Shockley's term for the reverse current through the diode; and the third term is the current back through the shunt resistance of the cell itself, with the series and shunt resistances R_{series} and R_{shunt} as identified in Figure 7.3. As the voltage, v, approaches the open circuit voltage, the diode no longer resists current and the net current output of the cell approaches zero.

A plot of this relation is called the "i-v curve," and is shown in Figure 7.4.

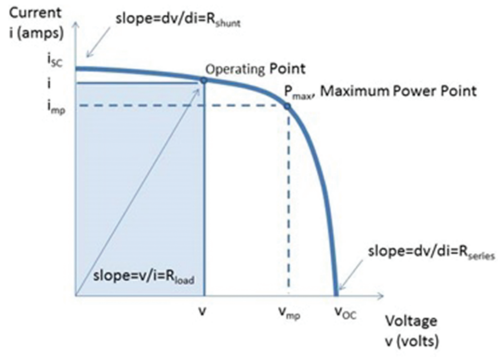

Figure 7.4. Current-voltage relation of photovoltaic cell (i-v curve) [4].

Examination of the i-v curve gives us important information regarding the performance of PV module. Voltage depends primarily on the band gap of the semiconductor material from which the PV cell was fabricated, but voltage goes down with increasing temperature. Voltage increases only very slightly with insolation. Voltage is not a function of cell area, A_c (m^2). Voltage is proportional to load resistance, $v = iR_{load}$. Current increases linearly with insolation (twice as many photons means twice as many electrons). Current increases linearly with cell area, A_c (m^2). Current is inversely proportional to load resistance, $i = v/R_{load}$.

Each PV cell produces about 0.6 V, so cells are wired in series to get to the desired voltage and then series strings are wired in parallel to provide the desired current and power. Modules often consist of almost 100 cells to bring the module voltage up to 60 V, and perhaps 10 of these modules could be connected in series for a voltage of 600V for the string. Six hundred volts is a common voltage in buildings, but increasing voltage reduces current and wire losses, so voltages of 1,000 volts are becoming more common, requiring that all components in a system be rated for the desired voltage.

These series strings are wired together in parallel which increases the current but does not increase the voltage above that of each series string. Thus large arrays of solar modules can be assembled creating a lot of power. The strings of each array would come together into a combiner box, and larger wires from there would run to an inverter which converts the power to alternating current, or AC, compatible with the utility system. Once we convert direct current to AC we can use a transformer to increase the voltage and send it over long distances, but wiring losses are a concern on the lower voltage DC side of the system, so once we get to around 500 kW of PV on one inverter, it makes more sense to start another system, then to add more PV to that inverter. So typically if you hear of a 1 MW system what you probably have is two 500 kW systems next to each other. Large central inverters in utility-scale PV systems can exceed 2 MW, but in buildings applications, and inverter on each PV module (microinverters) or on each string of modules (string inverters) have performance and reliability benefits, albeit at significantly higher cost than central inverters.

There are several types of PV devices. The oldest are the crystal technologies which grow a single cylindrical crystal of silicon and then saw it into round wafers. Multi-crystal are a variation on that which pours the silicon into an ingot and cool it at a rate that maximizes the size of the crystal grains. These crystalline devices are much thicker, and use more material, than thin-film technologies such as Cadmium Telluride. Thin film

devices can be much less expensive to manufacture but they have lower efficiency. Single crystal is currently the most efficient, with companies like SunPower producing modules in excess of 20% efficiency. Thin film silicon is the least expensive but there is not much benefit in reducing cost if the efficiency is low. Perhaps the best ratio of cost and efficiency is realized with the Cadmium Telluride technology, and First Solar has grown to be one of the largest manufacturers by using Cadmium Telluride technology. These technologies all compete in a market where $ per watt of rated capacity is the commodity. But high efficiency single crystal technology will take up less space where roof area is limited, and thin film technologies keep their efficiency better at the higher temperatures of hot climates. In addition to the technology type, the manufacturer and market conditions will impact which PV technology makes the most sense for your building project.

International Electrotechnical Commission (IEC) standard IEC 61853-1 requires that module performance be reported under 5 different sets of conditions. ASTM standard G173-03 solar radiation spectrum and "1.5 air mass," (1.5AM) is the standard atmosphere used in all five test conditions.

1. **Standard Test Conditions (STC):**
   For non-focusing modules for use on Earth, the specified STC insolation is I_c = 1000 W/m^2 and the cell temperature is T_{cell} = 25°C (78°F)
   For focusing collectors, the standard for insolation of direct beam radiation of 850 W/m^2 (IEC, 2006).
2. **Nominal Operating Cell Temperature (NOCT):**
   Insolation I_c = 800 W/m^2; ambient temperature $T_{ambient}$ = 20°C; wind speed = 1 m/s to specify air movement cooling the module.
3. **Low Irradiance Conditions (LIC):**
   Insolation I_c = 200 W/m^2; module temperature T_{cell} = 25°C
4. **High Temperature Conditions (HTC):**
   Insolation I_c = 1000 W/m^2; module temperature T_{cell} = 75°C
5. **Low Temperature Conditions (LTC):**
   Insolation I_c = 500 W/m^2; module temperature T_{cell} = 15°C

The first one, STC, is the commonly adopted definition of power rating in the PV industry. A PV module rated at 220W would typically mean that the module generates 220W under STC conditions; and an entire PV system rated at 2.2 MW would mean that it is comprised of 10,000 of such modules.

Roof racks can hold the PV up in an optimal orientation, but PV also does quite well when mounted flush with the roofline. Racks can penetrate the roof and attach to the structure, but non-penetrating systems are also available which sit on top of the roof and use ballast, or weight, to hold them down. PV modules can last more than 25 years, so avoid installing them on older roofs that may need significant repair or replacement within a 25 year period. If necessary, PV modules can be removed to replace a roof and then be reinstalled. Labor, however, is expensive-about half cost of PV — so this is a critical consideration for the long-term financial feasibility of a project. When installing solar panels on a roof, codes and standards related to fire protection require the installer to leave walkways for access to skylights, roof hatches, rooftop machinery, communications equipment, and other considerations to provide access and meet requirements imposed by a fire marshal. Fire marshals and local building officials may need to approve the layout of a rooftop solar array.

Conduct a thorough engineering study and roof structural analysis — the roof must be able to support the weight, but the design is usually governed by holding them down in the wind rather than holding them up, or by requirements related to seismic loads. Wind load is controlled by mounting panels at a low tilt angle and adding aerodynamic backsheets to the array. In windy areas, the amount of ballast weight required to resist wind loads can exceed the structural capacity of the roof. In such cases attached roof racks are indicated.

While many buildings have open areas on the roof that could be used for photovoltaic modules, some are crowded with HVAC and communications equipment, not structurally suitable, or limited by building codes or other regulations. Also, tracking systems have energy advantages but are very difficult to use on a rooftop because the wind loads are concentrated on the tracking mounts. In any of these cases, ground-mounted PV may be the best installation choice. Common ground-mounted foundation systems include:

- Piles driven into the ground by pile-drivers or vibrating machines. These are the simplest and least expensive, and consequently the most common.
- Screws drilled into the soil. These are simple and cost effective, and make sense in certain soil conditions. The shape of the screw itself will depend on soil conditions and loads.
- Concrete caissons and footers were more common before the pile and screw technologies were developed, and may make sense for certain ground conditions.

- Ballasted systems use heavy ballast weights on top of the ground or roof to hold down the PV modules. They are useful in areas where digging and drilling is a problem because of previous soil contamination, environmental concerns, capped landfills, or cultural concerns such as historic or archaeological sites that may have artifacts beneath the soul surface.

Building integrated PV or BIPV — is an interesting approach where PV can form part of the building itself and could be considered when structures are renovated, or are planned for new construction. PV technologies and materials can be made in an exceptional diversity of forms to fit any building type. Because of this, PV materials can be effectively integrated into building components such as windows and walls, shingles, flat roofs coverings, and standing seam metal roofs, among others. None of the building integrated examples to date have been hugely successful in the marketplace but new designs are deserving of consideration.

Most roof mounted systems keep a fixed orientation, but we can get about 40% more energy per day in the summer if we track the sun from east to west as it moves across the sky. In winter, any surface tilted toward the equator will have a good exposure, so tracking does not help much in winter and annual improvement of tracking compared to fixed tilt is on the order of 25%. Such tracking systems are becoming the norm for ground mounted systems. For ground mounted systems, the slope of the land should be minimal and construction techniques for the slope should be considered early and carefully. Driven piles require flat land to accommodate large hydraulic-driving machinery. PV can be installed on steeper slopes, but may require expensive hand construction and special foundations. PV can be mounted on monopoles to limit surface disturbance. If the land has to be graded, grading considerations include topsoil removal, surface treatment, and erosion control. Grading can have environmental impacts, and may require topsoil restoration. Some projects prefer to put down a groundcover like gravel so that they do not have to manage the vegetation growing up around the array over time.

Depending on the spacing of the photovoltaic modules, it is typical to estimate around 6 acres per MW of rated capacity. The row spacing or array spacing will vary for fixed flat plate modules depending on tilt angle and latitude, and additional space may be required for single or dual axis tracking to avoid shading and provide access.

A schematic diagram of a grid-connected PV system is shown in Figure 7.5. Components that make up a grid-connected PV system include:

- Photovoltaic modules, to convert sunlight into Direct Current electricity;
- Combiner box provides a fuse for each series string and combines small-dimensional wires from each series string to larger conductors which run to the DC disconnect. Recent safety requirements require "rapid shutdown" and arc-fault detection and interruption which can be accomplished by adding these features to the combiner box;
- DC disconnect to disconnect the PV system from the inverter. Notice that this keeps the power from the inverter but the DC side of this disconnect will be energized whenever the sun is shining on the array;
- Inverter to convert direct current to alternating current so that it can be compatible with utility power and used by modern electrical devices AC Disconnects on the AC side of the inverter;
- Transformer to convert the incoming voltage from the inverter to the voltage desired in your electrical system, 480 V three phase power is common for commercial buildings;
- An Electric Panel in the building or new electrical connection through which the Alternating Current can be delivered and distributed to your local power load and onto the grid;

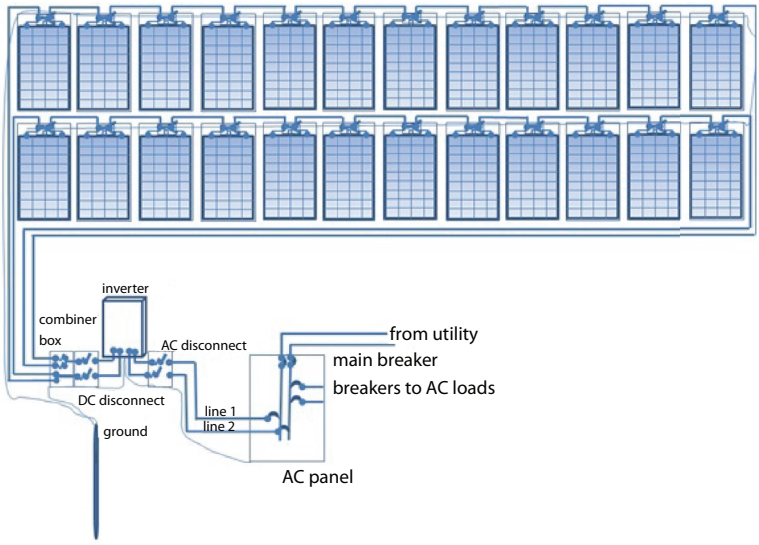

Figure 7.5. Schematic diagram of grid-connected PV system [4].

- Utility Meter to record power flow both to and from the Utility Grid; and
- Other Electrical Components such as wiring and conduit.

Figure 7.5 shows the schematic diagram for a simple grid connected systems with no batteries, but batteries could be added to provide energy when the sun is not shining, and in which case we would need the following additional components: a charge controller to keep the batteries from over-charging low voltage disconnect to keep them from discharging too much. A different type of off-grid inverter would also be required for use with batteries. A "dual mode" inverter could operate in either grid-connected or battery-only mode.

There are several inverter configurations:

- Micro-inverters are inverters on each module.
- String Inverters are inverters on each series string of PV modules.
- Central Inverters combine DC output a PV array into a single location for conversion to alternating current.
- DC Optimizers can optimize the output of each module or string for use with central inverters.

Each of these configurations has advantages and disadvantages. Micro-inverters optimize the power output by each module and can accommodate different levels of shading and different module orientations. Similarly, string inverters accommodate shading of strings and different orientations of strings. Micro-inverters and String-inverters minimize DC wiring and instead use more conventional AC wiring and switchgear to consolidate the solar power output. This has advantages in building applications where building codes, safety considerations, and O&M costs tend to favor the more conventional AC wiring. Requirements for rapid shutdown and arc-fault detection and interruption can be more easily satisfied with micro-inverters and string inverters. Central Inverters are often employed in large systems due to lower per-kW cost and in large ground mounted systems where safety considerations related to occupied buildings do not apply.

Costs change quickly and are hard to keep up to date. Major costs for the installation of a PV system in 2015 include the following [3]:

- PV Module Costs are around $0.69/W in 2015; $0.58/W for Chinese manufacturers, lower for large orders from some manufacturers.
- Cost of the inverter ranges from $0.08/Watt for large central inverter to $0.19/Watt for small residential size.

- Balance of system refers to rack and foundation which are $0.25/Watt; conductor and conduit which are about $0.14/Watt; and switches, disconnects, and other details which add up to $0.17/Watt. Installation labor is estimated at about $0.38/Watt.
- Soft costs such as design and construction management add about $0.15/Watt
- There might be about $0.20/Watt in general overhead and profit.
- Land & Infrastructure: In most cases, there will be no cost for the roof or land area to the building owner but there will likely be competing uses for that space and costs involved in preparing the location for a solar installation.
- Transmission, Distribution, and Interconnection costs occur if it is necessary to build or at least upgrade this infrastructure.
- Compliance: A PV facility may incur significant cost to comply with environmental, utility and cultural permitting regulations.

To design the desired size of a new PV system under predicted conditions, or to compare the actual power output of an existing PV system with what it should be producing under measured conditions, power output of a solar PV system may be calculated as a function of environmental conditions with Equation 7.2:

$$P_{solar} = P_{STC}\{\frac{(\eta_{bos} * degr)}{(1000W/m^2)} I_C(1-\delta((T_{ambient} + \frac{(NOCT-20C)}{(800W/m^2)} I_C)-25C))\} \quad (7.2)$$

P_{solar} = power output of the solar system in kW;

P_{STC} = rated size in kW, nameplate capacity; STC refers to Standard Test Conditions

h_{BOS} = balance of system efficiency; typically = 0.77 to 0.84 (NREL, 2011) [6];

degr = an age degradation factor that is 1.0 initially but degrades at 0.5 % per year. For an average over a 25 year period, a degradation factor of degr = 0.94 provides an estimate of the degradation levelized over the years. I_c = solar insolation in plane of array (W/m^2).

Table 7.1. Initial Cost, Operation and Maintenance Cost, and Lifetime for Different Sizes of PV System Deployment [5].

PV System Size	Mean Installed Cost ($/kW)	Installed Cost Std. Dev. (± $/kW)	Fixed O&M ($/kW-yr)	Fixed O&M Std. Dev. (± $/kW-yr)	Lifetime (yr)	Lifetime Std. Dev. (yr)
PV <10 kW	$3,897	± $889	$17	±$19	33	11
PV 10–100 kW	$3,463	± $947	$15	±$18	33	11
PV 100–1,000 kW	$2,493	± $774	$15	±$15	33	11
PV 1–10 MW	$2,025	± $693	$16	±$9	33	9

The factor δ = temperature coefficient of power (1/C), which is usually on the order of 0.004 1/C for Silicon PV modules and less for other technologies.

$T_{ambient}$ = ambient temperature (C);

NOCT = nominal operating cell temperature, which is a number found in the manufacturer's literature and is often around 47°C.

Conversely, if we know P_{solar} as the amount of power that we need to get from a system, we can use the above equation to calculate how many Watts rated at STC, P_{STC}, would provide that amount of power.

Scheduled PV maintenance requirements are very low and routine compared to other types of electricity generation. Still, it is very important to have an O&M plan in place, to do the preventative maintenance, and to do the monitoring to know when things go wrong and to have a plan to fix them. O&M costs vary from $0 to $40/kW/year with an average of $17/kW/year for small systems and $15 for larger [5]. The primary maintenance in some locations can be periodic inspection and performance test and washing the array. However, soiling is highly dependent on local conditions (bird populations; pollen; agricultural dust; construction dust; diesel soot) and if rainfall is sufficient, washing may not be required at all. Systems should be inspected annually to tighten electrical connections and remove debris, like vegetation, insect nests, dust, and leaves. Other maintenance items include the inspection of combiner boxes with an infrared camera to look for loose connections and cleaning of the air filter if your inverter includes a fan for cooling. Systems with trackers also require routine maintenance to keep moving parts working efficiently. It is possible that using a tracking system can double the maintenance costs. Unscheduled, or corrective maintenance costs may include servicing the inverter and replacing rusted components or other unpredictable costs that may be caused by theft, vandalism, or wildlife damage. You do not need to keep the cash on hand but you need to have a plan on how funds can be obtained to fix failures, such as a line of credit — otherwise your system may sit there for years without producing while you try to find money to make a simple replacement or repair.

Completed in 2008, the grid-connected PV system shown in Figure 7.6 was procured from the GSA Schedule and is rated at P_{STC} = 309 kW with an estimated cost of $2.9 million without incentives. There are 1584 * 195 watt PV modules with a 333kW inverter. Using Equation 1 with

Figure 7.6. Example of PV system: Veterans Administration, Jerry L. Pettis Memorial Medical Center Loma Linda, CA (photo courtesy of Larry Barrett, Veterans Administration).

an average solar resource of 5.5 kWh/m^2/day and a balance of system efficiency of h_{BOS} = 0.77 gives an estimated annual energy delivery of 477,459 kWh/year. In fact the first year of operation the system delivered 497,288 kWh/year, varying from 14,000 kWh in December to 60,000 kWh in May. The hospital was happy with the performance and is currently working on adding PV and constructing solar carports. Annual utility cost savings are estimated at approximately $62,000 per year. The project received a production incentive of $0.37/kWh for the first five years. The estimated payback period with incentives is approximately 17.6 years.

7.3 Daylighting

While often thought of as a lighting energy efficiency measure, daylighting offers perhaps the most direct potential for delivery of solar energy and associated energy savings in commercial buildings. Natural solar light can enhance a building aesthetically and also improve energy efficiency and reduce operating cost. Daylighting also adds to security and maintained use of a space if the power were to go out during daytime hours.

Daylighting is the controlled admission of natural light, both direct sunlight and diffuse skylight, into a building to reduce the need for electric lighting and save energy costs. A daylighting system consists

of apertures to admit daylight, measures to control glare and thermal discomfort, and controls to reduce use of the electric lighting system. Architectural considerations include: building orientation and shape, size and orientation of apertures, window glazing treatment, shading devices, and light redirection devices. Interior design considerations include color selection to balance contrast for ceilings, walls, floors, and office furniture, furniture layout and equipment placement, and occupant orientation relative to apertures. Control solutions involve zoning overhead or other ambient light fixtures for automatic or manual dimming or switching in response to the available daylight. Additionally, control solutions may involve occupant engagement strategies for tuning electric lighting, including task lighting, and shading or redirection devices.

By providing a direct link to the dynamic daily and seasonally changing patterns of outdoor illumination, daylighting helps create a visually stimulating and productive environment for building occupants, while reducing as much as 30 percent of total building energy costs. Daylighting is a viable, energy-efficient strategy in almost any climate, including typically overcast climates such as those found in parts of the Pacific Northwest. Daylighting can work in all building types as well, including office buildings, schools, hospitals, warehouses, and maintenance facilities. The architectural, interior design, and lighting control response to daylighting differs by building type, climate, siting constraints, and many other factors. Like PV, the first step in a daylighting evaluation is to understand the total solar resource at the building's location. This is necessary to get a sense of the potential for daylighting and the need to control solar gains into the space. As part of this first step, it is necessary to understand the type of resource at the site, including:

1. amount of overcast days versus clear and sunny days, and
2. the range of solar azimuth and altitude angles.

An optimized building footprint is a foundational element of a daylit building design. For example, a common daylit building shape starts with an articulated floor plan with a lot of access to the perimeter (rather than a dense core zone). A daylighting building has thinner floor plates, and courtyards or other voids to provide access to light. Frank Lloyd Wright said the floor plate should not exceed 45 ft, but by using reflectors to bounce light deeper into the space, a building at NREL has a 60-foot floor plate. These shapes are very common in historic buildings where daylight was the principal source of light. Light from the sun's relatively horizontal movement across the sky is reasonably simple to control with overhangs

or louvres on the side of the building that faces toward the equator (south side in the US). Diffuse light from the north is a great source of daylight because it does not entail a lot of glare and heat gain. However, the rays of eastern and western sunlight change radically on a daily, hour-by-hour basis and are extremely difficult to control and adapt for daylighting spaces with critical visual tasks. Because optimized daylighting depends on intentional design of the building footprint and orientation, this is usually only possible for new construction projects and additions, and typically does not apply to retrofits. Skylights can convey the soft gray-blue light of the overhead sky into a building but only on the top floor and they may introduce unwanted heat gain and glare in summer when the sun is directly overhead. "Active skylights" have moving reflectors to amplify sunlight into the skylight well. "Tubular daylighting devices," or solar tubes, use reflective coatings that allow sunlight and skylight to efficiently penetrate dropped ceilings and multiple floors of a building. Some of these systems also attempt to reduce the daylight ingress in the summer months to balance daylighting with cooling loads, as would roof monitors and vertical clerestory windows.

Regarding fenestration, the window-to-wall area ratio should be responsive to the climate and optimized for daylighting. Because even the most high-performance glazings do not have insulation ratings close to those of opaque wall constructions, the window area must be a careful balance between admission of daylight and thermal issues such as wintertime heat loss and summertime heat gain. It does not take a lot of window area to meet daylighting goals; the design challenge is to appropriately distribute the windows and limit unwanted heat gain and glare. Good daylighting fenestration practice dictates that an aperture should ideally be composed of two discrete components: a daylight window and a view window. The daylight window should be placed on the wall approximately 7.5 ft (2.3 m) above the finished floor and have a high visible transmittance 50% to 75%; the view window should be placed lower on the wall and have a visible transmittance of less than 40% in most climates.

Regarding window glass, the properties should depend on the application: whether it is a view window, a daylighting window, a skylight, or a window for a passive solar heating system. Key properties are heat transfer coefficient or U-value (W/m^2K) and Solar Heat Gain Coefficient (SHGC), and Visible Light Transmittance (VLT). A high-performance glazing system admits more light (high VLT) and less heat (low SHGC) than a typical window. Ways to reduce solar heat gain include:

1. Tinted glass: bronze, or green and light blue tints (the latter tends to have a higher light-to-solar heat gain ratio keeping a bright appearance in the space)
2. Coated glass, including:
    a. Reflective coating: a thin metallic layer reflects heat and much of the light
    b. Spectrally selective coating: a microscopically thin layer of metal and metal oxide or semiconductor absorbs ultraviolet and infrared radiation but allows visible light to pass through (this is often the same as a low-emissivity coating in glass specification)
3. Dynamic technologies, including:
    a. Electrochomic glass: changes SHGC and VLT with an applied electric voltage
    b. Thermochromic: changes SHGC and VLT with temperature
    c. Photochromic: changes SHGC and VLT with incident light level.

These glazings are typically configured as a double pane insulated glazing unit, with two 0.25 in. (6 mm) thick panes of glass that are separated by a 0.50 in. (12 mm) air gap, although the building I am writing this in has three panes for even less heat loss. A low-emissivity coating, which reduces emissivity (thermal radiant heat transfer), is often part of any high-performance glazing unit, which further lowers (improves) the U-value of the unit.

Solar shading devices are often employed on facades that receive direct sun, particularly on the equator-facing view windows. Shading devices minimize the amount of direct sun that enters the space. Horizontal shading elements are typically called overhangs and vertical elements are typically called fins.

Daylight redirection devices take incoming direct beam sunlight and reflect or refract it, generally onto the ceiling. These devices serve two functions. First they control glare, by redirecting the sunlight away from the eyes of occupants. Second, they cause the sunlight to penetrate deeper into a room, so sunlight is directed into a part of the floor plate that would not be otherwise have daylight. Daylight redirection devices generally take one of three forms and scales: a large horizontal interior element, called lightshelves, louvered systems that have an appearance similar to mini blinds, or films that look similar to diffuse or etched glass when applied to clear glass.

Electric lighting controls that respond to the amount of daylight are absolutely essential to any daylighting system. No daylighting design

will save energy unless the electric lights are dimmed or turned off when there is sufficient illumination from daylight. A typical control solution includes light level sensors (photocells) mounted on the ceiling to measure light reflected back up by a work surface. These sensors might send a low-voltage control signal to a relay for multi-level switching or to a dimmable ballast for continuous dimming. Switching controls are on-and-off controls that simply turn the electric lights off when there is ample daylight and turn them on when there is not. Multi-level switching controls determine the settings of individual lamps within a light fixture (luminaire) to provide intermediate levels of electric lighting. In multi-level switching, a fixture with three lamps could have 0, 1, 2 or 3 lamps on for four different lighting levels. Dimmable ballast typically reduce electric light output in a continuous fade to somewhere between 1% and 10% of the maximum power depending on the technology, and then turn off below that. The solutions discussed automatically adjust electric lighting by modulating the power input to lamps to complement the illumination provided by daylight.

In addition to completely automatic daylighting controls, a manual-on control element can be useful for increasing occupant comfort and energy savings by allowing occupants to take advantage of low daylighting levels in a space when they are working on a computer or performing non-critical tasks. In this approach, the occupant must choose to turn on the lights or increase the dim level after the electric lighting has been automatically reduced. Additional electric lighting control strategies should be incorporated where they are cost effective. These include:

- Occupancy controls that use infrared, ultrasonic, or microwave sensor technology to detect movement or object surface temperature and automatically turn off or dim luminaires when rooms are left unoccupied. Typical savings have been reported to be in the 10% to 50% range depending on the application.
- Timers are simple devices that turn lighting off or on at a set schedule. If spaces are known to be unoccupied during certain periods of time, timers are extremely cost-effective devices.

Even with good design, daylighting will not be uniform over time and throughout a space. Task lighting is provided to allow individual occupants to create lighted spaces to suit their specific needs while performing a specific task. For example, providing individual desk lamps at occupant workstations allow the occupants to control lighting levels in their own work areas.

A daylight-optimized environment complements and provides balanced daylight distribution and electric lighting. Interior design considerations include the arrangement of low-walled private interior offices, workstations pulled away from the perimeter wall to prevent glare, appropriate shading of the vision glass to maintain views for all occupants (exterior overhangs without interior shades is common), specification of furniture, selection of light color schemes to enhance daylight, and specification of electric lighting fixtures. Colors of walls and floors are selected to enhance daylight distribution onto walls and the ceiling to increase visual comfort and detection of objects in the general space. Room surfaces are generally finished with light colors–darker colors on poles, thresholds, and stair treads provide contrast that can increase visual comfort and safety. This integrated approach to rending the space with daylight and electric light allows for occupant comfort with lower ambient illuminance–task lighting then brings the additional lighting to work surfaces as needed by different occupants at different times of day.

With the exception of noisy or group work areas, the typical office cubicle partition heights will generally be low so that distribution of daylight is not blocked. This is especially true for those spaces running parallel to the south façade or along exterior walls. Enclosed office counts are kept to a minimum. The selection and design of open office furniture, especially workstation panels, requires a continued commitment to the preservation of daylight and views. Workstation panels must be kept low (42″ or less) and parallel to the direction of the daylight distribution to ensure the penetration of light and maintenance of views. Where higher panels (48″ or greater) are required for privacy or to create a sense of enclosure, they should be oriented perpendicular to the perimeter glazing. Sixty-five inch tall panels that are perpendicular to the direction of daylight distribution can enable privacy and allow for ample storage without compromising views or creating dark shadows.

Furniture design and placement also affects daylight. By positioning work surfaces at a distance from the south façade, solar control is easier with smaller overhangs or louvers than if a desk or office is placed directly against the south façade.

Workstations should be designed whenever possible so that the direction most occupants face while performing visual tasks (i.e., looking at a computer) is not directed toward daylight openings. This positioning helps avoid the visual discomfort occupants experience when looking into shadows, or worse, from the excessive contrast that occurs when a visual task

area is immediately surrounded by the brightness of a view to the exterior. The reflection of a window should not be visible in your computer screen.

The position and visual character of the "back" wall, the wall opposite a perimeter window, can serve a crucial role in receiving and reflecting daylighting that travels horizontally into the space. If this wall receives sufficient daylight, and is of a relatively high reflectance value, it will serve to balance the brightness of the view through the perimeter windows. Walls and ceilings should be as highly reflective as possible. This bounces and distributes the redirected daylight more fully and uniformly. In general, light finishes and interior colors support daylighting.

Many elements of an optimized daylighting system are exemplified by NREL's Research Support Facility open office design. The following section identifies relevant features of the architectural, interior, and electric lighting design.

We do not report here the cost of a daylighting system because it is not possible to separate it from the architectural elements of a building. Premium windows and shading elements do add cost, and dimmable ballasts are about $60 each compared to $20 for a non-dimming ballast, but daylighting has the potential to provide significant cost savings. Additionally, electric lighting accounts for 35% to 50% of the total electrical energy consumption in commercial buildings. By generating waste heat, lighting also adds to the loads imposed on a building's mechanical cooling equipment. The energy savings from reduced electric lighting through the use of daylighting strategies can directly reduce building cooling energy use by an additional 10% to 20%. Consequently, for many institutional and commercial buildings, total energy costs can be reduced by as much as one-third through the optimal integration of daylighting strategies.

As part of any routine building cleaning regimen, any windows and daylight redirection devices should be cleaned on a regular basis to ensure the optimal performance of the transmitting and reflecting surfaces. For commercial office spaces, most manufacturers of redirection devices recommend an annual cleaning cycle, with more frequent cleanings required for dirtier environments. Maintenance also should ensure that areas designed to admit daylight are not shaded by growth of landscaping or other obstructions. Initial landscape design should account for daylighting needs as landscape matures. However, if maturing landscape interferes with daylight levels, significant pruning or replanting may be needed to ensure that daylight levels are maintained as designed.

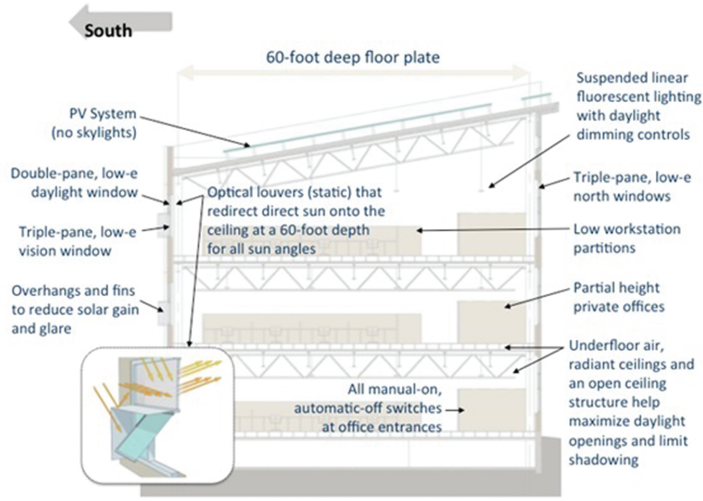

Figure 7.7. An example of the daylighting system an NREL Research Support Facility including apertures; louvers and overhangs for directing light; controls on artificial light (figure by RNL courtesy of NREL).

Tools to predict and evaluate annual daylighting distribution are advancing rapidly and include Radiance (accessed independently or as part of the OpenStudio platform); DAYSIM; IES-VE; 3Ds Max; and AGi32. Future tool enhancements will allow for improved prediction and understanding of occupant response to glare potential and nuances of integration between the architectural, interior design, electric lighting and control systems for optimized daylighting design. Simulation tools are further integrating daylighting and electric lighting with whole-building energy simulation. This integrated approach also allows for multiple-purpose daylighting solutions, including building-integrated PV systems. Tools such as IES-VE [http://www.iesve.com/] and OpenStudio [https://www.openstudio.net/] are tools with this capability.

The daylighting design landscape of evaluation tools, technologies, and approaches is evolving. Some new and innovative solutions include:

- Behavior-based control solutions that allow occupants to “opt-in” to use electric lighting or shading devices but set the system back to optimal energy efficiency settings at various points throughout a day
- Small-scale redirection devices such as prismatic films for daylighting windows
- Dynamic glazing such as electrochromic glass

- Light emitting diode (LED) fixtures with high-resolution sensor distribution and wireless controls for improved responsiveness to daylight contribution, especially in retrofit scenarios
- High-resolution energy use metering with automatic, initial and ongoing commissioning of daylight responsive electric lighting systems to ensure the expected performance is achieved.

7.4 Passive Solar Heating and Cooling Load Avoidance

Passive solar heating was widely used long ago, and probably well understood before the availability of central heating systems with continuous fuel delivery and automatic thermostats. But the passive solar approaches described here rely on modem advances in the performance of windows, insulation and storage systems. A building might not benefit from passive solar heat if it has a lot of internal heat sources such as lights and computers or is in a warm climate-but all buildings are exposed to the sun so understanding solar heat gain can also save energy by avoiding solar heat.

Passive Solar Heating is an architectural solution so it begins with programming the spaces within a building and layout on the site. An orientation with the long axis parallel to the equator is considered ideal. In the winter, the sun is low in the southern sky (in the northern hemisphere), and the extended south wall of the building is exposed to solar heat. But in the summer the path of the sun is more overhead and from east to west, so solar heat gain in summer is reduced by minimizing the east and west facades and having few windows on that side. The daylighting discussion above praised north facing windows for quality daylight, but the sun hits north windows rarely and at an oblique angle. The color of external surfaces can be selected to either absorb (dark) or reflect (light colors) solar heat. A building with the long axis stretched out from east to west is said to have a "high aspect ratio." An articulated floorplan can add solar heat gain to multiple wings, courtyards or atria, and the width of the floorplate rarely exceeds 20 m (60 ft) in passive solar buildings.

The heat loss coefficient (UA) Watts/m^2/C; is the heat loss per unit area of surface area to the ambient and per degree of temperature elevation above ambient temperature. The area A in the heat loss coefficient is the effective surface area of the room. The temperature difference driving the heat flow is the difference between the room temperature T_{room} and the ambient temperature, $T_{ambient}$. The overall (UA) of the room is determined

by adding up the heat loss from all the wall elements of the room and including a term for the infiltration of ambient air into the structure.

$$(UA) = \Sigma U_i A_i + M_{infiltration}\, c_p \tag{7.3}$$

where U_i is the thermal heat loss coefficient of each building element (roof, wall, floor, window, door, etc) in $W/m^2/C$ and A_i is the surface area of that element in m^2. The U-value of an element may be calculated from its thermal conductivity and its thickness. The mass flow rate of the infiltration air is $m_{infiltration}$.

Over the course of a day, the heating energy required is

$$E_{heat,day} = \int_{day} [(UA)(T_{room} - T_{ambient}) - P_{internal}]dt \tag{7.4}$$

where $P_{internal}$ is the "internal heat gain" from busy people and computers and lights within the space.

The solar heat gain through a window is proportional to the "Solar Heat Gain Coefficient" (SHGC) which is the fraction of the incident solar heat getting through the window to the inside of the room including both direct beams of sunlight coming through and sunlight absorbed in the glass that eventually makes it into the room. This is a property of the glazing assembly which is stamped on the label of every window, and is often on the order of 0.7. The energy coming through The energy coming through a window over the course of day would be

$$E_{solar,day} = \int_{day} A_c K I_c SHGC \; dt = A_c K I_{c,day} SHGC \tag{7.5}$$

Where $I_{c,day}$ equals the total solar insolation incident on the window over the day, usually on the order of 3 $kWh/m^2/day$ for a south-facing vertical window in the wintertime. K is the incident angle modifier accounting for increased reflection at high incident angles. Ac is the area of the window (m^2).

A window overhang is described by two dimensions; the "projection" distance that the overhang edge sticks out from the plane of the window and the vertical "offset" height from the top of the window to the edge of the overhang. There is no one overhang dimension that is perfect for all seasons. The sun is in the same position on both the spring and fall equinoxes, but in spring it is cold and we need heat and in fall it is hot and we do not. However, it is possible to design a single overhang which provides complete shade at noon on the summer solstice and complete

sun on the winter solstice which seems like a good design criteria. For example, the overhang over a 2 m (6.6 ft) tall window at a latitude of 41.2 degrees would have a vertical offset between overhang edge and top of window of 0.4 m (1.2 ft) and a horizontal projection from the plane of window to edge of overhang of 0.75 m (2.5 ft).

Thermal storage is needed to store the solar heat for use at night. "Sensible" storage media, such as concrete, brick, rock, or any mass, store heat associated with an increase in temperature. Phase change materials (PCMs) have been fabricated into shapes that can be added to building walls, floors, and ceilings. PCM's store heat through a change of phase rather than a sensible temperature increase. So if the transition temperature of the material is within the comfort range of the space, they keep the temperature very constant. The change of phase also stores a large amount of heat so less mass is required. The amount of heat stored as a storage media increases in temperature by an amount $\Delta T_{storage}$ is

$$Q_{stored} = M_{storage} \left[C_{p,storage} \, \Delta T_{storage} + \lambda_{storage} \right] \tag{7.6}$$

where $M_{storage}$ is the mass of the storage medium (kg or lbm), $C_{p,storage}$ is the specific heat (kJ/kg/K or Btu/lb/F), and where $\lambda_{storage}$ is the "latent heat" of the phase change material the amount of heat in J/kg or Btu/lb that is absorbed or released as the material changes from one phase to another, if its phase transition temperature is within the range of temperature increase.

The term "direct gain" means that sunlight is admitted directly into the living space. Direct gain designs are often implemented with standard construction of windows and massive floor slabs. Carefully implemented direct solar gain may contribute to daylighting objectives and allows views of the outdoors. Direct sunlight in the space causes some problems too: it can cause visual glare and thermal discomfort due to overheating or radiant asymmetry.

The temperature of a "sunspace" is allowed to get too hot during the day and too cold at night, but by doing so it makes a positive contribution to the heating load of the building that it is attached to. Significant mass in the wall between the sunspace and the room to be heated provides thermal storage and a transfer of heat from the sunspace in the daytime to the room at night. A thermal storage wall, or "Trombe Wall," is like a sunspace without the space. The massive concrete or masonry wall is built directly behind the glass of the window. A high surface temperature is required on the surface of the Trombe wall to drive the heat into the

mass by conduction. Diagrams and examples of each of these three passive solar heating strategies are illustrated in Figure 7.8.

The sizes of a the major components (window area, mass) of a passive solar system are best determined by optimizing life-cycle cost, and satisfying other constraints, using a computer program that takes into account the climate and details of the design. However, we must estimate at least a preliminary size before a design is created, and this may be accomplished by simple hand calculation. If our objective is to offset all of the heating requirements (SF = 1), then the collector area may be sized such that the average daily solar resource be equal to the average heating load.

$$E_{solar,day} = E_{heat,day} \tag{7.7}$$

The month with the greatest Heating Degree Days, $HDD_{day,max}$ (the coldest month, usually January or December in the northern hemisphere and June or July in the southern hemisphere) is chosen to make this balance. HDD_{month} has units of Cdays/month or Fdays/month. The daily solar resource coincident with this maximum heating load is $I_{c,min,day}$. The solar energy incident on the plane of the collector aperture (usually vertical window facing toward the equator) corresponding to the same month as the HDD is maximum. Then the required solar collector area window area, Ac, is calculated as in Equation 7.8.

$$A_c = \frac{\left[(UA) * \left(HDD_{month,max} \right) / \left(\frac{31 days}{month} \right) - P_{internal} * 24 hour/day \right])}{KI_{c,min,day} SHGC} s \tag{7.8}$$

We have adopted previously the convention that full sun is at a value of 1 kW/m^2, allowing us to calculate a "sunhours" per day by dividing $E_{solar,day}$ by 1 kW/m^2. We would like for the temperature in the space to be uniform, but if we can tolerate a $\Delta T_{storage}$, of, say 4°C (8°F) we can determine the amount of mass that would be required to store the daily solar resource.

$$M_{storage} = \frac{A_c KI_{c,min,day} SHGC \ - [UA(T_{room} - T_{ambient}) - P_{internal}] * sunhours}{C_{p,storage} \Delta T_{storage}} \tag{7.9}$$

Equations for passive solar heating analysis can be evaluated hourly by a computer program, but in this simple hand calculation we perform the comparison for an average day of each month. In any month, the amount of energy saved by the passive solar heating system directly during the day would be the minimum of the available solar energy and the require amount of heating

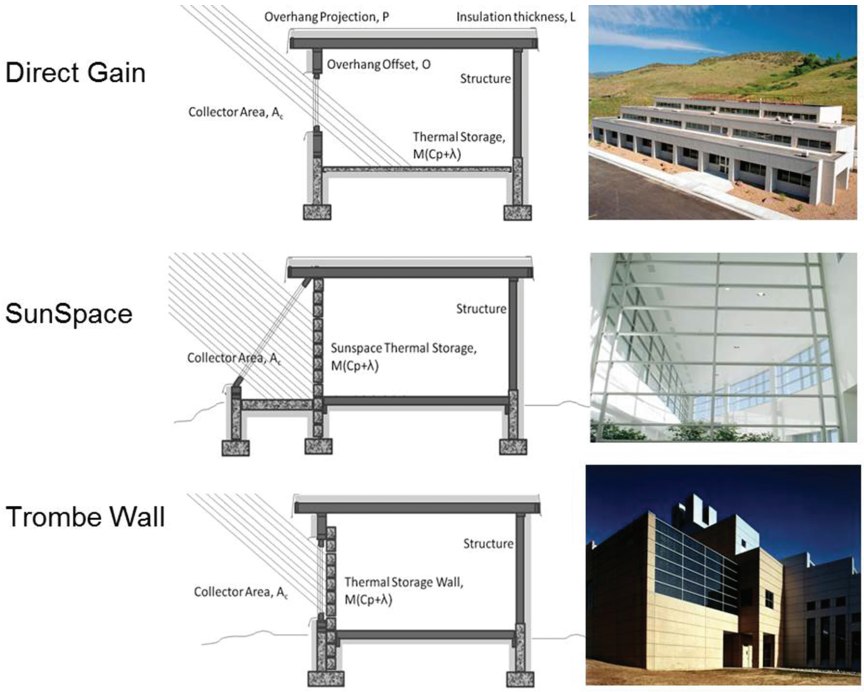

Figure 7.8. Three types of passive solar heating systems are: Direct gain; sunspace; and trombe wall (thermal storage wall) [4].

$$E_{saved\ daytime} = sunhours * MIN[(A_c K\ SHGC * \left(\frac{1kW}{m^2}\right), \\ UA(T_{room} - T_{ambient}) - P_{internal}] \tag{7.10}$$

Energy put into storage on an average day would be the minimum of solar energy available in excess of the daytime load and the limit imposed by a maximum temperature excursion, $\Delta T_{storage}$ of the mass within the space.

$$E_{into\ storage} = sunhours \\ *MIN\left[\left(A_c K\ SHGC * \left(\frac{1kW}{m2}\right) - UA(T_{room} - T_{ambient}) - P_{internal}\right), \\ (M_{storage} C_{storage} \Delta T_{storage} + \lambda_{storage})\right] \tag{7.11}$$

The solar energy delivered from storage to the heating requirement at night is the minimum of heat saved in storage and the nighttime load.

$$E_{saved\ nighttime} = MIN[(E_{into\ storage}), (UA(T_{room} - T_{ambient}) - P_{internal}) (24 - sunhours)] \quad (7.12)$$

The amount of solar heat ultimately delivered to offset the heating requirement of the space is calculated in Equation 7.13 as the sum of that delivered during the day and through storage at night. The amount of fuel saved would be this solar delivery divided by the efficiency of the heating system.

$$E_{FuelSavings} = \frac{(E_{saved\ daytime} + E_{saved\ nighttime})}{\eta_{heater}} \quad (7.13)$$

Where $E_{fuelSavings}$ is annual fuel energy savings (kWh/yr) and h_{heater} is the thermal efficiency of the fuel-fired or electric conventional heater. This calculation would be repeated for the 12 months of the year and the results summed to estimate annual energy savings

Computer Tools for analysis of Passive Solar Systems are "Whole Building" models that simulate the details of passive solar heat gain and heat loss from the building as well as details of the heating system and controls. The EnergyPlus program is one example of such a program [http://apps1.eere.energy.gov/buildings/energyplus/].

7.5 Solar Ventilation Air Preheating

Solar ventilation air preheating has the lowest cost and highest efficiency compared to other solar technologies such as photovoltaics or solar water heating, but it is only used for one thing, which is preheating ventilation air. It is also used for crop-drying in California and Latin America. It can be used to preheat air for conventional boilers in thermal and power plants, but not for gas-turbines since to do so would increase compressor work.

Maintenance requirements are minimal due to the simplicity of the technology. The technology has no moving parts other than the ventilation fan, so it lasts for decades.

Energy savings utilizing solar vent preheating technology varies based on both the solar energy available and the need for heat in each

location. The map of Figure 7.9 shows the maximum energy delivery from a solar ventilation air preheat system, and showing the greatest savings can be realized in locations where you can use the solar heat for most days. Rather than in warm, sunny climates, this technology is most cost effective where heating load dominates: along the Canadian border, and in the Rocky and Sierra mountains in the west, and also in the far Northeast. These locations have the best combination of available sun and high heating requirements for buildings. In fact, the only places that preheating ventilation air is not helpful are Florida, South Texas and other locations along the Gulf Coast, and Southern California. Even in warm climates the technology can be used to heat ambient air for crop drying or other industrial operations.

Solar ventilation air preheating is often cost effective in new construction and major renovations that include larger exterior walls on the south side of a building and where large amounts of ventilation air are needed. The best applications for solar ventilation preheat technology are larger industrial buildings that require a steady supply of ventilation air, such as vehicle maintenance facilities, aircraft hangers, and similar

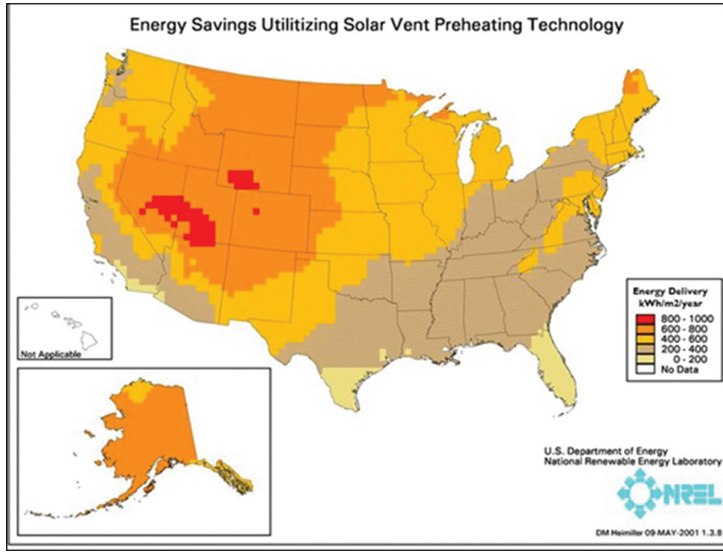

Figure 7.9. Map of potential energy delivery from solar ventilation preheat system in the US considering both solar resource and heating requirements (figure by Donna Heimiller, NREL).

facilities. These industrial buildings require a great amount of ventilation air, the building envelope matches well with the aesthetic of metal siding, and there are few windows or other types of fenestration required. However, the technology has also been used in applications where aesthetics are at a premium, including at visitor centers, office buildings, and apartment buildings.

A transpired solar collector is constructed of a perforated metal sheet, typically four feet wide and in any length. The collector is perforated with tiny holes and painted a dark color to absorb maximum solar radiation. The holes are about 1 mm in diameter and less than 1 cm apart — the ratio of open hole area to the total plate area is called the porosity. The operating principle of a transpired solar collector is based on a concept called the "boundary layer." Regardless of any amount of wind, the air in contact with the collector plate is not moving, because the wall is not moving. But within a layer of air about 1 millimeter thick, or about the thickness of a coin, the velocity increases to the exterior wind speed. Similarly, within this thin boundary layer, the temperature increases from the temperature of the plate to the temperature of the surrounding air. The principle of the transpired solar collector is such that the thin boundary layer of solar heated air enters in through small holes before it has a chance to mix with surrounding air.

In this thin boundary layer of air, the boundary layer results in an efficient transfer of heat from the collector plate to the air. The holes in the collector plate are close enough together to draw in this boundary layer of solar heated air before it has a chance to escape by convection. Big holes far apart will not work; they need to be tiny holes close together.

If the flow through the wall drops to less than 0.02 m^3/second per m^2 of collector, or 2 ft^3 per minute of air per square foot (CFM/ ft^2) of collector, then this heat has a chance to drift away and the collector efficiency drops dramatically. Or, if the flow rate is greater than 0.08 $m^3/m^2/s$ or 8 CFM/ft^2, then the fan power required to draw the air through the tiny holes can be excessive. Depending on the size and spacing of the holes in the collector, a flow rate of 0.04 $m^3/m^2/s$ 4 CFM/ft^2 may represent the optimum configuration.

The key is to specify porosity and/or a size of the collector that will maintain a 25 Pascal (Pa) pressure drop at the required flow rate. A pressure drop more than 25 Pa helps make the flow uniform through the holes across the face of the wall.

As illustrated in Figure 7.10, a solar ventilation air preheating system is comprised primarily of the following six components:

1. Transpired solar collector
2. Mounting brackets
3. Perimeter flashing
4. Ventilation fan
5. Ducts and ductwork, and
6. Actuated bypass dampers.

In the wintertime, or when the space is calling for heat, the bypass damper is closed and ventilation air is drawn in through the tiny holes of the transpired solar collector. The temperature might increase as much as 8 to 16°C, or 15 to 30°F on a sunny day. So instead of coming in at 0°F the air is coming in at 30°F, and that saves a lot on the fuel required to heat the ventilation air.

Then, in the summertime, or whenever the room is not calling for heat, the bypass damper opens and fresh ventilation air is brought in without passing through the solar collector.

If you have a building that is already heated by people, lights and computers on the inside, the solar heat might not be welcome and you could benefit from free cooling in winter. The applicability of this technology is reduced in buildings that have a lot of internal heat gain.

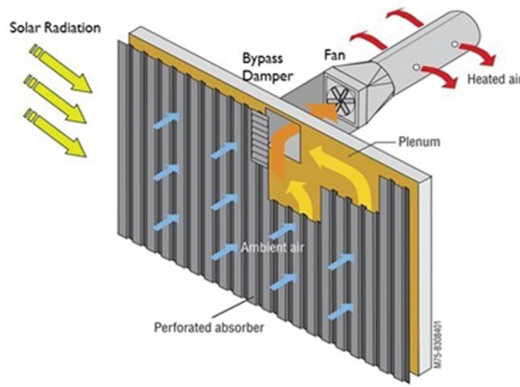

Figure 7.10. Schematic diagram of solar ventilation air preheat system.

The transpired collector is secured to the south-facing wall by mounting brackets that stand the transpired collector away from the wall to create a space to pass the pre-heated ventilation air. This space is referred to as a plenum. Proper installation of flashing is required around the perimeter of the transpired collector to keep air from going around it and bypassing the tiny holes.

The ventilation air is drawn through the holes in the collector and into the plenum by the action of a ventilation fan, which typically already exists in a building. The air is heated as it is drawn through the tiny holes and into the plenum and then it is drawn into the building.

If working with an air-handling unit, modifications can be made to introduce the preheated ventilation air into the mixing box which is the first stage of the air-handling unit. This stage would combine solar preheated air, outside air, and return air. Both the solar preheated air supply and the outside air supply would be fitted with actuated dampers. Often an air-handling unit recirculates some of the room air and mixes it with fresh air, and in this case it is the "mixed air temperature" that controls whether the bypass damper is open or closed. If the return air is hot enough to keep the mixed air temperature above the set point, then the solar damper would be closed and the outside air damper would be open.

If an air-handling unit is not involved, ductwork can be used to distribute hot air from the solar ventilation preheating system directly into a space, and then additional heat is added to the space by unit heaters or other means. Air can be introduced to the space with a stub duct, but often a fabric duct is used to deliver the air deeper into the space. A thermostatically controlled bypass damper would open when the space is not calling for heat to admit air without preheating.

The NREL Chemical Storage Facility, shown in Figure 7.11, was one of the first buildings to install the solar ventilation air preheat technology and was carefully monitored. The facility is a 1,300 square foot chemical waste storage

Table 7.2. Initial Cost, Operation and Maintenance Cost, and Lifetime of Solar Ventilation Preheat System [5].

Mean Installed Cost ($/ft^2)	Installed Cost Range (± $/ft^2)	Lifetime (yr)	Fuel and/or Water Cost ($/year)
$31	$15	25	1 W/ft^2 fan power

Figure 7.11. Photograph of transpired solar collector and bypass damper of solar ventilation air preheat system on NREL chemical storage building (photo by the author).

building that requires a ventilation rate of 3000 ft^3 per meter to maintain safe indoor conditions. Open flames are prohibited in this chemical storage building due to the danger of combustion; ventilation air is heated with electricity instead of gas. The Chemical Storage Facility has a large, south-facing wall area with only one penetration. Finally, the addition of the Transpired solar collector was an acceptable architectural change to the building.

The 300 square foot transpired collector saves about 14,310 kilowatt-hours annually, 25.7 percent of the energy required to heat the facility's ventilation air. In addition, the system annually avoids 14.9 tons of carbon dioxide and 52 pounds of nitrogen oxide emissions. With an installation cost of $20 per square foot and a utility cost of 5.4 cents per kilowatt hours, NREL saves 726 dollars a year in electric bills. This investment results in an 8.3-year simple payback.

Over the 25-year study period, the life-cycle savings are expected to equal 356,000-kilowatt-hours. Over its life cycle, the system will provide energy to the site at an equivalent energy rate of 2 cent per kilowatt-hours of heat. NREL's unglazed transpired solar collector has been in continuous operation for 15 years. Initial detailed measurements indicated that the average system efficiency was 63 percent. The collector was installed in front of an existing concrete wall. In general, each square foot of transpired collector will raise the temperature of 4 CFM of air by as much as 30°F, delivering approximately 240,000 British thermal

units (Btu) annually per square foot of installed collector. Typical annual efficiency for these systems is between 60 percent and 65 percent.

7.6 Solar Water Heating

There are a variety of different types of solar water heating systems, but the basic technology is a straightforward extension of a building's plumbing system. Solar collectors absorb heat from the sun and transfer that heat to water. A thermal storage tank stores water for use as needed. A conventional heating system provides backup if storage drops below the desired temperatures.

A typical solar system will reduce the need for conventional fuel for water heating by about two-thirds or three quarters. It is not cost effective to meet 100 percent of the water heating load on every day of the year; rather the optimal is to meet the load on an average sunny day, and use conventional fuel to top off the need for heat. But there have been many installations where solar is the only source of heat in developing countries or applications where reliable heat is not a requirement.

Solar hot water heating collector technologies vary based on temperature requirements. As shown in Figure 7.12, there are four basic types of solar water heating collectors: unglazed systems, glazed flat panels, evacuated tubes, and parabolic troughs. Collectors are installed in systems and also include thermal storage, pumps, controls, and features such as

Figure 7.12. Different types of solar water heating collectors.

pressure relief valves, temperature tempering valves, flush-and-fill valves, and any other required components. The controls turn any pump on and off in response to collector temperature. A back-up, conventional heater is still needed to meet 100 percent of the peak hot water demand generally, especially for cloudy days or for when the solar system is down for service.

7.6.1 Low Temperature Unglazed Collector

This type of collector is mainly used to heat swimming pools and consists of black colored matting or tubes made from plastic-based materials through which the pool water circulates. These panels can heat large volumes of water by a small temperature rise, perfect for swimming pools, during warm sunny conditions. Because this type of collector is not insulated, it cannot operate efficiently in cooler conditions or when hotter water is required. These collectors are often referred to as "unglazed" because they do not have a glass cover like flat plate or evacuated tube collectors. At low temperatures a glass cover can be counter-productive because it absorbs and reflects some solar heat.

7.6.2 Glazed Flat Plate Collectors

Flat-plate collectors consist of an insulated, weather-tight housing or box, a clear glass or plastic cover glazing, a black absorber plate, and a system of passages for the heat transfer fluid to pass through the collector. Special coatings called "selective surface" on the absorber maximize absorption of sunlight and minimize re-radiation of heat and are more durable than ordinary black paint. Gaskets and seals at the connections between the piping and the collector box and around the glazing insure a watertight system. With a cover glass and insulation, glazed flat plate collectors are able to provide heat at higher temperatures than unglazed collectors. Absorber plates are often made of metal — usually copper-because it is a good heat conductor. Copper is expensive, but is a better conductor and is less prone to corrosion than other materials.

The design is simply an insulated box with a absorber sheet welded to copper pipe through which the heat transfer liquid circulates through. While the basic design concept is fairly consistent amongst manufacturers, there are differences in aspects of the design that can improve performance, make the panels lighter, easier to install and suitable for different installation

formats, and ultimately impact the cost, efficiency and longevity. Flat plate collectors perform well in warm climates and when achieving temperature for basic domestic hot water use (<60°C/140°F). The fact that there is no insulation above the absorber is an inherent disadvantage of the design and leads to high heat loss. This heat loss means flat plates are unable to deliver hot efficiently at higher temperatures (>70°C/160°F), and performance is greatly reduced in cold weather.

7.6.3 Evacuated Tube Collectors

Evacuated tubes are comprised of an array of single or twin wall glass tubes with a vacuum that provides excellent insulation against heat loss. Radiation from the sun can pass through the vacuum but there is no air to convect or conduct heat out so heat loss is minimized. The design is very similar to a vacuum thermos bottle. Single wall evacuated tubes normally have a fin that contains the absorber coating, similar to that used in the flat plate collector.

Twin wall evacuated tubes have the absorber coating on the inner tube and the space between the two tubes is "evacuated" to form the vacuum. Evacuated-tube collectors are typically more efficient at higher temperatures than flat-plate collectors. In an evacuated-tube collector, sunlight enters through the outer glass tube and strikes the absorber, where the energy is converted to heat. The heat is transferred to the liquid flowing through the absorber, or to a heat pipe which transfers heat to fluid flowing through a header. A collector consists of rows of parallel evacuated tube assemblies. The absorber typically is of fin-tube design, with the fin treated with a selective surface, although cylindrical absorbers also are used. Most evacuated-tube collectors are modular — a single tube can fail without affecting the other tubes in a collector.

Due to the superior insulation, evacuated tube collectors are more efficient than flat-plate collectors under conditions of low solar radiation or low ambient temperature. This makes these collectors particularly useful in areas with cold, cloudy winters. While evacuated-tube collectors achieve higher temperatures than flat-plate collectors, they are also more expensive. Evacuated-tube collectors are competitive with flat plate collectors for most commercial and industrial applications, with the higher cost often offset by the higher performance.

7.6.4 Parabolic Trough Collectors

Parabolic-trough collectors use curved mirrors to focus sunlight on an evacuated tube receiver that run along the reflector's focal line. A mixture of pressurized water or perhaps other fluids that transfer heat is pumped through the tube. The fluids absorb solar heat and reach temperatures up to 570 degrees Fahrenheit. The hot water is sent to a thermal storage tank, or is used to create steam, which is directed through a turbine to generate electricity.

Parabolic-trough collectors use only direct radiation, and even though they use mechanical tracking systems to keep them facing the sun, they are most effective where there are very clear skies, such as the southwestern United States. If the sun hits the mirror at a random angle it is reflected at a random angle, so diffuse radiation is not collected.

Parabolic-trough collectors provide heat for industrial processes, commercial buildings, and electricity generation for utilities. Parabolic-trough collectors are more efficient for large facilities that require large quantities of hot water. They also require large areas for installation, yet they offset the need for conventional energy and provide energy savings and environmental benefits.

The Solar Rating & Certification Corporation, or SRCC is an independent third-party that tests and certifies solar energy equipment. The OG-100 collector certification program applies to the solar collector, and the OG-300 rating provides a certification for complete systems and determines whether systems meet minimum standards for system durability, reliability, safety and operation. Factors affecting total system design, installation, maintenance and service are also evaluated.

The SRCC solar collector thermal performance test is based on the American Society of Heating, Refrigerating, and Air Conditioning Engineers (ASHRAE) Standard 96-1980 and 93-1986 related to Methods of Testing to Determine the Thermal Performance of Solar Collectors, for glazed flat-plate liquid collectors, air collectors, linear tracking concentrators, and other collector devices which fall within the scope of the test standard. Based on the thermal performance data derived from the ASHRAE test methods, SRCC then calculates the collector rating.

SRCC measure the amount of heat delivered by a solar collector and correlates it to the measured environmental conditions. The amount of

useful heat collected is the radiant gains minus the thermal losses. Radiant gains are the intensity of the solar radiation times the solar collector area (m^2 or ft^2), times the transmissivity (tau) of the cover glass and times the absorptivity (alpha) of the absorber plate. The thermal losses are a loss coefficient times the collector area times the difference in temperature between the water entering the collector from the storage tank and the cold surrounding air.

The energy collected is calculated in Equation 7.14 as the optical gains minus thermal losses

$$Q_{useful} = t\ a\ I\ A_c - U_c\ A_c(T_s - T_{amb}) \tag{7.14}$$

Efficiency is what we get out, the useful heat, divided by what went in which is the intensity of the solar radiation times the solar collector area. Equation 7.15 is then a linear equation with a Y-intercept equal to the optical properties of the glass and absorber plate, transmissivity and absorbtivity, and a slope equal to the heat loss coefficient.

$$h_{solar} = Q_{useful}/I\ A_c = t\ a - U_c\ (T_s - T_{amb})/I, \tag{7.15}$$

Where

I_c = incident solar radiation (W/m^2) in the plane of the collector
t = transmissivity of cover glass
a = absorptivity of absorber plate
A_c = collector area (m^2)
Q_{useful} = useful heat from collector (W)
U_c = thermal loss coefficient of collector (W/C)
T_s = storage water temperature (C)
T_{amb} = outdoor ambient temperature (C)

The SRCC test results give us the slope and intercept for these efficiency lines. The efficiency curves for three collectors rated by SRCC is presented in Figure 7.13.

Materials and components used in solar water heating systems vary depending on the expected operating temperature range. As this chart shows, each collector type works most efficiently and at optimal performance at different temperature levels. This graph shows actual examples of SRCC testing results. The vertical axis of this chart shows the efficiency of the collector, the percentage of the incident solar energy

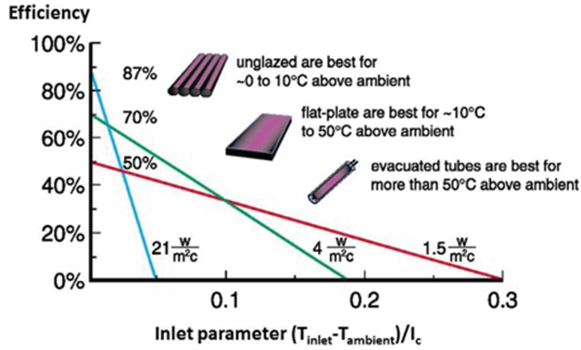

Figure 7.13. Efficiency curves of selected unglazed, glazed, and evacuated tube solar water heating collectors (figure by Jim Leyshon, NREL).

captured by the collector. The horizontal axis of this chart is temperature elevation above ambient temperature divided by solar radiation. So if the water temperature was 50 degrees Celsius, the ambient temperature zero degrees Celsius, and the solar radiation 500 watt per square meter, that would be the 0.1 on this chart. If the water temperature is hotter, the ambient temperature lower, or if there is less sun, we move to the right on this chart, and efficiency is decreased.

At very low temperatures the unglazed collector is not only least expensive, but also has the highest efficiency. There is no cover glass to absorb or reflect solar radiation and the heat loss is low because the temperature is low. Unglazed collectors are efficient up to about 10 degrees Celsius or 20 degrees Fahrenheit above ambient temperature

At higher temperatures we need a cover glass to attenuate heat loss off the collector. The glass itself reduces the optical gains of the collector, so the line starts at a lower efficiency, but there is less heat loss so the efficiency does not slope off as fast as we increase the temperature. Flat plate solar collectors are efficient up to, say, 50 degrees Celsius or 100 degrees Fahrenheit above ambient temperature.

For temperatures above that level, the superior insulation of an evacuated tube solar collector is required. The curved surface of the tube, and the space between tubes, reduces the optical gains considerably, but the low heat loss coefficient allows the evacuated tube collectors to efficiently delivery heat when temperature is high or solar radiation is low, once again, on the far right hand side of this figure.

Solar water heating system types are classified two following types, active and passive.

Passive systems included Integral collector storage and thermosyphon types. Active systems include direct or open loop systems or indirect or closed loop systems. Passive systems rely on buoyancy (natural convection) rather than electric power to circulate the heated water.

Integrated-collector-storage collectors place the storage inside the collector. An example of this is one with four-inch diameter copper tubes to store water inside the collector box. These have a lot of heat loss at night so are recommended only for warm climates.

Thermosyphon systems insulate the storage tank and place it above the solar collector, so that hot fluid rising in the collector causes a circulation to the storage tank.

Active systems involve electric power to activate pumps and/or controls.

Direct, or open loop systems, use a pump to circulate water from a tank to heat potable water directly in the collector. Mostly these are used in non-freezing climates like Hawaii but if used in a freezing climate they can drain water to drain when freezing is eminent, so called “drain down” systems.

Indirect, or closed loop systems, Heat an antifreeze solution like propylene glycol, in the collector and transfer the heat to potable water via a heat exchanger. In a “drain back” configuration this enclosed fluid drains from the collector into a small tank when the pump is not running. This protects the heat transfer fluid from both freezing and overheating.

Figure 7.14 shows an active, closed loop system, circulating an anti-freeze solution, which would be quite common in facilities such as barracks or dining halls.

The collector array consists of banks of solar collectors plumbed in parallel. Each bank that can be valved off must have a pressure relief valve, and air vents are often included at high points in the system to any let air out.

A controller compares the temperature at the collector outlet with that of the water storage tank. If the collector is sufficiently hotter than the

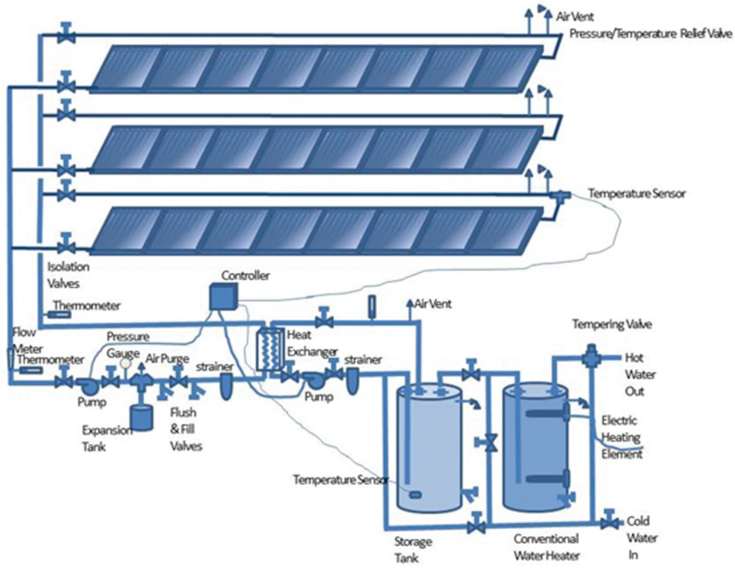

Figure 7.14. Schematic diagram of active, closed-loop solar water heating system [4].

water, the pumps turn off and if that temperature difference falls below a set point it turns the pumps off.

The heat transfer fluid and potable water are both circulated by pumps controlled by the temperature controller. Each pump has a strainer upstream to keep any objects from jamming in the pump.

The heat exchangers transfer the heat from the collector fluid to the potable water stored in the tanks. Double-walled heat exchangers prevent contamination of the potable water. Also the propylene glycol antifreeze used in this system is not toxic.

We do not want to send water that has been heated with gas or electricity to the solar collectors because the higher temperature results in a lower efficiency, so there is a separate pre-heat tank to store the potable water as it is heated by the sun. As water is used, it flows from the preheat tank into a conventional heater and if it is not hot enough, the conventional heater can add heat.

Table 7.3. Initial Cost, Operation and Maintenance Cost, and Lifetime of Glazed and Unglazed Types of Solar Water Heater [5].

Technology Type	Mean installed cost ($/ft^2)	Installed cost range (± $/ft^2)	O&M	Lifetime (yr)	Lifetime Std. Dev. (yr)
SWH, flat plate & evacuated tube	$141	$82	$0.75 to $1.50 per ft^2 per year	31	14
SWH, plastic collector	$59	$15	$0.60 to $1.20 per ft^2 per year	20	10

Flush and fill valves allow the fluid to be drained and replaced easily, and instruments such as temperature gauges, pressure gauges, and flow meters allow us to monitor the status of the system.

Finally, since the water could be heated by the sun up to a temperature hotter than we want it, a tempering valve is an important component of the system to mix the hot water with cold water to obtain the desired temperature.

Figure 7.14, shows a lot of detail, like pressure relief valves and controls, but you can see it is a pretty simple plumbing system and very similar to hydronic heating systems used for space heating.

Closed-loop glycol systems are popular in areas subject to extended freezing temperatures because they offer good freeze protection.

Nationwide, approximately 18 percent of energy use in residential buildings and 4 percent in commercial buildings is for water heating. Many estimates show that solar water heating system can efficiently serve up to 60 to 80 percent of hot water needs, but currently solar water heating represents around 1 percent of the potential U.S. water heating market. In other countries, solar technologies heats water on almost every building, but in the U.S. there is solar water heating in about 3 percent of buildings and for each building it provides about a third of the water heating needs. So there is tremendous potential for this technology to do more.

Solar water heating systems are the most cost effective where the following four characteristics exist:

1. Water heating load is constant throughout the week — for example, weekends require as much as weekdays.
2. Water heating load is constant throughout the year — for example, the building is not vacant in summer like a school might be.
3. A sunny climate is prevalent — this is helpful but not required — solar heat is available over most of the continental US and Hawaii.
4. Cost of fuel used to heat water is relatively high, more than 10 or 12 $/GJ ($10 dollars per Mbtu).

Solar water heating savings will cost effectively pay for system installation in three types of situations.

Any facility that pays high utility rates for conventional power water heating is a good candidate. Smaller facilities in rural areas served by only electric power are an example. Any of several mid-temperature solar water heating technologies can serve these facilities well. Off-the-shelf packages are available and systems that operate passively without pumps or electronic controls are often appropriate in warmer climates. Large facilities such as prisons, hospitals, and military bases with need for continually large volumes of hot water are excellent candidates. Even if conventional water heating costs are relatively low, economies of scale for larger mid-temperature or high-temperature systems can bring costs down to competitive levels.

Swimming pool systems will often pay for themselves in just a few years, particularly for pools that are used year round. Relatively inexpensive low-temperature systems are quite effective and can either greatly reduce conventional pool heating bills or extend the season where heating was considered too expensive.

Several factors must be weighed to determine whether a site has a good resource for solar water heating. Sites with an average solar radiation rate above 4.5 kWh/m^2/day are great candidates for solar water heating. But, even a site with a less attractive solar resource rating can have great potential for solar water heating if the energy rate it offsets is high enough, or other incentives are available.

Two solar water heaters, one of which is shown in Figure 7.15, were installed at the Mid-Atlantic Social Security Center in Philadelphia. The system design is to tap into the recirculation loop of the building and add solar heat to the water returning to the heating plant. This approach requires very well insulated collectors and evacuated tubes were specified.

Figure 7.15. Evacuated tube solar water heating system on Social Security Building, Philadelphia, PA (photo by the author).

Each system has 180 tubes that add up to 27 meters squared collector area. The cost was $37,000 dollars and each system delivered 36 GJ in the first year of operation.

Research has the ability to increase the potential for solar thermal technology. Plastic collectors can be manufactured at a lower cost than copper and glass ones, and products using materials that can tolerate higher temperatures are starting to come onto the market that maintain adequate performance and longevity.

Cross linked polyethene, or PEX, piping can also be less expensive than copper pipe and there are some types which can freeze and thaw out again without damage, which could simplify systems and reduce cost.

Small variable speed pumps are on entering the market to reduce pump power and also make sure the collector operates at an optimal efficiency.

7.7 Energy Systems Integration

In this final section, we will examine issues related to Energy System Integration (ESI), addressing how increasing amounts of intermittent solar energy generation can be accommodated to realize energy cost savings and improve system reliability. This section will discuss some of the challenges and solutions to ESI at the building,

substation, and grid level, as well as cost and process-related issues faced by the utility.

Historically, existing U.S. electric power utility systems were based on one-way power flow-real power always flowed from the central generation plant, through substations, and on to loads — and integration issues were not critical because solar energy projects were small and often located in off-grid applications. But Federal tax credits and other incentives introduced in 2005 made it profitable to install large renewable energy systems in grid-connected applications, many benefiting from a utility policy called "net metering." Challenges surfaced as buildings and campuses strived to integrate intermittent resources while still relying on the grid to meet demand at times when renewable energy resources were not producing.

As the amount of renewable generation in a system increases, system operation must be altered to accommodate the intermittent renewable power. These changes to the operation generally reduce the efficiency and cost-effectiveness of the conventional resources, although many advocates of renewable energy point out that distributed renewable energy might forestall the need for huge investment in central power generation.

Under a net metering policy, power from a renewable energy system in excess of the local load can be absorbed by the larger utility system and credited to the load's utility bill, with the load still able to consume power from the grid when the Renewable Energy is not generating. A building with enough PV might offset enough energy to bring its electric bill, which is based on consumption, to nearly zero. Yet the building is still using the utility on a daily basis even though it does not pay for that service. So we perceive net metering as an incentive for distributed generation that is offered at the expense of other rate-payers.

As of 2014, 44 of the 50 states have implemented net metering policies. But each has also imposed limits to net metering, either for each site or for the state as a whole, with the realization that there are both technical and economic reasons that not every utility customer can net meter. Utility companies, in conjunction with the state Public Utilities Commission (PUC), have established various threshold levels, also known as penetration limits, to regulate the amount of renewable energy on each circuit. Once penetration of distributed generation as a fraction of total electric load on each utility circuit reaches the limit (often 10 or 15%) an area already has too much PV for net metering — technically,

there is no additional load on the circuit for excess solar power from a new PV system to serve. This does not mean customers living in those areas cannot install PV systems, but it does trigger an Interconnection Requirement Study is required which costs about $3000 for residential PV systems, and up to say $40,000 for a large-scale system, can take months, and may include additional costly equipment before a building owner can install PV. The interconnection study tests the impact that proposed system will have on the entire utility circuit.

Challenges can occur for both the energy customer and the utility on the following scales when installing a large solar electric system:

1. Building and Electric Distribution System: limits to current-carrying capacity of utility circuit; location and setting of overcurrent protection (breakers, fuses); voltage out of limits;
2. Substation: routing of power from circuit with excess RE to load on other circuits; voltage fluctuations;
3. Generation Plant: increase in spinning reserve requirements; limits to sudden changes imposed by ramp-rates of generators;
4. Utility Operations: allocation of costs associated with RE integration among utility customers; equitable distribution of operating cost among ratepayers;
5. Investors: current model of a centralized utility in which guaranteed wholesale power rates return long-term investments (such as with baseload coal or nuclear plants) is challenged by on-site generation; wholesale prices are lowered by RE generation based on its low marginal cost compared to the fuel cost of fossil plants.

7.7.1 Building Level Challenges and Solutions

There are four areas of consideration related to the effects of high penetration of renewable energy on the electrical service to individual buildings.

1. **Sizing of Electrical Service to Building with Renewable Energy Generator**
   Challenge: The electrical service to a building is designed to accommodate the peak load expected of the building plus a safety factor for future load growth. For example, a building with a 1 MW load might have a 2 MW service. If, as many projects are

now doing, the building seeks to offset a 24 MWh/day of energy with on-site solar energy, which occurs only over 6 hours per day, a 4 MW PV system would be installed and the electrical service would not be sufficient to get the solar power OUT of the building. Solution: The electric service to the building would have to be upgraded from 2 MW to at least 3 MW to accommodate the flow of solar power OUT of the building during the day (4 MW − 1 MW = 3 MW).

2. **Overcurrent Protection on Electrical Service to Building with RE Generator**

   Challenge: Coordination of overcurrent protection is an important consideration in the addition of RE generation. During initial distribution system planning, a protection coordination study informed the location and settings of fuses, breakers, protective relays and synchronized other protective equipment to isolate electrical faults in a planned sequence. The additional current from an RE generator invalidates previous protection studies because it changes the amount of current available for conductors to carry and changes the location and setting of breakers to prevent excessive current flow. Consider for example an overcurrent protection situation shown in Figure 7.16 — a fuse limits the current coming from a transformer to a value which is less than the line is rated for … say 100 Amps in this example. Theoretically at least, a generator out on that line could add additional current and result in a current greater than the line is capable of carrying. In this example, the loads could be surveyed, and if lower than 100 Amps the fuse at the transformer could be changed out with one rated for 90 Amps. If the loads do indeed require 100 Amps then the service would have to be upgraded to a wire that could carry more current.

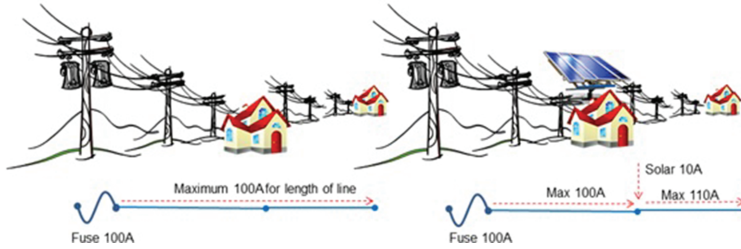

Figure 7.16. Introduction of electric current (Amps) onto a distribution system by an RE generator can increase current in the line beyond which the overcurrent protection was originally designed for.

Solutions: New studies may be required to determine how the maximum current from an RE generator increases currents flowing through the electrical system when a line becomes overloaded or when a fault (short-circuit) occurs. Results of this study include any required changes to the protective system used to detect and interrupt current and isolate faults.

The protective system may need to be reset or redesigned to properly set the coordination and timing of devices such as protective relays, reclosers, circuit-breakers and fuses in a system to detect and isolate faults. The renewable energy project should involve the utility to devise and review resulting modifications and plans for overcurrent protection.

3. **Voltage Regulation on Electric Service to Building with Renewable Energy**

Challenge: PV systems can increase the voltage at the point where they inject power, and they can also fool control systems which are based on load on the substation rather than actual voltage at the site. Voltage regulation is often cited as the primary concern of utilities when considering interconnection of an RE generator. Utilities are required to keep these voltages within a relatively narrow operating range for example 120V service may vary from 114V to 126V, RMS (Figure 7.17).

Since voltage drops along the powerline as the load increases, current technology changes the voltage at the transformer based on the load, by measuring current at the transformer. PV generation on a circuit defeats this "line drop compensation" because it

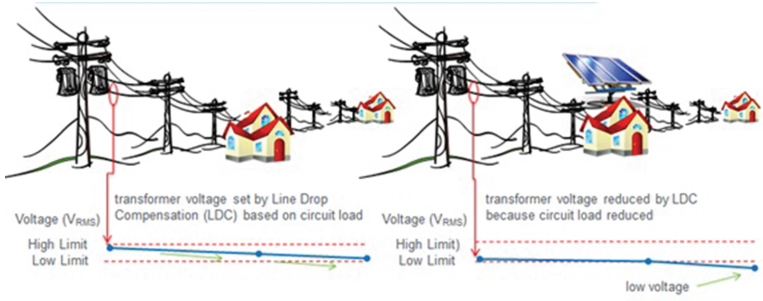

Figure 7.17. Voltage at the transformer is regulated by line drop compensation based on load rather than voltage. Distributed RE can reduce the load at the point of voltage regulation, which alters the voltage drop that the system was originally designed for.

reduces the load seen at the transformer, which results in a voltage lower than the imposed limits at the end of the line.

Solutions: Planning and modifications are needed to minimize deviations in voltage at various locations on the distribution system as PV inverters inject power at their locations. Also, at the substation, the utility will study the need to install new types of voltage regulation equipment (that is based on measured voltage rather than load). The intermittent operation of the RE generator may cause increased cycling on the new or existing voltage regulation equipment. Power-flow based software tools can determine cycle counts on voltage regulation equipment during changes in variable generation power output. If it is found to be excessive, one strategy to reduce cycling is increasing the delay time of the voltage regulators.

4. **Wear-and-Tear on Reactive Power Compensation Equipment Due to PV Systems**

Challenge: Equipment used to actively provide reactive compensation for power factor correction can also cycle excessively due to high-penetration of intermittent renewable energy generators. The reason for this is that most installed PV systems with static inverters supply power at unity power factor (PF = 1). This means that these PV systems can supply real power to loads but not reactive power, which must still be supplied by the substation.

The utility generally provides customers with both real power and also reactive power. The cosine of the angle between the two is the Power Factor. Reactive power is wasteful and the utility will impose charges and experience generator problems if the power factor is much lower than 1. Currently inverters are limited by standards to provide only real power, so the proportion of reactive power that the utility must provide could increase with addition of a PV system on the load, as shown in Figure 7.18.

Solution: The reactive power supplied by the utility must increase to accommodate each additional kW of PV as it varies widely and suddenly as the RE resource changes One solution is to specify inverters that provide reactive power if needed, as will soon be available under new inverter standards. The Institute of Electrical and Electronics Engineers implemented a National IEEE Standard 1547 for interconnecting distributed energy sources to utilities' distribution systems. This requirement has led to the uniform application of interconnection networks across the U.S. IEEE Standard 1547 is followed now by IEEE Standard 1547a, which provides for additional flexibility in the design which promises to

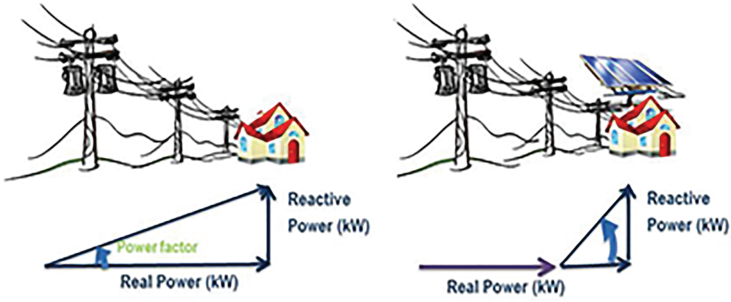

Figure 7.18. By supplying only real power (kW) and not Reactive Power (kVAR), an RE system can increase the Power Factor (PF) resulting in additional charges from a utility.

expand implementation strategies. These standards are important to designers of high penetration renewable energy systems and will allow for non-unity power factor, low voltage ride-through, and low-frequency ride through.

7.7.2 Substation-Level Challenges and Solutions

There are two areas of consideration related to the effects of energy system integration for substations.

1. **Effects of Renewable Energy on the Local Substation**
   Challenge: An electrical substation consists of a transformer by which voltage is converted from transmission to distribution voltage and a bus with circuit breakers, current transducers, and isolating switches on each circuit coming off of the bus. Configurations including transfer buses, double buses, and ring buses are available, but because they are simple and inexpensive, single bus configuration is common. This single bus may serve as a means to accept power from circuits with excess RE and deliver it back out to circuits with excess load.
   Solutions: Reconfigure Bus and Circuits: in configurations other than a single bus, sectionalizing switches or isolation switches must be positioned for this exchange of power to occur, and new legs between circuits may need to be added. Analysis of expected RE generation and loads may inform required reconfigurations to the buses and circuits. The intent of this reconfiguration

would be to allow power to flow from circuits with excess RE generations to other circuits with load to serve. A substation is not designed to conduct this transfer if it was designed for power to flow only out to circuits.

2. **Network Protectors in Network Systems**
   Challenge: Substations in networks (rather than purely radial) systems have "network protectors" on each circuit leaving the substation to prevent a reverse flow of power.
   Solutions: Integrating RE into a network power systems may require special controls to prevent the RE power from ever exceeding the load and potentially tripping the network protectors. This can be achieved most simply by installing an inverter with a capacity less than the minimum coincident load, but may also be achieved with advanced inverter features which allow the inverter to be turned off or modulate its output not to exceed the load. A network distribution system with network protectors may thus limit the size of RE at a Federal site to less than a size that would provide 100% net zero or even limit it to less than required for the 20% RE goal of the recent Presidential Memo. If the grid would not accept any excess power back, the only way to increase renewable energy use on-site would be to add energy storage to accept power in excess of the load.

7.7.3 Grid-Level Challenges and Solutions

There are two areas of consideration related to the effects of energy system integration for substations.

1. **Voltage Stability of Electric Grid**
   Challenge: Voltage stability refers to the ability of the grid to resume nominal voltage levels after disturbances such as sudden increase in load or sudden decrease in generator output or demands for reactive power that cannot be met. Renewable energy generators that are inverter-based have voltage set points, which could trip offline during abnormal voltage conditions and exacerbate a low-voltage problem.
   Solution: Consider new standards for static inverters out on a grid that play a role in voltage stability on large, complex power systems, with mutual agreement of the utility and the system owner. New inverter standards will allow inverters to contribute

to recovery from such a disturbance by "riding through" low voltage or low frequency conditions. These new inverter standards involve non-unity power factor, low voltage ride through, and low frequency ride through.

2. **Synchronization of Generation Equipment on the Electric Grid**
   Challenge: Rotor angle stability refers to the ability of the generators in a power system to maintain synchronism after disturbances, such as a drop in frequency caused by addition of a large load or drop in RE output due to natural fluctuation in the RE resource. Output of inverter-based RE generators can change very quickly in turn affecting generator dynamics. With high-penetration levels of inverter-based RE, effects on synchronization of all of the equipment on an electric grid may be significant.
   Solutions: Federal agencies working with utilities can hire consultants to use commercial software packages to simulate transient events, such as sudden loss of output from a renewable energy generator. These model the details of generator machines and controls and detailed electrical circuit and load models to determine if the system will return to stability following a transient event, such as sudden change in the output of a specific RE generator.

7.7.4 Utilities' Electrical Generation Systems

These are major issues faced by utility companies at the system level.

1. **Ramp-Rates and Spinning Reserve**
   Challenge: Building owners installing large renewable systems, especially on small utility grids such as on islands should realize that a kWh delivered does not generally equal a kWh saved at the generation plant. It takes time to start a generator and increase its power output, especially a big heavy coal or nuclear plant. The heat-engine portion of a generator is always operated with some extra reserve capacity to make up variations in the electrical demand. This operational overhead is called "spinning reserve." Without RE generation, the amount of spinning reserve must cover anticipated changes in the load. But with the addition of RE to a system, the amount of spinning reserve must cover both sudden increases in the load and sudden decreases in RE output and at the same time. Spinning reserve is undesirable since it consumes some fuel and

incurs run-time on the generator machine. Much maintenance is planned based on run-hours rather than power output.
Solutions: Several strategies have been identified to reduce, but not eliminate, the amount of waste associated with spinning reserve:

- Utilities' controls may implement sophisticated program logic that looks at the instantaneous contribution of RE and calculates the appropriate amount of spinning reserve.
- Storage alternatives to spinning reserve may be more cost effective.
- Demand side management (DSM) is another alternative to spinning reserve which controls the electrical loads on the system rather than aiming to meet all loads at any given time. However, DSM calls for at least some participation by the energy consumers by allowing the utility system operator to delay non-critical loads such as air conditioners and water heaters for several minutes at a time.
- Forecasting the output of a renewable energy generator minutes, hours or days in advance also can reduce the need for spinning reserve. Technical developments in forecasting software have allowed operators of utility transmission and distribution systems to predict in advance solar system or wind output.

2. **Allocating Costs and Investment**
Challenge: Utilities are faced with the challenge of coordinating generation resources and also controlling the load demand. Utilities incur costs as they implement the measures described in the previous section and provide the ongoing spinning reserve to accommodate distributed RE generation. Utilities argue that RE generation on their system saves them only some portion of the fuel they would otherwise use, and that all debt service, O&M expenses, and administrative costs remain the same. At the same time, the building owners that install large RE systems seek to minimize their financial payment to the utility. To equitably accommodate both the residential customers and commercial customers, utilities are faced with decisions of how to share costs. These discussions may impact the utilities openness to the high penetration of renewable energy. Also, RE is characterized as a high capital cost but a low operating cost; the marginal cost of solar and wind power is essentially zero, compared to substantial fuel costs for the fossil alternatives. This has the effect of suppressing

wholesale prices paid for fossil energy when renewable energy is generating. This affects the current investment model for utilities, and creates a problem for investors expecting a high rate of return on large coal and nuclear plants.
Solution: There is a necessity for a new business model that rewards low-carbon energy production, covers the cost of reliability, equitably assigns costs, and involves investors directly investing in required grid upgrades. Rather than recovering their costs based on how much energy you consume, utilities of the future might charge for the services, such as reliability of power and power quality, that you actually do use even when you generator your own on-site renewable energy.
Lets conclude with a recap of strategies to increase the amount of intermittent renewable energy generation that can be added to the utility system.

- Utility circuits can be reconfigured to allow power to get from distributed generators to a load, including locations and settings of network protectors, voltage regulation, and overcurrent protection devices.
- If PV is distributed over a large area rather than installed all in one place, there is less chance that a cloud could affect the output and the generation is smoothed out over a partly cloudy day.
- Fixed mounts facing south would all deliver their maximum power at noon, but by using tracking mounts and different PV orientations we can smooth out the daily delivery — less at noon but more in morning and evening hours.
- The new IEEE 1547a standard will allow for more advanced inverter features. These include: Low voltage ride-through; Low frequency ride-through; and Power-factor correction. Another capability is the ability of an inverter to curtail RE output in response to a signal from the utility or grid conditions.
- Forecasting of RE plant output would provide a utility system operator with enough advance notice to ramp up a fossil fueled generator rather than maintain such a large amount of spinning reserve. Even a few minutes warning could help out tremendously in this regard.
- Controlling the instantaneous demand of non-critical loads is also a good idea — it is less wasteful to turn off an appliance for the 15 minutes that it takes to ramp up a generator than it is to keep that generator running as spinning reserve.

- Energy Storage is the ultimate solution to almost all of these problems, and battery technology and cost are improving in response to this future need for a large amount of energy storage.

You can expect the ways that utility companies recover cost to evolve from purely commodity pricing based on how much energy you consume toward charging for services that support your RE generator and your load, such as stand-by charges that charge for the ability to serve your load should your RE generator fail to.
This section has described some of the most important hardware and operational measures that can be taken to resolve common challenges and achieve a higher level of RE penetration. Meeting our renewable energy goals is possible, but requires collaborating early with utilities and other stakeholders in the regulatory process.

7.8 Conclusion

In this chapter we considered the integration of solar energy technologies: photovoltaics, daylighting, passive solar heating and cooling, solar water heating, and solar ventilation air preheating. We considered how the solar resource varies predictably with time-of-day and day-of-year by location and also the unpredictable nature of clouds and weather. We considered the fundamental operating principle of each type of solar energy device, as well as how devices are assembled with other enabling components into complete systems. We case studies of real-world cost and performance reported by installed systems. Finally, we consider the measures that must be taken within a larger utility system in order to accommodate the distributed and intermittent nature of the solar resource. Both electric and thermal storage are enabling technologies for solar, with district heating enabling thermal storage on a seasonal scale.

While thermal loads are being increasingly electrified through the use of ground-source heat pumps, we conclude that a plurality of solar technologies can be used, and daylighting, photovoltaics, solar water heating, passive solar architecture, and solar ventilation air preheating might all feature in the strategy of achieving minimum use of fossil energy in a building. Growth in solar installations has been explosive in recent years, but to realize the potential of solar energy in buildings requires significant remaining research and development. A priority of this research is solar conversion efficiency, since a much higher efficiency affects so

many other aspects of implementation cost and site impacts (land use). Research is also required to develop the sophisticated control systems to forecast solar resources, forecast and control demand-loads, and optimize the dispatch of energy storage systems. While energy technologies and markets are constantly changing and surprising, this chapter presents reasons to extrapolate that solar energy will play an increasing role in the serving energy requirements in existing buildings as well as providing a new approach to meet much of the new load growth in the future.

References

References to websites that were sources of figures or data are referred to in the text.

Much of the text of this chapter results from research in preparing for the seven-part training series "Renewable Energy Technology Applications," delivered by Andy Walker and produced by Carl Costello of Greening America Inc. for the US DOE Federal Energy Management Program and available for free viewing at https://www4.eere.energy.gov/femp/training

[1] National Renewable Energy Laboratory, Q2/Q3 2015 Solar Industry Update; David Feldman, NREL; Daniel Boff, DOE; Robert Margolis, NREL. October 27, 2015, an unpublished quarterly brief.

[2] SolarGIS © 2015 GeoModel Solar. For more information see http://geomodelsolar.eu/

[3] National Renewable Energy Resource Atlas; http://maps.nrel.gov/re_atlas; April 9, 2014.

[4] *Solar Energy: Technologies and Project Delivery for Buildings* by Andy Walker, John Wiley and Sons Inc., Hoboken NJ; Sept 16 2013; ISBN 978-1-118-13924-0.

[5] Federal Energy Management Program (FEMP) RE Technologies Cost and Performance Matrix. http://www.nrel.gov/analysis/tech_lcoe_re_cost_est.html. Accessed 2/18/2015.

[6] NREL, 2011. PVWatts Changing System Parameters; DC to AC Derate Factor (http://rredc.nrel.gov/solar/calculators/PVWATTS/system.html).

[7] NREL, 2015 *2013 Renewable Energy Data Book*. Produced by Sean Esterly and Rachel Gelman, edited by Karin Haas, and designed by Stacy Buchanan and Alfred Hicks of the U.S. Department of Energy's National Renewable Energy Laboratory (NREL).

8 Energy Storage Systems for Buildings

Gang Li and Yunho Hwang

Abstract

Thermal energy storage (TES) systems could be used to reduce a building's peak power demand associated with heating or cooling by shifting the peak heating or cooling loads to the low power demanding hours. This chapter provides the overview of the recent energy storage research activities applicable to building applications. The information gathered in this chapter is divided into two storage technologies: sensible/latent TES and sorption TES. Sorption TES technology is summarized by improving working pair properties and enhancing sorption bed heat transfer. Investigation on the sensible/latent TES is tailored with more details for building storage system classification, its energy saving potential, phase change material (PCM) property improvement, and mathematical modeling of PCM storage system. In this chapter, several barriers that impede the commercialization of storage technology are identified, and possible solutions are then suggested. In addition, recommendations are made for the future TES technologies. This chapter is expected to be beneficial to researchers and engineers to design energy storage systems for building application and to access their merits.

8.1 Introduction

The continuous increase in the level of energy consumption and depleting energy resources leads to serious energy and pollution issues. According to the Energy Information Administration [1], the total energy consumption for developed countries like the United States, was 9.36 trillion kW·h in 1949, and then in 2011 increased to 28.5 trillion kW·h, about tripled in 62 years. A study from International Energy Agency (IEA) showed that fossil fuels, which have harmful environmental effects, such as causing air pollution and climate change, are still a dominant source of energy worldwide [2]. This study showed that CO_2 emissions increased from 20.9 gigatonnes (Gt) in 1990 to 28.8 Gt in 2007, and are projected to reach 34.5 Gt in 2020 and 40.2 Gt in 2030 with an average annual growth rate

of 1.5% over the full projection period. The building sector accounted for more than one third of the total energy consumption. The main energy uses in the building sector are space heating, space cooling, water heating, etc. In the United States, the building sector is responsible for approximately 41% of primary energy consumption in 2010 [3]. For the European Union, buildings account for 40% of the total energy consumption [4].

Facing the challenges of stable energy supply and pollution issues for buildings, it is necessary to develop and expand advanced technologies to reduce the energy demands in buildings, increase the energy supply while utilizing renewable energy effectively. In this context, the technology of thermal energy storage (TES) is proposed. TES is defined as the temporary holding of thermal energy in the form of hot or cold substances for later utilization. The TES applications cover the domestic hot water production [5, 6], space heating/cooling [6], airconditioning [7, 8], and even subzero applications [9]. To assist researchers and engineers for designing energy storage systems for building applications, this chapter provides the summary of different TES systems and technologies for building applications and evaluation of their benefits. In addition, several barriers that impede the commercialization of storage technology are identified, and possible solutions are then suggested. In addition, recommendations are made for the future TES technologies.

8.2 Sensible and Latent TES Systems for Buildings

8.2.1 Energy Storage System Classification

TES systems allow for efficient use of energy delivered and enhance occupant's thermal comfort in buildings. They can be used to reduce or even eliminate the electricity loads for buildings when coupled with different heating or cooling systems. TES can effectively utilize the building base load generating equipment or systems, and relieve the building's dependence on peak causing units that have higher operating costs. In this section, TES sensible and latent technologies coupled with different heating or cooling systems are introduced. The classification of sensible/latent TES systems applicable to buildings is shown in Figure 8.1, and such TES systems are introduced in this section.

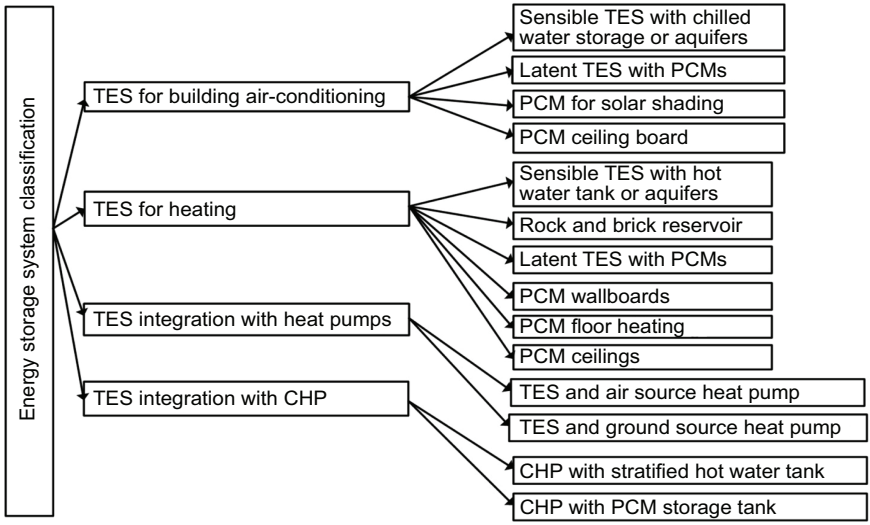

Figure 8.1. Sensible/latent TES system classification.

8.2.2 TES for Building Air conditioning

Application of cold TES for building air conditioning started in 1970s in the United States and storage technologies have been developed for a long time. It remains popular today in different countries for summer air conditioning applications in residential and commercial buildings. In this section, chilled water tank and aquifers, PCM storage tanks, PCM shutters and PCM ceiling boards are mainly introduced.

8.2.2.1 Sensible TES with Chilled Water Storage or Aquifers

Figure 8.2 shows the typical TES system with a chilled water tank or aquifers for air conditioning application. With a chilled water tank or aquifers, the refrigeration system can be operated during the off peak hours, when electricity price and cooling demand are lower. During the daytime, the cooling water stored in the chilled water tank or aquifers could be utilized to meet building loads instead of using the chiller unit. With TES, a smaller chiller unit can be designed based on the optimum efficiency for the majority of the working period.

Chilled water storage, which utilizes the sensible heat (4.184 kJ·$kg^{-1}\cdot K^{-1}$) to store cooling, needs a relatively larger volume storage tank

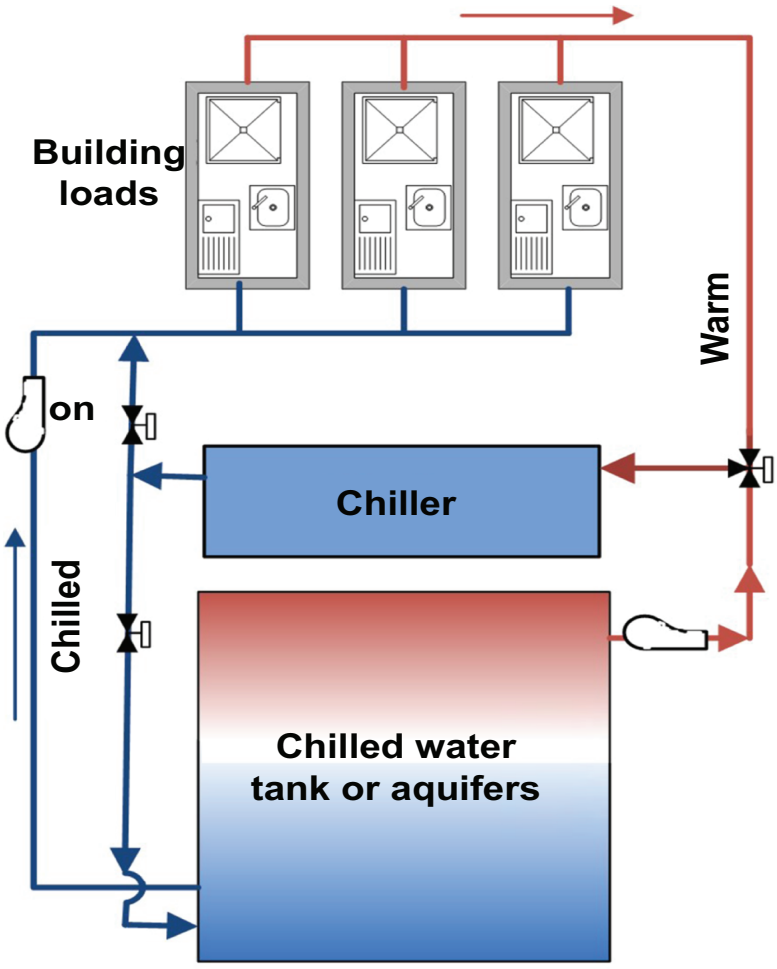

Figure 8.2. Typical TES system with chilled water tank or aquifers for air conditioning.

than other storage systems with a larger latent heat of fusion. However, it has been widely used because of its suitable cold storage temperature (4°C to 6°C). This characteristic enables its direct compatibility with conventional water chillers and distribution systems, and provides good unit efficiency with a low investment. Water is most dense at 4°C and becomes less dense at both higher and lower temperatures. Because of this density dependency on temperature, this kind of storage system has the phenomenon of a stratified temperature distribution in a storage tank. Effective chilled water storage requires that some form of separation

should be maintained between the stored cold water and the warmer return water. The mixing of two water streams at different temperatures, which is caused by the inlet diffuser during charge and discharge processes, significantly affects the temperature distribution in the tank. The two diffuser types most commonly used in today's commercial chilled water storage tanks are shown in Figure 8.3 [10]. Most studies related to this stratification tried to enhance the chilled water storage's performance,

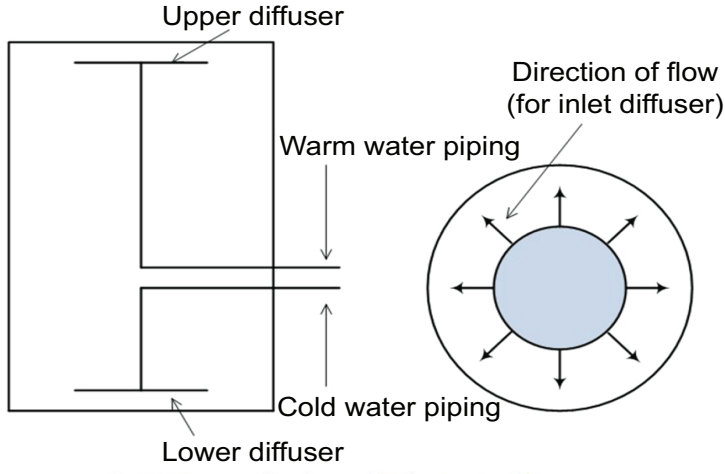

Figure 8.3. Stratified storage tank [10].

simplicity, cost, and reliability. In a single stratified tank storing both hot and cold water, diffusers are located at the top and bottom of the tank. Various physical methods, such as membranes, internal weirs, baffles, labyrinths, series tank, empty tanks, and thermally stratified systems, have been used to create the temperature stratification necessary for highly efficient storage [11].

One case study for energy savings and reductions in pollutant emissions was provided in ref. [12], a groundwater aquifer TES system was installed as part of a space-conditioning unit in a newly renovated office building of Anova Verzekering Co. (The Netherlands). Accounting for the subsidy of US $212,000 received from the Dutch government, which is equivalent to 20% of the total initial system cost, the reduced energy cost due to TES was expected to lead to a payback period of 6.5 years or less. In the case study, TES primary energy consumption was decreased over 44%, even though the electricity usage was increased by 21% as shown in Table 8.1.

8.2.2.2 Latent TES with PCMs

PCMs are designed to melt and freeze at a suitable phase change temperature range for their respective applications. With the superiority of their energy storage density to the conventional sensible heat energy storage systems, their storage system volume is smaller (in Figure 8.2, the chilled water tank can be replaced with the PCM storage tank). The most commonly used PCM is the ice. One ice harvesting system used for building air conditioning application is shown in Figure 8.4 [13]. During off-peak time, the ice can be produced and stored. During peak time, the chilled water can be obtained from the ice storage tank, further reducing

Table 8.1. Annual Energy Savings and Emission Reductions for the Case Study [12].

Commodity	Conventional system	TES-based system	Reduction for TES-based system
	Consumptions		
Natural gas (m^3)	215,800	95,500	120,300 (56%)
Electricity (kW·h)	395,550	511,500	−84,000 (−21%)
Primary energy (m^3)	322,000	179,000	143,000 (44%)
	Emissions		
CO_2 (kg)	608,000	346,000	262,000 (43%)

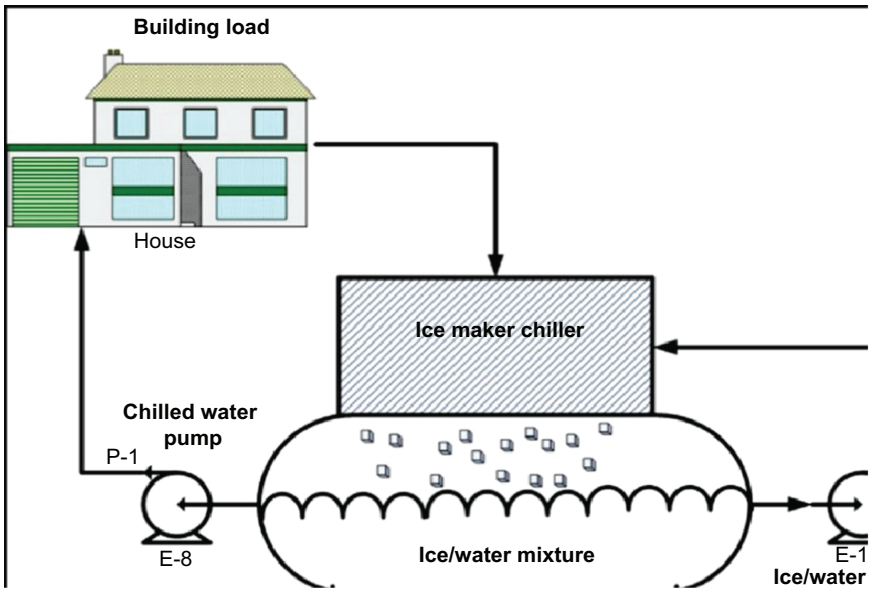

Figure 8.4. Schematic diagram of an ice TES system [13]

the water temperature to cope with the building load. For the other PCMs, current research is mainly focused on the salt hydrates and eutectics due to their high fusion heat and suitable phase change temperature range. To provide a general understanding for different storage systems, Hasnain [14] compared the primary features of chilled water, ice, and eutectic salt cold storage systems, as shown in Table 8.2.

According to one study [15], a mixture of paraffin wax and fatty acid was used as the PCM in an air distribution duct for an office building in Japan. The system capitalized the low electricity price in the nighttime for charging the PCM, as shown in Figure 8.5. The charging period was from (5.00–8.00), the stored energy would be released in the daytime when the peak cooling load occurred from (13.00–16.00). Simulation results indicated that the room temperature could be maintained around 19°C without cold operation sources.

One case study was conducted by using the ice thermal storage systems for office building applications [13]. The comparison results between the conventional AC system and the latent TES system indicate that a proper design could lead to lower energy consumption due to better utilization of the equipment. It shows that the load leveling strategy consumes around

Table 8.2. Comparison of Various Thermal Storage Systems [14].

Primary features	Chilled water storage	Ice storage	Eutectic salt storage
Specific heat ($kJ \cdot kg^{-1} \cdot K^{-1}$)	4.19	2.04	–
Latent heat of fusion ($kJ \cdot kg^{-1}$)	–	333	80–250
Maintenance	High	Medium	Medium
Warranty availability	Low	High	Medium
Tank interface	Open tank	Closed system	Closed tank
Discharge fluid	Water	Secondary coolant	Water
Charging temperature (°C)	4 to 6	−6 to −3	−20 to 4
Chiller	Standard water	Low temp. secondary coolant	Standard water
Packaged system	Medium	High	High
Heating capability	Low	High	Medium
Chiller charging efficiency	5.0–5.9 COP	2.9–4.1 COP	5.0–5.9 COP
Storage installZZed cost ($\$ \cdot kW^{-1} \cdot h^{-1}$)	8.5–28	14–20	28–43
Discharge temperature (°C)	Above 1–4	1–3	9–10

4% less energy than the conventional AC systems. The potential emission reduction when utilizing ice TES system was estimated based on the potential of the natural gas to produce CO_2 emission. The results show that the annual CO_2 emission reduction for load levelling strategy varies from 3000 to 60,000 tons for the total system capacities of 352 kW and 7034 kW.

8.2.2.3 PCM for Solar Shading

The PCM applied for solar shading system is shown in Figure 8.6. For the cases with significant daytime and nighttime temperature fluctuations, this system has the benefit of attenuating the temperature fluctuations inside the room. Usually, the PCM utilized in PCM assisted solar shading system is hydrated salt $CaCl_2 \cdot 6H_2O$.

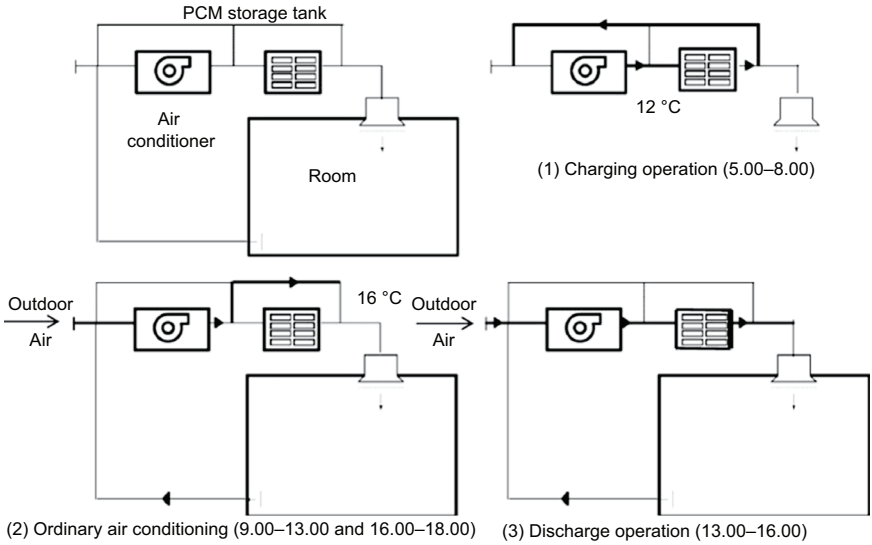

Figure 8.5. Schematics of free cooling systems [15].

Table 8.3. The Cumulative Energy Saving of the Load Levelling Strategy and Estimated Emission Reduction with Ice TES [13].

System Capacity (kW)	TotalAnnual Energy Consumption of Conventional System (kW·h)	Total Annual Energy Consumption Load Levelling Strategy (kW·h)	Total annual energy saving load levelling strategy (kW·h)	Total annual Onsite CO_2 Emission Reduction (ton)
352	1,165,565	1,161,133	4431	3000
1758	5,827,824	5,805,667	22,157	15,100
3517	11,655,648	11,611,333	44,314	30,300
5275	17,483,472	17,417,000	66,471	45,500
7034	23,311,295	23,222,667	88,629	60,600

One theoretical thermal analysis was performed for a window containing the PCM instead of blinder. The geometry configuration of window containing the PCM is shown in Figure 8.7 [16]. The objective of using PCM in the window is to utilize its high latent heat of fusion to reduce the heat gain by absorbing the heat through the melting process

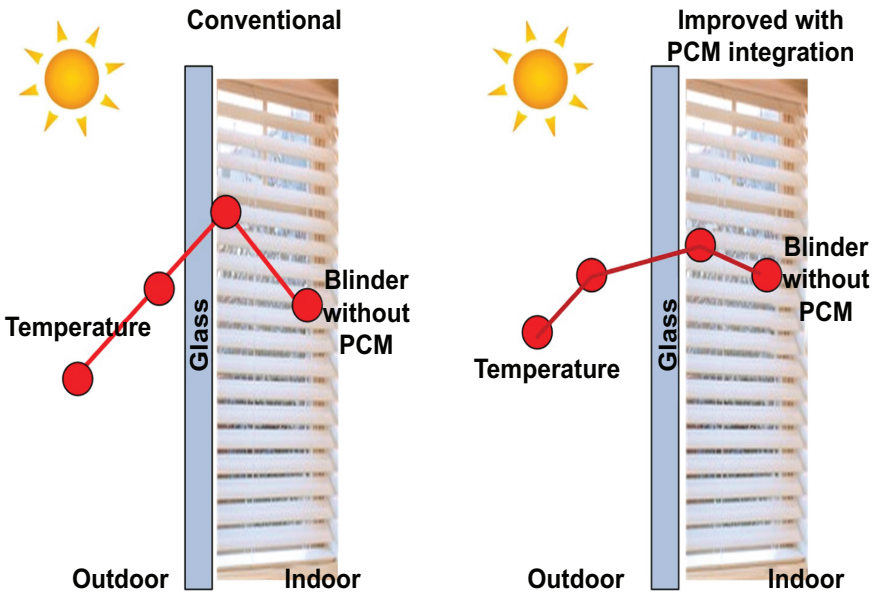

Figure 8.6. Diagram of PCM−assisted solar shading system.

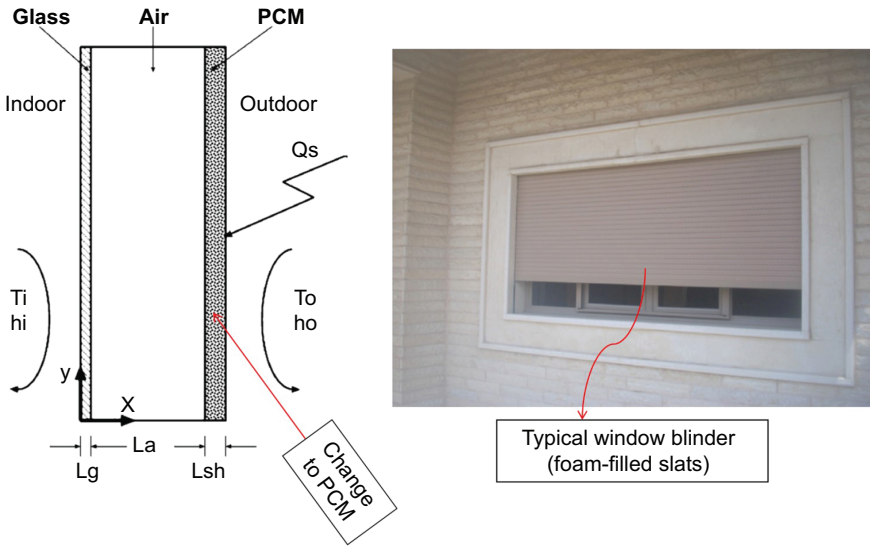

Figure 8.7. Schematic representation of the windows PCM system and the boundary conditions [16].

during the daytime before it reaches the indoor space. Heat gain through windows can be reduced by 23.29% when the PCM with thickness of 0.03 m is used, as shown in Table 8.4.

8.2.2.4 PCM Ceiling Board

One study [17] investigated the effect of a peak shaving control of air conditioning systems using PCM (micro-capsulate PCM melting point ~25.8°C, close to room temperature) for ceiling boards in an office building, as shown in Figure 8.8. The PCM ceiling board is used instead of a rock wool ceiling board. In the nighttime, the cool air from the AHU flows into the ceiling chamber space. And the PCM ceiling board is chilled and stored cooling. In the normal cooling operation period, the cool air

Table 8.4. The Effect of the PCM Thickness on the net Heat Flux during the Working Hours [16].

PCM thickness	0.01 m	0.015 m	0.02 m	0.03 m
Net heat flux ($W \cdot m^{-2}$)	44.79	38.65	36.33	33.18
Heat flux reduction (%)	−3.58	10.65	16.01	23.29

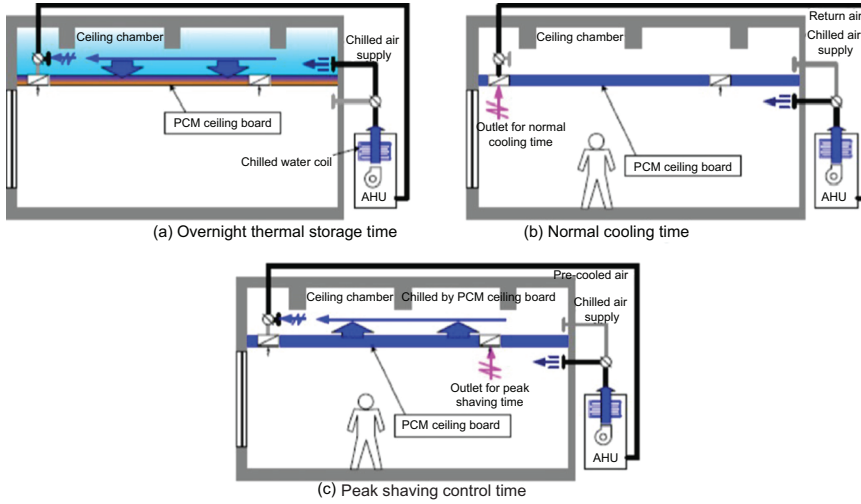

Figure 8.8. Schematic of the PCM ceiling board system [17].

from the AHU flows into the indoor space. During the peaking period, the air from the indoor space flows to the AHU via the ceiling chamber space, and is pre-cooled on its way back to the AHU. A PCM ceiling board system can be a good way to reduce the peak indoor temperature for the building occupants' thermal comforts [18].

8.2.3 TES for Heating

Compared with the cold TES and airconditioning systems, the TES integrated with heating systems have a more limited market. The main applications are space heating, domestic hot water supply, etc. Similarly, it is beneficial to manage the electric load, and shift on-peak demand to off-peak hours. In this section, the hot water tank and aquifers, rock and brick reservoirs, PCM storage tanks, PCM wallboards, PCM floor used for building heating are introduced.

8.2.3.1 Sensible TES with Hot Water Tank or Aquifers

Water is a favored material for heat storage in building application due to its high specific heat compared with other sensible heat storage media. Water tank (as shown in Figure 8.9) and aquifer storage systems are the two common water-based storage systems for building heating applications.

In water tanks, water naturally stratifies because of the increasing density at lower temperatures: the hot water flows to the top, the cold water remains at the bottom, and the intermediate region is the thermocline. For the sensible heat storage, typical temperature differences usually

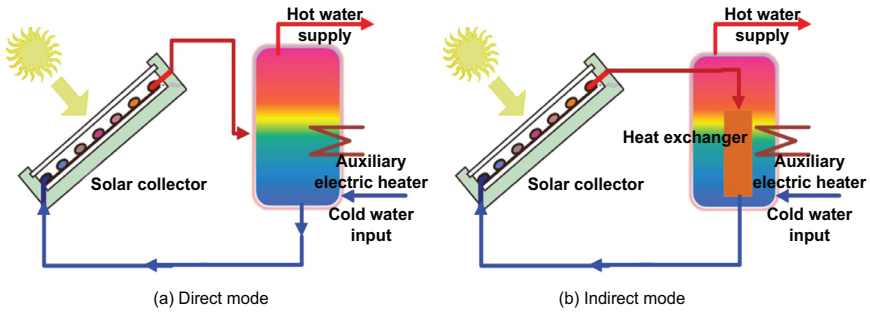

Figure 8.9. Schematic of domestic hot water system with auxiliary electrical heater.

range from 5°C to 10°C. The temperature scale for the space heating and domestic hot water production is usually at the operating range of 25°C to 80°C. One common application is the solar water heating, as shown in Figure 8.9. In the direct (open loop) configuration, the collector directly transfers the heat to the water in the tank without any intermediate heat exchanger, and water is the heat transfer fluid. Cold water enters at the bottom of the hot water tank and in turn passes through the solar collector, gets heated and delivers the heat at the top portion of water tank. In the indirect (closed loop) configuration, the heat transfer fluid does not mix with water in the tank. The hot water requirement is typically at a constant temperature, and solar radiation varies during the day. Therefore, it can be used with conventional heating and solar systems. The auxiliary heater installed in the tank is used to compliment the demand to maintain a constant water temperature.

The thermal stratification in the water storage tank is typically affected by several factors such as tank size and shape, location, geometry of inlets and outlets, temperature, and flow rates during charging and discharging. Similarly to the chilled water tank, strategies should be investigated to improve stratification. The water storage tank should be operated in a stratified manner so that hot water moves to the top from the bottom due to thermal buoyancy. It should be noted that the mixing effect caused by the temperature difference could degrade the heat source level and have negative effects on the system storage efficiency. The horizontally partitioned water tank achieved exceptional thermal stratification performance, and was efficient in heat storage application [19]. In addition, regarding the level of thermal stratification performance, it showed that in the forced-flow, direct solar water-heating systems, under realistic operating conditions, the fabric manifold is 4% more effective than the rigid manifold, and 48% more effective than the conventional drop-tube inlet [20]. More importantly, as a whole, various factors should be considered reasonably and one study [21] did the comprehensive investigation and summarized from the fluid mass flow rate, storage tank geometrical structure, fluid properties, fluid inlet temperature, etc. The study is beneficial for the researchers and engineers to design more efficient and optimized hot water storage systems. It should be noted that the water tank experiences heat loss. Effects of the water tank design and selection of the insulation materials (glass wool and polyurethane) on the reduction of heat loss should also be paid enough attention.

Aquifers are the geological formations containing ground water, and water in aquifers is sometimes mixed with the gravel or sand. Aquifers have the capacity to hold hot and cold temperatures for long periods,

especially when storage is available in large volumes. Heat storage in aquifers depends on extracting ground water from a well, heating this water with an available heat source, and then replacing it back into the aquifer in the other well, as illustrated in Figure 8.10. The groundwater that is extracted in summer time, is used for cooling by transferring heat from the building to the groundwater by means of a heat exchanger. Subsequently, the heated groundwater is injected back into the aquifer, which creates the storage of heated groundwater. In wintertime, the flow direction is reversed such that the heated groundwater is extracted and can be used for heating. Aquifer heat storage systems have lower investment and operating costs than classical water storage tanks. The allowable temperature change, the natural ground flow and potential environmental

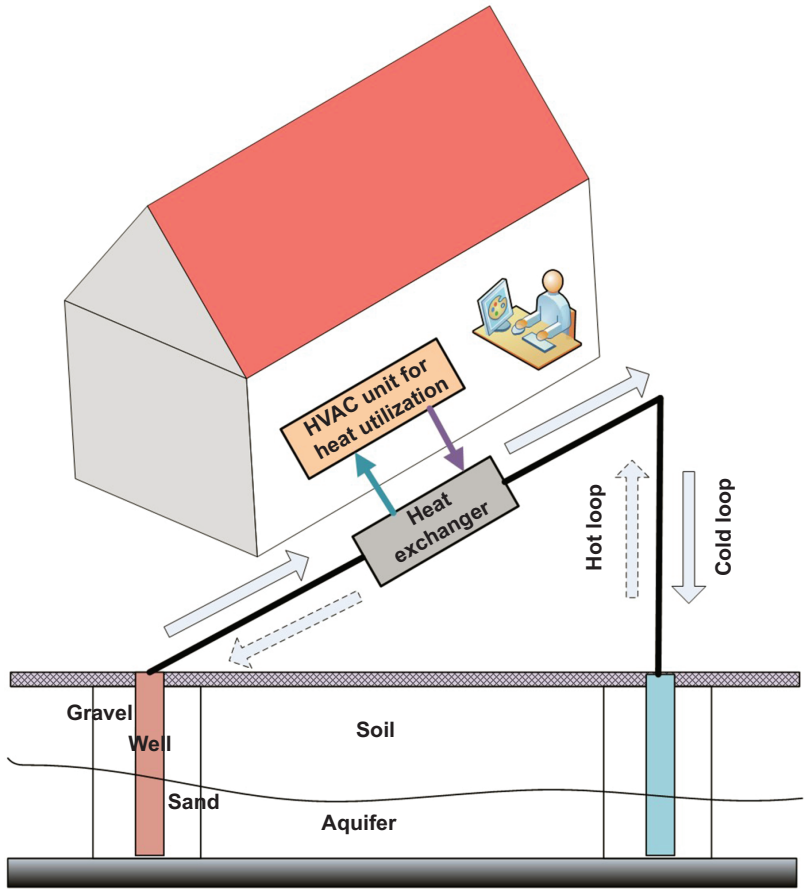

Figure 8.10. Schematic of aquifers [6].

factors should be considered for design and operation. Usually the hydrogeological conditions make the aquifer storage system quite complex and conditional. Now many countries and regions increase the use of aquifer TES to reduce greenhouse gas emissions and the number of aquifer TES has increased dramatically, especially in Europe. For example, in the Netherlands, a number of about 20,000 ATES systems could be achieved in 2020 was estimated [22]. This can possibly contribute the CO_2 emission reduction of about 11%, for the target of the Netherlands. Besides the Netherlands, Belgium, Germany, Turkey, and Sweden are also increasing the application of aquifer TES.

8.2.3.2 Rock and Brick Reservoir

In addition to the water, solid materials can also be used, such as the rock, metal, concrete, sand, brick, etc. The operating temperature range can be over 100°C. The solid storage has several inherent advantages over the water storage: it can withstand much higher temperatures, it has no leakage problems when contained, and the solid heat storage materials have good conductivity. Rock is the most commonly used heat storage material. Even though it has a lower volumetric thermal capacity, it is still effective at temperatures above 100°C. One example is Harry Thomason's technique using both water and stone as storage media, as shown in Figure 8.11 [23]. The collected heat can be stored both in the stone and water tank. The stored energy is then able to heat the cold air.

Another example is shown in Figure 8.12 [24]. During the off-peak periods (i.e., charging process) electric energy is converted to heat which is stored in the high mass units, or bricks, made of dense ceramic material. During the peak hours (i.e., discharging process), the power is shut off and an electric fan begins to transfer the heat from the brick to the house. The temperature is controlled by outside sensors. The sensors can adjust the amount of power intake so it can maintain a comfortable room temperature. In addition, sensible heat storage can use a large amount of water, such as the underground reservoirs or solar ponds.

In solid storage materials, the compatibility of the material and the heat transfer fluid used is very important. The storage performance is largely dependent on the solid material's size, shape, packing density, type of heat transfer fluid, etc. The main drawback of solid storage materials is their low specific heat capacity (~1200 $kJ \cdot m^{-3} \cdot K^{-1}$, where water is

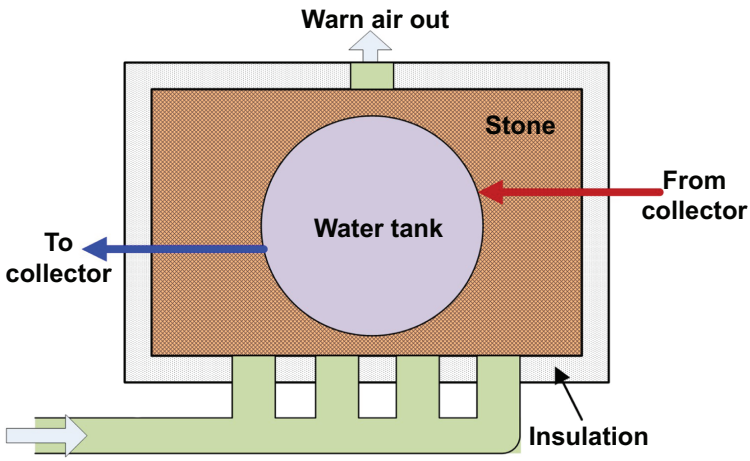

Figure 8.11. Harry Thomason's technique using both water and stone as storage media [23].

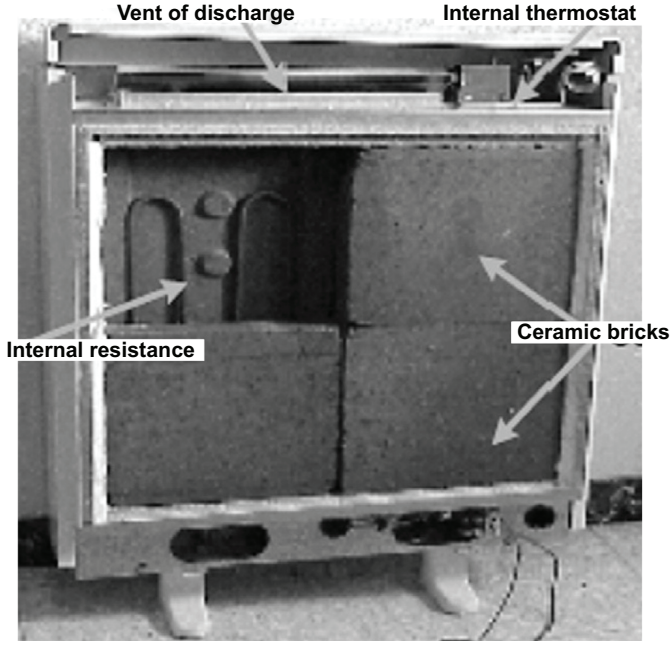

Figure 8.12. Sensible heat storage [24].

~4200 $kJ \cdot m^{-3} \cdot K^{-1}$), which causes a considerably low volumetric storage density. To achieve the same amount of heat storage, solid storage usually needs three times more volume than water-based storage system.

In another study, a pebble bed was used as the sensible storage material, as shown in Figure 8.13. This solar air heating system was designed for the water supply and space heating in a two-story building in Qinhuang Island, China [25]. The heating area was a 717 m^2 dormitory and a 2602 m^2 cafeteria. A 300 m^3 pebble bed was constructed to store surplus heat from the 473.2 m^2 solar collector during the daytime and was used as the primary heat source to meet the heat load during the night time. As shown in Figure 8.13, the heat from the solar air heating system flows to the indoor area and is then stored in the pebble bed. The experimental results revealed that the solar fraction achieved a mean value of 19.1%, and the highest value of 33.6% was observed in the second half of December 2010.

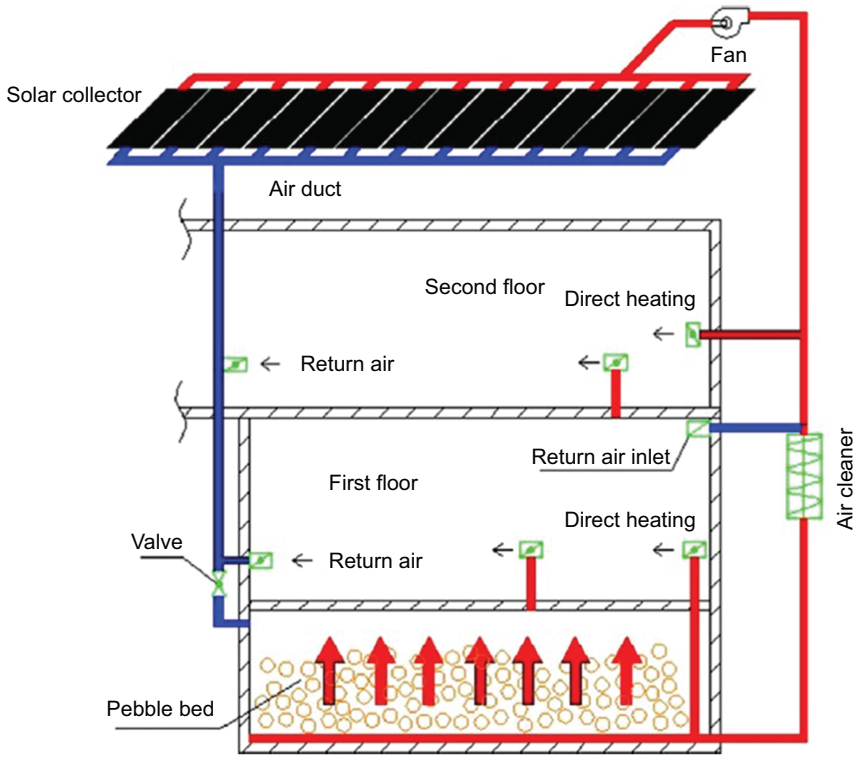

Figure 8.13. Schematic diagram of the solar air heating system in Qinhuang Island, China [25].

A Transient System Simulation Program (TRNSYS) modeling indicated that the designed system could reach an annual average solar fraction of 53% when operating under the optimal circumstances.

8.2.3.3 Latent TES with PCMs

Canbazoglu et al. [26] compared the PCM-charged solar water heating (SWH) systems to the conventional SWH systems without PCMs. The PCM-filled bottles were set in their storage system in three rows. The cross-sectional view of the system is shown in Figure 8.14. Without drawing off the hot water at night, the system could attain about 46°C. The storage time of hot water, the mass of the hot water produced, and

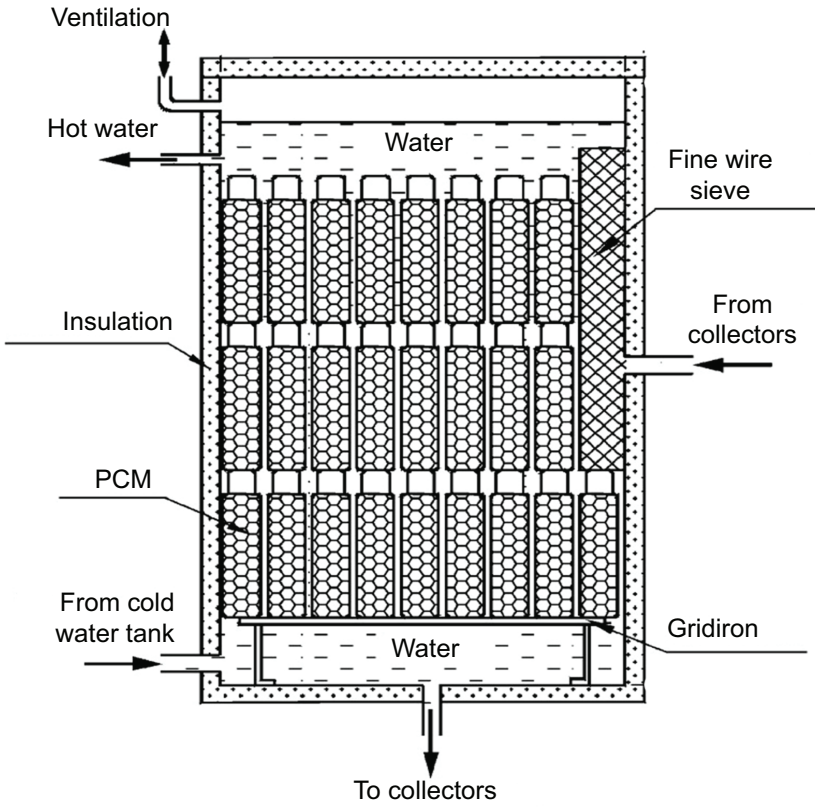

Figure 8.14. Cross-sectional view of heat storage tank integrated with PCM [26].

total heat accumulated in the solar water-heating system having the heat storage tank integrated with PCMs were approximately 2.59 to 3.45 times of that in the conventional SWH system.

One experimental evaluation using the PCM (6000 kg paraffin wax) unit for seasonal latent heat storage was performed for the heating system of a 180 m^2 greenhouse located in Turkey [27], as shown in Figure 8.15. There are five main parts in the system: flat plate solar air collectors, a latent heat storage unit, an experimental greenhouse, a heat transfer unit and a data acquisition system. Results indicated that the system reached an average efficiency of 40.4% for net energy.

8.2.3.4 PCM Wallboards

A PCM wall, which can capture a large portion of the incident solar radiation on the walls or roof of a building, has the benefit of minimizing the effect of large fluctuations in the ambient temperature on the indoor room temperature. With the high thermal mass of the PCM walls, it is very effective in shifting the cooling load to the off-peak electricity period. Usually the wall consists of glass, a transparent insulation material, a polycarbonate, a ventilation air layer, insulation, and an inside material (plaster) (as shown in Figure 8.16). Because of the glass and transparent insulation material, convective and radiative heat transfer can be prevented from the incoming short wave radiation. PCM can also absorb and store energy. The air for the house ventilation is heated in the air layer and then flows into the room.

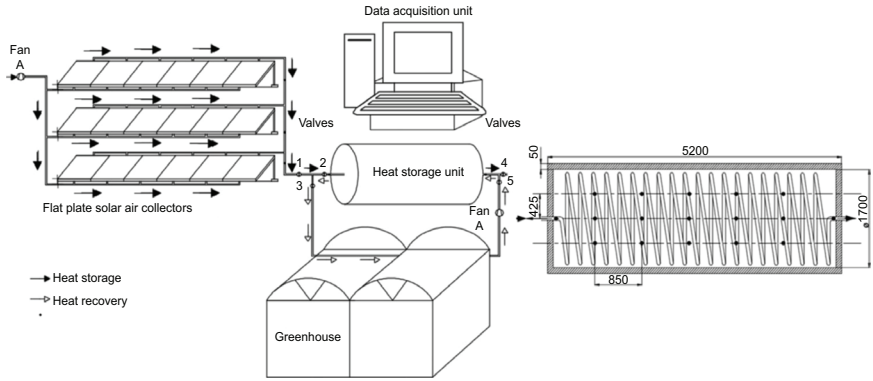

Figure 8.15. Schematic of thermal energy storage with paraffin wax in a greenhouse, Turkey [27].

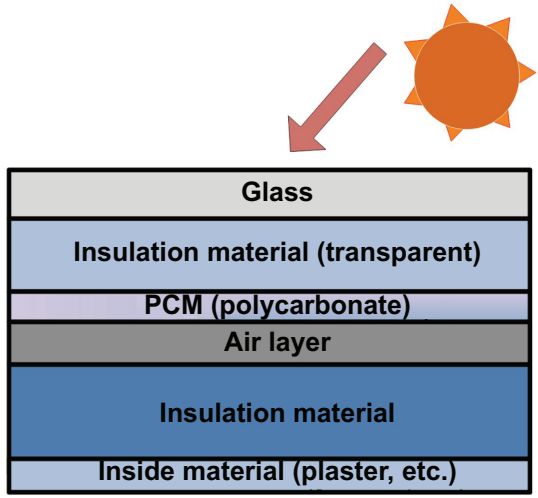

Figure 8.16. Elements of PCM solar wall.

8.2.3.5 PCM Floor Heating

An under-floor electric heating system with integrated PCM plate is shown in Figure 8.17 [28]. The under-floor heating system included polystyrene insulation, electric heaters, PCM, wooden supporter, air layer, and wood floor. Different from conventional PCMs, the shape-stabilized PCM can keep the shape unchanged during phase change process. Therefore, the risk of PCM leakage can be avoided. This system can charge heat by using inexpensive night time electricity and then discharges the stored heat in the day time.

8.2.3.6 PCM Ceilings

In the study for a space heating system with the PCM ceiling void [29], one passive solar unit was used to heat the perimeter zone of an office building during the less occupied hours (6:00 pm to 12:00 midnight) to decrease the use of perimeter heaters. The system integrated day light and PCMs for heat storage. Phase changing panels were embedded in the ceiling of an office space. The top of the light shelf was coated with a specularly reflective film such that 90% of the direct solar radiation incident upon it would be reflected toward the phase changing panel. The

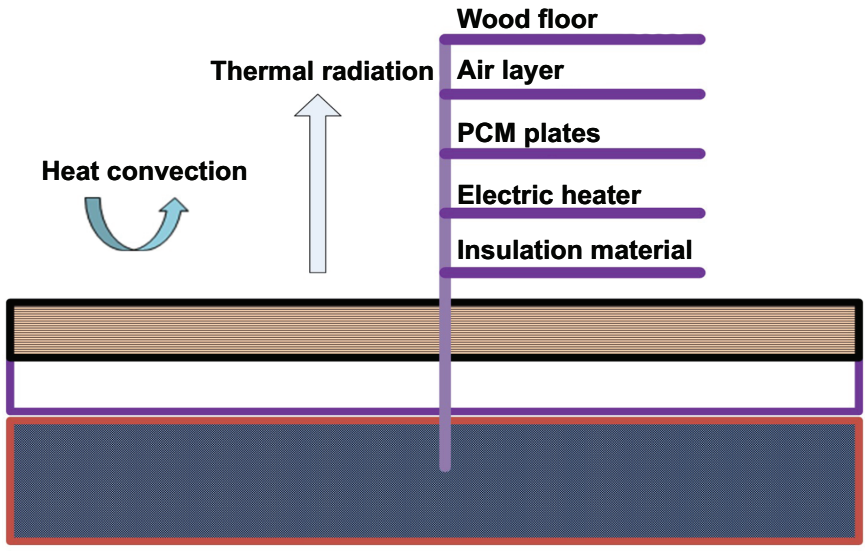

Figure 8.17. PCM assisted under-floor electric heating system [17].

main advantage of the system is that it allows a large area to be dedicated to heat storage without the need for large volumes of storage medium which would be required with sensible heat storage. The theoretically determined solar areas of the phase changing panel and the solar radiation data for the city of Montreal, Quebec, were used to determine the amount of solar energy available for passive storage for each daylight hour in an average day of each winter month (October to March). Simulation results showed it had the potential to recover 17% to 36% of heat lost over the initial gains.

8.2.4 TES and Heat Pumps

In this section, the heat pumps integrated with TES technologies are mainly introduced for heating or cooling in buildings. It is able to improve heat pump performance and decouple energy generation. The air-source heat pump remains popular in the market because it is less expensive, but its performance decreases when the external air temperature decreases. Unlike the air-source heat pump, which exchange heat with outside air, a geothermal heat pump utilizes the relatively shallow ground at relatively constant temperature. The ground at depths below the frost line

maintains such a stable temperature that geothermal systems are up to twice as efficient as air-source heat pumps, especially during cold weather. However, a geothermal heat pump is more expensive to install than an air source heat pump because of a ground heat exchanger installation.

A solar powered heat pump system incorporated with a cylindrical tank filled with 1090 kg $CaCl_2 \cdot 6H_2O$ as the PCM is shown in Figure 8.18 [30]. This system was used to supply heat for a floor heating system in a 75 m^2 area of a laboratory building in Turkey. Whenever solar radiation was available and space heating was required, the heat from the solar collector was charged into the PCM in storage tank. After that it could be used as a heat source for the water-source evaporator in the heat pump. Whenever solar radiation is not available, the PCM could supply heat for the heat pump system. In this way, the building energy consumption can be reduced by utilizing the renewable energy. However, the PCM is oversized to obtain the maximum energy that PCM could provide, which also leads to insufficient isolation for complete melting.

Another system with a ground source heat pump incorporated with a PCM (300 kg calcium chloride hexahydrate) storage tank, used for

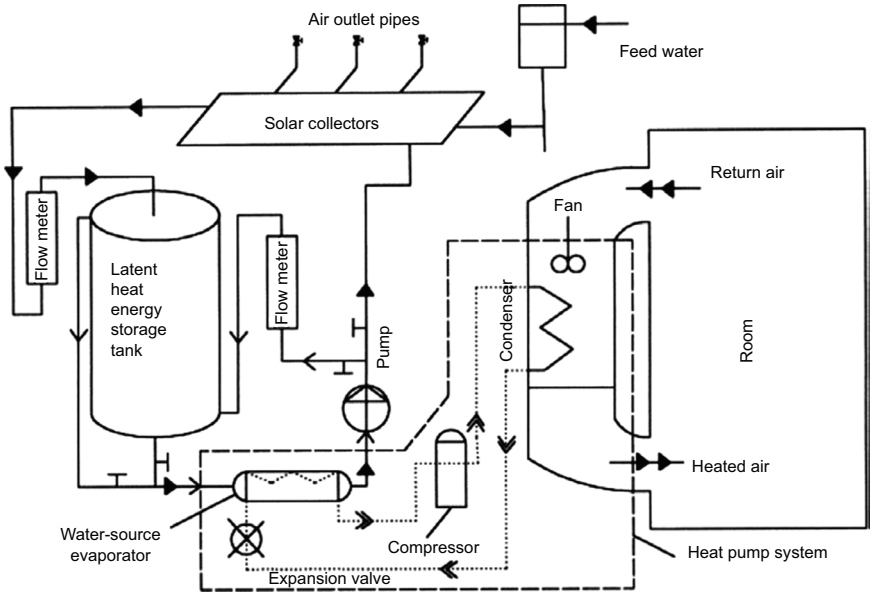

Figure 8.18. Solar assisted heat pump system with latent heat storage tank using $CaCl_2 \cdot 6H_2O$ [30].

space heating in a 30 m^2 glass greenhouse, was investigated in Turkey (as shown in Figure 8.19 [31]). The PCM storage unit could be charged from the solar radiation as well as from the heat pump. The PCM storage contributed to the rational heat distribution in the greenhouse due to its nearly constant phase changing temperature. Results obtained from October to May in the heating seasons of 2005 and 2006 showed that the COP of the ground-source heat pump varied from 2.3 to 3.8, and the combined COP of the whole system was 2 to 3.5.

In addition, Arteconi et al. [32] reviewed the thermal storage technologies for demand-side management and the application of reversible heat pumps in buildings. Reversible heat pumps are extensively used in the Asian and Pacific regions [33], where a lot of highly urbanized areas are characterized by hot summers and mild winters with temperatures that do not fall below 0°C, so the use of heat pumps for year round space conditioning is appropriate. Heat pump systems with TES, mostly heat pumps with the ice storage, have benefited from government subsidies and electric power utilities' promotions. When designing a heat pump system with TES, control strategies including the demand-side management with smart-grid concept, fuel cost and environmental protection benefit should also be considered [34].

The main barriers impeding the widespread use of the heat pumps are the large spaces required and the excessive drilling cost in the case

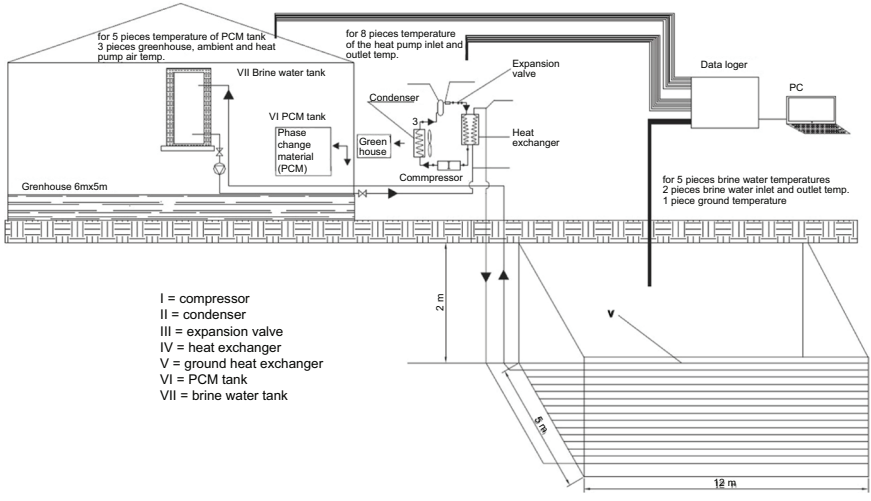

Figure 8.19. Schematic of the ground source heat pump with PCM tank [31].

of ground source heat pumps. There are also other issues such as noise, frosting on the evaporator, and insufficient performance of air source heat pumps at extreme ambient conditions. All these issues should be considered when using TES in heat pumps.

8.2.5 TES and CHP

The combined production of the heating and power (CHP) is the use of prime movers to simultaneously generate electricity and useful heat in a more efficient way than using two separate equipments. It can potentially reduce the operational cost, emissions, and the primary energy consumption. One issue for implementing CHP systems is a mismatch between the amount of the electricity and heat production by the CHP system and amount of electricity and heat demanded from buildings. In general, it is used when there is a low power-to-heat ratio (a ratio of the electric load to the thermal load) demanded by the building. Therefore, sometimes the surplus of heat production may not be used by buildings and would be wasted. In addition, the building demand varies under different ambient temperatures and climates, and this also adds the complexity of the design and application of CHP systems. TES can alleviate this issue by collecting surplus heat and delivering it to the building whenever a building thermal demand becomes higher, and could significantly reduce the size of the additional boiler needed to meet the building thermal demand. It may also result in the significantly reduced carbon dioxide emissions. TES devices help use of the residual heat better, which in turn results in better efficiency, economical operation, and lower economic risk [35–39]. In this section, the combined heating, cooling, and power (CCHP) and micro-CHP systems integrated with TES are introduced. In addition, there is one chapter on CHP included in Handbook.

The general layout of a CHP system with TES is shown in Figure 8.20. The prime mover is interconnected with the external electric network, the internal electric circuit, the TES system, the auxiliary boiler, and the heat distribution network. When the heat supplied is larger than the demand of the building loads, the surplus can be accumulated and stored in the TES system. The heat from the TES system can also form renewable or low-grade industry waste heat. When the instantaneous thermal demand is lower than the heat produced by the CHP prime mover, the stored energy can be utilized. The electricity produced by the prime mover can be sent to the buildings for electric loads, and the surplus of the electricity produced

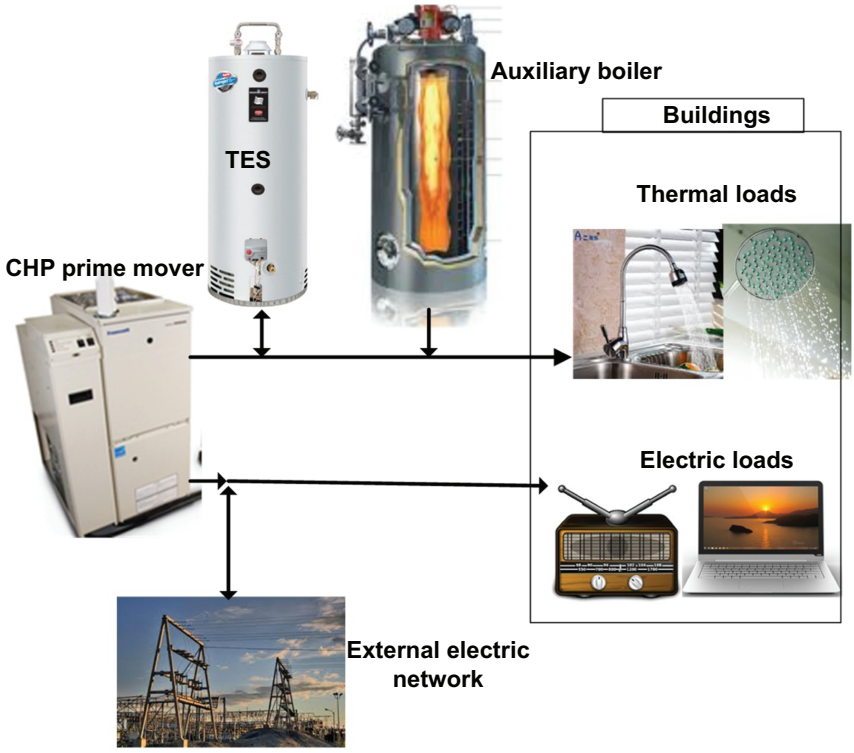

Figure 8.20. General layout of CHP system with TES.

can be exported to the external electric grid. When the instantaneous electrical demand is higher than the electric power provided by the prime mover, electricity is taken from the external grid. The function of the auxiliary boiler is to fulfill thermal demands whenever the combination of heat provided from the prime mover and the heat accumulated in the storage system is lower than that of building thermal loads.

One CCHP system integrated with TES was investigated for service buildings. The TES device was a stratified hot water tank, and supply and return temperatures were 90°C and 60°C, respectively. Figure 8.21 [40] depicts a CCHP system, which included a conventional gas engine, heat exchangers, an absorption chiller, and a TES tank. A single-effect absorption chiller was preferred over a double-effect absorption chiller because it was more cost-effective and, unlike the latter, it was able to work with heat sources at both low and high temperatures.

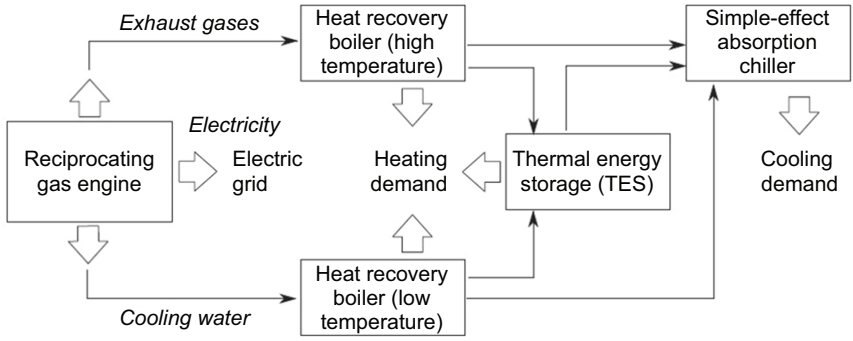

Figure 8.21. Diagram of the CCHP system with TES [40].

Optimal volume (vol_{opt}) and maximum TES volume (vol_{max}) were calculated for selected cases in to compare their values and the impact of both sizes on primary energy savings (PES) index of the plant. The obtained results are shown in Table 8.5 [40], which allows comparing the performance of the plant without TES device (columns 2 and 3), when a TES of optimal size is installed (columns 4, 5 and 6) and when the maximum feasible TES is considered (columns 7, 8 and 9). Results showed that in every case, the inclusion of a TES device of the system resulted in a significant improvement of the PES index, of similar magnitude for vol_{opt} than for vol_{max}. Regarding economic results, installing a TES unit can increase annual economic returns of the system (with both the optimal and the maximal volume) up to 15% in the cases analyzed.

Plants with PES <0 are not qualified to be considered as a special regimen for electricity sales so that they are unfeasible under the considered economic context. It was studied for the case without TES (columns 2 and 3), for the optimum TES size (columns 4–6) and for the maximum feasible TES (columns 7–9).

In another study, the CHP plant that incorporated a water TES system was installed for sustainable energy production [41]. This paper analyzed the economics and optimum size of CHP operating with gas engines and thermal stores in British market conditions. It revealed that the high variation in the electricity prices between day and night allows the thermal storage to improve the economics of CHP plants in the UK. It also showed that the thermal storage allows the engine to be operated as a priority during hours of high electricity prices. The economical size of CHP plant for a district or community heating load of 20,000 MW·h per year is found to be a 3 MW power gas engine with a 7.8 MW·h (250 m^3)

Table 8.5. Performance of the CCHP Plant for Different Demands and Operation Periods in Terms of Efficiency (PES: Primary Energy Savings) [40].

Operating hours (hr)	Without TES	With optimal TES		With maximal TES	
	PES^0 (%)	vol_{opt} (m^3)	$(PES)_{opt}$ (%)	vol_{max} (m^3)	$(PES)_{max}$ (%)
Hotel					
4000	12.4	20	14.0	47	14.3
5000	10.1	50	13.7	62	13.8
6000	7.2	40	9.9	59	10
7800	0.3	144	5.2	144	5.2
8760	−2.8	100	1.8	144	1.9
Shopping Center					
4000	5.8	40	8.6	70	8.8
5000	0.7	40	3.9	70	4.1
6200	−4.4	90	2.3	104	2.4
7200	−8.1	136	0.6	136	0.6
8760	−12.8	213	−1.4	213	−1.4
Hotel+Shopping Center					
4000	13.2	0	13.2	0	13.2
5500	13.3	10	13.8	32	14.1
6500	10.5	50	13.1	79	13.2
7300	7.1	80	12.4	103	12.5
8760	1.7	160	11.0	171	11.0

thermal storage. In this case the analysis revealed that the use of a thermal storage more than doubled the return of investments when compared with the same size of a plant without a thermal storage. It was concluded that thermal storage can improve the overall economics of CHP plants in present British markets.

One study was performed for a technical and of a cost analysis of residential micro-CHP plants in Italy with two different types of TES systems (hot water TES and PCM TES using sodium acetate trihydrate) [42]. For each micro-CHP system, when focused on the hot water system, the tank cost almost is accountable for the component's total cost, covering a percentage of about 98%. Otherwise, relative to each latent heat system, the heat exchanger and the PCM together represent about the 35% of the total cost of the latent heat thermal energy storage system's components. Results also showed that the total cost of the TES

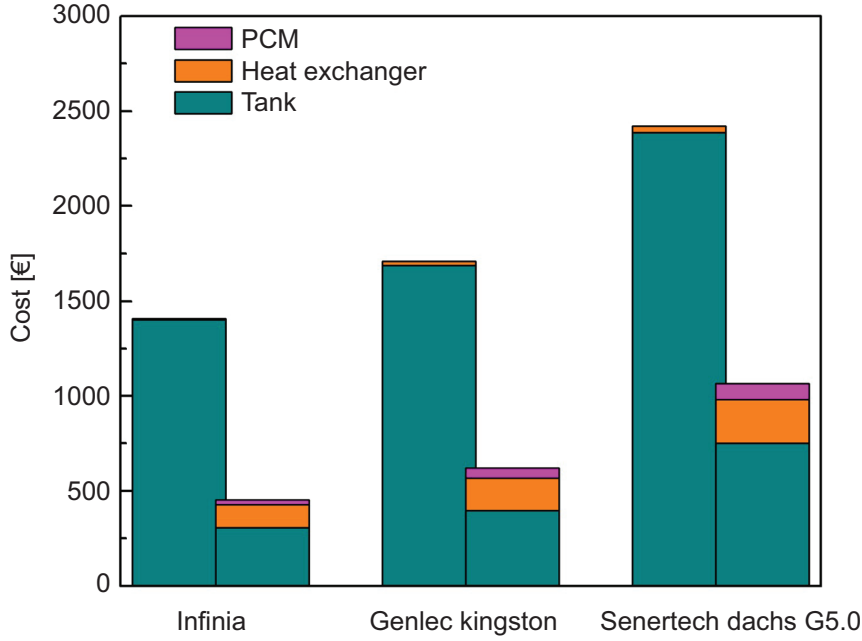

Figure 8.22. Sum of the hot water heat thermal energy storage systems components costs (left bar) and latent heat ones (right bar) for the micro-CHP systems relative to the single-family house [42].

components is consistently significantly lower for latent heat storage. This result is particularly noticeable in Figure 8.22 [42]. Furthermore, the difference in terms of the total cost of the components between the two types of thermal energy storage systems decreases as the storage system capacity increases. The tank volume of the latent heat TES system is about 30% of the volume of the corresponding hot water tank, due essentially to the significantly higher energy storage density of the PCM. It has also shown that the total heat transfer areas when compared with the heat exchangers of the latent heat thermal energy storage systems are more than four times larger than those of the corresponding heat exchangers relative to the hot water thermal energy storage systems, due to the very low thermal conductivity of the PCM, which represents the major limiting factor of this category of materials in heat storage applications.

An experimental study was carried out to evaluate the thermal behavior of different PCM TES units used in a micro-CHP system [43]. A cylindrical TES tank was used to compare the performance of two PCMs

with different melting temperatures and encapsulation methods, whereas using a water-filled unit as a reference scenario. The first concept consists of cylindrical PCM tubes, whereas the second uses small spherical PCM capsules. The analysis involves three different tests: constant inlet temperature, constant power, and partial capacity loading. Results showed that the PCM tubes were characterized by a higher capacity when a low thermal power was applied, whereas the PCM capsules were able to store more energy at higher power. The operating temperatures in partial loading tests indicated that the incorporation of PCM storage units in a smart grid environment may be beneficial to the effectiveness of the thermal system.

Another study by Dorer and Weber [44] investigated the performance of different micro-CHP in buildings with systems that incorporated low temperature floor heating and hot water tanks. It has been concluded that this technology had not been developed well enough and faced strong competition in the market with other innovative supply options such as heat pumps. Actually, TES can be a good way for load management for micro-CHP systems to manage the thermal loads of buildings [45].

8.2.6 Building with TES Integration Literature Summary

In section 8.2, different TES systems incorporated in buildings are introduced with examples demonstrating TES systems' energy savings and CO_2 emission reduction. Table 8.6 shows the available information that was collected for TES techniques integrated in buildings. Results showed that a large part of the studies in residential buildings were conducted using modeling basis. It is because the modeling simplifies the process used in prediction of a building's performance instead of the complicated experimental approaches. The possible performance improvements could be achieved by using TES in buildings, such as reducing energy expenses by introducing renewable energy (solar energy, free cooling, etc.), reducing the power required during heating/cooling peaks by using the water or PCMs, or making small changes to how indoor room temperature is controlled by using the PCM wallboards or the PCM ceiling board.

TES already became an important part of the building sector. Water storage tank for domestic hot water production paired with solar collectors and/or boilers has been actively used in buildings. Using PCMs to increase the thermal mass of buildings has become popularized. Commercial products are already available such as PCM plaster boards.

Table 8.6. Literature Summary for TES in Buildings [46].

Storage technique	Studied buildings	Methodology	Focus of studies	Main results	Ref.
Passive sensible storage	Single and multi-family buildings	Almost exclusively simulations.	Majority on energy savings, but also comfort and peak reduction	Most studies report small energy saving potential but more stable indoor temperature.	[47–50]
Sensible storage in tanks	Single and multi-family buildings	Single and multi-family buildings	Emission reduction, system evaluation, peak reduction	Emission reduction from boilers and heating peak load reduction possible.	[51–55]
Sensible storage in tanks	University	Case study on real building	Peak reduction	Significant peak demand reduction.	[55]
Storage in pits, buried tanks, etc.	Apartment complexes	Studies on real buildings	Switch in energy source	Possible to reach a high solar fraction. Heat losses from stores are fairly high.	[54, 56]
Borehole storage	Single family houses, residential complex	Studies on both real buildings and simulation	Evaluation of existing systems, switch in energy source	A seasonal borehole storage system is capable of meeting the heating demand even in severely cold areas.	[57–62]

(Continued)

Aquifer storage	Hospital	Case study in real building	Switch in energy source	Considerable reduction in use of fissile fuels as compared with a reference system.	[62]
Borehole storage	University complex	Case study in real buildings	Switch in energy source, energy evaluation	Potential for large reduction in purchased energy.	[63]
Snow storage	Office building, hospital	Prototype testing, case study in real building	Switch in energy source	Significant primary energy reduction. Construction cost reductions necessary. Large space requirement.	[64–66]
Passive latent storage	Single and multifamily buildings, test cubicles	Simulation and experiments	Majority on comfort, but also for energy savings and peak reduction	Reduction of excess temperatures and cooling demand, small reduction in heating demand.	[50, 67–69]
Latent storage in tanks	Solar low energy buildings	Simulation	Energy savings	No significant improvement of PCM compared with water for heating applications.	[70]

(Continued)

Table 8.6. Literature Summary for TES in Buildings [46]. (*Cont.*)

Latent storage in ventilation or AC unit	Single family houses	Simulation	Improved indoor climate, energy savings	Considerable reduction of excess temperatures. Reduced ventilation load.	[71, 72]
Passive latent storage	Single office	Simulation	Reduction of excess temperatures	Operative temperature can be reduced summer time but results show high dependence on climate and PCM properties.	[73]
Latent storage in tanks (ice storage)	Small and large office buildings	Case study in real buildings, simulation	Energy savings, peak reduction, energy evaluation	Efficiency of cooling system improved, large peak reductions. Benefits depend on climate and many other factors.	[74, 75]
Latent storage in ventilation or AC unit	Small office building, single offices, commercial complex, school	Experiments in real building, simulation, prototype testing	Heat transfer improvement of store, switch in energy source, excess temperature reduction	Cost and space reduction possible if heat transfer can be improved. CO_2 emission can be reduced.	[76–79]

Water storage tanks are already used successfully to a large extent for short term storage purpose. However, for long term storage in buildings, it is still difficult to apply due to heat loss through storage tank. It is possible to use seasonal storage (such as the borehole and aquifer storage) in larger residential complexes or in small communities while adopting good installation strategies and careful geological investigations. There are also many issues regarding PCMs, such as corrosion and supercooling issues for building applications, which need further investigation.

8.2.7 Materials for Sensible/Latent TES

Early in 1983, Abhat [80] suggested a useful classification of the substances used for thermal energy storage, as shown in Figure 8.23. The melting temperature and fusion heat of existing PCMs are shown in Figure 8.24 [81]. PCMs with high latent heat can show the ability to reduce the size of storage systems.

Requirements for TES materials, especially PCMs, which can be used for building applications, are summarized as follows:

- Large specific heat capacity for sensible materials;
- Proper phase change temperature range (it depends on cooling or heating requirement) and pressure (usually near atmospheric pressure);

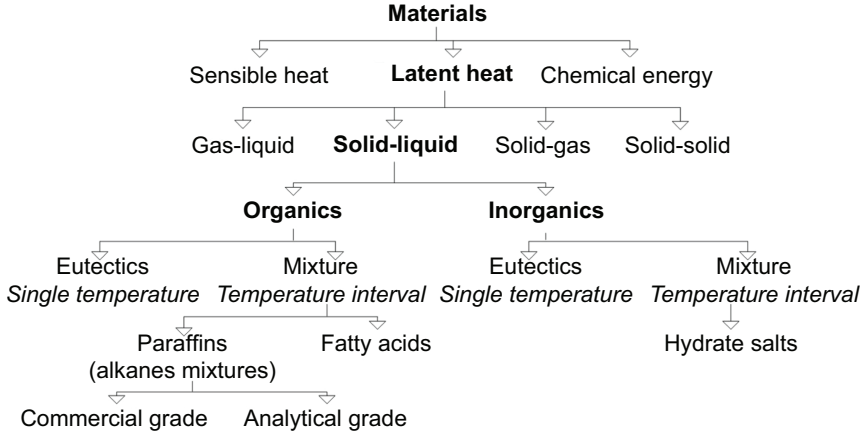

Figure 8.23. Classification of PCMs [80].

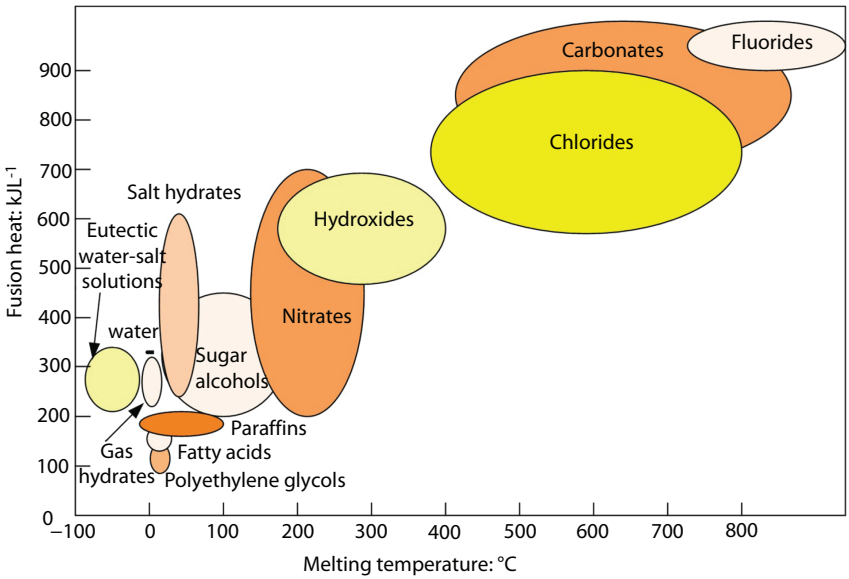

Figure 8.24. Melting temperature and fusion heat of existing PCMs [81].

- Large fusion heat, which allows for a more compact storage tank;
- Reproducible phase change, also called cycling stability, which can use the materials multiple times for storage and release of thermal energy with consistent performance;
- Good thermal conductivity helps speed up phase change progress, and low supercooling degree;
- Stable chemical properties, low corrosivity, and low environmental impact factors, such as zero Ozone Depletion Potential (ODP) and low Global Warming Potential (GWP); and
- Easy manufacturing and low cost.
- PCMs should be penetrated in the fireproofing and insulating materials, such as rock wool, fiber mineral wool, and silica aerogel. The adoption of passive fire protection materials (PFP), for example, installation of protective coatings able to withstand severe fire exposure conditions, may represent a highly safe and effective solution.

Generally it is difficult for a sensible material to satisfy all of the requirements listed, but chilled water is commonly used for cooling demand because it is inexpensive and available everywhere. Hot water, soil, and rock are common materials to meet heating demand in buildings. Table 8.7 lists a comparison of several commonly used sensible heat

Table 8.7. Comparison of Sensible Storage Concepts [82].

Hot-water	Gravel-water	Duct	Aquifer
Storage medium			
Water	Gravel-water	Ground material (soil/rock)	Ground material (sand/gravel-water)
Heat capacity (kW h·m^{-3})			
60–80	30–50	15–30	30–40
Storage volume for 1 m^3 water equivalent			
1 m^3	1.3–2 m^3	3–5 m^3	2–3 m^3
Geological requirements			
• Stable ground conditions • Preferably no groundwater • 5–15 m deep	• Stable ground conditions • Preferably no groundwater • 5–15 m deep	• Drillable ground • Groundwater favorable • High heat capacity • High thermal conductivity • Low hydraulic conductivity (k_f< 1.10 m/s) • Natural groundwater flow <1 m/a • 30–100 m deep	• Natural aquifer layer with high hydraulic conductivity (k_f>1.10 m/s) • Confining layers on top and below • No or low natural ground flow • Suitable water chemistry at high temperatures • Aquifer thickness 20–50 m

storage methods [82]. To choose a suitable storage medium, the relevant boundary conditions should be considered, such as available site size, local geological conditions, legal issues about drilling, temperature levels of the store, and investment costs. Duct and aquifer storages rely more heavily on the geological characteristics. Geological investigations should be performed in detail prior to designing a storage system because the hydraulic conductivity and natural groundwater flow can severely affect the system performance.

In Table 8.8, a comparison of the main features of common sensible and latent TES systems is provided [83]. The organic heat storage materials are mainly paraffin and non-paraffin (mainly fatty acids). Usually organic materials have negligible supercooling, non-corrosiveness, chemical stability, self-nucleation, no phase segregation, and low cost operation. However, they have issues of low thermal conductivity (~0.2 $W \cdot m^{-1} \cdot K^{-1}$), significant volume change, and flammability. Pure paraffin is very expensive, and therefore only technical grade paraffin (mixture of pure substances) is used for latent heat storage applications. Non-paraffin organic PCMs (fatty acids) also have corrosion issue. The organic heat storage materials should not be exposed to extreme heat sources or flames at high temperature. The inorganic storage materials are mainly salt hydrates. Salt hydrates have relatively high volumetric storage density and high thermal conductivity, and they are cheaper

Table 8.8. Comparison of Main Features of Different Methods of Heat Storage [83].

Property	Rock	Water	Organic PCM	Inorganic PCM
Density ($kg \cdot m^{-3}$)	2240	1000	800	1600
Specific heat ($kJ \cdot kg^{-1}$)	1.0	4.2	2.0	2.0
Latent heat ($kJ \cdot kg^{-1}$)	–	–	190	230
Latent heat ($kJ \cdot m^{-3}$)	–	–	152	368
Storage mass for 1 MJ (kg)	67,000	16000	5300	4350
Storage volume for 1 MJ (m^3)	30	16	6.6	2.7
Relative storage mass	15	4	1.25	1.0
Relative storage volume	11	6	2.5	1.0

than organic materials. However, they are poor in cycle stability, corrosion, and supercooling. The advantages and disadvantages of organic and inorganic materials are compared in Table 8.9, and possible solutions are also listed.

Figure 8.25 summarizes the possible techniques for enhancing heat transfer in latent heat material [84]. The performance of micro-encapsulated PCMs was expected to exceed conventional PCMs since small PCM particles provide larger heat transfer area per unit volume for a higher heat transfer rate. PCMs in metal structures have also proven to be a good way to enhance thermal conductivity. In addition, PCMs with highly conductive, porous materials and nanoparticles can still offer a promising alternative to improve the heat transfer processes in PCMs.

8.2.8 Mathematical Modeling of Storage System

Mathematical modeling of storage system is beneficial for improving performance and decreasing expenses. One problem that cannot be neglected is the Stefan problem for PCMs. Stefan problem (also Stefan task) is a particular kind of boundary value problem for a partial

Table 8.9. Comparison of PCM for TES Systems.

Organics (paraffin, fatty acids, etc.)	
Advantages	*Disadvantages and possible solutions*
No corrosives	Lower phase change enthalpy: adding inorganic PCMs
Low or none undercooling Chemical and thermal stability	Low thermal conductivity: adding high conductivity porous materials and nanoparticles. embedding graphite matrix in PCMs Inflammability: the shape-stabilized PCM composites using a polymer supporting material
Inorganics (salt hydrates, etc.)	
Advantages	*Disadvantages and possible solutions*
Large thermal conductivity	Corrosion: Use of corrosion resistant container
Large fusion heat Large density Low price	Phase separation: Adding another material such as water with a gelling or thickening agent can hinder the separation and sinking of heavier phases super-cooling: use of nucleating agents, cold finger, and porous heat exchange surfaces

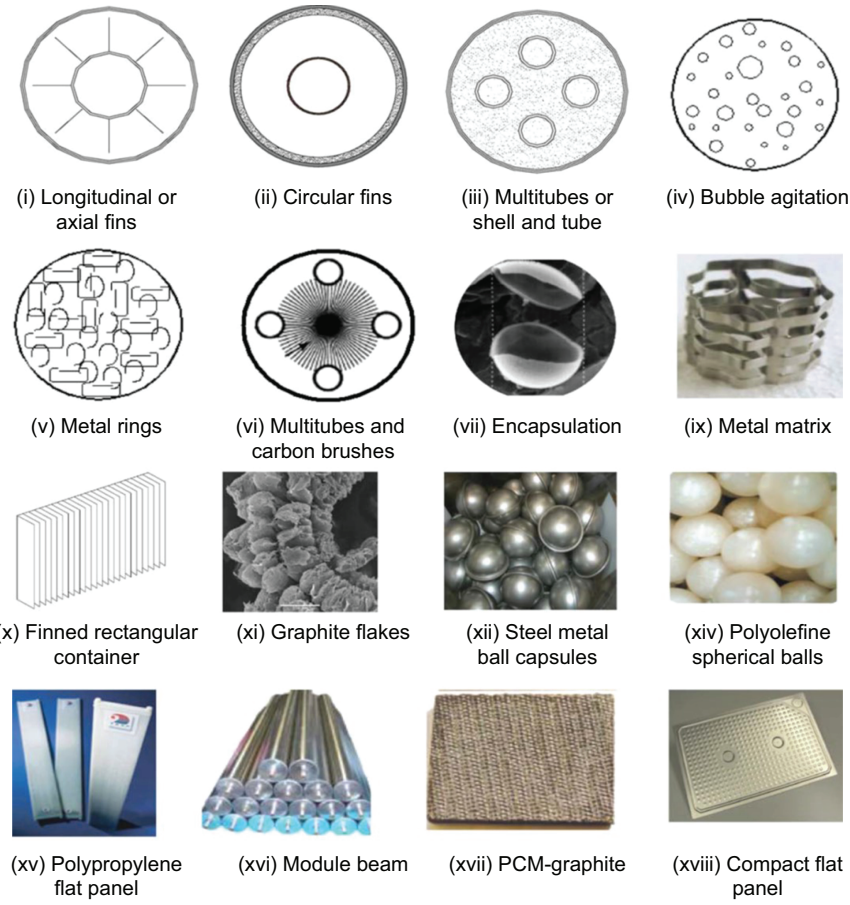

Figure 8.25. Heat transfer enhancement methods used in latent heat material research [84].

differential equation (PDE), adapted to cases in that a phase boundary can move with time. The classical Stefan problem aims to describe the temperature distribution in a homogeneous medium undergoing a phase change. For an example, ice melting problem can be solved with the heat transfer equation by imposing the initial temperature distribution on the whole medium, and a particular boundary condition, the Stefan condition, on the evolving boundary between its two phases. Note that this evolving boundary is an unknown (hyper-) surface: hence, Stefan problems are examples of free boundary problems. Usually there are very few analytical solutions in closed form. Currently there are many models established for PCM storage that consider boundary conditions. For most

cases, analytic expressions, simplified models, or correlation functions were developed to serve as practical guidelines in optimizing design of PCM storage in buildings. In addition, usually the numerical predictions are validated by means of appropriate experimental data, accompanied by addressing the issues of stability and convergence during the modeling process. Numerical methods for TES storage was collected by Dutil et al. [85], and the models in spherical geometries are shown in Table 8.10.

Regarding the mathematical modeling for TES storage, analytical solutions were involved in early studies to validate the model for selected problems which admit closed-form solutions. Recent studies rely more on commercial codes, and there is more discussion that relates to stability, convergence, grid independence, and other related numerical issues.

8.3 Sorption TES System for Buildings

Among several typical storage systems, the sensible TES technology is a mature technology and has already been implemented in many large-scale demonstration projects and plants. However, energy storage density (ESD) of the sensible TES is relatively low, leading to large storage volume. In contrast, the latent TES technology has a much higher ESD with a narrow temperature interval. However, the latent materials usually have the issues of crystallization, corrosion, etc. In addition, they can only store energy efficiently around phase transition temperature level. Regarding sorption TES technologies, sorption is the general phenomenon resulting from the interaction between an absorbent/adsorbent and a refrigerant, based on a reversible physical or chemical reaction process. In theory, sorption materials have a high ESD. Moreover, input and output temperature levels of the adsorption TES can be determined by practical demands and operating conditions, exhibiting some extent of flexibility. There are less moving components for sorption TES system so that it is quiet during its operation. In addition, the sorption heat can be stored for a long time without causing pollution and with negligible heat loss.

8.3.1 Working Principle of Sorption TES System

8.3.1.1 Absorption TES Working Principle

A schematic diagram of the basic principle of the absorption storage is shown in Figure 8.26. Using the working pair H_2O/LiBr as an example,

Table 8.10. Models for Spherical Geometry [85].

Model	Material	Numerical formulation		Comment	Validation
Roy and Sengupta [86]		MM FD	2D	Treatment of convection Two zones model	Numerical [99] [51−55]
Barba and Spriga [87]	37.5% NH_4NO_3 + 62.5% $Mg(NO_3)\cdot 6H_2O$	A	1D	Transient position of interface, temperature distribution, melting fraction, energy released, and duration of complete solidification	No
Fomin and Saitoh [88]	n-Octadecane	A	2D	Contact melting on unfixed solid phase	Experimental [100] Numerical [101, 102]
Adref and Eames [89] and [90]	Ice			Capsule filled a 80% with an air cell on the top	Eames and Adref [103]
Ismail and Henriquez [91]		MM FD	1D	Numerical correlation relating the working fluid temperature to the time has been produced	Numerical [104−106]
Ismail and Henriquez [91]	Ice	MM FD	1D	Analysis of the impact of thermal conductivity of the shell material	Yes

(*Continued*)

Table 8.10. Models for Spherical Geometry [85].

Veerappan et al. [93]	Various PCM	A	2D	Solidification and melting of sphere with conduction, natural convection, and heat generation	Experimental [103]
Regin et al. [94]	Paraffin wax	FD		Convective environment outside capsule	Yes
Bilir and Ilken [95]		FG	1D	Correlations which express the dimensionless total solidification time of the PCM in terms of Stefan Number, Biot Number and Superheat Parameter were derived	Numerical [92, 107, 108]
Assis et al. [96]	Parrafin wax RT27	MM CFD	2D	Partly filled capsule with open end	Yes+experimental [109, 110]
Khodadadi and Zhang [97]	Beeswax	FG	2D	Constrained melting	Yes
Tan et al. [98]	n-Octadecane	MM CFD	2D	Constrained and unconstrained melting	Experimental [111]

Note: A = analytic; CFD = Computed fluid dynamics; FD = finite difference; FE = finite element; FG = fixed grid and MM = moving mesh.

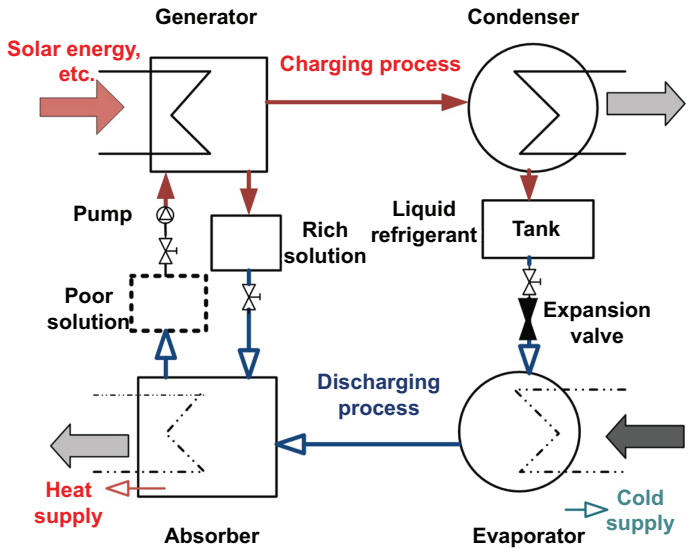

Figure 8.26. Schematic diagram of absorption TES.

with the shut-off valve after the poor solution opened, the poor solution (low concentration of absorbent) is pumped towards the high-pressure zone, and then the mixture is heated in the generator during the charging process. The contribution of heat (driving source) allows the separation of the refrigerant (H_2O) from the absorbent (LiBr solution). The refrigerant vapor is sent to the condenser, where it is condensed to liquid by a cooling fluid. The liquid refrigerant is stored in a container for TES, whereas the rich solution from the generator is also stored in a container. The liquid refrigerant in the container as the TES can be used to produce the cooling effect for air conditioning application in the evaporator or produce the heating effect for hot water in the absorber. During the discharging process, the shut-off valve after the poor solution is closed, the liquid refrigerant is expanded with the shut-off valve on the liquid refrigerant side opened and sent to the evaporator, and rich solution flows to the absorber with the shut-off valve on the rich solution side opened. Thus, the water vapor in the evaporator is absorbed by the rich solution and the cooling effect is produced in the evaporator at low pressures. And the rich solution absorbs the water vapor and releases absorption heat, which can be used for heating purposes. Gradually, the poor solution from the absorber is stored in a container. For an example, the solar energy can be utilized in the daytime in summer to store energy and release cold or heat whenever the demand is needed.

Absorption refrigeration technology is well developed and its systems are available in the market. Regarding the absorption TES, modification of the configuration of existing absorption refrigeration for energy storage purpose seems more attractive and realistic.

8.3.1.2 Adsorption TES Working Principle

To illustrate the working principle of adsorption TES for buildings, ref. [6] with working pair water/zeolite for residential application is used for convenience. It is a kind of physical adsorption cycle. In this study, Mitsubishi Plastic (MPI) FAM-Z01 made of zeolite was used for the adsorbent bed material and water as the refrigerant. Adsorption cold storage is shown in Figure 8.27. During the charging process, hot water (70°C) is used to regenerate the adsorbent in the desorption bed. The adsorbate vapor (i.e., refrigerant) is separated from the desorption bed and condensed into the ambient cooled coils (30°C) in the condenser. The liquid refrigerant flows to the evaporator and is stored there. Finally, the pressures of the desorption bed, condenser and evaporator are at the refrigerant saturation pressure of the ambient temperature. After the charging process is finished, all valves between chambers are closed. Then the adsorption bed is cooled at the ambient conditions (i.e., pre-discharging process at 30°C). Its pressure is greatly decreased below the refrigerant's saturation pressure at ambient temperature. As the discharging process begins (the valve between the adsorption bed and the evaporator chamber opens), the pressure difference between the evaporator and the adsorption bed forces the refrigerant flows from the evaporator to the adsorption bed. The decreased pressure in the evaporator chamber makes the evaporating temperature of falling film liquid refrigerant at the chamber bottom be decreased. It absorbs heat from the chiller water coil so that the cooling is produced in the evaporator to meet the loads.

The operating principle of the heat storage is introduced in Figure 8.28 (here it is a kind of short term heat storage). First, during the charging process, thermal energy (70°C) is used to regenerate the adsorbent in the desorption bed. The adsorbate vapor (i.e., refrigerant, here is water) is separated from the desorption bed and condensed by ambient cooled coils (30°C) in the condenser. The liquid refrigerant is stored in the condenser. At the beginning of the charging process, the pressure in the desorption bed and condenser increases greatly. Finally, the pressures of desorption bed and condenser are at the refrigerant saturation pressure of the ambient

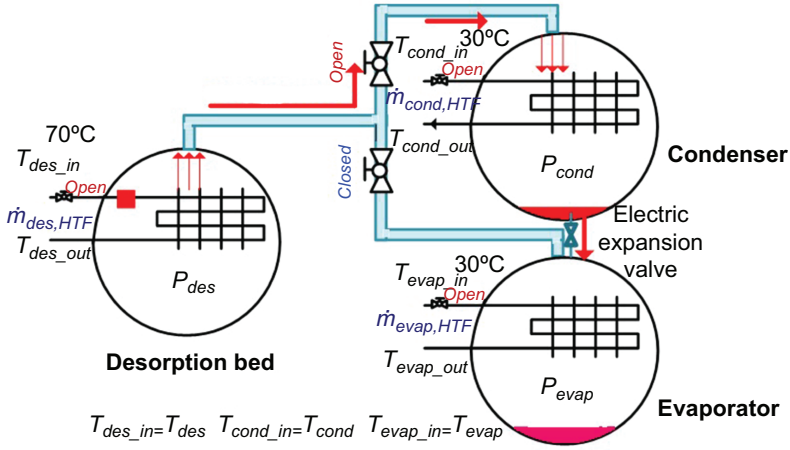

(a) Charging process

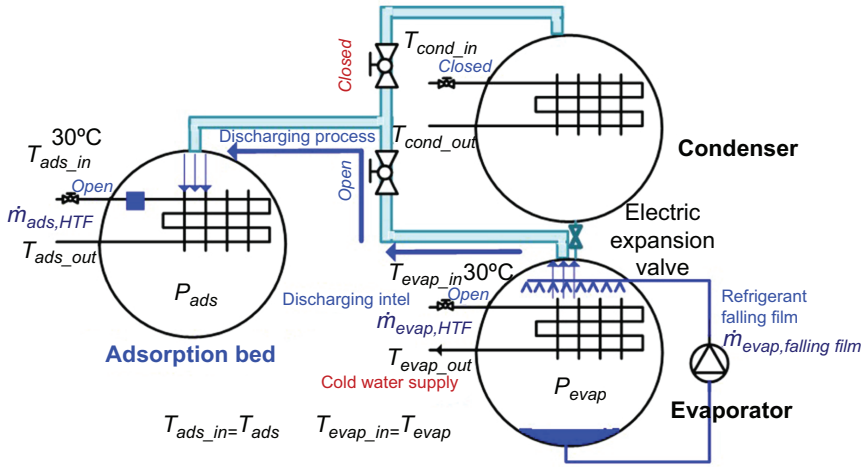

(b) Discharging process

Figure 8.27. Schematic of adsorption cold storage [6, 112].

temperature. The desorption bed and condenser worked during charging process changes their role as the adsorption bed and evaporator (evaporator is at the ambient temperature), respectively during discharging process. At the beginning of the discharging process, lower HTF temperature of the adsorption bed helps adsorbents adsorb more refrigerant vapor and thus make the adsorption chamber pressure lower than the refrigerant

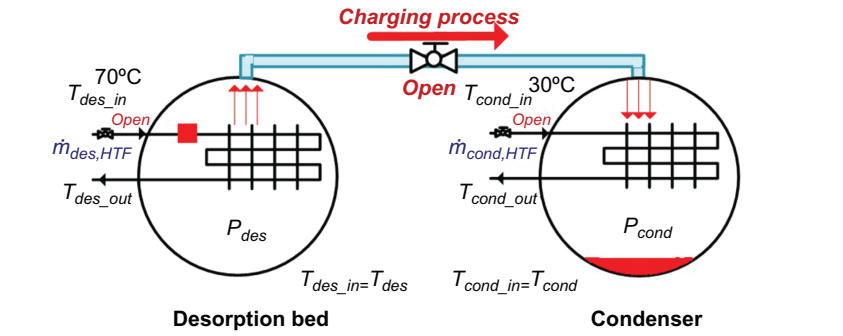

(a) Charging process

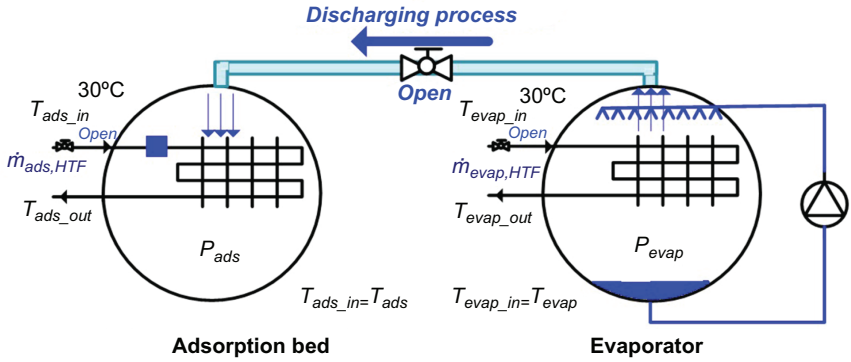

(b) Discharging process

Figure 8.28. Schematic of adsorption short term heat storage [6, 113].

saturation pressure of the ambient temperature. Here additional heat source can also be added into the evaporator chamber to make more refrigerant to flow into adsorption chamber if necessary. With the valve between the adsorption bed and the evaporator open, the pressures of two chambers decrease so that adsorbate (refrigerant) is forced to be in adsorption phase inside adsorbent and release the latent heat. This heat is carried by the heat transfer fluid to meet the building loads.

The working principles introduced above are all for closed sorption system. There are also open systems, which are connected with the ambient environment to allow the release and sorption of the sorbate. In general, water is commonly used in such systems. Figure 8.29 shows the working principle for open sorption TES. During the charging process, with solar

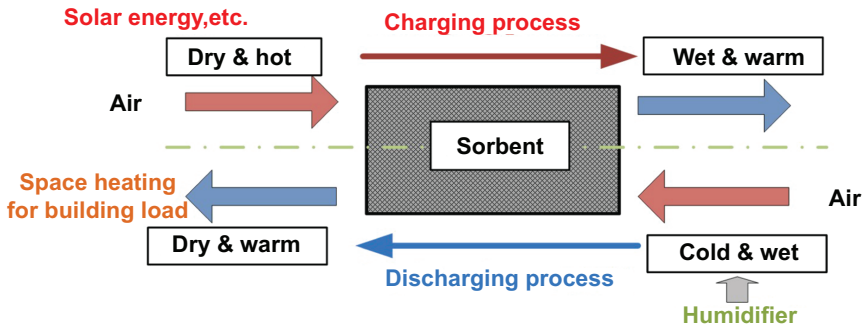

Figure 8.29. Schematic of open sorption TES.

energy heating, the dry and hot air stream flows into the sorbent reactor. The heat drives the water vapor inside sorbents to exit the sorption bed. When the air comes out of the sorbents, it becomes wetter and cooler. During the discharging process, the humid and cool air stream flows into the desorbed reactor again. Then part of the water vapor in the air stream is attracted by the sorbents. The released adsorption heat makes the air hotter. The hot air can be utilized for space heating in buildings. Regarding the open absorption TES, the main purpose is the dehumidification of the air. As compared with closed systems, the open systems have less components and better heat and mass transfer. However, it should be noted that some important factors such as ambient moisture condition, sufficient air stream flow rate, air stream duct distribution in buildings, etc., should be considered. In addition, under some conditions if the air is not wet enough, the humidifier may be adopted as needed.

8.3.2 Sorption Working Pairs

Generally the working pairs should meet the requirements of high thermal conductivity and heat transfer characteristics with the heat transfer fluid for sorption process. They also need to meet the requirements of environmental safety, non-toxicity, zero ODP and low GWP. In fact, there are no ideal materials available to satisfy all listed requirements. Here the commonly used working pairs are listed. In addition, Figure 8.30 shows the comparison of energy storage density for sensible, latent and sorption materials. It can be found that in general, sorption materials, especially the chemical reaction materials, have much higher energy storage density than

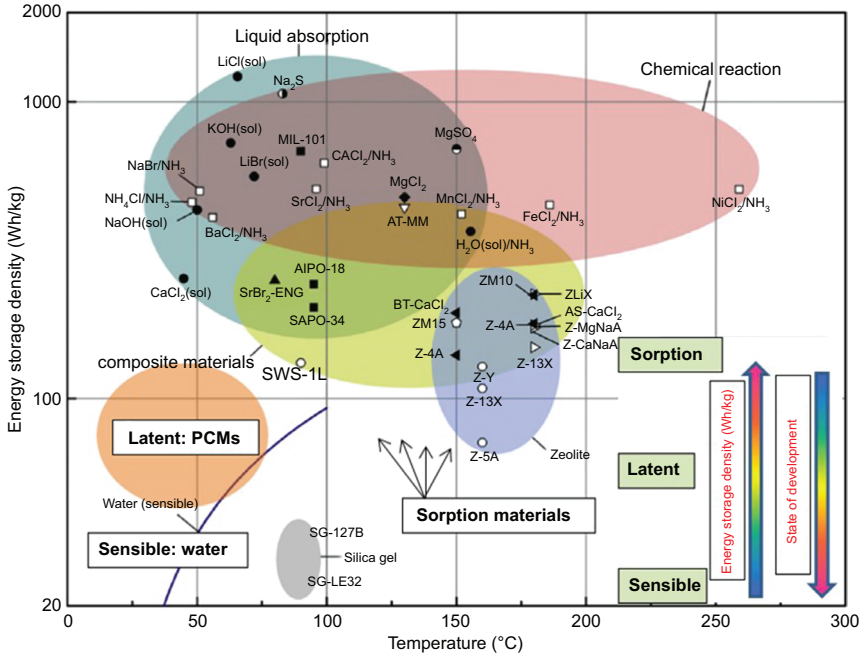

Figure 8.30. Energy storage density of different storage materials (combined from original figures in Ref. [114], latent material figure is added based on data from Ref. [6]).

sensible and latent storage materials. Currently the main development for sorption TES, especially the adsorption TES, is at the laboratory prototype level, which still needs in-depth investigation and efforts to promote its commercialization.

8.3.2.1 Absorption TES Working Pairs

Among the absorption absorbent/refrigerant pairs, H_2O/LiBr and NH_3/H_2O are the most common ones. The former is usually used for air conditioning application or heating purpose and the latter can be used for subzero applications, such as ice making. In addition, NH_3/H_2O has several disadvantages: (1) higher generator inlet temperature (about 90°C to180°C, whereas it is about 70°C to 90°C for H_2O/LiBr), (2) higher pressures and hence higher pumping power needed, (3) a

more complex system needed such as a rectifier to separate ammonia and water vapor at the generator outlet, and (4) health and fire hazard risks by the use of ammonia. Therefore, H_2O/LiBr is more suitable for air conditioning application. In addition, the comparison of working pairs, H_2O/LiBr, H_2O/NaOH, H_2O/LiCl, and H_2O/$CaCl_2$, has also been studied. As shown in Table 8.11, different working pairs are compared under the same conditions of a temperature of absorption of 25°C, a temperature of evaporation of 10°C and a temperature of condensation of 30°C [115]. From this table, and based on the analysis from literature [115], the H_2O/NaOH and H_2O/LiCl pairs have excellent performance on storage capacity. The NaOH has the advantage of being less expensive, but has the disadvantage of a high temperature requirement for solar energy utilization (84°C to 135°C). The $CaCl_2$ is the least expensive material, but its storage capacity is low so that the volume of storage tanks would be significantly larger than for the other pairs. The H_2O/NaOH could be the most economic material because of its low cost and high storage capacity. However, due to its high temperature requirement for solar energy utilization, the system's solar collector would be operated at low efficiency. This solution is also highly corrosive.

8.3.2.2 Adsorption TES Working Pairs

The commonly used working pairs, H_2O/silica gel and H_2O/zeolite are introduced in this section.

1. H_2O/silica gel

Based on literature by Faninger [116], the storage density of silica gel is up to four times that of water [116]. From the literature [117], the adsorption heat of H_2O/silica gel is about 2500 $kJ \cdot kg^{-1}$ and the desorption temperature can be very low, but above 50°C [117]. Normally the desorption temperature should not be higher than 120°C, and it is usually below 90°C. Approximately 4 to 6 wt.% water is connected with a single hydroxyl group on the surface of a silica atom to maintain the adsorption capacity. If the desorption temperature is too high (above 120°C), adsorption performance will decrease significantly, even to the point of losing its adsorption capacity. In addition, the adsorption quantity of this pair is low at about 0.2 $kg \cdot kg^{-1}$ [118].

2. H_2O/zeolite

Zeolites are alumina silicates with high microporosity [119], and are considered to be reliable even in the harshest environment [120]. Since

Table 8.11. Comparison of Different Absorption Working Pairs [115].

		Without crystallization			With crystallization		
Working pairs	**Absorbent price (Euro·ton^{-1})**	**Concentration maximum (%) (kg absorbent·kg solution^{-1})**	**Capacity (kJ·kg^{-1})**	**Temperature requirement for heat driving (°C)**	**Concentration maximum (%) (kg absorbent · kg solution^{-1})**	**Capacity (kJ·kg^{-1})**	**Temperature requirement for heat driving (°C)**
H_2O/LiBr	6,000	60	1,535	74	69	2,068	93
H_2O/LiCl	3,400	46	2,922	68	70	5,271	78
H_2O/NaOH	300	53	3,442	84	69	5,225	135
H_2O/$CaCl_2$	140	45	628	50	51	1,103	56

synthetic zeolites are expensive, Han et al. [121] conducted a contrast study of natural zeolites to the synthetic zeolite 13X. They reported that natural zeolites could be used as a storage material instead of the 13X synthetic zeolite when the heating temperature is below 100°C. For the H_2O/zeolite pair, the adsorption heat is about 3300 to 4200 kJ·kg^{-1} higher than that of H_2O/silica gel pair [118]. Additionally, with desorption temperature higher than 200°C, the H_2O/zeolite can still remain stable. The zeolites are usually used for air conditioning application with a heat source between 200°C and 300°C. Several kinds of crystal cell units of zeolite are shown in Figure 8.31 [117]. The volume of pores for type X and Y zeolites, whose void ratio can be as high as 50% when there is no water adsorbed, is larger than that of other types of pores. One crystal unit can have 235 molecules of water after adsorption, and most of the molecules would accumulate in the center pore.

In one study [6], Mitsubishi Plastic (MPI) FAM-Z01 made of zeolite was used as the adsorbent bed material and water was used as the refrigerant for residential application. It has the high durability that it can endure 200,000 cycles of water vapor adsorption and desorption process [122]. The isotherm curves in Figure 8.32 show the mass fraction (also named loading) of the adsorbate in equilibrium state as a function of pressure ratio (P/P_{sat}) between the adsorbate reservoir and the saturation pressure of the adsorbent bed. FAM-Z01 has a unique isotherm shape.

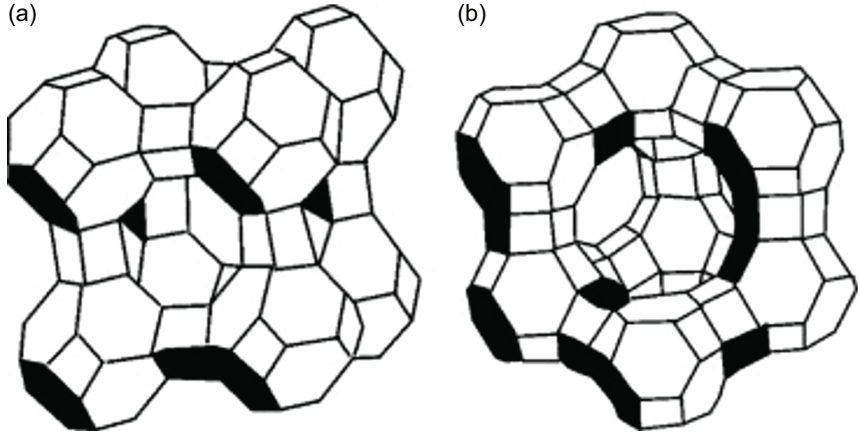

Figure 8.31. Crystal cell unit of zeolite [117].

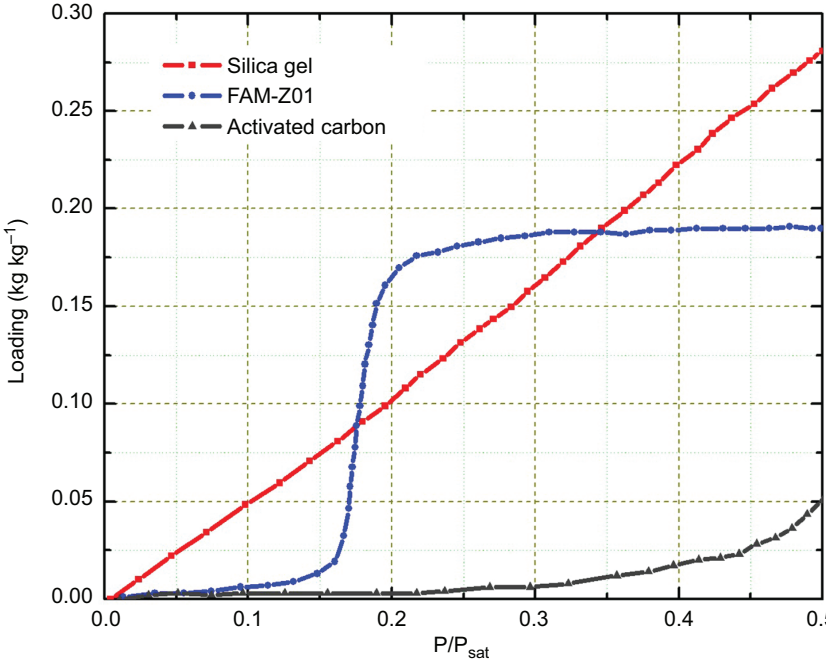

Figure 8.32. Different isotherm curves [112, 122].

As shown in Figure 8.32, it has the property and benefits of large amount of adsorption with changing the pressure ratio in a narrow range (0.15 to 0.2), as compared with Silica Gel and activated Carbon.

The adsorption process of the working pairs discussed above is physical adsorption, which is caused by the van de Walls force between the molecules of the adsorbent containing mesopores or micropores, and the refrigerant [123]. For details about chemical adsorption, please refer to literature [118].

8.3.3 Sorption TES Performance Improvement

8.3.3.1 Absorption TES Performance Improvement

Up to now, the absorption refrigeration technologies have been well developed, and various kinds of absorption chillers and heat pumps with single or double effect are commercially available in the market. How to

couple the absorption refrigeration cycles with thermal storage needs is one of directions to improve absorption TES performance. Figure 8.33 shows the absorption TES improvements with compressor integration [124], double stage discharging method [125], or three phase cycle discharging method [126].

Compressor integration can be used when heat source (such as solar energy or other heat sources) is not enough to drive the absorption machines, as shown in Figure 8.33(a) [124]. For the charging process, the refrigerant is regenerated from the rich solution and sucked in by the compressor. As a result, the refrigerant vapor pressure and temperature increased immediately. Then the hot vapor is condensed and stored in one tank. The condensation heat and compressor waste heat can be used to generate the weak solution in the desorber. During the charging process there is only the electricity power input to the system. For the discharging process, it is same to that conventional absorption TES process. The compressor integration systems aim to shift electricity demand from peak periods to off-peak periods as the compressor is driven by electricity.

The double stage absorption TES process, as shown in Figure 8.33(b) [125], can produce the same temperature of hot water as to the single stage process, but can be at a lower concentration of the NaOH lye (double-stage cycle 35 wt.%, single-stage cycle 50 wt.%) [125]. The double stage absorption TES is beneficial to the condition with a lower charging temperature, or a higher condensation temperature during the charging process, and for a higher discharging temperature or operating with lower

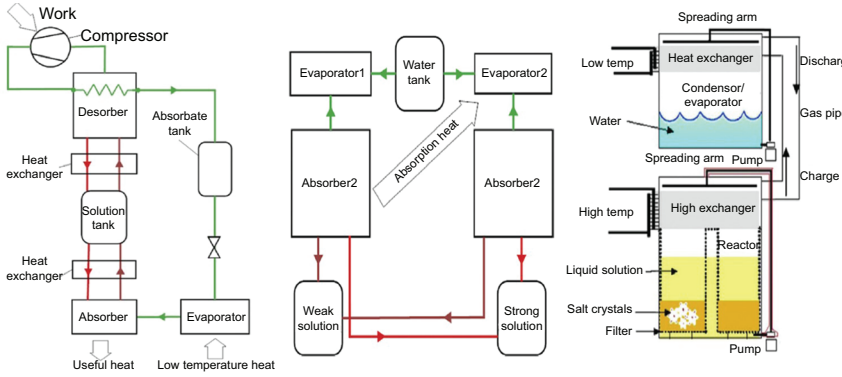

(a) Compressor integration [124] (b) Double stage discharging [125] (c) Thee phase cycle discharging [126]

Figure 8.33. Absorption TES performance improvement.

solution concentration during the discharging process. More details on the double stage absorption TES, please refer to literature [125].

Typically a larger concentration difference of liquid absorption couples can lead to a larger energy storage density. Conventional H_2O/LiBr absorption system cannot realize this because of the crystallization issue when expanding the concentration difference between the strong and weak solutions. In the three-phase absorption cycle, as shown in Figure 8.33(c) [126], salt crystals can be transformed from an obstacle to an enhancement to increase the energy density of the salt. Usually the energy is stored efficiently and, there is less thermal loss in the dried salt. During the charging process, the weak solution from the bottom of the reactor is pumped and sprayed over the heat exchanger. The solution is heated until it reaches the saturation point at the charging temperature.

As the water vapor is released from the solution, solid salt crystal is left continuously, flushed to the bottom of the vessel and stopped by a sieve. Three phases, including vapor, liquid solution and solid crystal, coexist simultaneously, so a monovariant process is ensured. For the discharging process, the process is reversed, and the solution becomes the poor solution at a lower temperature by absorbing the water vapor produced in the evaporator. The poor solution then flows down and meets with the solid crystal collected at the bottom where the crystal dissolves into the solution. Therefore, it can relieve the issue of crystallization.

8.3.3.2 Adsorption TES Performance Improvement

The main improvements of the adsorption TES performance focus on enhancing the heat and mass transfer of adsorption bed, especially for closed systems. Various extended surfaces have been used to enhance the sorption bed heat transfer, such as plate-fin heat exchangers [127], coated Spiro-tubes [128], coated fin-tube heat exchangers (as shown in Figure 8.34) [6, 112], etc. Regarding the open systems, a large contact surface area is needed between air stream and sorbents. In addition, it should also be mentioned that thermal capacity ratio between the metallic extended surfaces and the adsorbents should be considered when adopting heat/mass transfer enhancement methods.

There are some discussions on integrated reactors and separate reactors for adsorption TES performance for practical application. Regarding the integrated reactor, reaction occurs within the storage vessel, and this is

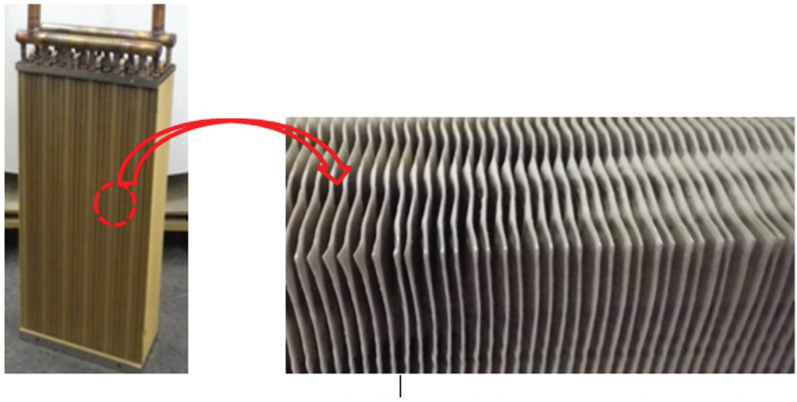

(a) Prototype of absorber heat exchanger

(b) Close-up adsorber heat exchanger with desiccant coated fins (1.8 mm fin spacing, 0.115 mm fin thickness, 0.25 mm zeolite coating thickness)

Figure 8.34. Desiccant coated fin adsorber heat exchanger used in sorption bed [6, 112].

the common type in solid adsorption systems. Regarding the separate reactor, when the reaction is complete, the sorbent is fed back to the storage vessel. More details can be referred to literature [129]. Simple construction is the main advantages of integrated reactors but separate reactors have the benefits of better optimization of the mass transport ability, the reduction of heat required for inert metallic components, etc.

8.3.3.3 Sorption TES Prototypes and Systems

In this section, several prototypes with sorption TES developed for building application are introduced. Table 8.12 shows the review of recent achievements of sorption TES prototypes.

One closed liquid absorption TES system using $CaCl_2$ solution is shown in Figure 8.35 [135, 136]. During the charging process in summer, diluted $CaCl_2$ solution is pumped to the solar collector, and it is heated up to 117 to 138°C. The concentrated $CaCl_2$ solution and condensed water are stored until the winter season to provide heating. Figure 8.35(b) shows the design and operation of the storage vessel to prevent mixing of solutions. An internal heat exchanger was used to add and discharge thermal energy in the tank. In particular, a heat exchanger and a stratification manifold are immersed in the storage tank, which can thermally stratify the solution

Table 8.12. Recent Achievements of Sorption TES Prototypes.

Reference	Sorption TES type	Working pair	Heat source temperature	Discharging temperature	Storage capacity	Storage density	COP
LOCIE-CNRS, France [130]	Closed liquid absorption	H_2O/LiBr	2–5 kW at 75–90°C	At 30–40°C	13 kWh		–
SERC, Sweden [131]	Closed absorption	H_2O/LiCl	15 kW at 87°C	8 kW at 30°C	35 kWh	M: 253 kWh·m^{-3} P: 86 kWh·m^{-3}	–
EMPA, Switzerland [131]	Closed liquid absorption	H_2O/NaOH	1 kW at 95°C	1 kW at 70°C	8.9 kWh	M: 250 kWh·m^{-3} Pc: 5 kWh·m^{-3}	–
AEE-INTEC, Austria [131]	Closed solid adsorption	H_2O/Silica gel 127B	1.0–1.5 kW	0.5–1.0 kW	13 kWh	M: 50 kWh·m^{-3} P: 33.3 kWh·m^{-3}	–
CEEE, University of Maryland, United States [6, 112, 113]	Closed solid adsorption	H_2O/FAM-Z01	At 70°C	~40°C (heat storage) ~15-20°C (space cooling)	–	M: 210 Wh·kg^{-1} M: 110 Wh·kg^{-1} (cold)	0.9 (heat) 0.45 (cold)
SPF, Switzerland [131]	Open solid adsorption	H_2O/Zeolite 13X	At 180°C	0.8–1.8 kW at 55°C	1 kWh	M: 180 kWh·m^{-3} P: 57.8 kWh·m^{-3}	–
ITW, Germany [131]	Open solid adsorption	H_2O/Zeolite 4A	2.0–2.5 kW at 180°C	1.0–1.5 kW 35°C	12 kWh	M: 160 kWh·m^{-3} P: 120 kWh·m^{-3}	–

(Continued)

Table 8.12. Recent Achievements of Sorption TES Prototypes. (*Cont.*)

ZAE Bayern, Germany [132]	Open solid adsorption	H_2O/Zeolite 13X	135 kW at 130°C	130 kW at 65°C 50 kW (cold) at 11°C	1300 kWh 1751 kWh (cold)	M: 124 $kWh \cdot m^{-3}$ M: 168 $kWh \cdot m^{-3}$ (cold)	0.9 (heat) 0.86 (cold)
Chiang Ma University, Thailand [133]	Closed composite sorption	H_2O/Na_2S–graphite	3.8 kW at 80–95°C	0.15–0.24 kW	0.56 kWh	M: 2240 $Wh \cdot kg^{-1}$	
ECN, the Netherlands [128]	Closed composite sorption	H_2O/Na_2S–cellulose	0.2–1.0 kW	0.5–0.7 kW at 5–20°C	3.2 kWh 2.1 kWh (cold)	M: 1070 Wh/kg M: 700 Wh/kg (cold)	0.56 (cold)
PROMES-CNRS, France [134]	Closed composite sorption	$H_2O/SrBr_2$–expanded natural graphite	At 80°C	2.5–4.0 kW	60 kWh 40 kWh (cold)	M: 321 $Wh \cdot kg^{-1}$ M: 214 $Wh \cdot kg^{-1}$ (cold)	–
PROMES-CNRS, France [139]	Closed composite sorption	$NH_3/BaCl_2$–expanded natural graphite	7 kW at 60–70°C	5kW (cold) at 4°C	20 kWh (cold)	M: 114 $Wh \cdot kg^{-1}$ (cold)	0.3-0.4 (cold)

Note: Cold: cold storage, others are heat storage; M: ESD based on material level and P: ESD based on prototype level.

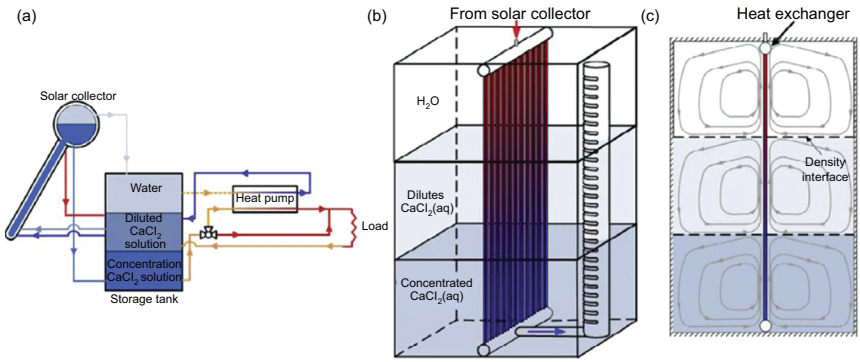

Figure 8.35. Closed $H_2O/CaCl_2$ absorption heating system with a single storage vessel: (a) system schematic [135]; (b) storage tank schematic [136]; (c) anticipated convective flow patterns during sensible charging [136].

and minimize mixing between regions of different $CaCl_2$ mass fractions. A storage tank of 1500 liters was built to elucidate mixing of solutions. The transient experimental characteristics of stable density interfaces and confined natural convection flows were shown via in Figure 8.35(c).

One adsorption TES system using H_2O/silica gel was developed within the framework of the EU-project MODESTORE [131, 137], as shown in Figure 8.36. The silica gel used here was microporous silica gel Grace 127B. A spiral heat exchanger containing silica gel was used and it is connected to an evaporator/condenser at the bottom of the vessel. Results showed that a storage capacity of the lab scale unit was only 13 kW·h, which was lower than initially expected. Further work is still needed to search for advanced sorption materials to get better storage performance.

One experimental adsorption TES for space cooling was investigated [6, 112], as shown in Figure 8.37. Cooling water at around 15°C can be produced for space cooling. The operation principle is introduced in Figure 8.27 in Section 8.3.1.2: Adsorption TES working principle. Chambers of the sorption beds, condenser and evaporator were housed in each own cylindrical vacuum chamber as shown in Figure 8.37. A steel flange on one side of each chamber supported a 2.5 cm thick plate of polycarbonate resin thermoplastic materials to enable viewing inside of the heat exchangers during adsorption thermal storage operation. The hot water was supplied by a 0.83 m^3 (approximately 833 liters) water storage thermal buffer tank, which is heated by the waste heat from the prime mover

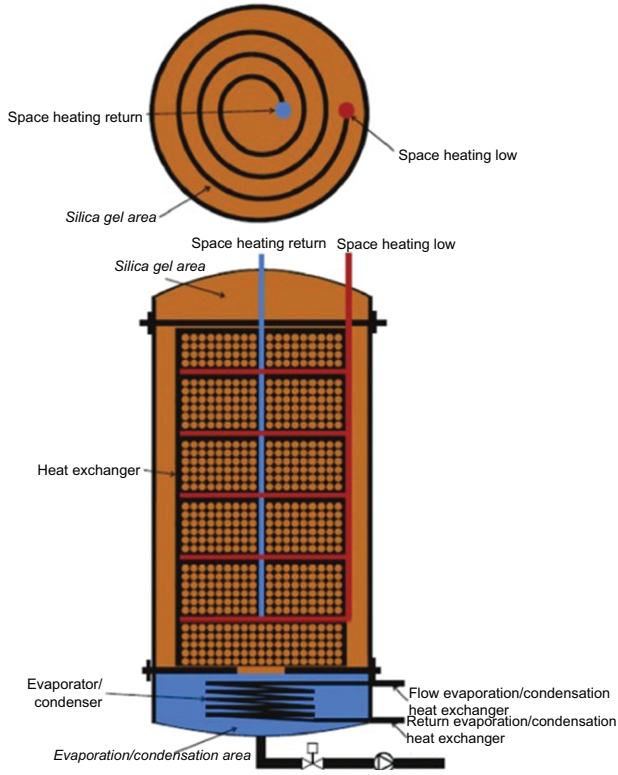

Figure 8.36. Schematic of H_2O/silica gel thermal storage prototype [137].

with an internal combustion spark ignition gas engine. Three constant speed pumps circulated HTF (water) for the sorption bed, condenser and evaporator. The heat transfer between components was regulated by electronically actuated mixing/diverting valves that control the amount of water recirculation. The adsorber heat exchanger (in Figure 8.37), which was placed inside the sorption bed, was a copper tube and aluminum plain fin type heat exchanger with 12 parallel four-pass circuits and a 0.25 mm thick coating of Z01 zeolite on all fin-and-tube surfaces. Regarding the evaporator chamber, the horizontal tubes were stacked vertically in two columns so that refrigerant dripping off would fall directly to the chamber bottom. The tubes were carefully leveled so that the refrigerant would fall in film form from one tube to other below. Distribution of the falling film was implemented with a combination of an orifice tube. Tests showed that the cold energy storage density of approximately 400 $kJ \cdot kg^{-1}$ was achieved with 44.6% energy efficiency under the operating conditions that regeneration, ambient, and evaporator HTF inlet temperatures were

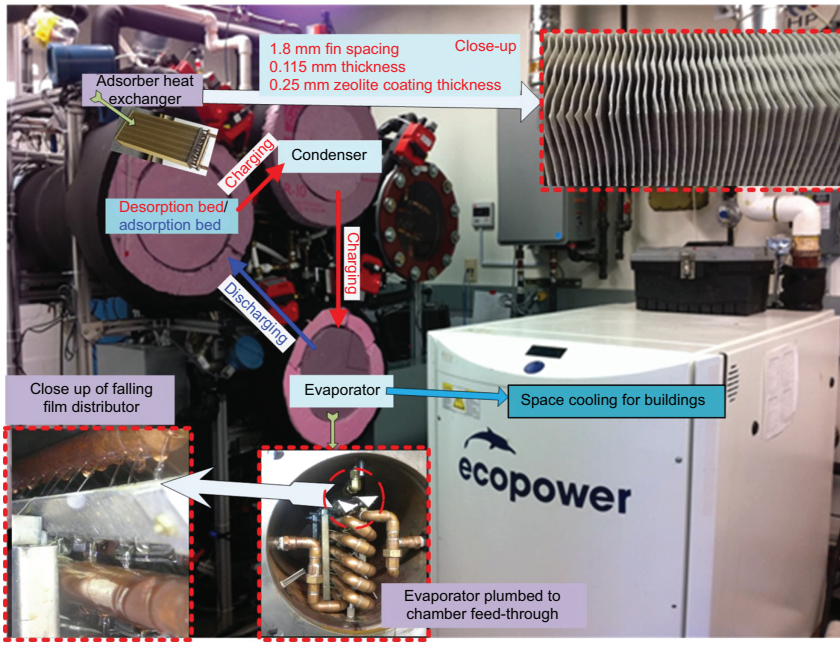

Figure 8.37. Schematic of adsorption TES test facility [6, 112].

70°C, 30°C, and 30°C, respectively. This system can also be used for short-term heat storage for residential application with flexible operating strategies, and the heat ESD was approximately 800 kJ·kg^{-1}. More details can be referred to literature [113].

An open type adsorption TES system using H_2O/13X zeolite was installed and studied by ZAE Bayern (Center for Applied Energy Research) [132, 138] to heat a school building in winter and to cool a jazz club in summer, as shown in Figure 8.38. The heating load is 130 kW for school and the cooling load is 50 kW for the club. During the night time, hot steam from the district heating system heats the zeolite to be 130°C to 180°C, and this is the charging process. During the day time, which is the discharging time, the zeolite bed is discharged in times of peak power demand. In addition, the cold recovery device, which consists of an exhaust air humidifier with an integrated heat exchanger and the supply air heat exchanger, is also added to in the cooling process for the jazz club. Results showed that the cold recovery device can exchange 83% of the maximum enthalpy difference from the exhaust air to the supply air. The storage densities were 124 kWh·m^{-3} for heating and 100 kWh·m^{-3} for cooling with COP of 0.9 and 0.86, respectively.

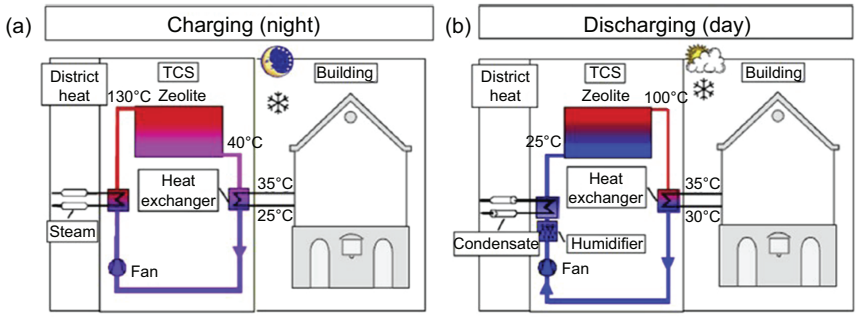

Figure 8.38. Open adsorption thermal storage system on district heating net in Munich: (a) charge mode for heating; (b) discharge mode for heating [138].

One system coupled with sorption and latent TES is shown in Figure 8.39 [139]. It is a solar air conditioning pilot plant built in 2006, which can provide a daily cooling capacity of 20 kWh. The heat source is from the flat plate solar collectors with temperature at 60°C to 70°C. There are four subsystems: a solar heating loop, a sorption unit using the working pair $NH_3/BaCl_2$, a ground cooling loop and a chilled water production loop.

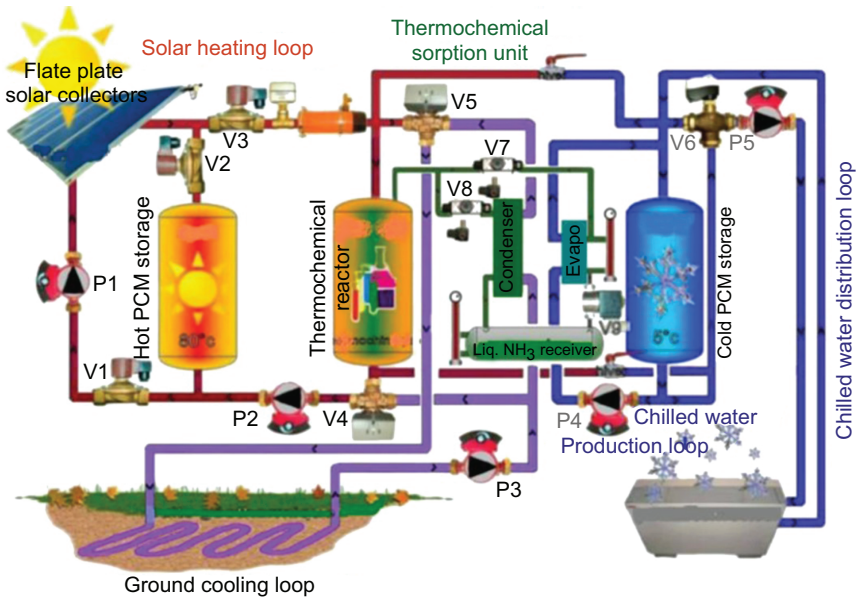

Figure 8.39. Solar sorption pilot plant for air conditioning [139].

The hot PCM storage tank can store the excess solar heat if the desorption reaction in the reactor is completed, and the cold PCM storage tank makes a necessary supply of cooling effect possible whenever the sorption effect is not available. It showed that an average yearly efficiency of solar collectors and a COP ranging from 0.4 to 0.5 and 0.3 to 0.4, respectively.

8.4 Conclusions and Perspective

The incorporation of TES systems in different methods into buildings is beneficial for saving energy and reducing CO_2 emissions by enabling utilization of recovered waste heat and renewable energies. It can lead to the reduction of heating/cooling peak demands and the indoor room temperature fluctuations. In this chapter, different types of TES systems and the development of energy-storing buildings have been introduced as a solution to the on-going quest for energy conservation and improving the indoor thermal comfort.

Sensible TES technologies have been well-developed, and the use of cooled water/stratified hot water, aquifers, rock storage, and ground storage have been investigated in detail. Currently there are many large-scale demonstration plants. The material is environmental-friendly and cheap, and the system is simple to design and easy to control. However, due to its low energy storage density, huge volumes are usually required, especially for district heating or cooling. Also with the growing global population, the land available for storage may be reduced, and site construction for large volume storage is very expensive. In addition, there are geological requirements for aquifers, rock storage, or ground storage. In the future, effort should be made to reduce the heat loss during storage periods. Proper system control policies to effectively use the renewable energy as heat source and optimization of storage temperatures to reduce the heat loss should be investigated. In addition, more reliable simulations and predictions for the feasibility of aquifer or ground storage geological conditions should be pursued to reduce the risk of heat losses and protect the ecological environment.

Latent TES systems have a higher energy storage density than sensible TES systems. PCMs have a high energy storage density, and can release the stored energy at a constant temperature. Currently there are several application examples of PCM storage tank integrated in buildings. Especially with ice storage, it remains popular today in different countries for summer air conditioning applications in commercial or residential

buildings. Of course, other kinds of PCMs, such as organics or inorganics, should continue to be investigated to evaluate their feasibility in TES for buildings. The performance of PCM construction materials suggests that they can significantly lower mean radiant temperatures, provide more thermal stability, and are less likely to overheat and experience temperature fluctuations. However, common issues of PCMs include supercooling or corrosion, which should be resolved in the future. The cost of PCMs except ice is still high. Thermal improvements in a building by the inclusion of PCMs depend on the type of PCMs, the melting temperature, the percentage of PCM mixed with conventional material, the climate, design, and orientation of the building. Therefore, for future work, the modeling, and optimization of these parameters is essential to demonstrate the potential success of the PCMs in building materials. In addition, searching for novel PCMs with higher fusion heat and fewer material issues should be investigated, and modeling and optimization work should be done to better predict and improve building performance and reduce the cost.

For sorption storage, absorption storage technology has been developed well, and adsorption storage technology has made a great progress towards a commercialization. Thermal energy can be stored with little heat loss for season long and the technique can also be used in buildings where the heating requirement is low (single family houses). However, sorption storage still has many issues that need to be solved before the technique can be more reliably used. Usually for sorption storage during discharging process, a low temperature heating source is required. This heat source can be ambient air or any other waste heat. How to obtain and integrate such heat sources reliably with sorption storage system should be investigated. Poor heat and mass transfer property of sorption bed under high density condition is another issue for sorption storage systems. Regarding the future work, optimization of sorption bed structure to improve heat and mass transfer performance, working pair selection with high sorption energy density and low cost, thermodynamic and kinetic study with noble reaction cycles, should be investigated.

Nomenclature

CHP	combined heating and power
CCHP	combined heating, cooling, and power
ESD	energy storage density
GWP	global warming potential
IEA	International Energy Agency
PCM	phase change material

PDE	partial differential equation
PES	primary energy savings
PFP	passive fire protection materials
MPI	Mitsubishi Plastic
ODP	ozone depletion potential
SWH	solar water heating
TES	thermal energy storage
TRNSYS	transient system simulation program
WHR	waste heat recovery

Acknowledgments

The authors gratefully acknowledge the support from the Center for Environmental Energy Engineering (CEEE) at the University of Maryland, College Park.

References

[1] Energy Information Administration, U.S. Department of Energy, 2011. Annual Energy Review 2011, Primary Energy Production by Source, Selected Years, 1949–2011.

[2] International Energy Agency, 2009. World Energy Outlook 2009.

[3] DOE, available at http://buildingsdatabook.eren.doe.gov/ChapterIntro1.aspx

[4] European Parliament, EU Directive on the Energy Performance of Buildings (recast) (2010/31/EU), 19 May 2010.

[5] Li, G., *Energy and exergy performance assessments for latent heat thermal energy storage systems*, Renewable and Sustainable Energy Reviews, 51:926–954, 2015.

[6] Li, G., 2013. *Review of Thermal Energy Storage Technologies and Experimental Investigation of Adsorption Thermal Energy Storage for Residential Application*, Master Thesis, University of .Maryland at College Park, United States. http://drum.lib.umd.edu/handle/1903/14698.

[7] Li, G., Hwang, Y., and Radermacher, R., 2012. *Review of Cold Storage Materials for Air Conditioning Application,* International Journal of Refrigeration, 35:2053–2077.

[8] Li, G., *Experimental Study on Growth Characteristics of New-Type Gas Hydrate for Cold Storage*, Master Thesis, University of Shanghai for Science and Technology, P. R. China 2009 (in Chinese).

[9] Li, G., Hwang, Y., Radermacher, R., and Chun, H.H., 2013. *Review of Cold Storage Materials for Subzero Applications*, Energy, 51: 1–17, 2013.

[10] Bahnfleth, W.P., Song, J., and Cimbala, J.M., *Thermal Performance of Single Pipe Diffusers in Stratified Chilled Water Storage Tanks*, Final report of ASHRAE, 1185-RP, 2003.

[11] Mackie, E.I., and Reeves, G., 1988. *EPRI Stratified Chilled-Water Storage Design Guide*, Electric Power Research Institute, Inc. Final report.

[12] Dincer, I., and Rosen, M.A., 2001. *Energetic, Environmental and Economic Aspects of Thermal Energy Storage Systems for Cooling Capacity*, Appl. Therm Eng, 21:1105–1117.

[13] Rismanchi, B., Saidur, R., Masjuki, H.H., and Mahlia, T.M.I., 2012. *Energetic, Economic and Environmental Benefits of Utilizing the Ice Thermal Storage Systems for Office Building Applications*, Energy and Buildings, 50:347–354.

[14] Hasnain, S.M., 1998. *Review on Sustainable Thermal Energy Storage Technologies*, *part II; Cool Thermal Storage*, Energy Conversion and Management, 24 (11):1139–1153.

[15] Yamaha, M., and Misaki, S., 2006. *The Evaluation of Peak Shaving by A Thermal Storage System Using Phase-Change Materials In Air Distribution Systems*. International Journal of Heating, Ventilating, Air-conditioning, and Refrigerating Research, 12(3c):61–869.

[16] Alawadhi, E.M., 2012. Using *Phase Change Materials in Window Shutter to Reduce The Solar Heat Gain*, Energy and Buildings, 47:421–429.

[17] Kodo, T., and Ibamoto, T., *Research on Using The PCM for Ceiling Board*, IEA ECESIA, Annex 17, 3rd workshop, Tokyo, Japan. October 1–2, 2002.

[18] BINE Information Service, *Concepts for Building Services Technology*, http://www.bine.info/en/publications/publikation /latentwaermespeicher-in-gebaeuden/pcm-konzepte-fuer-die -gebaeudetechnik/.

[19] Han, Y.M., Wang, R.Z., and Dai, Y.J., 2009. *Thermal Stratification within the Water Tank*, Renewable and Sustainable Energy Reviews, 13: 1014–1026.

[20] Davidson, J.H., and Adams, D.A., 1994. *Fabric Stratification Manifolds for Solar Water Heating*, ASME J. Solar Energy Engineering, 116: 130–136.

[21] Li, G., 2015. *Sensible Heat Thermal Storage Energy and Exergy Performance Evaluations*, Renewable and Sustainable Energy Reviews, doi:10.1016/j.rser.2015.09.006 (in press).

22] Godschalk, M., and Bakema, G., 2009. *20,000 ATES Systems in the Netherlands in 2020-Major Step Towards a Sustainable Energy Supply*. Proceedings Effstock.

[23] Dincer, I., and Rosen, M.A., 2011. *Thermal Energy Storage: Systems and Applications*. Wiley.

[24] Molina, A., Gabaldon, A., Alvarez, C., Fuentes, J.A., and Gomez, E., 2003. *Electrical Thermal Storage Modeling Tool to Evaluate New Opportunities and Bids for Residential Users in a Deregulated Market*, IEEE Power Tech Conference, Bologna.

[25] Zhao, D.L., Li, Y., Dai, Y.J., and Wang, R.Z., 2011. *Optimal Study of a Solar Air Heating System with Pebble Bed Energy Storage*. Energy Convers. Manage. 52:2392–2400.

[26] Canbazoglu, S., Sahinaslan, A., Ekmekyapar, A., Aksoy, Y.G., and Akarsu, F., 2005. *Enhancement of Solar Thermal Energy Storage Performance Using Sodium Thiosulfate Pentahydrate of a Conventional Solar Water-Heating System*, Energy and Buildings, 37(3):235–242.

[27] Öztürk, H.H., 2005. *Experimental Evaluation of Energy and Exergy Efficiency of a Seasonal Latent Heat Storage System for Greenhouse Heating*. Energy Convers. Manage., 46:1523–1542.

[28] Lin, K., Zhang, Y., Xu, X., Di, H., Yang, R., and Qin, P., 2005. *Experimental Study of Under-Floor Electric Heating System with Shape-Stabilized PCM Plates*. Energy and Buildings, 37:215–220.

[29] Gutherz, J.M., and Schiler, M.E., 1991. *A Passive Solar Heating System for the Perimeter Zone of Office Buildings*, Energy Sources, 13:39–54.

[30] Esen, M., 2000. *Thermal Performance of a Solar-Aided Latent Heat Store Used for Space Heating by Heat Pump*. Sol. Energy 69:15–25.

[31] Benli, H. 2011. *Energetic Performance Analysis of a Ground-Source Heat Pump System with Latent Heat Storage for a Greenhouse Heating*. Energy Convers. Manage., 52:581–589.

[32] Arteconi, A., Hewitt, N.J., and Polonara, F., 2012. *State of the Art of Thermal Storage for Demand-Side Management*, Applied Energy, 93:371–389.

[33] Nishimura, T., 2002.*"Heat Pumps-Status and Trends" in Asia and The Pacific*. Int. J Refrig 25:405–413.

[34] Hewitt, N.J., 2012. *Heat Pumps and Energy Storage–The Challenges of Implementation*, Appl. Energy, 89:37–44.

[35] Haeseldonckx, D., Peeters, L., Helsen, L., and D'haeseleer, W., 2007. *The Impact of Thermal Storage on the Operational Behaviour of Residential CHP Facilities and the Overall CO_2 Emissions*, Renew Sust. Energy Rev., 11:1227–1243.

[36] Cao, M., and Cao, J., 2006. *Optimal Design of Thermal-energy Stores for Boiler Plants*, Appl. Energy 83:55–68.

[37] Saverio, E., Melino, F., and Morini, M., 2012. *Influence of the Thermal Energy Storage on the Profitability of Micro-Chp Systems for Residential Building Applications*, Appl. Energy, 97:714–722.

[38] Streckiene, G., Martinaitis, V., Andersen, A.N., and Katz, J., 2009. *Feasibility of CHP-plants with Thermal Stores in the German Spot Market*, Appl. Energy, 86:2308–2316.

[39] Lai, S.M., and Hui, S.W., 2010. *Integration of Trigeneration System and Thermal Storage under Demand Uncertainties*, Appl. Energy, 87:2868–2880.

[40] Martínez-Lera, S., Ballester, J., and Martínez-Lera, J., 2013. *Analysis and Sizing of Thermal Energy Storage in Combined Heating, Cooling and Power Plants for Buildings*, Applied Energy, 106:127–142.

[41] Fragaki, A., Andersen, A.N., and Toke, D., 2008. *Exploration of Economical Sizing of Gas Engine and Thermal Store for Combined Heat And Power Plants in the UK*, Energy, Volume 33:1659–1670.

[42] Mongibello L, Capezzuto M, Graditi G. *technical and cost analyses of two different heat storage systems for residential micro-CHP plant*. Applied Thermal Engineering 2014; pp.636-642, vol.71.

[43] Nuytten, T., Moreno, P., Vanhoudt, D., Jespers, L., Solé, A., and Cabeza, L.F., 2013. *Comparative Analysis of Latent Thermal Energy Storage Tanks for Micro-CHP Systems*, Applied Thermal Engineering, 59:542–549.

[44] Dorer, V., and Weber, A., 2009. *Energy and CO_2 Emissions Performance Assessment of Residential Micro-cogeneration Systems with Dynamic Whole-building Simulation Programs*, Energy Convers Manag, 50:648–657.

[45] Matics, J., and Krost, G., 2008. *Micro Combined Heat and Power Home Supply: Prospective and Adaptive Management Achieved by Computational Intelligence Techniques*, Appl. Therm Eng, 28:2055–2061.

[46] Heier, J., 2013. *Energy Efficiency through Thermal Energy Storage: Possibilities for the Swedish Building Stock*, KTH Royal Institute of Technology, Licentiate thesis.

[47] Ståhl, F., 2009. *Influence of Thermal Mass on the Heating and Cooling Demands of a Building Unit*, PhD thesis, Chalmers tekniska högskola, Gothenburg.

[48] Hagentoft, C.-E., and Svensson, C., 2000. *Energieffektivitet och god termisk komfort genom värmelagring i byggnaden*. Bygg & Teknik, 5/00.

[49] Norén, A., Akander, J., Isfält, E., and Söderström, O., 1999. *The Effect of Thermal Inertia on Energy requirement in a Swedish Building—Results Obtained with Three Calculation Models*. International Journal of Low Energy and Sustainable Buildings, 1.

[50] Heier, J., Bales, C., and Martin, V., Year. 2012. *Thermal Energy Storage in Swedish Single Family Houses — A Case Study*. In: Proceedings of Innostock 2012, Lleida, Spain.

[51] Johansson, L.S., Leckner, B., Gustavsson, L., Cooper, D., Tullin, C., and Potter, A., 2004. *Emission Characteristics of Modern and Old-Type Residential Boilers Fired with Wood Logs and Wood Pellets*. Atmospheric Environment, 38:4183–4195.

[52] Papillon, P., Nielsen, J. E., Cholin, X., Letz, T., Thür, A., Kuhness, G., Bales, C., Albaric, M., Drueck, H., Ullmann, J., and Mette, B., 2010. *Solar Combisystems Promotion and Standardisation,* Final Report.

[53] Arteconi, A., Hewitt, N. J., and Polonara, F., 2013. *Domestic Demand-Side Management (DSM): Role of Heat Pumps and Thermal Energy Storage (TES) Systems*. Applied Thermal Engineering, 51:155–165.

[54] Schmidt, T., Mangold, D., and Müller-Steinhagen, H., 2004. *Central Solar Heating Plants with Seasonal Storage in Germany*, Solar Energy, 76:165–174.

[55] Boonnasa, S., and Namprakai, P., 2010. *The Chilled Water Storage Analysis for a University Building Cooling System*. Applied Thermal Engineering, 30:1396–1408.

[56] Bauer, D., Marx, R., Nußbicker-Lux, J., Ochs, F., Heidemann, W., and Müller-Steinhagen, H., 2010. *German Central Solar Heating Plants with Seasonal Heat Storage*, Solar Energy, 84:612–623.

[57] Nordell, B., and Hellström, G., 2000. *High Temperature Solar Heated Seasonal Storage System for Low Temperature Heating of Buildings*. Solar Energy, 69:511–523.

[58] Lundh, M., and Dalenbäck, J. O., 2008. *Swedish Solar Heated Residential Area with Seasonal Storage in Rock: Initial Evaluation*. Renewable Energy, 33:703–711.

[59] Heier, J., Bales, C., Sotnikov, A., and Ponomarova, G., 2011. *Evaluation of a High Temperature Solar Thermal Seasonal Borehole Storage*. ISES Solar World Congress. Kassel, Germany.

[60] Wang, H., and Qi, C., 2008. *Performance Study of Underground Thermal Storage in a Solar-ground Coupled Heat Pump System for Residential Buildings*. Energy and Buildings, 40:1278–1286.

[61] Wang, H., Qi, C., Wang, E., and Zhao, J., 2009. *A Case Study of Underground Thermal Storage in a Solar-Ground Coupled Heat*

Pump System for Residential Buildings. Renewable Energy, 34:307–314.

[62] Vanhoudt, D., Desmedt, J., Van Bael, J., Robeyn, N., and Hoes, H., 2011. *An Aquifer Thermal Storage System in a Belgian Hospital: Long-term Experimental Evaluation of Energy and Cost Savings*. Energy and Buildings, 43:3657–3665.

[63] Kizilkan, O., and Dincer, I., 2012. *Exergy Analysis of Borehole Thermal Energy Storage System for Building Cooling Applications*, Energy and Buildings, 49:568–574.

[64] Skogsberg, K., and Nordell, B., 2001. *The Sundsvall Hospital Snow Storage*. Cold Regions Science and Technology, 32:63–70.

[65] Skogsberg, K., 2002. *The Sundsvall Regional Hospital Snow Cooling Plant–Results from the First Year of Operation*. Cold Regions Science and Technology, 34:135–142.

[66] Hamada, Y., Kubota, H., Nakamura, M., Kudo, K., and Hashimoto, Y., 2010. *Experiments and Evaluation of a Mobile High-density Snow Storage System*. Energy and Buildings, 42:178–182.

[67] Peippo, K., Kauranen, P., and Lund, P. D., 1991. *A Multicomponent PCM Wall Optimized for Passive Solar Heating*. Energy and Buildings, 17:259–270.

[68] C. Castellón, M.N., J. Roca, M. Medrano and L.F. Cabeza. 2006. *Microencapsulated Phase Changing Materials (PCM) for Building Applications*. In: STILES, L., ed. Proceedings of the 10th International Conference on Thermal Energy Storage Stockton, 1–9.

[69] Yahay, N. A., and Ahmad, H., 2011. *Numerical Investigation of Indoor Air Temperature with the Application of PCM Gypsum Board as Ceiling Panels in Buildings*. Procedia Engineering, 20:238–248.

[70] Streicher, W., Schultz, J. M., Solé, C., Cabeza, L. F., Bony, J., Citherlet, S., and Heinz, A., 2008. *Final report of Subtask C "Phase Change Materials" The Overview — A Report of IEA Solar Heating and Cooling programme* — Task 32.

[71] Arkar, C., and Medved, S., 2007. *Free Cooling of a Building Using PCM Heat Storage Integrated into the Ventilation System*, Solar Energy, 81:1078–1087.

[72] Takeda, S., Nagano, K., Mochida, T., and Shimakura, K., 2004. *Development of a Ventilation System Utilizing Thermal Energy Storage for Granules Containing Phase Change Material*, Solar Energy, 77:329–338.

[73] Evola, G., Marletta, L., and Sicurella, F., 2013. *A Methodology for Investigating the Effectiveness of PCM Wallboards for Summer*

Thermal Comfort in Buildings, Building and Environment, 59:517–527.

[74] Rismanchi, B., Saidur, R., Masjuki, H. H., and Mahlia, T. M. I., 2012. *Thermodynamic Evaluation of Utilizing Different Ice Thermal Energy Storage Systems for Cooling Application in Office Buildings in Malaysia*, Energy and Buildings, 53:117–126.

[75] Sehar, F., Rahman, S., and Pipattanasomporn, M., 2012. *Impacts of Ice Storage on Electrical Energy Consumptions in Office Buildings*, Energy and Buildings, 51:255–262.

[76] Hamada, Y., and Fukai, J., 2005. *Latent Heat Thermal Energy Storage Tanks for Space Heating of Buildings: Comparison between Calculations and Experiments*. Energy Conversion and Management, 46:3221–3235.

[77] Turnpenny, J. R., Etheridge, D. W., and Reay, D. A., 2000. *Novel Ventilation Cooling System for Reducing Air Conditioning in Buildings: Part I: Testing and Theoretical Modelling*. Applied Thermal Engineering, 20:1019–1037.

[78] Turnpenny, J. R., Etheridge, D. W., and Reay, D. A., 2001. *Novel Ventilation System for Reducing Air Conditioning in Buildings. Part II: testing of prototype*. Applied Thermal Engineering, 21:1203–1217.

[79] Bellas, I., and Tassou, S. A., 2005. *Present and Future Applications of Ice Slurries*. International Journal of Refrigeration, 28:115–121.

[80] Abhat, A., 1983. *Low Temperature Latent Heat Thermal Energy Storage: Heat Storage Materials*. Solar Energy. 30:313–332.

[81] Dieckmann, J.H., 2006. *Latent Heat Storage in Concrete*. University of Kaiserslautern, Germany, http://www.eurosolar.org. [accessed on 11.11.2011].

[82] Schmidt, T., Mangold, D., and Müller-Steinhagen, H., 2003. *Seasonal Thermal Energy Storage in Germany*. In: ISES Solar World Congress, 14–19. June, Göteborg, Schweden.

[83] Farid, M.M., Khudhair, A.M., Razack, S.A.K., and Al-Hallaj, S., 2004. *A Review on Phase Change Energy Storage: Materials and Applications*. Energy Convers Manag, 45:1597–1615.

[84] Agyenim, F., Hewitt, N., Eames, P., and Smyth, M., 2010. *A Review of Materials, Heat Transfer and Phase Change Problem Formulation for Latent Heat Thermal Energy Storage Systems (LHTESS)*, Renewable & Sustainable Energy Reviews, 14:615–628.

[85] Dutil, Y., Rousse, D.R., Salah, N.B., Lassue, S., and Zalewski, L., 2011. *A Review on Phase-change Materials: Mathematical Modeling and Simulations*, Renewable and Sustainable Energy Reviews, 15:112–130.

[86] Roy, S.K., and Sengupta, S., 1989. *Melting of a Free Solid in a Spherical Enclosure: Effects of Subcooling*. J Solar Energy Eng, 111:32–36.

[87] Barba, A., and Spriga, M., 2003. *Discharge Mode for Encapsulated PCMs in Storage Tanks*. Solar Energy, 74:141–148.

[88] Fomin, S.A., and Saitoh, T.S., 1999. *Melting of Unfixed Material in Spherical Capsule with Nonisothermal Wall*. Int J Heat Mass Transfer, 42:4197–4205.

[89] Adref, K.T., 1995. *A Theoretical and Experimental Study of Phase Change in Encapsulated Ice Store*. Ph.D. thesis. England, UK: Department of Mechanical Engineering, Sheffield University.

[90] Adref, K.T., and Eames, I.W., 1998. *Freezing of Water within Spherical Enclosures: an Experimental Study*. In: Proceedings international conference on energy research development, 2:643–659.

[91] Ismail, K.A.R., Henriquez, J.R., and da Silva, T.M., 2003. *A Parametric Study on Ice Formation inside a Spherical Capsule*. Int J Therm Sci, 42:881–887.

[92] Ismail, K.A.R., and Henriquez, J.R., 2000. *Solidification of PCM inside a Spherical Capsule*. Energy Convers Manage, 41:173–187.

[93] Veerappan, M., Kalaiselvam, S., Iniyan, S., and Goic, R., 2009. *Phase Change Characteristic Study of Spherical PCMs in Solar Energy Storage*. Solar Energy, 83:1245–1252.

[94] Regin, A.F., Solanki, S.C., and Saini, J.S. 2006. *Experimental and Numerical Analysis of Melting of PCM inside a Spherical Capsule*. In: Proceedings of the 9th AIAA/ASME joint thermophysics and heat transfer conference (CD ROM). Paper AIAA 2006-3618; p. 12.

[95] Bilir, L., and Ilken, Z., 2005. *Total Solidification Time of a Liquid Phase Change Material Enclosed in Cylindrical/spherical Containers*. Appl Therm Eng, 25:1488–1502.

[96] Assis, E., Katsman, L., Ziskind, G., and Letan, R., 2007. *Numerical and Experimental Study of Melting in a Spherical Shell*. Int J Heat Mass Transfer, 50:1790–1804.

[97] Khodadadi, J.M., and Zhang, Y., 2001. *Effects of Buoyancy-driven Convection on Melting within Spherical Containers*. Int J Heat Mass Transfer, 44:1605–1618.

[98] Tan, F.L., 2008. *Constrained and Unconstrained Melting inside a Sphere*. Int Commun Heat Mass Transfer, 35:466–475.

[99] Mack, L.R., and Hardee, M.C. 1968. *Natural Convection between Concentric Spheres at Low Rayleigh Number*s. Int J Heat Mass Transfer, 11:387–396.

[100] Bahrami, P.A., and Wang, T.G., 1987. *Analysis of Gravity and Conduction Driven Melting in a Sphere*. ASME J Heat Transfer, 19:806–809.

[101] Hoshina, H., and Saitoh, T.S., 1997. *Numerical Simulation on Combined Close-contact and Natural Convection Melting in Thermal Energy Storage Spherical Capsule*. In Proceedings of the 34th national heat transfer symposium of Japan, 721–722.

[102] Yamada, K., 1997. *Numerical Simulation of the Latent Heat Thermal Energy Storage Tank*. Master thesis. Supervised by T.S. Saitoh, Tohoku University.

[103] Eames, I.W., and Adref, K.T., 2002. *Freezing and Melting of Water in Spherical Enclosures of the Type Used in Thermal (ice) Storage Systems*. Appl Therm Eng, 22:733–745.

[104] Shih, Y.P., and Chou, T.C., 1971. *Analytical Solution for Freezing a Saturated Liquid Inside or Outside Spheres*. Chem Eng Sci, 26:1787–1793.

[105] Pedroso, I.R., and Domoto, G.A., 1973. *Perturbation Solutions for Spherical Solidification of Saturated Liquids*. J Heat Transfer 95(1):42–46.

[106] Hill, J.M., and Kucera, A., 1983. *Freezing a Saturated Liquid inside a Sphere*. Int. J Heat Mass Transfer 26(11):1631–1637.

[107] Tao, L.C., 1967. *Generalized Numerical Solutions of Freezing a Saturated Liquid in Cylinders and Spheres*. AIChE J;13(1):165–169.

[108] Voller, V.R., and Cross, M., 1981. *Estimating the Solidification/ Melting Times of Cylindrically Symmetric Regions*. Int. J Heat Mass Transfer, 24(9):1457–1462.

[109] Katsman, L., June 2004. *Melting and Solidification of a Phase-Change Material (PCM)*, Graduation Project 16-04. Heat Transfer Laboratory, Department of Mechanical Engineering, Ben-Gurion University of the Negev.

[110] Assis, E., Katsman, L., Ziskind, G., and Letan, R., March 2004. *Experimental and Numerical Investigation of Phase Change in a Spherical Enclosure*. In: Proceedings of the fourth European thermal sciences conference.

[111] Tan, F.L., Hosseinizadeh, S.F., Khodadadi, J.M., and Fan, L., 2009. *Experimental and Computational Study of Constrained Melting of Phase Change Materials (PCM) inside a Spherical Capsule*, Int J Heat Mass Transfer, 52:3464–3472.

[112] Li, G., Hwang, Y., and Radermacher, R., 2010. *Experimental Investigation on Energy and Exergy Performance of Adsorption Cold Storage for Space Cooling Application*. International Journal of Refrigeration. 44:23–35.

[113] Li, G., Qian, S., Lee, H., Hwang, Y., and Radermacher, R., 2014. *Experimental Investigation of Energy and Exergy Performance of Short Term Adsorption Heat Storage for Residential Application*. Energy. 65, 675–691.

[114] Yu, N., Wang, R.Z., and Wang, L.W., 2013. *Sorption thermal storage for solar energy*. Progress in Energy and Combustion Science. 39, 489–514.

[115] Liu, H., Le Pierrès, N., and Luo, L., 2009. *Seasonal Storage of Solar Energy for House Heating by Different Absorption Couples.* 11th International Conference on Energy Storage, Effstock, Stockholm, Suède.

[116] Faninger, G., 2004. *Thermal Energy Storage*. www.etn.wsr.ac.at.

[117] Yang, R.T., 1991. *Gas Separation by Adsorption Methods*. Publishing House of Chemical Industry, Beijing, China.

[118] Wang, L.W., Wang, R.Z., and Oliveira, R.G., 2009. *A Review on Adsorption Working Pairs for Refrigeration.* Renewable and Sustainable Energy Reviews. 13(3), 518–534.

[119] Nielsen, K., 2003. *Thermal Energy Storage—A State-of-the-Art. A Report within the Research Program Smart Energy-Efficient Buildings at the Norwegian University of Science and Technology and SINTEF*.

[120] Zeolith-Technologie GmbH, 2008. *Clean Tech for Cooling, Heating and Drying.* www.zeo-tech.de.

[121] Han, B.Q., Yuan, H.Y., Yang, D.Q., and Liu, G.X., 1994. *Utilization of Natural Zeolites for Solar Energy Storage*, Lu N, Best G, Carvalho Neto CC. Editors, Integrated energy systems in China-the cold Northeastern region experience, FAO, Rome. www.fao.org.

[122] Mitsubishi Plastics. 2011. *Zeolitic Water Vapor Adsorbent*, AQSOA, Retrieved from: www.mpi.co.jp.

[123] Ponec, V., Knor, Z., and Cerny, S., 1974. *Adsorption on Solids*. Butterworth Group, London, England.

[124] Hans, V., 1985. *Heat Pumping and Transforming Processes with Intrinsic Storage*. Energy Conversion and Management. 25, 381–386.

[125] Weber, R., and Dorer, V., 2008. *Long-Term Heat Storage with NaOH*. Vacuum. 82:708–716.

[126] Bales, C., and Nordlander, S., 2005. TCA *Evaluation*: *Lab Measurements, Modelling and System Simulations*, Solar Energy Research Center Hogskolan Dalarna (Sweden).

[127] Liu, Y.L., Wang, R.Z., and Xia, Z.Z., 2005. *Experimental Study on a Continuous Adsorption Water Chiller with novel design*. Int J of Refrigeration; 28:218–230.

[128] Boer, R.d., Haije, W.G., Veldhuis, J.B.J., and Smeding, S.F., 2004. *Solid-Sorption Cooling with Integrated Thermal Storage: The SWEAT Prototype*. In: Proceedings of HPC 2004-3rd International Heat Powered Cycles Conference, Larnaca, Cyprus.

[129] Zondag, H.A., van Essen, V.M., Schuitema, R., Bleijendaal, L.P.J., Kalbasenka, A., van Helden, W.G.J., and Bakker, M., 2009. *Engineering Assessment of Reactor Designs for Thermochemical Storage of Solar Heat*. In: Proceedings of the 11th international conference on thermal energy storage (Effstock 2009), Stockholm, Sweden.

[130] N'Tsoukpoe, K.E., Le Pierrès, N., and Luo, L., 2013. *Experimentation of a LiBr-H_2O Absorption Process for Long-Term Solar Thermal Storage: Prototype Design and First Results*. Energy. 53, 179–198.

[131] Bales, C., 2013. *Laboratory Prototypes of Thermo-Chemical and Sorption Storage Units. IEA-SHC Task 32 Report B3 of subtask B "Chemical and sorption storage"*. http://members.iea-shc.org/publications/downloads/task32-Laboratory_Prototypes_of_Thermo-Chemical_and_Sorption_Storage_Units.pdf [accessed 08.01.2013].

[132] Hauer, A., 2007. *Adsorption Systems for TES-Design and Demonstration Projects*. In: HÖ Paksoy, editor. Thermal Energy Storage for Sustainable Energy Consumption. Netherlands: Springer; pp. 409–427.

[133] Lammak, K., Wongsuwan, W., and Kiatsiriroj, T., 2004. *Investigation of Modular Chemical Energy Storage Performance*. In: Proceedings of the Joint International Conference on Energy and Environment. Hua Hin, Thailand.

[134] Mauran, S., Lahmidi, H., and Goetz, V., 2008. *Solar Heating and Cooling by a Thermochemical Process. First Experiments of a Prototype Storing 60 kWh by a Solid/Gas Reaction*. Solar Energy. 82, 623–636.

[135] Quinnell, J.A., and Davidson, J.H., 2012. *Mass Transfer During Sensible Charging of a Hybrid Absorption/Sensible Storage Tank*. Energy Procedia. 30, 353–361.

[136] Quinnell, J.A., Davidson, J.H., and Burch, J., 2011. *Liquid Calcium Chloride Solar Storage: Concept and Analysis*. Journal of Solar Energy Engineering. 133: 011010e011011-8.

[137] Jaehnig, D., Hausner, R., Wagner, W., and Isaksson, C., 2006. *Thermo-Chemical Storage for Solar Space Heating in Single-Family House*. In: Proceedings of 10th International Conference on Thermal Energy Storage, New Jersey, USA.

[138] Hauer, A., 2002. *Thermal Energy Storage with Zeolite for Heating and Cooling Applications*. In: Proceedings of ISHPC 2002-International Sorption Heat Pump Conference. Shanghai, China.

[139] Stitou, D., Mazet, N., and Mauran, S., 2012. *Experimental Investigation of a Solid/Gas Thermochemical Storage Process for Solar Air-conditioning*. Energy. 41, 261–270.

9 Automated Fault Detection and Diagnosis in HVAC Systems

Marco E. Sanjuan, PhD, Cinthia Audivet, MSc, Horacio Pinzón, MSc

Abstract

As system integration becomes the norm in HVAC systems in buildings where energy conservation and efficiency are the main concern, more interdependency is built-in into system components, more variables are being monitored and controlled, and more data is available for equipment, system, and user domains. This increase in complexity and real-time information is leading toward new techniques and technologies for equipment and system level monitoring, supervision, and fault detection, some of which have emerged in commercial applications. However, there is a wealth of opportunities to enhance and integrate new and on-going research in automated fault detection techniques in building management systems (BMS), or stand-alone HVAC control and supervision applications, to increase system performance, efficiency, and quality of service.

This chapter presents a review of the different types of approaches of fault-detection techniques, state-of-the-art discoveries in the field, referenced applications to industrial and HVAC settings, commercial applications with embedded fault-detection ability, challenges to be addressed in this field, and a case study of implementation of automated fault detection in a district cooling application.

9.1 Introduction to Alarm Management and Fault Detection and Diagnosis

Control and supervision of processes and systems has become a hierarchical task where field devices interact with the process, and centralized or decentralized hardware carries out binary control functions (safety layer) and regulatory control functions (operations layer), while

communicating various types of data to a server where an industrial database resides. Linked to this database there are supervision or operator terminals with human-machine interfaces (HMIs) designed to allow for eventual, periodic or continuous observation of process behavior and performance.

One of the traditional views or screens available in such systems is the alarm management board, where a historic list of events is displayed for the system operator/supervisor to act upon it. However, as most system operators know, a distinction should be made between the annoying sound of an alarm panel and an actual process or system fault.

9.1.1 Process or System Fault Definition

A fault is considered as an abnormal operating condition developed within the process evidenced by an undesirable deviation of any characteristic property or variable from the acceptable values that define a standard behavior. Faults are usually related to changes in process parameters which the implemented control strategy cannot handle adequately and may be classified according to the nature of the atypical condition observed in each type of equipment. A general description of the most common fault types and some examples evidenced in HVAC systems are presented below.

A *process parameter change* is the most common source for faults within industrial processes. This type of fault is mostly developed on the main equipment and is related to aging or continuous operation. An example of process parameter changes affecting HVAC systems is the fouling condition on preheating, heating or cooling coils that leads to a reduction on heat transfer capabilities. Furthermore, a *Disturbance parameter change* is a deviation on a not-controlled variable larger than the identified maximum allowable magnitude driving the process outward the safe operating region determined by the control strategy set in place. Thermal load variations and several environmental changes are common disturbance sources affecting HVAC systems.

Actuator problems are directly related to an anomalous performance of any final control element such as dampers, fans or valves. Common HVAC

faults related to actuators include fan motor failure, damper or valve stiction, severe internal leakage, among others. On the other hand, *sensor problems* are related to erroneous measurements on the sensing element evidenced on biased or not steady signals produced by mechanical or electrical damage. Temperature, pressure or flow sensors exhibiting an offset or drifting behavior comprise the most common examples for this type of fault source.

Finally, *component failures* affecting the normal process dynamic response such as duct structural failures inducing air leakage or controller malfunctioning are common examples of faults and symptoms on major HVAC equipment. This type of mechanical or structural fault normally requires direct human intervention to isolate and recover the underlying faulty condition. Some examples of the most common faulty conditions developed in HVAC systems including type and process location are illustrated in Figure 9.1.

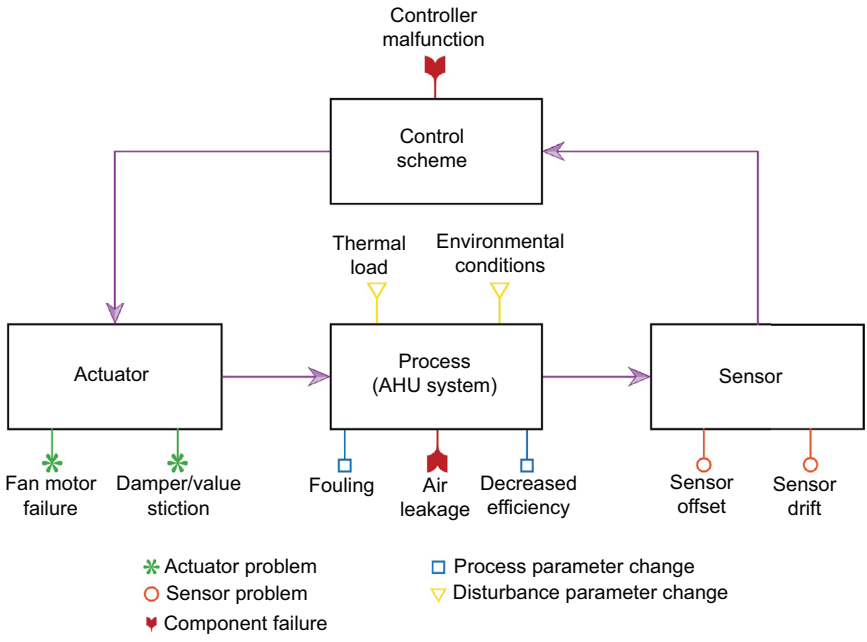

Figure 9.1. Common HVAC faults.

9.1.2 Process Monitoring Method

A process monitoring method, hereafter PMM, is considered a set of supervisory procedures implemented alongside a process control strategy to guarantee a proper system operation within safe and optimum limits, and given the presence of any abnormal condition, trigger the required procedures to mitigate the anomalous condition effectively. A PMM is comprised of four stages: Fault detection, identification and diagnosis followed by process recovery.

In the *fault detection* stage is determined whether a fault has occurred within the system. Its main goal is to acknowledge the presence of the abnormal condition at early or incipient phase and emit alarms to prevent major upsets within the process. Once detected, the rest of the process monitoring loop is triggered. The second stage pursues the *fault identification* isolating the process variables that contribute the most to the fault. Hence, the operating personnel may focus their attention on the main subsystem or a reduced set of variables facilitating the following diagnosis stage.

Fault diagnosis comprises the procedures required to determine the exact cause affecting the process. Once complete diagnosis is achieved,

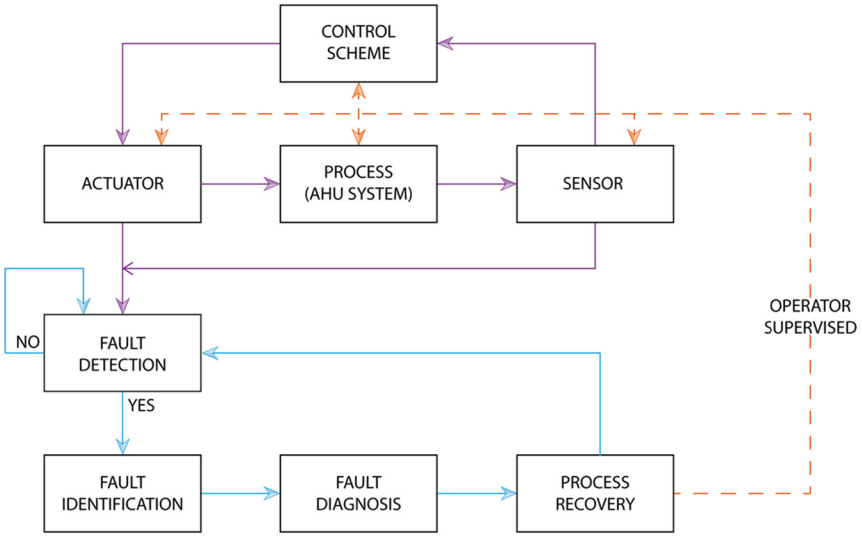

Figure 9.2. Process Monitoring Method and its implementation.

the main fault features such as nature, location and initiation time are completely acknowledged [1]. Finally, the last PMM stage is the *Process Recovery* where the operators intervene the process to implement actions to overcome the anomalous condition.

Although several researches have been conducted on each PMM stage to achieve a complete automated online solution, the fault diagnosis and process recovery stages still remain a partially automatic engineering supervised activities. The integration of the PMM procedures with the control strategy implemented in the process is illustrated in Figure 9.2.

9.2 Classification of Fault Detection Methods

Although intuition and experience are considered tools to detect a faulty condition, they are difficult to teach and even harder to encapsulate or embed in an automated system. In addition, they are not available in new processes or systems, or even in those with major innovative configurations. This leads to the need of formal methods to address fault detection as a specific task within an automated system. The successful implementation of a monitoring method for fault detection is highly dependent on:

- Process knowledge
- Overall process characterization approach (stochastic vs deterministic, first principle vs empirical, univariate vs multivariate)
- Amount and quality of available data
- Availability of an experienced operator willing to work in the development team

9.2.1 Traditional Alarm Management—A Prismatic Approach

One of the more intuitive, but formal, approaches to fault detection is to identify a set of key process variables, and identify for them lower and upper limits. This approach, commonly used in SCADA and DCS systems, reflects a non-interdependent view of variables within a process or system. If a single variable is chosen for monitoring, the feasible region of operation is described by a line segment. If two variables are chosen for monitoring, the feasible region of operation is described by a rectangle, if three variables are chosen; the feasible region becomes a tridimensional prism; if n variables are chosen, the feasible region becomes an nth

dimensional prism. Hence, we call this method of individual limits per variable, a prismatic approach to fault detection.

The main drawback from this approach is not only the lack of consideration of variables' interaction, but also the underlying assumption that feasible operation regions for industrial process or physical systems have linear frontiers with sharp edges. Process and system modelling analysis in physical domains commonly lead to nonlinear equations or models; therefore the inference of a nonlinear limiting operating region is more than reasonable.

Figure 9.3 illustrates the two possible prismatic boundaries that could be built given an actually nonlinear feasible operating region in a bi-dimensional process with temperature and pressure as monitored variables. The yellow region describes the feasible operation region or all possible pressure–temperature combinations that do not represent a hazard. Outside this region, humans, the environment, or equipment are at risk. Two prismatic regions may be defined on this region to create the alarm frontier: the circumscribed or outer prism (dashed lines) and the inscribed or inner prism (solid lines). The use of the outer prism makes no operational sense, since no alarm will be triggered outside the feasible region but inside the outer prism, leading to undetected faulty conditions.

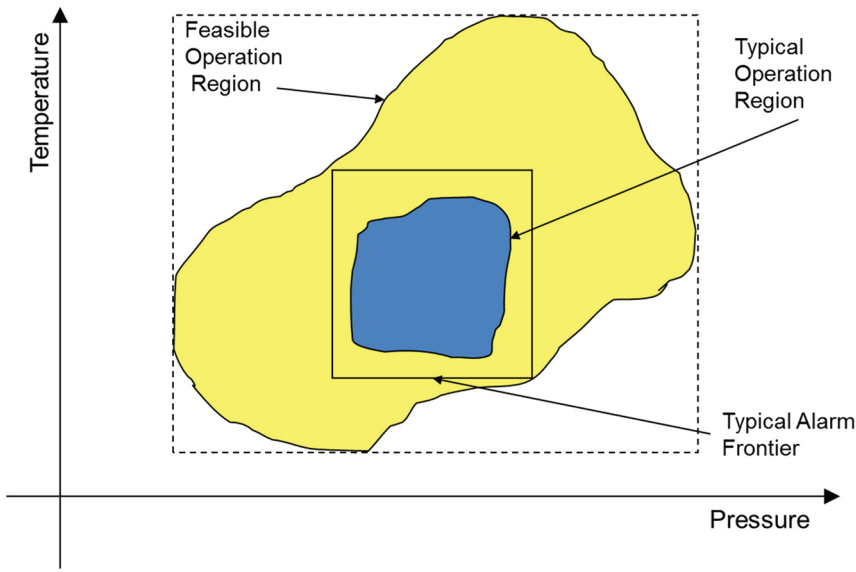

Figure 9.3. Feasible, typical and alarm region for a nonlinear process.

In practical sense, this outer prism leads to very low rate of false alarms, but very high rate of missed detections. The use of the inner prism, a common practice in SCADA and DCS configurations, almost makes sure that no faulty condition goes undetected, but induces a large set of false alarms, due to the prism's inability to better "fit" the feasible region.

If the inner prism is selected, no one should be surprised of monitoring systems generating alarms and most of them being discarded by the operator because no actual undesired behavior or performance is observed in the system under observation. As many process or system operators of highly automated and frequently monitored systems have seen, this is unfortunately common.

The need for a major shift in how industry approaches fault detection and alarm generation is supported by extensive research in this field, and a growing number of more sophisticated, and adapted to the "true" process shape, monitoring methods.

9.2.2 Most Commonly Used Fault Detection and Diagnosis Methods

As mentioned before, fault detection and diagnosis techniques are divided in three main approaches based on the nature of the available process information. Model based approaches are suitable when the *a priori* knowledge relies on a widespread comprehensive understanding of the fundamental physics and dynamics described by the process. Model-based methods are divided in qualitative-driven and quantitative-driven depending on the type of knowledge used for its development. On the other hand, the third approach, known as the data-driven approach, is suitable for large complex processes with a lot of available historical data and, due to the size and process features, a model-based approach is unfavorable.

The quantitative model-based methods are developed from a comprehensive knowledge of process physics, dynamics and chemistry achieving a descriptive analytics model using fundamental equations such as energy and mass balances, dynamic and momentum equations, among other mathematical functional relationships. The basic principle is to estimate states or parameters to develop analytic models and process features, and as a result of a comparison with actual online data, generate residuals to perform the fault detection and diagnosis procedures. The quantitative model-based techniques are usually clustered depending

on the use of input and output information and a general overview is illustrated in Figure 9.4. Venkatasubramanian et al. [2] and Isermann [1] performed an extensive review of quantitative model-based techniques.

On the other hand, the qualitative model-based methods translate the process knowledge to a non-mathematical set of qualitative functions centered around the main components of the process aiming to develop a logical framework to detect and diagnose abnormal conditions based on historic or deductive information. Its outcome is more limited than those provided by quantitative models in favor of a lighter required understanding of the process and a simpler structure. The early qualitative model-based methods were developed using an abductive approach relying on an if-then rules structure for fault detection with high computational demand and failing to diagnose any new faulty condition. Recent techniques use an inductive or deductive approach to include experimental knowledge to strengthen its database with an adaptive self-learning scheme and sum new information for fault and diagnosis procedures. Venkatasubramanian et al. [3] performed an extensive review of qualitative model-based techniques and a general overview is illustrated in Figure 9.5.

Finally, the data-driven methods use historic data to extract process features, especially of normal operating conditions, to develop a formal structure to perform the process monitoring. Their principal advantage relies on the independence of *a priori* process knowledge becoming the most diversified approach with the largest number of satisfactory implementations even though its performance is bounded by the quality of the historic data used.

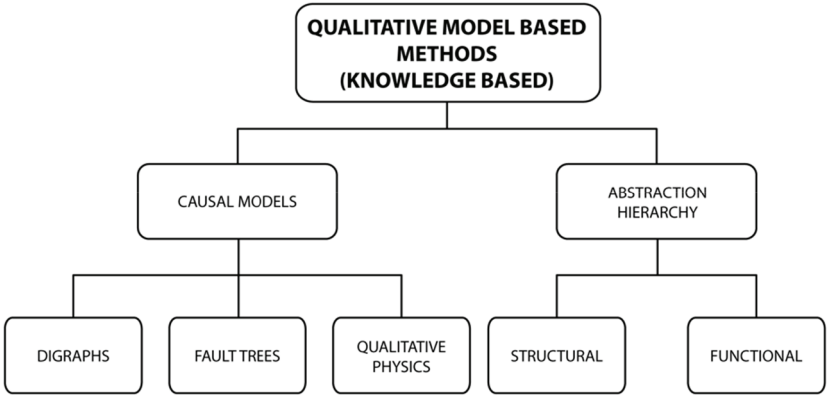

Figure 9.4. Qualitative Model-based Methods. Adapted from reference [3].

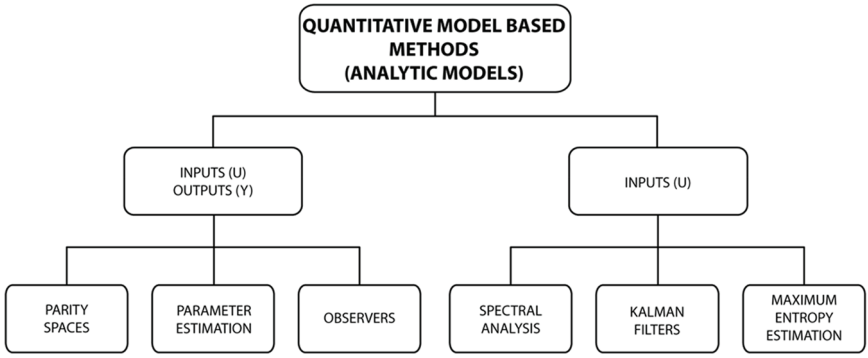

Figure 9.5. Quantitative model-based methods.

Data-driven techniques may be clustered in qualitative and quantitative approaches: Qualitative methods analyze the information to identify systematic trends on historic data to determine the presence of an abnormal condition whether quantitative methods are based on mathematical or statistical models extracted directly from data. Most of data-driven techniques are implemented in two steps: A feature extraction performed over offline historic data followed by an online process monitoring implementation. Venkatasubramanian [4] performed an extensive review of data-driven techniques and a general overview is illustrated in Figure 9.6.

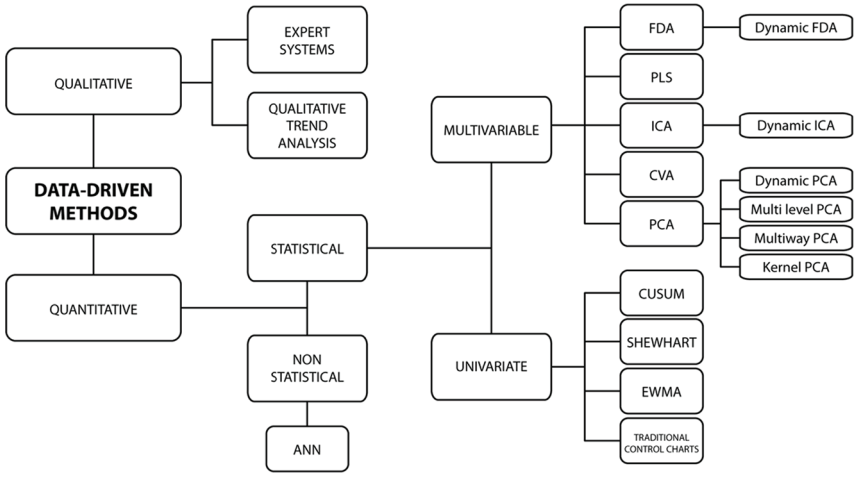

Figure 9.6. Data Data-driven methods.

9.2.2.1 Principal Component Analysis

The most popular data-driven technique used for fault detection purposes is known as Principal Component Analysis (PCA) and it is based on researches carried out by Pearson [5] and Hotelling [6] to develop a formal method to include the cross-correlation of process variables into multivariable statistical analysis.

PCA, as data-driven multivariate statistical technique, requires the application of data pretreatment operation prior its execution. Autoscaling is the main operation and may be defined as a standardization procedure applied over the observations matrix as follows:

Let $X_R \in \mathbb{R}^{n \times m}$ a data set consisting of m process variables and observations for each variable stacked in a matrix given by

$$X_R = \begin{bmatrix} x_{11} & x_{12} & \cdots & x_{1m} \\ x_{12} & x_{22} & \cdots & x_{2m} \\ \vdots & \vdots & \ddots & \vdots \\ x_{n1} & x_{n2} & \cdots & x_{nm} \end{bmatrix} \tag{9.1}$$

and let $\overline{x}_i$ y s_i the sample mean and standard deviation computed for the *i-th* column (variable) based on its n_i observations stored in two diagonal matrices $\overline{X}_R$ and $\Sigma_R \in \mathbb{R}^{m \times m}$ as follows,

$$\overline{X}_R = \begin{bmatrix} \overline{x}_1 & 0 & \ldots & 0 \\ 0 & \overline{x}_2 & \ldots & 0 \\ \vdots & \vdots & \ddots & \vdots \\ 0 & 0 & \ldots & \overline{x}_m \end{bmatrix} \tag{9.2}$$

$$\sum_X = \begin{bmatrix} s_1 & 0 & \ldots & 0 \\ 0 & s_2 & \ldots & 0 \\ \vdots & \vdots & \ddots & \vdots \\ 0 & 0 & \ldots & s_m \end{bmatrix} \tag{9.3}$$

An autoscaled observation matrix $X \in \mathbb{R}^{n \times m}$ may be computed using the following expression

$$X = (X_R - J_{nm} \cdot \overline{X}_R) \cdot \sum_X^{-1} \tag{9.4}$$

$$J_{nm} = \begin{bmatrix} 1 & 1 & \dots & 1 \\ 1 & 1 & \dots & 1 \\ \vdots & \vdots & \ddots & \vdots \\ 1 & 1 & \dots & 1 \end{bmatrix} \in \mathbb{R}^{n \times m} \tag{9.5}$$

where J_{nm} is the identity matrix on a Hadamard product [7]. Then the sample covariance matrix $S \in \mathbb{R}^{m \times m}$ of the autoscaled data set is equal to

$$S = \frac{1}{n-1} X^T X \tag{9.6}$$

As each entry of the covariance matrix is in general different of zero for an industrial process data set, this comprises a formal prove for variables cross-correlation. To decouple the observation space into a set of uncorrelated variables, an eigenvalue decomposition of the S matrix is carried out,

$$S = V \Lambda V^T \tag{9.7}$$

with

$$\Lambda = \begin{bmatrix} \lambda_1 & 0 & \dots & 0 \\ 0 & \lambda_2 & \dots & 0 \\ \vdots & \vdots & \ddots & \vdots \\ 0 & 0 & \dots & \lambda_m \end{bmatrix} \in \mathbb{R}^{m \times m} \tag{9.8}$$

$$V = [V_1 \, V_2 \dots V_m] \in \mathbb{R}^{m \times m} \tag{9.9}$$

where Λ is a diagonal matrix containing the eigenvalues of S, and V is an orthogonal matrix containing the corresponding eigenvectors and describes the principal directions of variation denoted by the observation space as depicted in Figure 9.7 (a).

In general, a matrix $Y \in \mathbb{R}^{n \times m}$ containing a set of uncorrelated variables is given by,

$$Y = XV$$

$$y = [y_1 \; y_2 \dots y_m]^T = V^T x \tag{9.10}$$

(Decorrelated Observation)

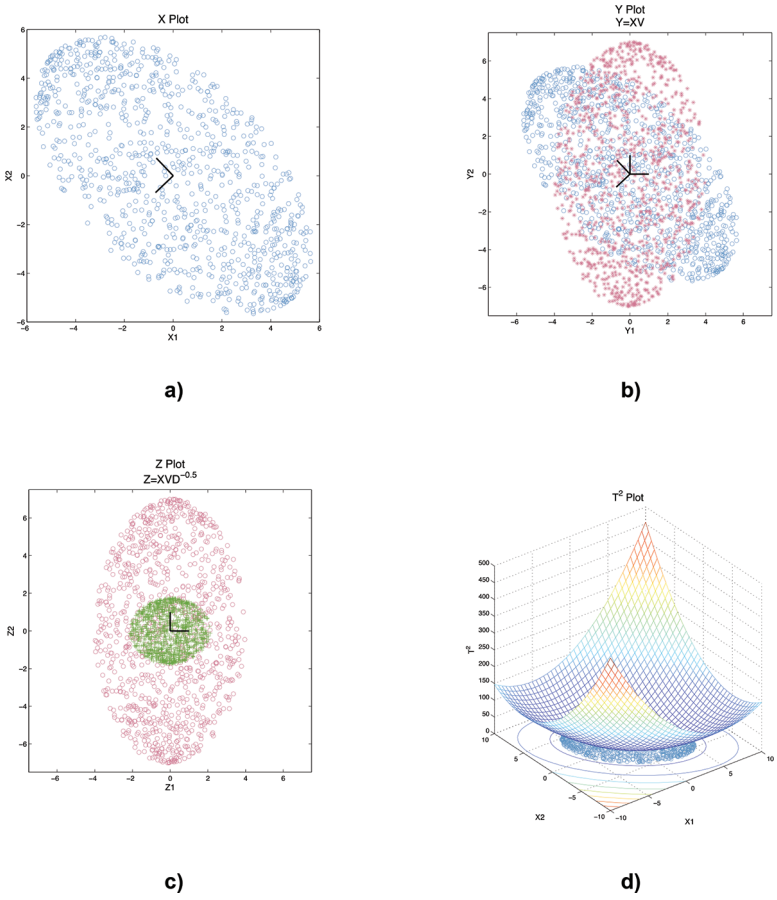

Figure 9.7. PCA Representation: (a) Original data X, (b) uncorrelated data Y, (c) scaled data Z, (d) de Hotelling's T^2 statistic.

and it may be understood as a transformation operation over the observation space X using V as rotation matrix to align its major axes to those of as depicted in Figure 9.7 (b). A second scaling operation is carried out to produce decorrelated variables with unity variance $Z \in \mathbb{R}^{n \times m}$, as presented in Figure 9.7 (c),

$$Z = XV\Lambda^{-1/2}$$

$$z = \left[\frac{y_1}{s_1} \quad \frac{y_2}{s_2} \quad \cdots \quad \frac{y_m}{s_m} \right] = \Lambda^{-1/2} V^T x \tag{9.11}$$

(Scaled Observation)

Finally, the Hotelling's T^2 statistic may be computed for each observation,

$$T^2 = z^T z \qquad \text{or} \qquad T^2 = \frac{y_1^2}{s_1^2} + \frac{y_2^2}{s_2^2} + \cdots + \frac{y_m^2}{s_m^2} \tag{9.12}$$

Hence, the Hotelling's T^2 statistic is a scaled squared norm of an observation vector and allows a scalar threshold to characterize the variability of the data in the entire-dimensional observation space [8]; its behavior on the observation space may be observed in Figure 9.7 (d).

PCA as a dimensionality reduction technique divides the entire observation space in two orthogonal subsets: a score subspace capturing the main systematic variability and a residual space associated with random noise. Order reduction is achieved by the application of any methodology or rule such as percentage variance test, scree test, parallel analysis and Kaiser's rule. Authors have studied the fault detection performance and main results points out that analysis parallel provides a superior outcome [9–11].

As a result, a subset of $a < m$ variables are selected yielding the original eigenvalues and eigenvectors matrices to $\Delta_a \in \mathbb{R}^{a \times a}$ and $P \in \mathbb{R}^{m \times a}$ as follows,

$$\Lambda_a = \begin{bmatrix} \lambda_1 & 0 & \dots & 0 \\ 0 & \lambda_2 & \dots & 0 \\ \vdots & \vdots & \ddots & \vdots \\ 0 & 0 & \dots & \lambda_a \end{bmatrix} \tag{9.13}$$

$$P = [V_1 V_2 \dots V_a] \tag{9.14}$$

Hence, the score T and E residual spaces are given by

$$t = P^T x \tag{9.15}$$

(Transformed uncorrelated Observation)

$$r = (I - PP^T)x \tag{9.16}$$

(Residual Observation)

Or

$$T = XP \tag{9.17}$$

$$E = X - XPP^T \tag{9.18}$$

The Hotelling's T^2 statistic is calculated as aforementioned based on the score matrix derived on the order reduction step and the reduced eigenvalues matrix.

The fault detection threshold for the Hotelling's T^2 static is given by

$$T_\alpha^2 = \frac{a(n-1)(n+1)}{n(n-a)} F_\alpha(a, n-a) \tag{9.19}$$

The residual space is monitored by the Q statistic, also known as the squared prediction error, and may be computed from a residual observation,

$$Q\ (SPE) = r^T r \tag{9.20}$$

The fault detection threshold for the squared prediction error is determined by Jackson and Mudholkar [12] as follows,

$$Q_\alpha = \theta_1 \left[\frac{h_0 c_\alpha \sqrt{2\theta_2}}{\theta_1} + 1 + \frac{\theta_2 h_0 (h_0 - 1)}{\theta_1^2} \right]^{1/h_0} \tag{9.21}$$

where,

$$\theta_i = \sum_{j=a+1}^{n} \sigma_j^{2i} \qquad h_0 = 1 - \frac{2\theta_1 \theta_3}{3\theta_2}$$

A flow diagram describing the main steps on the offline and online PCA implementation is illustrated in Figure 9.8.

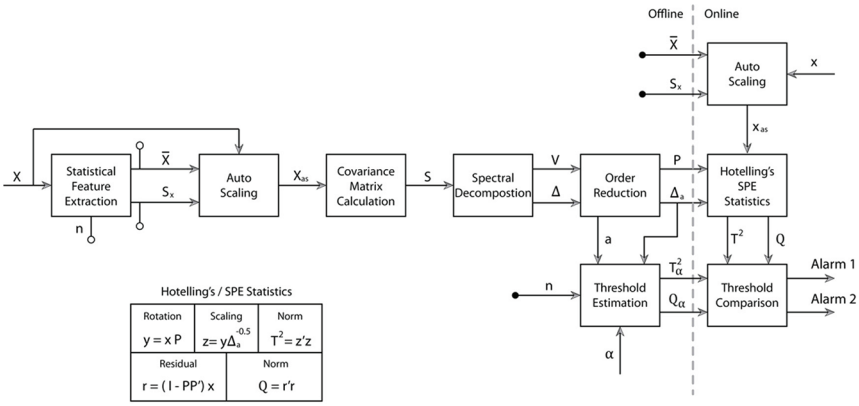

Figure 9.8. PCA Operational flow diagram.

9.2.2.2 Current Trends in Fault Detection Systems

Recent advances in data-driven methods focus on the development of robust techniques to address two main issues: The lack of adaptability of actual techniques to incorporate new available process states related to unknown faults or aged operating conditions, and the addition of diagnosis capabilities to the traditional statistical techniques (PCA, PLS, ICA, etc.) primarily designed for fault detection purpose only.

Adaptive fault detection has been mainly addressed using pattern recognition or clustering algorithms merged with traditional fault detection techniques (See section 3) to include new faulty conditions, or developing recursive schemes for traditional fault detection techniques to properly update the statistical structure given a new operating condition derived of slow dynamic trends related to aging. Jeng [13] and Li et al. [14] developed recursive update techniques for PCA-based fault detection, Portnoy et al. proposed an improved recursive update PCA-based fault detection technique with less computational complexity [15], Zhang et al. developed a recursive PCA based technique for adaptive fault detection for multi-mode processes [16], and Zhang et al. developed a recursive kernel PCA technique to include the time-varying and nonlinear process features with less computational demand [17].

The large amount of available fault detection and diagnosis techniques may rely on the fact that the performance of any method depends on the particular process conditions and the type of information available for these purposes. A recent trend on fault detection techniques is to integrate two or more techniques to obtain a more robust hybrid solution capable of overcome the individual limitations imposed by actual approaches.

Bin et al. [18] proposed a combination of PCA with a CUSUM univariate chart to expand the PCA capabilities achieving more sensible fault detection results over a Tennessee Eastman process and identifying new faults otherwise not detected. Cheng and Liao [19] proposed a technique combining artificial neural networks (ANN) and PCA developing a ANN-based model that compute residuals when compared with actual measurements and then feed a PCA-based strategy for fault detection and diagnosis. Lau et al. [20] proposed the integration of multi-scale PCA (MPCA) with an artificial neuro-fuzzy inference system (ANFIS) each one responsible for fault detection and diagnosis respectively. Sun et al. [21] proposed a combination of PCA with fault detection trees developing

a solution capable of performing fault detection and diagnosis with less training when compared to hybrid techniques using PCA and artificial neural networks (ANN). Venkatasubramanian et al. [22] developed an integrated hybrid framework including several techniques such as digraphs, observers, trend analysis and some statistical classifiers methods.

Beyond the aforementioned challenges particularly related to data-driven techniques, the major challenge in the process monitoring field is to develop an artificial self-controlled intelligent control system to assist human operators in this area, especially for fault identification and diagnosis and it is viewed as the next milestone in control systems research and its applications [2]. An Expert system is proposed as a specialized scheme that codifies knowledge gathered highly trained operating personnel with diagnosis capabilities over the domain of expertise to build a robust rule-based database and an inference engine [4,8,23]. Although it offers a transparent well supported explicit decision making process its major drawbacks also relies on the inherent dependency on the quality of the stored human expert knowledge, application-oriented implementation and its constantly increasing complexity when new information is added to the database and inference system [22].

Similar approaches are obtained with the implementation of artificial neural networks schemes exclusively. The main difference is to use a lower-level numerical model instead of a high-level logic model used by expert systems [24] with an adaptable underlying trainable weight structure. Fault detection and diagnosis ANN schemes ranges from one step multi-layer models (traditional ANN) to neuro fuzzy schemes featuring specialized networks for detection and diagnosis independently [25].

9.3 Recent Advances in Fault Detection for HVAC Systems

Heating, Ventilation and Air Conditioning System (HVAC) is considered the principal energy consumer in commercial and residential buildings. Usually, part of the energy is wasted due to improper design, poor maintenance, non-optimal operating conditions, poor performance of the control strategy and a complete or partial failure of its physical components. Faults can represent 20% to 30% of the total energy waste and may have other consequences such as inappropriate reference values for system operation, equipment life expectancy reduction, user thermal comfort reduction and poor indoor environmental quality. Fault detection

and diagnosis (FDD) methods have the potential to provide effective means to ensure more efficient and safe operation of HVAC systems [26–28]. A research performed in UK buildings confirmed that 25% to 50% of energy wasted is caused by faults in buildings HVAC systems. This range could be reduced below 15% whenever those faults could be detected and identified early before unacceptable damages occur.

Many researches have been conducted on fault detection and diagnosis implemented in HVAC systems primarily focused on faults developed in its physical components such as air handling units (AHU), variables air volume boxes and chillers, and their control instrumentation (sensors and valves) [29–31]. HVAC-oriented implementations may be divided in two major trends: The first trend comprises researches using a single technique and several examples are found in literature for both model-based and data-driven methods [32–40] while the second trend comprises hybrid methods combining two or more techniques from different approaches to enhance the performance of FDD systems in terms of robustness and efficiency, thus detecting and diagnosing a larger amount of faults with higher accuracy in a less time [26,41–51].

In the last 5 years, a wide range of statistical and machine learning techniques have been explored as a data driven methods for FDD in buildings. In general, statistical process history-based methods are preferred due to their dimensional reduction capabilities, the development of a process model from data exclusively [52–55] and their independency of a prior expert knowledge for fault identification and diagnosis depending only on the availability of classified training data. The use of hybrid techniques enhances the performance of an individual diagnosis approach in terms of robustness and efficiency. Table 9.1 summarizes the FDD methods developed in the last 5 years.

Furthermore, the vast majority of FDD HVAC-oriented methods are particularly developed to address the process monitoring activity of the water loop or the air loop equipment individually and future strategies are encouraged to analyze the overall system as a single unit. Air handling Units and Chillers are considered the most important components in the HVAC systems due to their energy consumption and the role maintaining comfortable and productive indoor air quality conditions. Several researches report advances in the development of FDD strategies in these components.

Najafi et al. [49] proposed a set of diagnostic algorithms for AHUs based on a comparative analysis between an online observed behavioral

Table 9.1. Recent Trends in FDD Methods for Buildings.

Approaches					
QKB	**QAM**	**DDM**	**System**	**Techniques**	**References**
X			AHU	Model based methods for isolation of sensor faults	[56,57]
X	X		AHU	Model based methods, Experts Rules based fault classifiers	[28,39]
X		X	Chiller	Statistical Process Control (SPC) + Kalman filtering based on gray-box models	[58]
	X		AHU	Ruled based methods	[59]
				Principal Component Analysis + Reconstruction based contribution approach + Decision tables	[41]
			Chiller	Tree-structured Fault Dependence Kernel + Learning techniques	[44]
				Radial Basis Function neural network + Exponentially Weighted Moving Average control charts + Rule based diagnostic techniques	[26]
	X	X		Exponentially Weighted Moving Average control charts + Rule based diagnostic techniques	[60]
			AHU	Rule-based expressions + Regression + One-class support vector machine (SVM) + Adaptive resonance theory (ART) + Lateral priming adaptive resonance theory (LAPART).	[61]

(*Continued*)

Table 9.1. Recent Trends in FDD Methods for Buildings. (*Cont.*)

	X	Chiller	Decoupling-based methods	[46]
			Support Vector Data Description.	[51,54,62]
			Linear discriminant Analysis	[63]
			Exponentially Weighted Moving Average (EWMA) control charts + Support Vector Regression	[50]
			Advanced Bayesian nonlinear state estimation techniques + Back-smoothing method	[64]
			Auto-regressive model with exogenous variables + Support Vector Machines	[65]
			Self-Adaptive Principal Component Analysis	[55]
			Regression Models + Adaptive Thresholds	[45]
			Combined Neural Networks, Subtractive Clustering Analysis	[48,66]
			Pattern Matching Methods and Bayesian probabilistic models.	[49]
			Nonlinear Autoregressive with Exogenous (NARX) method based on Least Squares Support Vector Machine (LS-SVM)	[67]
			Support Vector Machine techniques	[68]
		AHU	Principal Component Analysis + Cluster analysis	[69]
			Principal Component Analysis + Active Functional Testing	[42]
			Principal Component Analysis + Pattern Matching Methods	[43]
			Ensemble Rapid Centroid Estimation + Parallel Nonlinear Auto-Regressive Neural Network with exogenous inputs and distributed time delays	[47]
			Principal Component Analysis + Wavelet transform	[70]

Note: DDM: Data-driven Methods; QAM: Quantitative Analytic Models; QKB: Qualitative Knowledge-based Methods.

pattern with a set of predefined patterns extracted from different faults to find the closest match. Their approach can be formulated as an estimation of the posterior distribution of a Bayesian probabilistic model demonstrating less model accuracy dependency and more flexibility to measurement constraints.

Wen et al. [43] developed an hybrid fault detection strategy based on PCA and Pattern Matching method for AHU avoiding any requirement of priori knowledge and a minimal computer demand to implement the operating system. Authors proposed a preliminary screening of historical data to locate operation intervals that are similar to current operating conditions based on a PCA similarity factor and distance similarity factor estimating the degree of similarity between historical data window and current snapshot data. In general, the use of pattern recognition methods transforms a FDD problem into a classification problem as they extract the patterns' database from process data to create normal and faulty classes and optimizing the final diagnosis stage.

Zhao et al. [50] developed a robust statistical FDD method combining the EWMA chart with Support Vector Regression (SVR) models focused on the detection of incipient low-magnitude faults located at chillers. Their main idea is to create a benchmark reference model using SVR and then calculate a set benchmark performance indexes; finally, the same metrics are estimated for current process conditions and a set of residuals are monitored using the EWMA control charts to detect the faults. To extend detection capabilities to include fault diagnosis capabilities authors proposed in the use Support Vector Data Description (SVDD) algorithm [51]. The main idea is to find a minimum-volume hypersphere in a high dimensional feature space to enclose most of the data of an individual class and to transform the chiller FDD problem into a typical one-class classification problem. The results show that the proposed strategy can identify more than 90% data of their own classes to be inliers and also reject data of other classes.

A similar approach is proposed by Wen et al. [44] using a hierarchical kernel learning method instead of using traditional classification methods such as Multi-class SVM, decision trees, Ada Boost, Quadratic Discriminant Analysis or Logistic regression as these techniques ignore the relationship among different faults in chillers. Authors proposed a novel data-driven strategy that adopts structured labeling to include the dependency information and describe the severity level in a large margin learning framework.

Similar to pattern matching techniques, the artificial neural networks techniques have been used to improve the accuracy of fault detection and diagnosis methods. Du et al. [48] merged an artificial neural network with subtractive clustering analysis to detect abnormalities in a AHU. Authors used the first technique to detect a faulty condition while the second is used for fault diagnosis through adaptive classification. Authors also proposed a fault library with common abnormalities such as a fixed return water temperature sensor bias, fixed or drifting supply air temperature sensor bias, a complete supply temperature sensor failure and chilled water valve stiction.

Tran et al. [26] consider a chiller the main target for FDD in HVAC systems as this equipment consumes the major part of the power, hence "a highly effective approach" is necessary to improve its reliability. Authors proposed a hybrid strategy based on a Radial Basis Function (RBF) neural network, the Exponentially Weighted Moving Average (EWMA) control charts and a rule-based diagnostic technique. Results show that the proposed FDD strategy can effectively achieve a significant improvement in accuracy and reliability.

Beghi et al. [41] proposed a fault detection and diagnosis algorithm for HVAC water chillers employing a semi-supervised data-driven approach. Their method uses principal component analysis (PCA) to distinguish anomalies from normal operation variability and reconstruction-based contribution techniques to isolate variables related to faults. The algorithm performs the fault detection, fault identification, fault reconstruction and fault diagnosis, assuming the occurrence of one fault per time in chiller units.

9.4 Industrial and HVAC Applications of Fault Detection Methods

The concern for increased availability of HVAC systems, reducing operating time under sub-optimal conditions, and the increased concern for energy efficiency and quality of service has led to an increase in measured variables and user's willingness to pay for more than just "a working system", understanding that the proper monitoring and service strategy increase the system's life span and reduces the overall operating cost. This section discusses peripheral requirements and existing business models for automated fault detection systems.

9.4.1 Hardware/Software Requirements

The days of the lonely equipment are over. Even before the raise of IoT (Internet of Things), major equipment manufacturers were concerned about the system's ability to allow remote or onsite monitoring and performance analysis.

In HVAC systems, beyond the traditional sensor/transmitters, actuators, control valves, and control computer or system CPU, typically all of them in the field, the implementation of an automated fault detection strategy would require:

- An industrial communication network, or field bus, linking the system's controller to a SCADA (Supervisory Control and Data Acquisition), a DCS (Distributed Control System), or a local network where monitoring stations (PCs or Workstations) are connected. In HVAC systems BACnet has become the standard data communication protocol, although most automation systems allow for OPC connectivity,
- A server, running services and tasks, as well as an industrial data base, where process information is stored and made available for visualization, analysis and reporting,
- A networked computer, commonly a PC with robust specifications, where the operator's HMI runs, commonly based on windows, variables (or tags), scripts, and embedded code,
- A monitoring software, which could be from the HVAC system manufacturer, or open SCADA-type software with OPC connectivity to field controllers, and
- A software solution with the ability to carry the complex mathematical calculations demanded by the automated fault detection method, with connectivity to the industrial data base.

Most SCADA-type solutions (ISA 95 Level 2) will lack the embedded ability to perform matrix operations, calculate statistical functions, or run signal processing algorithms. In these cases, either a third-party solution is used, or an embedded Visual C++ or VBA program must be linked. One of the few SCADA-type solutions with enough intrinsic computational functions is LabView ® DSC (from National Instruments), and most state-of-the-art algorithms can be developed and embedded in this platform. DCS architectures have a more robust framework, suitable for a wide array of numerical calculations. In the past 10 years some DCS manufacturers have increased the

array of mathematical functions available for engineering calculations, and some advanced control software manufacturers, such as AspenTech, already have products with PCA and multivariate statistical analysis capabilities. The next section describes commercial solutions available for FDD by 2016, as well as business models under which they are being offered.

9.4.2 Business Models and Commercial Solutions

The implementation of Building Automation Systems (BAS) to provide automatic monitoring and control of building systems has stimulated the development of fault detection and diagnosis commercial software. These innovative solutions focus on the building's energetic efficiency, extended equipment life and performance, and maintenance services reduction [71]. Their incremental popularity relies on the effectiveness of these tools to monitor the HVAC components and mitigate the negative impact of a fault eventuality.

FDD software uses the existing operational data sources (Building Management & Control Systems (BEMS), Energy Management & Control systems, wireless sensors, weather data, and smart meters) to feed the underlying fault detection scheme such as rule-based inference systems, a residual estimation analytic model or a data-driven statistical model. Although any BEMS also provides a prismatic alarm approach to monitor HVAC components, their identification and diagnosis capabilities are very limited or nonexistent. The FDD software are capable to detect and diagnose faults at a component level and a system level in real time before they become an issue warranting such downtime [72], and some of them may include data trend analysis to improve its detection capabilities.

Table 9.2 summarizes the FDD commercial software emerged over the last years including its scope, the techniques used and its developer. Mostly, available FDD software has an underlying detection structure based on an expert rule system and a minority uses an artificial intelligence or statistical modelling approach. FDD software is administered by the developer under a subscription or a stand-alone license plan.

9.4.3 Review of Industrial and HVAC Implementations of FDD

A general overview of HVAC-oriented FDD researches indicates that these studies are mainly conducted by software developers or government

Table 9.2. FDD Commercial Software Released Over the Last Years.

Software	Company	FDD Methods	Scope	Acquisition Mode	Building Type
SkySpark	SkyFoundry	Rules based methods.	Based on rules, SkySpark looks for a correlation or match in new data and in historical data. If it finds a match then automatically generates visualizations, notifications and reports that show the issue (time, frequency and duration) [73,74].	Stand-alone Software.	Large commercial
Panoptix Continuous Diagnostic Advisor	Johnson Controls	Expert Rule based analysis Statistical analysis: Temporal, Regression and Peer analysis.	Panoptix reviews equipment performance, assesses effectiveness, and generates reports about energy efficiency and fault detection and it diagnostic [75,76].	Administered by Johnson Controls. The customers buy a subscription to access to the app.	Large commercial
ClockWorks	KGS Buildings	Rules based methods.	It performs a real-time automated fault detection and diagnostic, links to external management systems, informs about cost and energy saving opportunities and generates custom reports [77].	It is a cloud-based software application. Customers buy a subscription to access to the app.	Large commercial

SCIwatch®—Continuous Commissioning	Natural Logic strategic ally Scientific Conservation Inc.	Pattern recognition methods, Neural networks.	It is a platform that interfaces with BEMS for automatic data collection, fault diagnostics and work order issuance and tracking [78].	It is a cloud-based software application.	Large commercial
Trane Intelligent Services	Trane	Rules based methods.	In case of fault, Trane technical specialists respond immediately and remotely to any fault alarm, interrogate the system and perform system diagnostics [79,80].	Remote Trane service.	Large commercial
DABO™	ADMS Technologies	Rules based methods and performance indices.	It detects and diagnoses the operation inconsistencies and poor performances of systems and anticipates breakdowns. Its diagnoses enable long-term maintenance of an optimized operation and prevent comfort and energy waste problems [81,82].	Licensed software.	Large commercial

(*Continued*)

Table 9.2. FDD Commercial Software Released Over the Last Years.(*continued*)

Software	Company	FDD Methods	Scope	Acquisition Mode	Building Type
IBM TRIRIGA Energy Optimization	IBM—Intelligent Building Management	Rules based methods.	It captures data from Building Management & Control Systems and uses it for energy improvement and operating cost reducing. If anomalies are detected from application of analytical rules based on energy and operational data, it generates work order. Use historical data to compare trends and identify corrective actions [83,84].	Licensed software.	Large commercial
APAR & VPACC	NIST	Expert rules based methods.	The software can detect common mechanical faults and control errors in air handling units and variable air volume boxes. The software generates alarms, work order, fault codes [85].	Unknown	Medium/Large commercial

PACRAT	Facility dynamics	Expert rules based methods.	It is a commissioning analysis tool. It utilizes recorded system operational data to diagnose system problem and poor performance and identify energy wastes. Also, it generates reports of issues [86].	Unknown	Large commercial
FDD CX	NIST	Expert rules based methods.	Fault detection and diagnostic commissioning tool for residential air conditions and heat pumps [87].	Unknown	Residential

institutions using simulation platforms, experimental setups or using historic recorded data from an outdated experimental setup, and a very small group is based on real full-scale systems. This section presents a brief description of some cases studies about the implementation of FDD tools on large scale buildings.

- Advanced Automated HVAC Fault Detection and Diagnostics Commercialization project.

In California, over 28% of the electricity used by commercial buildings is consumed by HVAC systems and evidence suggest that at least 10% of this energy is wasted due to problems in physical components and control systems. The California Energy Commission's Public Interest Energy Research (PIER) supported the Advanced Automated HVAC Fault Detection and Diagnostics Commercialization project pursuing strategic alliances with manufacturers to develop more resistant and HVAC equipment and advanced FDD methods for HVAC systems yielding improvements and innovations for commercially available products.

Its third phase included the development of a robust FDD commercial application using APAR and VPACC rule set adapted to eight locations: a private office building, a large federal government office building, a private office building with some light industrial spaces, a federal government building with a combination of office and laboratory spaces, a large federal government office building, a classroom building on a community college campus, a museum building on a university campus, and a classroom and office building on a community college campus. Faults such as mixed air temperature sensor error, zone temperature sensor failure, incorrect cooling coil valve actuator configuration, disconnected VAV box supply air duct and AHU PID loop tuning error among others were detected and diagnosed effectively [88,89].

- Crown Casino Melbourne

Crown Casino and Entertainment Complex is a large casino located on the south bank of the Yarra River, in Melbourne, Australia. SkySpark was implemented in these installations as a part of a Building Optimization System program across the facility [90]. The HVAC equipment system under study includes 600 AHU, 2300 fan coil units, 27 chillers and 31 boilers. An algorithm containing a total of 150 SkySpark rules was implemented across the facility to detect

fault as failed dampers, VAV box failures, temperature set points not being achieved, invalid occupancy readings from room control sensors, heating and chilled water valves not closing or failed and pumps hunting. All the faults were detected and diagnosed achieving a 6% reduction in HVAC electrical consumption and 9% reduction in HVAC gas consumption.

- Fault Detection and Diagnosis in a commercial office building in Newcastle, Australia.

An operational office building in Newcastle, Australia with four floors, 15 zones and about 100 occupants was selected to study, detect and diagnose faults in its HVAC system. The study was supported by CSIRO Energy Transformed Flagship [91]. The faulty set comprised actuator stiction of exhaust air damper, cooling coil valve and outside air damper, heating coil valve and outside air damper leakage, fouling on supply air filter and other return air fan and cooling coil valve control faults. The FDD method implemented was based on the operational faults modelling using statistical machine learning and information theory computing probabilistic relationships between groups of points during both normal and faulty operation. Results concluded a successful operation of the developed tool as overall the faults were properly detected and diagnosed.

- Palais des congrès de Montréal, Montréal Canada

The Palais des congrès de Montréal is one of the first buildings in Canada to implement innovative continuous building optimization practices. It has an area of 130.000 m^2, a cooling capacity of 3.400 TR, a heating capacity of 18.000 kW, a peak electrical demand of 6 MW, 325 AHU, 4.740 control points and ventilation air requirements of 200.000 L/s. to diagnose any problem regard the building operation, the thermal comfort or the indoor air quality more quickly, this convention center implemented a fault detection and diagnose software (DABO^{TM}) based on 800 rules and 275 performance indices [92].

Based on daily analysis of individual components, 211 faults related to leaking chilled water valves, defective or undersized humidifiers, decalibrated sensors and unnecessary start-up of several HVAC systems during unoccupied periods were detected between 2008 and 2009 yielding a 25% energy savings.

9.5 Challenges in FDD Application to Buildings and HVAC Systems

Research referenced in Section 3 demonstrates significant progress in methods and systems for automated fault detection and diagnosis in HVAC applications, with an observable trend of increased preference for hybrid methods. Nevertheless, there is ample opportunity for new approaches, methods and technologies to be developed to better integrate FDD techniques into HVAC systems and to increase their performance. This section reflects the personal view of the authors regarding where these opportunities lie.

9.5.1 Technology Platforms Related Challenges

Significant progress has been made in control platforms and industrial networks, as well as in reduction of sensor prices and availability. However, we still find limitations for FDD originated by:

- Most small-scale HVAC systems are designed to be stand-alone units without the ability to communicate to hardware capable of running FDD algorithms. Although the per-user cost impact is not high, the aggregated effect of a huge number of isolated systems running under sub-optimal conditions has a major economic impact due to increased energy costs and the usually underestimated cost of out-of-comfort zone working or living rooms (mostly due to loss of productivity or health implications).
- Although the understanding of comfort in air-conditioned areas has evolved to include variables such as air speed and mean radiant temperature, in addition to the traditional temperature and humidity, sensing for most HVAC systems still remains mostly based on traditional dry-bulb temperature, with the occasional use of hygrometers. In addition, and judging by sensor location, there seems to be an across-the-board lack of concern for the "actual" user of the system, because most measures are focused on equipment properties or air-in-duct properties, rather than air-in-room properties, which tend to be assumed as lumped or average properties, contrary to what our experience as users dictates. From a FDD perspective this implies that most fault models are developed to detect/diagnose mechanical equipment failure, electronic equipment failure, or fluid in pipes or ducts failure, rather than abnormal temperature distributions, flow patterns, infiltrations, or loading conditions in the conditioned area.

- Fault detection and diagnosis algorithms are data intensive techniques, highly dependent for modeling, development and validation in historic data. Most users assume that the existence of an industrial database linked to their SCADA architecture guarantees the availability of relevant information. The true nature of system's operation is that the quality of stored data is seldom monitored, becoming evident in the rare instances when someone needs to use it. Frozen signals, missing values, or out-of-range values, are not uncommon. If a steady-state FDD algorithm is developed, the aforementioned events decrease the available set of vectors for model building and validation. However, is a dynamic FDD is being developed, this loss of information leads to losses of full dynamic transitions between states, with a major effect on false alarm rates if sufficient data is not made available.
- Fault detection and diagnosis algorithms tend to be computationally intensive, especially when adaptation rules are integrated to compensate for model aging or the appearance of a new normal operating pattern. Hence, it is highly relevant to work in computational complexity reduction of algorithms, to truly enable more on-line intelligence for FDD and operator assistance.

9.5.2 Strategy or Approach Related Challenges

Although the technology platform is certainly a limiting factor on how mathematically sophisticated and computationally intensive a fault detection strategy can by, it is certainly not the only source of challenges in FDD development and implementation. Some key identified challenges are:

- Fault diagnosis requires a clear relationship between a set of operation variables data (matrix) and the maintenance log. This way data can be validated as truly corresponding to an abnormal condition, and ideally, such condition is identified. However, most maintenance logs make reference to the intervention time, rather than faulty operation interval, limiting the ability to use past events to build knowledge both in fault detection models, as well as in fault diagnosis models.
- As every system tends to be its own unique kind, an effective FDD strategy requires the ability to adapt or learn beyond the initial configuration. One of the key pursues in contemporary research is the balance between supervised (assisted by operators and service engineers) and unsupervised learning (performed by embedded logic into the FDD strategy). The use of first principle

models allows for a more natural adaptation, but their reliability in complex settings and configurations increases the demand for a formal approach to adaptation.

- The cost of operating under a faulty condition is not a simple, deterministic issue. Although for HVAC systems most of the cost analysis address increased energy consumption and reduction of equipment life cycle, the cost of not satisfying appropriate comfort settings, especially in commercial and household applications still has plenty of room for improvement. How loss of comfort impacts productivity and health should drive more implementation of FDD systems in HVAC applications, and also promote the reconfiguration of fault models based on the actual HVAC system user, rather than the observed dominant perspective based on its operator.

9.6 Case Study Fault Detection System for a District Cooling Systems

Application of automated fault detection method reveals as much insight into a strategy as the formal mathematical analysis, but from a very different perspective. Access to validated and filtered historic data, event logs, and reliable sensor readings are necessary conditions for a successful implementation. In this section we present a case study at Universidad del Norte, Colombia, where the authors have been fortunate to have the support from maintenance and design engineers, as well as system operators.

9.6.1 Process Layout and Specifications

A district cooling system (DCS) is a system that produces and distributes thermal energy in form of chilled water from a central plant to a cluster of buildings for use in air conditioning applications. It consists in three parts: The central chiller plant, water distribution system and thermal consumers loop (Figure 9.9). In the recent years these systems have been widely used because a DCS offers massive cooling energy production with higher efficiency than the conventional plants at individual buildings, and represents a low cost. Furthermore, a district cooling system is financially beneficial for densely populated urban areas, high density building clusters and industrial complexes.

This case study exposed the implementation of a FDD system in a DCS, located in a tropical coastal city of Colombia. The weather is mainly

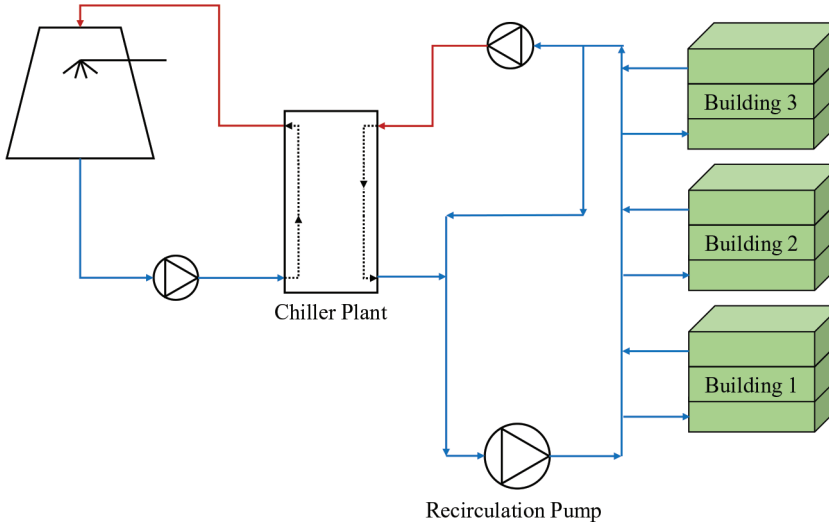

Figure 9.9. District cooling system.

hot and humid. The DCS feeds chilled water to a cluster of educational buildings where the thermal load varies along the day and the season of the year. The centrifugal chiller plant has a cooling capacity of 500 TR. The strategy is aimed to detect faults as cooling coil fouling and reduce chilled water flow in one of the buildings which conform the DCS. It is a three story building with a cooling capacity of 50 *TR*.

The building has one air handling unit (AHU) per floor, each one of these feed conditioned air to three classrooms with different thermal loads. The implemented HVAC system uses variable air volume (VAV) terminal boxes. It consists of the supply fans, the outdoor and recirculation dampers, the air handling units (filters and cooling coil), VAV terminal boxes and the local-loop controllers (Figure 9.10). The local loop controller is formed by the supply air temperature control, the duct static pressure at fan outlet control and the zone air temperature control. The supply air temperature is controlled by manipulating the flow rate of chilled water that enters the cooling coil. The duct static pressure at fan outlet is maintained at its desired value by modulating the fan speed. The zone air temperature is controlled by manipulating the VAV box damper opening [31]. There is a main control loop located in the recirculation pump that regulates the water pressure at its outlet by manipulating its velocity.

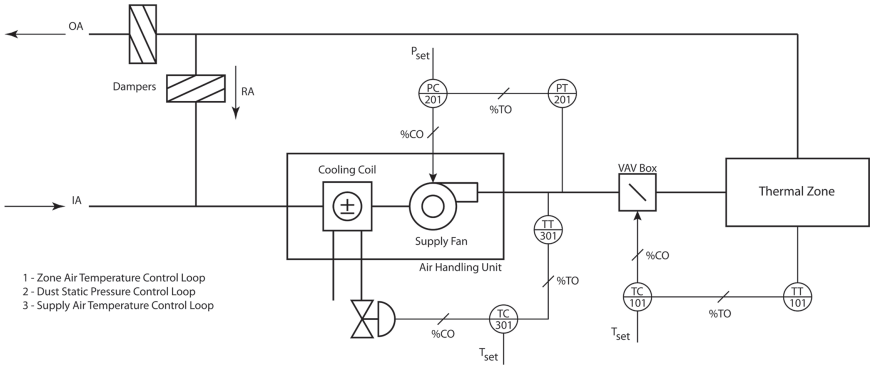

Figure 9.10. Air handing unit diagram.

9.6.2 FDD Design and Features

A hybrid strategy for early fault detection and diagnosis in cooling district systems is proposed based on unsupervised learning techniques, and principal components analysis. The aim is to develop and implement a novel online early fault detection strategy based on data driven approach, capable to be more sensitive than conventional PCA method in the detection of incipiently faults, like fouling in heat exchangers or ducts.

The techniques used in this research are: K-means clustering, and Principal Components Analysis. These two techniques are combined to: 1) Identify the operating states of the cooling district and evaluate the fault occurrence depending of its current operating state and 2) detect the fault more early than conventional PCA method.

The strategy includes two processes: Offline model training and online fault detection and diagnosis. In the offline model training process, the patterns present in the fault free training data or normal operating data set are recognized and put into clusters, the optimal number of clusters. When the data set is divided in two or more groups with a logical pattern, the possibility of increasing the sensitivity of the FDD method is greater because the observations that do not correspond to this cluster could be acting as noise or outliers. Then using PCA each cluster is statistically characterized and its thresholds of Hotelling statistic T^2 and Q statistic are defined. The confidence level of fault detection method is equal to 95%. It means 5% of fault free data are rejected as outliers.

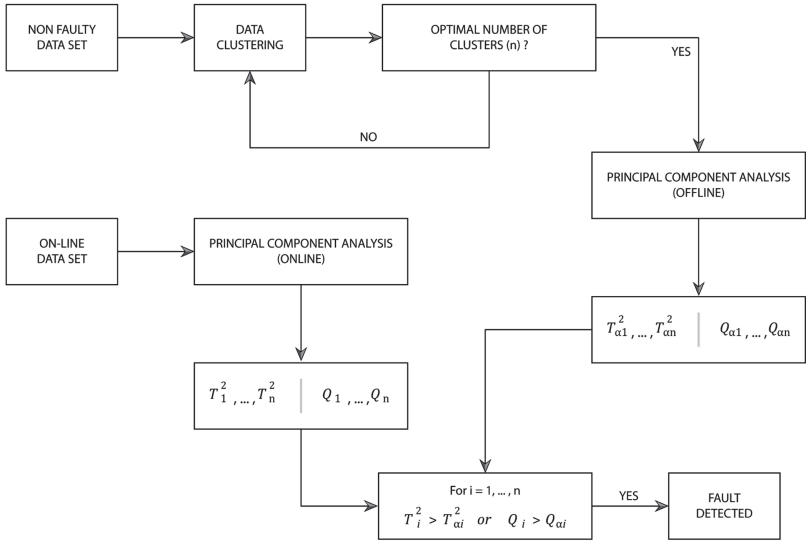

Figure 9.11. Structure of the proposed fault detection strategy.

In the online fault detection process, the belonging of each observation is evaluated in each one of the clusters with PCA. If the T^2 or Q statistic of each observation exceeds the corresponding threshold in all the clusters, the occurrence of a fault is considered and diagnosed. Figure 9.11 shows the structure of the proposed strategy.

9.6.3 Implementation Results

To validate the capability of the developed strategy to be more sensitive to the incipiently fault occurrence compared to Conventional PCA, a dynamic model of the process described previously was developed using mass and energy balances, and pressure equations in ducts and pipes. The dynamic model takes into account the interaction of the thermal zones with the environmental temperature, it means convection, conduction and radiation phenomenon, the variation of the thermal load along the day and the presence of the control loops to maintain the thermal comfort in the building.

There are 33 monitored variables in the system which are measured with a sample time of 5 minutes (Table 9.3). The non-faulty historical data set describes the performance of the DCS during 97 hours of operation, it means

Table 9.3 Monitored Variables.

Monitored Variables					
1	Supply air temperature AHU level 1	12	Room temperature 302	23	Room temperature controller signal 201
2	Supply air temperature AHU level 2	13	Duct pressure sensor level 3	24	Room temperature controller signal 202
3	Supply air temperature AHU level 3	14	Room temperature controller signal 300	25	Room temperature 100
4	Supply air temperature controller signal AHU level 3	15	Room temperature controller signal 301	26	Room temperature 101
5	Supply air temperature controller signal AHU level 2	16	Room temperature controller signal 302	27	Room temperature 102
6	Supply air temperature controller signal AHU level 1	17	Duct pressure controller signal level 3	28	Duct pressure sensor level 1
7	Water flow AHU level 3	18	Room temperature 200	29	Room temperature controller signal 100
8	Water flow AHU level 2	19	Room temperature 201	30	Room temperature controller signal 101
9	Water flow AHU level 1	20	Room temperature 202	31	Room temperature controller signal 102
10	Room temperature 300	21	Duct pressure sensor level 2	32	Duct pressure controller signal level 1
11	Room temperature 301	22	Room temperature controller signal 200	33	

1166 observation of each one of the monitored variables. The first step in the FDD proposed strategy is to identify how many clusters or system states are in the non-faulty historical data set. Using a K-means clustering algorithm two system states are recognized, a self-organizing map neighbor distances is used as data visual aid to validate cluster classification (Figure 9.12).

For each one of these clusters, a T^2 and a Q threshold is calculated, using PCA (Table 9.4).

The ability of the proposed strategy to detect faults is assessed considering the following two cases: Cooling coil fouling and reduced chilled water flow. Both faults were induced in the system at a specific time after a period of normal operation and were modeled as a ramp function with negative slope. For each observation, the corresponding T^2 and Q statistic is evaluated. It is assumed that a violation of the respective threshold (calculated off-line) is a

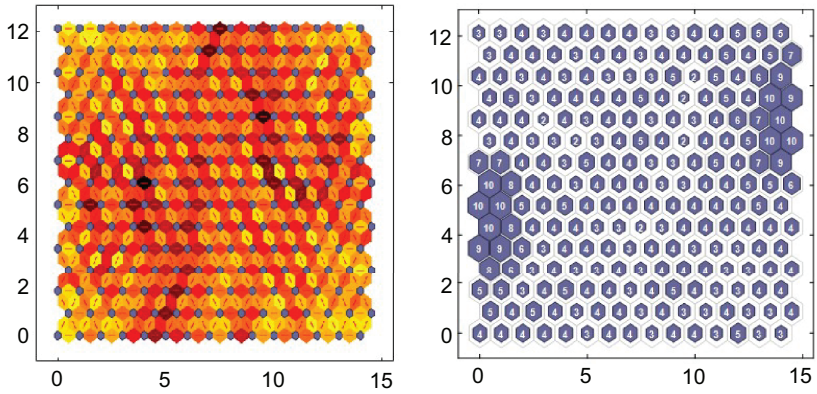

Figure 9.12. Historical data set clusters classification.

Table 9.4. Statistics Thresholds.

Proposed Strategy		
	Thresholds	
Cluster	T^2	Q
System state 1	3.8609	25.0669
System state 2	3.8875	31.7608
Conventional PCA		
Historical Data Set	3.8551	27.4146

fault occurrence signal. The results of the proposed strategy are compared to Conventional-PCA method, to identify the percentage of false alarms and calculate how much time takes the fault detection with the improvements. The Conventional PCA method refers to make the data dimensional reduction in the complete data set, it means without cluster classification and create just one threshold for each one of the statistics (Table 9.4).

a) Cooling Coil Fouling

Fouling is the accumulation of unwanted deposits on the surfaces of heat exchangers. These deposits cause a resistance to the transfer of heat and reduce the efficiency of the equipment. It is a common fault in HVAC systems especially in air handling units because a fraction of the air that is going to be cooled is extracted from the outside of the building and it could have particulate material that could pass the filters and arrive to the heat exchanger or blocked the air ducts causing pressure drops. This is an incipiently fault, it means that it can take much time to be detected by an operator, but small fractional performance degradations owing to fouling have the potential to cause large energy consequences. The early detection of this fault allow to reduce repair labor and parts, to increase the lifetime of equipment as heat exchangers and fans, and to eliminate preventative maintenance services.

The fault was induced in the cooling coil of the AHU located in first level of the building, 30 hours later of a normal operation state. It was modeled using the heat transfers coefficient of the equipment as a ramp function with a negative slope. In normal operation state, the equipment has a capacity of 10.2 TR. Under faulty conditions the heat transfer capacity decreases with a slope of 0.0012 TR, it means a reduction of 1%/*h* in the cooling capacity of the equipment. Figure 9.13 shows the performance of the main affected variables related to the faulty AHU. It is noticed the greater deviation of the performance of variables as supply air temperature controller signal, chiller water volumetric flow and principal pump pressure from their normal conditions. In the case of supply air temperature sensor signal there are peaks later the fault occurrence which do not fit to the normal performance of the variable. However, the controller achieves to regulate them, during the simulated time, and prevents the fault propagation in the overall system.

Figure 9.14 shows the performance of the proposed strategy and conventional PCA method in the fault detection. The red line indicates the T^2 and Q thresholds and the blue lines indicate the online performance of each statistic. When blue lines exceed the red line, it indicates a possible

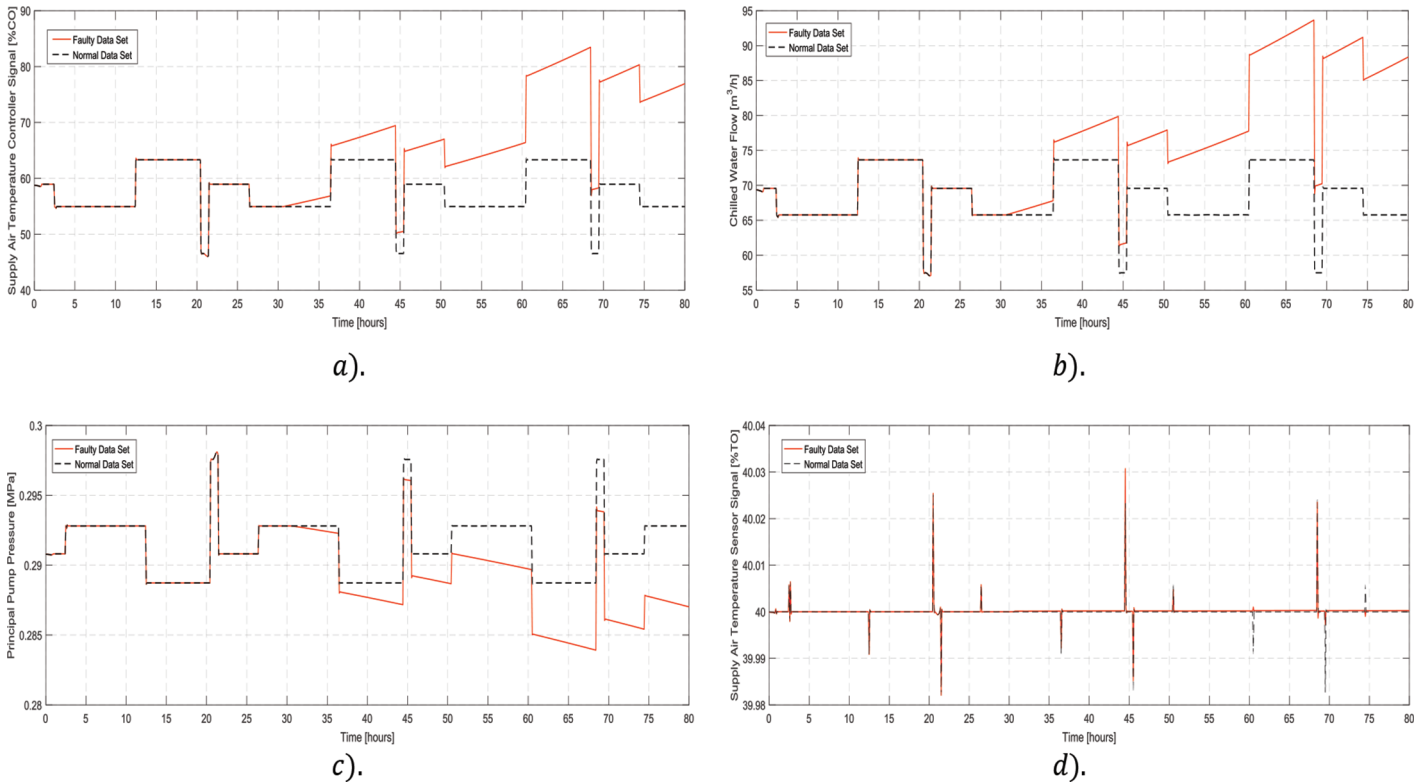

Figure 9.13. Main affected variables by fouling in AHU. (a) Supply air temperature controller signal, (b) chilled water flow, (c) principal pump pressure, and (d) supply air temperature sensor signal.

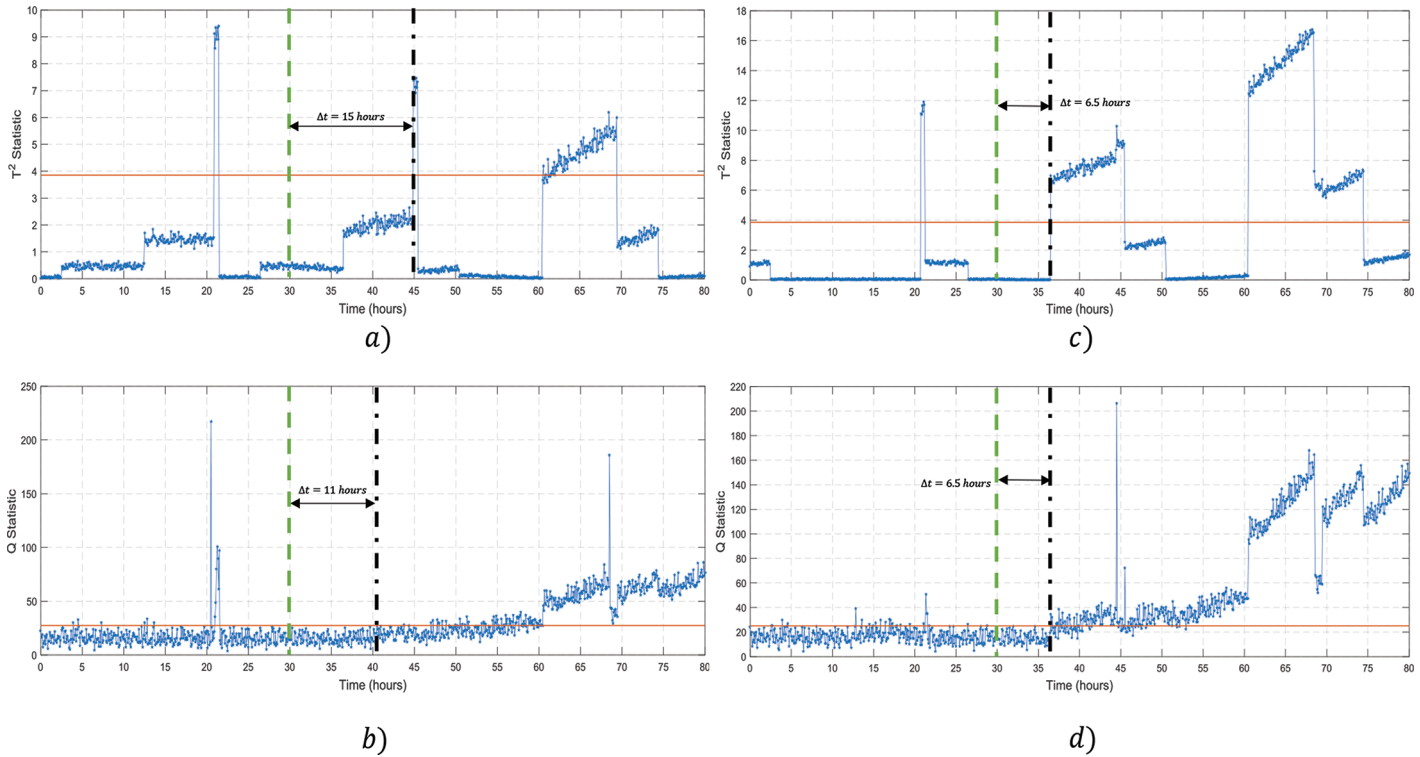

Figure 9.14. Fouling in detection. Conventional PCA: (a) T2 Statistic and (b) Q cstatistic. The proposed strategy: (c) T^2 Statistic and (d) Q Statistic.

fault occurrence. It is noticed that with conventional PCA method (black line), the T^2 statistic detects the fault 15 hours later than its occurrence (green line) with a 1.48% of false alarms, and Q statistic detects the fault 11 hours later than its occurrence with a 2.91% of false alarms. Although with the proposed strategy, the T^2 statistic and Q statistic detects the fault 6.5 hours later than its occurrence, with 1.36% and 2.28% of false alarms, respectively.

b) Reduced Chilled Water Flow.

It is a common symptom of faults as water pump failure, water control valve stuck or broken, leakage in water pipes or blocked pipes. Each one of these faults are very important because can affect the thermal comfort in the building and the lifetime of the overall system. In this case, the symptom was induced in the chilled water flow of the AHU located in third level of the building, 52 hours later of a normal operation state. It was modeled multiplying the inlet flow coming from the water pump by a ramp function with a negative slope. In normal operation state, the chilled water flow is 68.8178m^3/h, whereas under faulty conditions, it decreases with a slope of 1.2960m^3/h, it means a reduction approximately of 1.8%/h. Figure 9.15 shows the performance of the main affected variables related to the faulty AHU. It is noticed the deviation of the performance of variables as supply air temperature controller signal and sensor signal from their normal conditions. In the case of the first variable, it is noticed the saturation of the valve at 95% CO. This situation coincides with the deviation of the sensor signal.

Figure 9.16 shows the performance of the proposed strategy and conventional PCA method in the fault detection. It is noticed that with conventional PCA method, the T^2 statistic detects the fault 10 hours later than its occurrence with a 1% of false alarms and Q statistic detects the fault 3.5 hours later than its occurrence with a 2.39% of false alarile Although with the proposed strategy, the T^2 statistic detects the fault 8.5 hours later than its occurrence and Q statistic detects the fault 1.5 hours later than its occurrence, with 0.5% and 2.17% of false alarms respectively.

9.6.4 Conclusions and Recommendations

An online fault detection strategy for District Cooling Systems is proposed based on a data driven approach, especially on the implementation of pattern recognition techniques and principal components analysis. The strategy differentiates from previous reported ones as it incorporates

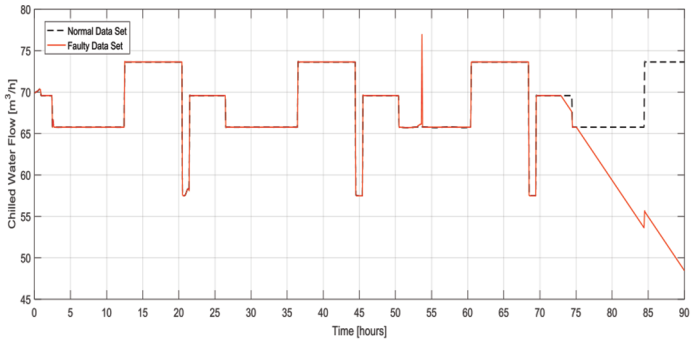

a).

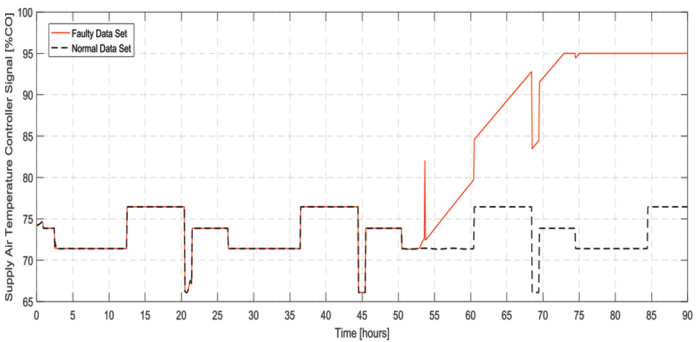

b).

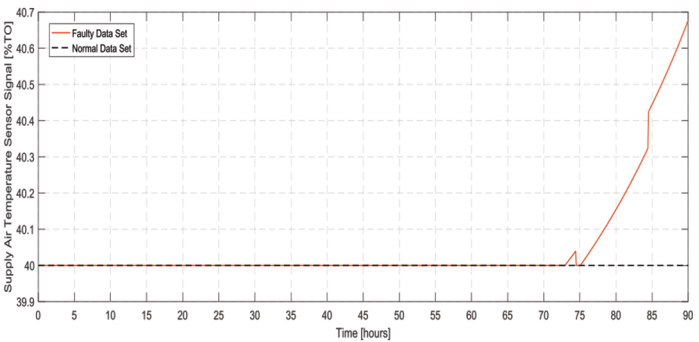

c).

Figure 9.15. Main affected variables by reduced chilled water in AHU. (a) Chilled water flow reduction, (b) Supply air temperature control signal and (c) Supply air temperature sensor signal.

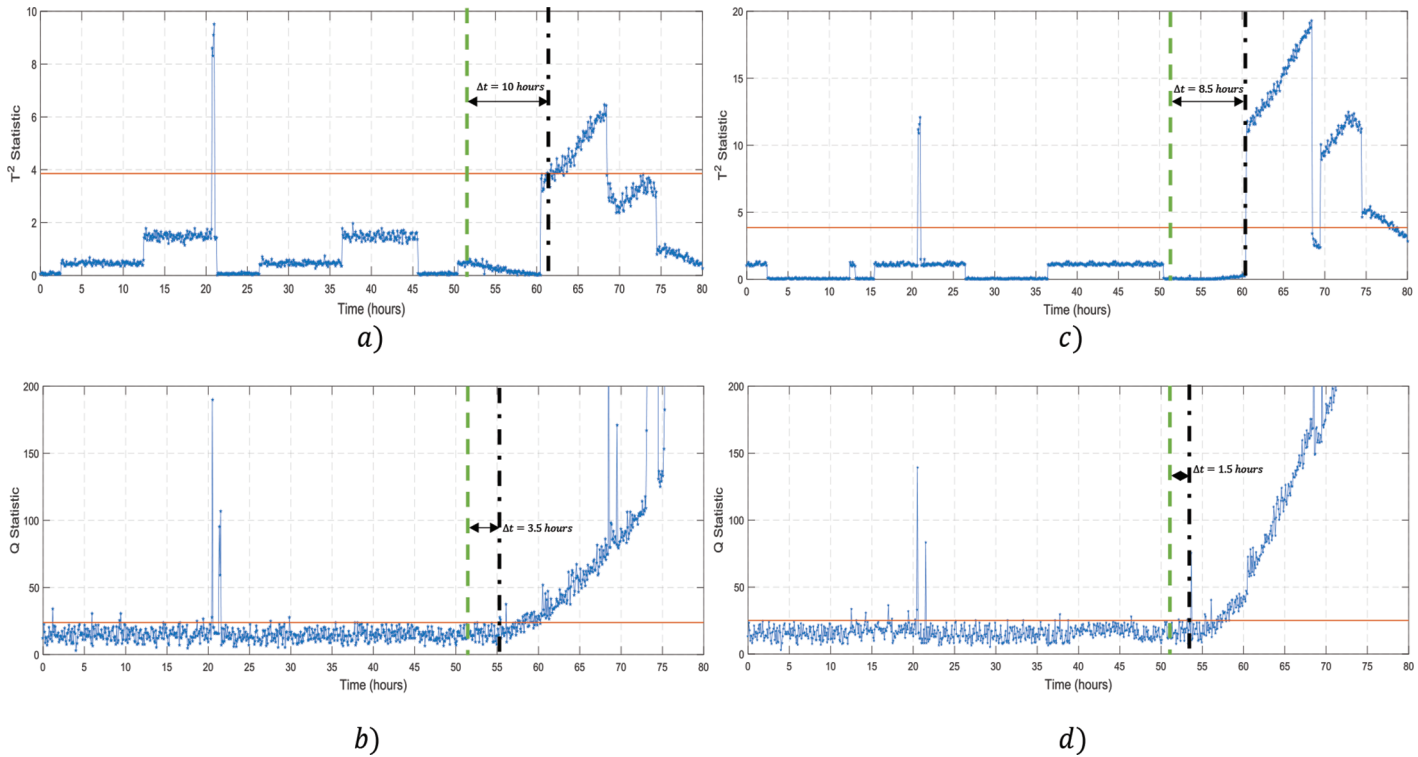

Figure 9.16. Reduced chilled water flow detection. Conventional PCA: a)T^2 statistic and b)Q statistic. The proposed strategy: c) T^2 Statistic and d)Q statistic.

static grouping techniques to identify correlations and interactions among measured variables during normal operational conditions. The classification of data sets in clusters (patterns) is beneficial to the fault detection process because it allows capturing more variability in the data sets and reducing the number of missed detection events and false alarms. The clustering step further tunes the outliers (atypical data) removal step improving the diagnosis reliability. The proposed fault detection strategy shows a superior performance with respect to Conventional-PCA. The inherent ability of the strategy to classify operational states according to performance patterns is especially useful because the observations that do not correspond to each cluster could be acting as noise or outliers and delay the detection.

9.7 Conclusions and Future Works

Although much progress has been made in design and architecture of HVAC systems, the constant need for reducing energy consumption, detect faults before they have propagated through the system, and better supervision of the distributed infrastructure system is an ever ongoing effort. This chapter has presented a broad array of approaches that are being taken both in industry and research to address these needs. Based on the above sections we may conclude that:

- Early fault detection strategies, either data-driven or model-driven, provide a useful approach for monitoring and supervision of large HVAC systems (building scale or district scale), leading to energy savings and shorter detection times compared to human supervision.
- It is very common in HVAC systems, due to their cyclical nature, to find patterns of operation. When such variability is integrated into a single model it leads to a larger detection limit, hence detection times are increased. A patter-recognition layer leads to several normal OC models (one for each pattern), improving the system's sensitivity to changes without inducing a significant increase in false alarm rates.
- Fault diagnosis should be a target but major limitations arise from fixed-structure algorithms unable to "learn" from previous experiences or limited by inaccuracy or vagueness in maintenance logs. The design of the FDD system is as critical as its operation, as it must be a target to continuously enhance the knowledge base or the model base upon which the system operates.

Acknowledgments

Getting access to data, system design and blueprints was significant for the case study that has been presented. Our gratitude goes to the team from the Administrative Service Office and the Planning Office at Universidad del Norte, and the SCADA system contractor, K Ingeniería, for supporting our work with their knowledge and professionalism. We also want to thank COLCIENCIAS for partially supporting the development of the case study, under the Young Researchers grant in 2015.

References

[1] Isermann, R., Model base fault detection and diagnosis methods, in: Proc. 1995 Am. Control Conf.—ACC'95, American Autom Control Council, 1995: pp. 1605–1609. doi:10.1109/ACC.1995.529778.

[2] Venkatasubramanian, V., Rengaswamy, R., Yin, K., Kavuri, S.N., A Review of Process Fault Detection and Diagnosis: Part I: Quantitative Model-Based Methods, *Computers and Chemical Engineering* 27 (2003): 293–311. doi:10.1016/S0098-1354(02)00160-6.

[3] Venkatasubramanian, V., Rengaswamy, R., Kavuri, S.N., A Review of Process Fault Detection and Diagnosis: Part II: Qualitative Models and Search Strategies, *Computers and Chemical Engineering* 27 (2003): 313–326. doi:10.1016/S0098-1354(02)00161-8.

[4] Venkatasubramanian, V., Rengasamy, R., Kavuri, S., Yin, K., A Review of Process Fault Detection and Diagnosis: Part III: Process History Based Methods, *Computers and Chemical Engineering* 27 (2003): 327–346.

[5] Pearson, K., LIII. On Lines and Planes of Closest Fit to Systems of Points in Space, *Philosophical Magazine Series* 6 2 (1901): 559–572. doi:10.1080/14786440109462720.

[6] Hotelling, H., Multivariate Quality Control-Illustrated by Air Testing of Sample Bombsights, in: C. Eisenhart, M.W. Hastay, W.A. Wallis (Eds.), Sel. Tech. Statistical Anal., McGraw Hill, New York, 1947: pp. 11–184.

[7] Million, E., The Hadamard Product, (2007) 1–7. http://buzzard.ups.edu/courses/2007spring/projects/million-paper.pdf.

[8] Russel, E., Chiang, L.H., Braatz, R.D., *Data-Driven Techniques for Fault Detection and Diagnosis in Chemical Processes*, 1st ed., Springer London, London, 2000.

[9] Zwick, W.F., William, R., Velicer, Comparison of Five Rules for Determining the Number of Components to Retain, *Psychological Bulletin* 99 (1986): 432–442.

[10] Franklin, S.B., Gibson, D.J., Robertson, P.A., Pohlmann, J.T., Fralish, J.S., Parallel Analysis: A Method for Determining Significant Principal Components, *Journal of Vegetation Science* 6 (1995): 99–106. doi:10.2307/3236261.

[11] Ledesma, R.D., Universidad, C., De Mar, N., Valero-Mora, P., De Valencia, U., Determining the Number of Factors to Retain in EFA: An Easy-to-Use Computer Program for Carrying Out Parallel Analysis, *Pract. Assessment, Res. Eval.* 12 (2007): 2–11. doi:http://pareonline.net/getvn.asp?v=12&n=2.

[12] Jackson, J.E., Mudholkar, G.S., Control Procedures for Residuals Associated with Principal Component Analysis, *Technometrics* 21 (1979): 341–349. doi:10.1080/00401706.1979.10489779.

[13] Jeng, J.C., Adaptive Process Monitoring Using Efficient Recursive PCA and Moving Window PCA Algorithms, Journal of the *Taiwan Institute of Chemical Engineering* 41 (2010): 475–481. doi:10.1016/j.jtice.2010.03.015.

[14] Li, W., Yue, H.H., Valle-Cervantes, S., Qin, S.J., Recursive PCA for Adaptive Process Monitoring, *Journal of Process Control* 10 (2000): 471–486.

[15] Portnoy, I., Melendez, K., Pinzon, H., Sanjuan, M., An Improved Weighted Recursive PCA Algorithm for Adaptive Fault Detection, *Control Engineering Practice* 50 (2016): 69–83. doi:10.1016/j.conengprac.2016.02.010.

[16] Zhang, Z., Peng, B., Xie, L., Peng, L., Process Monitoring Based on Recursive Probabilistic PCA for Multi-mode Process**The work is supported by National Natural Science Foundation of China (No.61374047, No.61202473) and Fundamental Research Funds for Central Universities (JUSRP51322B, JUSRP111, IFAC-PapersOnLine. 48 (2015): 1294–1299. doi:10.1016/j.ifacol.2015.09.147.

[17] Zhang, Y., Li, S., Teng, Y., Dynamic Processes Monitoring Using Recursive Kernel Principal Component Analysis, *Chemical Engineering Science* 72 (2012): 78–86. doi:10.1016/j.ces.2011.12.026.

[18] Bin Shams, M.A., Budman, H.M., Duever, T.A., Fault Detection, Identification and Diagnosis Using CUSUM Based PCA, *Chemical Engineering Science* 66 (2011): 4488–4498. doi:10.1016/j.ces.2011.05.028.

[19] Chen, J., Liao, C.-M., Dynamic Process Fault Monitoring Based on Neural Network and PCA, *Journal of Process Control* 12 (2002): 277–289. doi:10.1016/S0959-1524(01)00027-0.

[20] Lau, C.K., Ghosh, K., Hussain, M.A., Che Hassan, C.R., Fault Diagnosis of Tennessee Eastman Process With Multi-Scale PCA and ANFIS, *Chemometrics and Intelligent Laboratory Systems* 120 (2013): 1–14. doi:10.1016/j.chemolab.2012.10.005.

[21] Sun, W., Chen, J., Li, J., Decision Tree and PCA-Based Fault Diagnosis of Rotating Machinery, *Mechanical Systems and Signal Processing* 21 (2007): 1300–1317. doi:10.1016/j.ymssp.2006.06.010.

[22] Uraikul, V., Chan, C.W., Tontiwachwuthikul, P., Artificial Intelligence for Monitoring and Supervisory Control of Process Systems, *Engineering Applications of Artificial Intelligence* 20 (2007): 115–131. doi:10.1016/j.engappai.2006.07.002.

[23] Butler, K.L., An Expert System Based Framework for an Incipient Failure Detection and Predictive Maintenance System, in: Proc. Int. Conf. Intell. Syst. Appl. to Power Syst., IEEE, 1996: pp. 321–326. doi:10.1109/ISAP.1996.501092.

[24] Wang, Y., Li, Q., Chang, M., Chen, H., Zang, G., Research on Fault Diagnosis Expert System Based on the Neural Network and the Fault Tree Technology, *Procedia Engineering* 31 (2012): 1206–1210. doi:10.1016/j.proeng.2012.01.1164.

[25] Mok, H.T., Chan, C.W., Yang, Z.Y., Online Fault Detection and Isolation of Nonlinear Systems Based on Neurofuzzy Networks, *IFAC Proc.* 39 (2006): 246–251. doi:10.3182/20060829-4-CN-2909.00040.

[26] Tran, D.A.T., Chen, Y., Chau, M.Q., Ning. B., A Robust Online Fault Detection and Diagnosis Strategy of Centrifugal Chiller Systems for Building Energy Efficiency, *Energy and Buildings* (2015). doi:10.1016/j.enbuild.2015.09.044.

[27] Zhao, X., Lab Test of Three Fault Detection and Diagnostic Methods' Capability of Diagnosing Multiple Simultaneous Faults in Chillers, *Energy and Buildings* 94 (2015): 43–51. doi:10.1016/j.enbuild.2015.02.039.

[28] Wang, H., Chen, Y., Chan, C.W.H., Qin, J., Wang, J., Online Model-Based Fault Detection and Diagnosis Strategy for VAV Air Handling Units, *Energy and Buildings* 55 (2012): 252–263. doi:10.1016/j.enbuild.2012.08.016.

[29] Katipamula, S., Brambley, M., Review Article: Methods for Fault Detection, Diagnostics, and Prognostics for Building Systems—A Review, Part II, *HVAC&R Res.* 11 (2005): 169–187. doi:10.1080/10789669.2005.10391133.

[30] Katipamula, S., Brambley, M., Review Article: Methods for Fault Detection, Diagnostics, and Prognostics for Building Systems—A Review, Part I, *HVAC&R Res.* 11 (2005): 3–25. doi:10.1080/10789669.2005.10391123.

[31] Yu, Y., Woradechjumroen, D., Yu, D., A Review of Fault Detection and Diagnosis Methodologies on Air-Handling Units, *Energy and Buildings* 82 (2014): 550–562. doi:10.1016/j.enbuild.2014.06.042.

[32] Navarro-Esbrí, J., Torrella, E., Cabello, R., A Vapour Compression Chiller Fault Detection Technique Based on Adaptative Algorithms. Application to On-Line Refrigerant Leakage Detection, *International Journal of Refrigeration* 29 (2006): 716–723. doi:10.1016/j.ijrefrig.2005.12.008.

[33] Sreedharan, P., Haves, P., *Comparison of Chiller Models for Use in Model-Based Fault Detection*, Lawrence Berkeley Natl. Lab. (2001).

[34] Lee, W.-Y., Park, C., and Kelly, G.E., Fault Detection in an Air-Handling Unit Using Residual and Recursive Parameter Identification Methods, *ASHRAE Transactions* 102 (1996): 1–12.

[35] Yang, H., Cho, S., Tae, C.-S., Zaheeruddin, M., Sequential Rule Based Algorithms for Temperature Sensor Fault Detection in Air Handling Units, *Energy Converservation and Management* 49 (2008): 2291–2306. doi:10.1016/j.enconman.2008.01.029.

[36] Usoro, P.B., Schick, I.C., Negahdaripour, S., An Innovation-Based Methodology for HVAC System Fault Detection, *Journal of Dynamic Systems Measurement and Control*. 107 (1985): 284. doi:10.1115/1.3140737.

[37] Yoshida, H., Iwami, T., Yuzawa, H., Suzuki, M., Typical Faults of Air Conditioning Systems and Fault Detection by ARX Model and Extended Kalman Filter, (1996).

[38] Salsbury, T., Diamond, R., Fault Detection in HVAC Systems Using Model-Based Feedforward Control, *Energy and Buildings* 33 (2001): 403–415. doi:10.1016/S0378-7788(00)00122-5.

[39] Yang, X.-B., Jin, X.-Q., Du, Z.-M., Zhu, Y.-H., A Novel Model-Based Fault Detection Method for Temperature Sensor Using Fractal Correlation Dimension, *Building and Environment* 46 (2011): 970–979. doi:10.1016/j.buildenv.2010.10.030.

[40] Gao, Z., Cecati, C., Ding, S.X., A Survey of Fault Diagnosis and Fault-Tolerant Techniques—Part I: Fault Diagnosis With Model-Based and Signal-Based Approaches, *IEEE Transactions on Industrial Electronics* 62 (2015): 3757–3767. doi:10.1109/TIE.2015.2417501.

[41] Beghi, A., Brignoli, R., Cecchinato, L., Menegazzo, G., Rampazzo, M., Simmini, F., Control Engineering Practice Data-Driven

Fault Detection and Diagnosis for HVAC Water Chillers, *Control Engineering Practice* 53 (2016): 79–91. doi:10.1016/j .conengprac.2016.04.018.

[42] Padilla, M., Choinière, D., A Combined Passive-Active Sensor Fault Detection and Isolation Approach for Air Handling Units, *Energy and Buildings* 99 (2015): 214–219. doi:10.1016/j .enbuild.2015.04.035.

[43] Li, S., Wen, J., Application of Pattern Matching Method for Detecting Faults in Air Handling Unit System, *Automation in Construction* 43 (2014): 49–58. doi:10.1016/j.autcon.2014.03.002.

[44] Li, D., Zhou, Y., Hu, G., Spanos, C.J., Fault Detection and Diagnosis for Building Cooling System With A Tree-structured Learning Method, *Energy and Buildings* 127 (2016): 540–551. doi:10.1016/j.enbuild.2016.06.017.

[45] ce Gao, D., Wang, S., Shan, K., Yan, C., A System-Level Fault Detection and Diagnosis Method for Low Delta-T Syndrome in the Complex HVAC Systems, *Applied Energy* 164 (2016): 1028–1038. doi:10.1016/j.apenergy.2015.02.025.

[46] Zhao, X., Yang, M., Li, H., Field Implementation and Evaluation of a Decoupling-Based Fault Detection and Diagnostic Method for Chillers, *Energy and Buildings* 72 (2014): 419–430. doi:10.1016/j .enbuild.2014.01.003.

[47] Yuwono, M., Guo, Y., Wall, J., Li, J., West, S., Platt, G., Su, S.W., Unsupervised Feature Selection Using Swarm Intelligence and Consensus Clustering for Automatic Fault Detection and Diagnosis in Heating Ventilation and Air Conditioning systems, *Applied Soft Computing* 34 (2015): 402–425. doi:10.1016/j .asoc.2015.05.030.

[48] Du, Z., Fan, B., Jin, X., Chi, J., Fault Detection and Diagnosis for Buildings and HVAC Systems Using Combined Neural Networks and Subtractive Clustering Analysis, *Building and Environment* 73 (2014): 1–11. doi:10.1016/j.buildenv.2013.11.021.

[49] Najafi, M., Auslander, D.M., Bartlett, P.L., Haves, P., Sohn, M.D., Application of Machine Learning in the Fault Diagnostics of Air Handling Units, *Applied Energy* 96 (2012): 347–358. doi:10.1016/j.apenergy.2012.02.049.

[50] Zhao, Y., Wang, S., Xiao, F., A Statistical Fault Detection and Diagnosis Method for Centrifugal Chillers Based on Exponentially-Weighted Moving Average Control Charts and Support Vector Regression, *Applied Thermal Engineering* 51 (2013): 560–572.

[51] Zhao, Y., Xiao, F., Wen, J., Lu, Y.H., Wang, S.W., A Robust Pattern Recognition-Based Fault Detection and Diagnosis (FDD) Method

for Chillers, *HVAC&R Res*. 20 (2014): 798–809. doi:10.1080/10789669.2014.938006.

[52] Lo, C.H., Chan, P.T., Wong, Y.K., Rad, A.B., Cheung, K.L., Fuzzy-Genetic Algorithm for Automatic Fault Detection in HVAC Systems, *Applied Soft Computing* 7 (2007): 554–560. doi:10.1016/j.asoc.2006.06.003.

[53] Chen, Y., Lan, L., A Fault Detection Technique for Air-Source Heat Pump Water Chiller/Heaters, *Energy and Buildings* 41 (2009): 881–887. doi:10.1016/j.enbuild.2009.03.007.

[54] Zhao, Y., Wang, S., Xiao, F., Pattern Recognition-Based Chillers Fault Detection Method Using Support Vector Data Description (SVDD), *Applied Energy* 112 (2013): 1041–1048. doi:10.1016/j.apenergy.2012.12.043.

[55] Hu, Y., Chen, H., Xie, J., Yang, X., Zhou, C., Chiller Sensor Fault Detection Using a Self-Adaptive Principal Component Analysis Method, *Energy and Building* 54 (2012): 252–258. doi:10.1016/j|.enbuild.2012.07.014.

[56] Papadopoulos, P.M., Reppa, V., Polycarpou, M.M., Panayiotou, C.G., Distributed Adaptive Estimation Scheme for Isolation of Sensor Faults in Multi-Zone HVAC Systems, *IFAC-PapersOnLine* 48 (2015): 1146–1151. doi:10.1016/j.ifacol.2015.09.681.

[57] Zimmermann, G., Lu, Y., Lo, G., Automatic HVAC Fault Detection and Diagnosis System Generation Based on Heat Flow Models, *HVAC&R Res*. (2012).

[58] Sun, B., Luh, P.B., Jia, Q.-S., O'Neill, Z., Song, F., Building Energy Doctors: An SPC and Kalman Filter-Based Method for System-Level Fault Detection in HVAC Systems, *IEEE Transactions on Automation Science and Engineering* 11 (2014): 215–229. doi:10.1109/TASE.2012.2226155.

[59] Bruton, K., Raftery, P., O'Donovan, P., Aughney, N., Keane, M.M., O'Sullivan, D.T.J., Development and Alpha Testing of a Cloud Based Automated Fault Detection and Diagnosis Tool for Air Handling Units, *Automation in Construction* 39 (2014): 70–83. doi:10.1016/j.autcon.2013.12.006.

[60] Wang, H., Chen, Y., A Robust Fault Detection and Diagnosis Strategy for Multiple Faults of VAV Air Handling Units, *Energy and Buildings* 127 (2016): 442–451. doi:10.1016/j.enbuild.2016.06.013.

[61] Jones, C.B., Fault Detection and Diagnostics of an HVAC Sub-System Using Adaptive Resonance Theory Neural Networks, (2015).

[62] Beghi, A., Cecchinato, L., Corazzol, C., Rampazzo, M., Simmini, F., Susto, G.A., A One-Class SVM Based Tool for Machine Learning

Novelty Detection in HVAC Chiller Systems, *IFAC Proc.* 47 (2014): 1953–1958. doi:10.3182/20140824-6-ZA-1003.02382.

[63] Li, D., Hu, G., Spanos, C.J., A Data-Driven Strategy for Detection and Diagnosis of Building Chiller Faults Using Linear Discriminant Analysis, *Energy and Building* 128 (2016): 519–529. doi:10.1016/j.enbuild.2016.07.014.

[64] Bonvini, M., Sohn, M.D., Granderson, J., Wetter, M., Piette, M.A., Robust On-Line Fault Detection Diagnosis for HVAC Components Based on Nonlinear State Estimation Techniques, *Applied Energy* 124 (2014): 156–166. doi:10.1016/j.apenergy.2014.03.009.

[65] Yan, K., Shen, W., Mulumba, T., Afshari, A., ARX Model Based Fault Detection and Diagnosis for Chillers Using Support Vector Machines, *Energy and Buildings* 81 (2014): 287–295. doi:10.1016/j.enbuild.2014.05.049.

[66] Du, Z., Fan, B., Chi, J., Jin, X., Sensor Fault Detection and Its Efficiency Analysis in Air Handling Unit Using the Combined Neural Networks, *Energy and Buildings* 72 (2014): 157–166. doi:10.1016/j.enbuild.2013.12.038.

[67] Gao, Y., Liu, S., Li, F., Liu, Z., Fault Detection and Diagnosis Method for Cooling Dehumidifier Based on LS-SVM NARX Model, *International Journal of Refrigeration* 61 (2016): 69–81. doi:10.1016/j.ijrefrig.2015.08.020.

[68] Mulumba, T., Afshari, A., Yan, K., Shen, W., Norford, L.K., Robust Model-Based Fault Diagnosis for Air Handling Units, *Energy and Buildings* 86 (2015): 698–707. doi:10.1016/j.enbuild.2014.10.069.

[69] Yan, R., Ma, Z., Kokogiannakis, G., Zhao, Y., A Sensor Fault Detection Strategy for Air Handling Units Using Cluster Analysis, *Automation in Construction* (2016). doi:10.1016/j.autcon.2016.06.005.

[70] Li, S., Wen, J., A Model-Based Fault Detection and Diagnostic Methodology Based on PCA Method and Wavelet Transform, *Energy and Buildings* 68 (2014): 63–71. doi:10.1016/j.enbuild.2013.08.044.

[71] Wiggins, M., Brodrick, J., HVAC Fault Detection, *ASHRAE Journal* 54 (2012): 78–80.

[72] Bruton, K., Raftery, P., Kennedy, B., Keane, M.M., O'Sullivan, D.T.J., Review of Automated Fault Detection and Diagnostic Tools in Air Handling Units, *Energy Efficiency*. 7 (2014): 335–351. doi:10.1007/s12053-013-9238-2.

[73] SkyFoundry, SkySpark: Analytics Software for a World of Smart Devices, (2014). https://www.skyfoundry.com/file/8/SkySpark-Overview-Brochure.pdf (accessed July 20, 2016).

[74] SkyFoundry, SkySpark, (2009). https://www.skyfoundry.com/skyspark/.
[75] BuildingIQ, BuildingIQ and Johnson Controls to offer Predictive energy Optimization™ through Panoptix™Platform, (2012). https://buildingiq.com/2012/11/13/buildingiq-and-johnson-controls-to-offer-predictive-energy-optimization-through-panoptixplatform/.
[76] Johnson Controls, Johnson Controls Announces Panoptix™—A New Approach To Building Efficiency, (2011). http://investors.johnsoncontrols.com/news-and-events/press-releases/2011/04-10-2011.
[77] KGS Buildings, ClockWorks, (2016). http://www.kgsbuildings.com/clockworks.
[78] Natural Logic, SCIwatchTM—Continuous Commissioning, (n.d.). http://natlogic.com/resources/tools/sciwatch/.
[79] Trane, Trane ® Intelligent Services, (2015). http://commercial.trane.com/content/dam/Trane/micro-sites/building-advantage/intelligent-services/brochures/TRANE15005G_ISPortfolioBrchr_F_LR.pdf (accessed July 20, 2016).
[80] TRANE, Trane Building Advantage, (2015). http://commercial.trane.com/content/dam/Trane/micro-sites/building-advantage/intelligent-services/intelligentServices.html?cid=tisexperience.
[81] VPC, Ongoing Commissioning, (n.d.). http://www.vpc.gr/en/ongoing-commissioning.
[82] Poirier, M., DABO Adds Intelligence and Memory to a Building's Operating System, (2010). https://www.nrcan.gc.ca/sites/www.nrcan.gc.ca/files/canmetenergy/files/pubs/DABO_EN.pdf (accessed July 22, 2016).
[83] IBM, IBM TRIRIGA, (n.d.). http://www-03.ibm.com/software/products/en/ibmtrir.
[84] IBM, IBM TRIRIGA Energy Optimization, (n.d.). http://www-03.ibm.com/software/products/en/tririga-energy-optimization.
[85] Schein, J., Results From Field Testing of Embedded Air Handling Unit and Variable Air Volume Box Fault Detection Tools., 2006. http://fire.nist.gov/bfrlpubs/build06/art033.html.
[86] Facility Dynamics, PACRAT, (2016). http://www.facilitydynamics.com/software/pacrat/.
[87] Heo, J., Payne, W.V., Domanski, P.A., FDD CX: A Fault Detection and Diagnostic Commissioning Tool for Residential Air Conditioners and Heat Pumps, (2012). doi:10.6028/NIST.TN.1774.

[88] Architectural Energy Corporation, Advanced Automated HVAC Fault Detection And Diagnostics Commercialization Program, 2008. http://www.energy.ca.gov/2013publications/CEC-500-2013-054/CEC-500-2013-054.pdf (accessed July 21, 2016).
[89] Burton, P., Case Study: Automated Fault Detection and Diagnostic Software, 2005.
[90] SkyFoundry, Crown Casino Melbourne: Energy and Operational Savings Across a Multi-Use Entertainment Complex, (2015). http://www.skyfoundry.com/file/136/Case-Study-Crown-Melbourne—Driving-Savings-in-an-Entertainment-Complex.pdf (accessed July 21, 2016).
[91] West, S.R., Guo, Y., Wang, X.R., Wall, J., Automated fault detection and diagnosis of HVAC subsystems using statistical machine learning, in: 12th Conf. Int. Build. Perform. Simul. Assoc., 2011.
[92] Natural Resources Canada, Dabo, Palais Des Congrès De Montréal: A More Intelligent and Efficient Building because of Dabotm, (2009). https://www.nrcan.gc.ca/sites/www.nrcan.gc.ca/files/canmetenergy/files/pubs/DABO_Palais_des_congr%C3%A8s_Montr%C3%A9al_en.pdf (accessed July 22, 2016).

10 Modeling Building Air Conditioning Energy Consumption in Dense Urban Environments

Jorge E. Gonzalez, Yehisson Tibana, Luis Ortiz, and Estatio Gutierrez

Abstract

Dense urban environments are exposed to the combined effects of rising global temperatures and urban heat islands, a thermal gradient between the urban centers and the less urbanized surroundings suburbs. This combination results in increasing energy demands in cities, associated mostly to air conditioning, to maintain indoor human comfort conditions. Cities are becoming denser as population from rural areas is migrating towards urban centers worldwide. Given the anticipated increased of energy demands from cities in the future, it is imperative to develop new methodologies to quantify energy demands from buildings in very dense urban environments.

10.1 Chapter Summary

The purpose of this chapter is to precisely present a methodology to quantify thermal loads of buildings located in very dense urban environment taking of New York City as case study. To quantify thermal loads of buildings for this city; a single building energy model (SBEM), the US Department of Energy EnergyPlus™, and an urbanized weather forecasting model (uWRF) coupled to a building energy model are used. The SBEM is driven by Typical Meteorological Year (TMY) weather file and by a customized weather file built from uWRF's weather data for the specific days of the heat wave in July 2010. A series of simulations were conducted with the SBEM software to model building energy consumption data due to air conditioning for two locations in Uptown and Midtown Manhattan, NY, which represented a low density and a high density building area within the city. Assumptions were made regarding the building's floor plans and operation schedule to simplify the model and provide a close comparison to uWRF.

Results of the ensemble of SBEM indicate there is an increase in energy demand during the July 2010 heat-wave with uWRF weather

generated data when compared with the Central Park TMY case. The uptown location consumed 52% more energy during the heat wave event, whereas the midtown location showed an increased in energy demand of 65% when compared with a typical July three day period, reaching total peak loads of close to 14000 kW for a 75 m height building. Comparison of the results directly from uWRF for the energy demand for same locations, indicate that for the midtown location the SBEMs underestimated the total energy demand at a 57% difference. This may be due to the fact that uWRF energy model takes into account urban microclimate parameters, such as anthropogenic sources and waste heat interactions between surrounding buildings.

10.2 Introduction

The electrical energy consumption from commercial and residential buildings during summer periods in subtropical climates, and year round in tropical climates, is mostly associated to the use of air conditioning to maintain indoor human comfort conditions. It was estimated by the Energy Information Administration (EIA) that about 11% of total U.S. electricity consumption was used for cooling by the residential and commercial sectors in 2011 [1]. The energy demand in cities is further magnified during extreme heat events. The frequency of these heat waves is projected to increase over the 21st century [2, 3] as well as its duration, and severity [4–7].

Coupled with higher temperatures of summer seasons, the urban heat island (UHI) effect present in dense urbanized regions creates a significant additional source of heat. The main contributing factors to the UHI are changes in the physical characteristics of the surface such as albedo, thermal capacity, and heat conductivity, due to replacement of vegetation by asphalt and concrete; decrease of surface moisture available for evapotranspiration; anthropogenic heat; and changes in the radiative fluxes and in the near surface flow, due to the complex geometry of streets and tall buildings. Denser sections of a city can experience higher temperatures, up to 4°C warmer [8–9] as seen in Figures 10.1 and 10.2. Several studies have reported UHI as a local environmental impact such as cases in Atlanta, Georgia [10], Sacramento, California [11], San Juan, Puerto Rico [12], and Houston, Texas [13]. Gedzelman et al. [14] found that around New York City, the urban-rural temperature difference is greatest on clear nights with low humidity throughout the troposphere and

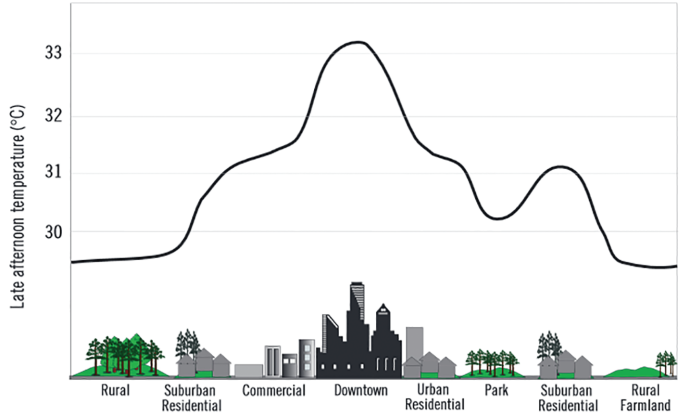

Figure 10.1. Urban Heat Island Profile [24].

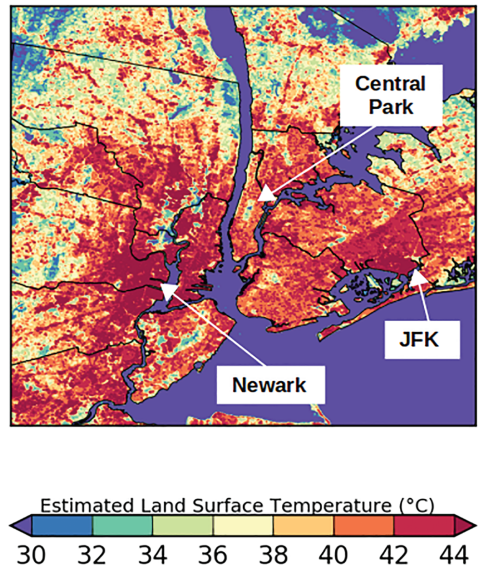

Figure 10.2. Example of UHI for New York City of San Juan, Puerto Rico. Thermal gradients urban-rural are as high as 10°C. (Taken from NASA/ Landsat Sensor as reported in Cox et al.).

gentle northwest winds and it is strongly reduced by sea breezes and back door cold fronts during spring and summer. In this area, wind speed has strongly declined over the century due to the increase of building heights intensifying the UHI [15]. Table 10.1 summarizes urban heat island intensities for various cities in the U.S. and around the world.

Table 10.1. Urban Heat Island Intensities for Various Cities.

City	Summer UHI Intensity (℃)
New York	3.5–5.5 [15]
Atlanta	2.5–5.0 [10]
Phoenix	9.4–12.9 [16]
Mexico City	1.0–7.8 [17]
Beijing	−1.59 to 5.34 [18]

In addition to the higher temperatures experienced in cities, global warming may further influence energy demand during the summer period in cities. Recent studies show energy demand will increase by 15% for cooling of buildings over the 21st century [19], and summer loads will increase by 10% for most building in the United States [20]. Table 10.2 displays US National and regional studies of cooling energy demands change over the century due to increasing temperatures. In short, the high temperatures during summers in dense urban areas may result in significant increases of energy consumption to a point where the electrical grid may be at risk. Therefore, it is imperative to develop accurate methodologies to quantify energy demands from buildings in very dense urban environments.

The relevance of this topic is increasingly growing as population migration trends are to move urban areas. According to the 2010 US census, 80.7% of the US populations are living within urban areas [21] and as of 2012, 52.6% of the world's populations lived in urban zones; this has seen an average annual growth of 2.1% in the last ten years [22]. Moreover, accurate quantification of energy consumption can reduce power outages and potentially lessen the extreme heat related deaths in these environments which have been shown to increase in U.S. cities [23].

The main purpose of this chapter is to quantify thermal loads of buildings located in the very dense urban environment using New York City during a summer season (2010) as a case study to illustrate the need for new developments to quantify energy demands in very dense urban environments.

10.3 Case Study Sites

Two New York City locations are considered for the analysis: a low density uptown Manhattan area as seen in Figures 10.4, and the high-density midtown site in Figure 10.5. The uptown location is a mix of

Table 10.2. National and Regional Studies of Cooling Energy Demands due to Increasing Temperatures.

Study	Change in Cooling Energy Consumption (%)	Temperature Change (°C) and Date for Change
	National Studies	
Rosenthal et al. 1995 [25]	+20% (residential) +15% (commercial)	+1°C (2010)
Scott et al. 2005 [26]	+8% to 39% (residential) +6% to 30% (commercial)	+1.7°C median (2020)
Belzer et al. 1996 [27]	+53.9% (commercial)	+3.9°C (2030)
	Regional	
Sailor, 2001 (New York) [28]	+0.9% per capita residential +1.6% per capita commercial	2°C (N/A)
Ruth and Lin, 2006 (Maryland) [29]	+2.5% (residential) +10% (per employee commercial)	1.7°C–2.2°C (residential) +2.2°C (commercial) (2025)
Amato et al. 2005 (Massachusetts) [30]	+10% to +40% (residential) +4% to +10% (per employee commercial)	+24.1% in cooling degree-days (2030)

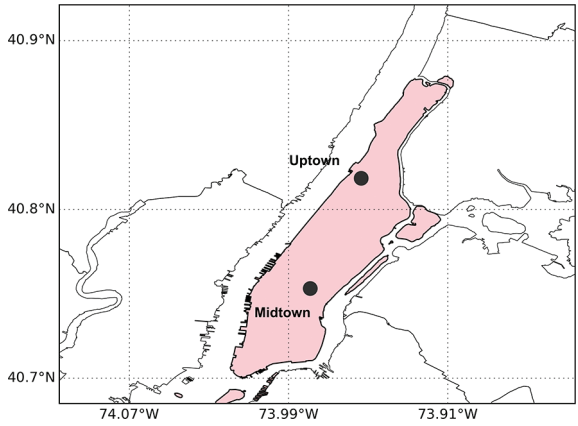

Figure 10.3. Locations of study. Shaded area denotes New York County, which is mostly comprised of Manhattan.

Figure 10.4. Uptown Manhattan. Coordinates: 40.822631, −73.951367 ***Source:*** **Google Earth.**

mid-rise residential buildings and commercial sites. The Midtown location is a more urbanized area with high-rise residential and commercial buildings. The urban fraction of the midtown zone is nearly one. In contrast, the uptown area has a greater visible amount of urban vegetation. Temperature differences between both locations are shown in Figure 10.6.

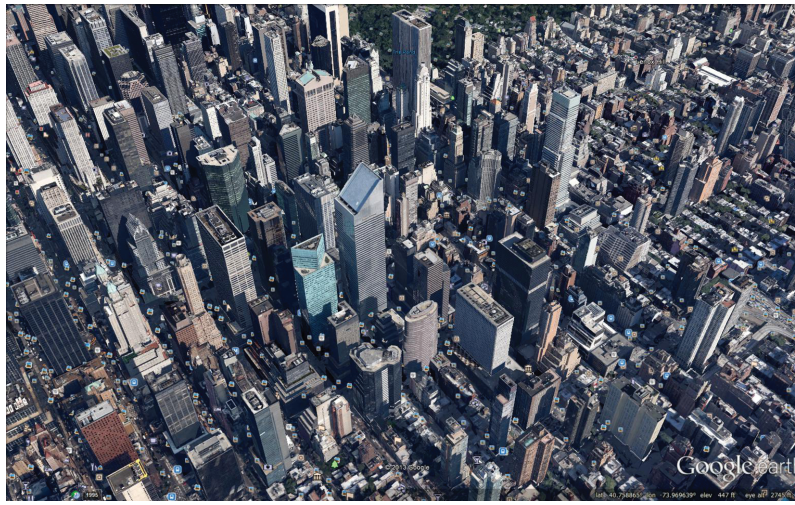

Figure 10.5. Midtown Manhattan Coordinates: 40.759302, −73.969148 ***Source:*** **Google Earth.**

10.4 Description of the Summer 2010 Heat Wave Event

We choose a heat wave event to better illustrate the differences between city scale and single building energy models. A heat wave is a prolonged period of temperatures considered abnormally high for a particular area. The National Weather Service (NWS) declares heat watches and warnings on a region when the daytime heat index, an expression that combines temperature and relative humidity [31], is greater than or equal to 40.6°C (105°F), with nighttime lows greater than or equal to 26.7°C (80°F), for at least two consecutive days [32]. In the summer heat wave of 2006, the high temperatures caused power outages in several areas including Queens, New York [8]. Several studies have found that the duration, severity, and frequency of heat waves may increase by the end of the century as consequence of global warming. The number of heat waves days is projected to double in the Los Angeles area [4], and Quadruple in Chicago [5]. Heat wave severity is expected to increase with a temperature greater than 3°C in the western and southern regions of the United States [3]. Other models show a heat wave frequency increase of 36% and duration of individual events by 27% [2].

The 2010 July heat wave took place after persistent anticyclonic conditions predominated the North East region. The peak of the heat event

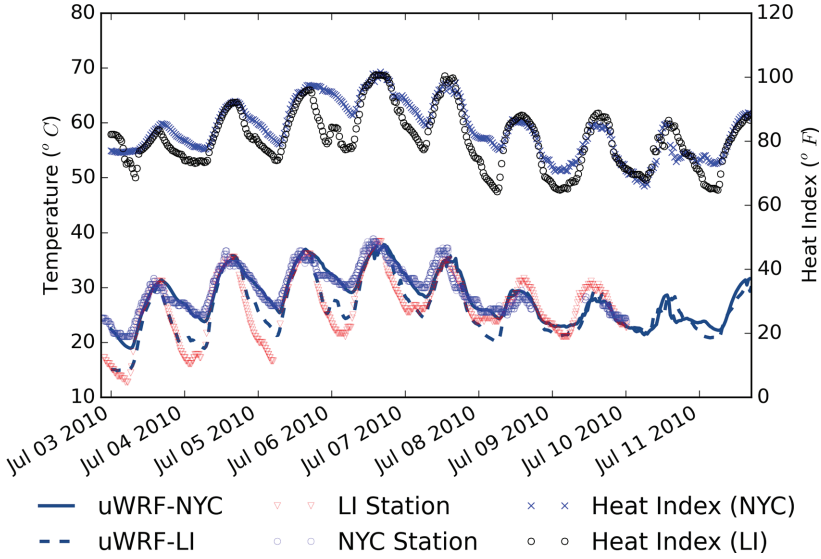

Figure 10.6. NYCMetNet observations during heat wave event.

was characterized by an intense high pressure system over the east coast and part of the ocean that induced a weak westerly wind that advected warm air into the area. Following the trajectory of the upper level subtropical ridge, the surface high showed a westward movement dissipating by the end of July 8, 2010.

Mean observed hourly surface temperature values for the heat event in New York City in July 4 to 8, 2010, were measured from the ground network of stations referred as NYCMetNet[1]. Maximum surface temperatures exceeding 32°C were recorded with the highest temperature registered by NYCMetNet stations reaching 39.4°C in Manhattan on July 6th at 1500 ET (Figure 10.6). The heat index time series obtained from observations showed maximum index of 107, 119, and 112°F and minimum values of 85, 87, and 83°F for three consecutive days in clear correspondence with the NWS service heat wave definition[2]. The UHI was recorded at a maximum of 4°C in the night and a magnitude of 2°C during the hottest day [33]. Figure 10.6 also shows the validation of the urbanized weather model for the same two locations, this will be discussed later in the chapter.

[1] http://nycmetnet.ccny.cuny.edu/
[2] http://www.nws.noaa.gov/os/heat/index.shtml

10.5 Methodology for Case Study

The approach used to model thermal loads of buildings for the duration of the heat wave is a single building energy model (SBEM) using US Department of Energy EnergyPlus™, and an urbanized weather forecasting model coupled to a building energy model (uWRF). The SBEM software was driven by Typical Meteorological Year (TMY) weather file and by a customized weather file built from uWRF's weather data for the specific days of the heat wave.

10.5.1 City Scale Model-uWRF

uWRF is a mesoscale numerical weather prediction system coupled to a multilayer urban parameterization [34]. The urban model is composed of a Building Energy Parameterization (BEP) and Building Energy Model (BEM) as described in Salamanca and Martilli [35] and Martili et al. [36]. BEP accounts for impacts from horizontal and vertical building surfaces in the momentum, heat, and turbulent kinetic energy equations. On the other hand, BEM, for each building floor, considers the diffusion of heat through walls, roofs and floor; natural ventilation; radiation exchange between indoor surfaces; generations of heat due to occupants and equipment, and the energy consumption due to air conditioning (AC) systems. Both BEP and BEM work together, along with the uWRF dynamical core (Figure 10.7) to predict urban weather and energy demands.

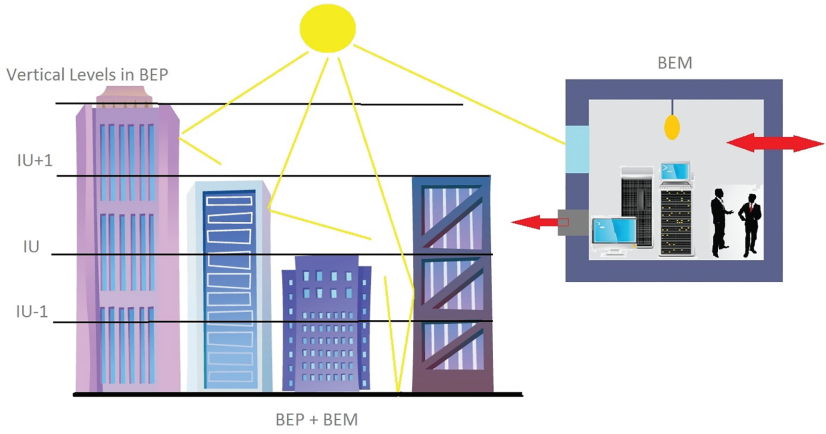

Figure 10.7. UWRF's BEP and BEM.

10.5.2 Building Energy Parameterization (BEP)

BEP included in WRF version 3.1 accounts for impacts from ground surfaces, as well as from horizontal and vertical building surfaces in the prognostic momentum, heat, and turbulent kinetic energy (TKE) equations [34].

These equations, in Reynolds averaged form, are defined as follows:

Momentum:

$$\frac{\partial \rho U_i}{\partial t} = \frac{-\partial P}{\partial x_i} - \frac{\partial \rho U_i U_j}{\partial x_j} - \frac{\partial \rho u_i' w}{\partial x_j} - \rho \frac{\theta'}{\theta_o} g \delta_{i3} - 2\varepsilon_{ijk}\Omega_j (U_k - U_k^G) + D_{ui}, \tag{10.1}$$

Where U (as well as u and w) represent flow velocities, ρ is the air density, θ_o is the reference state potential temperature, θ' is the change of the actual potential temperature from the base reference state, g is the gravitational constant, Ω is the angular velocity of the earth's rotation, U_k^G is the geostrophic wind, and D_{ui} are the forces due to the solid-fluid interactions.

Energy:

$$\frac{\partial \rho\, \theta}{\partial t} = \frac{-\partial \rho \theta U_i}{\partial x_i} - \frac{\partial \rho \overline{w\theta}}{\partial z} + D_\theta - \frac{1}{C_p}\left(\frac{P_o}{P}\right)^{\frac{R}{C_p}} \frac{\partial R_{lwave}}{\partial z}, \tag{10.2}$$

Here, P_o is the reference pressure of the system (1000 hPa), R is the gas constant of air, C_p is the specific heat at constant pressure of air, R_{lwave} is the longwave radiation, and D_θ is the sensible heat flux from solid surfaces to the fluid.

Air Humidity:

$$\frac{\partial \rho H}{\partial t} = \frac{-\partial \rho H U_i}{\partial x_i} - \frac{\partial \rho \overline{wh}}{\partial x_i} + D_h, \tag{10.3}$$

Here, H is the absolute humidity of air, h is the turbulent fluctuation of humidity, and D_h is the latent heat flux from the solid surfaces.

Turbulent Kinetic Energy:

$$\frac{\partial \rho E}{\partial t} = \frac{-\partial \rho U_i E}{\partial x_i} - \frac{\partial \rho \overline{ew}}{\partial z} + \rho K_z \left[\left(\frac{\partial U_x}{\partial z} \right)^2 + \left(\frac{\partial U_y}{\partial z} \right)^2 \right]$$

$$- \frac{g}{\theta_o} \rho K_z \frac{\partial \theta}{\partial z} - \rho C_\varepsilon \frac{E^{\frac{3}{2}}}{l_\varepsilon} + D_E, \tag{10.4}$$

Finally, here E is the turbulent kinetic energy, and its turbulent fluctuation is e. K_z is the vertical diffusion coefficient, and C_ε, and l_ε are model parameters, and D_E is the source of turbulent kinetic energy due to solid-fluid interactions. Although traditional approaches confine momentum sinks to the surface, BEP distributes the sinks to different vertical levels within the PBL. Urban grid cells are assumed to have of an array of buildings of the same width located at the same distance from each other, but with different heights. The D^* terms in equations 10.1–10.4 represents the combined fluxes to the presence of buildings and background fluxes (from non-building sources) for each variable and are computed as

$$D_{A_I} = \frac{F_{a_I^H} + F_{a_I^V}}{V_I^A}, \tag{10.5}$$

where V_I^A is the grid cell air volume, and F_I^V and F_I^H are average fluxes from buildings' vertical and horizontal surfaces, respectively.

10.5.3 Building Energy Model (BEM)

The Building Energy Model [35] estimates indoor temperature evolution due to change in the total sensible heat and latent loads. Consequently, BEM calculates the amount of heat (H_{out} and E_{out}) per floor that has to be extracted or added to maintain indoor temperature at a target value. The removed heat load excess is released on each floor level as sensible heat having a direct impact on air temperature. The system discharges small amounts of latent heat to the atmosphere produced by human metabolism inside the building. BEM is coupled with BEP and it was incorporated in WRF in version 3.2. Room temperature and moisture change with time are defined by:

$$\rho V_B \frac{\partial q_{V_r}}{\partial t} = E_{in} - E_{out} \tag{10.6}$$

Where heat (H_{in}) and humidity (E_{in}) sources are calculated as follows:

$$H_{in} = \sum_j A_i^{wind} h_{wind,j}(T_{wind,j} - T_r) + A_i^{wind} h_{wind,j}(T_{wall,j} - T_r) \tag{10.7}$$

$$+ (1-\beta) C_p \rho V_a (T_a - T_r) + A_f q_E + A_f P \varphi_P q_{hs},$$

$$E_{\text{in}} = (1-\beta) l \rho V_a (q_{V_a} - q_{V_r}) + A_f P \varphi_P q_{hl}, \tag{10.8}$$

Here, Q_B is the total heat capacity, V_B is the total volume of air inside the building, A_i is the building surface area, h_{wind} is the external heat transfer coefficient, β is the thermal efficiency of the heat exchanger, V_a is the total ventilation rate, l is the latent heat of evaporation, q_E is the equipment sensible heat gain, φ is the ratio of hourly occupants to peak occupancy, q_{hs} is the sensible heat gain from occupancy, q_V is the specific humidity of air (indoor and outdoor), and q_{hl} is the occupancy latent heat. The 2010 heat wave simulations using uWRF were conducted and reported in a previous study by Gutierrez et al. [33] showing excellent agreement with surface weather observations. The building parameters used in such simulation and for this study are listed in Table 10.3. Martilli et al. [36] and Salamanca and Martilli [35] conducted extensive validation simulations, and available in their respective publications. Detailed validation of BEM was performed by Salamanca and Martilli [37] using data collected during a measurement campaign in Basel, Switzerland. BEM is shown to improve the model results when compared to air conditioning demand observations.

uWRF utilizes Primary Land Use Tax Lot Output (PLUTO), created by the Department of City Planning. PLUTO is used to derive several of the necessary urban morphology parameters for NY: the mean building height, height histograms, gross area, garage floor area, total surface area, building width, among others. Adaptation of the model for use in other cities requires this data, either from publicly available databases or from observational studies. Projects, such as the World Urban Database and Access Portal Tools (WUDAPT) [38–39], have developed methodologies that incorporate satellite and local observations to derive urban parameters. The building height distributions for both grid

Table 10.3. uWRF Building Parameters for locations.

Building Parameter	Midtown	Uptown
Shape	Square	Square
Floor Area	1346.9 m^2	580.8 m^2
Street Width (SW)	52.4 m	54.7 m
Building Width (BW)	36.7 m	24.1 m
Urban Fraction (UF)	0.95	0.85
Zones	1/floor	1/floor
Cooling System	DX Cooling Coil	DX Cooling Coil
Cooling COP	3.5	3.5
Thermal Conductivity of Walls, Ceiling	0.67 W/m-K	0.67 W/m-K
Equipment gain	26 W/m^2	20 W/m^2
People gain	0.05 W/m^2	0.025 W/m^2
Window Fraction	33%	33%

locations are shown in Figure 10.8. A sample distribution for the grids is shown in Figure 10.9.

To accurately compare the SBEM solutions to uWRF, the simulations were conducted for each building height shown in Figure 10.8. The BEM component of uWRF computes the air conditioning energy demand for each floor as follows:

$$E_{floor} = \frac{|SensibleHeat| + |Latentheat|}{COP} \tag{10.9}$$

The sensible and latent heat is the energy that needs to be removed to meet the target temperature and humidity. This energy consumption is equivalent

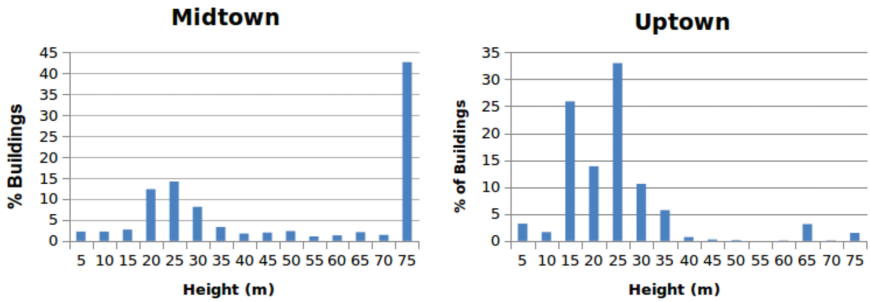

Figure 10.8. Building height distribution of a 1-km grid from PLUTO.

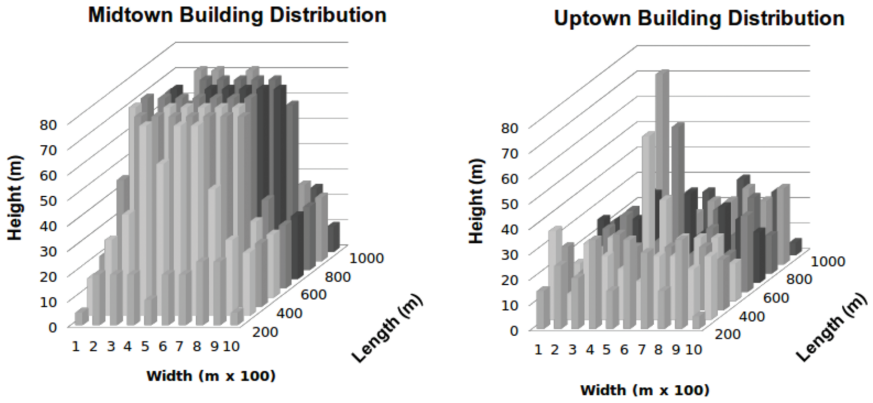

Figure 10.9. 1 km grid building height distribution for NYC.

to the AC compressor work calculated in the SBEMs. To represent the total consumption in each grid, the sum of consumption for all floors and for each building is multiplied by the probability of that type of building, in Figure 10.8, times a scaling factor to link the urban and the meso-scales:

$$E_{Total} = E_{Total,i} + Meso * E_{floor} * PB \tag{10.10}$$

Where

$$Meso = \frac{UF}{2 * (BW + SW) * BW} \tag{10.11}$$

Where, *UF* is the urban fraction within the grid, *BW* and *SW* are the building and street widths, respectively, and *PB* is the building height probability.

Energy demand for cooling for the 1 km grid is reported as W/m^2. The SBEM results for all building heights were scaled to match uWRF grid results by calculating total energy demand for all buildings. The previously listed equations were used in the process.

10.5.4 Single Building Energy Model-EnergyPlus™

EnergyPlus™ is an energy analysis and thermal load simulation developed by the US Department of Energy as a tool intended for analyzing energy dynamics of single buildings and useful for the design and sizing of HVAC

equipment [40]. This SBEM simulates the thermal zones, the air handling systems, and the central plant equipment simultaneously. Simulations involve the numerical computation of heat and moisture (mass) balance equations that describes the building components. Figure 10.10, display the heat sources that a typical SBEM software such as EnergyPlus™ takes into account.

Energy Plus is also able to incorporate the effects of shadows created by the surfaces of the building due to the changing position of the Sun. If an external surface is created, shadow effects are also applied as well as radiation reflectance from these external surfaces.

The model used for both uptown and midtown locations are a three-floor building with a floor area of 1346.9 m^2 and 580.8 m^2, respectively (Figure 10.11). External surfaces are modeled to simulate adjacent building shadow and radiation reflectance.

All building heights (Figure 10.8) simulations are accomplished with this simple three floor model. To reproduce the number of floors, the middle floor (thermal zone) is multiplied. A separate model was used to simulate the one floor and two floor building. The parameters of the model are chosen to match uWRF's (Table 10.3) as close as possible. Assumptions were made regarding the building's floor plans and operation schedule to simplify the model and provide a closer comparison to uWRF. Each floor

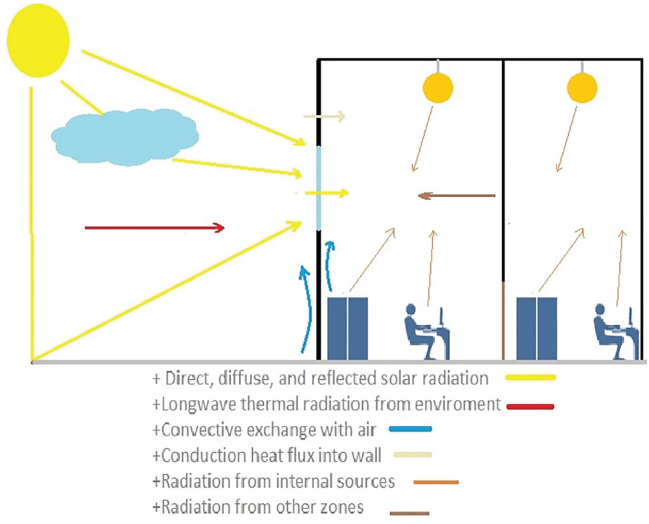

Figure 10.10. Typical SBEM energy sources interaction.

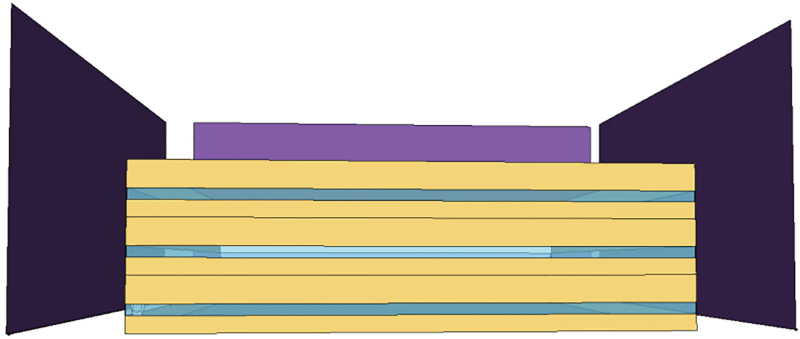

Figure 10.11. EnergyPlus™ Model.

is taken as a single thermal zone. Thermal set points were set to closely imitate a 24 hour always on schedule.

10.6 Results and Discussion

Custom weather files were developed for each location in New York City for the 3-day heat wave event from uWRF outputs. They contained accurate temperature, humidity, wind magnitude and direction, and solar radiation profiles for each location using data produced from uWRF weather outputs. Results for the location of uptown and midtown Manhattan temperatures obtained from uWRF weather outputs data are compared with TMY records and shown in Figure 10.12. The uWRF output exhibits higher temperatures for both the Midtown and Uptown locations. These higher temperatures more closely match the observed values at various locations in New York City, as shown in Figure 10.6. The closest temperatures are obtained from an airport weather station 6 miles away from midtown.

This is a substantial temperature difference, bearing in mind that SBEM are driven primarily by TMY weather files, which are statistical construct of typical weather for a given time of the year in a location [41]. Although TMY data is designed to capture some of the variability, the nature of using historical data prevents it from capturing extreme events such as the heat wave used in this study. Figure 10.13 displays the relative humidity comparison between the Manhattan's TMY weather file and weather data from the heat wave. Data from a typical year weather file overstimates the humidity experienced during this extreme weather period.

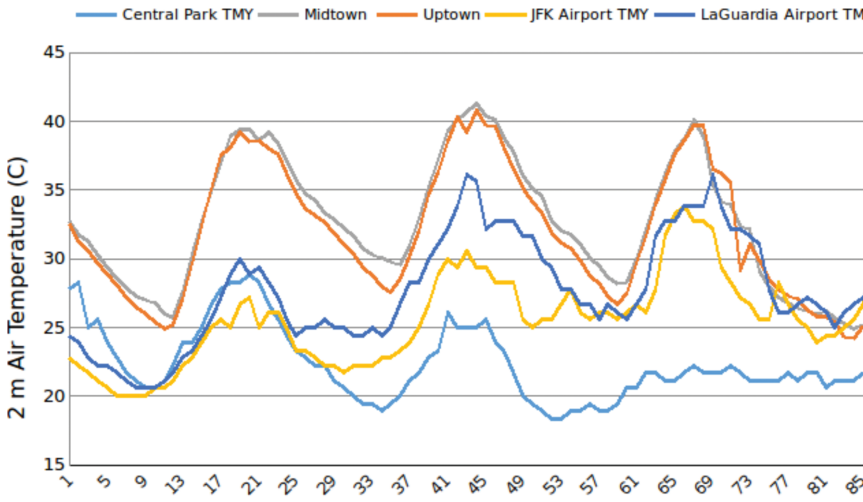

Figure 10. 12. uWRF Modeled and TMY Air Temperatures during heat wave at midtown and uptown locations.

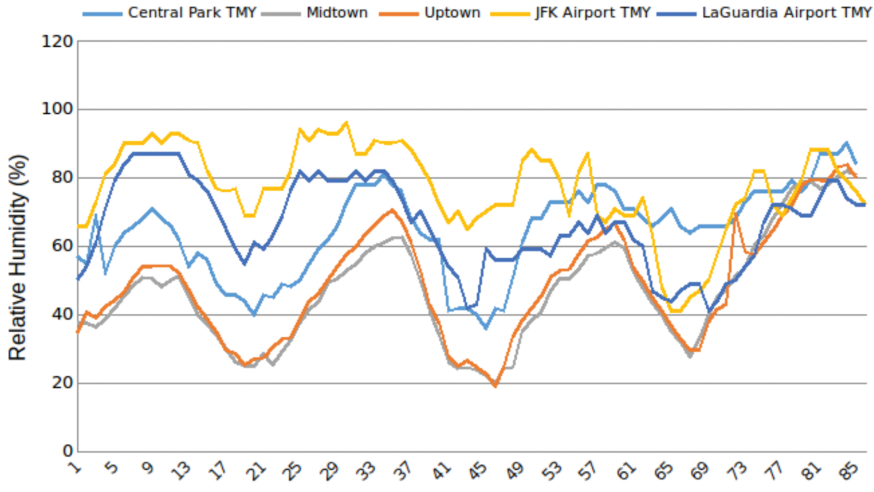

Figure 10.13. uWRF and TMY Relative Humidity during heat wave at midtown and uptown locations.

Analysis of the energy consumption for cooling during the 2010 heat wave conducted with uWRF [33], showing higher values in both midtown and downtown areas of Manhattan (Figure 10.14). This is in agreement with higher urban density of the location and higher building heights.

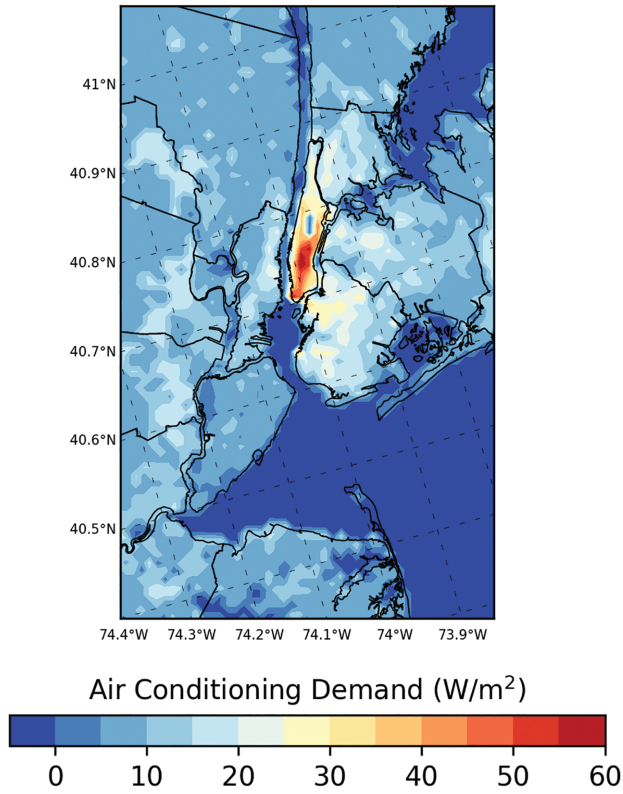

Figure 10.14 Dark roof AC energy consumption simulation on July 6, 2010 15ET [33].

Figure 10.15 displays the total energy demand simulated in EnergyPlus™, for the heat wave event using both TMY and uWRF customized weather files for different locations in New York City. The analysis was conducted on a 75 meters height building with the same parameters listed in Table 10.3. The figure shows that the midtown location exhibited the greatest consumption with 9812 kWh. The plot emphasizes the differences of the single building energy model output when using customized weather files instead of TMY weather files. The TMY files use average weather data collected from previous average years from nearby locations, whereas uWRF produces weather outputs specific to the location and days. From the total demand we may note that the weather data clearly varies, producing different TMY results. The lowest consumption at 1800 kWh is derived from Central Park TMY weather file which happens to be the closest location to the area of study and the most probable chosen weather file for a typical SBEM analysis of a Manhattan building.

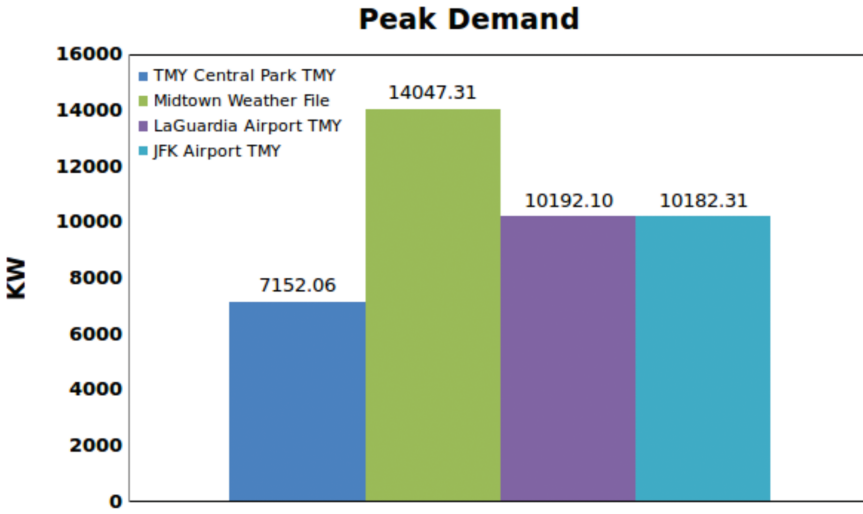

Figure 10.15. Total energy demand from A/C during the 3-day heat wave. Custom weather File vs TMY for 75 m High Building using EnergyPlus™.

Figure 10.16 show comparisons between the energy consumption for the SBEM and uWRF for Midtown and Uptown, New York City, respectively. For uptown (Figure 10.17), the total energy demand per meter square results in a 10.8 % difference when compared to uWRF. Through the day the results closely parallel each other. Overall there seems to be agreement between the two approaches. In the midtown simulations, however, EnergyPlus™ significantly underestimated the HVAC electrical demand per square meter at a startling 56.9% lower total demand. The atmospheric mesoscale modeled estimated midtown entire electrical energy demand to be 2372.9 W/m^2 through the heat wave event.

The major difference between the SBEM and uWRF is that the SBEM fails to accurately estimate the energy consumption in a dense urban location as seen in the case of midtown Manhattan. The single building model do not consider the urban microclimate effects such as canyon and UHI effects experienced in a dense location. Some sources of anthropogenic heat are also not taken into account in SBEM that may influence the energy exchange between the urban environment and individual buildings. Sources of anthropogenic heat include human metabolism heat emission by vehicles and buildings that are taken into account by the urbanized weather model [42–43]. SBEM only considers

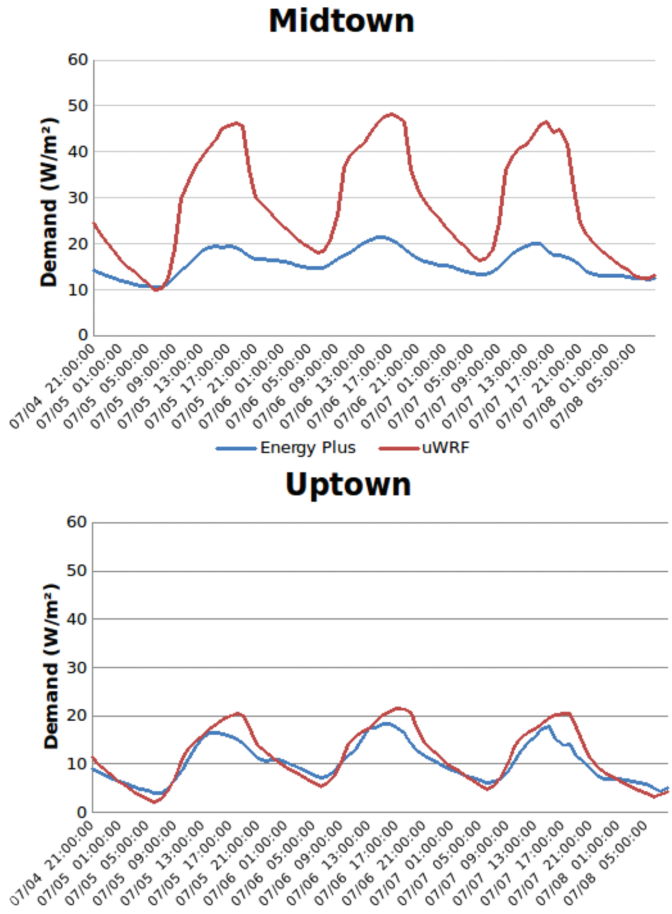

Figure 10.16. SBEM vs. uWRF for Midtown, New York during the heat wave event.

the human heat loads in the heat balance calculations (Figure 10.9). It is estimated that buildings contribute over 60% of the total urban anthropogenic heat [44]. Heat interactions between buildings specifically waste heat from AC equipment into the environment can be significant [45] and are not accounted for in TMY weather files or by SBEMs. Therefore, it is safe to assume that uWRF is more accurate in predicting the effects of microclimate conditions on energy consumptions in very dense environments. This can be seen in Figure 10.16, as the densest location (midtown) is shown to demand more energy than the SBEM results. For a less dense area such as uptown the two models, more or less, produce similar results as seen in Figure 10.16.

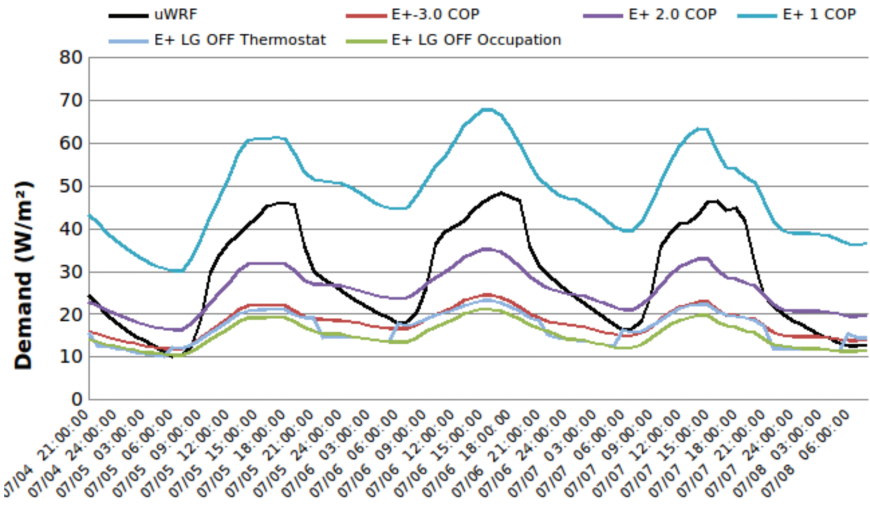

Figure 10.17. SBEM sensitivity analysis using energy plus for Midtown, New York.

Sensitivity analyses were conducted for the SBEMs in Midtown, New York City using various building parameters to achieve simulations with similar energy consumption results to uWRF. These parametric studies involved changes to the COP of the cooling systems, large office building thermostat set points, and large office building occupation. The parametric studies for EnergyPlus™ can be seen in Figure 10.17.

10.7 Conclusions and Future Work

Temperature rises due to global warming, added to the urban heat island present in dense cities is resulting in increasing trends of energy consumption in cities. This energy consumption from buildings during summer times is mostly associated with the use of air conditioning to maintain indoor human comfort conditions. The energy demand is further magnified during extreme heat events. Given the forecasted increased frequency of extreme heat events for the future, it is imperative to develop methodologies to quantify energy demands from buildings in dense urban areas, particularly during extreme heat events. Energy models that take into account microclimate effects, such as uWRF, need to be implemented in the energy analysis and design efforts of dense urban locations. These models could prove to be more accurate in estimating energy demand and its associated cost.

Our future goals are the following: (1) conduct a similar analysis for a full year for New York City; (2) Validate the electrical energy demand results from uWRF with actual data from New York's utility companies and building owners, and (3) extend this city-scale energy analysis for other cities worldwide.

Acknowledgments

Funding for this research was provided by US The Department of Education — Earth Science and Environmental Sustainability Graduate Initiative Grant P031M105066 and by The National Oceanic and Atmospheric Administration — Cooperative Remote Sensing Science and Technology Center (NOAA-CREST). NOAA CREST — Cooperative Agreement No: NA11SEC481000.

Nomenclature

BEM — Building Energy Model

BEP — Building Energy Parameterization

BW — Buildings Width (m)

COP — Coefficient of Performance

E — Energy Consumption (W/m^2)

PB — Building Height Probability (%)

SBEM — Single Building Energy Model

SW — Street Width (m)

TMY — Typical Meteorological Year weather file

UF — Urban Fraction

uWRF — Urbanized Weather Forecasting Model

References

[1] U.S. Energy Information Administration (EIA), September 2013 Monthly Energy Review, DOE/EIA-0035 (2013/09), Washington, DC.

[2] Ebi, K., and Meehl, G. 2007. "The Heat is On: Climate Change and Heat Waves in the Midwest" Regional Impacts of Climate Change: Four Case Studies in the United States. Arlington, VA: the Pew Center on Global Climate Change.

[3] Meehl, G.A., and Tebaldi, C. 2004. "More Intense, More Frequent, and Longer Lasting Heat Waves in the 21st Century," Science, 305(5686), 994−997.

[4] Vavrus, S., and van Dorn, J. 2008. "Projected Future Temperatures and Precipitation Extremes in Chicago," Journal of Great Lakes Research, in press.

[5] Hayhoe, K., Cayan, D., Field, C.B., Frumhoff, P.C., Maurer, E.P., Miller, N.L., Moser, S.C., Schneider, S.H., Cahill, K.N., Cleland, E.E., Dale, L., Drapek, R., Hanemann, R.M., Kalkstein, L.S., Lenihan, J., Lunch, C.K., Neilson, R.P., Sheridan, S.C., and Verville, J.H. 2004. "Emissions Pathways, Climate Change, and Impacts on California," Proceedings of the National Academy of Sciences, 101(34), 124−127.

[6] Kunkel, K.E., Bromirski, P.D., Brooks, H.E., Cavazos, T., Douglas, A.V., Easterling, D.R., Emanuel, K.A., Groisman, P.Ya., Holland, G.J., Knutson, T.R., Kossin, J.P., Komar, P.D., Levinson, D.H., and Smith, R.L. 2008. "Weather and Climate Extremes in a Changing Climate: Regions of Focus: North America, Hawaii, Caribbean, and U.S. Pacific Islands," Synthesis and Assessment Product 3.3 U.S. Climate Change Science Program, Washington, DC, pp. 35−80.

[7] Gutowski, W.J., Hegerl, G.C., Holland, G.J., Knutson, T.R., Mearns, L.O., Stouffer, R.J., Webster, P.J., Wehner, M.F., and Zwiers, F.W. 2008. "Weather and Climate Extremes in a Changing Climate: Regions of Focus: North America, Hawaii, Caribbean, and U.S. Pacific Islands," Synthesis and Assessment Product 3.3. U.S. Climate Change Science Program, Washington, DC, pp. 81−116.

[8] Thomas, R.K., Melillo, J.M., and Peterson, T.C. 2009. Global Climate Change Impacts in the United States, Cambridge University Press, pp. 89−98.

[9] Lemmen, D.S., and Warren, F.J. 2004. "Climate Change Impacts and Adaptation: A Canadian Perspective," Climate Change Impacts

and Adaptation Program, Natural Resources Canada, Ottawa, ON, p. 174. http://adaptation.nrcan.gc.ca/perspective/pdf/report_e.pdf.
[10] Bornstein, R., and Lin, Q. 2000. "Urban Heat Islands and Summertime Convective Thunderstorm in Atlanta: Three Cases Studies," Atmospheric Environment, 34, 507−516.
[11] US EPA Heat Island Website. http://www.epa.gov/heatislands/pilot /index.htm.
[12] González, J.E., Luvall, J.C., Rickman, D., Comarazamy, D.E., Picón, A.J., Harmsen, E.W., Parsiani, H., Ramírez, N., Vázquez, R., Williams, R., Waide, R.B., and Tepley, C.A. 2005. "Urban Heat Islands Developing in Coastal Tropical Cities," EOS Transactions, AGU, 86(42), 397 & 403.
[13] Houston Shepherd, J.M., and Burian, S.J. 2003. "Detection of Urban-Induced Rainfall Anomalies in a Major Coastal City," Earth Interactions, 7, 1−17.
[14] Gedzelman, S.D., Austin, S., Cermak, R., Stefano, N., Partridge, S., Quesenberry, S., and Robinson, D.A. 2003. "Mesoscale Aspects of the Urban Heat Island around New York City," Theoretical and Applied Climatology, 75, 29–42.
[15] Gaffin, S.R., Rosenzweig, C., Khanbilvardi, R., Parshall, L., Mahani, S., Glickman, H., Goldberg, R., Blake, R., Slosberg, R.B., and Hillel, D. 2008. "Variations in New York City's Urban Heat Island Strength over Time and Space," Theoretical and Applied Climatology, 94, 1−11.
[16] Hawkins, T., Brazel, A., Stefanov, W., Bigler, W., and Saffel, E. 2004. "The Role of Rural Variability in Urban Heat Island Determination for Phoenix Arizona," Journal of Applied Meteorology, 43, 476−486.
[17] Jauregui, E. 1997. "Heat Island Development in Mexico City," Atmospheric Environment, 31(22), 3821−3831.
[18] Miao, S., Chen, F., LeMone, M., Tewari, Li, Q., and Wang, Y. 2009. "An Observational and Modeling Study of Characteristics of Urban Heat Island and Boundary Layer Structures in Beijing," Journal of Applied Meteorology and Climatology, 48, 484−501.
[19] Crawley, D. 2008. "Estimating the Impacts of Climate Change or Urbanization on Building Performance," Journal of Building Performance Simulation, 1(2), 91–115.
[20] Lu, N., Leung, L., Wong, P., Paget, M., Taylor, Z., Correia, J., Mackey, P., Jiang, W., and Xie, Y. 2008. "Climate Change Impacts on Residential and Commercial Loads in the Western U.S. Grid," National Technical Information Service, U.S. Department of Commerce.

[21] U.S. Census Bureau, “Geography,” 2010 Urban Area Facts, http://www.census.gov/geo/reference/ua/uafacts.html.
[22] The World Bank. “Urban population (% of total),” United Nations, World Urbanization Prospects. http://data.worldbank.org/indicator/SP.URB.TOTL.IN.ZS/countries?
[23] Zanobetti, A., and Schwartz, J. 2008. “Temperature and Mortality in Nine US Cities,” Epidemiology, 19(4), 563−570.
[24] Akbari, H. et al. 1992. Cooling Our Communities, Report to U.S. EPA. Office of Policy Analysis.
[25] Rosenthal, D.H., Gruenspecht, H.K., and Moran, E. 1995. “Effects of Global Warming on Energy Use for Space Heating and Cooling in the United States,” Energy Journal, 16(2), 77−96.
[26] Scott, M.J., Dirks, J.A., and Cort, K.A. 2005. “The adaptive value of energy efficiency programs in a warmer world: Building energy efficiency offsets effects of climate change,” PNNL-SA-45118. In: Reducing Uncertainty Through Evaluation, Proceedings of the 2005 International Energy Program Evaluation Conference, August 17–19, 2005, Brooklyn, New York.
[27] Belzer, D.B., Scott, M.J., and Sands, R.D. 1996. “Climate Change Impacts on U.S. Commercial Building Energy Consumption: An Analysis Using Sample Survey Data,” Energy Sources, 18(2), 177–201.
[28] Sailor, D.J. 2001. “Relating Residential and Commercial Sector Electricity Loads to Climate: Evaluating State Level Sensitivities and Vulnerabilities,” Energy, 26(7), 645–657.
[29] Ruth, M., and Lin, A.-C., 2006. “Regional Energy and Adaptations to Climate Change: Methodology and Application to the State of Maryland,” Energy Policy, 34, 2820−2833.
[30] Amato, A.D., Ruth, M., Kirshen, P., and Horwitz, J. 2005. “Regional Energy Demand Responses to Climate Change: Methodology and Application to the Commonwealth of Massachusetts,” Climatic Change, 71, 175–201.
[31] Robinson, P. 2001. “On the Definition of a Heat Wave,” Journal of Applied Meteorology, 40, 762−775.
[32] NWS (National Weather Service). 1994. Excessive heat watch, warning and advisory heat index criteria. Regional Operations Manual Letter E-5-94, Eastern Region, NWS, Bohemia, NY. 3 pp.
[33] Gutierrez, E., Gonzalez, J.E., Bornstein, R., Arend, M., and Martilli, A. 2013. “A New Modeling Approach to Forecast Building Energy Demands During Extreme Heat Events in Complex Cities,” J. of Solar Energy Engineering, 135, doi: 10.1115/1.4025510.

[34] "The Weather Research & Forecasting Model." WRF. http://www.wrf-model.org/index.php.
[35] Salamanca, F., and Martilli, A. 2010. A New Building Energy Model Coupled with an Urban Canopy Parameterization for Urban Climate Simulations — Part I. Formulation, Verification and a Sensitive Analysis of the Model," Theoretical and Applied Climatology, 99, 331–344.
[36] Martilli, A., Clappier, A., and Rotach, M.W. 2002a. "An Urban Surface Exchange Parameterization for Mesoscale Models," Boundary-Layer Meteorology, 104, 261–304.
[37] Salamanca, F., and Martilli, A. 2009. "A New Building Energy Model Coupled with an Urban Canopy Parameterization for Urban Climate Simulations — Part II. Validation with One Dimension Off-Line Simulations," Theoretical and Applied Climatology, 99(3), 345−356.
[38] Bechtel, B., Alexander, P., Böhner, J., Ching, J., Conrad, O., Feddema, J., Mills, G., See, L., and Stewart, I. 2015. "Mapping Local Climate Zones for a WorldWide Database of Form and Function of Cities," International Journal of Geographic Information, 4(1), 199−219.
[39] Burian, S.J., Han, W.S., Velugubantla, S.P., Maddula, S.R.K. 2003. Development of Gridded Fields of Urban Canopy Parameters for Models-3/CMAQ/MM5. Department of Civil and Environmental Engineering, University of Utah.
[40] "About EnergyPlus." EnergyPlus Energy Simulation Software. http://apps1.eere.energy.gov/buildings/energyplus/energyplus_about.cfm.
[41] Hall, I.J., Prairie, R.R., Anderson, H.E., and Boes, E.C. 1978. "Generation of a typical meteorological year," Conference: Analysis for solar heating and cooling, San Diego, CA.
[42] ASHRAE standard: energy standard for buildings except low-rise residential buildings. (SI ed.). (2010). Atlanta, GA: ASHRAE.
[43] Sailor, D.J., and Lu, L. 2004. "A Top-Down Methodology for Developing Diurnal and Seasonal Anthropogenic Heating Profiles for Urban Areas," Atmospheric Environment, 38, 2737–2748.
[44] Quah, A., and Roth, M. 2012. "Diurnal and Weekly Variation of Anthropogenic Heat Emissions in a Tropical City," Singapore Atmospheric Environment, 46, 92−103.
[45] Ohashi, Y., Genchi, Y., Kondo, H., Kikegawa, Y., Yoshikado, H., and Hirano, Y. 2007. "Influence of Air-Conditioning Waste Heat on Air Temperature in Tokyo During Summer: Numerical Experiments Using an Urban Canopy Model Coupled With a Building Energy Model," Journal of Applied Meteorology and Climatology, 46(1), 66.

Index

Page numbers followed by f and t indicate figures and tables, respectively.

A

Absorption chillers; *see also* Chillers
  cost estimates for, 266, 266t
  double-effect (2E), 371
    exhaust absorption chiller, 277, 278f
    Li-Br, 273, 277
  schematic, 266, 267f
  single-effect (1E), 264–265, 265f, 371
  types, 277, 278t
  water/LiBr, 266
Absorption cooling systems, 97–100
Absorption TES
  performance improvement, 397–399, 398f
  working pairs, 393–394, 395t
  working principle, 385, 388–389, 388f
Active systems, solar water heating systems, 331, 331f
Active thermal energy storage systems, 240–243
Actuator problems, 423
Actuators, 192
Adaptive fault detection, 435
Adsorption TES
  performance improvement, 399–400, 400f
  for space cooling, 403–404, 405f
  test facility, 403–404, 405f
  working pairs, 394, 396–397
    silica gel and water, 394
    zeolites and water, 394, 396–397, 396f, 397f
  working principle, 389–392, 390f, 391f, 392f
Advanced Automated HVAC Fault Detection and Diagnostics Commercialization project, 448
AFUE (annual fuel utilization efficiency), 113–114, 117
Aggregated thermal demand (ATD) method, extended, 270–271
Air conditioning energy consumption, 475–496
  case study sites, 478, 480, 480f, 481f, 482f
  future work, 495–496
  methodology for case study, 483–490
    BEM, 485–488, 487f, 487t, 488f
    BEP, 484–485
    SBEM, EnergyPlus™, 488–490, 489f, 490f
    uWRF, city scale model, 483, 483f
  overview, 475–478, 477f, 478t, 479t
  results and discussion, 490–495
    dark roof AC energy consumption simulation, 490, 492f
    SBEM sensitivity analysis, 493–495, 495f
    SBEM *vs.* uWRF, 493, 494f
    TMY weather file, 490, 491f
    total energy demand, 492, 493f
    uWRF weather outputs data, 490, 491f
  summer 2010 heat wave event, 481, 482
  US National and regional studies, 478, 479t
Air conditioning (A/C) technology, building, 349–358
  chilled water storage/aquifers, 349–352, 350f, 351f, 352t
  PCMs, 352, 353–354
    ceiling board, 357, 357f, 358
    cumulative energy saving of load levelling strategy, 355t
    free cooling systems, 355f

ice TES system, schematic diagram, 353f
for solar shading, 354, 355, 356f, 357, 357t
various thermal storage systems, 354t
Air conditioning (A/C) technology, solid desiccant, 268–269
Air-cooled condensers, 104–105
Air handling units (AHU), 124–127
diagnostic algorithms for, 437, 440
diagram, 453, 454f
FDD methods, 438t–439t
fresh air ventilation rates, 126–127
Air humidity, 484
Air supply temperature control loop, 131
Alarm functions, 206
Alarm management, 421–424
PMM, 424, 425f
process/system fault definition, 422–423, 423f
Algorithms for recovery times estimation, 219–220
Allocation, costs and investment, 344–345
AM10 Natural Ventilation in Non-Domestic Buildings, 154
Analysis
economic and feasibility, CCHP systems, 279–283
cost, 282, 283t
detailed electricity and natural gas usage, 280, 280t
electric and natural gas costs, 281, 283t
electric output, 281, 281t
heat output, 281, 282t
Anova Verzekering Co., 352
APAR & VPACC, 446t
Applications
FDD, challenges in, 450–452
strategy/approach related, 451–452
industrial and HVAC, fault detection methods, 441–449
business models and commercial solutions, 443
commercial software, 443, 444t–447t
hardware/software requirements, 442–443
implementations, review of, 443, 448–449
solar ventilation air preheating, 320
TES, 348
Aquifers
chilled water storage, 349–352, 350f, 351f, 352t
hot water tank, 358–361, 358f, 360f
Arizona Public Service (APS), 281
Artificial lighting, annual use of, 214
Artificial neural networks (ANN), 202; *see also* Intelligent control systems
PCA and, 435–436
Artificial neuro-fuzzy inference system (ANFIS), 435
ASHRAE 62.1, 150
ASHRAE (American Society of Heating, Refrigerating, and Air-Conditioning Engineers), 113, 127, 260, 328
ASHRAE 188: Prevention of Legionellosis Associated with Building Water Systems, 161
ASHRAE 62.1 standard, 150
ASHRAE Standard 52, 161
ASHRAE Standard 55, 149
ASHRAE Standard 62, 221, 226
ASHRAE Std. 189.1, 10
ASME Boiler and Pressure Vessel Code, 115
ASME ISBES Workshop, 8–10
AspenTech, 443
Automated fault detection and diagnosis, in HVAC systems, *see* Fault detection and diagnosis (FDD)
Autoscaling, defined, 430
Azeotrope, 96

B
BACnet, 442
BACnet device, 209
Bahnfleth's solution, 35
Bayesian-Emulator approach, 86–88
BEM (building energy model), 483, 483f, 485–488, 487f, 487t, 488f
Benefits, TES, 270–271
BEopt™ (Building Energy Optimization) software, 5
BEP (building energy parameterization), 483, 483f, 484–485
Bishop, 42
BLAST, 42, 84
Boiler Efficiency Institute, 117
Boilers, 110–124
 control for, 236
 electric heat pumps, 120–121
 electric resistance heating, 119
 low-temperature radiant heating systems, 121–124
 selection, 115–116
Bottoming cycle, CCHP systems, 271
Boundary layer
 defined, 320
 temperature, 321
Building automation systems (BAS), 204
 implementation, 443
Building Description Language (BDL), 83
Building energy model (BEM), 483, 483f, 485–488, 487f, 487t, 488f
Building Energy Modeling, 4–5
Building energy parameterization (BEP), 483, 483f, 484–485
Building integrated PV (BIPV), 299
Building integration, CCHP (case studies), 271–279
Building level challenges and solutions, ESI, 337–341
 overcurrent protection, 337f, 338, 339
 sizing, 337, 338
 voltage regulation, 338f, 339
 wear-and-tear on reactive power compensation equipment, 340–341, 340f
Building load coefficient (BLC), 76, 82
Building loads, 240
Building management & control systems (BEMS), 443
Building management systems (BMS), 204
Building Optimization System program, 448
Building systems control strategies, 5–6
Building thermal mass, precooling of, 236–239
Buildings
 CCHP in, *see* Combined cooling, heating and power (CCHP) systems
 energy storage systems for, *see* Energy storage systems
 FDD application, challenges in, 450–452
  strategy/approach related, 451–452
 sorption TES system for, 385, 388–407
  working principle, 385, 388–392
 with TES integration literature summary, 375–379, 376t–378t
Buoyancy-driven natural ventilation, 143, 153–154
Business models, industrial and HVAC application, 443

C
C ratio, defined, 258
Cadmium telluride, 296–297
Caissons, concrete, 298
Calcium chloride, 107
California Energy Commission, 448
Carnot cycle method, 120

Carnot Refrigeration Cycle, 94–97
Case studies; *see also* District cooling systems (DCS), fault detection system for (case study); Fault detection system for DCS (case study); Passive cooling, case studies
 air conditioning energy consumption methodology, 483–490
 sites, 478, 480, 480f, 481f, 482f
 CCHP sizing options, building integration, operation and system controls, 271–279
 fault detection system for DCS
  design and features, 454–455, 455f
  implementation results, 455–461, 456t, 457f, 457t, 459f, 460f
  process layout and specifications, 452–453, 453f, 454f
 fault detection system for district cooling systems, 452–464
Cast-iron boilers, 115
CCHP, *see* Combined cooling, heating and power (CCHP) systems
Ceiling board, PCM, 357, 357f, 358
Center for Research and Technology Development (CRTD), 2
Central communications controller (CCC), 205
Central control unit (CCU), 205
Central inverters, 301
Challenges
 building level, ESI, 337–341
  overcurrent protection, 337f, 338, 339
  sizing, 337, 338
  voltage regulation, 338f, 339
  wear-and-tear on reactive power compensation equipment, 340–341, 340f
 in FDD application, 450–452
  strategy/approach related, 451–452
 substation-level, ESI
  grid-level, 342–343
  network protectors in systems, 341–342
  RE on local substation, 341
Chilled water storage/aquifers, sensible TES with, 349–352, 350f, 351f, 352t
Chiller water loops and VAV systems, 127–133
 energy recovery systems, 132–133
Chiller-priority control strategy, 240
Chillers, 100; *see also* Absorption chillers
 control for, 235
 recommendations for chiller system operation in commercial buildings, 105–106
 set-point temperature, 244, 245
Chlorofluorocarbons (CFCs), 96
City scale model, uWRF, 483, 483f
Classification
 fault detection methods, 424, 425–436
  commonly used methods, 427–429, 428f, 429f
  current trends, 435–436
  overview, 424, 425
  PCA, 430–434, 432f, 434f
  traditional alarm management, prismatic approach, 425–427, 426f
 sensible/latent TES systems, 348, 349f
Climate change and sustainable buildings, 17–18
Climate Consultant, 145–146
ClockWorks, 444t
Closed loop system, 192
Coefficient of performance (COP), 98–99
 GAX with, 265
 ground-source heat pump, 369
 Li-Br 2E absorption chiller, 277
 space cooling/heating, 268
 standalone solid desiccant systems, 269
Collectors, solar water heating
 efficiency curves, 329, 329f
 evacuated tube, 326–327, 334–335
 glazed flat plate, 326, 332t
 integrated-collector-storage collectors, 330

parabolic-trough, 327–328
types, 324–335, 325f
unglazed, low temperature, 325–326, 330, 332t
Combined cooling, heating and power (CCHP) systems, 251–284
absorption chillers
cost estimates for, 266, 266t
double-effect (2E), 273, 277, 278f
schematic, 266, 267f
types, 277, 278t
water/LiBr, 266
bottoming cycle, 271
building integration, case studies, 271–279
combined cycle, 271
conventional systems *vs.*, 252–253, 253f
cooling technology, matching, 261
datacenter
electric and cooling demand for, 272–273, 273f
electric LDC of, 274, 274f
two-dimensional LDC for, 275–276, 275f, 276f
economic and feasibility analysis, 279–283
cost analysis, 282, 283t
detailed electricity and natural gas usage, 280, 280t
electric and natural gas costs, 281, 283t
electric output, 281, 281t
heat output, 281, 282t
future, 284
goal, 271
heat recovery, 254, 261, 262–264, 263t
installation, 281, 282f
operation, case studies, 271–279
overview, 252–253, 253f
prime movers, 260–261, 260f, 262t
sizing options, case studies, 271–279
system controls, case studies, 271–279
technology, state-of-the-art review, 254–260
basic elements, 254
commercial application, 256
general diagram, 254–255, 254f
key system parameters and characteristics, 259, 259t
large-scale CCHP systems, 258
micro-CCHP systems, 256–257
overall efficiency, 255
performance, evaluation, 256
schematic diagram, 255, 255f
technical potential, 256, 257f
tri-generation, 259
TES requirements/benefits, 270–271
thermally activated, 264–269
absorption and vapor-compression chillers, 265–266, 266t, 267f
category, 264
ejector heat pump cycle, 269, 270f
single-effect (1E) absorption cycle, 264–265, 265f
solid desiccant A/C technology, 268–269
standalone liquid desiccant A/C, 269
topping cycle, 271
Combined production of heating and power (CHP), TES and, 370–375
CCHP system
diagram of, 371, 372f
hot water heat TES systems, 373–374, 374f
performance, 372, 373t
general layout, 370, 371f
Commercial building lighting and window designs, 16–17
Commercial solutions, industrial and HVAC application, 443
Communication protocol, 209–210; *see also* Supervisory controllers
Compressor integration, absorption TES performance, 398, 398f
Concrete caissons and footers, 298
Conduction transfer functions (CTFs), 34, 41–43

Constant-air volume (CAV), 225
Contaminants in buildings, 126
Control modes, 198–201
Control strategies
  applications
    about, 210–211
    electrical systems, 211–218, 212t, 215t, 218t
    HVAC equipment operation, 221–236, 223t
    HVAC systems with thermal storage, 236–246
    optimal start of HVAC systems, 218–221
  control modes, 198–201
  control system components, 190–198, 191t, 195t
  intelligent control systems
    about, 201
    artificial neural networks, 202
    expert controls, 202
    fuzzy control, 202
  overview, 189–190
  supervisory controllers
    communication protocol, 209–210
    components of EMCS, 204–206
    design considerations of EMCS, 207–209
    functions of ECMS, 206–207
  types of, 202–203
Controller bias, 199
Conventional systems, CCHP systems *vs.*, 252–253, 253f
Cool tower ventilation, 152
Cooling by desiccant equipment, 106–109
Cooling coil fouling, 457, 458, 461, 459f, 460f
Cooling demands
  building heating and, 272
  for data center, 272–273, 273f
Cooling load avoidance, 313–319, 317f
Cooling towers, 101–103
Cooling vapor compression systems, 94–97
Cooling/heating central plant optimization, 234–236
Cost(s)
  CCHP systems
    analysis, 282, 283t
    electric and natural gas, 281, 283t
  of daylighting system, 311
  energy, TES and, 352
  estimates, for absorption and vapor-compression chillers, 266, 266t
  installation of PV system, 301–302
  Interconnection Requirement Study, 336
  solar ventilation air preheating, 319, 320, 323t
  solar water heating systems, 332t, 333, 334–335
  utilities' electrical generation systems, 344–345
Crop drying, solar ventilation air preheating, 319
Crown Casino and Entertainment Complex, 448–449
CSIRO Energy Transformed Flagship, 449
Current-voltage relation, of PV cell, 295–296, 295f
Cycling stability, defined, 380

D

DABO™, 445t, 449
Data centers, 17
  in commercial sector, 256
  cooling LDC of, 274–275, 275f
  electric and cooling demand, 272–273, 273f
  electric LDC of, 274, 274f
  two-dimensional LDC for, 275–276, 275f, 276f
Data transmission medium (DTM), 206
Data-driven approach
  defined, 427
  review, 429, 429f
Daylighting, 305–313, 312f

Daylighting control system, 213–218, 213f, 214f, 215t, 218t; *see also* Electrical systems
Daylighting simulation tool, 216
DCS, *see* District cooling systems (DCS)
Dehumidification, 106–107, 125
  solid desiccant, 268
Demand controlled ventilation (DCV), 225–228, 228t
Demand side management (DSM), 343
Dense urban environments, air conditioning energy consumption in, *see* Air conditioning energy consumption
Department of Energy (DOE), 256
Desiccant equipment, cooling by, 106–109
Designs
  direct gain, 315–316
  FDD, 454–455, 455f
Desorber, defined, 265
Detection, fault, *see* Fault detection and diagnosis (FDD)
Diagnosis, fault, *see* Fault detection and diagnosis (FDD)
Dichlorodi-fluoromethane, 97
Dimensionality reduction technique, PCA as, 433
Direct digital control (DDC) systems, 202, 203
Direct gain
  defined, 315
  designs, 315–316, 317f
Discharging method
  double stage, 398–399, 398f
  three phase cycle, 398f, 399
Discussion, air conditioning energy consumption, 490–495, 491f, 492f, 493f, 494f, 495f
District cooling systems (DCS), fault detection system for (case study), 452–464
  design and features, 454–455, 455f
  implementation results, 455–461
    cooling coil fouling, 457, 458, 461, 459f, 460f
    historical data set clusters classification, 457, 457f
    monitored variables, 455, 456t
    recommendations, 461, 464
    reduced chilled water flow, 457, 461, 462f, 463f
    statistics thresholds, 457, 457t
  process layout and specifications, 452–453, 453f, 454f
Disturbance parameter change, 422
DOE-2, 76, 83, 84–85, 87, 88
Double skin facade, 168–173; *see also* Passive cooling
  design considerations, 170–173
  performance, 169–170
  principle, 168–169
Double stage discharging method, 398–399, 398f
Double-effect (2E) absorption chillers, 371; *see also* Chillers
  exhaust absorption chiller, 277, 278f
  Li-Br, 273, 277
Downflow furnace, 111–112
“Drain down” systems, 331
Duty cycling, 210

E

Earth cooling, 143
Economic analysis, CCHP systems, 279–283; *see also* Costs
  cost analysis, 282, 283t
  detailed electricity and natural gas usage, 280, 280t
  electric and natural gas costs, 281, 283t
  electric output, 281, 281t
  heat output, 281, 282t
Economizer systems, 222
Ecotect, 145–146
Efficiency curves, for solar water heating collectors, 329, 329f
Ejector heat pumps, 269, 270f
Electric devices, 202

Electric grid, synchronization of generation equipment on, 342–343
Electric service, to building with RE
overcurrent protection, 337f, 338, 339
sizing, 337, 338
voltage regulation, 338f, 339
Electrical generation systems, utilities, 343–345
Electrical power (maximum), defined, 241–242
Electrical systems; *see also* Control strategies
daylighting control system, 213–218, 213f, 214f, 215t, 218t
motor duty cycling controls, 211–213
Electronic devices, 202
Electronic thermal anemometer, 222
Electronicto-pneumatic (E/P) transducers, 203
EMCS, *see* Energy management and control systems (EMCS)
Emerging Technologies (ET), 2
Energy analysis methods, detailed, 70–76
heat balance method, 70–73
thermal network method, 73–74
weighting factors, 74–76
Energy analysis methods, simplified, 60–70
transient thermal network analysis, 67–70
variable base degree days method, 60–66
Energy cost savings, 237–238, 239f
Energy Information Administration (EIA), 475
Energy management and control systems (EMCS)
about, 189
communication protocol, 209–210
components of, 204–206
cost benefits of, 208
design considerations of, 207–209
functions of, 206–207
size categories, 204
Energy Management System (EMS), 204
EnergyPlus, 42, 71–72, 76, 84–85, 87, 233, 243
EnergyPlus™, SBEM and, 319, 483, 488–490
energy sources interaction, 489, 489f
model, 489, 490f
parametric studies for, 495, 495f
SBEM *vs.* uWRF for Midtown, 493, 494f
total energy demand, 492, 493f
Energy savings from daylighting controls, 213
Energy storage density (ESD)
comparison of, 392, 393f
of sensible TES, 385
Energy storage systems, for buildings, 347–408
overview, 347–348
sorption TES system for buildings, 385, 388–407
performance improvement, 397–407; *see also* Performance improvement
working pairs, 392–397; *see also* Working pairs
working principle, 385, 388–392
TES systems, sensibility and latency, 348–385
air conditioning, 349–358
ceiling board, PCM, 357, 357f, 358
ceilings, PCM, 366, 367
chilled water storage/aquifers, 349–352, 350f, 351f, 352t
CHP and, 370–375, 371f, 372f, 373t, 374f
classification, 348, 349f
floor heating, PCM, 366, 367f
for heating, 358–367
heat pumps and, 367–370, 368f, 369f
hot water tank/aquifers, 358–361, 358f, 360f

integration literature summary, building with, 375–379, 376t–378t
latent TES with PCMs, 352, 353–354, 364–365; *see also* Phase change materials (PCMs)
materials, 379–383; *see also* Materials, for sensible/latent TES
mathematical modeling of storage system, 383, 384–385, 386t–387t
PCMs, 352–355, 357–358, 364–367; *see also* Phase change materials (PCMs)
rock and brick reservoir, 361–364, 362f, 363f
solar shading, PCM for, 354, 355, 356f, 357, 357t
wallboards, PCM, 365, 366f
Energy system integration (ESI), 335–345
challenges, 336–337
challenges and solutions, building level, 337–341
overcurrent protection, 337f, 338, 339
sizing, 337, 338
voltage regulation, 338f, 339
wear-and-tear on reactive power compensation equipment, 340–341, 340f
challenges and solutions, grid-level, 342–343
synchronization of generation equipment, 342–343
voltage stability, 342
challenges and solutions, substation-level, 341–342
network protectors in systems, 341–342
RE on local substation, 341
net metering policies, 335–336
utilities, electrical generation systems, 343–345
allocating costs and investment, 344–345
ramp-rates and spinning reserve, 343–344
EQUEST, 83
Error transfer function, 197
ESI, *see* Energy system integration (ESI)
Ethernet local area networks, 209
Evacuated tube collectors, 326–327, 334–335
Evaporative cooling, direct/indirect, 158–162; *see also* Passive cooling
design considerations, 160–162
performance, 159–160
principle, 158–159
Evaporative cooling systems, 143
Expert controls, 202; *see also* Intelligent control systems
Exponentially Weighted Moving Average (EWMA) control charts, 440, 441

F

Facility loads, 190
Fanger comfort model, 232, 233, 234
Fatty acid, as PCM, 353
Fault detection and diagnosis (FDD), automated, 421–464
alarm management, 421–424
PMM, 424, 425f
process/system fault definition, 422–423, 423f
application, challenges in, 450–452
strategy/approach related, 451–452
classification, 424, 425–436
current trends, 435–436
most commonly used methods, 427–429, 428f, 429f
overview, 424, 425
PCA, 430–434, 432f, 434f
traditional alarm management, prismatic approach, 425–427, 426f
for DCS, case study
design and features, 454–455, 455f

implementation results, 455–461, 456t, 457f, 457t, 459f, 460f
process layout and specifications, 452–453, 453f, 454f
for district cooling systems, case study, 452–464
industrial and HVAC applications, 441–449
business models and commercial solutions, 443
commercial software, 443, 444t–447t
hardware/software requirements, 442–443
implementations, review of, 443, 448–449
recent advances, 436–441, 438t–439t
design and features, 454–455, 455f
implementation results, 455–461
cooling coil fouling, 457, 458, 461, 459f, 460f
historical data set clusters classification, 457, 457f
monitored variables, 455, 456t
recommendations, 461, 464
reduced chilled water flow, 457, 461, 462f, 463f
statistics thresholds, 457, 457t
process layout and specifications, 452–453, 453f, 454f
Fault detection system for district cooling systems (case study), 452–464
FDD, *see* Fault detection and diagnosis (FDD)
FDD CX, 447t
Feasibility analysis, CCHP systems, 279–283
cost analysis, 282, 283t
detailed electricity and natural gas usage, 280, 280t
electric and natural gas costs, 281, 283t
electric output, 281, 281t
heat output, 281, 282t
Features, FDD, 454–455, 455f
Feedback control system, 192
Feed-forward networks, 244
Field interface devices (FID), 205, 206
Fins, defined, 308
Fire marshals, 298
Fire-tube boilers, 115
First Solar, 297
Flat-plate collectors, glazed, 326, 332t
Floor heating, PCM, 366, 367f
Footers, concrete, 298
Fouling, cooling coil, 457, 458, 461, 459f, 460f
Fourier's law of heat conduction, 28
Fuel cells, chemical reaction in, 254–255
Fuel oil, 112
Furnaces, 110–124
electric heat pumps, 120–121
electric resistance heating, 119
low-temperature radiant heating systems, 121–124
Fusion heat, of PCMs, 379, 380f
Fuzzy control, 202; *see also* Intelligent control systems

G

Gas-to-liquid heat exchangers, 264
Gaussian Process (GP) emulator, 87–88
Gauss-Jordan Matrix Solver, 41
Generator–Absorber heat eXchange (GAX), 265
Glazed flat plate collectors, 326, 332t
Grid-connected PV system, 300–301, 300f, 305, 305f
Grid-level challenges and solutions, 342–343
synchronization of generation equipment, 342–343
voltage stability, 342
Ground-coupled heat transfer, 229f

H

Hardware requirement, industrial and HVAC application, 442–443
Harry Thomason's technique, 361, 362f

Heat exchanger materials, 134
Heat flux modulation techniques, 229
Heat generation and transfer equipment, 109–124
  furnaces and boilers, 110–124
  introduction, 109–110
Heat pumps, TES and, 367–370, 368f, 369f
Heat rates, 115
Heat recovery, CCHP systems, 254, 261, 262–264, 263t
Heat recovery steam generator (HRSG), 258
Heat recovery unit (HRU), 255
Heat rejection equipment, 101–105
Heat transfer concepts, 24–30
  transient heat transfer from building envelope, 26–30
Heat transfer enhancement methods, 383, 384f
Heat wave event (summer 2010), 481, 482
Heating Degree Days (HDD), 316
Heating energy
  savings, 234
  use, 231
Heating, TES for, 358–367
  hot water tank/aquifers, 358–361, 358f, 360f
  PCMs
    ceilings, 366, 367
    floor heating, 366, 367f
    latent TES with, 364–365, 364f, 365f
    wallboards, 365, 366f
  rock and brick reservoir, 361–364, 362f, 363f
Heating, ventilation and air conditioning (HVAC) systems, automated FDD in, *see* Fault detection and diagnosis (FDD)
Helmholtz equation, 35–36
Hierarchical kernel learning method, 440
High efficiency system integration, 127–133
  chiller water loops and VAV systems, 127–133
High temperature conditions (HTC), 297
Hittle, 42
Horizontal furnaces, 112
Hot water heat TES systems, 373–374, 374f
Hot water tank/aquifers, sensible TES with, 358–361, 358f, 360f
Hotelling T^2 statistics, 431–432, 432f, 433, 434, 454
Houghton Hall Office Building in Luton, UK, 179–180
Humidification, 162
HVAC equipment operation
  cooling/heating central plant optimization, 234–236
  demand controlled ventilation (DCV), 225–228, 228t
  outdoor air intake controls, 221–225, 223t–224t
  radiant slab heating systems, 228–234, 234t
HVAC mechanical systems, 133–135
  heat exchanger materials, 134
  supervisory control systems, 133–134
  surface enhancing heat transfer, 134–135
HVAC system
  control systems used in, 202
  optimal start of, 218–221
  sensors used for, 191t
  with thermal storage
    neural network controls of, 243–246
    passive/active thermal energy storage systems, 240–243
    precooling of building thermal mass, 236–239
Hybrid ventilation, 153–154
Hydraulic systems, 203

I

IBM TRIRIGA Energy Optimization, 446t
Ice storage system, 242

Identification, fault, 424, 425f
IES-VE, 313
Implementations, industrial and HVAC, 443, 448–449
Indoor air quality (IAQ), 207, 221, 225
Industrial and HVAC applications, fault detection methods, 441–449
 business models and commercial solutions, 443
 commercial software, 443, 444t–447t
 hardware/software requirements, 442–443
 implementations, review of, 443, 448–449
Industrial heat pumps, 121
Institute of Electrical and Electronics Engineers (IEEE), Standard 1547, 340–341, 345
Integral gain constant, 200
 derivative control, 200
Integrated building automation system (IBAS), 189, 204
Integrated-collector-storage collectors, 330
Integrated/Sustainable Building Equipment and Systems (ISBES) Initiative, 2
Integration
 literature summary, TES, 375–379, 376t–378t
 solar energy systems, *see* Solar energy systems
Intelligent control systems; *see also* Control strategies
 about, 201
 artificial neural networks, 202
 expert controls, 202
 fuzzy control, 202
Interconnection Requirement Study, 336
International Electrotechnical Commission (IEC) standard, 297
International Energy Agency (IEA), 347
Inverters, dual mode, 301
Investment, utilities' electrical generation systems, 344–345
I-v curve, of PV cell, 295–296, 295f

J

Journal of Solar Energy Engineering, 2

K

Kathabar, 107–108
K-means clustering algorithm, 457, 457f

L

LabView, 442
Laplace transform, 193–194
Latency, TES, 348–385
 air conditioning, building, 349–358
  chilled water storage/aquifers, 349–352, 350f, 351f, 352t
  PCM ceiling board, 357, 357f, 358
  PCM for solar shading, 354, 355, 356f, 357, 357t
  PCMs, 352, 353–354, 353f, 354t, 355f, 355t
 CHP and, 370–375
  CCHP system, diagram of, 371, 372f
  general layout, 370, 371f
  hot water heat TES systems, 373–374, 374f
  performance of CCHP plant, 372, 373t
 classification, 348, 349f
 for heating, 358–367
  hot water tank/aquifers, 358–361, 358f, 360f
  PCM ceilings, 366, 367
  PCM floor heating, 366, 367f
  with PCMs, 364–365, 364f, 365f
  PCM wallboards, 365, 366f
  rock and brick reservoir, 361–364, 362f, 363f

heat pumps and, 367–370, 368f, 369f
materials, 379–383
heat transfer enhancement methods, 383, 384f
main features, 382, 382t
PCM for TES systems, comparison, 383, 383t
PCMs, classification of, 379, 379f
PCMs, melting temperature and fusion heat, 379, 380f
sensible storage concepts, 380–381, 381t
mathematical modeling of storage system, 383, 384–385, 386t–387t
TES integration literature summary, building with, 375–379, 376t–378t
Lawrence Berkeley National Laboratory (LBNL), 83
Lighting energy use savings, 216
Lightshelves, defined, 309
Limitations, for FDD, 450–451
Liquefied propane gas (LPG), 112
Liquid desiccant air conditioners (LDACs), 269
Lithium chloride, 107
Load anticipation, 190
Load duration curve (LDC)
for data centers
cooling, 274–275, 275f
electric, 274, 274f
two-dimensional, 275–276, 275f, 276f
sizing and evaluating building electric power, 273f, 274, 274f
Load tracking, 190
Local substation, RE on, 341
Losses, thermal, 328
Low irradiance conditions (LIC), 297
Low temperature conditions (LTC), 297

M

Materials
for sensible/latent TES, PCMs, 379–383
classification of, 379, 379f
comparison, 383, 383t
heat transfer enhancement methods, 383, 384f
main features, 382, 382t
melting temperature and fusion heat, 379, 380f
sensible storage concepts, 380–381, 381t
in solar water heating systems, 329, 330
Mathematical modeling, of storage system, 383, 384–385, 386t–387t
Mean air temperature (MAT), 229, 232
Mean radiant temperature (MRT), 229
Measurement and verification (M&V) of energy savings, 78
Mechanical cooling equipment, 100
Mechanical draft towers, 103
Melting temperature, of PCMs, 379, 380f
Methodology for case study, air conditioning energy consumption, 483–490
BEM, 485–488, 487f, 487t, 488f
BEP, 484–485
SBEM, EnergyPlus™, 488–490, 489f, 490f
uWRF, city scale model, 483, 483f
Micro-inverters, 301
Mitalas, 42
Modeling
building air conditioning energy consumption, *see* Air conditioning energy consumption
mathematical, of storage system, 383, 384–385, 386t–387t
Modules, defined, 294
Montreal Protocol, 96
Motor duty cycling controls, 211–213; *see also* Electrical systems
Multi-level switching controls, 309
Multiple boilers, control for, 235
Multiple chillers control, 235; *see also* Chillers

Multiplexer (MUX), 206
Multi-scale PCA (MPCA), 435

N
National Electrical Manufacturers Association (NEMA), 211
National Weather Service (NWS), 481
Natural gas, 258
Natural ventilation, 147–154; *see also* Passive cooling
 design considerations, 150–154
 performance, 148–150
 principle, 147–148
Net metering
 defined, 335
 policies, 336
 PV for, 336
Neural network controls, 243–246
Neurons, 202
Night cooling, 143
Night cooling with thermal mass, 154–157; *see also* Passive cooling
 design considerations, 155–157
 performance, 154–155
 principle, 154
NN-based optimal controller, 244, 245, 245f
Nominal operating cell temperature (NOCT), 297, 304
NREL Chemical Storage Facility, 323–324, 324f
NYCMetNet, 482, 482f

O
Offline model training, 454
One-zone controls of carbon-di-oxide, 228
Online FDD, 454
Open loop systems, 192
OpenStudio, 313
Operating differential, 198
Operation, CCHP (case studies), 271–279
Operative temperature (OT), 229
Optimal daylighting controller, 216
Outdoor air flow, 227
Outdoor air intake controls, 221–225, 223t–224t
Overcurrent protection, on electrical service, 337f, 338, 339
Overhangs
 defined, 308
 window, 315

P
PACRAT, 447t
Palais des congrés de Montréal, 449
Panoptix Continuous Diagnostic Advisor, 444t
Parabolic-trough collectors, 327–328
Paraffin
 organic heat storage materials, 382
 wax, as PCM, 353
Parallel duty cycling, 212
Parameter change
 disturbance, 422
 process, 422
Passive cooling, 142–143
 case studies, 179–184
 direct/indirect evaporative cooling, 158–162
 double skin facade, 168–173
 natural ventilation, 147–154
 night cooling with thermal mass, 154–157
 overview, 143–145
 phase change material, 173–179
 prescreening feasibility, 145–147
 Sunspace, 165–168
 Trombe Wall, 162–165
Passive design strategies, 6, 8
Passive solar heating, 143–144, 313–319
 computer tools for, 319
 direct gain, 315–316, 317f
 equations for, 318
 sunspace, 316, 317f
 Trombe Wall, 316, 317f
 window overhang, 315

Passive systems, solar water heating systems, 330
Passive thermal energy storage systems, 240–243
Pattern matching method, 440
PCMs, *see* Phase change materials (PCMs)
Penetration limits, defined, 336
Performance, of CCHP plant, 372, 373t
Performance improvement, sorption TES system, 397–407
  absorption, 397–399, 398f
  adsorption, 399–400, 400f
  prototypes and systems, 400–407
    adsorption TES test facility, 403–404, 405f
    closed $H_2O/CaCl_2$, 400, 403, 403f
    H_2O/silica gel, 403, 404f
    H_2O/13X zeolite, 405, 406f
    recent achievements, 400, 401t–402t
    solar sorption pilot plant, 406, 406f
Phase change materials (PCMs), 173–179; *see also* Passive cooling
  ceiling board, 357, 357f, 358
  ceilings, 366, 367
  classification of, 379, 379f
  design considerations, 177–179
  floor heating, 366, 367f
  latent heat of, 315
  latent TES with, 352, 353–354, 364–365
    cross-sectional view of heat storage tank, 364f
    cumulative energy saving, 355t
    free cooling systems, 355f
    paraffin wax, 365f
    schematic diagram, 353f
    thermal storage systems, comparison, 354t
  melting temperature and fusion heat, 379, 380f
  performance, 174–177
  principle, 173–174
  for solar shading, 354, 355, 356f, 357, 357t
  Stefan problem for, 383, 384
  TES units, 374
  wallboards, 365, 366f
Photo-sensor system, 216, 217f
Photovoltaics (PVs), 292–305
  BIPV, 299
  cadmium telluride, 296–297
  cells, equivalent circuit diagram, 294, 295f
  effect, 292
  grid-connected, 300–301, 300f, 305, 305f
  IEC standard, 297
  initial, operation and maintenance costs, 303t
  i-v curve, 295–296, 295f
  roof racks, 298
  short-circuit operating current, 294
  solar insolation, map of, 292, 293f
  solar resource, map of, 292–294, 293f
  wear-and-tear on reactive power compensation equipment, 340–341, 340f
Pierce two-node model, 233, 234
Piles, 298
Pitot-tube array station, 222
Plenum, defined, 322
Plenum pressure control, 225
Pneumatic devices, 202
Policies, net metering, 336
Polycarbonate, 365
Polymer electrolyte membrane fuel cells (PEFC/PEMFC), 258
Polynomial transfer function, 48
Porosity, defined, 320
Power combustion furnaces, 112
Power generation unit (PGU), 254, 255
Power-to-heat ratio, defined, 370
Pre-cooling control strategy, 237–238, 237f
Pre-cooling energy savings, 239t
Precooling of building thermal mass, 236–239

Predicted mean vote (PMV), 232
Predicted mean vote modified by effective temperature (PMVET), 233
Predictive control strategy, 243
Preheating, ventilation air, *see* Solar ventilation air preheating
Primary land use tax lot output (PLUTO), 486, 487f
Prime movers, for CCHP systems, 254, 260–261, 260f, 262t
Principal component analysis (PCA)
 ANN and, 435
 fault detection method, 430–434, 432f, 434f
 FDD design and feature, 454–455, 455f
 MPCA, 435
 operational flow diagram, 434, 434f
Prismatic approach, traditional alarm management, 425–427, 426f
Prismatic regions, defined, 426
Process monitoring method (PMM), 424, 425f
Process parameter change, 422
Proportional control system, 199–200
Proportional gain constant, 199
Proportional-plus-integral control (PI control), 200
Proportional-plus-integral-plus derivative (PID) control, 200, 201f, 226, 228
Propylene glycol, 331, 332
Protectors, in network systems, 341–342
Protocol implementation conformance statement (PICS), 210
Prototypes, sorption TES system, 400–407
 adsorption TES test facility, 403–404, 405f
 closed $H_2O/CaCl_2$, 400, 403, 403f
 H_2O/silica gel, 403, 404f
 H_2O/13X zeolite, 405, 406f
 recent achievements, 400, 401t–402t
 solar sorption pilot plant, 406, 406f
PRRMSE indicators, 88
Public Interest Energy Research (PIER), 448
Public Utilities Commission (PUC), 336
PVs, *see* Photovoltaics (PVs)

Q

Qualitative model-based methods, FDD, 428–429, 428f
Quantitative model-based methods, FDD, 427–429, 429f

R

Racks, roof, 298
Radial Basis Function (RBF) neural network, 441
Radiant gains, 328
Radiant slab heating systems, 228–234, 234t
Radiant systems, 121–124
Ramp-rates, 343–344
RC thermal network technique, 67–69
Reactive power compensation equipment, 340–341, 340f
Recent trends, in FDD methods, 436–441, 438t–439t
Reciprocating engines, 258, 261
Recovery time, 219
Reduced chilled water flow, 457, 461, 462f, 463f
Regeneration process, 98, 268
Regression analysis, 219
Renewable energy (RE) systems
 advantages, 291
 electric service to building with overcurrent protection, 337f, 338, 339
  sizing, 337, 338
  voltage regulation, 338f, 339
 on local substation, 341
Requirements
 hardware/software, industrial and HVAC application, 442–443
 TES, 270–271

Resources, solar, 292–294, 293f
Results, air conditioning energy consumption, 490–495, 491f, 492f, 493f, 494f, 495f
RETScreen, 279
Reynolds averaged form, defined, 484
RMI Headquarters Building: Amory Lovins Uber Solar Home in Colorado, US, 180, 182–184
Rock and brick reservoir, 361–364, 362f, 363f
Roof racks, 298
Rotor angle stability, defined, 342

S

Salt hydrates, 382
Saturation enthalpy, 108–109
SBEM, *see* Single building energy model (SBEM)
SCIwatch®, 445t
Screws, 298
Secondary systems, 124–127
  fresh air ventilation rates, 126–127
Sensibility, TES, 348–385
  air conditioning, building, 349–358
    chilled water storage/aquifers, 349–352, 350f, 351f, 352t
    PCM ceiling board, 357, 357f, 358
    PCM for solar shading, 354, 355, 356f, 357, 357t
    PCMs, 352, 353–354, 353f, 354t, 355f, 355t
  CHP and, 370–375
    CCHP system, diagram of, 371, 372f
    general layout, 370, 371f
    hot water heat TES systems, 373–374, 374f
    performance of CCHP plant, 372, 373t
    TES integration literature summary, building with, 375–379, 376t–378t
  classification, 348, 349f
  ESD of, 385
  for heating, 358–367
    hot water tank/aquifers, 358–361, 358f, 360f
    PCM ceilings, 366, 367
    PCM floor heating, 366, 367f
    PCM wallboards, 365, 366f
    rock and brick reservoir, 361–364, 362f, 363f
  heat pumps and, 367–370, 368f, 369f
  materials, 379–383
    heat transfer enhancement methods, 383, 384f
    main features, 382, 382t
    PCM for TES systems, comparison, 383, 383t
    PCMs, classification of, 379, 379f
    PCMs, melting temperature and fusion heat, 379, 380f
    sensible storage concepts, 380–381, 381t
  mathematical modeling of storage system, 383, 384–385, 386t–387t
Sensors, 191
Shaft energy, 254
Shockley, William, 294, 295
Short-circuit operating current, of PV module, 294
Sick Building Syndrome (SBS), 140, 149–150
Silica gel, water and, 394, 403, 404f
Single building energy model (SBEM)
  AC compressor work in, 488
  energy consumption for, 493
  Energy Plus, 489
  energy sources interaction, 489f
  ensemble of, 475–476
  sensitivity analysis, 493, 495f
  solutions to uWRF, 487
  thermal zones, 489
  by TMY weather file, 475, 490, 494
  using US Department of Energy, 483
  uWRF *vs.*, 493, 494f
Single chiller control, 235
Single-effect (1E) absorption chillers, 264–265, 265f, 371

Sizing
of electrical service to building, 337, 338
options, CCHP (case studies), 271–279
SkySpark, 444t, 448
Software requirement, industrial and HVAC application, 442–443
Sol-air temperature, 71–72
Solar energy systems, integration of, 291–345
cooling load avoidance, 313–319, 317f
daylighting, 305–313, 312f
ESI, 335–345
allocating costs and investment, 344–345
building level challenges and solutions, 337–341; *see also* Building level challenges and solutions
challenges, 336–337
grid-level challenges and solutions, 342–343
net metering policies, 335–336
ramp-rates and spinning reserve, 343–344
substation-level challenges and solutions, 341–342
utilities, electrical generation systems, 343–345
overview, 291–292
passive solar heating, 313–319
computer tools for, 319
direct gain, 315–316, 317f
equations for, 318
sunspace, 316, 317f
Trombe Wall, 316, 317f
window overhang, 315
photovoltaics, 292–305
BIPV, 299
cadmium telluride, 296–297
cells, equivalent circuit diagram, 294, 295f
effect, 292
grid-connected, 300–301, 300f, 305, 305f
IEC standard, 297
initial, operation and maintenance costs, 303t
i-v curve, 295–296, 295f
roof racks, 298
short-circuit operating current, 294
solar insolation, map of, 292, 293f
solar resource, map of, 292–294, 293f
ventilation air preheating, 319–324
applications, 320
components, 321, 322f
costs, 319, 320, 323t
maintenance requirements, 319
NREL Chemical Storage Facility, 323–324, 324f
potential energy delivery, map of, 319, 320f
transpired solar collector and bypass damper, 323, 324f
water heating systems, 324–335
active systems, 331, 331f
collectors, types, 324–335, 325f
costs, 332t, 333, 334–335
efficiency curves, 329, 329f
evacuated tubes, 326–327, 334–335, 334f
glazed flat plate collectors, 326, 332t
integrated-collector-storage collectors, 330
materials and components, 329, 330
parabolic-trough collectors, 327–328
passive systems, 330
SRCC, 328–329
unglazed collector, low temperature, 325–326, 330, 332t
Solar heat gain coefficient (SHGC), 308, 314
Solar insolation, map of, 292, 293f
Solar Rating & Certification Corporation (SRCC), 328–329

Solar resource, map of, 292–294, 293f
Solar shading, PCMs for, 354, 355, 356f, 357, 357t
Solar ventilation air preheating, 319–324
  applications, 320
  components, 321, 322f
  cost, 319, 320
  initial cost, operation and maintenance cost, 323t
  maintenance requirements, 319
  NREL Chemical Storage Facility, 323–324, 324f
  potential energy delivery, map of, 319, 320f
  transpired solar collector and bypass damper, 323, 324f
Solar water heating (SWH) systems, PCM-charged, 364–365, 364f, 365f
Solid desiccant A/C technology, 268–269
Solid oxide fuel cells (SOFC), 258
Solutions
  building level challenges and, ESI, 337–341
    overcurrent protection, 337f, 338, 339
    sizing, 337, 338
    voltage regulation, 338f, 339
    wear-and-tear on reactive power compensation equipment, 340–341, 340f
  substation-level challenges, ESI
    grid-level, 342–343
    network protectors in systems, 341–342
    RE on local substation, 341
Sorption TES system for buildings, 385, 388–407
  performance improvement, 397–407
    absorption, 397–399, 398f
    adsorption, 399–400, 400f
    prototypes and systems, 400–407, 401t–402t, 403f, 404f, 405f, 406f
  working pairs, 392–397
    absorption, 393–394, 395t
    adsorption, 394, 396–397, 396f, 397f
    ESD, comparison of, 392, 393f
  working principle, 385, 388–392
    absorption, 385, 388–389, 388f
    adsorption, 389–392, 390f, 391f, 392f
Southwest Gas Corporation (SWG), 281
Spherical geometry, models for, 385, 386t–387t
Spinning reserve, 343–344
Squared prediction error, defined, 434
Stack ventilation, 151, 152
Staggered duty cycling, 212
Standalone solid desiccant A/C technology, 268–269
Standard, IEC, 297
Standard test conditions (STC), 297
Steel boilers, 115
Stefan-Boltzmann equation, 123
Stefan problem, for PCMs, 383, 384
Stephenson, 42
Storage-priority control strategy, 240
Strategy/approach related challenges, FDD application, 451–452
String inverters, 301
Substation-level challenges and solutions, ESI
  network protectors in systems, 341–342
  RE on local substation, 341
Summer 2010 heat wave event, 481, 482
Sun Shot program, 134
SunPower, 297
Sunspace, 165–168; *see also* Passive cooling
  design considerations, 167–168
  passive solar heating strategy, 316, 317f
  performance, 166–167
  principle, 165–166
  temperature of, 316

Supervisory control and data acquisition (SCADA), 442
Supervisory control systems, 133–134
Supervisory controllers; *see also* Control strategies
  communication protocol, 209–210
  components of EMCS, 204–206
  design considerations of EMCS, 207–209
  functions of ECMS, 206–207
Support vector data description (SVDD) algorithm, 440
Support vector regression (SVR) models, 440
Surface enhancing heat transfer, 134–135
Switching controls, 309
System(s)
  controls, CCHP (case studies), 271–279
  sorption TES, 400–407
    adsorption TES test facility, 403–404, 405f
    closed $H_2O/CaCl_2$, 400, 403, 403f
    H_2O/silica gel, 403, 404f
    H_2O/13X zeolite, 405, 406f
    recent achievements, 400, 401t–402t
    solar sorption pilot plant, 406, 406f

T

Temperature-modulation control, 229
Temperatures
  solar water heating system, 331–332
  unglazed collector, 330, 332t
Tennessee Eastman process, 435
TES, *see* Thermal energy storage (TES)
Thermal comfort, 232, 233
Thermal energy storage (TES)
  applications, 348
  defined, 348
  requirements/benefits, 270–271
  sensibility and latency, 348–385
    air conditioning, 349–358
    ceiling board, PCM, 357, 357f, 358
    ceilings, PCM, 366, 367
    chilled water storage/aquifers, 349–352, 350f, 351f, 352t
    CHP and, 370–375, 371f, 372f, 373t, 374f
    classification, 348, 349f
    floor heating, PCM, 366, 367f
    for heating, 358–367
    heat pumps and, 367–370, 368f, 369f
    hot water tank/aquifers, 358–361, 358f, 360f
    integration literature summary, building with, 375–379, 376t–378t
    latent TES with PCMs, 352, 353–354, 364–365; *see also* Phase change materials (PCMs)
    materials, 379–383; *see also* Materials, for sensible/latent TES
    mathematical modeling of storage system, 383, 384–385, 386t–387t
    PCMs, 352–355, 357–358, 364–367; *see also* Phase change materials (PCMs)
    rock and brick reservoir, 361–364, 362f, 363f
    solar shading, PCM for, 354, 355, 356f, 357, 357t
    wallboards, PCM, 365, 366f
  sorption TES system for buildings, 385, 388–407
    performance improvement, 397–407
    working pairs, 392–397
    working principle, 385, 388–392
Thermal energy storage (TES) systems
  active and passive systems, 240–243
  neural network controls of, 243–246
Thermal losses, 328
Thermally activated cooling systems, 264–269
  absorption and vapor-compression chillers, 265–266, 266t, 267f
  category, 264
  ejector heat pump cycle, 269, 270f
  single-effect (1E) absorption cycle, 264–265, 265f

solid desiccant A/C technology, 268–269
standalone liquid desiccant A/C, 269
Thermal mass, 154, 157
Thermal sensation vote (TSV), 233
Thermocline, 358
Three phase cycle discharging method, 398f, 399
Topping cycle, CCHP systems, 271
Traditional alarm management, prismatic approach, 425–427, 426f
Trane Intelligent Services, 445t
Transfer function, 194, 197f
Transient building envelope energy analysis, 30–59
conduction transfer function (CTF) methods, 41–44
finite difference methods, 31–34
frequency-domain regression (FDR) method, 45–53
interzone temperature profile estimation (ITPE) techniques, 34–41
response factors, 53–59
Transient System Simulation Program (TRNSYS) modeling, 364
Triethylene glycol, 107
Trigeneration, defined, 252
TRNSYS, 42, 76, 85
Trombe Wall, 162–165, 316, 317f; *see also* Passive cooling
design considerations, 164–165
performance, 163–164
principle, 162–163
Turbulent kinetic energy, 485
Two-position control system, 198–199
Two-zone controls of carbon-di-oxide, 228
Typical Meteorological Year (TMY), 319, 483, 490, 491f, 492

U

Unglazed collector, low temperature, 325–326, 330, 332t
Upflow furnace, 111
Urban heat island (UHI) effect, 476–477, 477f, 478t
Urbanized weather forecasting model (uWRF)
building parameters for locations, 486–487, 487t
city scale model, 483, 483f
PLUTO and, 486
SBEM *vs.*, 493, 494f
TMY and, 492
weather outputs, 490, 491f
Utilities, electrical generation systems, 343–345
allocating costs and investment, 344–345
ramp-rates and spinning reserve, 343–344
UWRF, *see* Urbanized weather forecasting model (uWRF)

V

Vapor-compression chillers, 266, 266t
Variable air volume (VAV), 221, 225
Variable air volume (VAV) systems and chiller water loops, 127–133
energy recovery systems, 132–133
Variable air volume (VAV) terminal boxes, 453
Ventilation, 125
Ventilation air, preheating, *see* Solar ventilation air preheating
Visible light transmittance (VLT), 308
VisualDOE, 83
Voltage regulation, on electric service to building with RE, 338f, 339
Voltage stability, of electric grid, 342

W

Wallboards, PCM, 365, 366f
Water heating systems, solar, 324–335
active systems, 331, 331f
collectors, types, 324–335, 325f
evacuated tube, 326–327
glazed flat plate collectors, 326, 332t

integrated-collector-storage collectors, 330
parabolic-trough collectors, 327–328
unglazed collector, low temperature, 325–326, 330, 332t
costs, 332t, 333, 334–335
efficiency curves, 329, 329f
evacuated tube, 334–335, 334f
materials and components, 329, 330
passive systems, 330
SRCC, 328–329
Water tank, hot water, 358–361, 358f, 360f
Water/ammonia (NH_3/H_2O), 98
Water/LiBr absorption chillers, 266
Water/lithium-bromide (H2O/LiBr), 98
Water-tube boilers, 115
Wear-and-tear on reactive power compensation equipment, 340–341, 340f
Web-bulb depression efficiency (WBDE), 159–160
Whole-building energy models, 76–89
forward modeling methods, 81–86
inverse modeling methods, 77–81
meta-modeling approach, 86–89
Wind-driven natural ventilation, 143, 150–151
Working pairs, sorption TES system, 392–397
absorption, 393–394, 395t
adsorption, 394, 396–397, 396f, 397f
silica gel and water, 394
zeolites and water, 394, 396–397, 396f, 397f
ESD, comparison of, 392, 393f
Working principle, of sorption TES system, 385, 388–392
absorption, 385, 388–389, 388f
adsorption, 389–392, 390f, 391f, 392f
World urban database and access portal tools (WUDAPT), 486
Wright, Frank Lloyd, 307

Z

Zeolites, water and, 394, 396–397, 396f, 397f, 405, 406f
Zero-input response, 43
Zion National Park Visitor Center, 152